ADVANCES IN IMMUNOTHERAPEUTIC APPROACHES TO TUBERCULOSIS

EDITED BY: Rogelio Hernandez Pando, Iris Estrada-Garcia and Juraj Ivanyi
PUBLISHED IN: Frontiers in Immunology and Frontiers in Microbiology

IUIS

frontiers Research Topics

frontiers

ISSN 1664-8714
ISBN 978-2-88966-901-1
DOI 10.3389/978-2-88966-901-1

About Frontiers

Frontiers is more than just an open-access publisher of scholarly articles: it is a pioneering approach to the world of academia, radically improving the way scholarly research is managed. The grand vision of Frontiers is a world where all people have an equal opportunity to seek, share and generate knowledge. Frontiers provides immediate and permanent online open access to all its publications, but this alone is not enough to realize our grand goals.

Frontiers Journal Series

The Frontiers Journal Series is a multi-tier and interdisciplinary set of open-access, online journals, promising a paradigm shift from the current review, selection and dissemination processes in academic publishing. All Frontiers journals are driven by researchers for researchers; therefore, they constitute a service to the scholarly community. At the same time, the Frontiers Journal Series operates on a revolutionary invention, the tiered publishing system, initially addressing specific communities of scholars, and gradually climbing up to broader public understanding, thus serving the interests of the lay society, too.

Dedication to Quality

Each Frontiers article is a landmark of the highest quality, thanks to genuinely collaborative interactions between authors and review editors, who include some of the world's best academicians. Research must be certified by peers before entering a stream of knowledge that may eventually reach the public - and shape society; therefore, Frontiers only applies the most rigorous and unbiased reviews.
Frontiers revolutionizes research publishing by freely delivering the most outstanding research, evaluated with no bias from both the academic and social point of view. By applying the most advanced information technologies, Frontiers is catapulting scholarly publishing into a new generation.

What are Frontiers Research Topics?

Frontiers Research Topics are very popular trademarks of the Frontiers Journals Series: they are collections of at least ten articles, all centered on a particular subject. With their unique mix of varied contributions from Original Research to Review Articles, Frontiers Research Topics unify the most influential researchers, the latest key findings and historical advances in a hot research area! Find out more on how to host your own Frontiers Research Topic or contribute to one as an author by contacting the Frontiers Editorial Office: frontiersin.org/about/contact

ADVANCES IN IMMUNOTHERAPEUTIC APPROACHES TO TUBERCULOSIS

Topic Editors:
Rogelio Hernandez Pando, Instituto Nacional de Ciencias Médicas y Nutrición Salvador Zubirán (INCMNSZ), Mexico
Iris Estrada-Garcia, Instituto Politécnico Nacional de México (IPN), Mexico
Juraj Ivanyi, King's College London, United Kingdom

We acknowledge the initiation and support of this Research Topic by the International Union of Immunological Societies (IUIS). We hereby state publicly that the IUIS has had no editorial input in articles included in this Research Topic, thus ensuring that all aspects of this Research Topic are evaluated objectively, unbiased by any specific policy or opinion of the IUIS.

Citation: Pando, R. H., Estrada-Garcia, I., Ivanyi, J., eds. (2021). Advances in Immunotherapeutic Approaches to Tuberculosis. Lausanne: Frontiers Media SA. doi: 10.3389/978-2-88966-901-1

Table of Contents

frontiers in Immunology

EDITORIAL
published: 22 April 2021
doi: 10.3389/fimmu.2021.684200

Editorial: Advances in Immunotherapeutic Approaches to Tuberculosis

Iris Estrada García[1], *Rogelio Hernández Pando*[2*] *and Juraj Ivanyi*[3]

[1] Department of Immunology, National School of Biological Sciences, ENCB-IPN, Mexico City, Mexico, [2] Experimental Pathology Section, Department of Pathology, National Institute of Medical Sciences and Nutrition 'Salvador Zubiran', Mexico City, Mexico, [3] Centre for Host–Microbiome Interactions, Guy's Campus of Kings College, London, United Kingdom

Keywords: Tuberculosis, Intracellular infection, pulmonary infection disease, mycobacterial infections, Immunotherapies

Editorial on the Research Topic

Advances in Immunotherapeutic Approaches to Tuberculosis

OPEN ACCESS

Edited and reviewed by:
Ian Marriott,
University of North Carolina at Charlotte, United States

****Correspondence:***
Rogelio Hernández Pando
rhdezpando@hotmail.com

Specialty section:
This article was submitted to Microbial Immunology, a section of the journal Frontiers in Immunology

Received: *22 March 2021*
Accepted: *07 April 2021*
Published: *22 April 2021*

Citation:
Estrada García I, Hernández Pando R and Ivanyi J (2021) Editorial: Advances in Immunotherapeutic Approaches to Tuberculosis. Front. Immunol. 12:684200. doi: 10.3389/fimmu.2021.684200

Tuberculosis (TB) has been a widespread infectious disease since ancient times and still remains a major worldwide health problem. Significant progress in drug development during the last decade greatly contributed to TB therapy, while immunotherapies represent an interesting opportunity for further improving the control of TB. However, particular attention needs to be given to the increasing emergence of drug-resistant strains of *M. tuberculosis* (Mtb) and the association of TB with HIV infection and with chronic degenerative diseases such as type 2 diabetes. This special issue of the Frontiers contains a collection of 15 papers that advance various aspects that are relevant to TB immunotherapy. They can be grouped into three categories, concerning: i) role of innate immune cytokines, ii) recognition of specific antigenic determinants and iii) improvement of diagnostic assays. These papers are being briefly reported in the text and quoted in **Table 1**, listing the number of registered views so far for each.

Much of the Mtb infection cycle is fulfilled in the cytoplasm of macrophages, which represent the key innate immune cellular element involved in the infection. A study of glycolysis and proinflammatory cytokines is reported on Mtb infected human lung macrophage populations *in vitro* (Cox et al.). Inhibition of histone deacetylase by suberanilohydroxamic acid increased interleukin (IL-1b) and reduced IL-10 production, thus enhancing interferon-γ, (IFN-γ), tumour necrosing factor-α (TNF–α) and granulocyte-macrophage colony-stimulating factor (GM-CSF) co-production in responding T helper cells. These results indicate that modulation of innate immunometabolic processes in macrophages can promote subsequent adaptive proinflammatory responses. A study of Linezolid chemotherapy in mice and macaques investigated reducing its IL-1 mediated bone marrow toxicity and TB pathology. Lung inflammation could be reduced using an IL-1 receptor antagonist Anakinra (Winchell et al.), without being immunosuppressive and retaining its therapeutic impact on TB

pathology The role of GM-CSF for innate resistance against TB was suggested on the grounds of its higher production by Mtb-infected human macrophages (Mishra et al.). The increased expression of genes involved in the GM-CSF signalling pathway was associated with diminished Mtb growth, hence indicating its translational potential as a host directed therapy. A subset of lung macrophages, linked to higher Th1 and Th17 responses, has been associated with better protection in Bacillus Calmette Guerin (BCG) vaccinated mice (Yang et al.). The role of sex influences on adjunctive anti-inflammatory therapies of TB has been examined, using monocyte derived macrophages (Dutta and Schneider).

Bacterial or immune cell derivatives could represent another form of immunotherapy. The immunogenicity of 15 secreted O-mannosylated glycoproteins of BCG was examined following their purification and expression in *Mycobacterium smegmatis* and *Escherichia coli* recombinants (Deng et al.). Two glycoproteins, BCG_0470 and BCG_0980 (PstS3), were proposed for vaccine development on the grounds of inducing higher immunodominant Th1 responses. A novel approach is represented by the demonstration of single domain antibody ligands with T-cell receptor (TcR)-like specificity (Ortega et al.). A clone, selected from a phage display library, recognised an HLA-A*0201 bound peptide, which is known to be an immunodominant epitope of the Ag85B antigen for human T cells. This proof-of-principle for generating antibodies with TcR-like specificity against epitopes on the surface of both replicating and dormant Mtb infected macrophages, warrants further investigation, since such antibodies, particularly when conjugated with apoptosis-inducing ligands, could lead to passive immunotherapy in immunocompromised HIV-infected TB patients. Further synergistic benefit may come from agents, e.g. IFNg, which enhance the surface expression of major histocompatibility complex (MHC) -bound epitope targets. Vaccination, through respiratory delivery of a whole cell inactivated vaccine, showed improved polymeric Ig receptor (i.e. pIgA dependent) protection in mice and non-human primates (Aguilo et al.). The immunotherapeutic potential of 'unconventional T cells' has been considered for cell transfer therapy of severe multidrug resistant infection (La Manna et al.). This included CD1–restricted T cells, MHC-related protein-1–restricted mucosal-associated invariant T cells, MHC class Ib–reactive T cells, and γδ T cells. A review of therapeutic vaccines covered several aspects of their construction. Potentials for faster disease resolution (Afkhami et al.) and shortening of chemotherapy for drug-resistant strains, fragmented/incomplete therapy and against relapsing disease, have been evaluated. The mechanisms discussed pertain to distinct immune responses induced by the infection versus the vaccines, as well as their efficacy in HIV co-infected individuals. The importance of non-recirculating, lung-residing immunity was suggested by the finding that IFN-γ secreting PD-1+ T cells accumulate in the lungs following aerosol and intratracheal delivery, but not in the lymph nodes and not after subcutaneous inoculation of BCG (Basile et al.). Single chain T cell receptor and light chain domain antibody ligands produced by phage display technology recognized the Mtb-specific sulfoglycolipid Ac_2SGL, complexed with the monomorphic CD1b cellular receptor, which are recognized by T cells in both active and latent TB (Camacho et al.). Molecular modelling suggested better recognition of the natural complex than it's synthetic analogue and this difference was interpreted as support for the therapeutic and diagnostic targeting of Mtb infected cells.

The prospects for IGRA and QTF-Plus tests distinguishing between active and latent TB has been reviewed with the aim of improving the specificity of tuberculin skin testing, which is obscured by BCG vaccination (Carranza et al.). Moreover, the frequency of the proportion of TNF-a only T_{EFF} cells, with an effector memory phenotype ($CD45RA^{-}CCR7^{-}CD127^{-}$) was associated with a higher risk of progression to active TB. However, expansion of immature myeloid-derived suppressor cells has been linked to both active TB and recently acquired latent TB. Differential diagnosis involved both cellular and antibody responses to the DosR regulon encoded latency-associated antigens and IFN-γ signalling, and miRNA and molecular signatures of the blood transcriptome. A study of circRNA microarray expression profiles identified circRNA_051239, circRNA_029965, and circRNA_404022 as potential biomarkers for TB diagnosis (Liu et al.). The expression of the CD69 biomarker of T-cell activation in active and latent TB cohorts was shown to distinguish latently infected subjects from

TABLE 1 | Review of Topic publications.

Category	Authors*	Subject	Views**
Role of innate immune cytokines	Cox–Keane	High IL-1b/low IL10 due to Histone deacetylase inhibitor	2,313
	Winchell–Flynn	IL-1 blockade, adjunct to chemotherapy	2,079
	Mishra–Khan	Protection by GM-CSF	1,515
	Yang–Dou	Protection by M1-cytokines	1,631
	Dutta–Schneider	Sex differences to therapies	784
Antigen-specific immunotherapy and prophylaxis	Deng–Yang	Mannosylated vaccine antigens	1,858
	Ortega–Espitia	Antibodies against T-cell epitopes	1,760
	Aguilo–Martin	Protective mucosal sIgA	1,597
	La Manna–Caccamo	Immunotherapy by genotype-unrestricted T cells	1,498
	Afkhami–Xing	Design of therapeutic vaccines	1,246
	Basile–Rottenberg	Protection by PD-1^{+} lung-resident T cells	1,110
	Camacho–Acosta	Sulfoglycolipid-CD1b specific antibodies	1,089
Diagnosis	Carranza–Torres	Distinguishing between active and latent TB	2,515
	Liu–Wang	New CirRNA biomarkers	1,409
	Chen–Fan	Low CD69+T cells post infection	1,517

*First and last authors; **Views registered on 2nd April, 2021.

those who were uninfected, despite continuous exposure to infection (Chen et al.).

In conclusion, the present collection provides further evidence that the immune system is a significant factor in both the containment and cure of Mtb infection. Immunotherapy based on the augmentation of protective immunity or decreasing the immune modulatory responses during late progressive disease can be of value as an adjunctive agent in TB treatment. In this respect, novel combinations of both new and old drugs need to be evaluated for their efficacy, when combined with various forms of immunotherapy. The goals of future immunotherapies must be to shorten chemotherapy use, prevention latent TB reactivation and prevent transmission of the infection.

AUTHOR CONTRIBUTIONS

IEG, RHP, and JI wrote and reviewed the manuscript. All authors contributed to the article and approved the submitted version.

Conflict of Interest: The authors declare that the research was conducted in the absence of any commercial or financial relationships that could be construed as a potential conflict of interest.

frontiers in Microbiology

ORIGINAL RESEARCH
published: 13 March 2020
doi: 10.3389/fmicb.2020.00407

Identification of Secreted O-Mannosylated Proteins From BCG and Characterization of Immunodominant Antigens BCG_0470 and BCG_0980

Guoying Deng[1†], Wenli Zhang[2†], Na Ji[3], Yunpeng Zhai[4], Xiaoxia Shi[5], Xin Liu[1] and Shufeng Yang[1]*

[1] Department of Microbiology, College of Basic Medical Sciences, Dalian Medical University, Dalian, China, [2] Department of Biochemistry and Molecular Biology, College of Basic Medical Sciences, Dalian Medical University, Dalian, China, [3] Department of Clinical Laboratory, Dalian Third People's Hospital, Dalian, China, [4] Department of Clinical Laboratory, Dalian Municipal Women and Children's Medical Center, Dalian, China, [5] Department of Occupational and Environmental Health, Dalian Medical University, Dalian, China

OPEN ACCESS

Edited by:
Juraj Ivanyi, King's College London, United Kingdom

Reviewed by:
Mahavir Singh, LIONEX GmbH, Germany
Andre Kipnis, Universidade Federal de Goiás, Brazil

***Correspondence:**
Shufeng Yang
shufengyang@dmu.edu.cn

[†] *These authors have contributed equally to this work*

Specialty section:
This article was submitted to Microbial Immunology, a section of the journal Frontiers in Microbiology

Received: *23 December 2019*
Accepted: *26 February 2020*
Published: *13 March 2020*

Citation:
Deng G, Zhang W, Ji N, Zhai Y, Shi X, Liu X and Yang S (2020) Identification of Secreted O-Mannosylated Proteins From BCG and Characterization of Immunodominant Antigens BCG_0470 and BCG_0980. Front. Microbiol. 11:407. doi: 10.3389/fmicb.2020.00407

Bacterial glycoproteins have been investigated as vaccine candidates as well as diagnostic biomarkers. However, they are poorly understood in *Mycobacterium bovis* strain bacille Calmette-Guérin (BCG), a non-pathogenic model of *Mycobacterium tuberculosis*. To understand the roles of secreted O-mannosylated glycoproteins in BCG, we conducted a ConA lectin-affinity chromatography and mass spectra analysis to identify O-mannosylated proteins in BCG culture filtrate. Subsequent screening of antigens was performed using polyclonal antibodies obtained from a BCG-immunized mouse, with 15 endogenous O-mannosylated proteins eventually identified. Of these, BCG_0470 and BCG_0980 (PstS3) were revealed as the immunodominant antigens. To examine the protective effects of the antigens, recombinant antigens proteins were first expressed in *Mycobacterium smegmatis* and *Escherichia coli*, with the purified proteins then used to boost BCG primed-mice. Overall, the treated mice showed a greater delayed-type hypersensitivity response *in vivo*, as well as stronger Th1 responses, including higher level of IFN-ɣ, TNF-α, and specific-IgG. Therefore, mannosylated proteins BCG_0470 and BCG_0980 effectively amplified the immune responses induced by BCG in mice. Together, our results suggest that the oligosaccharide chains containing mannose are the antigenic determinants of glycoproteins, providing key insight for future vaccine optimization and design.

Keywords: bacille Calmette-Guérin, glycoprotein, O-mannosylated protein, vaccine, oligosaccharide chains

INTRODUCTION

Tuberculosis (TB), caused by *Mycobacterium tuberculosis* (*M. tuberculosis*), remains a major threat to public health, with ever increasing morbidity and mortality rate worldwide (WHO, 2019). As reported by the World Health Organization in 2019, *M. tuberculosis* causes active TB disease in 10.0 million individuals each year, amongst whom approximately 1.5 million will die

(WHO, 2019). Current TB health interventions include treatment of latent TB infection and childhood immunization using the bacille Calmette-Guérin (BCG) vaccine (Martinez et al., 2017; WHO, 2019). However, latent TB infection prevention services are often not accessible to eligible patients, BCG vaccination coverage generally achieves a rate of at least 90% (WHO, 2019). Thus, the efficient prevention resulting from the vaccine confirms its importance in fight against TB.

BCG, an attenuated *Mycobacterium bovis* strain developed as a vaccine by Calmette and Guérin in 1921, is the only licensed TB vaccine approved by the World Health Organization. Nowadays, BCG still is widely applicable in epidemic regions, especially for the prevention of extrapulmonary TB in infants (Toida, 2000; WHO, 2019). Although its efficacy is varied, nearly 100 years of BCG use confirms that this living bacilli alone inducessubstantial immune protection against TB (Pym et al., 2003; Nieuwenhuizen and Kaufmann, 2018). It is thought that the alive bacilli secret protective antigens once injected, promoting T-lymphocyte based immune responses and eliciting humoral immunity against TB (Horn et al., 1999; Pym et al., 2003). Therefore, identifying and characterizing the most immunogenic and efficient antigens in the BCG vaccine may help to completely eliminate TB infection.

Currently, many protein-based subunit vaccines have been developed based on highly immunodominant antigens secreted by the replicating *M. tuberculosis* or latency-associated proteins expressed by persistent bacilli (Kebriaei et al., 2016; Nandakumar et al., 2016; Khademi et al., 2018). A large number of secreted mycobacterial proteins have also been investigated as diagnostic biomarkers and vaccine candidates (Wolfe et al., 2010; Facciuolo and Mutharia, 2014). Some secreted *M. tuberculosis* proteins including alanine and proline-rich protein (Apa/Rv1860), Rv0934 (PstS-1), Rv3763 (LpqH), Rv1887, and Rv1096, are reportedly modified by O-linked mannosylation, the most common type of the post-translational modifications (Gonzalez-Zamorano et al., 2009; Sanchez et al., 2012; Nandakumar et al., 2013; Smith et al., 2014). Homologous glycoproteins in various other mycobacteria show structural diversity in their glycosyl moieties. For example, native Apa protein, secreted by *M. tuberculosis*, *M. bovis*, and BCG, contain one to nine mannose residues, while recombinant Apa expressed by *Mycobacterium smegmatis* contains seven to nine mannose residues. Interestingly, Apa from *Escherichia coli* does not contain mannose (Horn et al., 1999). Differences in mannosylation patterns are related to the T-cell antigenicity of Apa (Horn et al., 1999; Nandakumar et al., 2013), with mannosylated Apa proteins eliciting more robust lymphoproliferation response than those without mannose modification (Horn et al., 1999). Additionally, a key enzyme involved in the modification process, protein mannosyl transferase (Pmt, Rv1002c), is crucial for the virulence of *M. tuberculosis* (Liu et al., 2013). Together, these findings demonstrated the antigenic significance of mannosylated proteins in mycobacteria, and suggested mannose linked to mycobacterial proteins represents a potential antigenic determinant.

However, the significance of mannosylation in glycoproteins of BCG and the role of oligosaccharide chains linked to O-glycoproteins are poorly understood. To examine the

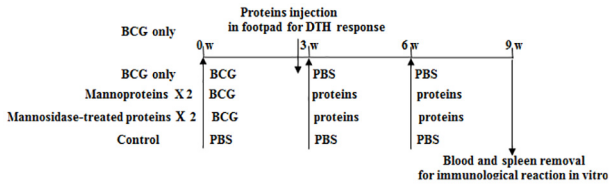

FIGURE 1 | Schematic diagram of immunization. Female BALB/c mice were primed with 1 × 10^5 CFU of BCG by intravenous injection, then boost twice at 3 weeks intervals with recombinant proteins (BCG_0980 and BCG_0470) in presence or absence of mannose modification.

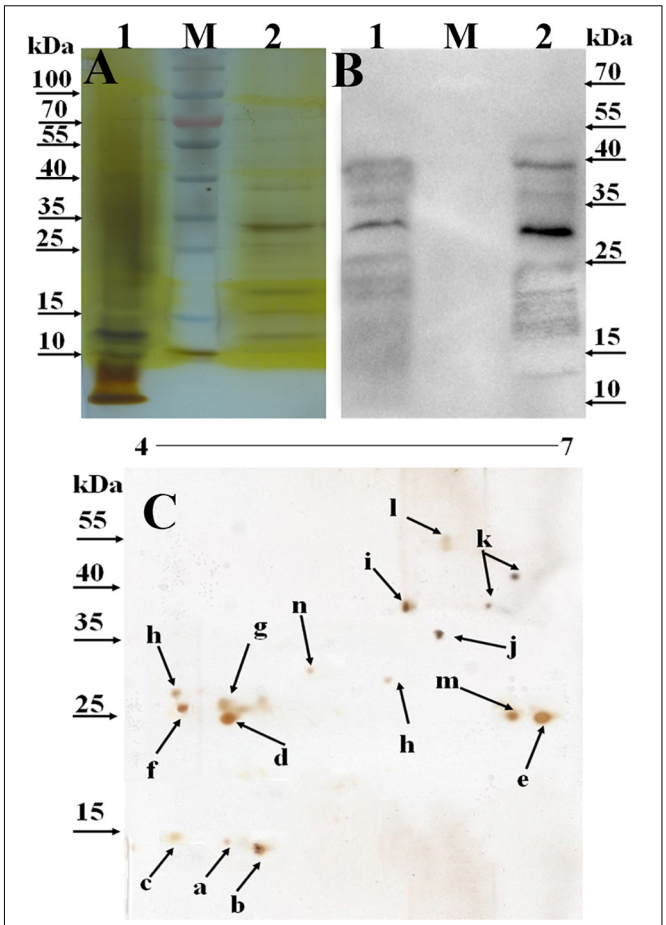

FIGURE 2 | Identification of secreted O-mannosylated proteins in BCG using SDS-PAGE, 2D-PAGE, and Western blot. M, PageRuler prestained protein ladder (Thermo Scientific, Lithuania). 1, the total secreted proteins precipitated by $(NH4)_2SO_4$; 2, ConA-dragged O-mannosylated proteins from BCG CF. (A) SDS-PAGE analysis of the secreted O-mannosylated proteins in BCG. The gel was visualized using sliver staining kit. (B) Western blot analysis of the secreted O-mannosylated proteins in BCG. The membranes were blotted with ConA, and visualized using ECL. (C) 2D-PAGE analysis of the secreted O-mannosylated proteins in BCG. The gel was visualized using sliver staining kit. a–n, the spots selected for MALDI-TOF identification. Five microgram proteins were loaded.

mannosylated proteins of BCG, and understand their roles in eliciting an immune responses in the host, we carried out lectin affinity chromatography assays followed by mass spectra (MS)-based identification. The findings of this study will help us to understand the importance of mannosylated proteins and oligosaccharide chains containing mannose residues of BCG, and reveal the effective antigens for use in BCG vaccines.

MATERIALS AND METHODS

Bacteria and Culture Conditions

Bacille Calmette-Guérin G Danish strain was reactivated on Middlebrook 7H10 agar (BD, Franklin Lakes, NJ, United States) supplemented with 10% OADC (oleic albumin dextrose catalase) at 37°C for 20 days. A single colony was picked up and inoculated in 5 ml of Proskauer and Beck modified synthetic medium (Gonzalez-Zamorano et al., 2009) and cultured to mid-log phase at 37°C. This starter culture was transferred into 200 ml of fresh Proskauer and Beck modified synthetic medium, and incubated without shaking until surface pellicles were visible. Bacterial cells were then removed by filtration using a 0.22-μm polyethersulfone filter, leaving only the culture filtrate. Proteins were precipitated by incubation with ammonium sulfate at 4°C overnight, and then collected by centrifugation at 10,300 × *g* for 30 min at 4°C. Protein pellets were resuspended in distilled water and dialyzed completely against distilled water at 4°C for 72 h. The dialyzed proteins were lyophilized and stored at −80°C.

Animal Care

This study was carried out in accordance with the principles of the Basel Declaration and the Dalian Medical University recommendations for laboratory animals. The protocol was approved by the Animal Ethics Committee of Dalian Medical University.

ConA-Affinity Chromatography

A 1 ml ConA-agarose column (Sigma-Aldrich, Stainheim, Sweden) was prewashed with five column volumes of wash solution (1 M NaCl, 5 mM $MgCl_2$, 5 mM $MnCl_2$, and 5 mM $CaCl_2$) and the resin equilibrated with equilibrating buffer (20 mM Tris, 0.5 M NaCl, pH 7.4). Protein solution containing 2.0 mg of total protein from CF (1 mg/ml, free of particulates) was then loaded onto column and washed with equilibration buffer until the eluent solution was free of protein. The target proteins were eluted with solution containing 200 mM methyl-D-glucopyranoside (Sigma-Aldrich, Stainheim, Sweden). Samples were dialyzed, lyophilized and stored at −80°C until use.

One-Dimensional and Bidimensional Gel Electrophoresis and Western Blot Analysis

Purified glycoproteins were subjected to 12% sodium dodecyl sulfate-polyacrylamide gel electrophoresis (SDS-PAGE) using a vertical electrophoresis apparatus. Gels were silver-stained according to the manufacturer's instructions. In addition, bidimensional gel electrophoresis (2D-DIGE) was performed as described previously (Chen et al., 2019). Briefly, samples were processed using a Bio-Rad clean-up kit as per the manufacturer's instructions (Hercules, CA, United States). The protein pellets were then dissolved in 50 μl of isoelectric focusing buffer (30 mM Tris, pH 8.0, 7 M urea, 2 M thiourea, 2% CHAPS). Soluble mannoproteins (30 μg) were separated in the first dimension using Immobiline DryStrips (11 cm, pH 4–7, Bio-Rad) and in the second dimension using 12% SDS-PAGE gels. The gels were stained using a ProteoSilver Plus SilverStain Kit (Sigma-Aldrich, MO, United States).

The proteins were then transferred from the SDS-PAGE gels onto polyvinylidene fluoride (PVDF) membrane (Millipore, Prod, pore size 0.45 μm) using Trans-Blot machine (Bio-Rad, Hercules, CA). The parameters were setting at 110 V and 35 min. The membrane was blocked with 2% (w/v) bovine serum albumin (BSA) in phosphate-buffered saline (PBS) and then incubated with 10 μg/ml biotinylated ConA (Sigma-Aldrich, Stainheim, Sweden) for 2 h at room temperature. The membrane was then incubated with streptavidin-peroxidase (1:5000, Sigma-Aldrich, St. Louis, MO, United States) solution as per the manufacturer's instructions. The target bands were visualized using enhanced chemiluminescence reagents (Millipore, Burlington, MA, United States).

MS Analysis

Matrix-Assisted Laser Desorption/Ionization Time-of-Flight (MALDI-TOF)

Selected silver-stained proteins were manually excised from the 2D-PAGE gels for MS-based analysis. Gel digestion and MS analysis (5800 MALDI-TOF, AB SCIEX, Foster City, CA, United States) were performed as described previously (Yang et al., 2018). Data were acquired using Mascot 2.2 software (Matrix Science)[1].

Liquid Chromatography Tandem Mass Spectrometry (LC-MS/MS)

Whole glycoproteins digested with trypsin were also examined using a Q Exactive Mass Spectrometer (Thermo Fisher Scientific, Waltham, MA, United States) coupled with an Easy nLC liquid chromatography system (Thermo Fisher Scientific). LC was operated by a C18 reverse phase trap column (Scientific Acclaim PepMap100, 100 μm × 2 cm, nanoViper, Thermo Fisher Scientific) connected to a C18 reversed-phase analytical column Easy Column, 10 cm long, 75 μm inner diameter, 3 μm resin, Thermo Fisher Scientific) in 0.1% formic acid and separated with a linear gradient of buffer (acetonitrile and 0.1% formic acid). The flow rate was at 300 ml/min and the system was controlled using IntelliFlow technology. The MS system was operated in positive ion mode. The optimal source/gas parameters were as follows: automatic gain control target, 3e6; maximum inject time, 10 ms. The dynamic exclusion duration was 40.0 s and the normalized collision energy was 30 eV. The survey scan for higher-energy collisional dissociation (HCD) fragmentation was set at 300–1800

[1]http://www.matrixscience.com

TABLE 1 | Profiles of the identified mannosylated proteins secreted by BCG.

ID	BCG gene	Access No.*	Protein name	Protein MW (D)	Matched peptides	Sequence coverage %	NetOglyc hits[#]	Predicted Lpp[&]	*M. bovis* ortholog	*M. tuberculosis* ortholog	Identified MS methods[1/2]
a	0086	A1KEM3	30S ribosomal protein S18 rpsR1	9543.1	1	8.33	1		Mb0056	Rv0055	[1]
b	1237c	A0A0H3MC91	SA5K secreted antigen	10881.2	2	9.09			Mb1207c	Rv1174c	[1]
c	RN06_2923	A0A109S8K1	Resuscitation-promoting factor RpfD	15678.6	1	3.08	3		Mb2410c	Rv2389c	[1]
d	2967c	A0A0K2HZQ7	Putative phthiocerol dimycocerosate transporter LppX	24139.9	2	8.58	6	yes	Mb2970c	Rv2945c	[1]
e	1472c	A0A0H3M3S8	Lipoarabinomannan carrier protein LprG	24547.5	1	2.97	1	yes	Mb1446c	Rv1411c	[1]
f	0470	A0A0H3M1J1	Putative tuberculin related peptide	16865.3	1	8.39	11		Mb0439	Rv0431	[1]
g	3419c	A0A0H3MEK7	Probable transposase	26630.2	1	9.08	9		Mb3382c	Rv3349c	[1]
h	1154	A0A0H3MC31	Possible acyl-[acyl-carrier protein] desaturase (desA2)	31359.1	1	3.64	2		Mb1124	Rv1094	[1]
i	0980	A0A0H3MBK5	Phosphate-binding protein3 (PstS3)	37952.7	4	7.57	7	yes	Mb0951	Rv0928	[1]
j	1156	A0A0H3M373	Possible glycosyl hydrolase	31099.1	2	2.69	3		Mb1126	Rv1096	[1]
k	1896	P80069	Alanine and proline-rich secreted protein Apa	32686.3	6	9.23	16		Mb1891	Rv1860	[1]
l	3277c	A1KNQ0	Adenosylhomocysteinase (ahcY)	54323.3	1	2.82	4		Mb3276c	Rv3248c	[1]
m	3652c	A0A0H3MBJ4	Probable conserved membrane protein	27001. 5	1	4.94	14		Mb3618c	Rv3587c	[1]
n	3955c	A0A0H3MFZ4	Uncharacterized protein	29993.6	1	2.39	23		Mb3928c/ Mb3829c	Rv3899c	[1]
	3252	A0A0G2Q9I2	Possible short-chain dehydrogenase/reductase	29814.1	1	3.55	0		Mb3251	Rv3224	[2]

[1]*Identified by both MALDI-TOF and LC-MS/MS.* [2]*only identified by LC-MS/MS.* **UniprotKB access number.* [#]*According to NetOglyc predictions (http://www.cbs.dtu.dk/services/NetOGlyc/, NetOGlyc 4.0 Server).* [&]*According to the predictions of lipoproteins (https://services.healthtech.dtu.dk/service.php?LipoP, LipoP1.0 Server).*

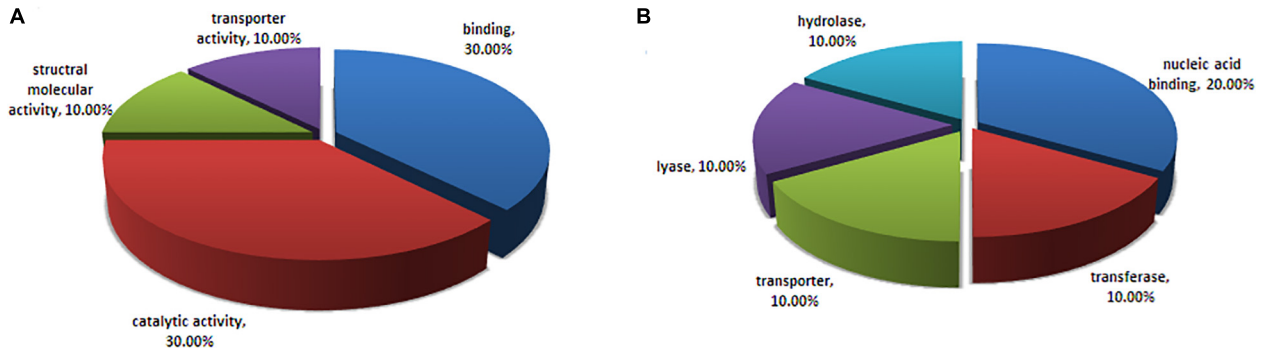

FIGURE 3 | Classification analysis of the 15 identified glycoproteins in BCG using the online PANTHER database. Representative pie charts display the enrichment percentage of proteins. **(A)** Proteins are classified based on molecular functions. **(B)** Proteins are categorized based on protein classes.

m/z, with HCD spectra set to 17,500 at m/z 200, and an isolation width was of 2 m/z. The instrument was run with an enabled mode of peptide recognition.

Preparation of Murine Anti-Serum Against BCG

BALB/c female mice (8 mice per group) were subcutaneously immunized with 5 × 10^5 colony-forming units (CFU) of log-phase BCG in normal saline). The control group was injected with equal volume of normal saline. At 3 weeks post-inoculation, whole blood were collected and centrifuged with 1,000 × *g* for 10 min. The sera were then collected for the detection of mannosylated antigens.

Detection of Mannosylated Antigens

Glycoproteins separated by SDS-PAGE and 2D-PAGE were transferred onto PVDF membrane as described. After blocking with 5% BSA (w/v) in PBS, the membranes were blotted with the prepared polyclonal antibodies (1:1,000) overnight at 4°C. Following incubation, the membranes were washed three times with PBS and then incubated with the secondary antibody (1:5000, rabbit anti-rat IgG, HRP conjugated; Sigma-Aldrich, MO, United States) for 1.5 h at room temperature. Protein bands and spots were visualized using enhanced chemiluminescence. Target bands and spots were then excised manually and stripped using Restore Western Blot Stripping Buffer (Thermo Fisher Scientific, United States) at 37°C for 40 min to remove affinity-bound primary and secondary antibodies. After washing with tris-buffered saline with 0.1% Tween 20, the target proteins were identified by LC-MS/MS as described previously.

Expression, Purification, and Treatment of the Identified BCG Antigens, Including BCG_0470 and BCG_0980

The *BCG_0470* and *BCG_0980* coding sequences were amplified from BCG genomic DNA using *Pfu* High Fidelity DNA Polymerase (Invitrogen, Carlsbad, CA, United States) and the following primers: BCG_0470-F (5′-CATATGGTGCTGGTTACAGTGGGCTC-3′, *Nde*I site is underlined), paring with BCG_0470-R (5′-AAGCTTTCAGCCGGTCACCACGAC-3′, *Hin*dIII site is underlined); and BCG_0980-F (5′-CATATGTTGAAACTCAACCGATTTGG-3′, *Nde*I site is underlined), pairing with BCG_0980-R (5′-AAGCTTTCAGGCGATCGCGTTGACCG-3′, *Hin*dIII site is underlined). The amplified products were then ligated into the pJET (Thermo Fisher Scientific, Lithuania) cloning vectors. Following sequence confirmation, the amplicons were excised from the vectors using the appropriate restriction enzymes and ligated into pCold II (Takara, Dalian, China),which carries a hexa-histidine tag at the C-terminus and a cold start promoter, generating recombinant the expression vectors pCold II-*BCG_0470* and pCold II-*BCG_0980*. For expression, the plasmids were transformed into *E. coli* BL21 (DE3). In addition, recombinant plasmids pVV2-*BCG_0470* and pVV2-*BCG_098* were constructed to allow expression of the two proteins in *M. smegmatis*. The vectors were transformed into *M. smegmatis* by electroporation as described previously (Yang et al., 2014). Cell lysates were then prepared to purify recombinant BCG_0470 and BCG_0980 as described previously (Yang et al., 2018). The recombinant proteins were assessed by 12% SDS-PAGE and further confirmed by western blot using anti-His monoclonal antibody (Sigma-Aldrich, St. Louis, MO, United States) or ConA lectin (Sigma-Aldrich, St. Louis, MO, United States) as a probe. In addition, the recombinant mannosylated proteins were treated with α-mannosidase (Sigma-Aldrich, St. Louis, MO, United States) as per the manufacturer's instructions. Mannosidase-treated proteins were collected using magnetic agarose beads as described previously (Chen et al., 2019).

Immunization of BCG-Primed Mice Using the Recombinant Antigens

Female BALB/c mice (five mice per group) were primed with 1 × 10^5 CFU of BCG by intravenous injection as shown in **Figure 1**. At 3 weeks post-inoculation, 5 μg of the recombinant proteins (with or without mannose modification) were subcutaneously injected into the BCG-primed mice,

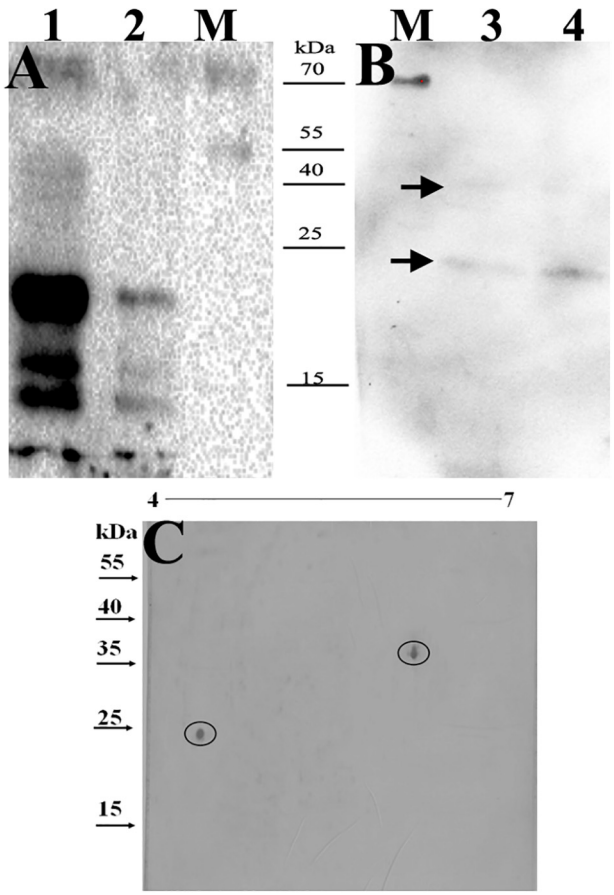

FIGURE 4 | Identification of the immunodominant glyco-antigens by BCG ploycolonal antibody using immunoblotting. 5μg proteins were loaded. M, PageRuler prestained protein ladder (Thermo Scientific, Lithuania). **(A,B)** the samples were separated by SDS-PAGE. 1, whole BCG cell-lysates; 2, crude protein extracts precipitated by the addition of $(NH4)_2SO_4$; 3 and 4, mannosylated proteins purified from BCG CF. Arrows indicated two targeting bands with molecular masses of approximately 38 kDs and 25 kDa, respectively. **(C)** Samples were separated by 2D-PAGE analysis. Circles indicate two targeting spots with molecular masses of approximately 38 kDs and 25 kDa, respectively.

followed by a second twice dose at 6 weeks post-inoculation. An additional group of mice were injected with an equal volume of PBS as a negative control. At 3 weeks after the final booster, the animals were sacrificed to evaluate immune responses *in vitro*.

Evaluation of Delayed-Type Hypersensitivity (DTH) Responses

The DTH responses of mice to recombinant protein with or without mannose modification were evaluated in mice inoculated with BCG only (no recombinant protein booster) as previously described (Tong et al., 2018). Briefly, as shown in **Figure 1**, at 2 weeks 4 days post-BCG immunization, 5 μg of recombinant protein (four groups: BCG_0470, mannosidase-treated BCG_0470, BCG_0980, and mannosidase-treated BCG_0980) in 40 μl of PBS were injected into the left hind footpad, while the same volume of PBS was injected into the right hind footpad as a control. Differences in footpad swelling between the protein-challenged and PBS-injected feet were measured at 24, 48, and 72 h post-protein injection to assess protein-specific DTH responses. In addition, at 48 h post-protein injection, three mice of every group were then sacrificed and equal amounts of the left hind footpads were collected and homogenized in 1 ml of protein extraction buffer with protease inhibitor cocktail (Thermo Fisher Scientific). The homogenates were centrifuged at 10,000 × *g* for 10 min to collect the supernatants, which were then tested to determine the levels of various cytokines, including IFN-γ, IL-4, and TNF-α, using an enzyme-linked immunosorbent assay (ELISA) kit (Abcam, Hong Kong, China) as per manufacturer's instruction (Aguilar et al., 2007).

Detection of Antigen Specific Antibodies Using ELISA

Whole blood from sacrificed mice was centrifuged at 1,000 × *g* for 10 min at 4°C, with the resulting serum collected and immediately used to assess the specificity of antibodies against their corresponding antigens. Briefly, 150 μl of each (2 μg/ml) recombinant antigen was incubated overnight at 4°C in a 96-well plate. After blocking with 3% BSA in PBS, the plate was incubated with diluted (1:1,000) murine serum for 2 h at 37°C, before being incubated with horseradish peroxidase-conjugated anti-mouse IgG (1:5000 dilution) at room temperature for 1 h. Tetramethylbenzidine was added to each well for color development, which was then stopped with 2 M sulfuric acid. The optical density of each well was then measured at 450 nm.

Detection of Cytokine Secretion in Mouse Splenocytes by ELISA

Spleens from the sacrificed mice were aseptically removed, and the single-cell suspensions were prepared as reported previously (Rao et al., 2017). The freshly isolated splenocytes were resuspended in RPMI 1640 medium (Gibco, Suzhou, China) enriched with 10% fetal calf serum and antibiotics (penicillin and streptomycin) at concentration of 1×10^6 cells/ml. The cells were then seeded in a 96-well sterilized plate and stimulated with 2 μg/ml antigen mixture (BCG_0980 and BCG_0470) *in vitro* for 72 h at 37°C with 5% CO_2. The plate was then centrifuged at 1,600 × *g* for 10 min to collect supernatant, which was subsequently used to measure the levels of various cytokines including TNF-α, IFN-γ, and IL-2, using ELISA kits (Abcam, Hong Kong, China).

Statistical Analysis

All the data were are presented as mean ± SEM from at least three independent experiments. Statistical analyses were performed

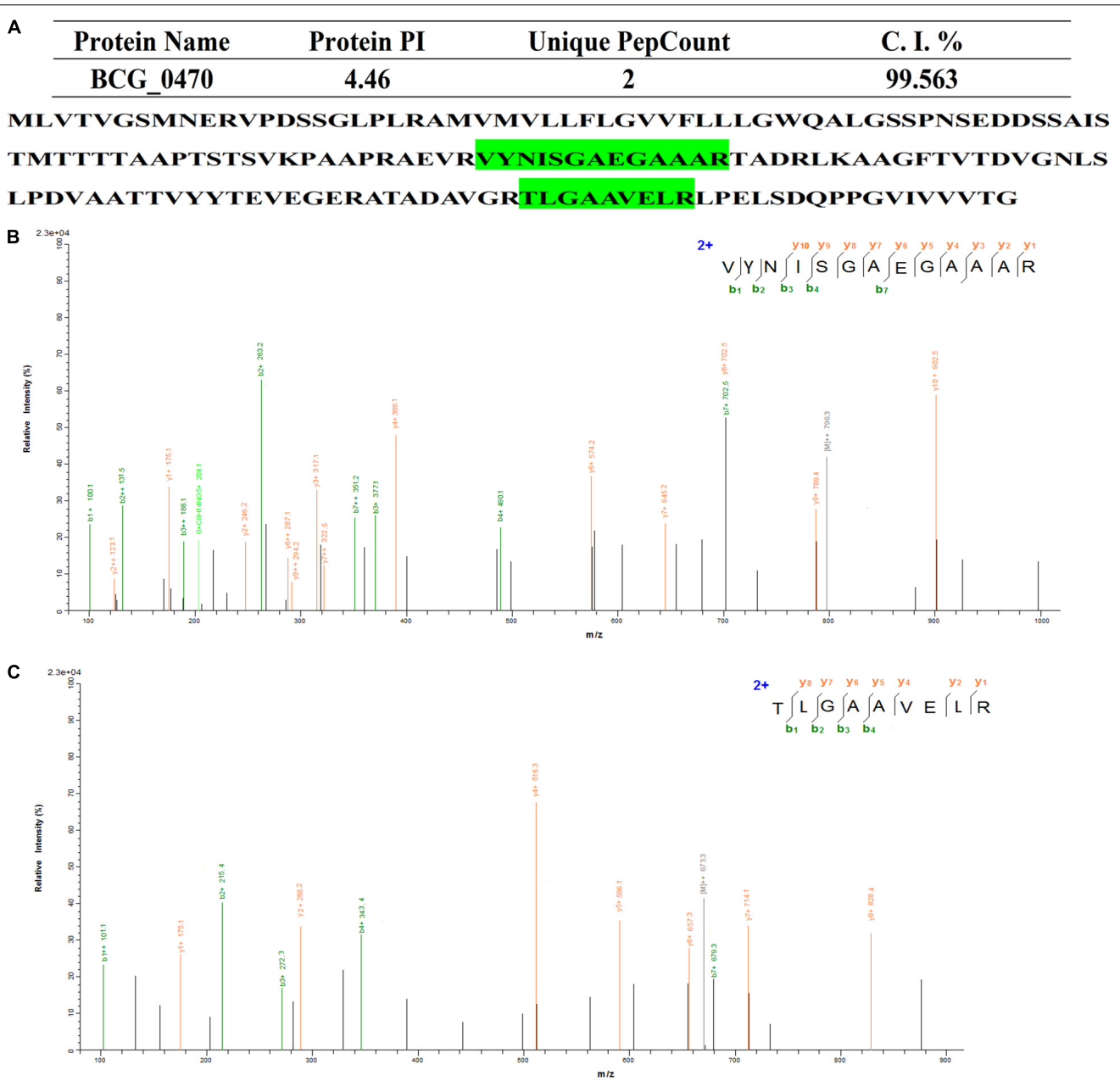

FIGURE 5 | Identification of BCG_0470 via LC-MS/MS-based analysis. **(A)** Profiles of BCG_0470. **(B,C)** Tandem mass spectrometry (MS/MS) spectrum of the trypsin-digested BCG_0470. **(B)** Peptide fragment ions with m/z 929.5441: sequence TLGAAVELR. **(C)** Peptide fragment ions with m/z 1278.6677: sequence VYNISGAEGAAAR.

using a Student's unpaired *t*-test or one-way ANOVA. Unless stated, $p < 0.05$ was considered statistically significant.

RESULTS

Recognition of the Mannosylated Proteins in BCG

To identify O-mannosylated proteins in the BCG CF, ConA-lectin affinity chromatography was used. The glycoproteins were eluted using the solution containing a high concentration of methyl-α-mannopyranoside. SDS-PAGE and 2D-PAGE analyses were utilized to separate the purified glycoproteins. Bands and spots corresponding to the glycoproteins on the SDS-PAGE (**Figure 2A**) and 2D-PAGE (**Figure 2C**) were visualized by silver-staining. In total, 9 protein bands with a molecular mass of 10–70 kDa were observed on the SDS-PAGE gel. While 14 proteins spots (**Figure 2Ca–n**) were selected from the 2D-PAGE gel. Western blot analysis confirmed the binding activity of the observed proteins with ConA. As shown in **Figure 2B**, the

A

Protein Name	Protein PI	Unique PepCount	C. I. %
BCG_0980	5.75	3	37.6

MKLNRFGAAVGVLAAGALVLSACGNDDNVTGGGATTGQASAKVDCGGKKTLKASGSTAQANAMTRFVNVFEQACPGQTLNYTANGSGAGISEFNGNQTDFGGSDVPLSKDEAAAAQRRCGSPAWNLPVVF
GPIAVTYNLNSVSSLNLDGPTLAKIFNGSITQWNNPAIQALNRDFTLPGERIHVVFRSDESGTTDNFQRYLQAASNGAWGKGAGKSFQGGVGEGARGNDGTSAAAKNTPGSITYNEWSFAQAQHLTMANIVTSA
GGDPVAITIDSVGQTIAGATISGVGNDLVLDTDSFYRPKRPGSYPIVLATYEIVCSKYPDSQVGTAVKAFLQSTIGAGQSGLGDNGYIPIPDEFKSRLSTAVNAIA

B

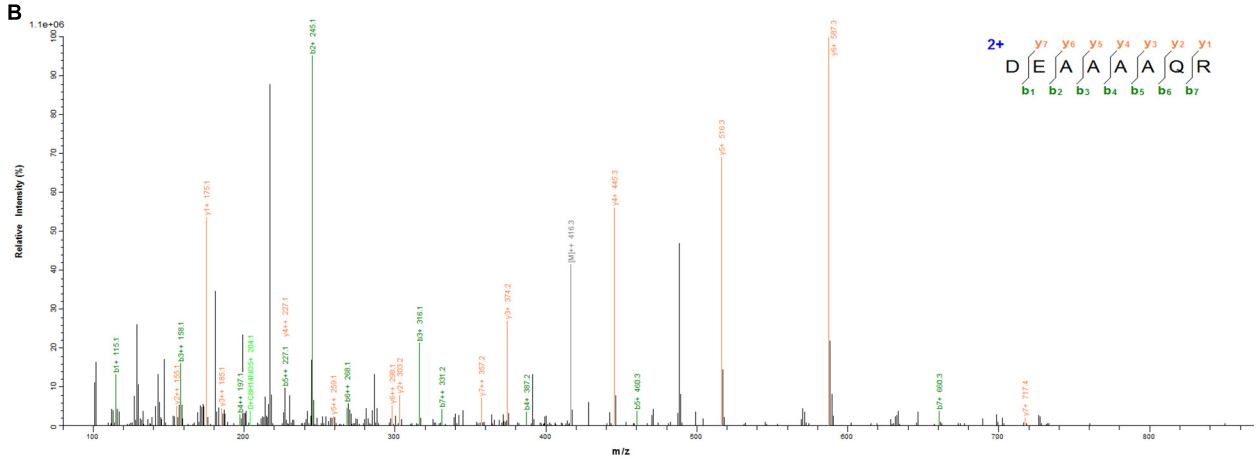

C

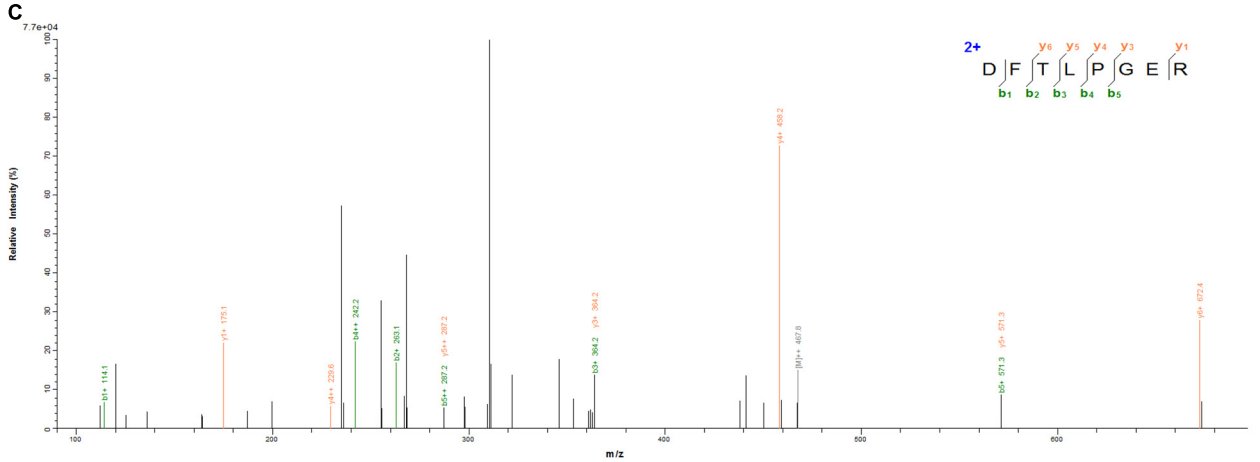

D

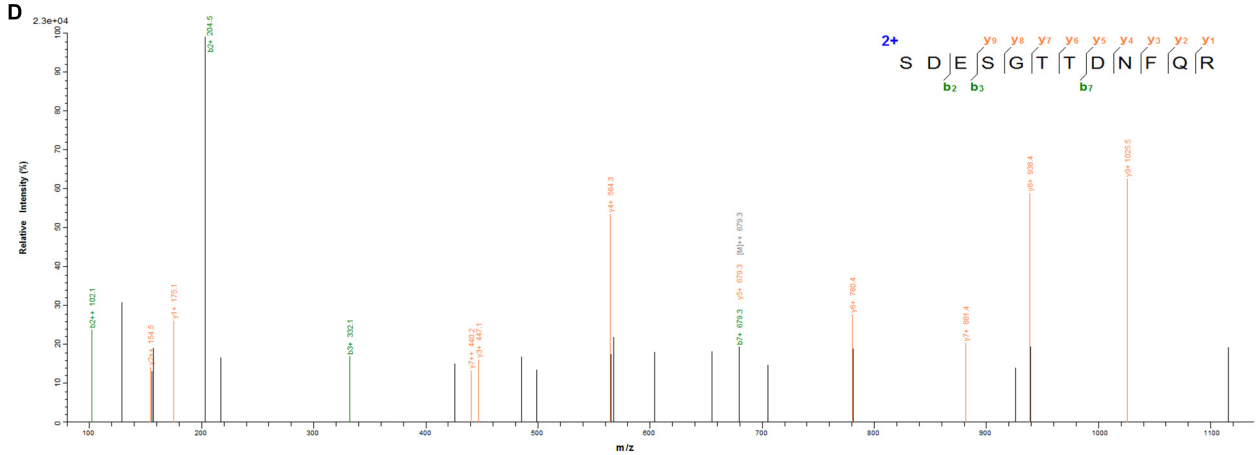

FIGURE 6 | Identification of BCG_0470 via LC-MS/MS-based analysis. **(A)** Profiles of BCG_0980. **(B–D)** Tandem mass spectrometry (MS/MS) spectrum of the trypsin-digested BCG_0980. **(B)** Peptide fragment ions with m/z 831.3955: sequence DEAAAAQR. **(C)** Peptide fragment ions with m/z 934.46287: sequence DFTLPGER**. (D)** Peptide fragment ions with m/z1356.56624: sequence SDESGTTDNFQR.

majority of mannoproteins present in the CF were identified using ConA-lectin.

Identification of the Mannosylated Proteins in BCG

Fourteen visible spots on the silver-stained 2D-PAGE gel (**Figure 2Ca–n**) were excised for MALDI-TOF-based identification, while whole glycoproteins were characterized by LC-MS/MSanalysis. Overall, 15 glycoproteins were identified (**Table 1**), amongst which BCG_2967c (LppX), BCG_0980 (PstS3) and BCG_1472c (LprG) were shown to be lipoproteins with potential sites for type II signal peptidase binding. Further, BCG_3277c, BCG_3252, BCG_1154, and BCG_1564 were predicted to be involved in degradation and metabolism of nutrients, BCG_1896 (Apa) was associated with cell adhesion, and BCG_RN06_2923 and BCG_1237c were predicted to play a role in bacterial growth. All identified proteins were predicted to have potential signal peptides. Most of them were evaluated to possess between 1 and 23 potential O-glycosylated sites. Result of the classification analysis of 15 identified glycoproteins based on molecular function and protein class are shown in **Figure 3**.

Confirmation of BCG_0470 and BCG_0980 as Immunodominant Antigens

Based on the possible involvement of the identified glycoproteins in immune responses, BCG ploycolonal antibody was used as a probe to screen potential immunogenic antigens (v:v, 1:1,000). **Figure 4A** shows that at least seven bands were detected in the whole BCG cell lysates, while four bands were detected in crude protein extracts, which were precipitated by the addition of ammonium sulfate. Among the antigens, two proteins with molecular masses of approximately 25 and 38 kDa, respectively were detected. In addition, the polyclonal antisera showed cross-reactivity with BCG between whole BCG cell lysates and ConA-dragged proteins (**Figure 4A**), and bands with molecular masses approximately 25 kDa and 38 kDa were also detected among the ConA-dragged proteins (**Figure 4B**). Because bands observed on SDS-PAGE gels can comprise more than one protein, immunoblotting of ConA-dragged proteins separated by 2D-PAGE analysis was performed. Results confirmed the presence of only two target spots (**Figure 4C**).

We then further characterized the 15 identified glycoproteins with immunogenic activities, we analyzed the 15 identified proteins. As a consequence, Glycoproteins BCG_2967, BCG_1472c, BCG_0470, BCG_3419c, BCG_1154, and BCG_3652c (spot IDs d, e, f, g, h, and m, respectively, in **Figure 2C**) were all found to be ∼25kDa, while BCG_0980 was ∼38 kDa. To further confirm the targeting glycoproteins detected in **Figures 4B,C**, the reactive spots were excised and stripped for LC-MS/MS-based analysis. MS analysis confirmed that the target proteins were BCG_0470 (spot ID f in **Figure 2C**, 25 kDa) and BCG_0980 (spot ID i in **Figure 2C**, 38 kDa). The MS profiles of BCG_0470 and BCG_0980 are shown in **Figures 5**, **6**.

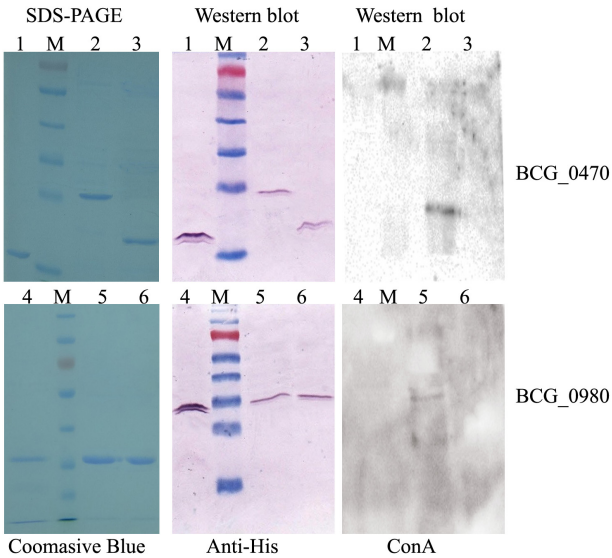

FIGURE 7 | Characterization of BCG_0470 and BCG_0980 as mannosylated proteins. 1, Recombinant BCG_0470 from *E. coli*. 2, Recombinant BCG_0470 from *M. smegmatis*. 3, Recombinant BCG_0470 from *M. smegmatis* treated by α-mannosidase. 4, Recombinant BCG_0980 from *E. coli*. 5, Recombinant BCG_0980 from *M. smegmatis*. 6, Recombinant BCG_0980 from *M. smegmatis* treated by α-mannosidase.

Characterization of Mannosylated BCG_0470 and BCG_0980

To further characterize the mannosylation of BCG_0470 and BCG_0980, the proteins were expressed in both *E. coli* and *M. smegmatis*, respectively. Previous studies have shown that expressed proteins are non-glycosylated in *E. coli*, but are glycosylated in *M. smegmatis* (Coddeville et al., 2012). As shown in **Figure 7**, the soluble proteins were successfully expressed in both *E. coli* and *M. smegmatis* in this study. The molecular mass of BCG_0470 was much higher when expressed in *M. smegmatis* (∼25 kDa) than in *E. coli* (∼ 18 kDa). Non-glycosylated BCG_0470 has a predicted molecular mass of 18 kDa, which agreed with the mass of protein expressed in *E. coli*. In addition, western blot analysis showed that BCG_0470 expressed in *M. smegmatis* reacted strongly with ConA-lectin (**Figure 7**). In comparison, SDS-PAGE and western blot analysis showed that the molecular mass of recombinant BCG_0980 was similar in both *E. coli* and *M. smegmatis*, and was consistent with the predicted molecular mass ∼38 kDa. Western blot analysis blotted with ConA showed a weak band corresponding to BCG_0980 when expressed in *M. smegmatis*. Therefore, these findings suggested that BCG_0470 is highly mannosylated while BCG_0980 is mannosylated to a lesser extent.

To examine mannose linkage in BCG_0470 and BCG_0980, α-mannosidase, which hydrolyzes the terminal non-reducing α-D-mannose residues of glycoproteins, was used to digest the recombinant BCG_0470 and BCG_0980 proteins expressed in *M. smegmatis*. Western blot analysis showed no ConA binding, suggesting complete loss of mannose residues from

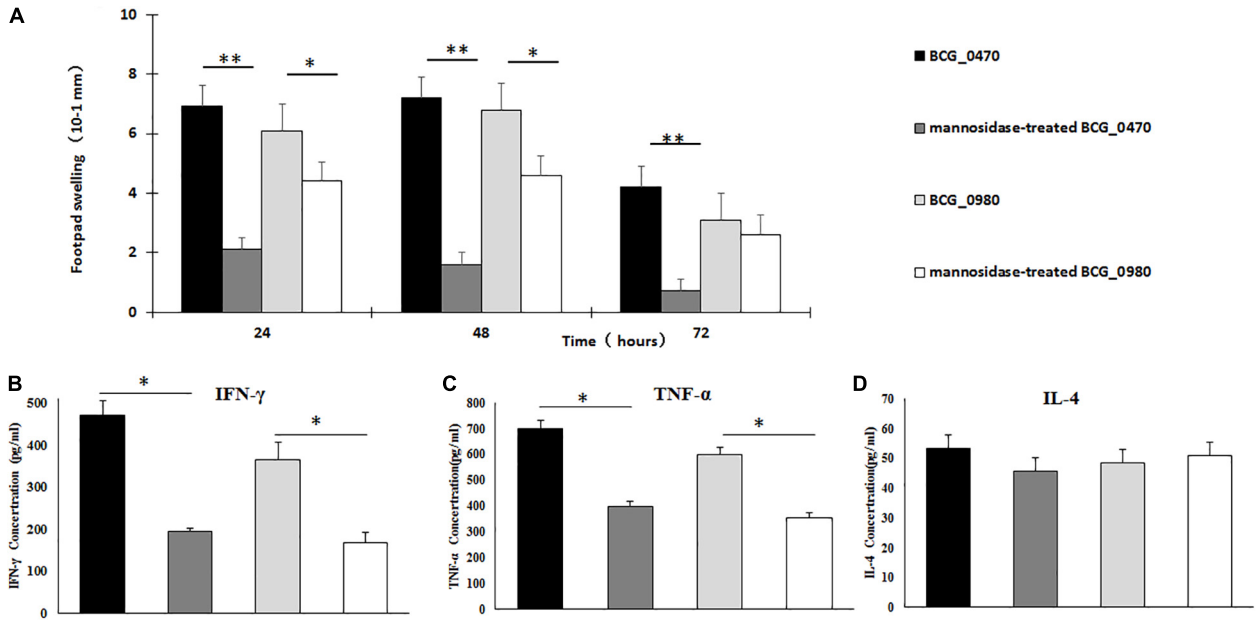

FIGURE 8 | Detection of T-cell activity in the BCG-sensitized BALB/c mice via DTH responses. **(A)** Measurement of swelling in protein-challenged footpad. Both mannosylated BCG_470 and BCG_0980 could elicit increased swelling-responses than non-mannosylated proteins, especially in BCG_0470 (*t*-test, $^{*}p < 0.05$, $^{**}p < 0.01$). **(B–D)** Cytokines including IFN-γ **(B)**, TNF-α **(C)**, and IL-4 **(D)** in 48 h post protein-challenged footpad. Both mannosylated BCG_0470 and BCG_0980 could induce higher level of IFN-γ, IFN-α than non-mannosylated proteins. The level of IL-4 showed no difference between the paired groups (*t*-test, $^{*}p < 0.05$, $^{**}p < 0.01$).

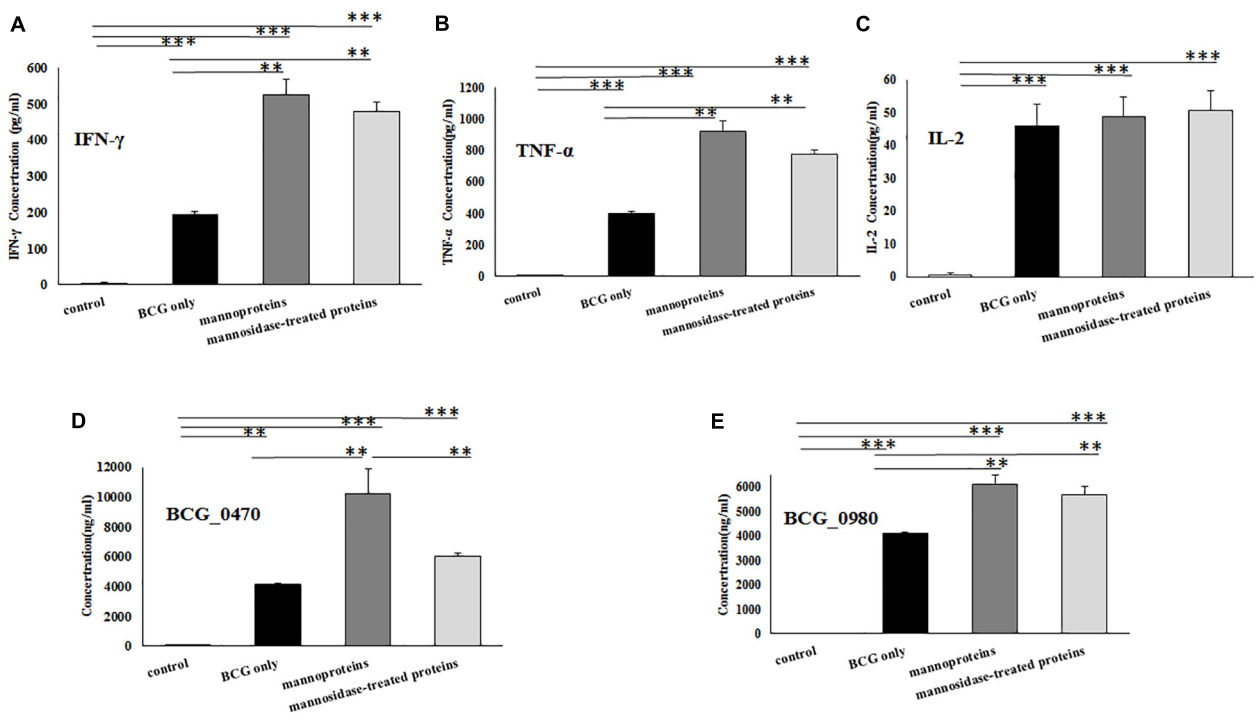

FIGURE 9 | Detection the levels of splenocytes cytokines and serum antigenic-specific IgG using ELISA. **(A)** IFN-γ. **(B)**TNF-α. **(C)**IL-2. **(D)** BCG_0470-specific IgG. **(E)** BCG_0980-specific IgG. Mice were primed with BCG and received two boosts of BCG_0470 and BCG_0980 proteins with or without mannose modification. Differences between the groups were calculated by One Way ANOVA. Asterisks represented statistical difference (one-way ANOVA, $^{*}p < 0.05$, $^{**}p < 0.01$, $^{***}p < 0.001$).

the α-mannosidase-digested BCG_0470 and BCG_0980 proteins. Thus, the examined mannosylated proteins, including BCG_0470 and BCG_0980, are likely to contain a terminal non-reducing α-D-mannose.

Confirmation T-Cell Activator by BCG_0470 and BCG_0980 via DTH Responses *in vivo*

Recombinant BCG_0470 and BCG_0980 proteins with or without mannose modification were injected intradermally into the hind footpads of BCG-sensitized BALB/c mice. Footpad swelling was then recorded at 24 h intervals. As shown in **Figure 8A**, increased swelling response was observed in mice injected with the mannosylated proteins compared with those injected with non-mannosylated proteins. Additionally, a significant difference in footpad swelling was observed at 24 h and 48 h post-injection time points, especially in BCG_0470-injected mice. To further determine whether the footpad swelling resulted from DTH or simple tissue edema, three mice of every group were sacrificed at 48 h post-injection time point, the levels of DTH-associated cytokines in the protein-injected footpads were assessed. As shown in **Figures 8B,C**, higher levels of IFN-γ and TNF-α were observed in the mannoprotein-injected footpads compared with those injected with mannosidase-treated proteins, but the level of IL-4 showed no difference between the paired groups (**Figure 8D**). Thus, footpad swelling was mainly attributed to DTH-associated Th1 cytokines, which attract cells to the injection site. Additionally, analysis of the DTH response demonstrated the T-cell activity of mannosylated BCG_0470 and BCG_0980 in the BCG-sensitized BALB/c mice, suggesting that mannose residues play an important role in immune responses *in vivo*.

Detection of BCG_0470- and BCG_0980-Induced Splenocyte Cytokines and Antigen-Specific IgG

BCG-primed BALB/c mice were subcutaneously injected at two separate time points with recombinant BCG_0470 and BCG_0980 proteins with or without mannose modification. At three weeks post final immunization, splenocytes were isolated for detection of cytokines including IFN-γ, TNF-α, and IL-2while the serum was collected and assayed to determine the levels of antigen-specific IgG. As shown in **Figure 9**, all immunized mice showed dramatically increased levels of cytokines and antigen-specific IgG compared with PBS-injected mice, confirming the antigenicity of BCG and two boosting proteins. In addition, compared with the mice only received BCG injection, mice treated with mannosylated or non-mannosylated protein booster injections showed increased levels of IFN-ɤ and TNF-α (**Figures 9A,B**). In comparison, no significant differences in IL-2 levels were detected between the paired groups (**Figure 9C**). Further, mice that received either mannosylated or non-mannosylated proteins boosts showed increased level of BCG_0980-specific IgG, compared with mice received BCG only (**Figure 9E**). Interestingly though, only mice treated with mannosylated protein boosters showed increased production of BCG_0470-specific antibody, with no significant increase in specific IgG antibody in non-mannosylated protein-treated mice compared with the BCG-only group (**Figure 9D**). Overall, these results suggested that BCG_0470 and BCG_0980 amplify the immune responses induced by BCG, and imply that the mannose oligosaccharide of BCG_0470 is indispensable for promoting high levels of BCG_0470-specific IgG.

DISCUSSION

Protein O-mannosylation process occurs in both eukaryotes and prokaryotes, including the important human pathogen *M. tuberculosis*, the etiological agent of TB (Espitia and Mancilla, 1989). O-mannosylated proteins play an important role in bacterial physiology and host-pathogen interactions (Liu et al., 2013; Alonso et al., 2017). Since the initial discovery of mycobacterial glycoproteins such as Apa, PstS1, and LpqH (Espitia and Mancilla, 1989), many studies have focused on this subclass of proteins. To date, more than 40 proteins secreted by *M. tuberculosis* have been identified as mannoproteins (Gonzalez-Zamorano et al., 2009; Smith et al., 2014), while Sec-dependent translocation has been shown to be required for the export of *M. tuberculosis* mannoproteins (VanderVen et al., 2005). In addition, the glycosylation sites and the structural linkage of O-linked glycoproteins have been reported (Horn et al., 1999; Smith et al., 2014; Alonso et al., 2017). In the current study, we identified 15 mannosylated proteins from BCG CF. The proteins had a wide range of predicted functions, including catalytic activity, solute binding, cell wall biosynthesis, and ABC transporters (**Table 1** and **Figure 3**). Of the 15 identified glycoproteins, lipoprotein BCG_2967c (LppX) has been confirmed as a B-cell immunogenic protein expressed on the BCG cell surface (Lefevre et al., 2000). *M. tuberculosis* PstS3 is reportedly an excellent immunomodulator involved in both Th1 and Th17 responses (Palma et al., 2011), and is also a promising sera-diagnostic marker for latent tuberculosis

TABLE 2 | Bioinformatic B-cell Epitopic analysis of BCG 0470 and BCG_0980.

Protein	Peptide predicted to be a B-cell epitope (underlined is the potential mannosylated site)
BCG_0470	8MNERVPDSSGL18 42LGSSPNSEDDSSAISTMTTTTAAPTSTSVKPAAPRA77 85SGAEGAAARTADRL98 125EVEGERATADAVGR138 150ELSDQPPG157
BCG_0980	24GNDDNVTGGGATTGQASAKVDCGGKKTLKASGSTAQAN61 73ACPGQTLNYTANGSGAGISEFNGNQTDFGGSDVPLSKDEAAA AQRRCGSPAW124 161TQWNNP166 189DESGTTDN196 204ASNGAWGKGAGKSFQGGVGEGARGNDGTSAAAKNTPGSIT Y244 262TSAGGDPVAI271 278QTIA281 285ISGV288 299FYRPKRPGSY308 322YPDSQVGT329 339IGAGQSGLGDNGYIPIPDEFKS360

Common B-cell Epitopes were predicted using Bepipred Linear Epitope Prediction (IEDB Analysis Resource v2.15.1, http://tools.immuneepitope.org). Only the epitope including ≥4 residues in length was considered. The O-mannosylated sites were predicted using NetOglyc predictions (http://www.cbs.dtu.dk/services/NetOGlyc/, NetOGlyc 4.0 Server).

infection (Baumann et al., 2013, 2015). BCG_1472c (LprG) is another important lipoprotein identified in this work. Its ortholog in *M. tuberculosis*, coded by *Rv1141c*, is described as a lipoarabinomannan carrier protein with Toll-like receptor 2 (TLR-2) agonist activity (Drage et al., 2010). LprG is also thought to be a virulence factor because a *M. tuberculosis Rv1141c* deletion mutant showed reduced virulence in a mouse model of infection (Gaur et al., 2014). In addition, LprG is the key target glycoprotein responsible for the impaired growth and attenuated virulence associated with *pmt* (*Rv1002c*) deletion in *M. tuberculosis* (Yang et al., 2014; Alonso et al., 2017). The impaired growth and virulence of the *pmt* mutant was also observed in the corresponding *Mycobacterium abscessus* mutant strain (Becker et al., 2017). Furthermore, secreted antigen SA5K (also called TB8.4 low molecular weight T-cell antigen), encoded by *BCGsa5k*, is associated with BCG intracellular adaption and survival (Bottai et al., 2006), while resuscitation-promoting factor RpfD, encoded by *RN06_2923* in BCG, demonstrates strong immunogenicity in many mycobacterial infection models (Romano et al., 2012). Taken together, these findings suggested that the O-mannosylated proteins identified in the current study were potentially antigenic, and could be used to promote the immune responses induced by BCG.

Polyclonal antisera from mycobacterial-infected patients or animals could be used to screen for the immunogenic proteins (Wieles et al., 1994; Facciuolo et al., 2013) (Tsibulkin et al., 2016). In the current work, two immunodominant glycoproteins, BCG_0980 and BCG_0470, were identified using antisera against BCG-immunized mice (as shown in **Figure 4**). Orthologs of these two glycoproteins (Rv0928 (PstS3) and Rv0431, respectively) were identified in *M. tuberculosis*, and we found that the serum-reactivity of PstS3 was consistent with the previous reports (Baumann et al., 2013, 2015). We have previously shown that mannosylation of Rv0431 may play a role in mediating bacterial immune evasion (Deng et al., 2016). Recently, Rv0431 was reported to be a vesiculogenesis and immune response regulator (virR) involved in regulating the release of *M. tuberculosis*-derived material via the TLR-2 pathway (Rath et al., 2013). However, the current work is the first to identify the potential antigenicity of Rv0431 (BCG_0470).

Several mycobacterial mannoproteins including Apa, LpqH and LprG are involved in host immune regulations. Of these proteins, Apa the best-studied of these proteins, the placement of its mannose modifications have been shown to determine its ability to stimulate a T-lymphocyte response (Horn et al., 1999). Furthermore, Apa mannosyl appendages act as binding sites for host receptors including lung surface protein A and DC-SIGN, and are important for *M. tuberculosis* survival (Pitarque et al., 2005; Ragas et al., 2007). LpqH, another well-studied glycoprotein in *M. tuberculosis,* plays a role in antigen processing. The binding activity of LpqH with host receptors also relies on the integrated mannosyl residues (Herrmann et al., 1996). LprG, a glycoprotein found in *Mycobacterium leprae*, activates MHC II-restricted T-lymphocytes in patients with lepromatous leprosy. Complete mannosylation is required for T-lymphocyte activation (Sieling et al., 2008). Therefore, we hypothesized that the two immunodominant antigens identified in the current work (BCG_0470 and BCG_0980) were potential targets to regulate the immune responses induced by BCG, and that the manosyl appendages of these glycoproteins were essential for high-level antigenicity.

In the present study, mice were immunized with BCG by intravenous injection, which has been shown to elicit stronger immune responses than other routine immunization routes (Darrah et al., 2020). DTH responses *in vivo* along with various immune factors were assessed. We found that the presence of mannose modifications may be responsible for a stronger DTH response. It is well known that a Th1-driven DTH response is associated with protective immunity against mycobacterial infection (Nadler et al., 2003). The detection of DTH-associated cytokines in the footpads of inoculated mice confirmed that the stronger DTH responses were the result of Th1 cytokines such as IFN-γ and TNF-α rather than Th2 cytokine such as IL-4. However, the exact T-regulatory and effector cells involved in the DTH response, as well as the underlying pathway evoked during the response, need to be explored further. Our results also showed that both BCG_0470 and BCG_0980 could induce stronger Th1 responses, including IFN-γ and TNF-α, and stimulate higher concentrations of specific IgG compared with BCG treatment alone. Further investigation is now required to determine whether an immune response is triggered by these two glycoproteins alone.

High level of mannosylation of BCG_0470, which accounted for nearly 7 kDa in molecular mass (**Figure 7**) was a focus of this study. Because mannosylated protein induced higher levels of BCG_0470-specific IgG in the mice compared with un-mannosylated protein, we concluded that the mannoses oligosaccharides linked with BCG_0470 was an important determinant of B-cell antigenicity. We also analyzed the B-cell Epitopes for BCG_0470 and BCG_0980 using Bepipred Linear Epitope Prediction[2]. As shown in **Table 2**, there were five common B-cell epitopes (≥4 residues in length) for BCG_0470. In addition, all of the potentially O-mannosylated sites for BCG_0470 were included within one B-cell epitope (**Table 2**). Thus, it may be possible for the mannose oligosaccharides of BCG-0470 to act as antigenic determinants. Recently, several glycoconjugate vaccines and specific antibodies have been inducibly produced by the carbohydrate-recognizing T cells (Tcars), a subclass of T-helper cells that recognize the carbohydrate of glycopeptides presented by MHC-II molecules, aiding B-cell maturation and specific memory (Sun et al., 2019). Our results regarding BCG_0470-specific IgG production are consistent with the above findings.

In summary, we identified a total of 15 O-mannosylated proteins secreted by BCG. Of these, two glycoproteins (BCG_0980 and BCG_0470) were identified as immunodominant glyco-antigens. We found that mannose linkages on both proteins contributed to the stimulation of a T-cell response via DTH *in vivo*, and were necessary for inducing high level of antigenic IgG. These findings imply that mannose linkages maybe the antigenic determinants. Therefore, a further exploration of BCG glycoproteins will contribute

[2]http://tools.immuneepitope.org

to a better understanding of the protective mechanism of the BCG vaccine, allowing the development of subunit vaccine to optimize BCG.

DATA AVAILABILITY STATEMENT

The datasets generated for this study can be found in the ProteomeXchange (http://www.proteomexchange.org/) (PXD017576).

ETHICS STATEMENT

The animal study was reviewed and approved by the Animal Ethics Committee of the Dalian Medical University.

AUTHOR CONTRIBUTIONS

All authors have read and approved the manuscript and contributed significantly to this work. GD, WZ, and SY have contributed to the conception and design and were in charge of writing. GD, WZ, NJ, and XS performed the experiments. GD, YZ, and XL contributed to the data analysis and figure preparation.

FUNDING

This work was supported by the National Natural Science Foundation of China (81801981) and the Doctoral Scientific Research Starting Foundation of Liaoning Province (2019-BS-067).

REFERENCES

Aguilar, D., Infante, E., Martin, C., Gormley, E., Gicquel, B., and Hernandez Pando, R. (2007). Immunological responses and protective immunity against tuberculosis conferred by vaccination of Balb/C mice with the attenuated *Mycobacterium tuberculosis* (phoP) SO2 strain. *Clin. Exp. Immunol* 147, 330–338. doi: 10.1111/j.1365-2249.2006.03284.x

Alonso, H., Parra, J., Malaga, W., Payros, D., Liu, C. F., Berrone, C., et al. (2017). Protein O-mannosylation deficiency increases LprG-associated lipoarabinomannan release by *Mycobacterium tuberculosis* and enhances the TLR2-associated inflammatory response. *Sci. Rep.* 7:7913. doi: 10.1038/s41598-017-08489-7

Baumann, R., Kaempfer, S., Chegou, N. N., Nene, N. F., Veenstra, H., Spallek, R., et al. (2013). Serodiagnostic markers for the prediction of the outcome of intensive phase tuberculosis therapy. *Tuberculosis* 93, 239–245. doi: 10.1016/j.tube.2012.09.003

Baumann, R., Kaempfer, S., Chegou, N. N., Oehlmann, W., Spallek, R., Loxton, A. G., et al. (2015). a subgroup of latently *Mycobacterium tuberculosis* infected individuals is characterized by consistently elevated IgA responses to several mycobacterial antigens. *Mediators Inflamm.* 2015:364758. doi: 10.1155/2015/364758

Becker, K., Haldimann, K., Selchow, P., Reinau, L. M., Dal Molin, M., and Sander, P. (2017). Lipoprotein glycosylation by protein-o-mannosyltransferase (MAB_1122c) contributes to low cell envelope permeability and antibiotic resistance of mycobacterium abscessus. *Front. Microbiol.* 8:2123. doi: 10.3389/fmicb.2017.02123

Bottai, D., Batoni, G., Esin, S., Florio, W., Brancatisano, F. L., Favilli, F., et al. (2006). The secretion antigen SA5K has a role in the adaptation of Mycobacterium bovis bacillus Calmette-Guerin to intracellular stress and hypoxia. *Microbes Infect.* 8, 2254–2261. doi: 10.1016/j.micinf.2006.04.020

Chen, Y., Xu, Y., Yang, S., Li, S., Ding, W., and Zhang, W. (2019). Deficiency of D-alanyl-D-alanine ligase A attenuated cell division and greatly altered the proteome of *Mycobacterium smegmatis*. *Microbiol. Open* 8:e00819. doi: 10.1002/mbo3.819

Coddeville, B., Wu, S. W., Fabre, E., Brassart, C., Rombouts, Y., Burguiere, A., et al. (2012). Identification of the *Mycobacterium marinum* Apa antigen O-mannosylation sites reveals important glycosylation variability with the M. *tuberculosis Apa homologue*. *J. Proteomics* 75, 5695–5705. doi: 10.1016/j.jprot.2012.07.017

Darrah, P. A., Zeppa, J. J., Maiello, P., Hackney, J. A., Wadsworth, M. H., Hughes, T. K., et al. (2020). Prevention of tuberculosis in macaques after intravenous BCG immunization. *Nature* 577, 95–102. doi: 10.1038/s41586-019-1817-8

Deng, G., Zhang, F., Yang, S., Kang, J., Sha, S., and Ma, Y. (2016). *Mycobacterium tuberculosis* Rv0431 expressed in *Mycobacterium smegmatis*, a potentially mannosylated protein, mediated the immune evasion of RAW 264.7 *macrophages*. *Microb. Pathog.* 100, 285–292. doi: 10.1016/j.micpath.2016.10.013

Drage, M. G., Tsai, H. C., Pecora, N. D., Cheng, T. Y., Arida, A. R., Shukla, S., et al. (2010). *Mycobacterium tuberculosis* lipoprotein LprG (Rv1411c) binds triacylated glycolipid agonists of Toll-like receptor 2. *Nat. Struct. Mol. Biol.* 17, 1088–1095. doi: 10.1038/nsmb.1869

Espitia, C., and Mancilla, R. (1989). Identification, isolation and partial characterization of *Mycobacterium tuberculosis* glycoprotein antigens. *Clin. Exp. Immunol* 77, 378–383.

Facciuolo, A., Kelton, D. F., and Mutharia, L. M. (2013). Novel secreted antigens of Mycobacterium paratuberculosis as serodiagnostic biomarkers for Johne's disease in cattle. *Clin. Vaccine Immunol.* 20, 1783–1791. doi: 10.1128/CVI.00380-13

Facciuolo, A., and Mutharia, L. M. (2014). Mycobacterial glycoproteins: a novel subset of vaccine candidates. *Front. Cell Infect. Microbiol.* 4:133.

Gaur, R. L., Ren, K., Blumenthal, A., Bhamidi, S., Gonzalez-Nilo, F. D., Jackson, M., et al. (2014). LprG-mediated surface expression of lipoarabinomannan is essential for virulence of *Mycobacterium tuberculosis*. *PLoS Pathog.* 10:e1004376. doi: 10.1371/journal.ppat.1004376

Gonzalez-Zamorano, M., Mendoza-Hernandez, G., Xolalpa, W., Parada, C., Vallecillo, A. J., Bigi, F., et al. (2009). *Mycobacterium tuberculosis* glycoproteomics based on ConA-lectin affinity capture of mannosylated proteins. *J. Proteome Res.* 8, 721–733. doi: 10.1021/pr800756a

Herrmann, J. L., O'Gaora, P., Gallagher, A., Thole, J. E., and Young, D. B. (1996). Bacterial glycoproteins: a link between glycosylation and proteolytic cleavage of a 19 kDa antigen from *Mycobacterium tuberculosis*. *EMBO J.* 15, 3547–3554. doi: 10.1002/j.1460-2075.1996.tb00724.x

Horn, C., Namane, A., Pescher, P., Riviere, M., Romain, F., Puzo, G., et al. (1999). Decreased capacity of recombinant 45/47-kDa molecules (Apa) of *Mycobacterium tuberculosis* to stimulate T lymphocyte responses related to changes in their mannosylation pattern. *J. Biol. Chem.* 274, 32023–32030.

Kebriaei, A., Derakhshan, M., Meshkat, Z., Eidgahi, M. R., Rezaee, S. A., Farsiani, H., et al. (2016). Construction and immunogenicity of a new Fc-based subunit vaccine candidate against *Mycobacterium tuberculosis*. *Mol. Biol. Rep.* 43, 911–922. doi: 10.1007/s11033-016-4024-9

Khademi, F., Derakhshan, M., Yousefi-Avarvand, A., Tafaghodi, M., and Soleimanpour, S. (2018). Multi-stage subunit vaccines against *Mycobacterium tuberculosis*: an alternative to the BCG vaccine or a BCG-prime boost? *Expert Rev. Vaccines* 17, 31–44. doi: 10.1080/14760584.2018.1406309

Lefevre, P., Denis, O., De Wit, L., Tanghe, A., Vandenbussche, P., Content, J., et al. (2000). Cloning of the gene encoding a 22-kilodalton cell surface antigen of Mycobacterium bovis BCG and analysis of its potential for DNA vaccination against tuberculosis. *Infect. Immun.* 68, 1040–1047. doi: 10.1128/iai.68.3.1040-1047.2000

Liu, C. F., Tonini, L., Malaga, W., Beau, M., Stella, A., Bouyssie, D., et al. (2013). Bacterial protein-O-mannosylating enzyme is crucial for virulence of *Mycobacterium tuberculosis*. *Proc. Natl. Acad. Sci. U.S.A.* 110, 6560–6565. doi: 10.1073/pnas.1219704110

Martinez, L., Shen, Y., Mupere, E., Kizza, A., Hill, P. C., and Whalen, C. C. (2017). Transmission of *Mycobacterium Tuberculosis* in households and the community: a systematic review and meta-Analysis. *Am. J. Epidemiol.* 185, 1327–1339. doi: 10.1093/aje/kwx025

Nadler, R., Luo, Y., Zhao, W., Ritchey, J. K., Austin, J. C., Cohen, M. B., et al. (2003). Interleukin 10 induced augmentation of delayed-type hypersensitivity (DTH) enhances Mycobacterium bovis bacillus Calmette-Guerin (BCG) mediated antitumour activity. *Clin. Exp. Immunol.* 131, 206–216. doi: 10.1046/j.1365-2249.2003.02071.x

Nandakumar, S., Kannanganat, S., Dobos, K. M., Lucas, M., Spencer, J. S., Amara, R. R., et al. (2016). Boosting BCG-primed responses with a subunit Apa vaccine during the waning phase improves immunity and imparts protection against *Mycobacterium tuberculosis*. *Sci. Rep.* 6:25837. doi: 10.1038/srep25837

Nandakumar, S., Kannanganat, S., Dobos, K. M., Lucas, M., Spencer, J. S., Fang, S., et al. (2013). O-mannosylation of the *Mycobacterium tuberculosis* adhesin Apa is crucial for T cell antigenicity during infection but is expendable for protection. *PLoS Pathog.* 9:e1003705. doi: 10.1371/journal.ppat.1003705

Nieuwenhuizen, N. E., and Kaufmann, S. H. E. (2018). Next-Generation vaccines based on bacille calmette-guerin. *Front. Immunol.* 9:121. doi: 10.3389/fimmu.2018.00121

Palma, C., Spallek, R., Piccaro, G., Pardini, M., Jonas, F., Oehlmann, W., et al. (2011). The *M. tuberculosis* phosphate-binding lipoproteins *PstS*1 and PstS3 induce Th1 and Th17 responses that are not associated with protection against M. tuberculosis infection. *Clin. Dev. Immunol.* 2011:690328. doi: 10.1155/2011/690328

Pitarque, S., Herrmann, J. L., Duteyrat, J. L., Jackson, M., Stewart, G. R., Lecointe, F., et al. (2005). Deciphering the molecular bases of *Mycobacterium tuberculosis* binding to the lectin DC-SIGN reveals an underestimated complexity. *Biochem. J.* 392(Pt 3), 615–624. doi: 10.1042/bj20050709

Pym, A. S., Brodin, P., Majlessi, L., Brosch, R., Demangel, C., Williams, A., et al. (2003). Recombinant BCG exporting ESAT-6 confers enhanced protection against tuberculosis. *Nat. Med.* 9, 533–539. doi: 10.1038/nm859

Ragas, A., Roussel, L., Puzo, G., and Riviere, M. (2007). The *Mycobacterium tuberculosis* cell-surface glycoprotein apa as a potential adhesin to colonize target cells via the innate immune system pulmonary C-type lectin surfactant protein A. *J. Biol. Chem.* 282, 5133–5142. doi: 10.1074/jbc.m610183200

Rao, M., Cadieux, N., Fitzpatrick, M., Reed, S., Arsenian, S., Valentini, D., et al. (2017). *Mycobacterium tuberculosis* proteins involved in cell wall lipid biosynthesis improve BCG vaccine efficacy in a murine TB model. *Int. J. Infect. Dis.* 56, 274–282. doi: 10.1016/j.ijid.2017.01.024

Rath, P., Huang, C., Wang, T., Wang, T., Li, H., Prados-Rosales, R., et al. (2013). Genetic regulation of vesiculogenesis and immunomodulation in *Mycobacterium tuberculosis*. *Proc. Natl. Acad. Sci. U.S.A.* 110, E4790–E4797. doi: 10.1073/pnas.1320118110

Romano, M., Aryan, E., Korf, H., Bruffaerts, N., Franken, C. L., Ottenhoff, T. H., et al. (2012). Potential of *Mycobacterium tuberculosis* resuscitation-promoting factors as antigens in novel tuberculosis sub-unit vaccines. *Microbes Infect.* 14, 86–95. doi: 10.1016/j.micinf.2011.08.011

Sanchez, A., Espinosa, P., Garcia, T., and Mancilla, R. (2012). The 19 kDa *Mycobacterium tuberculosis* lipoprotein (LpqH) induces macrophage apoptosis through extrinsic and intrinsic pathways: a role for the mitochondrial apoptosis-inducing factor. *Clin. Dev. Immunol.* 2012:950503. doi: 10.1155/2012/950503

Sieling, P. A., Hill, P. J., Dobos, K. M., Brookman, K., Kuhlman, A. M., Fabri, M., et al. (2008). Conserved mycobacterial lipoglycoproteins activate TLR2 but also require glycosylation for MHC class II-restricted T cell activation. *J. Immunol.* 180, 5833–5842. doi: 10.4049/jimmunol.180.9.5833

Smith, G. T., Sweredoski, M. J., and Hess, S. (2014). O-linked glycosylation sites profiling in *Mycobacterium tuberculosis* culture filtrate proteins. *J. Proteomics* 97, 296–306. doi: 10.1016/j.jprot.2013.05.011

Sun, X., Stefanetti, G., Berti, F., and Kasper, D. L. (2019). Polysaccharide structure dictates mechanism of adaptive immune response to glycoconjugate vaccines. *Proc. Natl. Acad. Sci. U.S.A.* 116, 193–198. doi: 10.1073/pnas.1816401115

Toida, I. (2000). Development of the Mycobacterium bovis BCG vaccine: review of the historical and biochemical evidence for a genealogical tree. *Tuber. Lung Dis.* 80:291.

Tong, J., Hu, X. J., Cai, W. Q., Dai, X., and Wang, L. (2018). Puerarin alleviates delayed-type hypersensitivity via cytokine inhibition by modulating Th1/Th2 balance. *Exp. Ther. Med.* 15, 4441–4447. doi: 10.3892/etm.2018.5990

Tsibulkin, A. P., Khaertinova, I. M., Urazov, N. G., and Khaertinov, K. S. (2016). the screening of diagnostic potential of native protein fractions of *Mycobacterium Tuberculosis* using technique of immune blotting. *Klin. Lab. Diagn.* 61, 91–102.

VanderVen, B. C., Harder, J. D., Crick, D. C., and Belisle, J. T. (2005). Export-mediated assembly of mycobacterial glycoproteins parallels eukaryotic pathways. *Science* 309, 941–943.

WHO, (2019). *Global Tuberculosis Report 2019*. Geneva: WHO.

Wieles, B., van Agterveld, M., Janson, A., Clark-Curtiss, J., Rinke de Wit, T., Harboe, M., et al. (1994). characterization of a *Mycobacterium leprae* antigen related to the secreted *Mycobacterium tuberculosis* protein MPT32. *Infect. Immun.* 62, 252–258.

Wolfe, L. M., Mahaffey, S. B., Kruh, N. A., and Dobos, K. M. (2010). Proteomic definition of the cell wall of *Mycobacterium tuberculosis*. *J. Proteome Res.* 9, 5816–5826. doi: 10.1021/pr1005873

Yang, S., Zhang, F., Kang, J., Zhang, W., Deng, G., Xin, Y., et al. (2014). *Mycobacterium tuberculosis* Rv1096 protein: gene cloning, protein expression, and peptidoglycan deacetylase activity. *BMC Microbiol.* 14:174. doi: 10.1186/1471-2180-14-174

Yang, S., Xu, Y., Wang, Y., Ren, F., Li, S., Ding, W., et al. (2018). The biological properties and potential interacting proteins of d-Alanyl-d-alanine Ligase A from *Mycobacterium tuberculosis*. *Molecules* 23:324 doi: 10.3390/molecules23020324

Conflict of Interest: The authors declare that the research was conducted in the absence of any commercial or financial relationships that could be construed as a potential conflict of interest.

frontiers in Immunology

ORIGINAL RESEARCH
published: 12 May 2020
doi: 10.3389/fimmu.2020.00891

Evaluation of IL-1 Blockade as an Adjunct to Linezolid Therapy for Tuberculosis in Mice and Macaques

*Caylin G. Winchell[1], Bibhuti B. Mishra[2,3], Jia Yao Phuah[2], Mohd Saqib[3], Samantha J. Nelson[2], Pauline Maiello[1], Chelsea M. Causgrove[1], Cassaundra L. Ameel[1], Brianne Stein[1], H. Jacob Borish[1], Alexander G. White[1], Edwin C. Klein[4], Matthew D. Zimmerman[5], Véronique Dartois[5], Philana Ling Lin[6], Christopher M. Sassetti[2] and JoAnne L. Flynn[1]**

[1] Department of Microbiology and Molecular Genetics, University of Pittsburgh School of Medicine, Pittsburgh, PA, United States, [2] Department of Microbiology and Physiological Systems, University of Massachusetts Medical School, Worcester, MA, United States, [3] Department of Immunology and Microbial Disease, Albany Medical College, Albany, NY, United States, [4] Division of Laboratory Animal Research, University of Pittsburgh, Pittsburgh, PA, United States, [5] Center for Discovery and Innovation, Hackensack Meridian Health, Nutley, NJ, United States, [6] Department of Pediatrics, UPMC Children's Hospital of the University of Pittsburgh, Pittsburgh, PA, United States

OPEN ACCESS

Edited by:
Juraj Ivanyi, King's College London, United Kingdom

Reviewed by:
Rajko Reljic, St George's, University of London, United Kingdom
Katalin A. Wilkinson, Francis Crick Institute, United Kingdom

***Correspondence:**
JoAnne L. Flynn
joanne@pitt.edu

Specialty section:
This article was submitted to Microbial Immunology, a section of the journal Frontiers in Immunology

Received: *07 February 2020*
Accepted: *17 April 2020*
Published: *12 May 2020*

Citation:
Winchell CG, Mishra BB, Phuah JY, Saqib M, Nelson SJ, Maiello P, Causgrove CM, Ameel CL, Stein B, Borish HJ, White AG, Klein EC, Zimmerman MD, Dartois V, Lin PL, Sassetti CM and Flynn JL (2020) Evaluation of IL-1 Blockade as an Adjunct to Linezolid Therapy for Tuberculosis in Mice and Macaques. Front. Immunol. 11:891. doi: 10.3389/fimmu.2020.00891

In 2017 over 550,000 estimated new cases of multi-drug/rifampicin resistant tuberculosis (MDR/RR-TB) occurred, emphasizing a need for new treatment strategies. Linezolid (LZD) is a potent antibiotic for drug-resistant Gram-positive infections and is an effective treatment for TB. However, extended LZD use can lead to LZD-associated host toxicities, most commonly bone marrow suppression. LZD toxicities may be mediated by IL-1, an inflammatory pathway important for early immunity during *M. tuberculosis* infection. However, IL-1 can contribute to pathology and disease severity late in TB progression. Since IL-1 may contribute to LZD toxicity and does influence TB pathology, we targeted this pathway with a potential host-directed therapy (HDT). We hypothesized LZD efficacy could be enhanced by modulation of IL-1 pathway to reduce bone marrow toxicity and TB associated-inflammation. We used two animal models of TB to test our hypothesis, a TB-susceptible mouse model and clinically relevant cynomolgus macaques. Antagonizing IL-1 in mice with established infection reduced lung neutrophil numbers and partially restored the erythroid progenitor populations that are depleted by LZD. In macaques, we found no conclusive evidence of bone marrow suppression associated with LZD, indicating our treatment time may have been short enough to avoid the toxicities observed in humans. Though treatment was only 4 weeks (the FDA approved regimen at the time of study), we observed sterilization of the majority of granulomas regardless of co-administration of the FDA-approved IL-1 receptor antagonist (IL-1Rn), also known as Anakinra. However, total lung inflammation was significantly reduced in macaques treated with IL-1Rn and LZD compared to LZD alone. Importantly, IL-1Rn administration did not impair the host response against Mtb or LZD efficacy in either animal model. Together, our data support that inhibition of IL-1 in combination with LZD has potential to be an effective HDT for TB and the need for further research in this area.

Keywords: tuberculosis, MDR-TB, IL-1, linezolid, host-directed therapy

INTRODUCTION

Tuberculosis (TB) remains the top cause of death by a single infectious agent, with an estimated 10 million new cases of active TB and 1.3 million deaths in 2017 alone (1). Antibiotic treatment regimens are long and multi-drug resistant (MDR) and extensive-drug resistant (XDR) *Mycobacterium tuberculosis* (Mtb) strains have emerged, complicating treatment. Even those patients that are cured of the infection can suffer permanent deficits in lung function that result from inflammation and fibrosis (2). Host-directed therapies (HDTs) have been proposed as a potential option for improving therapy. Depending on the strategy, HDTs can function to enhance antimicrobial immune responses and shorten therapy, or inhibit pathological inflammation (3). Since HDTs would be used as part of a multi-drug regimen, targeting mechanisms that increase drug exposure or decrease toxicity are also possible. While some HDT strategies hold promise, very few have been rigorously tested in pre-clinical models (4).

Interleukin-1 (IL-1) has been implicated in TB disease severity and inflammation, making it a possible target of HDT. This cytokine plays an important yet complicated role in TB disease progression. The susceptibility of mice lacking critical mediators of IL-1 signaling indicates that initial production of IL-1 upon Mtb infection is essential for establishing protective immune responses necessary for disease control (5–8). In contrast, IL-1 production is regulated after the onset of adaptive immunity, via multiple mechanisms including IFNγ production (8), which acts via the induction of nitric oxide synthase 2 (NOS2)-dependent nitric oxide to inhibit IL-1β processing (9). Persistent IL-1 signaling can contribute to the accumulation of disease-promoting neutrophils in susceptible mice, and genetic variants that result in higher IL-1β production are associated with increased disease severity and neutrophil accumulation in humans (9–11). Given that HDT is designed to be administered to chronically infected patients during treatment when persistent IL-1 production can play a pathological role, it could be beneficial to block the inflammation and disease promoting activities of this cytokine.

IL-1 may also play a role in the toxicity of linezolid (LZD), an increasingly important antibiotic for the treatment of drug-resistant TB, highlighted by its recent inclusion in a newly approved therapy for MDR-TB (12). While LZD has shown efficacy against XDR and MDR-TB, its wide-spread use has been limited by severe host toxicities that occur after more than 4 weeks of treatment (13, 14). Over the 6–20 month treatment course necessary to treat resistant TB, both reversible bone marrow suppression and irreversible neuropathies are common clinical manifestations (15). LZD-associated toxicities are generally attributed to the inhibition of mitochondrial translation and LZD-mediated bone marrow suppression is promoted by the subsequent mitochondrial damage. This damage acts on the NOD-like receptor family, pyrin domain containing 3 (NLRP3) protein that has been shown to be necessary for LZD-mediated bone marrow suppression in mice (16). NLRP3 forms an inflammasome complex containing caspase-1, which cleaves a number of substrates resulting in cell death and/or the release of active of IL-1β. While the importance of NLRP3 in bone marrow suppression is clear, the relative roles of inflammasome activation and IL-1 signaling remain uncertain.

Based on these studies, inhibiting the IL-1 pathway as a potential HDT could serve two purposes: first, to alleviate LZD-associated host toxicity and second, to reduce the pathology associated with unchecked IL-1 signaling during TB disease. Due to the pro-inflammatory nature of the IL-1 pathway, strict regulatory mechanisms exist within the host to quell this pathway. IL-1 receptor antagonist (IL-1Rn) is a protein produced constitutively at low levels that can increase in response to a variety of cytokine signals. IL-1Rn serves as a decoy ligand for the IL-1receptor type 1 (IL-1R1), blocking signal transduction and subduing activation of downstream pro-inflammatory pathways (17). Anakinra is an FDA-approved recombinant IL-1Rn that is used to treat rheumatoid arthritis and other inflammatory disorders. As there are no FDA approved drugs to inhibit inflammasome activation, inhibition of the IL-1 pathway with biologics like Anakinra is currently the only feasible strategy to modulate this pathway in humans (18).

We hypothesized that the combination of Anakinra (herein referred to as IL-1Rn) with LZD for treatment of active TB disease would reduce LZD-associated toxicities and host inflammation. While there is little rationale to expect IL-1 blockade to enhance bacterial clearance by the antibiotic, suppression of both inflammation and LZD toxicity could provide a significant benefit. To test this concept, we employed two established TB animal models to assess differing aspects of host responses to LZD and IL-1R1 blockade. We used multiple strains of mice to model distinct disease states and dissect the relative importance of the inflammasome and IL-1 signaling in evaluating HDT efficacy. As a translational model, we used cynomolgus macaques in combination with [^{18}F] FDG PET CT serial imaging to track TB disease progression, including inflammation, before and during drug regimens (19). Cynomolgus macaques present a similar spectrum of Mtb infection as humans with pathology, granuloma structure and diversity, that recapitulates human TB (20–22). Importantly, we designed our study in macaques to reflect clinical standards, adhering to FDA guidelines for dosage and time frame of LZD and IL-1Rn administration. Together, our data indicate that IL-1 blockade alleviates LZD-mediated bone marrow (BM) suppression in mice and may accelerate the resolution of inflammation in both mice and macaques with TB.

MATERIALS AND METHODS

Ethics Statement

All experimental manipulations, protocols, and care of the animals were approved by the University of Pittsburgh School of Medicine Institutional Animal Care and Use Committee (IACUC). The protocol assurance number for our IACUC is A3187-01. Our specific protocol approval numbers for this project are 15117082, 16017370, 18124275, 13011368, and 16027525. The IACUC adheres to national guidelines established in the Animal Welfare Act (7 U.S.C. Sections 2131 - 2159) and the Guide for the Care and Use of Laboratory Animals (8th Edition) as mandated by the U.S. Public Health Service Policy.

All macaques used in this study were housed at the University of Pittsburgh in rooms with autonomously controlled temperature, humidity, and lighting. Animals were singly housed in caging at least 2 square meters that allowed visual and tactile contact with neighboring conspecifics. The macaques were fed twice daily with biscuits formulated for non-human primates, supplemented at least 4 days/week with large pieces of fresh fruits or vegetables. Animals had access to water *ad libitum*. Because our macaques were singly housed due to the infectious nature of these studies, an enhanced enrichment plan was designed and overseen by our non-human primate enrichment specialist. This plan has three components. First, species-specific behaviors are encouraged. All animals have access to toys and other manipulata, some of which will be filled with food treats (e.g., frozen fruit, peanut butter, etc.). These are rotated on a regular basis. Puzzle feeders foraging boards, and cardboard tubes containing small food items also are placed in the cage to stimulate foraging behaviors. Adjustable mirrors accessible to the animals stimulate interaction between animals. Second, routine interaction between humans and macaques are encouraged. These interactions occur daily and consist mainly of small food objects offered as enrichment and adhere to established safety protocols. Animal caretakers are encouraged to interact with the animals (by talking or with facial expressions) while performing tasks in the housing area. Routine procedures (e.g., feeding, cage cleaning, etc.) are done on a strict schedule to allow the animals to acclimate to a routine daily schedule. Third, all macaques are provided with a variety of visual and auditory stimulation. Housing areas contain either radios or TV/video equipment that play cartoons or other formats designed for children for at least 3 h each day. The videos and radios are rotated between animal rooms so that the same enrichment is not played repetitively for the same group of animals.

All animals are checked at least twice daily to assess appetite, attitude, activity level, hydration status, etc. Following *M. tuberculosis* infection, the animals are monitored closely for evidence of disease (e.g., anorexia, weight loss, tachypnea, dyspnea, coughing). Physical exams, including weights, are performed on a regular basis. Animals are sedated prior to all veterinary procedures (e.g., blood draws, etc.) using ketamine or other approved drugs. Regular PET/CT imaging is conducted on most of our macaques following infection and has proved very useful for monitoring disease progression. Our veterinary technicians monitor animals especially closely for any signs of pain or distress. If any are noted, appropriate supportive care (e.g., dietary supplementation, rehydration) and clinical treatments (analgesics) are given. Any animal considered to have advanced disease or intractable pain or distress from any cause is sedated with ketamine and then humanely euthanized using sodium pentobarbital.

Mice, Infection and Treatment

C57BL/6 (stock no. 000664), *Nos2*$^{-/-}$ (B6.129P2-Nos2^{tm1Lau}/J, stock no. 002609), C3HeB/FeJ (stock no. 00658), and *Nlrp3*$^{-/-}$ (B6.129S6-*Nlrp3*^{tm1Bhk}/J, stock no. 021302) were purchased from the Jackson Laboratory. Breeding pairs of Caspase-1/11 double knock-out mice were kindly provided by Prof. Katherine Fitzgerald of the Department of Infectious Diseases at University of Massachusetts (UMASS) Medical School and bred in house. Mice were housed under specific pathogen-free conditions, and in accordance with the UMASS Medical School, IACUC guidelines.

Unless otherwise indicated, all mice used in this study were of C57BL/6 background, male, and 8–12 weeks of age at the time of infection.

The wild type strain of *M. tuberculosis* (Mtb) Erdman was used in these studies. Bacteria were cultured in 7H9 medium containing 0.05% Tween 80 and OADC enrichment (Becton Dickinson). For infections, mycobacteria were suspended in phosphate-buffered saline (PBS)-Tween 80 (0.05%); clumps were dissociated by sonication, and ∼100 CFU were delivered via the respiratory route using an aerosol generation device (Glas-Col, Terre Haute, IN). At indicated time points mice were treated with 200 mg/kg of Linezolid (LZD). These drugs were prepared in 0.5% carboxymethyl cellulose (CMC) and Polyethylene glycol 300 solution as the vehicle. Cohorts of mice were treated with anti-IL-1R1 antibody (InVivoMab, anti-mouse IL-1R, Clone JAMA147, BioXcell), either alone or in combination with LZD. 0.5% CMC and Polyethylene glycol was used as vehicle control. All antibiotic treatment was done by daily oral gavage. Anti-IL-1R1 (100 μg/mouse/0.2 mL) was administered every alternate day by subcutaneous and intraperitoneal route. All data from these studies are available in the **Supplementary Data Sheet**.

Macaque Pharmacokinetic Study and Analytical Method

Uninfected macaques designated for other studies ($n = 3$) were given 20 mg/kg or 40 mg/kg of LZD by oral gavage and plasma acquired at 0, 5, 19, 15, 20, 25, and 30 h post LZD administration. High pressure liquid chromatography coupled to tandem mass spectrometry (LC/MS-MS) analysis was performed on a Sciex Applied Biosystems Qtrap 4000 triple-quadrupole mass spectrometer coupled to an Agilent 1260 HPLC system to quantify LZD in macaque plasma. LZD chromatography was performed on an Agilent Zorbax SB-C8 column (2.1 × 30 mm; particle size, 3.5 μm) using a reverse phase gradient elution. Milli-Q deionized water with 0.1% formic acid was used for the aqueous mobile phase and 0.1% formic acid in acetonitrile for the organic mobile phase. Multiple-reaction monitoring (MRM) of parent/daughter transitions in electrospray positive-ionization mode was used to quantify the analytes. Sample analysis was accepted if the concentrations of the quality control samples were within 20% of the nominal concentration. Data processing was performed using Analyst software (version 1.6.2; Applied Biosystems Sciex).

Neat 1 mg/mL DMSO stocks for all compounds were serial diluted in 50/50 Acetonitrile water to create standard curves and quality control spiking solutions. Twenty microliter of neat spiking solutions were added to 20 μL of drug free plasma or control tissue homogenate, and extraction was performed by adding 180 μL of Acetonitrile/Methanol 50/50 protein precipitation solvent containing the internal standard (10 ng/mL verapamil and deuterated LZD-d3). Extracts were vortexed

for 5 min and centrifuged at 4,000 RPM for 5 min. Hundred microliter of supernatant was transferred for LC-MS/MS analysis and diluted with 100 μL of Milli-Q deionized water.

Rhesus macaque plasma (Lithium Heparin, Bioreclamation IVT, NY) was used as a surrogate to cynomolgus macaque plasma to build standard curves. LZD-d3 internal standard and verapamil were purchased from Toronto Research Chemical. The lower and upper limits of quantitation (LLOQ and ULOQ) were 1 and 50,000 ng/mL, respectively. The following MRM transitions were used for LZD (338.00/235.00), LZD-d3(341.20/297.20), and verapamil (455.40/165.20).

Macaques, Infection and Treatment

All housing, care, and experimental procedures were approved by the University of Pittsburgh School of Medicine Institutional Animal Care and Use Committee (IACUC). Examination of animals was performed in quarantine to assess physical health and confirmation of no previous *M. tuberculosis* infections as previously described (23). Cynomolgus macaques (*Macaca fascicularis*) ($N = 10$) were purchased for this study from (Valley Biosystems). Bone marrow control (non-drug treated) samples were taken from Mtb-infected cynomolgus macaques in unrelated ongoing studies ($N = 5$). For the current study, all 10 animals were infected bronchoscopically with 12 CFU of Mtb strain Erdman. After active disease developed (3–5 months), NHPs were randomized to LZD only ($N = 5$) or LZD+IL-1Rn ($N = 5$) treatment groups. For randomization, macaques were paired based on total FDG activity in lungs (a surrogate for total thoracic CFU), and then assigned to treatment by coin flip (20). LZD was administered twice a day orally with food (30 mg/kg), while IL1-Rn was given at 2 mg/kg once each day by subcutaneous injection. All animal data are provided in **Supplementary Table 1**. Medication compliancy was monitored at every administration and pharmacokinetic analysis performed at select times. Drug treatments were administered for 4 weeks prior to necropsy. Bronchoalveolar lavages (BAL) were performed prior to drug-treatment and 3 weeks-post start of treatment for CFU, flow cytometry and multiplex assays.

Macaque PET/CT Imaging

Positron emission tomography (PET) with computed tomography (CT) imaging was performed with 2-deoxy-2-[^{18}F]-D-deoxyglucose (FDG) throughout the study as previously described (19). Serial scans were performed throughout the study to track disease progression and changes during drug treatment. Total FDG activity of the lungs was measured over the course of infection and drug treatment as previously described (19). Granulomas identified on scans were denoted, measured (mm) and standard uptake values (SUVR) were determined to assess metabolic activity, a readout for inflammation. SUVR values were normalized to muscle and SUVR and size measurements were determined at each scan over time to compare pre-and post-drug treatment. Each animal was scanned prior to necropsy to identify granulomas for matching at necropsy; granulomas $\geq$1 mm are distinguishable by PET/CT.

Macaque Necropsy

Necropsies were performed as previously described. In short, multiple tissues (granulomas, lung lobes, thoracic lymph nodes, peripheral lymph nodes, liver, spleen, bone marrow) were excised and homogenized into single-cell suspensions for assessment of bacterial burden and immunological assays. Granulomas were individually excised (PET/CT identified and others not identified on scans) and split (size permitting) with one-half for homogenization and single cell suspension and the other half processed for histological analysis. Bone marrow samples were obtained from the sternum, with a portion sent for histological analysis while single cell suspensions were acquired as previously described (24). Bacterial burden was assessed from each tissue by plating serial dilutions on 7H11 agar plates and incubated at 37°C in 5% CO_2 for 21 days before enumeration of Mtb CFU.

Flow Cytometry and Immunoassays

Mice

Single cell suspensions were prepared from the infected mouse organs. Briefly, lung tissue was digested with Collagenase type IV/DNaseI and passed through 40 μm cell strainers to obtain single cell suspension. Red blood cells were lysed using Tris-buffered Ammonium Chloride (ACT) Non-specific antibody binding sites were blocked by Fc-Block CD16/32 (Clone 93, cat. no. 101319) and the cells were stained with anti-CD3-PE (Clone 17A2, cat. no. 100205), anti-CD11b-PerCP Cy5.5 (Clone M1/70, cat. no.101227), anti-Ly-6G-FITC (Clone 1A8, cat. no.127605), anti-Ly-6C-PE (Clone HK1.4, cat. no.128007), anti-Gr1-APC (Clone RB6-8C5, cat. no.108411), anti-Ter119-PE (Clone TER119, cat. no.116208), anti-CD71-FITC (clone RI7217, cat. no. 113806). Antibodies were purchased from BioLegend. All analyses were performed on live cells only after staining them with fixable live dead stain conjugated with eFlour780, purchased from eBiosciences. All the staining was done according to the manufacturer's instructions. Lung, spleen and bone marrow cells were surface stained for 30 min at room temperature, fixed for 20 min at 4°C using the Cytofix buffer (BD-Biosciences, cat. no. 554655). Data were acquired in a BD LSRII flow cytometer in the flow cytometry core facility at UMASS medical school and analyzed with FlowJo Software (Treestar, Inc.). Gating strategies are provided in applicable figures.

Macaques

Single cell suspensions acquired from homogenization of granulomas, lung lobes, and lymph nodes were subjected to intracellular cytokine staining (ICS). Prior to staining, cells were incubated in RPMI 1640 containing 1% HEPES, 1% L-glutamine, 10% human AB serum, and 0.1% brefeldin A (Golgiplug; BD Biosciences) for 3 h at 37°C in 5% CO_2. After viability staining (Invitrogen), surface antigens and intracellular cytokines were assessed using standard protocols. Surface markers include CD3 (SP34-2; BD Pharmingen), CD4 (L200; BD Horizon), CD8 (RPA-T8; BD Horizon) for T cells and CD11b (ICRF44; BD Pharmingen), CD206 (19.2; BE Pharmingen) for macrophages/neutrophils. Calprotectin (27E10; ThermoFisher) was stained intracellularly to identify neutrophils. For bone marrow, single cell suspensions underwent

red blood cell lysis (BD Pharm Lyse) before incubation in alpha-MEM + 10% Stasis^{TM} FBS (Gemini Bio-Products) + MitoTracker^{TM} Red CMXRos (Invitrogen) for 30 min to stain for membrane potential of mitochondria. Cells were then stained for viability (Invitrogen) and surface stained to distinguish erythroid progenitor populations by CD34 (581; Biolegend), CD235a (HIR2; BD Pharmingen), CD71 (L01.1; BD Pharmingen), and CD45 (D058-1283; BD Pharmingen). All samples were acquired on an LSR II (BD) and analyzed with FlowJo Software (Treestar, Inc.). Gating strategies are provided in applicable figures.

For the multiplex assays, all samples and supernatants were stored at −80°C from time of necropsy until time of assay. Five representative granuloma supernatants were randomly selected from each animal using JMP Pro v12 (SAS Institute Inc.). Supernatants were thawed and filtered with a 0.22 μM syringe filter to remove infectious bacteria and debris, then kept on ice throughout the assay. For BAL samples, supernatants were concentrated using regenerated cellulose centrifugal filter tubes (3,000 NMWL, Millipore Sigma) to a final 10X concentration (5 to 0.5 mL). Both granuloma and BAL supernatants were evaluated with a ProcartaPlex multiplex immunoassay (Invitrogen) that assesses thirty cytokines and chemokines specific for NHPs. We followed the manufacturer's protocol with one modification in which we diluted the standard out an extra dilution to increase the range of detection. Results were analyzed by a BioPlex reader (BioRad).

Histopathology and Immunofluorescence

Mice

Lung tissues were fixed in 10% buffered formalin and embedded in paraffin. Five micrometer-thick sections were stained with hematoxylin and eosin (H&E). Tissue staining was done by the Diabetes and Endocrinology Research Center histopathology core facility at the University of Massachusetts Medical School or immunology core facility of Albany medical college, NY. Brightfield images were acquired in Abaxis VETSCAN HD microscope. Lesion size in the histopathological sections were measured using the Image J image analysis software, and percentage of lesion area was calculated relative to the total lung area.

Paraffin embedded lung tissue sections were cut at 5 μm thickness, mounted on ultraclean glass slides covered in silane, deparaffinized, then dehydrated and rehydrated using the following steps: Ethanol solutions (30, 50, 70, 90, 95, and 100 % for 3 min each), xylenes (2 different solutions for 10 min each) and ethanol solutions (100, 95, 90, 70, 50, and 30 for 3 min each). The slides were washed once in Tris buffer saline (TBS) for 5 min. Slices were subjected to antigen retrieval by boiling in sodium citrate buffer at pH = 6.0 for 20 min and incubated in 0.1% Triton-X 100 for 5 min. Slices were removed and allowed to equilibrate to room temperature for at least 20 min and rinsed with distilled water. Tissue sections were blocked (blocking solution; 0.5 M EDTA, 1% BSA, in PBS) and incubated overnight in primary antibodies against the proteins related to our studies. Sections were stained for nuclei (DAPI, blue staining), anti-mouse CD3e (cat.no. ab16669, green staining), anti-mouse Ly-6G (clone 1A8, cat. no. 127602) to identify neutrophil granulocytes (Cy3, red staining). As controls, pre-immune serum and isotype matched controls were used. After incubation, the tissues were washed several times with sterile TBS at room temperature and incubated in the respective secondary antibodies (anti-rabbit conjugated to Alexa-488, anti-rat conjugated to Cy3) for at least 2 h at room temperature. Tissue sections were mounted using Prolong Gold Antifade reagent (Invitrogen, grand Island, NY) with DAPI, and the tissue sections were examined in ECHO Revolve 4 microscope. Isotype matched control antibodies were used for checking antibody specificity.

Macaques

As previously described, samples acquired at necropsy were formalin fixed, paraffin embedded, cut into ∼5 μm serial sections and stained with H&E (23). A study-blinded veterinary pathologist assessed and characterized each granuloma, indicating size, type, distribution and cellular composition. Sterna for bone marrow analysis were excised and formalin fixed then transected longitudinally into 1 to 2 sternebral unites and placed in Cal-Ex Hydrochloric acid decalcification solution for 2–4 h. Upon removal, specimens were washed and trimmed to test for adequate mineral removal, then submitted for routine tissue processing with other tissue specimens as described above.

Statistical Analysis

Mouse Studies

Equal variance between samples was assessed by Brown-Forsythe test. Experiments in which variances were equivalent were analyzed by one-way ANOVA with Sidak's multiple comparisons test. Those with unequal variances were analyzed by Welch ANOVA and Dunnett's multiple comparisons test. $P < 0.05$ was considered significant.

Macaque Studies

Nonparametric *U*-tests (Mann-Whitney) were performed for two-group comparisons and Kruskal-Wallis tests were performed for three-group comparisons as indicated on data sets with non-normal distributions. Wilcoxon signed rank tests were performed for matched pairs. Fisher's exact test was run on any categorical data. $P < 0.05$ were considered significant. Total lung FDG activity was $\log_{10}$-transformed. Note that for any log-transformed data, a $\log_{10}(x + 1)$ transform was implemented so that zeroes were not excluded from the graphs or analyses. A two-way ANOVA was utilized to test whether treatment or time (or an interaction between these factors) had an effect on total lung inflammation. Time was found to be a statistically significant effect ($p = 0.0046$); therefore, Dunnett's multiple comparison tests were then used to compare each time point to pre-drug treatment within each treatment group. For bivariate data, a linear regression was used to test the linear relationship between the variables and the R^2 and *p*-value for the *F*-test are reported in the accompanying figure legend. Statistical analyses were performed in GraphPad Prism 8 (GraphPad Software, San Diego, CA). A regression equation created from control animals from previous studies was used to create a 95% prediction interval for total thoracic bacterial burden using total lung FDG activity on the scan just before drug treatment (20). The lower

and upper bounds and the mean of this prediction interval were subtracted from each animal's total CFU to estimate change in CFU over the course drug treatment. All statistical analyses are referenced in the corresponding figure legends.

RESULTS

IL-1 Receptor Blockade Reduces Inflammation in Mouse Models of TB Disease

Given the complex role played by IL-1 during TB, we initially sought to determine the effect of inhibiting this cytokine during TB disease in mice. We used a blocking antibody to the murine IL-1 receptor type 1 (αIL-1R1) since this reagent has been shown to alter TB disease in mice (25), and we previously found that recombinant human IL-1Rn (Anakinra) has little effect in this mouse model. Two mouse strains were employed to assess the effects of these treatments in animals with different amounts of IL-1 activity. In relatively resistant C57BL/6 animals, mature IL-1 production is controlled by IFNγ-dependent nitric oxide production, whereas unregulated IL-1 drives inflammatory disease characterized by increased number of neutrophils (PMNs), bacterial burden (CFU) in the lungs and significant weight loss observed in Mtb-infected *Nos2*$^{-/-}$ mice that lack this regulatory pathway (9, 10).

αIL-1R1 was administered to the animals between days 14 and 28 post infection after the onset of adaptive immunity. In both resistant (C57BL/6) and susceptible (Nos2$^{-/-}$) mice, αIL-1R1 treatment significantly reduced PMN numbers in the lungs. In addition, this treatment reversed the weight loss observed in *Nos2*$^{-/-}$ animals (**Figures 1A,B**). Somewhat surprisingly, this regimen also modestly reduced the mean bacterial burden in lungs and spleens, with this reduction meeting statistical significance in the spleens of *Nos2*$^{-/-}$ mice (**Figures 1C,D**). This generally beneficial effect of αIL-1R1 treatment was consistent with qualitatively improved histopathological disease (**Figures 1E,F**). By no metric did this αIL-1R1 treatment exacerbate disease in either mouse strain.

IL-1 Blockade Alleviates Lung Inflammation and Hematopoietic Suppression During LZD Treatment in Mice

The IL-1R1 blocking antibody was next tested in combination with LZD to determine whether the efficacy or toxicity of the antibiotic was altered. C3HeB/FeJ mice, which are relatively susceptible to Mtb and develop histopathological lesions that more closely resemble human disease, were used for these studies. To model established disease, mice were treated between days 28 and 46 post-infection with vehicle alone, LZD, αIL-1R1 or a combination of the two. As previously reported, LZD was effective in this model, reducing lung neutrophil numbers, bacterial burden and weight loss (**Figures 2A–D**) (26). The addition of αIL-1R1 to this regimen further reduced lung neutrophil numbers. IL-1 blockade had very little effect on bacterial burdens in lung or spleen, whether given alone or in conjunction with LZD. The mean CFU burden in αIL-1R1-treated animals was within 2.3-fold of the untreated groups, and only the αIL-1R1-associated decrease in the spleens of LZD treated animals approached significance. As IL-1β production in response to both Mtb infection (9) and LZD treatment (16) depends largely on the NLRP3 inflammasome, we also investigated a regimen in which LZD and a small molecule NLRP3 inhibitor (MCC950) was administered between days 56 and 77 post-infection. As observed with αIL-1R1, the addition of MCC950 reduced PMN numbers in the lung, relative to LZD alone, and did not significantly alter bacterial killing (**Figures 2E–G**). Using a more rapid treatment protocol and C57BL/6 mice with genetic deficiencies in Caspase 1 or NLRP3, we confirmed that the antimicrobial activity of LZD was unaffected by inflammasome activation (**Supplementary Figures 1A–D**). Mice were treated between days 14 and 28 post-infection and the effect of LZD on bacterial burden and lung neutrophil number was at least as large in the knockout animals as the wild type controls.

Next, we evaluated the hematopoietic suppression caused due to LZD treatment in the bone marrow and spleens of C3HeB/FeJ mice. In small animals, bone marrow serves as the primary site of hematopoiesis, but during infection or stress, the spleen functions as an extramedullary hematopoietic organ to compensate for the increasing demand of blood cells in the periphery (27). As LZD did not alter the myeloid cells in the bone marrow (data not shown), and previous reports have shown its effects on erythropoiesis (16), we investigated the effect of this oxazolidinone on erythroid lineage cells in both these organs. Using flow cytometry, erythroid progenitors can be divided into a progression of precursors: pro-erythrocyte (ProE), EryA, EryB, and EryC (**Figure 3A**). These populations were quantified in each tissue of Mtb-infected animals treated with LZD and/or αIL-1R1. In both bone marrow and spleen, LZD had a profound effect, nearly eliminating early erythroid progenitors of the ProE, EryA, and EryB classes (**Figures 3B–G**). Simultaneous treatment with αIL-1R1 largely reversed the effect of LZD in the spleen, restoring these immature precursors to approximately half of their untreated levels. While αIL-1R1 also significantly increased the number of erythroid precursors in the BM, the suppression of LZD toxicity was less pronounced at this site.

In sum, studies in the mouse model indicated that the addition of αIL-1R1 to an LZD regimen could reduce the number of lungs PMN and ameliorate hematopoietic toxicity, while not compromising antimicrobial activity. These observations justified further studies in a non-human primate model.

Changes in TB Disease in Macaques Treated With LZD and HDT by PET/CT

Previously we published the efficacy and pharmacokinetics of LZD in cynomolgus macaques treated for 8 weeks with a single daily dose of 30 mg/kg (14). To adhere to FDA guidelines for LZD administration at the time we initiated this study and reproduce clinical exposure at 600 mg twice daily (b.i.d.), we shortened treatment duration to 4 weeks and increased the dosing frequency to 30 mg/kg b.i.d. Dose finding studies were carried out in uninfected cynomolgus macaques to ensure that adequate drug

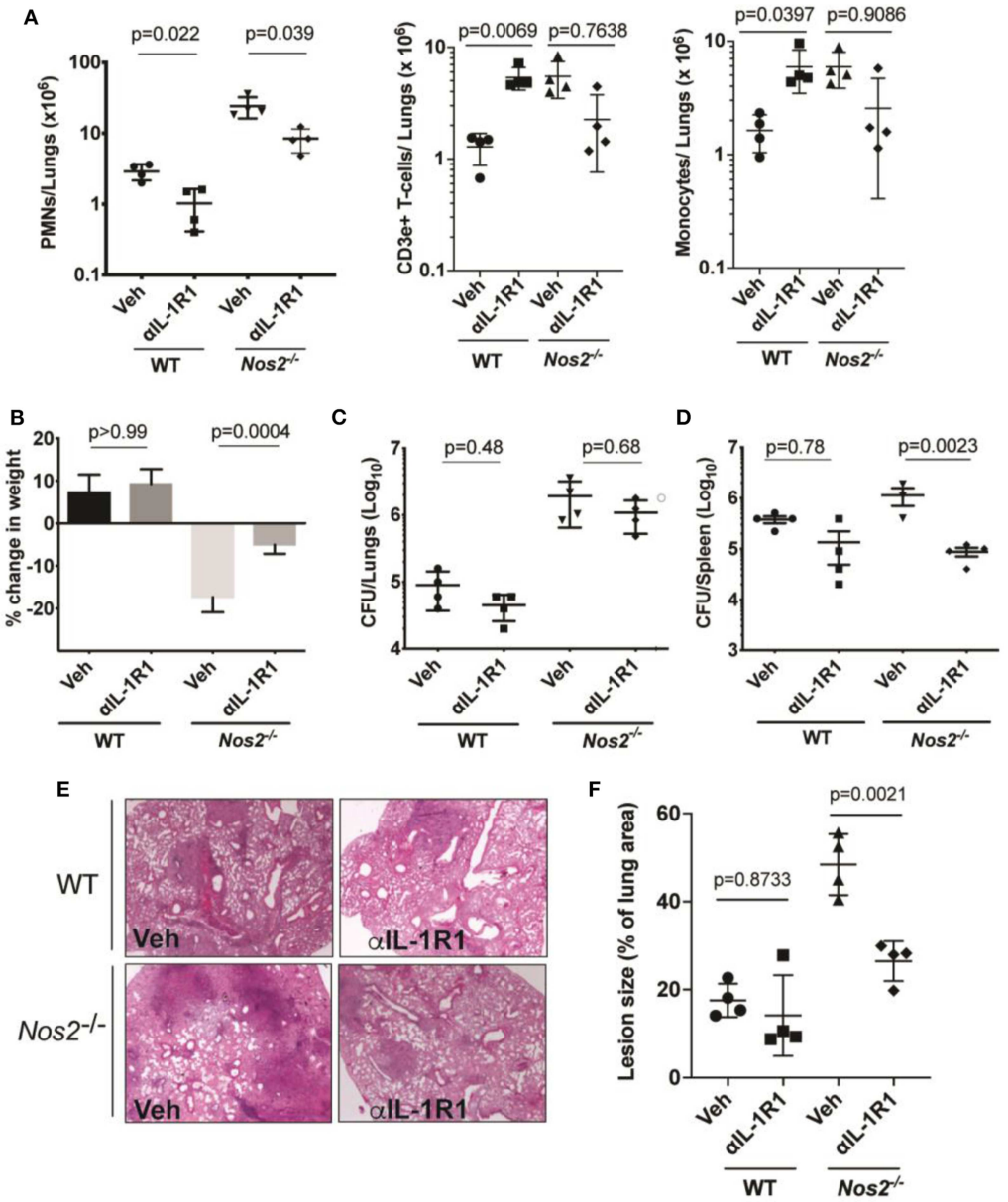

FIGURE 1 | IL-1 inhibition in susceptible mice reduces inflammation with no effect on lung bacterial burden. Wild type C57BL/6 and *Nos2*$^{-/-}$ mice were infected with Mtb Erdman for 2 weeks and treated with anti-IL-1R1 (αIL-1R1) for the subsequent 2 weeks. **(A)** Lung neutrophil/PMN (CD45^{+} CD11b^{+} Ly-6C^{-} CD3e^{-}Ly-6G^{+}), T-cell (CD45^{+} Ly6C^{-}LyG^{-}CD3e^{+}), and Monocyte/macrophage (CD45^{+} CD11b^{+} Ly-6G^{-} CD3e^{-} Ly6C^{+}) recruitment to the lung among different treatment groups were quantified by flow cytometry. **(B)** Weight loss and **(C)** CFU in lung and **(D)** spleen are shown. Data shown (mean ± SD) are representative of two independent experiments. One-way ANOVA with Sidak's multiple comparisons-test was used. $N = 4$ mice per treatment cohorts. **(E)** Histopathology analysis of a single lung lobe from WT or *Nos2*$^{-/-}$ mice was performed by Hematoxylin-eosin (H&E) staining and **(F)** Lesion size was quantified by analyzing the histopathological images from each mouse lung among treatment groups ($n = 4$). Data shown are expressed as Mean ± SD. One-way ANOVA with Tukey's multiple comparison test was applied to calculate the *p*-value.

concentrations similar to those achieved in patients at 600 mg b.i.d. were reached in the blood (**Supplementary Figure 2**).

To assess this LZD regimen and HDT with IL-1Rn, we infected 10 cynomolgus macaques with Mtb strain Erdman and monitored development of active TB disease (**Supplementary Table 1** and **Supplementary Figure 2**). Infected macaques were then randomized to a 4 week drug regimen of LZD ($n = 5$) or LZD+IL-1Rn ($n = 5$) (**Supplementary Figure 2**). Our model has the advantage of tracking disease progression throughout infection and treatment using serial ^{18}F-FDG PET CT scans (14, 28). Lung inflammation quantified by total FDG activity in the lungs is correlated with total thoracic bacterial

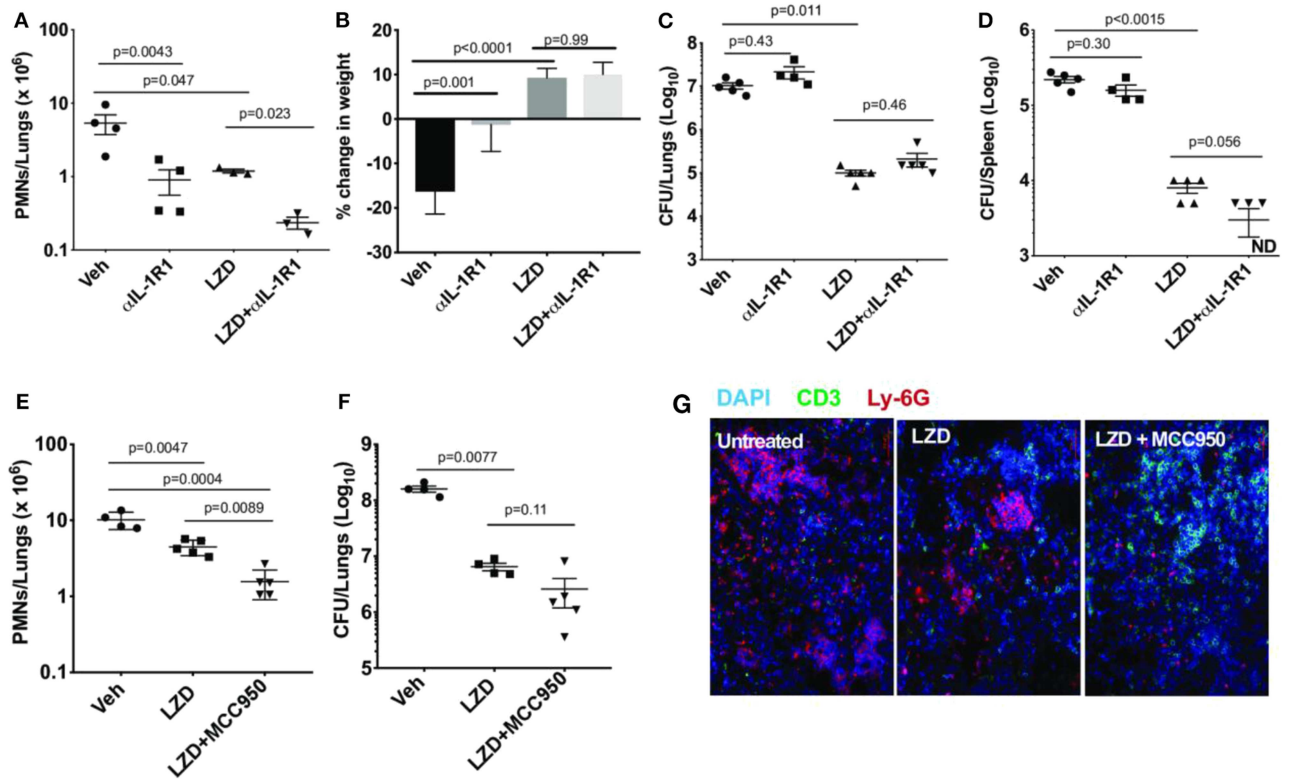

FIGURE 2 | IL-1R1 blockade combined with Linezolid ameliorates TB disease. **(A–D)** C3HeB/FeJ mice were infected with Mtb Erdman for 4 weeks and treated with linezolid (LZD) and/or anti-IL-1R1 (αIL-1R1) for the following 18 days. **(A)** Lung neutrophils were quantified by flow cytometry; **(B)** Percent change in body weight is shown and **(C)** Bacterial burden in the lung and **(D)** spleen were quantified as CFU. Data shown (Mean ± SD) are representative of two independent experiments. Welch ANOVA with Dunnett's post-test was used to calculate statistical significance where each treatment group was compared to the vehicle as control group. $N = 3$–5 mice per treatment group. **(E–G)** C3HeB/FeJ mice were infected with *M. tb* Erdman for 8 weeks and treated with linezolid (LZD) and/or an inhibitor of the NLRP3 inflammasome (MCC950) for the following 21 days. **(E)** Lung neutrophils were quantified by flow cytometry. **(F)** Bacterial burden in the lung was quantified by CFU. Data shown (Mean ± SD) are from one experiment. One-way ANOVA with Tukey's multiple comparison test was used to calculate the *p*-value. $N = 4$–5 mice/group. **(G)** Representative immunofluorescence images of the lungs from different treatment groups. Cell nuclei stained with DAPI (blue), T-cells stained with anti-mouse CD3ε (green) and neutrophils stained with anti-mouse Ly-6G (red).

burden as previously described (19). Here we quantified total lung FDG activity before and during treatment. 3D rendered images provide a visual for changes in overall lung inflammation in the "best" and "worst" animals for both treatment groups (**Figure 4A**). Quantification of total lung FDG showed no significant difference in inflammation at time of necropsy between LZD and LZD+IL-1Rn treatment groups (**Figure 4B**), however a slight change in slope with IL-1Rn treatment was observed. To expand on this finding and test if LZD+IL-1Rn reduced total lung FDG activity more effectively than LZD alone over time, we compared the change in FDG activity between 0, 2, and 4 weeks post treatment. In LZD only treated macaques, there was no significant decrease in total lung FDG activity after 2 ($p = 0.0857$) and 4 weeks of treatment ($p = 0.2876$) (**Figure 4B**). In contrast, LZD+IL-1Rn treatment resulted in a significant reduction in total lung FDG activity after 2 and 4 weeks ($p = 0.0242$, $p = 0.0237$, respectively). To assess whether these changes in lung inflammation were reflected in individual granulomas, we used PET CT scans acquired pre-treatment and at 4 weeks post-treatment to determine changes in granuloma physical size (mm) and metabolic activity as Standard Uptake Value (SUVR) of FDG per granuloma (**Figures 4C,D**) (19). Differences in size and SUVR as presented as the fold change from pre-treatment to necropsy. SUVR indicates the inflammatory state of each individual granuloma, allowing us to track specific lesions throughout treatment for changes in activity. After treatment, while the majority of granulomas decreased in size and SUVR, there was variability within an animal and between animals resulting in no significant differences between LZD and LZD+IL1-Rn treated animals. These data indicate that blocking of IL-1R in combination with LZD reduces total lung inflammation more efficiently than LZD alone.

Addition of IL-1Rn Does Not Alter LZD Bacterial Clearance

IL-1Rn does not have direct bactericidal activity, therefore addition of IL-1Rn to LZD treatment should not directly influence bacterial killing and burden. However, to ensure immunomodulation with IL-1Rn did not have detrimental

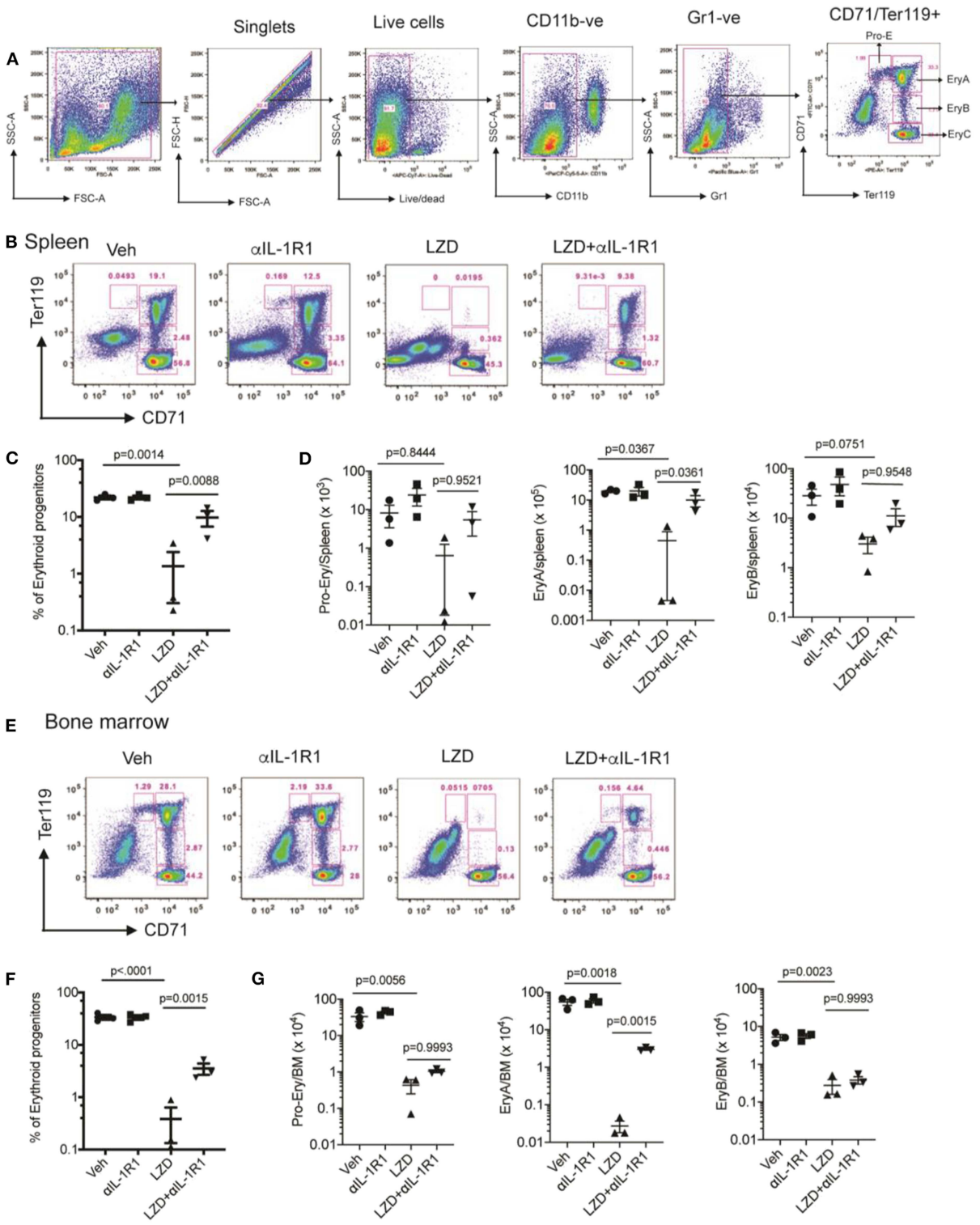

FIGURE 3 | Erythropoiesis associated with LZD treatment was partially relieved after IL-1R1 blockade. C3HeB/FeJ mice were infected with Mtb Erdman for 4 weeks, and treated with LZD either alone or in combination with anti-IL-1R1 antibody for the subsequent 18 days. **(A)** Gating strategy for detecting erythroid progenitors is shown. Erythroid progenitors in the spleen **(B–D)** and bone marrow **(E–G)** were quantified by flow cytometry as described in Materials and Methods. Representative flow cytometry plots, percent, and total numbers of the early erythroid progenitors (sum of Pro-Ery, EryA, EryB) among different treatment groups are shown **(C,F)**. Cell numbers in each subset are also shown **(D,G)**. Data shown (Mean ± SD) are from two independent experiments. One-way ANOVA with Dunnett's post-test was applied to calculate the *p*-value by comparing the mean of each group with that of LZD treated group. $N = 3$–5 mice per group.

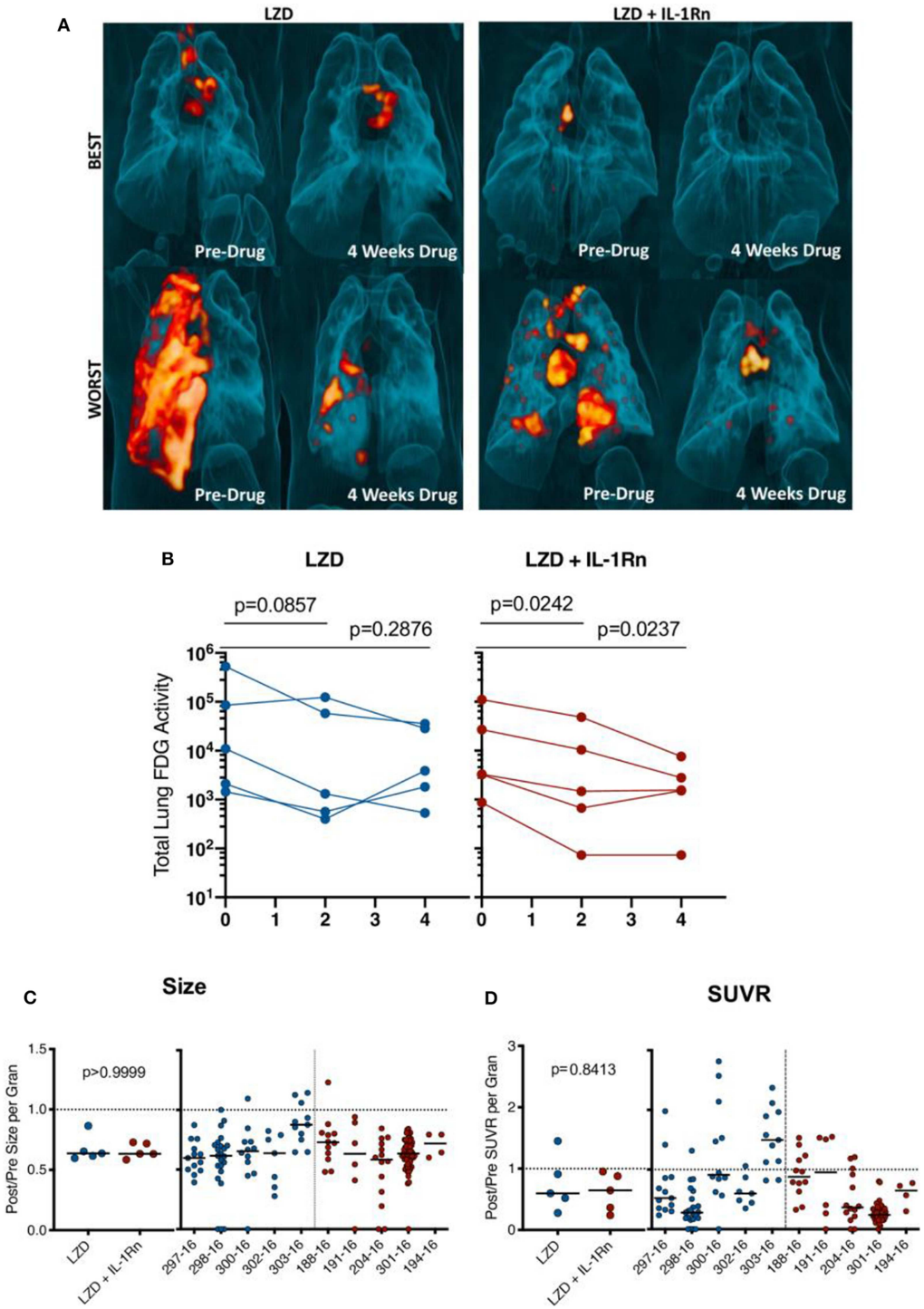

FIGURE 4 | HDT reduces granuloma inflammation by PET/CT in macaques. Cynomolgus macaques were infected with *Mtb* Erdman for approximately 4 months (see **Supplementary Table 1**) and randomized to treatment with LZD or LZD+IL-1Rn for an additional 4 weeks. PET CT scans were performed pre-treatment 0, 2, and 4 weeks post-treatment with 4 week scans as the last prior to necropsy. **(A)** 3-D renderings of PET/CT scans from pre-treatment and 4 weeks post-treatment are depicted, with "best" and "worst" of each group referring to TB disease prior to drug administration. **(B)** Total lung FDG activity of each macaque throughout treatment with LZD (left) or LZD+IL-1Rn (right). Two-way ANOVA with Dunnett's adjusted *p*-values are reported. **(C)** Individual granulomas were identified pre-treatment and tracked post-treatment by PET/CT. Change in size (by CT) was determined for granulomas from each animal; the median (left) change in granuloma size from each animal and individual granulomas per animal (right). **(D)** Standard uptake value (SUVR) of ^{18}F-FDG was calculated for each granuloma, representing inflammation. The median fold change in SUVR of all granulomas (left) and change in SUVR of individual granulomas from each animal (right) are shown. Mann-Whitney tests determined *p*-values for **(C,D)**, with $p < 0.05$ considered significant.

effects on host antibacterial immune responses, we performed comprehensive bacterial burden analysis at necropsy as previously described (20). In short, we acquired individual granulomas identified by PET CT as well as other TB pathologies, thoracic lymph nodes, uninvolved lung tissue and extrapulmonary lesions for bacterial plating and CFU determination. Total thoracic CFU (lung + lymph nodes) was not significantly different between LZD and LZD + IL-1Rn in macaques ($p = 0.1508$). Similarly, separate analysis of lung CFU excluding thoracic lymph nodes did not demonstrate significant differences between groups ($p = 0.5476$) (**Figure 5A**). We did not have untreated control macaques available in this study, therefore we provide total thoracic CFU for 3 historical control animals that were similarly infected and necropsied at a similar time point; these data serve as reference for expected CFU at this time point and were not included in statistical analyses. While the treatment groups had similar frequencies of sterilized granulomas (LZD = 68.42%, LZD+IL-1Rn = 72.22%), it is important to note that the majority of granulomas were sterilized during the short 4 week course of LZD or LZD+IL-1Rn treatment. We previously reported that a 2-month lower dose regimen of LZD could reduce bacterial burden compared to untreated controls, with ∼80% sterilized granulomas in treated animals and ∼20% sterilized in untreated (14). This supports that high dose LZD as a single drug is effective at killing bacteria even in a short (4 week) regimen. The lymph nodes are a recently identified reservoir for Mtb and a hub for immune cell interactions (29), therefore we assessed HDT effects on bacterial burden in thoracic lymph nodes after treatment. We saw no significant difference in overall lymph node CFU nor CFU per lymph node (**Figure 5B**), indicating addition of IL-1Rn did not measurably alter LZD efficacy or antibacterial immunity in lymph nodes. To better understand the efficacy of high dose LZD for 4 weeks, we estimated the pre-treatment total thoracic CFU for each macaque using the total lung FDG by PET CT as previously described (20), and compared the true bacterial burden post-treatment against the estimated pre-treatment value (**Figure 5C**). This analysis allows us to estimate the magnitude of LZD bacterial killing during LZD and LZD+IL-1Rn treatment. All macaques had lower total thoracic CFU at necropsy compared to the estimated total thoracic CFU prior to treatment start and on average the total CFU was ∼100-fold lower than estimated CFU prior to treatment (**Figure 5C**). Our data indicate that while IL-1Rn did not significantly enhance bacterial killing, it did not impair LZD-mediated bacterial clearance, an important observation for HDT development.

Lack of LZD-induced Bone Marrow Suppression in Macaques

In humans, LZD is associated with host toxicities during extended treatment periods of >4 weeks (30) resulting in the FDA limitation of LZD to <4 weeks for most indications. We designed our study in macaques to follow FDA-guidelines for transition to possible human trials, therefore the potential for bone marrow toxicity to occur within this timeframe in macaques was unknown. To determine whether bone marrow suppression occurred during the 4 week high dose LZD therapy and whether IL-1Rn could modulate any observable host toxicities, we isolated bone marrow at necropsy from the sternum of each macaque and assessed erythropoietic progenitor populations and mitochondrial function by flow cytometry (**Figure 6A**). During homeostatic erythropoiesis, a 1:8 ratio is maintained between ProE and EryC progenitor populations. Changes in this ratio can be used to indicate disruption of erythropoiesis. In macaques, there was no significant difference in ProE:EryC ratios between the treatment groups (**Figure 6B**). We also analyzed control bone marrow from untreated Mtb-infected macaques involved in other on-going studies (TB only), which showed no significant difference between ProE:EryC ratios compared to treatment groups. To determine whether LZD was affecting mitochondrial function, we stained bone marrow cells with MitoTracker™ Red CMXRos which only stains mitochondria with active membrane potential, indicating function of those organelles (**Figure 6B**). Regardless of treatment, the MitoTracker MFI remained similar, indicating that mitochondrial function is the same among groups. To confirm our observations, a pathologist evaluated bone marrow tissue sections and found no observable differences between TB only, LZD and LZD+IL-1Rn groups in terms of cellularity (myeloid:erythroid ratios) or abnormalities (**Figure 6C**). We could not consistently identify progenitor populations in blood or spleen, therefore we performed complete blood counts (CBCs) during treatment to identify signs of bone marrow suppression (i.e., anemia, thrombocytopenia). There were no observable differences between LZD and LZD+IL-1Rn treatments (**Supplementary Figure 3**). In conclusion, 4 weeks of LZD was not sufficient to induce observable bone marrow suppression in cynomolgus macaques and blocking of IL-1R did not alter bone marrow status during LZD treatment of TB.

Reduction in Neutrophil Signatures in the Lung During LZD and LZD_IL-1Rn Treatment

To determine whether addition of IL-1Rn to LZD treatment modulated immune populations similar to observations in the mouse model, bronchoalveolar lavages (BAL) were acquired prior to the start of treatment and 3 weeks post treatment. Innate and adaptive immune cell populations were identified and frequencies were assessed by flow cytometry (**Figure 7A**). Population frequencies of CD4 T cells, CD8 T cells, neutrophils (PMNs) and macrophages remain similar between LZD or LZD+IL-1Rn, indicating that IL-1Rn did not significantly alter the frequencies of immune populations in the airways. However, we observed a possible reduction in neutrophils post treatment in both groups. Therefore, we pooled LZD and LZD+IL-1Rn treated animals and compared pre and post treatment immune populations. Although macrophage populations were relatively unchanged, there was a significant reduction in neutrophil frequency in the BAL after 3 weeks of treatment with LZD, regardless of IL-1Rn ($p = 0.0098$). To determine whether the cytokine milieu in the airways changed during treatment, a subset of 3 animals per group were chosen at random for analysis by multi-plex using 10X concentrated BAL fluid

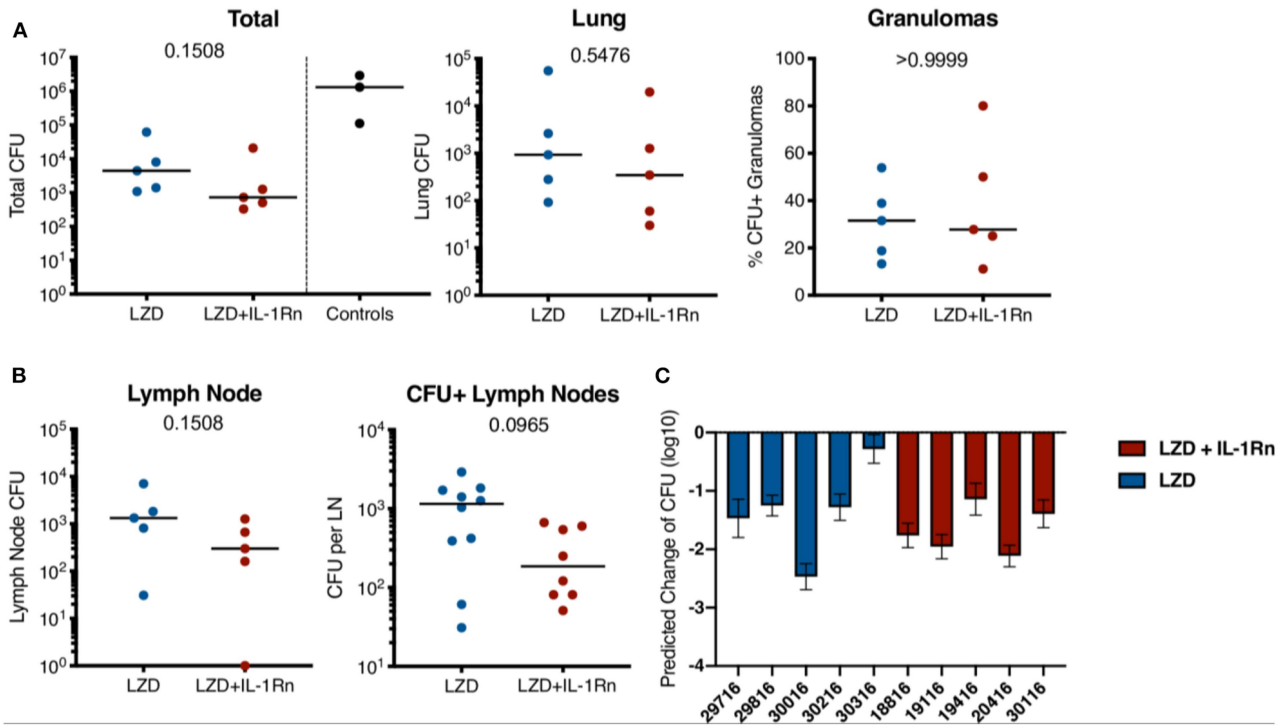

FIGURE 5 | Addition of IL-1Rn does not modify efficacy of LZD-bacterial killing. Bacterial burden is shown after 4 weeks of LZD (blue) or LZD+IL-1Rn (red) treatment. **(A)** Total thoracic (lung + lymph nodes) and lung CFU; each data point represents one macaque. Total thoracic CFU from three similarly infected untreated historical control macaques (black) are included as reference for untreated CFU at this time point but excluded from statistical analysis. Lung (granulomas and lung tissue) are shown separately. The percent of all lung granulomas that were CFU+ per monkey is shown. **(B)** CFU of all thoracic lymph nodes with data points representing CFU from one macaque. CFU+ lymph nodes show the CFU from each thoracic lymph node in any animal that was Mtb+. For **(A,B)**, *p*-values were determined by Mann-Whitney test. **(C)** PET CT scans from pre-treatment were used to model predicted CFU prior to HDT initiation and compared to actual CFU determined at time of necropsy. The predicted change in CFU was determined by: Actual total thoracic CFU post-treatment—Predicted total thoracic CFU interval (predicted from pre-drug-treatment scan). Bars represent mean of prediction intervals and error whiskers represent the lower and upper bounds of the difference between final total CFU and predicted CFU prior to drug treatment.

(**Figure 7B**). Statistical analysis was performed on combined treatment groups to only compare pre- and post-treatment changes. We assessed IL-1β and IL-1RA and saw no significant changes after treatment (IL-1β $p = 0.1562$, IL-1RA $p = 0.1250$). Interferon-inducible T cell alpha chemoattractant (I-TAC) is upregulated in response in interferons and IL-1 and is generally an indicator of inflammation, which appeared to be reduced post treatment, however was not statistically significant ($p = 0.0625$). IL-8, a neutrophil chemoattractant, was significantly reduced after treatment, mirroring the reduction in neutrophil frequency observed by flow cytometry and the mouse data. These data suggest that treatment with either LZD or LZD+IL-1Rn rapidly reduces inflammatory signatures associated with TB disease in the airways.

IL-1 Blockade Modulates Granuloma Environment and Pathology

To determine whether IL-1Rn modulated immune responses at the site of infection, we chose at random 5 granulomas per animal (25 per treatment group) and performed a multi-plex analysis of granuloma supernatants (**Figure 8A**). There were no significant differences in IL-1β, IL-1RA, or IL-18 levels in either treatment group. IL-2 and IL-17 are correlated with protective immune responses during TB (31) and while IL-2 levels in LZD+IL-1Rn treatment were not statistically higher ($p = 0.0882$), a statistically significant increase in IL-17a in LZD+IL-1Rn treated animals was observed. While there are granulomas that have no detectable IL-17, this results are still biologically significant given that only 5 of 25 granulomas from LZD only treated macaques had detectable IL-17, while 11 of 25 granulomas from LZD+IL-1Rn treated macaques had detectable IL-17. Interestingly, G-CSF/CSF-3 levels were also significantly higher in LZD+IL-1Rn treated granulomas ($p = 0.0004$). These results indicate IL-1Rn immune modulation occurs in the granuloma environment. While we did not see a significant difference in granuloma inflammation by FDG SUVR between treatment groups (**Figure 4C**), we next questioned whether the changes in cytokines observed in multiplex assays could be associated with change in SUVR by PET CT. Therefore, we performed linear regression analyses comparing cytokines detected by multiplex and granuloma inflammation (FDG SUVR) and found a positive correlation between IL-1β and fold change of SUVR in LZD+IL-1Rn granulomas (**Figure 8B**). These data indicate that change in inflammation (fold change of FDG SUVR) is correlated

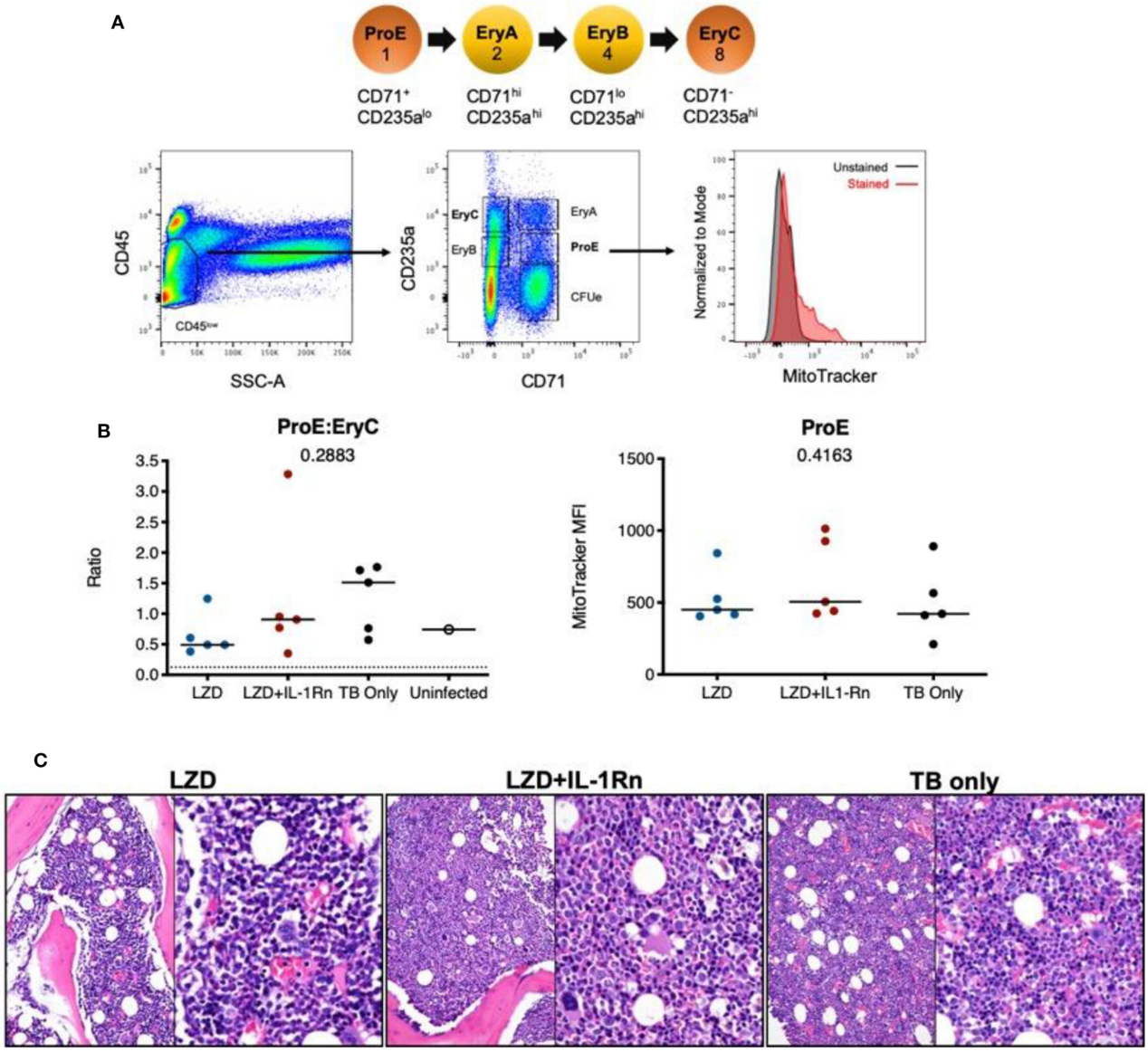

FIGURE 6 | Linezolid-associated bone marrow suppression was not observed in macaques. Bone marrow was acquired from the sternum of all macaques at necropsy after 4 weeks LZD or LZD+IL-1Rn. A portion was used for flow cytometric analysis of erythroid progenitor populations and the rest for histopathology analysis. **(A)** A schematic of erythropoiesis indicating the stage of differentiation and corresponding expression levels of phenotyping markers (CD235a and CD71) and progenitor ratios (1:2:4:8). Included is the gating strategy to identify progenitor populations and an example of MitoTracker staining. **(B)** The ProE:EryC ratio (left) of each animal, including untreated TB only macaques (black) from other ongoing unpublished studies. A single uninfected animal (open circle) is shown as reference, the dotted line indicates the homeostatic ratio of 1:8. MitoTracker MFI (right) is shown for each macaque per treatment group. Kruskal-Wallis test was performed to compare the three groups (excluding uninfected macaque) and *p*-values are shown in the graphs. **(C)** Representative H&E images from sternal bone marrow acquired at necropsy, 20x (left) and 40x (right) are shown.

with levels of IL-1β in the granuloma. The IL-1 pathway is associated with fibrosis, which increases in granulomas during drug treatment (32). Furthermore, IL-17 and G-CSF are also associated with fibrosis (33). To determine whether immunomodulation by IL-1Rn changed granuloma pathology, granulomas suitable for histological analysis were evaluated by a study blinded pathologist and lesions were categorized based on treatment groups and descriptive qualities (**Figure 8C**). Of lesions acquired from LZD only animals, ∼71% were identified as fibrotic (n = 40/56), while those treated with LZD+IL-1Rn had ∼85% fibrotic lesions (n = 39/46) with no significant difference in frequency of fibrotic lesions between treatment groups. We also compared the frequency of granulomas that were deemed necrotizing or non-necrotizing ("other" indicates neither categorization). Granulomas from LZD+IL-1Rn treated animals had significantly more non-necrotizing granulomas (∼74%,

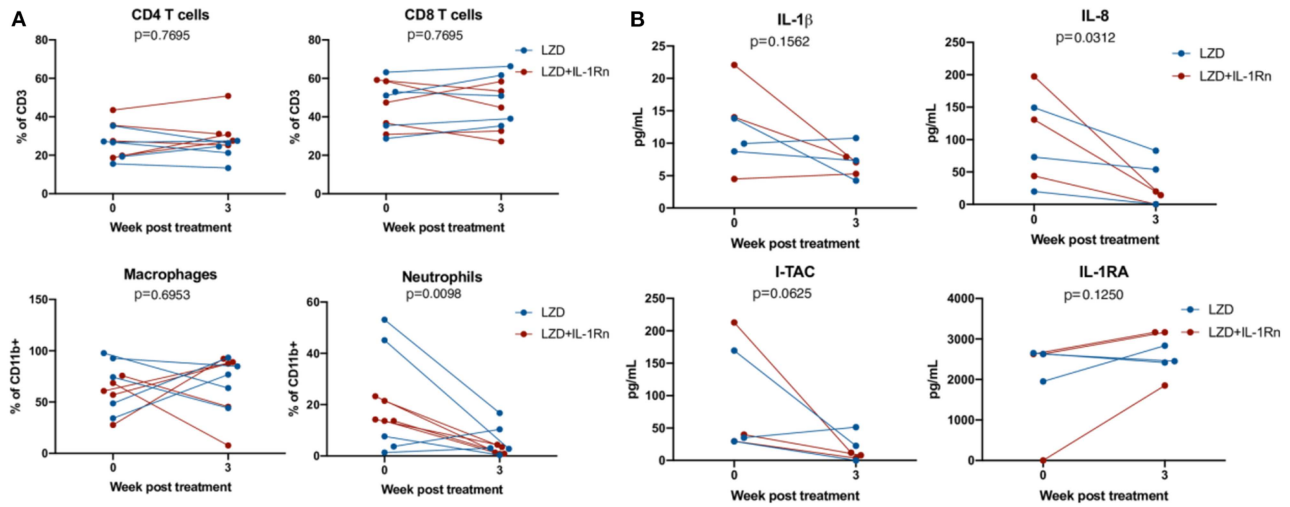

FIGURE 7 | LZD and LZD_IL-1Rn reduce inflammatory signatures in BAL. Bronchoalveolar lavages (BAL) were acquired pre-treatment and 3 weeks post-treatment with LZD (blue) or LZD+IL-1Rn (red). **(A)** Cells were analyzed by flow cytometry to determine frequency changes in CD4 T cells (CD3+CD4+), CD8 T cells (CD3+CD8+), macrophages (CD11b+CD206+), and neutrophils (CD11b+Calprotectin+). Wilcoxon signed rank test was performed to determine differences before and after drug treatment, regardless of group (LZD and LZD+IL-1Rn combined). **(B)** BAL fluid was concentrated 10X and assessed by multiplex assay for changes in inflammatory cytokines and chemokines for a random subset of samples ($n = 3$ per treatment group). Wilcoxon signed rank test was performed to determine differences before and after drug treatment, regardless of group (LZD and LZD+IL-1Rn combined).

$n = 34/46$), compared to those from LZD alone treated macaques (∼46%, $n = 26/56$). The proportion of necrotizing granulomas was significantly lower in the LZD+IL-1Rn treatment group (13.04%, $n = 6/56$) compared to LZD alone (30.36%, $n = 17/56$) ($p = 0.0151$). These data suggest that addition of IL-1Rn influences inflammation and antibiotic-associated pathology dynamics of granulomas.

DISCUSSION

HDTs are a tantalizing solution to improve TB therapy, however the complexities of host-pathogen interactions and host variability call for rigorous pre-clinical testing before implementation in humans. Here, we sought to determine the efficacy and safety of an HDT for TB comprised of LZD and IL-1Rn. IL-1 plays a complex role during TB, as IL-1 is important for early control of infection (5, 7, 8, 34, 35), yet is also associated with pathology at later times (10, 11). To validate the safety of IL-1Rn in this context, we first assessed the effects of IL-1 inhibition on TB disease progression in mice, using treatment regimens designed to concentrate on established disease. In C57BL/6, Nos2$^{-/-}$ and C3HeB/FeJ mice, αIL-1R1 blockade reduced PMN infiltrates that are associated with pathological inflammation and did not impair bacterial control. The effect on bacterial control differs from a recent report in which lung bacterial burdens were increased by a similar αIL-1R1 treatment in C57BL/6 or C57BL/6 animals carrying the super susceptibility to tuberculosis-1 (Sst1) allele (25). We hypothesize that these differences are related to the timing of treatment, relative to the onset of adaptive immunity. Once infection is established, bacterial control is mediated predominantly via T cell functions, potentially reducing the importance of IL-1 dependent mechanisms (36). According to this model, the effect of IL-1 inhibition will depend on the timing of administration, as well as experimental factors that alter the timing of T cell priming and expansion, such as bacterial strain and dose. Regardless, our data indicate that IL-1 blockade can be beneficial in the context of established disease.

Any HDT will be administered in conjunction with antimicrobial therapy. When co-administered with LZD, blockade of IL-1R1 reduced PMN infiltrates in the mouse models, compared to the antibiotic alone. Despite differences between animal models and the IL-1 antagonists used in each model, we observed a similar anti-inflammatory effect in both mouse and primate systems. In macaques, IL-1Rn in conjunction with LZD significantly reduced overall lung inflammation as assessed by PET CT while LZD alone was more variable. IL-1Rn did not significantly enhance bacterial clearance compared to LZD alone, which was not surprising as we did not expect IL-1Rn to have direct antibacterial functions. However, it was important to assess bacterial burden during IL-1Rn treatment to ensure IL-1 blockade did not modulate host-mediated antibacterial mechanisms in granulomas and lymph nodes. In CFU positive lymph nodes, we observed a slight reduction in bacterial burden with IL-1Rn that approached significance ($p = 0.0965$). Further studies should include assessing the influence of drug treatment and immunomodulation in lymph nodes, as thoracic lymph nodes are recognized as a site of Mtb persistence (29).

To further assess the effects of IL-1Rn modulation of immune responses, we observed a decrease in neutrophils (PMNs) and a corresponding decrease in IL-8 in the airways of both treatment group (LZD or LZD+IL-1Rn). This indicated LZD alone was

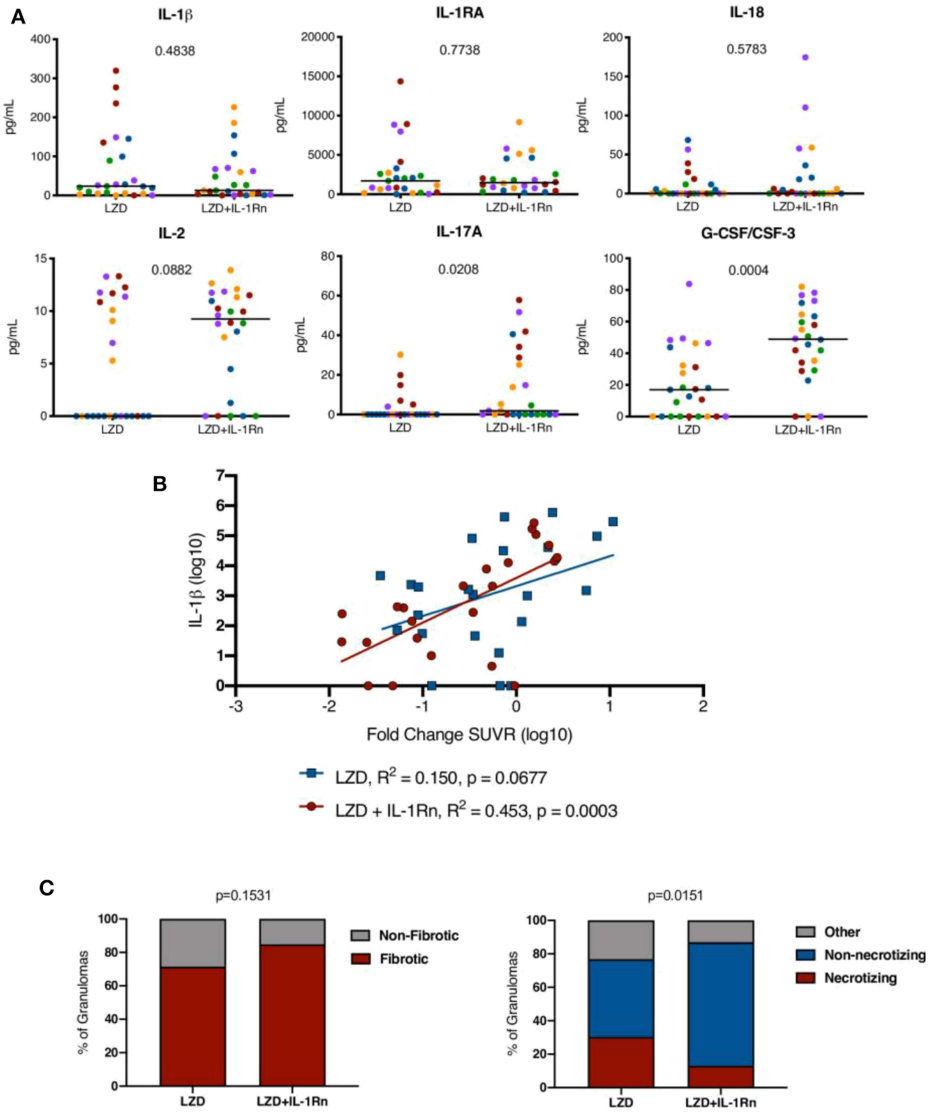

FIGURE 8 | Inflammation modulation by HDT influences granuloma resolution. **(A)** Randomly selected granulomas ($n = 5$ per macaque, $n = 25$ per treatment group) were subjected to multiplex cytokine analysis to determine differences between treatment groups (colors indicate lesions from a single animal). p-values shown determined by Mann-Whitney test. **(B)** A linear regression analysis of IL-1β levels and fold change in SUVR is depicted for LZD (blue) and LZD+IL-1Rn (red) granulomas. R^2 and p-values are provided in the legend. **(C)** Granulomas from LZD ($n = 57$) and LZD+IL-1Rn ($n = 45$) were examined by a pathologist (EK) and categorized. We compared fibrotic (red) vs. non-fibrotic (gray) (left) frequencies between treatment groups. The right compares necrotizing (red) vs. non-necrotizing (blue) and other (gray) granuloma frequencies. Fisher's exact test p-values are reported.

efficacious in reducing PMN inflammatory signatures, likely due to the reduction in bacterial burden. In granulomas, levels of IL-1β, IL-1RA, and IL-18 were not affected by IL-1Rn treatment in the subset examined. As IL-1Rn does not affect inflammasome formation and function it is not surprising that IL-1β and IL-18 production were minimally modulated by IL-1Rn. IL-1RA levels remained unchanged between treatment groups, which could be due to our method of detection or kinetics of consumption. Our multiplex analysis is specific for non-human primates and may not recognize recombinant human IL-1RA like Anakinra. In LZD+IL-1Rn treated granulomas we found a strong positive correlation between IL-1β levels and fold-change in SUVR, a surrogate for inflammation. These data highlight the relationship between IL-1β and inflammation in granulomas, further supporting the potential of IL-1 blockade as an HDT. In TB, IL-2 and IL-17A have protective functions however are primarily expressed by T cells (31). While IL-1β has been reported to enhance IL-17A production by T cells in mice, these studies have primarily used model-antigen systems and may not reflect a chronic infection like TB (37). IL-1 exacerbates pathology later in TB infection, indicating the effects of IL-1 on adaptive immunity are complex and likely

dependent on the host system and infection model being used. G-CSF was increased in granulomas from LZD+IL-1Rn treated macaques which, combined with our observations of reduced PMN infiltrates in mouse lungs and macaque airways, indicates a paradoxical role of G-CSF as a neutrophil differentiation factor (38). However, in a model of LPS-induced lung injury G-CSF blockade induced accumulation of PMNs and increased inflammation in the lungs, indicating pulmonary inflammation may not follow dogmatic rules of canonical inflammatory pathways (38).

Lung fibrosis is modulated by the IL-1 pathway and while fibrosis is associated with healing tissue, lung fibrosis can cause secondary complications after TB disease resolution (2). We have shown in previous studies that TB drug therapy induces fibrosis in granulomas (32, 39). These studies in combination with the correlation between IL-1β and SUVR led us to assess whether LZD+IL-1Rn was associated with changes in granuloma pathology. While we did not observe a difference in fibrosis, there was a significant decrease in frequency of necrotizing granulomas with IL-1Rn in addition to LZD therapy. Thus, while there is no synergistic effect between IL-1Rn and LZD in promoting fibrosis associated with drug clearance, the reduction in neutrophils observed in mice and macaques could skew granuloma resolution toward a non-necrotizing lesion (40). Further studies with IL-1Rn alone could elucidate these dynamics, however we designed this macaque study with intention to be translatable to humans. We could not justify an IL-1Rn only treated group as TB-patients would receive anti-microbial therapy with any HDT or immunomodulatory intervention. However, our findings give precedence for further exploration of the potential of IL-1Rn as an HDT for TB and will require additional studies to determine mechanism and safety.

Our second goal was to abrogate LZD-associated bone marrow suppression with IL-1Rn therapy, thereby increasing the efficacy and therapy potential of LZD in TB. While we designed our HDT to match the current FDA guidelines for LZD and IL-1Rn schedules, this resulted in a lack of observable bone marrow suppression in macaques. In hindsight, extending LZD treatment beyond 4 weeks to induce bone marrow suppression would have allowed assessment of IL-1Rn abrogation of LZD-toxicity, however we initially designed the NHP studies to reflect FDA guidelines for the therapeutics used at the time of study initiation. In mice however, LZD-induced bone marrow suppression was reduced with the addition of IL-1R1 antagonist, supporting our initial hypothesis of the therapeutic potential of IL-1Rn in reducing LZD toxicity. The role of IL-1 signaling is consistent with the ability of IL-1 to suppress erythropoiesis in mice by reducing the number of progenitors (41). The remaining deficit in erythropoiesis during IL-1 blockade could reflect either incomplete inhibition by IL-1Rn or an independent role of inflammasome activation. Optimizing this effect will require further work to understand the relative roles of IL-1 signaling and inflammasome activation.

Overall, our data support previous findings in macaques that LZD has superb efficacy against TB, administered here as a single-drug given for only 4 weeks, supporting LZD as an antimicrobial for MDR/XDR-TB cases (42). IL-1Rn therapy in conjunction with LZD was successful in reducing TB-associated inflammation with no negative effects on bacterial clearance. Reduction in inflammation with IL-1 blockade could have beneficial effects in quelling more pathological inflammation due to IL-1 during active disease (11). While we observed changes in granuloma resolution (necrotizing vs. non-necrotizing), these effects long-term are unknown. Fibrosis is associated with healing and is observed in NHPs after drug treatment (32), however excess fibrosis in the lung may not result in the best outcome for TB patients' long term. Given the link between fibrosis and IL-1, perhaps other inflammatory pathways could be targeted to reduce inflammation and enhance disease resolution. We know TNF is essential for controlling TB disease, and less specific anti-inflammatory agents can also inhibit the protective immune response, which has left many hesitant to modulate host inflammation as a therapy (43). However, our data support the idea that immunomodulation during TB is not always detrimental and suggests that more specific agents may be beneficial.

The differences in bone marrow suppression between mice and macaques highlights the importance of assessing HDTs in multiple models prior to human trials, as there are clear biological differences between the two models. Anakinra (IL-1Rn) is already FDA-approved for adult and pediatric treatment of other inflammatory disorders and our data provide pre-clinical evidence for IL-1Rn consideration as potential therapy in TB. Further safety and mechanism assessments in translatable animal models are required, but one could envision IL-1Rn therapy to limit destructive inflammation for severe cases of TB. While our study emphasizes the importance of rigorous testing of HDTs for TB in multiple translational models prior to implementation in human trials, we also show that immunomodulation of the IL-1 pathway did not exacerbate TB disease.

DATA AVAILABILITY STATEMENT

All datasets generated for this study are included in the article/**Supplementary Material**.

ETHICS STATEMENT

The animal study was reviewed and approved by University of Pittsburgh School of Medicine Institutional Animal Care and Use Committee University of Massachusetts Medical School Institutional Animal Care and Use Committee.

AUTHOR CONTRIBUTIONS

CW, BM, CS, and JF drafted and edited this manuscript. BM, JP, MS, and SN contributed to mouse experiments and/or figures. CW, PM, CC, CA, BS, HB, AW, EC, MZ, VD, PL, and JF contributed to macaque experiments and data and statistical analysis and/or figures. All authors approved the final version of this manuscript.

FUNDING

These studies were funded by NIH UH2AI122295 (JF and CS). CW was supported by NIH T32AI049820.

ACKNOWLEDGMENTS

We thank all members of the Flynn, Sassetti, Mattila, and Lin laboratories for their collaborative efforts during this study. We are grateful for intellectual contributions from Dr. Clifton Barry III and Dr. Robert Wilkinson. Special thanks to all the veterinary and research staff for their efforts, expertise and dedication to these studies. This manuscript has been released as a pre-print at bioRxiv Winchell et al. (44).

SUPPLEMENTARY MATERIAL

The Supplementary Material for this article can be found online at: https://www.frontiersin.org/articles/10.3389/fimmu.2020.00891/full#supplementary-material

REFERENCES

1. World Health Organization. *Global Tuberculosis Report* 2018. Geneva: World Health Organization. Report No.: Licence: CC BY-NC-SA 3.0 IGO (2018).
2. Pasipanodya JG, Miller TL, Vecino M, Munguia G, Garmon R, Bae S, et al. Pulmonary impairment after tuberculosis. *Chest*. (2007) 131:1817–24. doi: 10.1378/chest.06-2949
3. Tobin DM. Host-directed therapies for tuberculosis. *Cold Spring Harb Perspect Med*. (2015) 5:a021196. doi: 10.1101/cshperspect.a021196
4. Baindara P. Host-directed therapies to combat tuberculosis and associated non-communicable diseases. *Microb Pathog*. (2019) 130:156–68. doi: 10.1016/j.micpath.2019.03.003
5. Fremond CM, Togbe D, Doz E, Rose S, Vasseur V, Maillet I, et al. IL-1 receptor-mediated signal is an essential component of myd88-dependent innate response to *mycobacterium tuberculosis* infection. *J Immunol*. (2007) 179:1178–89. doi: 10.4049/jimmunol.179.2.1178
6. Di Paolo NC, Shafiani S, Day T, Papayannopoulou T, Russell DW, Iwakura Y, et al. Interdependence between Interleukin-1 and tumor necrosis factor regulates tnf-dependent control of *Mycobacterium tuberculosis* infection. *Immunity*. (2015) 43:1125–36. doi: 10.1016/j.immuni.2015.11.016
7. Juffermans NP, Florquin S, Camoglio L, Verbon A, Kolk AH, Speelman P, et al. Interleukin-1 signaling is essential for host defense during murine pulmonary tuberculosis. *J Infect Dis*. (2000) 182:902–8. doi: 10.1086/315771
8. Mayer-Barber KD, Andrade BB, Barber DL, Hieny S, Feng CG, Caspar P, et al. Innate and adaptive interferons suppress IL-1alpha and IL-1beta production by distinct pulmonary myeloid subsets during Mycobacterium tuberculosis infection. *Immunity*. (2011) 35:1023–34. doi: 10.1016/j.immuni.2011.12.002
9. Mishra BB, Rathinam VA, Martens GW, Martinot AJ, Kornfeld H, Fitzgerald KA, et al. Nitric oxide controls the immunopathology of tuberculosis by inhibiting NLRP3 inflammasome-dependent processing of IL-1beta. *Nat Immunol*. (2013) 14:52–60. doi: 10.1038/ni.2474
10. Mishra BB, Lovewell RR, Olive AJ, Zhang G, Wang W, Eugenin E, et al. Nitric oxide prevents a pathogen-permissive granulocytic inflammation during tuberculosis. *Nat Microbiol*. (2017) 2:17072. doi: 10.1038/nmicrobiol.2017.72
11. Zhang G, Zhou B, Li S, Yue J, Yang H, Wen Y, et al. Allele-specific induction of IL-1beta expression by C/EBPbeta and PU.1 contributes to increased tuberculosis susceptibility. *PLoS Pathog*. (2014) 10:e1004426. doi: 10.1371/journal.ppat.1004426
12. Conradie F, Diacon AH, Ngubane N, Howell P, Everitt D, Crook AM, et al. Treatment of highly drug-resistant pulmonary tuberculosis. *N Engl J Med*. (2020) 382:893–902. doi: 10.1056/NEJMoa1901814
13. Tan TQ, Yogev R. Clinical pharmacology of linezolid: an oxazolidinone antimicrobial agent. *Expert Rev Clin Pharmacol*. (2008) 1:479–89. doi: 10.1586/17512433.1.4.479
14. Coleman MT, Chen RY, Lee M, Lin PL, Dodd LE, Maiello P, et al. PET/CT imaging reveals a therapeutic response to oxazolidinones in macaques and humans with tuberculosis. *Sci Transl Med*. (2014) 6:265ra167. doi: 10.1126/scitranslmed.3009500
15. Lee M, Lee J, Carroll MW, Choi H, Min S, Song T, et al. Linezolid for treatment of chronic extensively drug-resistant tuberculosis. *N Engl J Med*. (2012) 367:1508–18. doi: 10.1056/NEJMoa1201964
16. Iyer SS, He Q, Janczy JR, Elliott EI, Zhong Z, Olivier AK, et al. Mitochondrial cardiolipin is required for Nlrp3 inflammasome activation. *Immunity*. (2013) 39:311–23. doi: 10.1016/j.immuni.2013.08.001
17. Weber A, Wasiliew P, Kracht M. Interleukin-1 (IL-1) pathway. *Sci Signal*. (2010) 3:cm1. doi: 10.1126/scisignal.3105cm1
18. Furst DE. Anakinra: review of recombinant human interleukin-I receptor antagonist in the treatment of rheumatoid arthritis. *Clin Ther*. (2004) 26:1960–75. doi: 10.1016/j.clinthera.2004.12.019
19. White AG, Maiello P, Coleman MT, Tomko JA, Frye LJ, Scanga CA, et al. Analysis of 18FDG PET/CT imaging as a tool for studying Mycobacterium tuberculosis infection and treatment in non-human primates. *J Vis Exp*. (2017) 56375. doi: 10.3791/56375
20. Maiello P, DiFazio RM, Cadena AM, Rodgers MA, Lin PL, Scanga CA, et al. Rhesus macaques are more susceptible to progressive tuberculosis than cynomolgus macaques: a quantitative comparison. *Infect Immun*. (2018) 86:e00505-17. doi: 10.1128/IAI.00505-17
21. Lin PL, Maiello P, Gideon HP, Coleman MT, Cadena AM, Rodgers MA, et al. PET CT identifies reactivation risk in cynomolgus macaques with latent *M. tuberculosis*. *PLoS Pathog*. (2016) 12:e1005739. doi: 10.1371/journal.ppat.1005739
22. Cadena AM, Fortune SM, Flynn JL. Heterogeneity in tuberculosis. *Nat Rev Immunol*. (2017) 17:691–702. doi: 10.1038/nri.2017.69
23. Lin PL, Pawar S, Myers A, Pegu A, Fuhrman C, Reinhart TA, et al. Early events in *Mycobacterium tuberculosis* infection in cynomolgus macaques. *Infect Immun*. (2006) 74:3790–803. doi: 10.1128/IAI.00064-06
24. Phuah JY, Mattila JT, Lin PL, Flynn JL. Activated B cells in the granulomas of nonhuman primates infected with *Mycobacterium tuberculosis*. *Am J Pathol*. (2012) 181:508–14. doi: 10.1016/j.ajpath.2012.05.009
25. Ji DX, Yamashiro LH, Chen KJ, Mukaida N, Kramnik I, Darwin KH, et al. Type I interferon-driven susceptibility to *Mycobacterium tuberculosis* is mediated by IL-1Ra. *Nat Microbiol*. (2019) 4:2128–35. doi: 10.1038/s41564-019-0578-3
26. Driver ER, Ryan GJ, Hoff DR, Irwin SM, Basaraba RJ, Kramnik I, et al. Evaluation of a mouse model of necrotic granuloma formation using C3HeB/FeJ mice for testing of drugs against *Mycobacterium tuberculosis*. *Antimicrob Agents Chemother*. (2012) 56:3181–95. doi: 10.1128/AAC.00217-12
27. Boettcher S, Manz MG. Regulation of inflammation- and infection-driven hematopoiesis. *Trends Immunol*. (2017) 38:345–57. doi: 10.1016/j.it.2017.01.004
28. Lin PL, Coleman T, Carney JP, Lopresti BJ, Tomko J, Fillmore D, et al. Radiologic responses in cynomolgus macaques for assessing tuberculosis chemotherapy regimens. *Antimicrob Agents Chemother*. (2013) 57:4237–44. doi: 10.1128/AAC.00277-13
29. Ganchua SKC, Cadena AM, Maiello P, Gideon HP, Myers AJ, Junecko BF, et al. Lymph nodes are sites of prolonged bacterial persistence during mycobacterium tuberculosis infection in macaques. *PLoS Pathog*. (2018) 14:e1007337. doi: 10.1371/journal.ppat.1007337
30. Fung HB, Kirschenbaum HL, Ojofeitimi BO. Linezolid: an oxazolidinone antimicrobial agent. *Clin Ther*. (2001) 23:356–91. doi: 10.1016/S0149-2918(01)80043-6
31. Gideon HP, Phuah J, Myers AJ, Bryson BD, Rodgers MA, Coleman MT, et al. Variability in tuberculosis granuloma T cell responses exists, but a balance

of pro- and anti-inflammatory cytokines is associated with sterilization. *PLoS Pathog.* (2015) 11:e1004603. doi: 10.1371/journal.ppat.1004603
32. DiFazio RM, Mattila JT, Klein EC, Cirrincione LR, Howard M, Wong EA, et al. Active transforming growth factor-beta is associated with phenotypic changes in granulomas after drug treatment in pulmonary tuberculosis. *Fibrogenesis Tissue Repair.* (2016) 9:6. doi: 10.1186/s13069-016-0043-3
33. Borthwick LA. The IL-1 cytokine family and its role in inflammation and fibrosis in the lung. *Semin Immunopathol.* (2016) 38:517–34. doi: 10.1007/s00281-016-0559-z
34. Mayer-Barber KD, Barber DL, Shenderov K, White SD, Wilson MS, Cheever A, et al. Caspase-1 independent IL-1beta production is critical for host resistance to mycobacterium tuberculosis and does not require TLR signaling *in vivo*. *J Immunol.* (2010) 184:3326–30. doi: 10.4049/jimmunol.0904189
35. Cooper AM, Mayer-Barber KD, Sher A. Role of innate cytokines in mycobacterial infection. *Mucosal Immunol.* (2011) 4:252–60. doi: 10.1038/mi.2011.13
36. Scanga CA, Mohan VP, Yu K, Joseph H, Tanaka K, Chan J, et al. Depletion of CD4(+) T cells causes reactivation of murine persistent tuberculosis despite continued expression of interferon gamma and nitric oxide synthase 2. *J Exp Med.* (2000) 192:347–58. doi: 10.1084/jem.192.3.347
37. Ben-Sasson SZ, Hu-Li J, Quiel J, Cauchetaux S, Ratner M, Shapira I, et al. IL-1 acts directly on CD4 T cells to enhance their antigen-driven expansion and differentiation. *Proc Natl Acad Sci USA.* (2009) 106:7119–24. doi: 10.1073/pnas.0902745106
38. Bajrami B, Zhu H, Kwak HJ, Mondal S, Hou Q, Geng G, et al. G-CSF maintains controlled neutrophil mobilization during acute inflammation by negatively regulating CXCR2 signaling. *J Exp Med.* (2016) 213:1999–2018. doi: 10.1084/jem.20160393
39. Warsinske HC, DiFazio RM, Linderman JJ, Flynn JL, Kirschner DE. Identifying mechanisms driving formation of granuloma-associated fibrosis during *Mycobacterium tuberculosis* infection. *J Theor Biol.* (2017) 429:1–17. doi: 10.1016/j.jtbi.2017.06.017
40. Flynn JL, Chan J, Lin PL. Macrophages and control of granulomatous inflammation in tuberculosis. *Mucosal Immunol.* (2011) 4:271–8. doi: 10.1038/mi.2011.14
41. Johnson CS, Pourbohloul SC, Furmanski P. Negative regulators of *in vivo* erythropoiesis: interaction of IL-1 alpha and TNF-alpha and the lack of a strict requirement for T or NK cells for their activity. *Exp Hematol.* (1991) 19:101–5.
42. Maxmen A. Treatment for extreme drug-resistant tuberculosis wins US government approval. *Nature.* (2019). doi: 10.1038/d41586-019-02464-0. [Epub ahead of print].
43. Dorhoi A, Kaufmann SH. Perspectives on host adaptation in response to *Mycobacterium tuberculosis*: modulation of inflammation. *Semin Immunol.* (2014) 26:533–42. doi: 10.1016/j.smim.2014.10.002
44. Winchell CG, Mishra BB, Phuah JY, Saqib M, Nelson SJ, Maiello P, et al. Evaluation of IL-1 blockade as an adjunct to linezolid therapy for tuberculosis in mice and macaques. *bioRxiv [Preprint].* (2019). doi: 10.1101/792390

Conflict of Interest: The authors declare that the research was conducted in the absence of any commercial or financial relationships that could be construed as a potential conflict of interest.

frontiers in Microbiology

ORIGINAL RESEARCH
published: 09 June 2020
doi: 10.3389/fmicb.2020.01215

A Panel of CircRNAs in the Serum Serves as Biomarkers for *Mycobacterium tuberculosis* Infection

Hengjun Liu[1†], Geng Lu[1†], Weixiang Wang[1,2,3†], Xinrui Jiang[1], Shuangshuang Gu[1], Jin Wang[3], Xin Yan[2*], Fei He[1*] and Jun Wang[1*]*

[1] Department of Emergency, Nanjing Drum Tower Hospital, The Affiliated Hospital of Nanjing University Medical School, Nanjing, China, [2] Department of Respiratory Medicine, Nanjing Drum Tower Hospital, The Affiliated Hospital of Nanjing University Medical School, Nanjing, China, [3] School of Life Sciences, Nanjing University, Nanjing, China

Tuberculosis (TB), one of the ancient and deadliest diseases, is a chronic immune disorder caused by *Mycobacterium tuberculosis* (Mtb) infection. Due to the lack of ideal diagnostic and therapeutic markers, TB is still posing a major health, social, and economic burden worldwide. Circular RNA (circRNA), a newly discovered endogenous RNA, is abundant and stable in the cytoplasm and has tissue specificity. More and more studies suggested circRNA is involved in a variety of human pathological and physiological processes. Recently, several studies have confirmed circRNAs not only existed in the serum but also could serve as ideal biomarkers for detecting diseases since the circRNAs have continuous, stable, and covalently closed circular structures and are not easily degraded by nucleases. In this study, we screened the circRNA expression profiles in active TB serum samples and healthy volunteers serum samples by circRNA microarrays. Then, we performed qRT-PCR to verified the dysregulated circRNAs and ROC curve analysis to evaluate the value of circRNAs for TB diagnosis. The results showed circRNA_051239, circRNA_029965, and circRNA_404022 could serve as biomarkers for TB diagnosis.

Keywords: biomarker, circRNA, serum, tuberculosis, infection

OPEN ACCESS

Edited by:
Rogelio Hernandez Pando, Salvador Zubirán National Institute of Medical Sciences and Nutrition (INCMNSZ), Mexico

Reviewed by:
Won Fen Wong, University of Malaya, Malaysia
Hazel Marguerite Dockrell, University of London, United Kingdom

****Correspondence:***
Jin Wang
wjgaogou@aliyun.com
Fei He
hefei1201@163.com
Xin Yan
yanxin8612@126.com
Jun Wang
wjgaogou@aliyun.com

† These authors have contributed equally to this work

Specialty section:
This article was submitted to Microbial Immunology, a section of the journal Frontiers in Microbiology

Received: *27 February 2020*
Accepted: *12 May 2020*
Published: *09 June 2020*

Citation:
Liu H, Lu G, Wang W, Jiang X, Gu S, Wang J, Yan X, He F and Wang J (2020) A Panel of CircRNAs in the Serum Serves as Biomarkers for Mycobacterium tuberculosis Infection. Front. Microbiol. 11:1215. doi: 10.3389/fmicb.2020.01215

INTRODUCTION

Tuberculosis (TB) is the ninth leading cause of death worldwide with 1.5 million deaths and 10 million new cases worldwide in 2018 (Reinhart et al., 2012). Despite advances in the effective treatment of TB in recent years, the number of annual deaths and infections remains almost unchanged (Reinhart et al., 2012). The prevention, diagnosis and treatment of tuberculosis are mostly important for TB control. Since there are millions of infected people around the world, timely and effective isolation patients and treatment is the key factors to reduce the transmission

of TB. This is based on the effectively simple and cheap early diagnosis of TB. Currently, the commonly used diagnosis technologies for TB are imaging inspection, bacteriological inspection, molecular biological detection, and immunological experimental inspection. However, all of these methods have some unavoidable limitation. For example, typical imaging inspection (such as X-ray) is useful for the diagnosis of TB, but the specificity is too low to distinguish the TB infection from the other lung disease, such as cancer, pneumonia (Bhalla et al., 2015). The bacteriological inspection is still the gold standard for TB diagnosis, but it requires 4–8 weeks for the growth of *M. tuberculosis*. Therefore, identifying novel appropriate biomarkers for early diagnosis of TB is an urgent.

Circular RNAs (circRNAs) are a novel class of RNAs that participate in almost all the physiological and pathological processes by acting as competing endogenous (ceRNAs) RNAs to block the functions of their target microRNAs (miRNAs) by binding target miRNAs to relieve the suppression of miRNAs for their target gene (Thomson and Dinger, 2016). CircRNAs are highly stable and resistant to debranching and exonuclease-mediated degradation since they could form a circular structure closed by covalent bonds. Recently, several studies have provided circRNAs could not only exist in the body fluids, such as plasma/serum, interstitial fluid, and saliva, but also could serve as molecular biomarkers in the diagnosis and prognosis of many diseases (Zhang et al., 2018). For example, Sonnenschein et al. (2019) found circDNAJC6, circTMEM56, and circMBOAT2 in the serum could distinguish between healthy and hypertrophic cardiomyopathy patients. Ye et al. (2019) identified hsa_circ_0082182, hsa_circ_0000370 were significantly upregulated in colorectal cancer plasma, and the hsa_circ_0035445 was down-regulated.

In this study, we firstly investigated the circRNA expression profiles in serum samples from active TB patients and healthy controls by circRNA microarrays. Subsequently, the dysregulated circRNAs was verified by qRT-PCR, and three circRNAs (circRNA_051239, circRNA_029965, and circRNA_404022) showed significantly increases in the serum from the active TB patients, compared to the healthy controls. The ROC curve analysis showed these three circRNAs could serve as biomarkers for TB diagnosis. More interestingly, we found circRNA_051239 was significantly upregulated in serum derived from drug-resistant TB patients compared to drug-susceptible patients.

MATERIALS AND METHODS

Patients and Healthy Controls

Patients (n = 131) with active pulmonary TB, patients (n = 50) with community acquired pneumonia (CAP), and healthy controls (n = 53) were collected from the Nanjing Drum Tower Hospital. Serum samples were collected at the patients' first admission to the hospital. All the TB patients were clinically diagnosed as active pulmonary TB by positive AFB smear staining or sputum culture. For CAP patients, they shared similar symptoms similar to TB infection (such as fever and chills, loss of appetite, shortness of breath), but didn't have pulmonary TB by sputum smear or/and TB culture. The age- and sex-matched healthy controls, who had no clinical symptoms and normal physical examination, and sputum smear or/and TB culture for pulmonary TB were negative, were collected from the physical examination center of Nanjing Drum Tower Hospital. Patients and controls were matched based on age and gender. All the participants provided their written informed consent to participate in the study and the protocol was approved by the Institutional Research Board of the Nanjing Drum Tower Hospital. Protocols were designed and performed according to the principles of the Helsinki Declaration. Patient characteristics are summarized in **Table 1**. In order to identify serum circulating circRNAs which could serve as novel biomarkers for active TB diagnosis, a multiphase, case-control study was conducted (**Figure 1**).

CircRNA Microarray

Total RNA was isolated from serum with TRIzol reagent (Invitrogen, Carlsbad, CA, United States) according to the manufacturer's protocol. The concentration and quality of total RNA of each sample were determined with NanoDrop ND-1000 spectrophotometer (NanoDrop, Wilmington, DE, United States). CircRNA expression profiles of serum for three active pulmonary TB patients and three healthy controls were generated using the 074301 Arraystar Human CircRNA microarray V2. The data processing and quantile normalization were performed by R (Version 3.4.1) software.

qRT-PCR

For qRT-PCR, cDNA was synthesized with SuperScript First-Strand Synthesis System (Invitrogen, Carlsbad, CA, United States) from RNA extracted from serum. Subsequently, qRT-PCR reaction was performed by an ABI 7500 real-time PCR System according to the manufacturer's protocol. Briefly, PCR reactions were performed in a total volume of 10 μL, including 3 μL cDNA, 5 μL 2 × SYBR Green, 0.25 μL primer forward (10 μmol/L) and 0.25 μL primer reverse (10 μmol/L) at 95°C for 10 min, followed by 40 cycles of 95°C for 15 s and 60°C for 60 s. The synthetic *Caenorhabditis elegans* miRNA cel-miR-39 (5′-*UCACCGGGUGUAAAUCAGCUUG*-3′) (RiboBio, Guangzhou, China) was spiked into the serum as a normalization control

TABLE 1 | The demographic and clinical characteristics of active TB patients, community acquired pneumonia (CAP) patients, and healthy individuals in training and validation sets.

Variable	TB (n = 128)	CAP (n = 50)	HC (n = 50)
Age, years[a]	43.5 (19.84)	45.3 (18.25)	44.4 (18.43)
Sex, n			
Male	87	31	29
Female	41	19	21
History of TB treatment			
Yes	32		
No	96		

[a]*Age data are present as the mean (SD).*

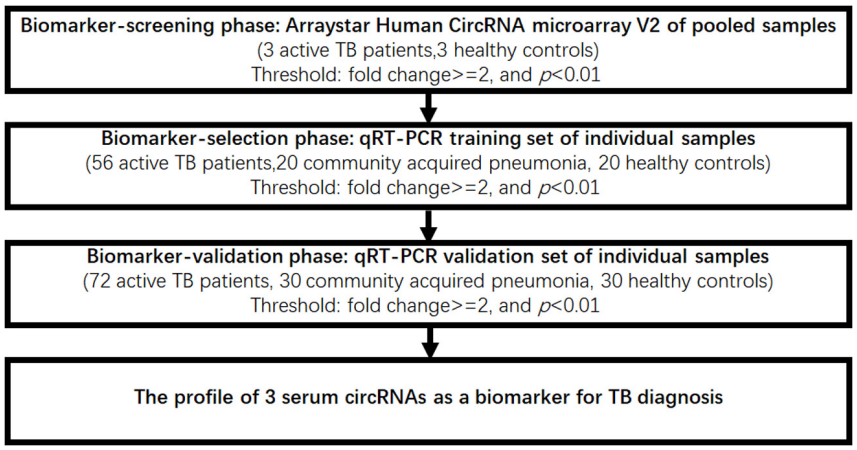

FIGURE 1 | Flow chart of the experimental design.

TABLE 2 | circRNAs selected in Biomarker-screening phase by Arraystar Human CircRNA microarray V2 of pooled samples (three active TB patients, three healthy controls) with fold change = 2, and $p < 0.01$.

CircRNA	Chrom	Strand	txStart	txEnd	CircRNA_type	Best_transcript	Gene symbol	FC (TB vs. HC)	*p*
hsa_circRNA_051239	chr19	–	41938372	41945481	Exonic	uc010xwb.2	ATP5SL	5.358899153	0.007123
hsa_circRNA_029965	chr13	+	33306237	33344899	Exonic	NM_015032	PDS5B	5.174550937	0.004866
hsa_circRNA_404022	chr8	+	41466934	41469511	Exonic	NM_178819	AGPAT6	3.985615857	0.004119
hsa_circRNA_102116	chr17	–	47388673	47389404	Exonic	NM_014897	ZNF652	3.809132132	0.00888
hsa_circRNA_065793	chr3	+	50131152	50131308	Exonic	NM_005778	RBM5	3.175970107	0.004918
hsa_circRNA_104588	chr8	–	37727937	37735069	Exonic	NM_025151	RAB11FIP1	2.993253915	0.004175
hsa_circRNA_048148	chr19	+	1037623	1039064	Exonic	uc002lqu.3	CNN2	2.99009157	0.008405
hsa_circRNA_406174	chr22	–	28249524	28269803	Sense overlapping	NM_012399	PITPNB	2.934103983	0.002732
hsa_circRNA_100823	chr11	–	58317258	58322413	Exonic	NM_004811	LPXN	2.286347985	0.005376
hsa_circRNA_029301	chr12	–	124832370	124835283	Exonic	NM_006312	NCOR2	2.123749587	0.00054

(Kroh et al., 2010). The primers for circRNAs and cel-miR-39 were synthesized at Genscript (Nanjing, China). All reactions were analyzed in triplicate. Receiver operating characteristic (ROC) curve analysis was utilized to estimate the diagnostic value of serum circRNA.

Expression and Statistical Analyses

SPSS 18.0 software was used for statistical analyses, and GraphPad Prism 6.0 (GraphPad Software, San Diego, CA, United States) was used to generate graphs. To compare significant differences in serum circRNA expression, the Mann-Whitney *U* test was used. A *P*-value of < 0.05 was regarded as statistically significant.

RESULTS

Dysregulated CircRNAs Expression Profile in TB Patients

To explore whether serum circRNAs are potential biomarkers for TB infection, the landscape of expressed circular transcripts and their expression pattern in serum was investigated by performing the Agilent-069978 Arraystar Human CircRNA microarray V1 for six serum samples (three active TB patients and three healthy controls) in the biomarker-screening phase (**Supplementary Table S1**). As showed in **Figures 2A,B**, Hierarchical clustering and scatter plots indicated that the serum circRNA expression patterns had the potential possibility to distinguish TB patients from HCs. Only 10 circRNAs showed significantly upregulated in TB patients (fold change > 2; $p < 0.01$) (**Table 2**). The 10 upregulated circRNAs were selected for further analysis by qRT-PCR in the serum of 56 active TB patients, 20 community acquired pneumonia and 20 healthy controls during the Biomarker-selection phase. Compared with healthy controls and community acquired pneumonia, the expression level of circRNA_051239, circRNA_029965, and circRNA_404022 was significantly upregulated in TB patients ($P < 0.01$), while no significant difference in the other seven circRNAs was found (all $P > 0.05$, shown in **Figure 3**).

Biomarker-Validation Phase of the Serum CircRNAs for TB

Next, these three circRNAs (circRNA_051239, circRNA_029965, and circRNA_404022) was further validated in a larger cohort,

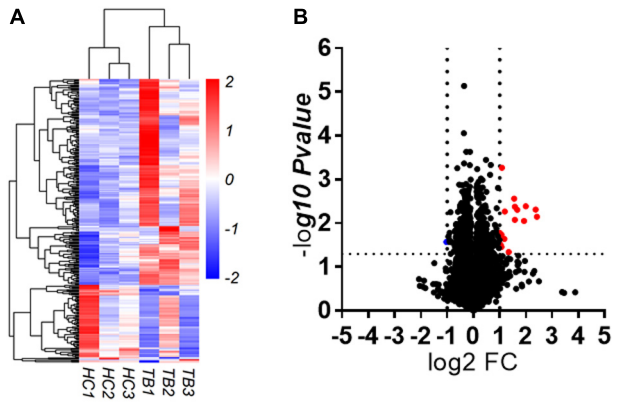

FIGURE 2 | circRNAs expression in serum derived from active TB patients and healthy controls (HC). **(A)** Heatmap. **(B)** Volcano plot.

comprising 72 active TB patients, 30 community acquired pneumonia, 30 healthy controls by qRT-PCR (**Figure 1**). As the results in the Biomarker-selection phase, the concentrations of these three circRNAs (circRNA_051239, circRNA_029965, and circRNA_404022) in TB patients were significantly increased in the TB patients, compared to the community acquired pneumonia and healthy controls (**Figures 4A–C**).

ROC Curve Analysis of Dysregulated CircRNAs

To assess the diagnostic value of these three serum circRNAs for TB detection, the ROC curve analysis was subsequently performed. As showed in **Figures 4D–F**, the area under the curve (AUC) values of these circRNAs were 0.9738 (95% CI, 0.9582–0.9893) for circRNA_051239, 0.9443 (95% CI, 0.9165–0.9721) for circRNA_029965, and 0.9682 (95% CI, 0.9496–0.9868) for circRNA_404022. Then, the diagnostic value of the combination of these three circRNAs was evaluated by a logistic regression model and found that the AUC was 0.9920 with $p < 0.01$ (**Figure 4G**). These results suggested circRNA_051239, circRNA_029965, and circRNA_404022 in the serum could serve as ideal potential biomarkers for TB diagnosis.

CircRNA_051239 Was Significantly Upregulated in Drug-Resistant TB Patients

In the 128 TB patients, we found 20 patients were resistant to at least one drug, while 31 samples were pan-susceptible TB patients. We further analyzed the expression level of circRNA_051239, circRNA_029965, and circRNA_404022 in these drug-resistant TB patients and pan-susceptible TB patients. As the results showed in **Figure 5A**, circRNA_051239 was significantly increased in the drug-resistant group (**Figure 5A**), while the expression level of the other two circRNAs has no difference. More interestingly, Cui et al. (2017) reported levels of miR-320a were decreased in the drug-resistant group, compared to the pan-susceptible TB patients. We also evaluated the miR-320a level in our samples. As for the results reported by Cui et al. (2017), miR-320a significantly decreased in the drug-resistant group, compared to the pan-susceptible TB patients (**Figure 5B**). We conducted Spearmen correlation analysis to explore the correlation between levels of circRNA_051239 and miR-320a, the negative correlation was observed for circRNA_051239 and miR-320a ($R = -0.9296$, $p = 0.0022$) (**Figure 5C**).

We speculated circRNA_051239 might act as a ceRNA for miR-320a, and play a vital role in the TB drug-resistant progress. As predicted by RNAhydrid, miR-320a have three binding sites with circRNA_051239 (**Figure 5D**).

DISCUSSION

As newly discovered endogenous non-coding RNAs with covalently closed loop structures are resistant to RNase digestion

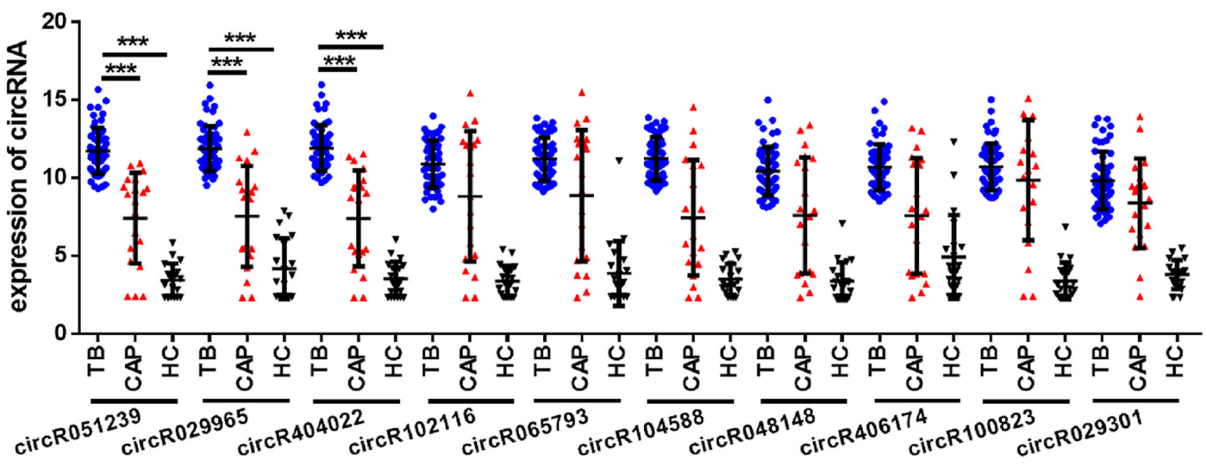

FIGURE 3 | The expression of circRNAs in serum from active TB patients ($N = 56$), CAP patients ($N = 20$), and healthy controls ($N = 20$) by qRT-PCR. Each point represents the mean of triplicate samples. Each P-value was calculated with a nonparametric Mann-Whitney test. $^{***}P < 0.001$.

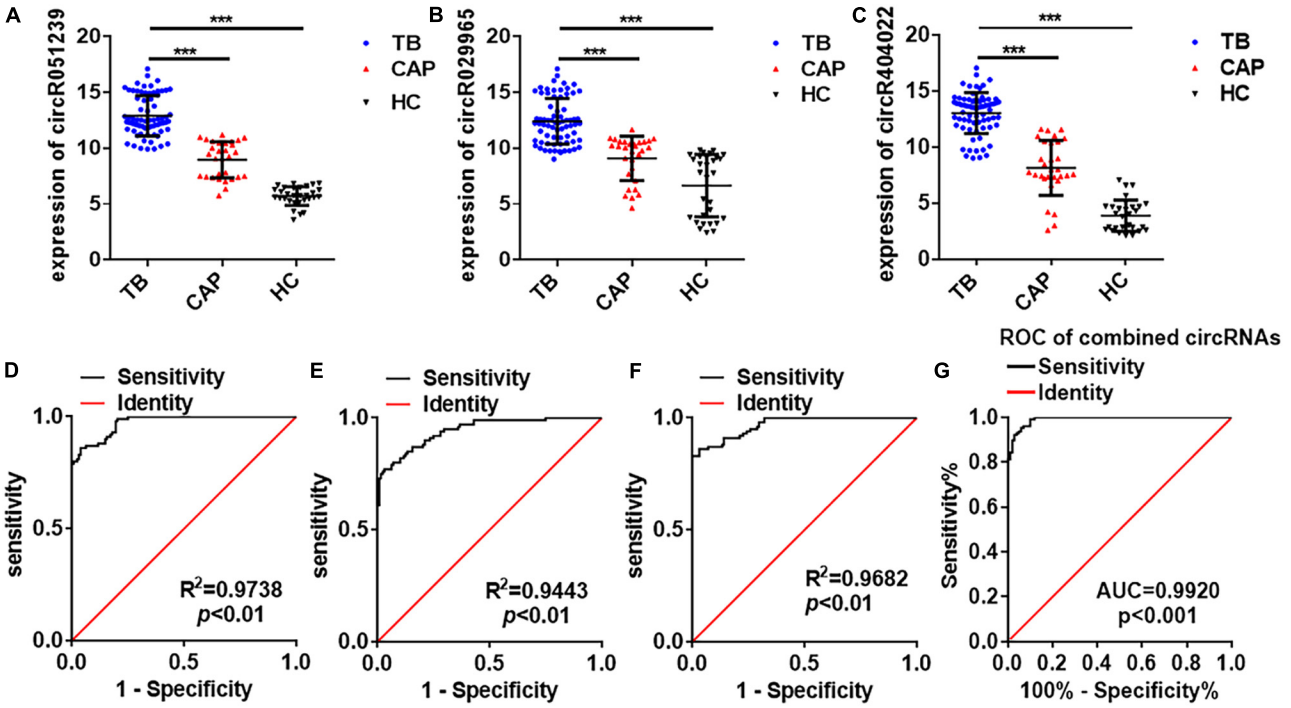

FIGURE 4 | Serum circRNA expression signature for TB diagnosis in the validation phase. **(A–C)** The expression of circRNA_051239, circRNA_029965, and circRNA_404022 in serum from active TB patients (*N* = 72), CAP patients (*N* = 30), and healthy controls (*N* = 30) by qRT-PCR. **(D–F)** ROC curve analysis for circRNA_051239, circRNA_029965, and circRNA_404022 in serum from active TB patients (*N* = 128, including training set and validation set), CAP patients (*N* = 50, including training set and validation set), and healthy controls (*N* = 50, including training set and validation set). **(G)** ROC curve analysis for the combined circRNAs panel in serum from active TB patients (*N* = 128, including training set and validation set), CAP patients (*N* = 50, including training set and validation set), and healthy controls (*N* = 50, including training set and validation set). Each value is the mean ± SD; ***$P < 0.001$.

(Memczak et al., 2013), circRNAs have been proved could serve as ideal potential biomarkers for tumors, Alzheimer's disease, cardiovascular disease, and other diseases (Abu and Jamal, 2016). Recently, Fu et al. (2019) found circRNA_103017, circRNA_059914, and circRNA_101128 were increased in the peripheral blood mononuclear cells (PBMCs) from active tuberculosis (TB) patients, while circRNA_062400 was decreased in TB samples. Huang et al. (2018a) also identified the dysregulated circRNAs in the PBMCs from TB patients, and confirmed hsa_circRNA_001937, hsa_circRNA_009024, and hsa_ circRNA_005086 were significantly elevated and hsa_circRNA_102101, hsa_circRNA_104964, and hsa_circRNA_104296 were significantly reduced in PBMCs from TB patients as compared to healthy controls. Subsequently, they compared the expression level of circRNAs in the plasma from TB patients and healthy controls, the results showed the expression level of hsa_circ_0001204 and hsa_circ_0001747 were significantly decreased in the plasma of TB patients (Huang et al., 2018b), and hsa_circ_0001953 and hsa_circ_0009024 were remarkably increased in the plasma of TB patients (Huang et al., 2018c). Yi et al. (2018) reported hsa_circRNA_103571 exhibited significant decrease in the plasma of active TB patients and showed potential interaction with active TB-related miRNAs, such as miR-29a and miR-16. As for the RNA isolation, transportation and preservation of PBMCs and plasma is too complexity to do quality control, the circRNAs in the PBMC and plasma could not serve as ideal biomarkers for TB diagnosis in clinical application. Compare to PBMCs and plasma, serum is an ideal material for molecular diagnosis. In order to investigate the potential diagnosis value of circRNAs in the serum for TB diagnosis, we characterized the profile of differentially expressed circulating circRNAs in the serum of active TB patients, CAP patients and healthy controls by circRNA microarray and qRT-PCR. As the results in the PBMCs and plasma, the expression profile of circulating circRNAs in the serum of active TB patients showed significantly different from the healthy controls, and we found that circRNA_051239, circRNA_029965, and circRNA_404022 significantly increased in the serum of TB patients and could serve as ideal biomarkers for TB diagnosis with the AUC of all of the three circRNAs is larger than 0.9.

Drug-resistant TB is one of the biggest threats for global TB control and remains a major public health concern in many developing countries. In 2018, more than 500,000 new cases of multidrug-resistant TB and an additional 100,000 cases with rifampicin-resistant TB were identified (Reinhart et al., 2012). Until now, there is still no biomarker to identify whether the TB patients was drug-resistant. In 2017, Cui et al. (2017) reported miR-320a in the plasma significantly decreased in the

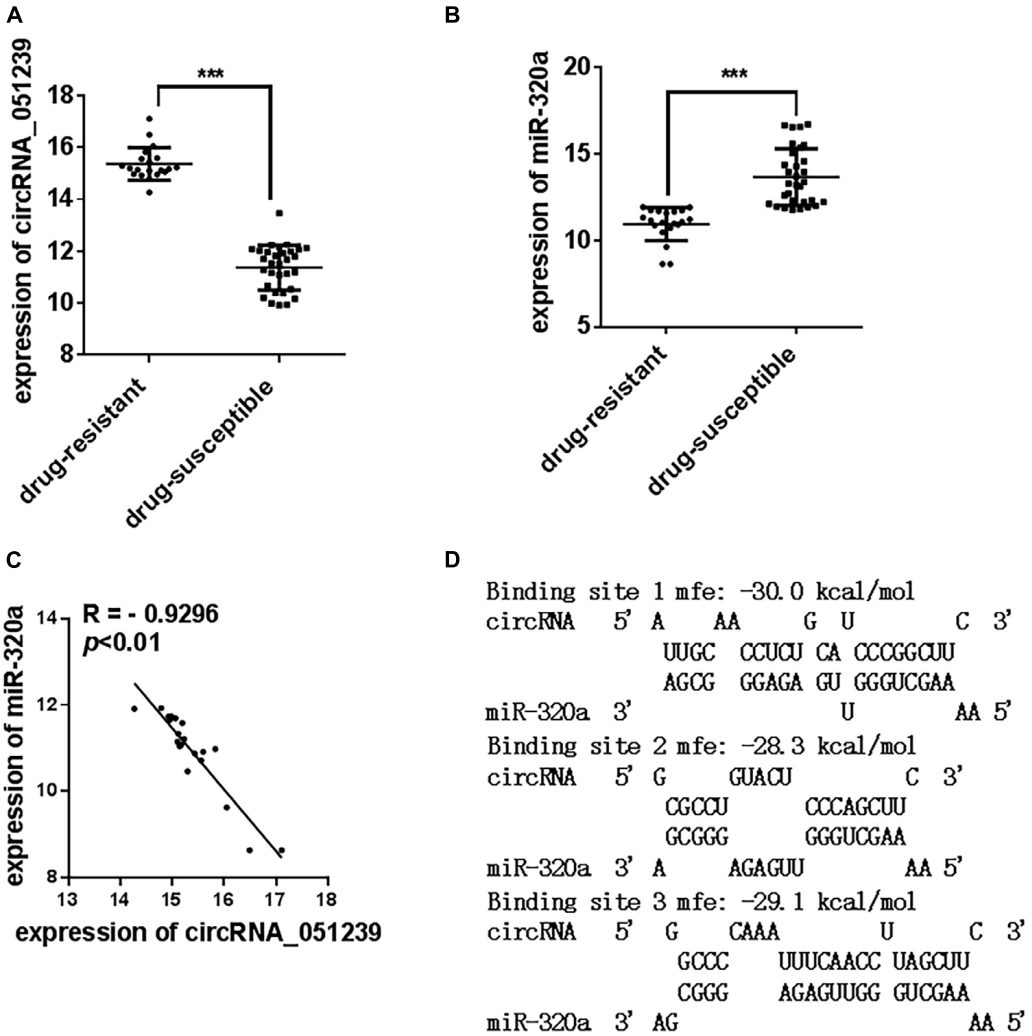

FIGURE 5 | The expression level of circRNA_051239 and miR-320a in the serum of drug-resistant TB patients and drug-susceptible patients. **(A,B)** The expression level of circRNA_051239 and miR-320a in the serum of drug-resistant TB patients and drug-susceptible patients. **(C)** Spearman's rank correlation scatter plot of circRNA_051239 and miR-320a in the serum of drug-resistant TB patients. Each value is the mean ± SD; ***$P < 0.001$. **(D)** Schematic descriptions of the hypothetical duplexes formed by miR-320a with circRNA_051239.

drug-resistant TB patients. We also evaluated the expression level of miR-320a in the serum and found miR-320a in the serum also significantly decreased in the drug-resistant TB patients. However, the expression level of miR-320a in the serum/plasma altered in kinds of diseases. Such as, plasma miR-320a showed significantly decreased in the Arrhythmogenic CardioMyopathy (ACM), compared to the healthy controls (Sommariva et al., 2017). The concentrations of plasma miR-320a were decreased in patients with colorectal cancer and benign lesions (polyps and adenoma) compared with healthy controls, but increased in inflammatory bowel disease (IBD) (Fang et al., 2015). In the present study, circRNA_051239 was significantly upregulated in serum derived from drug-resistant TB patients compared to drug-susceptible patients, implying circRNA_051239 as a potential marker for discriminating drug-resistant TB patients. Moreover, we found the expression levels of circRNA_051239 and miR-320a showed negative correlation (**Figure 5C**). Recent studies have confirmed circRNAs play essential roles in various physiological and pathological processes via acting as a ceRNA for miRNAs to relive the repression of miRNAs for their target genes (Thomson and Dinger, 2016). Here, circRNA_051239 was speculated to sponge miR-320a to release the target genes of miR-320a, and play a vital role in the TB drug-resistant progress. However, it needs to be further confirmed.

In summary, our study firstly provided a profile of circulating circRNAs in the serum of TB patients and healthy controls. We found circRNA_051239, circRNA_029965, and circRNA_404022 significantly increased in the serum of TB patients and could serve as ideal biomarkers for TB diagnosis. Moreover, circRNA_051239 could distinguish drug-resistant TB patients from pan-susceptible TB patients.

DATA AVAILABILITY STATEMENT

All datasets generated for this study are included in the article/**Supplementary Material**. Raw and processed data are stored in the laboratory and are available upon request.

ETHICS STATEMENT

The studies involving human participants were reviewed and approved by Medical Ethics Committee, Nanjing Drum Tower Hospital, The Affiliated Hospital of Nanjing University Medical School. The patients/participants provided their written informed consent to participate in this study.

AUTHOR CONTRIBUTIONS

FH and JW designed the experiments. HL, GL, WW, XJ, SG, and XY performed the experiments and analyzed the results. JW helped to analyze the microarray of circRNA and made critical reading of the manuscript. XY wrote the manuscript.

SUPPLEMENTARY MATERIAL

The Supplementary Material for this article can be found online at: https://www.frontiersin.org/articles/10.3389/fmicb.2020.01215/full#supplementary-material

TABLE S1 | The circRNA expression profile in the serum of TB patients and healthy controls by circRNA Microarray.

REFERENCES

Abu, N., and Jamal, R. (2016). Circular RNAs as promising biomarkers: a mini-review. *Front Physiol* 7:355. doi: 10.3389/fphys.2016.00355

Bhalla, A. S., Goyal, A., Guleria, R., and Gupta, A. K. (2015). Chest tuberculosis: radiological review and imaging recommendations. *Indian J. Radiol. Imaging* 25, 213–225. doi: 10.4103/0971-3026.161431

Cui, J. Y., Liang, H. W., Pan, X. L., Li, D., Jiao, N., Liu, Y. H., et al. (2017). Characterization of a novel panel of plasma microRNAs that discriminates between *Mycobacterium tuberculosis* infection and healthy individuals. *PLoS One* 12:e0184113. doi: 10.1371/journal.pone.0184113

Fang, Z. X., Tang, J., Bai, Y. Y., Lin, H. Y., You, H. Y., Jin, H. W., et al. (2015). Plasma levels of microRNA-24, microRNA-320a, and microRNA-423-5p are potential biomarkers for colorectal carcinoma. *J. Exp. Clin. Cancer Res.* 34:86. doi: 10.1186/s13046-015-0198-6

Fu, Y. R., Wang, J. D., Qiao, J. J., and Yi, Z. J. (2019). Signature of circular RNAs in peripheral blood mononuclear cells from patients with active tuberculosis. *J. Cell Mol. Med.* 23, 1917–1925. doi: 10.1111/jcmm.14093

Huang, Z. K., Su, R., Qing, C., Peng, Y. P., Luo, Q., and Li, J. M. (2018a). Plasma circular RNAs hsa_circ_0001953 and hsa_circ_0009024 as diagnostic biomarkers for active tuberculosis. *Front Microbiol* 9:2010. doi: 10.3389/fmicb.2018.02010

Huang, Z. K., Su, R. G., Yao, F. Y., Peng, Y. P., Luo, Q., and Li, J. M. (2018b). Circulating circular RNAs hsa_circ_0001204 and hsa_circ_0001747 act as diagnostic biomarkers for active tuberculosis detection. *Int. J. Clin. Exp. Pathol.* 11, 586–594.

Huang, Z. K., Yao, F. Y., Xu, J. Q., Deng, Z., Su, R. G., Peng, Y. P., et al. (2018c). Microarray expression profile of circular RNAs in peripheral blood mononuclear cells from active tuberculosis patients. *Cell Physiol. Biochem.* 45, 1230–1240. doi: 10.1159/000487454

Kroh, E. M., Parkin, R. K., Mitchell, P. S., and Tewari, M. (2010). Analysis of circulating microRNA biomarkers in plasma and serum using quantitative reverse transcription-PCR (qRT-PCR). *Methods* 50, 298–301.

Memczak, S., Jens, M., Elefsinioti, A., Torti, F., Krueger, J., Rybak, A., et al. (2013). Circular RNAs are a large class of animal RNAs with regulatory potency. *Nature* 495, 333–338. doi: 10.1038/nature11928

Reinhart, K., Bauer, M., Riedemann, N. C., and Hartog, C. S. (2012). New approaches to sepsis: molecular diagnostics and biomarkers. *Clin. Microbiol. Rev.* 25, 609–634.

Sommariva, E., D'Alessandra, Y., Farina, F. M., Casella, M., Cattaneo, F., Catto, V., et al. (2017). MiR-320a as a potential novel circulating biomarker of arrhythmogenic CardioMyopathy. *Sci. Rep.* 7:4802. doi: 10.1038/s41598-017-05001-z

Sonnenschein, K., Wilczek, A. L., de Gonzalo-Calvo, D., Pfanne, A., Derda, A. A., Zwadlo, C., et al. (2019). Serum circular RNAs act as blood-based biomarkers for hypertrophic obstructive cardiomyopathy. *Sci. Rep.* 9:20350. doi: 10.1038/s41598-019-56617-2

Thomson, D. W., and Dinger, M. E. (2016). Endogenous microRNA sponges: evidence and controversy. *Nat. Rev. Genet.* 17, 272–283. doi: 10.1038/nrg.2016.20

Ye, D. X., Wang, S. S., Huang, Y., and Chi, P. (2019). A 3-circular RNA signature as a noninvasive biomarker for diagnosis of colorectal cancer. *Cancer Cell Int.* 19:276. doi: 10.1186/s12935-019-0995-7

Yi, Z. J., Gao, K. S., Li, R. F., and Fu, Y. R. (2018). Dysregulated circRNAs in plasma from active tuberculosis patients. *J. Cell Mol. Med* 22, 4076–4084. doi: 10.1111/jcmm.13684

Zhang, Z., Yang, T., and Xiao, J. (2018). Circular RNAs: promising biomarkers for human diseases. *EBioMedicine* 34, 267–274. doi: 10.1016/j.ebiom.2018.07.036

Conflict of Interest: The authors declare that the research was conducted in the absence of any commercial or financial relationships that could be construed as a potential conflict of interest.

frontiers in Microbiology

ORIGINAL RESEARCH
published: 18 June 2020
doi: 10.3389/fmicb.2020.01339

Respiratory Immunization With a Whole Cell Inactivated Vaccine Induces Functional Mucosal Immunoglobulins Against Tuberculosis in Mice and Non-human Primates

Nacho Aguilo[1,2†], Santiago Uranga[1,2], Elena Mata[1,2], Raquel Tarancon[1,2], Ana Belén Gómez[1,2], Dessislava Marinova[1,2], Isabel Otal[1,2], Marta Monzón[3], Juan Badiola[3], Dolores Montenegro[4], Eugenia Puentes[4], Esteban Rodríguez[4], Richard A. W. Vervenne[5], Claudia C. Sombroek[5], Frank A. W. Verreck[5†] and Carlos Martín[1,2,6†]*

[1] Grupo de Genética de Micobacterias, Universidad de Zaragoza, Zaragoza, Spain, [2] CIBER Enfermedades Respiratorias, Instituto de Salud Carlos III, Madrid, Spain, [3] Research Centre for Encephalopathies and Transmissible Emerging Diseases, Universidad de Zaragoza, Zaragoza, Spain, [4] Biofabri, Porrino, Spain, [5] Biomedical Primate Research Centre (BPRC), Rijswijk, Netherlands, [6] Servicio de Microbiología, Hospital Universitario Miguel Servet, ISS Aragón, Zaragoza, Spain

Vaccination through the natural route of infection represents an attractive immunization strategy in vaccinology. In the case of tuberculosis, vaccine delivery by the respiratory route has regained interest in recent years, showing efficacy in different animal models. In this context, respiratory vaccination triggers lung immunological mechanisms which are omitted when vaccines are administered by parenteral route. However, contribution of mucosal antibodies to vaccine- induced protection has been poorly studied. In the present study, we evaluated in mice and non-human primates (NHP) a novel whole cell inactivated vaccine (MTBVAC HK), by mucosal administration. MTBVAC HK given by intranasal route to BCG-primed mice substantially improved the protective efficacy conferred by subcutaneous BCG only. Interestingly, this improved protection was absent in mice lacking polymeric Ig receptor (pIgR), suggesting a crucial role of mucosal secretory immunoglobulins in protective immunity. Our study in NHP confirmed the ability of MTBVAC HK to trigger mucosal immunoglobulins. Importantly, *in vitro* assays demonstrated the functionality of these immunoglobulins to induce *M. tuberculosis* opsonization in the presence of human macrophages. Altogether, our results suggest that mucosal immunoglobulins can be induced by vaccination to improve protection against tuberculosis and therefore, they represent a promising target for next generation tuberculosis vaccines.

Keywords: whole-cell vaccine, pulmonary vaccination, animal models, mucosal immunoglobulins, opsonization, tuberculosis

OPEN ACCESS

Edited by:
Rogelio Hernandez Pando, Salvador Zubirán National Institute of Medical Sciences and Nutrition (INCMNSZ), Mexico

Reviewed by:
Prosper N. Boyaka, The Ohio State University, United States
Armando Acosta, Universiti Sains Malaysia Health Campus, Malaysia

***Correspondence:**
Nacho Aguilo
naguilo@unizar.es

†These authors share senior authorship

Specialty section:
This article was submitted to Microbial Immunology, a section of the journal Frontiers in Microbiology

Received: *25 November 2019*
Accepted: *25 May 2020*
Published: *18 June 2020*

Citation:
Aguilo N, Uranga S, Mata E, Tarancon R, Gómez AB, Marinova D, Otal I, Monzón M, Badiola J, Montenegro D, Puentes E, Rodríguez E, Vervenne RAW, Sombroek CC, Verreck FAW and Martín C (2020) Respiratory Immunization With a Whole Cell Inactivated Vaccine Induces Functional Mucosal Immunoglobulins Against Tuberculosis in Mice and Non-human Primates. Front. Microbiol. 11:1339. doi: 10.3389/fmicb.2020.01339

INTRODUCTION

Tuberculosis (TB) disease causes one and a half million deaths per year, and is one of the leading infectious diseases affecting mainly developing and underdeveloped countries. The rising spread of multidrug resistant strains with increasing human migration makes TB an alarming global health problem, according to World Health Organization (WHO). Therefore, there is an urgent need for new effective TB vaccines.

Vaccination through the natural route of infection represents an attractive strategy for priming the natural host immunity. In the case of TB, respiratory mucosal tissue is the primary site for establishment of infection. It has been well described in different preclinical models that vaccination with BCG by the respiratory route confers a substantially improved protection in comparison to subcutaneous or intradermal immunization (Lagranderie et al., 1993; Aguilo et al., 2016; Dijkman et al., 2019). Indeed, in the last few years, it has raised an interest in exploring new vaccination approaches delivered through respiratory routes of administration. These strategies include attenuated *M. tuberculosis* (Kaushal et al., 2015) in addition to BCG, as well as subunit vaccines formulated with adjuvants or non-replicative virus (Stylianou et al., 2015; Woodworth et al., 2019). In 2014, the first clinical trial of an aerosol tuberculosis vaccine was reported (Satti et al., 2014).

It is assumed that inactivation of whole-cell tuberculosis vaccines reduces their immunogenic and protective potential. Nevertheless, and likely based on safety concerns described for live BCG under specific conditions (e.g., immunodeficiencies), researchers have explored the use of inactivated vaccine approaches for tuberculosis. To overcome the loss of immunogenicity, different strategies have been conducted, such as the use of inactivated whole-cell vaccines as booster for BCG (Von Reyn et al., 2017).

The present work describes vaccination with a heat-killed (HK) version of the live attenuated *M. tuberculosis* vaccine MTBVAC (Arbues et al., 2013) both in mice and non-human primates (NHP). MTBVAC is the first and only live attenuated tuberculosis vaccine based on *M. tuberculosis* that has reached clinical stages of development, and it has shown an excellent safety profile both in adults and newborns, as well as stronger immunogenicity compared to BCG (Spertini et al., 2015; Tameris et al., 2019). Results in the present study demonstrate improved efficacy of MTBVAC HK when given by intranasal route to mice previously vaccinated with subcutaneous BCG. In addition, we interrogated lung humoral immune responses elicited by MTBVAC HK in mice and NHP, finding an induction of tuberculosis-specific mucosal immunoglobulins with functional activity against *M. tuberculosis*.

RESULTS

Intranasal MTBVAC HK Enhances Protection Conferred by Subcutaneous BCG

We and others have previously demonstrated an advantageous vaccine-induced protection of whole-cell live vaccines when given by respiratory route, compared to subcutaneous or intradermal administration in immunologically naïve subjects (Aguilo et al., 2016). Since respiratory airways could be a sensitive organ for exacerbated inflammatory response caused by live bacteria in the pre-exposed, we chose to evaluate the efficacy of an inactivated whole cell vaccine as a booster strategy after primary BCG. To this end, we inactivated MTBVAC building upon the promising immunogenic profile shown by the live version of this vaccine both in animal models and in humans (Marinova et al., 2017). MTBVAC was inactivated by heating the vaccine at 100°C for 30 min. Bacterial inactivation was confirmed by plating on 7H10 solid agar medium (data not shown). Bacteria visualization using electron microscopy confirmed that MTBVAC maintained their bacillary shape upon heat treatment (**Supplementary Figure S1**). Then, we characterized MTBVAC HK-conferred protection in mice under different experimental conditions. First, 10^7 MTBVAC HK bacteria were inoculated intranasally in naïve or in BCG-primed mice. One month later, mice were challenged intranasally with a low dose (150 CFU) of the H37Rv Mtb strain. After one month, mice were sacrificed and lung bacterial load evaluated by plating in solid medium. Our data showed that MTBVAC HK alone did not confer protection compared to unvaccinated control. However, when combined with subcutaneous BCG priming, protection was about one-log higher than that provided by BCG only (**Figure 1A**), indicating the need of a BCG prime to trigger a MTBVAC HK-induced protective response.

We also evaluated protection induced by MTBVAC killed with formalin, since this method of inactivation had been shown in a previous study with other inactivated vaccines to better preserve immunogenicity compared to heating (Cryz et al., 1982). However, in this case, we did not find any difference in efficacy between both MTBVAC inactivation methods (**Supplementary Figure S2**). Since heat-inactivation is easier to implement, we continued vaccine characterization using this method of inactivation. MTBVAC HK induced better protection only when given by intranasal route, but did not improve BCG when administered subcutaneously (**Figure 1B**). Ultimately, our data show that the MTBVAC HK booster effect was dose-dependent, as we only observed improved protection with a high dose of MTBVAC HK (10^7), whereas no effect was obtained using 10^4 bacteria (**Figure 1C**). We and others have previously reported the lack of protection induced by BCG subcutaneous in the mouse strain DBA/2 (Aguilo et al., 2016). Interestingly, MTBVAC HK also induced protection in BCG-vaccinated DBA/2 mice, suggesting that this vaccination approach could confer protective efficacy in cases in which BCG is ineffective (**Supplementary Figure S3**). Comparison of different independent lots of MTBVAC HK provided a similar protective profile, superior to BCG only, evidencing the reproducibility of our results (**Supplementary Figure S4**).

Considering that BCG is primarily administered in the clinic in newborn populations, we used a neonatal mouse model in which BCG was inoculated at birth, and MTBVAC HK given 8 weeks later, when the immune system has reached a mature status. Protection by Mtb reduction in lungs was

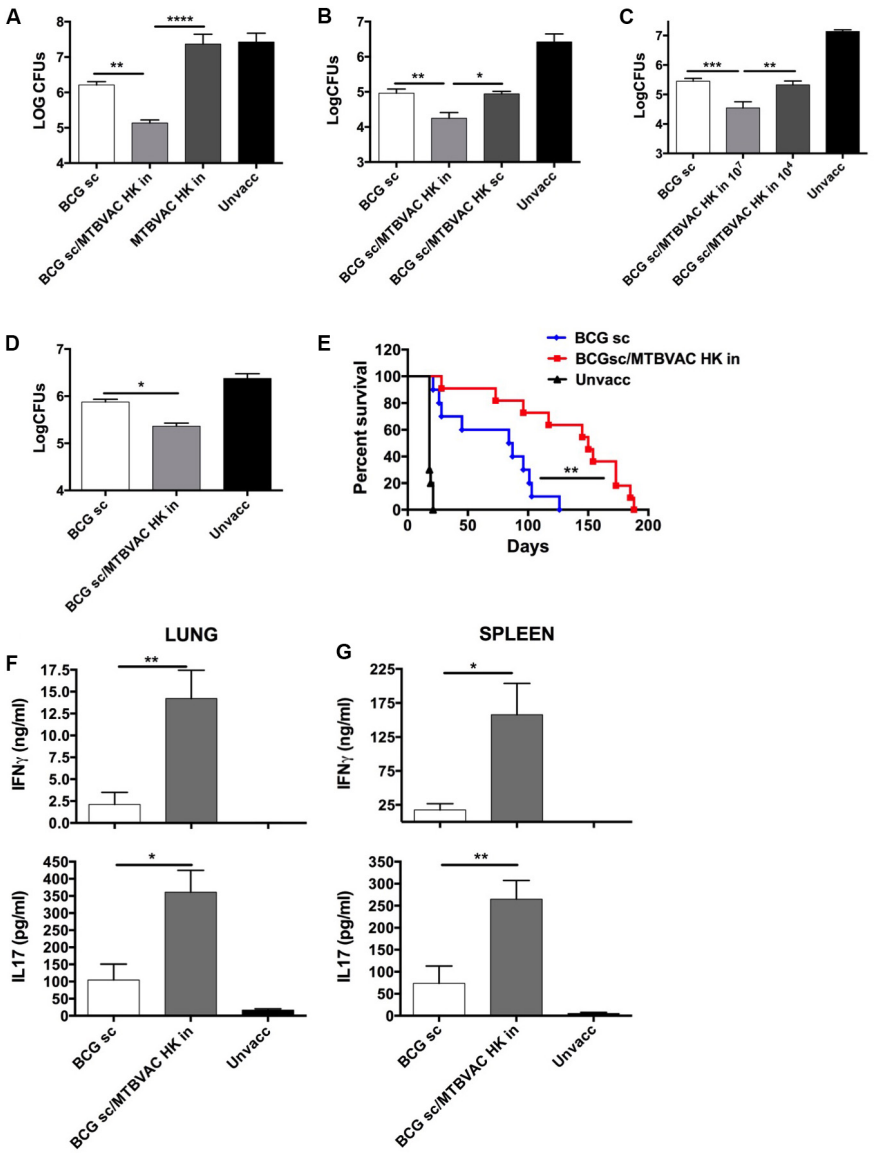

FIGURE 1 | Improved protection induced by intranasal MTBVAC HK as boost of subcutaneous BCG. **(A–C)** Groups of C57BL/6 adult mice where vaccinated with BCG and MTBVAC HK 4 weeks apart (107 MTBVAC HK dose when not specified). After one month, mice were intranasally challenged with H37Rv and lung bacterial load analyzed one month later. **(D,E)** Newborn mice were vaccinated with BCG and 8 weeks later boosted intranasally with 107 MTBVAC HK. Mice were challenged with a low-dose **(D)** or a high-dose **(E)** H37Rv inoculation and lung CFUs or survival analyzed, respectively. **(F,G)** Antigen-specific IFNg and IL17A production one month after MTBVAC HK vaccination, following PPD stimulation of cells from lungs **(F)** and spleen **(G)**. **(A–D, F,G)** Data are shown as mean ± SEM and are representative of at least two independent experiments. (n = 6 mice/group). *$p < 0.05$; **$p < 0.001$; ***$p < 0.001$; ****$p < 0.0001$ by one-way ANOVA and Bonferroni post-test. **(E)** Data from one experiment (n = 10 mice/group) are represented in a Kaplan-Meier survival curve and statistical significance calculated by a LogRank test. **$p < 0.01$.

significantly improved in the MTBVAC HK booster group (**Figure 1D**), and comparable to the protection level observed in adult mice immunized with BCG. We also evaluated vaccine efficacy by survival as a readout in a high-dose, mouse challenge model and found that intranasal MTBVAC HK boosting substantially extended mouse survival in comparison to BCG sc immunization (**Figure 1E**).

Although we did not investigate other administration routes, our results suggest that the beneficial effect of MTBVAC HK boosting specifically depends on its interaction with the respiratory mucosal immune system. Therefore we analyzed cellular responses in lungs as well as in spleen after *ex vivo* stimulation with *M. tuberculosis* secreted antigens (Purified protein derivative: PPD). Data revealed that MTBVAC HK intranasal boosting enhanced antigen-specific IFNγ and IL17 induction in lungs (**Figure 1F**). In addition, spleen response profiling also revealed a higher IFNγ and IL17 production at a systemic level elicited by MTBVAC HK boosting (**Figure 1G**).

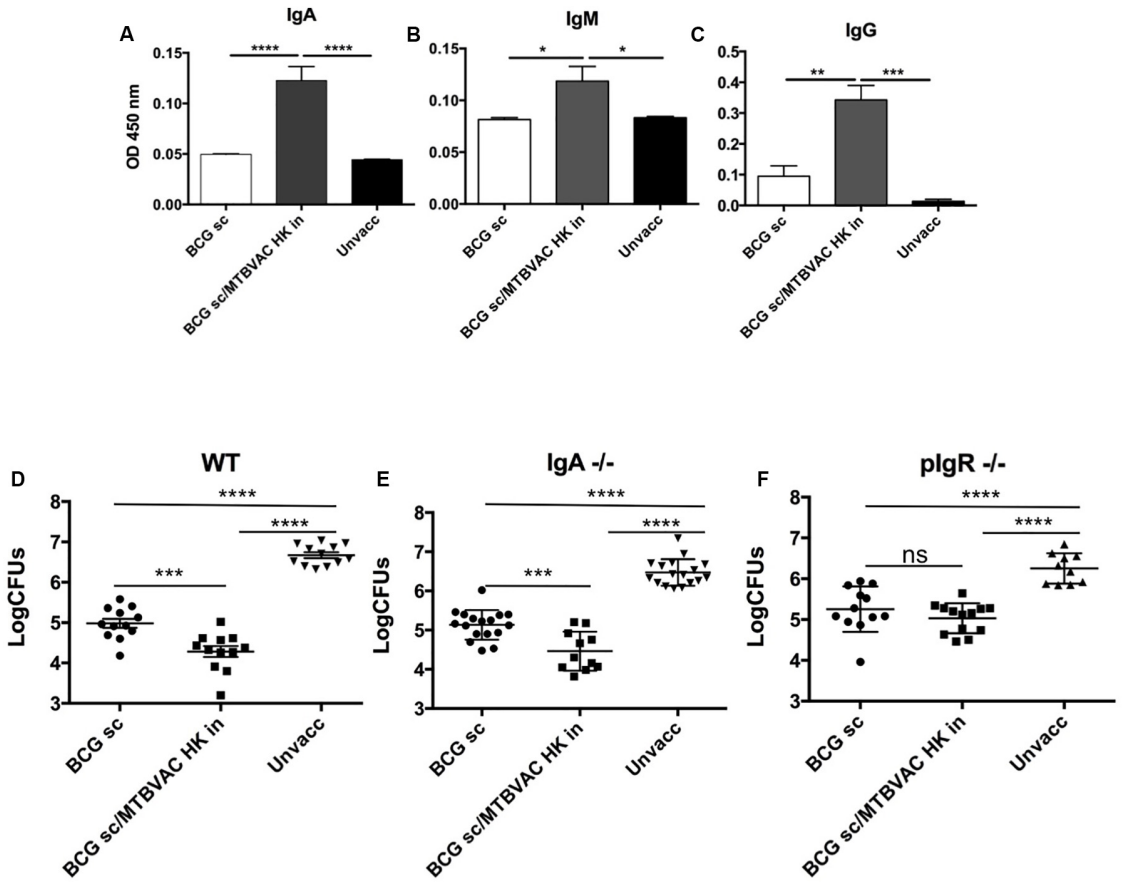

FIGURE 2 | Intranasal MTBVAC HK induces mucosal immunoglobulins in respiratory airways. **(A–C)** Groups of C57BL/6 adult mice where vaccinated with BCG and MTBVAC HK 4 weeks apart. One month later PPD- specific IgA, IgM, IgG in BAL samples. **(D–F)** One month after MTBVAC HK boosting, wild-type, IgA-/- and pIgR-/- mice were intranasally challenged with H37Rv and lung bacterial load analyzed one month later. All data are mean ± SEM **(A–C)** Data are representative of two independent experiments (n = 6 mice/group). **(D–F)** Data in the graphs represent a pool of two independent experiments (n = 12 mice/group). *$p < 0.05$; **$p < 0.01$; ***$p < 0.001$; ****$p < 0.0001$ by one-way ANOVA and Bonferroni post-test.

Intranasal MTBVAC HK Induces Protective Secretory Immunoglobulins

We have previously reported that respiratory, but not subcutaneous live BCG, triggered IgA production in respiratory airways (Aguilo et al., 2016). Thus, we next assessed whether intranasal MTBVAC HK induced PPD-specific immunoglobulins, including IgA, IgM and IgG subtypes, in bronchoalveolar lavage (BAL) (**Figures 2A–C**). MTBVAC HK booster vaccination triggered an increase of the three types of antibodies compared to unvaccinated and BCG only control groups.

To assess contribution of mucosal secretory immunoglobulins (sIg) to MTBVAC HK-mediated protection, we tested vaccine-conferred protective efficacy in mice deficient by genetic knockout for IgA (igha-/-) or for the polymeric immunoglobulin receptor (pIgR-/-). This latter molecule is a protein transporter highly expressed in mucosal tissues, which binds to J chain to actively translocate multimeric IgA or IgM across mucosal epithelium, and therefore lack of pIgR leads to retention of multimeric sIg in the mucosal lamina propria, preventing their active transport over the mucosal barrier (Kaetzel et al., 1991). Our results revealed a similar protection provided by intranasal MTBVAC HK in igha-/- mice when compared to wild type (**Figures 2D,E**) suggesting no specific protective role of IgA. Conversely, MTBVAC HK-specific protection was completely abrogated in the absence of pIgR (**Figure 2F**). Altogether, this result would indicate a crucial contribution of sIg to protective efficacy mediated by MTBVAC HK, suggesting a substantial contribution of sIgM rather than sIgA. Remarkably, pIgR-/- mice did not show less protection by BCG s.c, suggesting that sIg has no role in systemic vaccine-induced protection.

Mucosal MTBVAC-HK Booster Vaccination in NHP

MTBVAC-HK was further evaluated as a booster vaccine in a non-human primate (NHP) vaccination and infection study to address tolerability, immunogenicity and protective efficacy in the primate host. Adult rhesus macaques (*Macaca mulatta*) were vaccinated either with BCG only, or with BCG followed by a MTBVAC-HK booster by pulmonary mucosal instillation

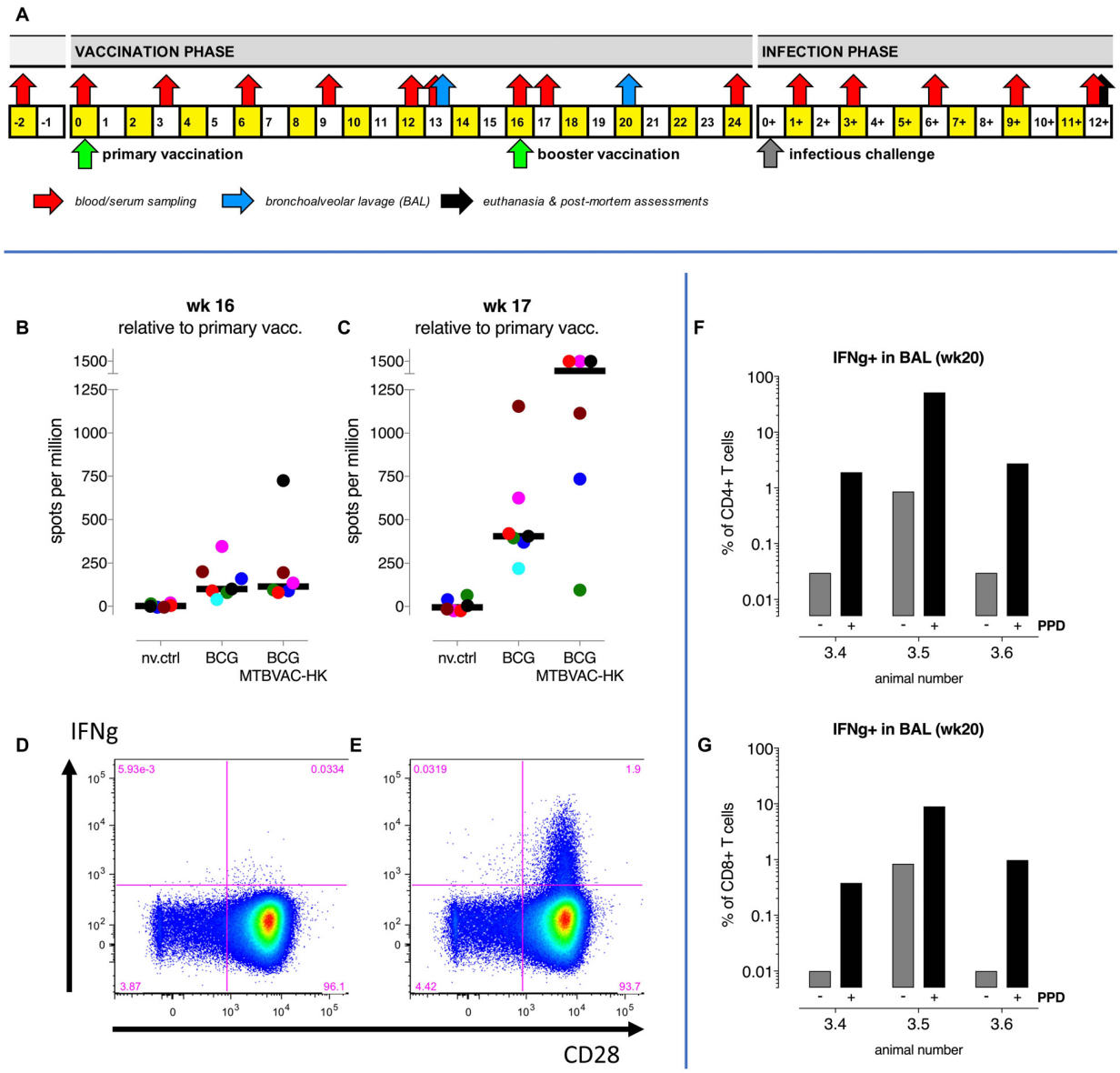

FIGURE 3 | Intrabronchial MTBVAC HK boosting induces local and systemic tuberculosis-specific cellular responses in NHP. **(A)** A study design schematic shows the time lines on a weekly basis relative to primary BCG vaccination and infectious challenge with *M. tuberculosis*, including booster immunization and biosampling events. **(B,C)** PPD-specific IFNg responses in peripheral blood were measured by ELISPOT immediately prior to and 1 week after MTBVAC HK boosting, at week 16 and 17, respectively. Individual data points are consistently colored according to the **Supplementary Table 1**; fat horizontal lines indicate group medians. Also, flow cytometry after intracellular cytokine staining was used to analyze IFNg responses. Dot plots of CD28 versus IFNg specific fluorescence signals of CD4 + T lymphocytes from a representative BAL sample illustrate local IFNg production **(D)** in the absence and **(E)** in the presence of PPD recall stimulation *in vitro*. Percentages per individual of PPD-induced IFNg-positive **(F)** CD4+ and **(G)** CD8+T lymphocytes from BAL are depicted.

16 weeks later (**Figure 3A**). One group was left untreated as non-vaccinated controls. Twenty-five weeks after primary vaccination all animals were challenged by endobronchial instillation of 50 colony forming units (CFU) of *Mtb* strain Erdman, with a follow-up of 12 weeks until study endpoint and post-mortem evaluation of infection and disease (**Figure 3A**). (See **Supplementary Table 1** for an overview of animals per treatment group).

Within the limits of observation, animals tolerated mucosal MTBVAC-HK boosting well; we did not observe any adverse events. Measuring vaccine-induced responses by specific interferon-gamma (IFNg) ELISPOT, using PBMC and antigenic recall stimulation with PPD, MTBVAC-HK boosting induced a transient elevation of the frequency of IFNg producing cells in the periphery at week 17 (one week post MTBVAC HK immunization) relative to the response induced by BCG (p = 0.0997 by non-parametric Mann-Whitney testing; **Figures 3B,C**). This increase was found to be transient since MTBVAC HK-specific T cell response dropped sharply at week

20 (**Supplementary Figure S5A**). Locally, and examining three pre-assigned animals out of six of the MTBVAC-HK boosted animals only (comparing week 13 versus week 20 post-BCG), we registered a clear influx of cells into the lung lumen upon mucosal MTBVAC-HK boosting and the induction of IFNg-positive CD4+ and CD8+ T lymphocytes (**Figures 3D–G**).

Upon infectious challenge with *Mtb*, highest pathology scores and lung bacterial counts were obtained in 3 non-vaccinated control (nv.ctrl) animals (**Figures 4A–D**, and **Supplementary Figures S5B,C**). However, there was an unexpected large spread in pathological involvement, with three out of six unvaccinated controls showing relatively mild disease levels (for which we have no explanation at this point), which altered all the statistical comparisons. Both BCG vaccinees and the MTBVAC-HK boosted animals revealed lower pathology scores by group median values (except for extrathoracic dissemination), but without statistical significance (**Figures 4A–C**). Likewise, there was no statistically significant vaccine effect by enumeration of *Mtb* at necropsy from lung (**Figure 4D**) or hilar lymph node and spleen (**Supplementary Figures 4B,C**, respectively). Despite the lack of statistically significant improvement, by various parameters there appears some positive trend by group median scores of improved TB disease outcome after MTBVAC-HK boosting relative to BCG alone: for total pathology score (**Figure 4A**), body weight development, and infection-associated anemia by hematological mean corpuscular hemoglobin (MCH) and mean corpuscular volume (MCV) development (**Supplementary Figures S5D,F,G**, respectively).

Most notably, MTBVAC-HK boosting significantly suppressed the PPD-specific IFNg response up until 6 weeks after infection (**Figures 4E–H**). Also, the *Mtb*-specific response against an ESAT6-CFP10 fusion protein (covering antigens which are absent from *M. bovis*-derived BCG vaccine) is significantly suppressed up until 6 weeks post-infection by MTBVAC-HK boosting (**Figures 4I–K**). While we have recently established the correlation between lower anti-*Mtb* IFNg responses following challenge and protective immunity against infection and disease in a repeated limiting dose (RLD) infection model in rhesus macaques (Dijkman et al., 2019), we consider that these unprecedented, suppressed PPD and ESAT6-CFP10 specific responses might reflect the protective effect of MTBVAC-HK boosting in this NHP model under relatively high-dose challenge condition. Most likely because of the relatively high challenge dose of 50 CFU of *Mtb*, we anticipate that, from 6 weeks post-infection onward, disease in these highly susceptible rhesus macaques can no longer be controlled. As a consequence, pathology scores and mycobacterial counts at endpoint may have converged to a similar outcome leaving a trend of improvement by MTBVAC-HK boosting only.

MTBVAC HK Vaccination Induces Mucosal Immunoglobulins in Vaccinated NHP

MTBVAC HK mucosal vaccination induced a strong cellular response both systemically and locally. However, considering the results obtained in mice we focused further analyses on systemic and local antibodies. To this end, we used sera and BAL samples from vaccinated monkeys obtained along the study time line to characterize humoral immune responses. PPD-specific IgG, IgM and IgA kinetics were monitored in serum samples from MTBVAC HK group during vaccination phase (from week 0 to week 20). Specific IgG showed a significant increase at week 20, which was particularly pronounced in 4 of the 6 animals, indicating a correlation between PPD-specific IgG and MTBVAC HK vaccination (**Figure 5A**). In the case of IgM, no significative changes were observed at the timepoints analyzed, although a slight transitory increase was observed in two animals at week 17, one week after MTBVAC HK inoculation (**Figure 5B**). Finally, the PPD-specific IgA profile showed a decrease that correlated with the administration of MTBVAC HK (**Figure 5C**).

We obtained BAL samples of three monkeys from the MTBVAC HK group at two different timepoints: at week 13 (before MTBVAC HK booster immunization), and at week 20 (4 weeks after MTBVAC HK administration). Our results clearly indicate that mucosal vaccination with MTBVAC HK induced a substantial increment of PPD-specific IgA, IgG, and IgM in the three animals studied, similar to the observations in mice. In addition, we also observed an increase in J chain presence, suggesting the presence of multimeric secretory IgA and IgM (**Figures 5D–G**).

Our data demonstrate the induction of PPD-specific immunoglobulins by MTBVAC HK. However, PPD comprises the secreted fraction of *M. tuberculosis* proteome. Thus, we next aimed to elucidate whether MTBVAC HK-induced mucosal Ig could bind to *M. tuberculosis* bacilli. To this end, we incubated H37Rv bacteria with BAL fluid samples, followed by biotin-conjugated secondary antibodies specific for human IgM, IgG and IgA. A final incubation step with PE-bound streptavidin allowed visualization of Ig binding by flow cytometry. Our data show a positive shift of the fluorescence signal for either of the three immunoglobulin families, IgA, IgM, and IgG, when bacteria had been incubated with BAL fluid from MTBVAC HK-vaccinated animals, indicating the presence of IgA, IgM, and IgG, able to bind to Mtb directly. This binding was substantially higher in the case of IgM, which would correlate with the pentameric conformation of this immunoglobulin. While for the BCG only-vaccinated animals, the binding was similar to that measured in BAL samples from unvaccinated animals, the highest signals were obtained after MTBVAC HK boosting specifically (**Figure 5H**).

H37Rv Opsonization Following Incubation With MTBVAC HK-Derived BAL

Phagocytosis mediated by antibody-dependant opsonization represents a major bactericidal mechanism triggered by immunoglobulins. To evaluate opsonization in our study, we added H37Rv to human monocyte cells THP1, after it had been incubated with the different BAL samples. We used GFP-expressing bacteria in order to monitor internalization by flow cytometry. Our data demonstrate about a two-fold increase of infected cells when H37Rv had been previously incubated with

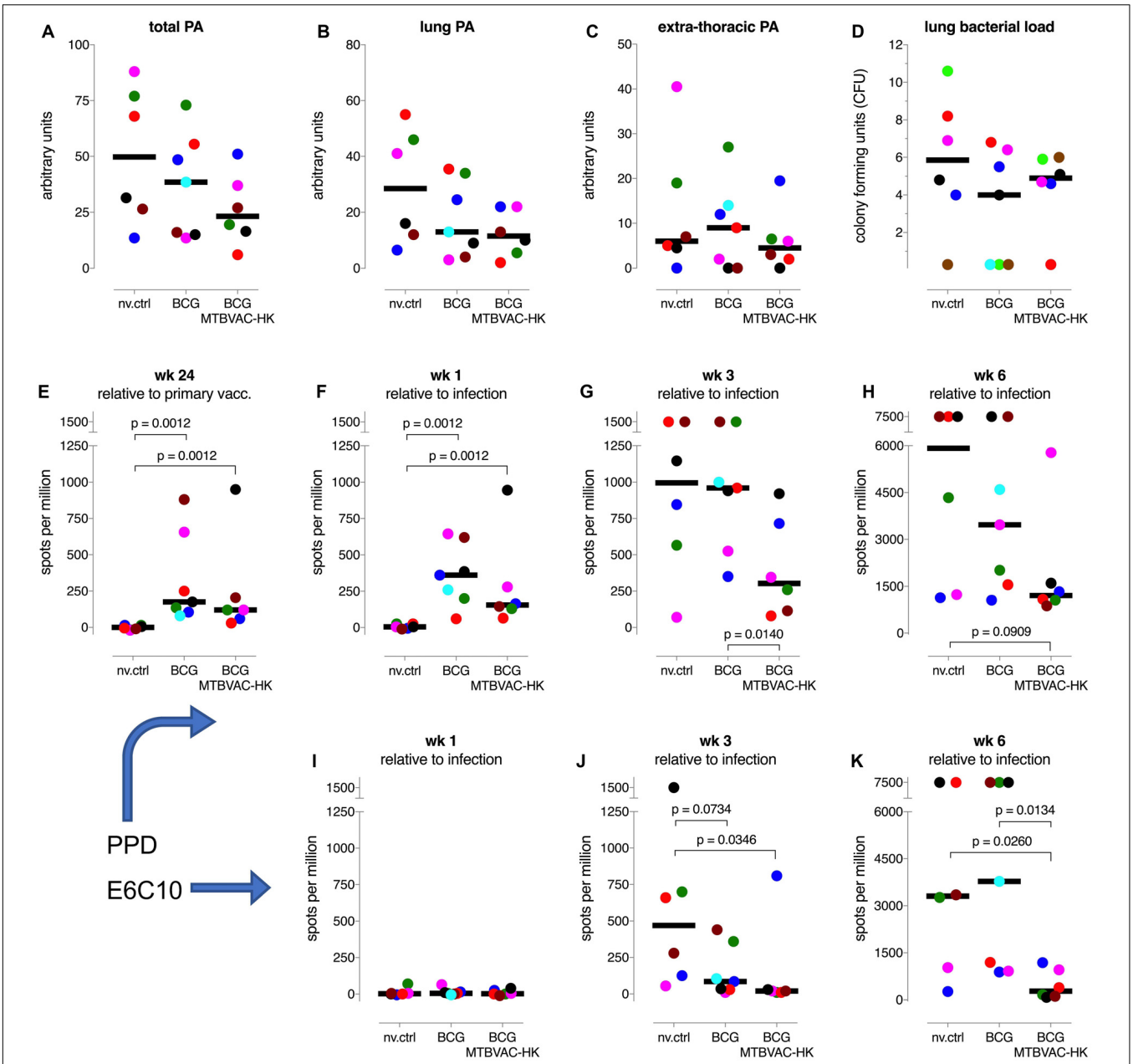

FIGURE 4 | TB disease measures and IFNg responses after infectious challenge. **(A–C)** Total arbitrary score of pathological involvement at endpoint and for lung and extra-thoracic disseminated disease, respectively. **(D)** Post-mortem enumeration of bacterial burden in the lung. **(E–H)** PPD-specific and **(I–K)** ESAT6-CFP10 fusion protein (E6C10) specific IFNg responses by specific ELISPOT analysis of PBMC, at indicated timepoints relative to primary vaccination or infectious challenge. Individual data points are consistently colored according to the **Supplementary Table 1**; fat horizontal lines indicate group medians.

BAL fluid from MTBVAC HK-vaccinated monkeys compared to control groups (**Figure 6A**). Opsonization has been associated with an increase in the capacity of macrophages to restrict bacteria into acidic compartments. To assess this, we analyzed intracellular colocalization of H37Rv with lysotracker, a probe that becomes fluorescent under acidic conditions. In the three monkeys analyzed, our results showed an increased bacterial colocalization following pre incubation of H37Rv with BAL from week 20 compared to those from week 13 (**Figure 6B**).

Our results showed great ability of BAL IgM and IgG to bind Mtb surface. Complement activation in respiratory airways has been previously reported, and therefore, since IgM and IgG is a very efficient complement activators, we evaluated the role of C3b, one of the major opsonins released during complement activation, for MTBVAC HK vaccination-induced opsonization. We incubated H37Rv with the different BAL samples and then we added a C3b-specific antibody to detect binding of this protein to Mtb surface by flow cytometry. In

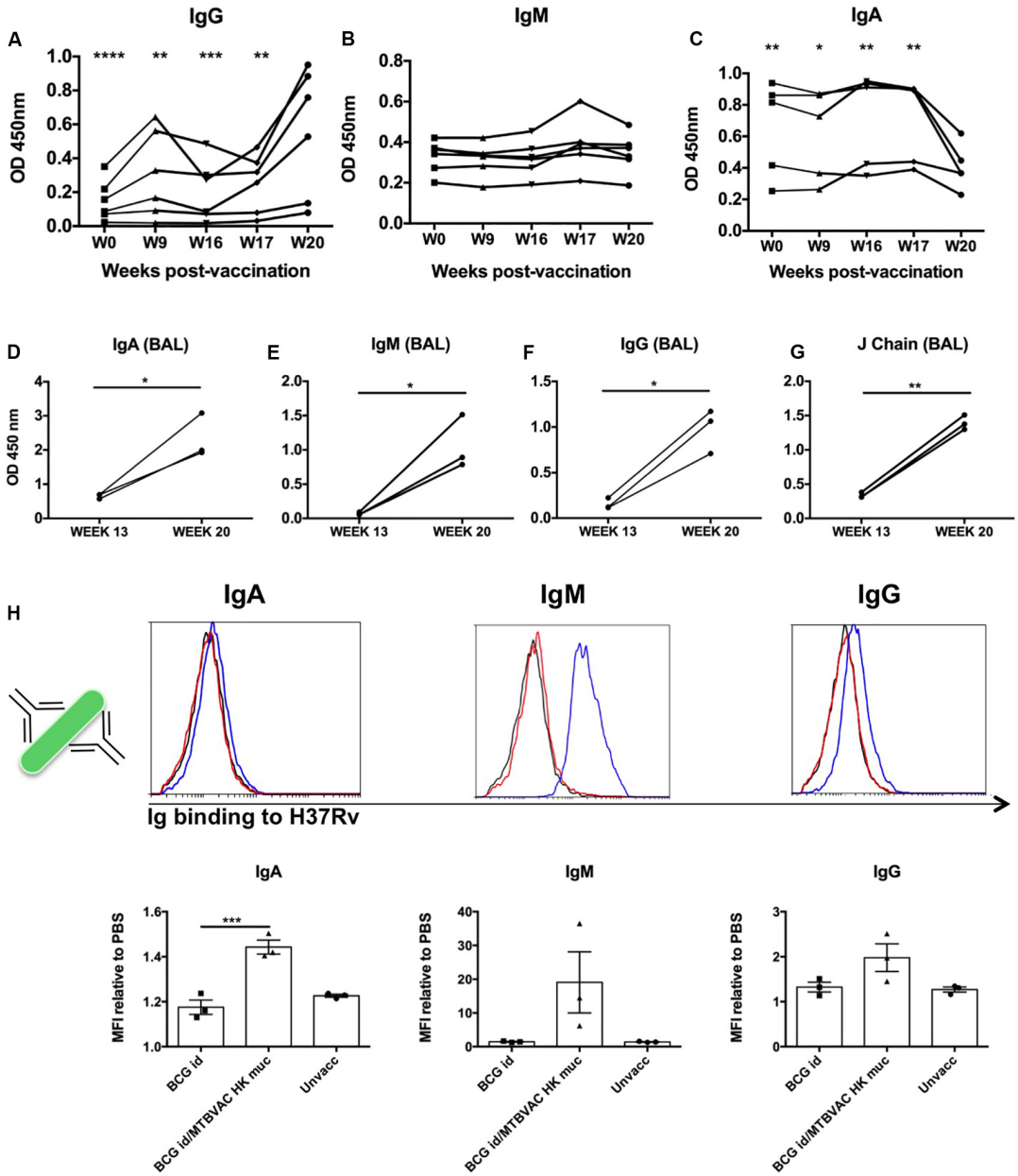

FIGURE 5 | Intrabronchial MTBVAC HK induces mucosal immunoglobulins in respiratory airways from non-human primates. **(A–C)** PPD-specific IgG, IgM, and IgA were measured in sera samples from the different individuals throughout the vaccination phase (until week 20). **(D–G)** PPD- specific IgA, IgM, IgG, as well as J chain were analyzed in BAL samples harvested at week 13 (before MTBVAC HK) and week 20 (after MTBAVC HK) from three individuals from the MTBVAC HK group. Data in the graphs show values for each individual **(H)** Direct binding of IgA, IgM, and IgG to Mtb surface. H37Rv bacteria were incubated with BAL samples and immunoglobulin binding measured by flow cytometry using specific secondary antibodies. Representative overlay histograms are shown. Black line: unvaccinated; Red line: BCG vaccinated; Blue line: BCG/MTBVAC HK vaccinated. Data in the graphs show the mean fluorescence intensity (MFI) obtained with each BAL compared to the measured when bacteria are incubated with PBS. **(A–G)** Data show individual from one experiment. **(F)** Data are shown as mean ± SEM and are representative of two independent experiments. **(A–C, H)** $*p < 0.05$; $**p < 0.01$; $***p < 0.001$; $****p < 0.0001$ by one-way ANOVA and Bonferroni post-test. **(A–C)** Comparisons of the different timepoints with week 20 are shown. **(D–G)** $*p < 0.05$; $**p < 0.01$ by paired *t*-student test.

line with what was observed for the different immunoglobulin subtypes previously, we detected a higher fluorescence peak of C3b binding with the BAL from week 20 compared to week 13 (**Figure 6C**). Interestingly, preincubation of week 20 BAL from two different individuals with anti-C3b partially prevented Mtb phagocytosis, suggesting a functional role of this opsonin in enhanced uptake (**Figure 6D**). These results do not rule out that other opsonins released during complement activation play a role in the enhanced uptake of Mtb after MTBVAC HK booster vaccination.

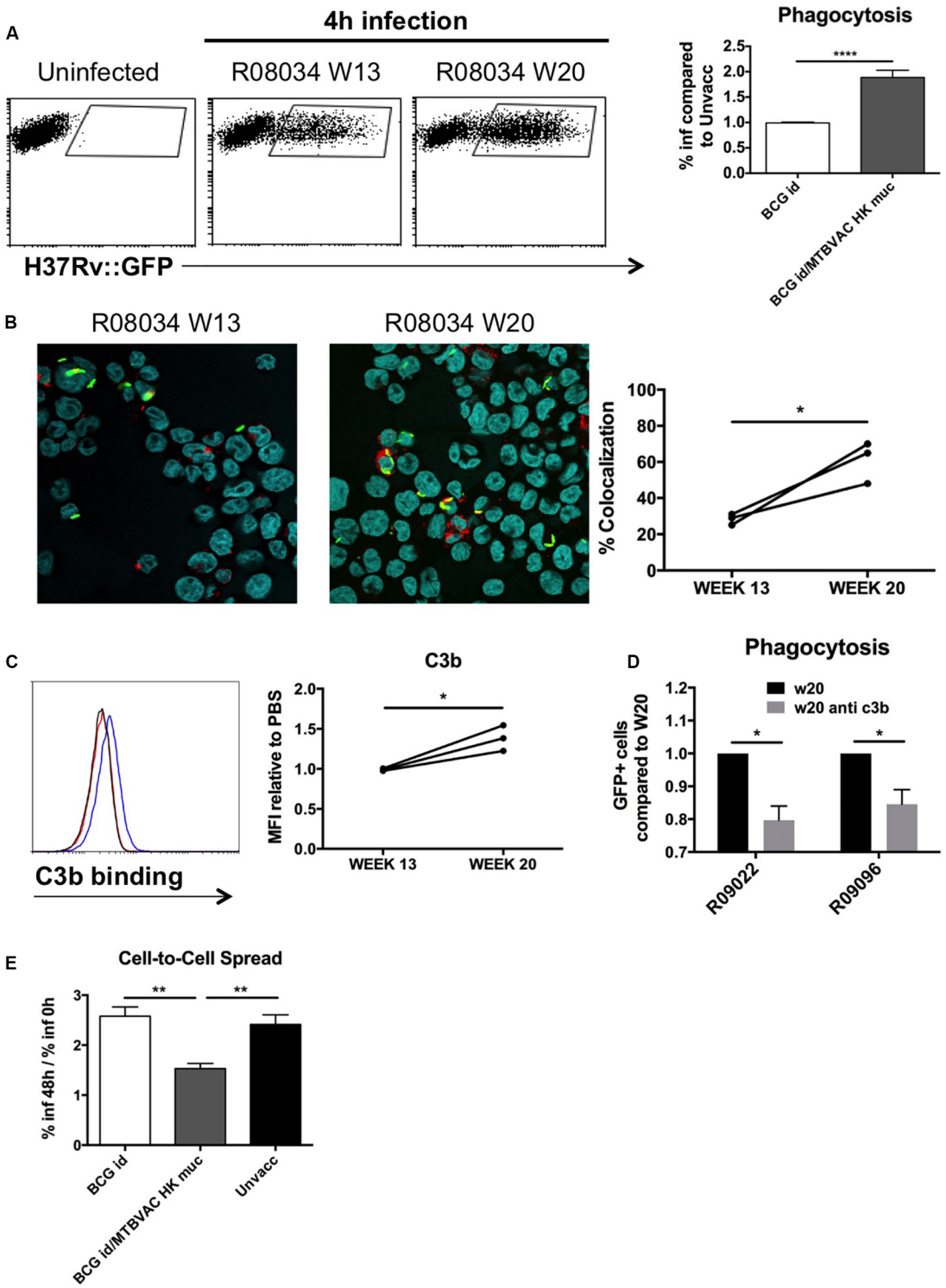

FIGURE 6 | Mucosal immunoglobulins induced by MTBVAC HK opsonize Mtb *in vitro*. GFP-expressing H37Rv coated with BAL samples were added to THP-1 human monocytes. **(A)** Percentage of infected cells was determined by flow cytometry 4 h post-infection. Representative dot-plots from one individual are shown in the left panel. Data in the graph is represented as the fold-change of the percentage obtained with the BAL from BCG-only or BCG/MTBVAC HK compared with the BAL from unvaccinated NHP. **(B)** Representative images of infected cells stained with lysotracker and Hoechst reagents. Data in the graph show colocalization values for each individual from MTBVAC HK group comparing colocalization obtained with BAL from week 13 and 20. **(C)** C3b binding to H37Rv surface was analyzed by flow cytometry using an antibody against C3b. A representative overlay histogram is shown. Black line: unvaccinated; Red line: BCG vaccinated; Blue

(Continued)

FIGURE 6 | Continued
line: BCG/MTBVAC HK vaccinated. Data in the graph show the MFI fold-change obtained following incubation with BAL from week 13 and 20 compared to the measured with the value when bacteria are incubated with PBS. **(D)** THP1 cells were infected with H37Rv previously incubated with BAL from week 20 in the presence or absence of a neutralizing antibody antiC3b. **(E)** Fold-change comparison of infected- THP1 cells at 48 h versus 0 h for each experimental condition. **(A,E)** Data in the graphs are mean ± SEM from a pool of three independent experiments. $^{**}p < 0.01$; $^{****}p < 0.0001$ by one-way ANOVA and Bonferroni post-test. **(B)** Data show mean values of at least six images for each experimental condition from one experiment. **(C)** Data show individual from one experiment. **(B,C)** $^{*}p < 0.05$ by paired *t*-student test. **(D)** Data in the graphs are mean ± SEM from a pool of two independent experiments. $^{*}p < 0.05$ by two-way ANOVA and Sidak's multiple comparison test.

Finally, we analyzed the capacity of internalized bacteria to spread from cell to cell. Our data indicate that percentage of infected cells at 48 h of infection was about 2.5-fold higher when compared to initial infection rate in cases where H37Rv had been incubated with control BAL fluid (unvaccinated or BCG only), whereas this ratio dropped to 1.5 with the BAL from MTBVAC HK boosted animals (**Figure 6E**). This result suggests that the ability of Mtb to spread to bystander cells was impaired when bacteria were opsonized.

DISCUSSION

During the last years there is rising interest to elucidate the role of immunoglobulins in tuberculosis infection. Different studies using animal models have shown that pulmonary delivery of monoclonal antibodies targeting certain Mtb surface proteins leads to a reduction of bacterial load following challenge (Achkar and Casadevall, 2013). In addition, results from clinical vaccine trials suggest a correlation between Mtb-specific IgG in sera and lower risk of TB disease (Fletcher et al., 2016). An elegant study recently demonstrated differences in glycosylation of immunoglobulin Fc fractions between latent and active TB individuals, and the importance of these signatures for antibody interaction with different cellular subsets, suggesting a role of antibodies in natural prevention of TB reactivation (Lu et al., 2016). Altogether, these studies provide substantial support for the potential contribution of antibodies to natural or vaccine-induced protection against tuberculosis.

Nevertheless, there is a poor understanding about the processes that drive to generation of protective antibodies during tuberculosis infection, and vaccine strategies that specifically exploit humoral responses are underrepresented in the tuberculosis vaccine pipeline. In the present work, we identify a novel vaccine approach that induces mucosal protective antibodies in the lungs. We describe in mice how a single intranasal immunization with a inactivated whole-cell *M. tuberculosis* vaccine triggers lung protective immunity when given as boost over previously BCG immunized animals. Data from NHP studies also showed a tendency in the MTBVAC HK-immunized group to improve protection in certain disease-associated parameters, even though differences were not statistically significant. Remarkably, results in NHP showing MTBVAC HK-induced inhibition of PPD- and ESAT6/CFP10-specific responses following Mtb challenge suggest a protective role of MTBVAC HK in this animal model. However, high dose challenge experimental conditions used in this study may be obscuring the full protective potential of MTBVAC HK boosting.

We show that mucosal administration of MTBVAC HK induces strong cellular and humoral responses at both systemic and local lung level, which correlates with an improved protection compared to animals immunized only with BCG by parenteral route. Our data evidence the importance of the mucosal route of administration to trigger mucosal immunoglobulins in the lungs. In this regard, we demonstrate that intradermal BCG, the current vaccine regimen used in the clinic, does not generate antibodies in the lung lumen, which is in agreement with our previous observations (Aguilo et al., 2016).

Remarkably, MTBVAC HK fails to protect in the absence of pIgR, a transporter protein that mediates release of secretory Ig (sIg) to respiratory airways, suggesting a crucial role of mucosal antibodies in the protective mechanism triggered by this vaccination strategy. sIg comprise polymeric IgA (dimer) or IgM (pentamer) molecules, covalently linked to J chain, and the secretory component (SC), which corresponds to a pIgR extracellular domain that is cleaved following translocation. This complex conformation provides more stability to the immunoglobulin, making it less susceptible to proteolytic digestion and more mucophilic (Rojas and Apodaca, 2002). Our results in mice suggest no contribution of IgGs to MTBVAC HK-mediated protection, despite their presence in BAL following immunization. Monomeric immunoglobulins have lower capacity to neutralize pathogens in mucosal tissues compared to polymeric conformations (Renegar et al., 1998). In this regard, our results suggest a strong capacity of sIgA and sIgM to impair *M. tuberculosis* infection.

Even though our data do not demonstrate greater susceptibility of IgA-/- and pIgR-/- mice to Mtb infection *per se* and therefore, no apparent role of sIg in natural TB protection, the scenario changes when Mtb-specific sIg are present in the respiratory airways prior to pathogen encounter. Our *in vitro* functional assays using BAL fluid samples from MTBVAC HK-vaccinated NHP indicate the capacity of vaccine-induced sIg to bind directly to Mtb surface and to modulate pathogen interaction with macrophages. Mtb incubation with BAL from MTBVAC HK-immunized monkeys led to an increase of the phagocytosis rate, a higher colocalization of intracellular Mtb with acidic compartment tracer, and an impaired capacity of bacteria to spread from cell to cell. Thus, our data suggest antibody-mediated opsonization as a plausible protective mechanism of MTBVAC HK vaccination.

Our results indicate similar MTBVAC HK-induced protection in IgA-/- mice (where IgM is the only secretory immunoglobulin available) compared to wild-type animals,

suggesting a primordial role of sIgM in vaccine-induced protective efficacy. However, our results are not sufficient to determine that IgA have not contribution to vaccine-induced protective response. A good approach to elucidate this point could be the use of a mouse strain unable to produce secretory IgM. This experiment should be performed in the future to clarify this question. Unlike IgG and IgA, it is not well defined up-to-date which receptor for IgM could drive IgM-specific opsonization. However, IgM, including secretory IgM (Michaelsen et al., 2017), is a strong complement activator, and IgM-dependent opsonization by complement-derived opsonins is well reported (Guidry et al., 1993). In addition, our results also revealed an important binding of IgG to *Mtb* surface. Since IgG is a strong complement activator, these antibodies might also play a role in the bacterial opsonization events described in this study. One of the major opsonins activated during this process is C3b, released as a consequence of the C3 proteolization by the enzyme C3-convertase. C3b presents strong avidity of binding to bacterial surfaces directly, and it mediates opsonization following recognition by CD35, a surface receptor on macrophages, including the THP1 cells used in the present study (Baqui et al., 1999). Our results suggest that, at least partially, C3b generated following MTBVAC HK vaccination has a role in Mtb opsonization. Although complement proteins are mostly generated in the liver, lungs can be a local source of complement proteins. In particular, alveolar epithelial cells, as well as alveolar macrophages can secrete complement proteins (Strunk et al., 1988; Huber-Lang et al., 2002).

Despite the lower immunogenicity and poorer protective efficacy conferred by inactivated whole-cell tuberculosis vaccines in comparison to their live counterparts, there is an interest in the development of this type of vaccination strategies. As inactivation is associated with an improved safety profile, such vaccines are considered in particular for target populations to which live vaccines might be harmful, such as immunosuppressed individuals. Limited immunogenicity of inactivated vaccines is usually overcome by other strategies, such as the formulation of inactivated vaccines with adjuvants (Haile et al., 2004) or repeated administration by multiple immunizations (Opie and Freund, 1937; Von Reyn et al., 2017). In the case of intranasal MTBVAC HK, our data indicate that it is not protective by itself, but it needs of a previous BCG prime to trigger a response in the lungs and confer protection. Even though we have not fully studied the mechanisms behind this result, it could be interesting to address the cross-talk between mucosal and systemic immune compartments in the future. For now, we speculate that the mucosal delivery of MTBVAC HK might be pulling the systemic cellular response elicited by subcutaneous BCG toward the lungs. Secondary targeting of the lung compartment with inactivated bacilli, would be a relatively safe way of boosting the cellular response and inducing specific antibodies locally against whole-cell bacteria.

Our results do not clarify whether the present vaccination approach is effective only when we use an *M. tuberculosis*-based vaccine as MTBVAC, or whether it can be translated to other whole-cell vaccines like inactivated BCG. In this regard, a previous study reported no additional protection in the lungs conferred by intranasal heat-killed BCG given as booster of subcutaneous live BCG immunization (Haile et al., 2005). This failure of boosting with inactivated BCG could highlight the importance of the differential antigens expressed by MTBVAC relative to BCG (Marinova et al., 2017), which are shared with the *M. tuberculosis* pathogen. Indeed, contribution of differential antigens to MTBVAC-conferred protection has been previously reported in the case of live MTBVAC (Aguilo et al., 2017). Nevertheless, comparison between inactivated MTBVAC and BCG should be done head-to-head in order to confirm this difference under the same experimental conditions.

The results from the present study indicate that a plausible mechanism of protection of mucosal MTBVAC HK is mediated by the generation of specific antibodies in the respiratory airways, with capacity to opsonize live Mtb bacteria. We do not discard that another inflammatory events mediated by the vaccine as production of certain cytokines could also contribute to protection. To our knowledge, this is the first tuberculosis vaccine approach based on whole-cell bacteria that targets to elicit protective mucosal antibodies.

MATERIALS AND METHODS

Bacteria

BCG Danish (Statens Serum Institute) and H37Rv (Institut Pasteur Paris) strains were grown at 37°C in Middlebrook 7H9 broth (Difco) supplemented with ADC 10% (Difco) and 0.05% (v/v) Tween-80 (Sigma), or on solid Middlebrook 7H11 (Difco) supplemented with ADC 10%. Bacterial suspensions for vaccination or infection were prepared in PBS from glycerol stocks previously quantified by plating serial dilutions. MTBVAC HK vaccines were prepared by heating a log-phase MTBVAC culture at 100°C during 30 min. In the case of formalin inactivation, MTBVAC culture was incubated with 0.5% (vol/vol) formalin during 48 h. Culture viability was checked for each vaccine lot. Bacterial density was determined by plating prior to heat treatment, and was used to calculate MTBVAC HK dose for *in vivo* studies.

Cell Lines

THP-1 cells were purchased to European Collection of Cell Cultures (ECACC) (Lot Number 10/016). All the experiments were done using cells with less than five passages from its thawing. Mycoplasma absence in the cultured cells was confirmed after finalizing the experiments using the MycoAlert PLUS Mycoplasma Detection Kit (Lonza).

Animal Studies Approval

Mouse studies were conducted in agreement with European and national directives for protection of experimental animals and with approval from the Ethics Committee from University of Zaragoza (approved protocols PI14/14, PI50/14, and PI33/15).

Ethical approval for NHP study was obtained from the Dutch authorities prior to start, under dossier registration number DEC726subB.

Mouse Study

All mice were kept under controlled conditions and observed for any sign of disease.

Protective Efficacy

Female, 8–10 weeks-old C57BL/6 (Janvier Biolabs), pIgR-/- (a kind gift from Gerard Eberl, Institut Pasteur Paris), IgA-/- (MMRRC repository), or DBA/2J (Janvier Biolabs) mice were vaccinated subcutaneously with 5×10^5 CFU BCG vaccine in 100 μl PBS. Four weeks post-vaccination, mice were intranasally vaccinated with 10^7 MTBVAC HK bacteria in 40 μl of PBS. Four weeks later, mice were challenged intranasally with 150 CFUs H37Rv. Bacterial burden was assessed four weeks post-challenge by plating homogenized lungs and spleen on solid medium. A group of infected mice was sacrificed 1 day after challenge in order to determine the initial bacterial load in lungs, which resulted in approximately 20 CFU in all experiments. In the experiments involving newborn animals, mice were vaccinated subcutaneously with 2.5×10^5 BCG CFU in 50 μl PBS in the first three days after birth. Unvaccinated controls were inoculated with 50 μl of PBS. 10^7 MTBVAC HK was administered intranasally eight weeks later (or 10^4 when indicated). Four weeks later, mice were challenged with 150 CFUs of H37Rv for bacterial burden determination, or 10^4 CFUs for survival evaluation. In this latter case, disease-associated symptoms (including weight, aspect and individual/social behavior) were monitored weekly, and mice were humanely euthanized according to pre-established endpoint criteria.

Immunogenicity

Four weeks after MTBVAC HK vaccination, mice were euthanized and splenocytes and lung cells collected. 10^6 cells per experimental timepoint were stimulated with Purified Protein Derivative (PPD) (Statens Serum Institute, SSI) 5 μg/ml during 48 h for supernatants collection and cytokine detection by ELISA. IL17A or IFNγ concentrations were determined with specific ELISA commercial kits (MabTECH). For bronchoalveolar lavage (BAL) collection, trachea was cannulated and BAL was performed with 0.8 ml of ice-cold PBS. Supernatant was separated from cells by centrifugation and frozen at −80°C for further protein detection analysis. For antibodies or J chain determination in BAL, maxisorp ELISA plates (NUNC) were coated with 10 μg/ml of PPD and incubated overnight at 4°C. After a washing step with PBS-Tween20 0.05% (v/v) buffer, plate was blocked with Bovine Serum Albumin 1% (w/v) in washing buffer for 1 h at 37°C. Then, plates were incubated with 100 μl of BAL during 90 min at 37°C. Following washing, plates were incubated for 1 h at 37°C with the corresponding anti IgA, IgG, or IgM antibodies conjugated with Horseradish Peroxidase (HRP) (Sigma Aldrich) at a 1:10000 dilution. Finally, enzyme-substrate reaction was developed using 3,3′,5,5′-Tetramethylbenzidine (TMB) (Sigma Aldrich) as substrate, and reaction was stopped with H_2SO_4 0.1N.

NHP Study

Bacteria, Vaccination and Infectious Challenge

For primary vaccination of NHPs, clinical grade BCG Danish 1331 (SSI, Copenhagen, Denmark) was reconstituted according to manufacturer's protocol and applied at a single, standard human dose (of 5×10^5 CFU on average) by intradermal injection.

Inactivated MTBVAC-HK booster vaccination in NHP was established by endobronchial instillation of 1.95×10^8 CFU-equivalent/10 mL/dose, targeting the lower left lung lobe. To this end, one mL of MTBVAC-HK suspension (provided by Biofabri) was added to 9 mL of sterile, isotonic saline solution (Eurovet Animal Health B.V., Bladel, Netherlands) immediately prior to administration.

M. tuberculosis (Mtb) strain Erdman K01 was prepared at 50 colony forming units (CFU) per 3 mL sterile, isotonic saline per dose, for infectious challenge of NHPs by endobronchial instillation targeting the lower left lung lobe. NHPs were challenged in random order in a single session within 3 h from the preparation of the inoculum, using a pool of 3 vials of Mtb Erdman from −80°C frozen stock.

Study Design, Handling and Sampling

Purpose-bred, adult, healthy, Indian-genotype rhesus macaques (Macaca mulatta) were selected from BPRC's breeding colonies and stratified into treatment groups. Males and females were represented at a 2:1 ratio per group (unless indicated otherwise; see **Supplementary Table 1**). Animals, per gender, were socially housed throughout the experiment in BPRC's experimental animal facilities at biosafety level three. Enrichment was provided in the form of food and non-food items and welfare was monitored by daily observation.

A schematic diagram of the study design is provided in **Figure 3A**. After a brief period of acclimatization and baseline measurements, animals were primed with BCG – or left untreated as non-vaccinated controls – and BCG vaccinees were either or not boosted with MTBVAC-HK 16 weeks later. Another 9 weeks later – that is 25 weeks post-priming – all animals received an infectious challenge with 50 CFU of Mtb Erdman into the lower left lung lobe. Twelve weeks post-infection, animals were sedated and euthanized by intravenous pentobarbital injection, and subsequently submitted to full post-mortem evaluation and assessment of pathological and bacteriological parameters of infection and disease. Two animals of the non-vaccinated control group reached a premature, humane endpoint due to acute progressive disease development and were euthanized for full post-mortem evaluation 6 and 11 weeks post-infection, respectively (see **Supplementary Table 1**).

All animal handling was performed under ketamine sedation (10 mg/kg, by intra-muscular injection). For pulmonary endoscopic installation and additional relaxation, intramuscular ketamine (5 mg/kg) was supplemented with medetomidine (0.04 mg/kg) and an analgesic was sprayed into the larynx.

Peripheral blood was sampled by venepuncture at various time points, as indicated in the Results section. For immunological assays, peripheral blood mononuclear cells (PBMC) were isolated from heparinized blood by standard Ficoll®-based gradient centrifugation using Lymphoprep™ (Axis-Shield, United Kingdom). Serum tubes were spun for 10 min at 1000 g to harvest and store cell-free serum at −80°C for further

analysis at later time point. Serum samples were filter-sterilized using 0.2 μm PVDF-membrane plates (Fisher Scientific) before immune response analysis.

Standard hematological parameters were measured in fresh EDTA blood on a Sysmex2000i system (Siemens). Standard clinical chemistry values were determined in fresh serum samples on a Cobas^{TM} Intregra 400+ platform (Roche Diagnostics).

Bronchoalveolar lavage (BAL) was collected by three times consecutive instillation-and-harvesting of 20 mL prewarmed, sterile 0.9% saline, targeting the lower left lung lobe with an endoscope. BAL was collected 3 weeks before and 4 weeks after MTBVAC-HK boosting from $N = 3$ pre-assigned animals of the MTBVAC-HK booster group, and 3 weeks before boosting also from $N = 3$ pre-assigned animals of the non-vaccinated controls (see also **Supplementary Table 1** and **Figure 3A**). After passage over a 100 μm filter and centrifugation for 10 min at 400 g, supernatant was decanted and stored as BAL fluid at −80°C pending further analysis. BAL cell pellet was resuspended in fetal calf serum-, glutamax- and penicillin/streptomycin-supplemented RPMI culture medium for immediate use in immune assays. BAL fluid samples were filter-sterilized using 0.2 μm PVDF-membrane plates (Fisher Scientific) before immune response analysis.

NHP Post-mortem Evaluation

At study endpoint, gross pathology was arbitrarily scored utilizing a predefined algorithm, adapted from Lin et al. (2009). Lung lobes were slabbed into approximately 0.5 cm slices for ample inspection and lesions were scored by size, frequency and appearance. Extrathoracic organs (typically spleen, liver and kidneys) were scored similarly, and lymph node involvement was graded by size and appearance.

After gross pathological examination, lung lobes were minced and spleen and lung-draining lymph nodes were passed over a 100 μm cell strainer (Greiner Bio One International), prior to further homogenization using GentleMACS M tubes (Miltenyi Biotec). Homogenates were frozen stored at -80°C and later thawed and serially diluted onto Middlebrook 7H10 plates for enumeration of bacterial tissue burden.

NHP Immune Analyses

Immunogenicity of vaccination was measured by a lymphocyte stimulation test using a specific NHP IFNg ELISPOT kit (U-CyTech) for the readout of the frequency of IFNg producing cells. In brief, 2×10^5 PBMC in supplemented RPMI culture medium were incubated in triplicate in microtiter flat-bottom plates for 24 h at 37°C and 5% CO2, either or not in the presence of specific antigen. Mtb-derived protein purified derivative (PPD, Statens Serum Institute, Denmark) or Mtb-specific, recombinant ESAT6-CFP10 fusion protein (E6C10, for short; a gift from K. Franken, LUMC, Leiden) were used for *in vitro* recall stimulation as indicated, both at a final concentration of 5 μg/mL. After overnight incubation cells were transferred to specific anti-IFNg-coated filter plates (PVDF, Millipore) for an additional overnight incubation. Spots were developed using tetra-methylbenzidine substrate (MAbTech) and quantified on an AELVIS automated reader.

Flow cytometry was used to measure intracellular IFNg cytokine levels in CD4+ and CD8+ T lymphocytes from BAL. In brief, BAL cells (at least 1×10^6 cells) were either or not stimulated with PPD at a final concentration of 5 μg/mL in supplemented RPMI for 3 h in the presence of costimulatory antibodies against CD28 (PE-Cy7 conjugated) and CD49d. Subsequently, Golgiplug (BD Biosciences) was added and cells were incubated for another 15 h at 37°C and 5% CO2. Cells were then stained by standard procedures using Cytofix/Cytoperm and PermWash buffer (all from BD Bioscience), using the following antibody conjugates: anti-CD20-V450, anti-CD3-V500, anti-CD4-PerCP-Cy5.5, anti-CD8a-APC-Cy7, and anti-IFNg-AF700. T lymphocytes were gated as singlets, CD20-negative, CD3-positive cells. Within this population CD4+ and CD8+ cells were interogated for cytokine production (**Supplementary Figure S6**). Cells were measured in a LSR-II flowcytometer (BD Biosciences); data were analyzed using FlowJo software.

PPD-specific IgA, IgM and IgG in sera and BAL samples, as well as J chain in BAL, were determined following a protocol similar to the one described above for mice. For J chain determination, plates were incubated with a primary monoclonal antibody anti J chain (Santa Cruz Biotechnology, sc-271967) at a 1:1000 dilution, followed by incubation with secondary anti mouse IgG. Serum samples were diluted 1:500 in all cases, whereas BAL fluid was used undiluted. Anti human IgA, IgG or IgM antibodies were all conjugated with HRP (Sigma Aldrich) and diluted 1:10000. Primary anti J chain antibody was the same as described above for mice.

Functional Studies With BAL Samples

To evaluate direct Ig binding to Mtb, 10^7 GFP-expressing H37Rv in 50 μl of PBS were added to 50 μl of BAL (or PBS as control) and incubated for 1 h at room temperature. Then, anti human IgA, IgG or IgM antibodies, all biotin-conjugated (Mabtech), were added in 50 μl at a final dilution of 1:200 (30 min at room temperature). Finally, streptavidin conjugated with APC (Miltenyi Biotech) was added in 50 μl at a final dilution of 1 μg/ml (30 min at room temperature). Bacteria were fixed adding 300 additional μl of paraformaldehyde (PFA) (final concentration 4%) and acquired with a flow cytometry Gallios (Beckman Coulter). Use of GFP-expressing H37Rv allowed discerning bacteria from BAL-derived debris. To assess C3b binding, we used an anti C3b as primary antibody (Millipore, clone 3E7) diluted at 1:25. Biotin-conjugated anti mouse IgG (Bethyl), diluted 1:200, and APC-conjugated streptavidin were used to detect fluorescence by flow cytometry.

THP-1 cells (Sigma-Aldrich) were cultured at 37°C and 5% CO_2 in DMEM medium (Invitrogen) supplemented with 10% inactivated foetal bovine serum (Biological industries) and 2 mM glutamine (Biological industries). 5×10^5 cells were seeded in 24-plate wells and incubated overnight with PMA 10 ng/ml. GFP-expressing H37Rv were incubated with the different BAL samples (or PBS as control) as described above. When indicated, anti C3b at 300 μg/ml was added to BAL suspensions. Then, bacterial suspensions were prepared in DMEM complete medium and put in contact with cells for 4 h at a MOI or five bacteria per cell. Cells were washed three times with PBS and detached

with trypsin to evaluate internalization by flow cytometry. In some of the experiments, fresh media was added and GFP-positive cells analyzed 48 h later. To assess bacterial colocalization with acid compartments, cells seeded over microscopy slides were incubated with 1 μM lysotracker red (Invitrogen). Then, they were fixed with PFA and nuclei stained with Hoechst 33342 10 μg/ml. Images were acquired with an Olympus FV10-i confocal microscopy. Colocalization was quantified using FV10-ASW 3.0 software (Olympus), and was calculated as the proportion of pixels that were both green and red compared to those that were green. Percentage of colocalization was determined analysing at least six images randomly taken for each experimental condition.

Statistical Analysis

Results from this study were not blinded for analysis. No randomization specific methodology was applied to this study. No statistical method was used to calculate sample size in animal experiments. GraphPad Prism six software was used for statistical analysis. Statistical tests used for each experiment are indicated in the figure legends. All statistical tests were two-tailed. Outlier values were determined applying the Grubb's test to all data sets, and were discarded from the final statistical analysis. Differences were considered significant at $p < 0.05$.

DATA AVAILABILITY STATEMENT

The datasets generated for this study are available on request to the corresponding author.

ETHICS STATEMENT

The animal study was reviewed and approved by Comisión Ética de Experimentación Animal de la Universidad de Zaragoza.

AUTHOR CONTRIBUTIONS

NA, EP, ER, FV, and CM designed the experiments and directed the study. NA, SU, EM, RT, DoM, AG, IO, RV, and CS performed the experiments. MM and JB provided material and facilities crucial for the execution of the experiments. NA, DeM, EP, FV, and CM wrote the manuscript. All authors contributed to the article and approved the submitted version.

FUNDING

This work was supported by "Spanish Ministry of Economy and Competitiveness" (grant number IPT-2012-0327-090000), "Ministry of Science, Innovation and Universities" (grant number RTI2018-097625-B-I00), "European Commission H2020 program" (grant number TBVAC2020 643381), and "Gobierno de Aragón/Fondo Social Europeo." NHP study was supported by a grant from the Bill and Melinda Gates Foundation (BMGF) to the TuBerculosis Vaccine Initiative (TBVI, Lelystad, Netherlands), and was co-sponsored by BPRC. The funders had no role in study design, data collection and analysis, decision to publish or preparation of the manuscript.

ACKNOWLEDGMENTS

The authors acknowledge the Scientific and Technical Services from Instituto Aragonés de Ciencias de la Salud and Universidad de Zaragoza, as well as expert support from the staff of the Veterinary Care, Animal Care, Clinical Lab and Pathology units, all from BPRC's Animal Science Department. *M. tuberculosis* strain Erdman K01, that was used for infectious challenge in NHPs, was obtained through the NIH Biodefense and Emerging Infections Research Repository (BEI Resources NIAID-NIH, (VA) United States; TMC107, NR-15404). The recombinant ESAT6-CFP10 fusion protein used for immune analysis post-infection in NHPs was a generous gift by Kees Franken from the laboratory of Prof. Dr. T. Ottenhoff, Department of Infectious Diseases, Leiden University Medical Center (LUMC, Leiden, Netherlands).

SUPPLEMENTARY MATERIAL

The Supplementary Material for this article can be found online at: https://www.frontiersin.org/articles/10.3389/fmicb.2020.01339/full#supplementary-material

REFERENCES

Achkar, J. M., and Casadevall, A. (2013). Antibody-mediated immunity against tuberculosis: implications for vaccine development. *Cell Host Microb.* 13, 250–262. doi: 10.1016/j.chom.2013.02.009

Aguilo, N., Alvarez-Arguedas, S., Uranga, S., Marinova, D., Monzon, M., Badiola, J., et al. (2016). Pulmonary but not subcutaneous delivery of BCG vaccine confers protection to tuberculosis-susceptible mice by an interleukin 17-Dependent mechanism. *J. Infect. Dis.* 213, 831–839. doi: 10.1093/infdis/jiv503

Aguilo, N., Gonzalo-Asensio, J., Alvarez-Arguedas, S., Marinova, D., Gomez, A. B., Uranga, S., et al. (2017). Reactogenicity to major tuberculosis antigens absent in BCG is linked to improved protection against *Mycobacterium tuberculosis*. *Nat. Commun.* 8:16085.

Arbues, A., Aguilo, J. I., Gonzalo-Asensio, J., Marinova, D., Uranga, S., Puentes, E., et al. (2013). Construction, characterization and preclinical evaluation of MTBVAC, the first live-attenuated *M. tuberculosis*-based vaccine to enter clinical trials. *Vaccine* 31, 4867–4873. doi: 10.1016/j.vaccine.2013.07.051

Baqui, A. A., Meiller, T. F., Kelley, J. I., Turng, B. F., and Falkler, W. A. (1999). Antigen activation of THP-1 human monocytic cells after stimulation with lipopolysaccharide from oral microorganisms and granulocyte-macrophage colony-stimulating factor. *J. Periodontal Res.* 34, 203–213. doi: 10.1111/j.1600-0765.1999.tb02243.x

Cryz, S. J. Jr., Furer, E., and Germanier, R. (1982). Effect of chemical and heat inactivation on the antigenicity and immunogenicity of *Vibrio cholerae*. *Infect. Immun.* 38, 21–26. doi: 10.1128/iai.38.1.21-26.1982

Dijkman, K., Sombroek, C. C., Vervenne, R. A. W., Hofman, S. O., Boot, C., Remarque, E. J., et al. (2019). Prevention of tuberculosis infection and disease by local BCG in repeatedly exposed rhesus macaques. *Nat. Med.* 25, 255–262. doi: 10.1038/s41591-018-0319-9

Fletcher, H. A., Snowden, M. A., Landry, B., Rida, W., Satti, I., Harris, S. A., et al. (2016). T-cell activation is an immune correlate of risk in BCG vaccinated infants. *Nat. Commun.* 7:11290.

Guidry, A. J., Berning, L. M., and Hambleton, C. N. (1993). Opsonization of *Staphylococcus aureus* by bovine immunoglobulin isotypes. *J. Dairy Sci.* 76, 1285–1289. doi: 10.3168/jds.s0022-0302(93)77458-5

Haile, M., Hamasur, B., Jaxmar, T., Gavier-Widen, D., Chambers, M. A., Sanchez, B., et al. (2005). Nasal boost with adjuvanted heat-killed BCG or arabinomannan-protein conjugate improves primary BCG-induced protection in C57BL/6 mice. *Tuberculosis* 85, 107–114. doi: 10.1016/j.tube.2004.09.013

Haile, M., Schroder, U., Hamasur, B., Pawlowski, A., Jaxmar, T., Kallenius, G., et al. (2004). Immunization with heat-killed *Mycobacterium bovis* bacille Calmette-Guerin (BCG) in Eurocine L3 adjuvant protects against tuberculosis. *Vaccine* 22, 1498–1508. doi: 10.1016/j.vaccine.2003.10.016

Huber-Lang, M., Younkin, E. M., Sarma, J. V., Riedemann, N., Mcguire, S. R., Lu, K. T., et al. (2002). Generation of C5a by phagocytic cells. *Am. J. Pathol.* 161, 1849–1859. doi: 10.1016/s0002-9440(10)64461-6

Kaetzel, C. S., Robinson, J. K., Chintalacharuvu, K. R., Vaerman, J. P., and Lamm, M. E. (1991). The polymeric immunoglobulin receptor (secretory component) mediates transport of immune complexes across epithelial cells: a local defense function for IgA. *Proc. Natl. Acad. Sci. U.S.A.* 88, 8796–8800. doi: 10.1073/pnas.88.19.8796

Kaushal, D., Foreman, T. W., Gautam, U. S., Alvarez, X., Adekambi, T., Rangel-Moreno, J., et al. (2015). Mucosal vaccination with attenuated *Mycobacterium tuberculosis* induces strong central memory responses and protects against tuberculosis. *Nat. Commun.* 6:8533.

Lagranderie, M., Ravisse, P., Marchal, G., Gheorghiu, M., Balasubramanian, V., Weigeshaus, E. H., et al. (1993). BCG-induced protection in guinea pigs vaccinated and challenged via the respiratory route. *Tuber. Lung Dis.* 74, 38–46. doi: 10.1016/0962-8479(93)90067-8

Lin, P. L., Rodgers, M., Smith, L., Bigbee, M., Myers, A., Bigbee, C., et al. (2009). Quantitative comparison of active and latent tuberculosis in the cynomolgus macaque model. *Infect. Immun.* 77, 4631–4642. doi: 10.1128/iai.00592-09

Lu, L. L., Chung, A. W., Rosebrock, T. R., Ghebremichael, M., Yu, W. H., Grace, P. S., et al. (2016). A functional role for antibodies in tuberculosis. *Cell* 167:e414.

Marinova, D., Gonzalo-Asensio, J., Aguilo, N., and Martin, C. (2017). MTBVAC from discovery to clinical trials in tuberculosis-endemic countries. *Expert Rev. Vacc.* 16, 565–576. doi: 10.1080/14760584.2017.1324303

Michaelsen, T. E., Emilsen, S., Sandin, R. H., Granerud, B. K., Bratlie, D., Ihle, O., et al. (2017). Human secretory IgM antibodies activate human complement and offer protection at mucosal surface. *Scand. J. Immunol.* 85, 43–50. doi: 10.1111/sji.12508

Opie, E. L., and Freund, J. (1937). An experimental study of protective inoculation with heat killed tubercle bacilli. *J. Exp. Med.* 66, 761–788. doi: 10.1084/jem.66.6.761

Renegar, K. B., Jackson, G. D., and Mestecky, J. (1998). In vitro comparison of the biologic activities of monoclonal monomeric IgA, polymeric IgA, and secretory IgA. *J. Immunol.* 160, 1219–1223.

Rojas, R., and Apodaca, G. (2002). Immunoglobulin transport across polarized epithelial cells. *Nat. Rev. Mol. Cell Biol.* 3, 944–955.

Satti, I., Meyer, J., Harris, S. A., Manjaly Thomas, Z. R., Griffiths, K., Antrobus, R. D., et al. (2014). Safety and immunogenicity of a candidate tuberculosis vaccine MVA85A delivered by aerosol in BCG-vaccinated healthy adults: a phase 1, double-blind, randomised controlled trial. *Lancet Infect. Dis.* 14, 939–946. doi: 10.1016/s1473-3099(14)70845-x

Spertini, F., Audran, R., Chakour, R., Karoui, O., Steiner-Monard, V., Thierry, A. C., et al. (2015). Safety of human immunisation with a live-attenuated *Mycobacterium tuberculosis* vaccine: a randomised, double-blind, controlled phase I trial. *Lancet Respir. Med.* 3, 953–962. doi: 10.1016/s2213-2600(15)00435-x

Strunk, R. C., Eidlen, D. M., and Mason, R. J. (1988). Pulmonary alveolar type II epithelial cells synthesize and secrete proteins of the classical and alternative complement pathways. *J. Clin. Invest.* 81, 1419–1426. doi: 10.1172/jci113472

Stylianou, E., Griffiths, K. L., Poyntz, H. C., Harrington-Kandt, R., Dicks, M. D., Stockdale, L., et al. (2015). Improvement of BCG protective efficacy with a novel chimpanzee adenovirus and a modified vaccinia Ankara virus both expressing Ag85A. *Vaccine* 33, 6800–6808. doi: 10.1016/j.vaccine.2015.10.017

Tameris, M., Mearns, H., Penn-Nicholson, A., Gregg, Y., Bilek, N., Mabwe, S., et al. (2019). Live-attenuated *Mycobacterium tuberculosis* vaccine MTBVAC versus BCG in adults and neonates: a randomised controlled, double-blind dose-escalation trial. *Lancet Respir. Med.* 7, 757–770. doi: 10.1016/s2213-2600(19)30251-6

Von Reyn, C. F., Lahey, T., Arbeit, R. D., Landry, B., Kailani, L., Adams, L. V., et al. (2017). Safety and immunogenicity of an inactivated whole cell tuberculosis vaccine booster in adults primed with BCG: a randomized, controlled trial of DAR-901. *PLoS One* 12:e0175215. doi: 10.1371/journal.pone.0175215

Woodworth, J. S., Christensen, D., Cassidy, J. P., Agger, E. M., Mortensen, R., and Andersen, P. (2019). Mucosal boosting of H56:CAF01 immunization promotes lung-localized T cells and an accelerated pulmonary response to *Mycobacterium tuberculosis* infection without enhancing vaccine protection. *Mucosal Immunol.* 12, 816–826. doi: 10.1038/s41385-019-0145-5

Conflict of Interest: NA, SU, DeM, EP, ER, and CM are co-inventors of the patent "inactivated tuberculosis vaccine" filled by the University of Zaragoza and Biofabri.

The remaining authors declare that the research was conducted in the absence of any commercial or financial relationships that could be construed as a potential conflict of interest.

The handling editor declared a past co-authorship with one of the authors CM.

frontiers in Immunology

ORIGINAL RESEARCH
published: 23 June 2020
doi: 10.3389/fimmu.2020.01298

Activation of M1 Macrophages in Response to Recombinant TB Vaccines With Enhanced Antimycobacterial Activity

*Shiu-Ju Yang[1], Yih-Yuan Chen[2], Chih-Hao Hsu[1], Chia-Wei Hsu[1], Chun-Yu Chang[1], Jia-Ru Chang[1] and Horng-Yunn Dou[1]**

[1] National Institute of Infectious Diseases and Vaccinology, National Health Research Institutes, Zhunan, Taiwan, [2] Department of Biochemical Science and Technology, National Chiayi University, Chia-Yi, Taiwan

Pulmonary tuberculosis (TB) is a difficult-to-eliminate disease. Although the Bacille Calmette–Guérin (BCG) vaccine against *Mycobacterium tuberculosis* (MTB) has been available for decades, its efficacy is variable and has lessened over time. Furthermore, the BCG vaccine no longer protects against newly emerged Beijing strains which are responsible for many current infections in adults. Development of a novel vaccine is urgently needed. In this study, we first tested the efficacy of our recombinant BCG vaccines rBCG1 and rBCG2, compared to parental BCG, against MTB strain H37Ra in mice. Both the bacterial load and the level of lymphocyte infiltration decreased dramatically in the three groups treated with vaccine, especially rBCG1 and rBCG2. Furthermore, the Th1 and Th17 responses increased and macrophage numbers rose in the vaccination groups. Th1-mediated production of cytokines TNF-α, IFN-γ, and MCP-1 as well as M1-polarized cells all increased in lung tissue of the rBCG1 and rBCG2 groups. Clodronate-induced depletion of macrophages reduced the level of protection. Based on these results, we conclude that rBCG vaccines induce a significant increase in the number of M1 macrophages, which augments their potential as TB vaccine candidates.

Keywords: recombinant Bacille Calmette–Guérin, *Mycobacterium tuberculosis*, innate immunity, macrophage, vaccine

OPEN ACCESS

Edited by:
Juraj Ivanyi, King's College London, United Kingdom

Reviewed by:
Hazel Marguerite Dockrell, University of London, United Kingdom
Marc Jacobsen, Heinrich Heine University of Düsseldorf, Germany

***Correspondence:**
Horng-Yunn Dou
hydou@nhri.edu.tw

Specialty section:
This article was submitted to Microbial Immunology, a section of the journal Frontiers in Immunology

Received: *06 March 2020*
Accepted: *22 May 2020*
Published: *23 June 2020*

Citation:
Yang S-J, Chen Y-Y, Hsu C-H, Hsu C-W, Chang C-Y, Chang J-R and Dou H-Y (2020) Activation of M1 Macrophages in Response to Recombinant TB Vaccines With Enhanced Antimycobacterial Activity. Front. Immunol. 11:1298. doi: 10.3389/fimmu.2020.01298

INTRODUCTION

Tuberculosis is a difficult-to-treat disease that causes millions of deaths worldwide (1, 2). The disease is a major public health problem in many countries, consuming considerable societal and financial resources. The bacille Calmette–Guérin (BCG) vaccine, created in 1921, is the only licensed vaccine against *Mycobacterium tuberculosis* (MTB) (3). When administered during childhood, the vaccine provides ∼10–15 years of protection, but this immunity wanes in adulthood (4). However, the protective efficacy of the BCG vaccine varies widely, from 0 to 88% (5–7). Based on this epidemiological evidence, BCG appears to lose its protective effect over time (4–7). Although most studies did not find any association, a study that subdivided Beijing MTB strains into typical and atypical lineages found typical Beijing strains to be more frequent among BCG-vaccinated persons compared to non-vaccinated persons (8), suggesting that BCG vaccination is less protective against typical Beijing strains, which has also been reported in animal models (9, 10). For these reasons, development of a novel, effective vaccine is urgently needed.

Antigen 85B (Ag85B) and culture filtrate protein 10 (CFP-10) are two candidates for effective MTB vaccine development. Ag85B, part of the Ag85 complex with antigens B and C, functions as a mycolyl transferase in MTB cell wall assembly (11). This major protective protein is recognized by T cells and is a strong MTB antigen (12, 13). Ag85B binds fibronectin, which then stimulates human monocytes to produce TNF-α (14). Overexpression of Ag85B reduces bacterial load (15) and protects mice against MTB infection (16). Recently, Prendergast et al. showed that Ag85B-deficient BCG had reduced capacity to infect macrophages, whereas an Ag85B-overexpressing BCG strain had improved uptake by macrophages (17). CFP-10, a secreted protein encoded by the RD-1 region of MTB, combines with the 6-kDa early secreted antigen target 6 (ESAT-6) protein to form a heterodimer (18). Loss of both Ag85B and CFP-10 has been associated with attenuated MTB infection (19, 20). Therefore, these targets have been used as trial vaccine candidates for years. However, some studies show that Ag85B and CFP-10 do not provide adequate protection (17) or do not have enough long-term data to support their efficacy (21, 22).

Recombinant BCG vaccines can be engineered to express immunodominant antigens such as Ag85 complex (Ag85A-C) and ESAT-6. Notably, CD8+ T cells recognizing CFP-10 are elicited following MTB infection in humans (23–26). Therefore, our strategy is to combine Ag85B and CFP-10 into a fusion protein that is expressed in BCG hosts. Human IL-12 provides a robust immune response to such fusion proteins and could enhance vaccine efficacy. Recently, our recombinant BCG vaccines rBCG1 and rBCG2 demonstrated higher stimulation of IFN-γ secretion compared to parental BCG vaccine (27). rBCG1 is BCG containing a fusion protein of Ag85B and CFP-10, whereas rBCG2 is BCG containing the same fusion protein plus human IL-12 (27). Prior to the present study, we had not tested the protective efficacy of these two recombinant vaccines in an animal infection model. In order to establish the efficacy of our rBCG vaccines in mice, we tested them against MTB strain H37Ra administered intravenously and compared their effects to that of the parental BCG vaccine; in this trial, the mice were given two vaccinations 2 weeks apart and then challenged with H37Ra 2 weeks later. This study was designed to evaluate rBCG1 and rBCG2 efficacy and long-term protection against MTB compared to the parental BCG vaccine. The study included characterization of immune cell responses, including cytokine-release profiles.

MATERIALS AND METHODS

Bacterial Strains and Cultures

Parental BCG is *Mycobacterium bovis* BCG (Tokyo172) and was used to construct the recombinant BCG strains rBCG1 and rBCG2 in a previous study (27). Briefly, rBCG1 was constructed using MTB antigens Ag85B and CFP-10 in an *M. bovis* BCG Tokyo 172 strain, and rBCG2 was constructed using MTB antigens Ag85B and CFP-10 plus human IL-12 also in *M. bovis* BCG Tokyo 172. rBCG1 and rBCG2 were compared to *M. tuberculosis* strain H37Ra. H37Ra and BCG (Tokyo 172) were maintained on Middlebrook 7H9 medium (Difco Laboratories, Detroit, MI, USA) and supplemented with 0.5% glycerol, 0.05% Tween 80, and 10% albumin- dextrose-catalase or on solid Middlebrook 7H11 medium (Difco Laboratories) supplemented with oleic acid-albumin-dextrose-catalase. rBCG1 and rBCG2 were maintained on the media described above with 25 μg/ml kanamycin.

Mice and Immunization

Female C57BL/6 and SCID mice aged 6–8 weeks were purchased from the National Laboratory Animal Center (Taipei, Taiwan). All mice were kept in individually ventilated cage environments at the Animal Center of the National Health Research Institutes (Maoli, Taiwan). The temperature was maintained at 20–24°C with a relative humidity of 40–70% and a 12-h light/dark cycle. Animal experiments were reviewed and approved by the National Health Research Institutes Institutional Animal Care and Use Committee (NHRI-IACUC). We conducted experiments according to guidelines set out by the Association for Assessment and Accreditation of Laboratory Animal Care International (AAALAC). Mice were given a two-dose vaccination of parental BCG, rBCG1, or rBCG2 (5×10^5 colony forming units [CFUs] per mouse) subcutaneously at weeks 0 and 2. Mice were then challenged with 10^6 CFU of H37Ra per mouse at week 4 by intravenous injection. For macrophage depletion, mice were given a two-dose vaccination of parental BCG, rBCG1, or rBCG2 (5×10^5 CFU per mouse) subcutaneously at weeks 0 and 2, and they received one drop of encapsome® (control) or clodrosome® (Encapsula Nano Sciences, TN, USA) intratracheally weekly for 8 weeks. For the biosafety assay, C57BL/6 and SCID mice aged 6–8 weeks were given a two-dose vaccination of parental BCG, rBCG1, or rBCG2 (5×10^5 CFU per mouse) subcutaneously at weeks 0 and 2, and then challenged with H37Ra at week 4. The mice were closely monitored and their body weights were measured every week until week 40 (or a humane endpoint).

Multiple Cytokine Testing

After sacrifice, blood was collected and plasma was stored at −20°C until use. Murine inflammatory cytokine testing was performed using a multiple mouse cytometric bead array (CBA) mouse inflammation kit (BD Biosciences, San Jose, CA, USA).

Immunohistochemical Staining (IHC) and Pathologic Score

Samples of lung tissue were fixed in formalin and embedded in paraffin using routine methods, and the sections were then stained with hematoxylin and eosin (H&E). Tissue processing was performed by the core pathology facility at the National Health Research Institutes (Maoli, Taiwan). Histopathologic parameters (i.e., peribronchiolitis, perivasculitis, alveolitis, and granuloma formation) were each semi-quantitatively scored as absent, minimal, slight, moderate, marked, or strong using numerical scores of 0, 1, 2, 3, 4, and 5, respectively (28). Lesion frequency and severity were incorporated into these scores. For each time point, lung tissue from six or seven animals was examined, and the mean score for each slide of five or six random views was calculated. For IHC, paraffin sections

were rehydrated and retrieved with 100 mM citrate buffer (pH 6.0) at 100°C for 5 min. After blocking the peroxidase activity and background (IHC/ICC kit, BioVision, Milpitas, CA, USA), the serial sections were incubated with primary antibody anti-iNOS (Abcam, ab15323, Cambridge, UK, **RRID:AB_301857**) and anti-mannose receptor (Abcam, ab64693, Cambridge, UK, **RRID:AB_1523910**), and stained following the manufacturer's protocol (BioVision). Finally, the sections were colored with the chromogen DAB and counterstained with hematoxylin. For determination of positive cells, the number of DAB-positive plus hematoxylin- positive cells in six randomly selected fields per slide (each an area of 8.4×10^3 μm^2) was calculated and analyzed.

Bacterial Culture

Half of each lung tissue sample was minced and passed through a MACS C tube to produce single-cell suspensions in 5 ml of saline (cell survival rate >99.5% by hemocytometer). CFU values were determined by using 100 μl of cell mixture dilution on 7H10 agar plates. Each plate contained 100 μl of tissue homogenate, and each sample was titrated for three dilutions (10×, 100× and 1000×) performed in triplicate. Plates were kept at 37°C for 3–4 weeks. The colony number was counted and presented as a value per one lung (one mouse).

Flow Cytometry

Lung and spleen tissues were minced and passed through a MACS C tube to produce single-cell suspensions (cell survival rate >99.5% by hemocytometer). The cells were incubated in 50 μl of RPMI medium that contained 2% fetal bovine serum (FBS) with Fc receptor for 15 min and then with several antibodies: CD4-FITC (cat. 553046, **RRID:AB_394582**), CD4-PerCP-Cy5.5(cat. 553052, **RRID:AB_394587**), CD8-PerCP-Cy5.5 (cat. 551162, **RRID:AB_394081**), CD25-BB515(cat.564424, **RRID:AB_2738803**), F4/80-PE(cat. 565410, **RRID:AB_2687527**), CD49b-APC, (cat.558295, **RRID:AB_398658**), IFN-γ-FITC(cat.554411), IL-17A-AF647(560184, **RRID:AB_1645204**), IL-4-PE(cat. 554435, **RRID:AB_395391**), Foxp3-PE(cat. 560408, **RRID:AB_1645251**) (all from BD Biosciences), and CD317-PerCP-Cy5.5 (pDCs; 120G8, Dendritics, San Diego, CA, USA, **RRID:AB_2566646**). For intracellular cytokine labeling, cells were stimulated with MTB-specific peptides (5 μg/ml of CD4 peptide $Ag85B_{241-255aa}$ QDAYNAAGGHAVFN (Mission Biotech, Taiwan, cat. 991172), CD8 peptide $Ag85B_{1-19aa}$ FSRPGLPVEYLQVPSMG, Mission Biotech, Taiwan, cat. 991171) for 68 h and then Golgi-stop (BD Biosciences) was added for an additional 4 h [28). Cells were then fixed, permeabilized and stained with cytokine antibodies (IFN-γ-FITC, IL-17A-AF647, IL-4-PE and Foxp3-PE) for 1 h following standard procedures. The gating strategy involved $CD4^+$ T cells, and other relevant cell populations were gated from the single cell lymphocyte population in the forward scatter (FSC) and side scatter (SSC) sections (29). The samples were acquired and analyzed using a FACSCalibur system and CellQuest software (BD Biosciences).

TABLE 1 | Sequences of primers used for quantitative PCR.

Primer name	Sequence (5'–3')	
mTNF-α	Forward	AAGCCTGTAGCCCACGTCGTA
	Reverse	GGCACCACTAGTTGGTTGTCTTTG
mIFN-γ	Forward	CATTGAAAGCCTAGAAAGTCTGAATAAC
	Reverse	TGGCTCTGCAGGATTTTCATG
mIL-4	Forward	CCTCACAGCAACGAAGAACA
	Reverse	TGGACTCATTCATGGTGCAG
mIL-5	Forward	CGCTCTTCCTTTGCTGAAG
	Reverse	TAGGGACAGGAAGCCTCATC
mIL-6	Forward	AAGTCGGAGGCTTAATTACACATGT
	Reverse	AAGTGCATCATCGTTGTTCATACA
mIL-10	Forward	GCTCTTACTGACTGGCATGAG
	Reverse	CGCAGCTCTAGGAGCATGTG
mIL-12	Forward	GGAAGCACGGCAGCAGAATA
	Reverse	AACTTGAGGGAGAAGTAGGAATGG
mIL-17	Forward	ATCCACCTCACACGAGGCAC
	Reverse	ACCTTCACATTCTGGAGGAA
mIFN-α1	Forward	AGTGAGCTGACCCAGCAGAT
	Reverse	CAGGGGCTGTGTTTCTTCTC
mIFN-β1	Forward	CCCTATGGAGATGACGGAGA
	Reverse	CTGTCTGCTGGTGGAGTTCA
miNOS	Forward	AAAGTGACCTGAAAGAGGAAAAGGA
	Reverse	TTGGTGACTCTTAGGGTCATCTTGTA
mGAPDH	Forward	GTTGTCTCCTGCGACTTCA
	Reverse	GGTGGTCCAGGGTTTCTTA
mIDO1	Forward	TGGCACTCAGTAAAATATCTCCT
	Reverse	CAGGCAGATTTCTAGCCACA
mIDO2	Forward	ATGGAGCCTCAAAGTCAGAGC
	Reverse	CGCTGCTCACGGTAACTCTTTA
mMCP-1	Forward	CCCACTCACCTGCTGCTACT
	Reverse	TCTGGACCCATTCCTTCTTG

RNA Extraction and Quantitative PCR

Total mRNA was extracted by Trizol reagent, and cDNA was prepared by using a reverse transcription kit (ThermoFisher Scientific, CA, USA). Primer sequences are shown in **Table 1**. The mRNA levels of TNF-α, IFN-γ, MCP-1, various transcription factors and GAPDH were detected by real-time quantitative PCR analysis using the ABI vii7 system (Applied Biosystems, Foster City, CA, USA). Cytokine and GAPDH levels were calculated relative to amounts found in a standard sample, and cytokine levels were corrected for GAPDH mRNA levels to normalize for RNA input. Relative expression (Relative index) is presented as $2^{-\Delta CT}$.

Statistical Analysis

All results are presented as mean ± SEM for six or seven mice per group. The statistical significance between the experimental groups was assessed using a two-tailed unpaired Student's *t*-test, non-parametric analysis, one-way and two-way analysis of variance (ANOVA) with a Tukey or Bonferroni *post hoc* test. The differences were considered significant for $P < 0.05$.

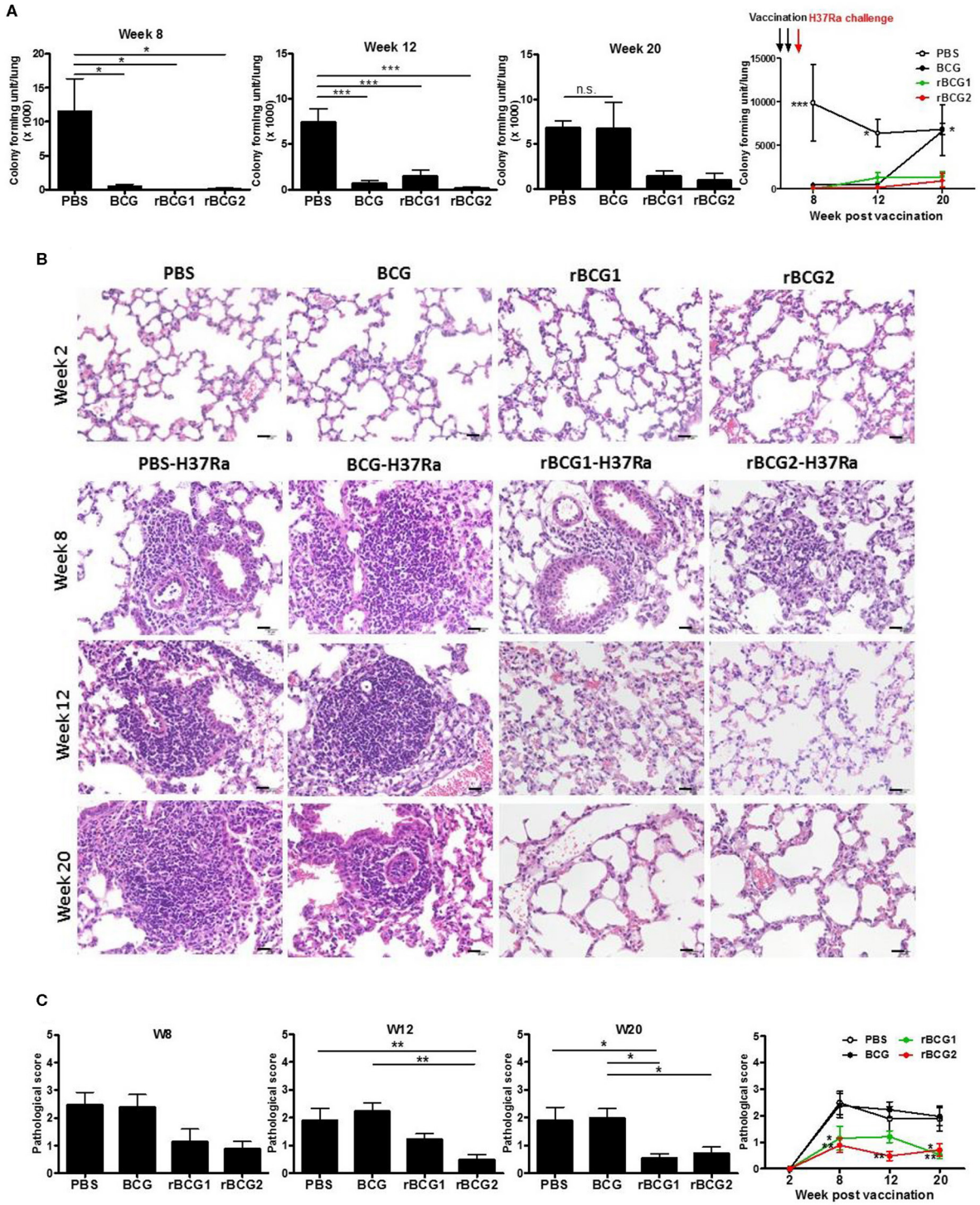

FIGURE 1 | Protection provided by recombinant BCG vaccines rBCG1 and rBCG2 against *Mycobacterium tuberculosis* H37Ra in mice. C57BL/6 mice were immunized with BCG, rBCG1, or rBCG2 at weeks 0 and 2, and then challenged with H37Ra at week 4 ($n = 6$–7, in two independent experiments). At 2, 8, 12, and 20 weeks, the mice were sacrificed. One lung from each mouse was homogenized and the other was fixed in 3.7% formaldehyde. **(A)** Colony forming units (CFU) of bacterial growth in murine lung. Each plate contained 100 μl of tissue homogenate, and each sample was titrated for two dilutions (5 × and 50×) and repeated in triplicate. **(B)** Lung samples were fixed in 3.7% formaldehyde, embedded in paraffin, sectioned, and stained with H&E; scale bar = 20 μm. Differences among groups were determined using a one-way, non-parametric test, or two-way ANOVA with a Tukey or Bonferroni *post hoc* test (*$P < 0.05$; **$P < 0.01$; ***$P < 0.001$; ns, non-significant). **(C)** Pathologic scores were determined and analyzed by H&E staining. For each time point, lung tissue from six or seven animals was examined and the mean score for each slide of five or six random views was calculated. Differences among groups were determined by one-way or two-way ANOVA with a Tukey or Bonferroni *post hoc* test (*$P < 0.05$, **$P < 0.01$).

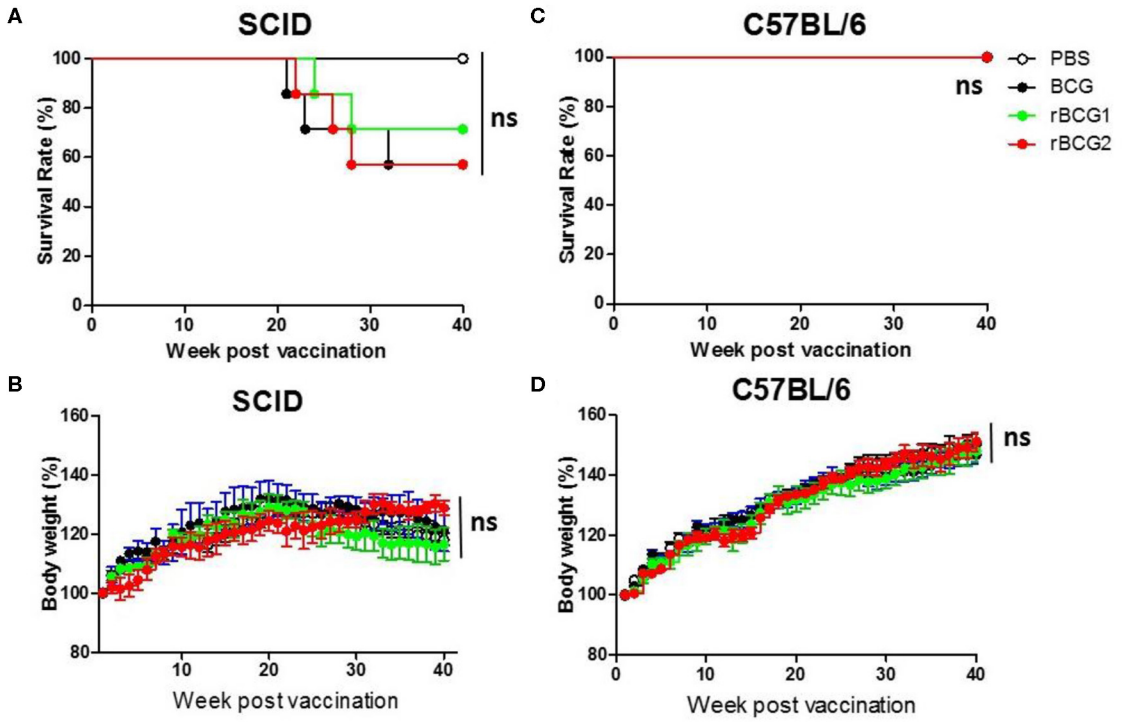

FIGURE 2 | Test of rBCG vaccine safety in immunodeficient and immunocompetent mice. SCID and C57BL/6 wild-type mice were immunized with BCG, rBCG1, or rBCG2 at weeks 0 and 2 ($n = 10$). **(A,C)** Survival rate of SCID and C57BL/6 mice after vaccination. **(B,D)** The body weights of SCID and C57BL/6 mice were recorded every week. Body weight (%) was calculated as: weight (week n)/weight (week 0) per mouse. Survival curves were plotted by the Kaplan-Meier method. The Log-rank test was performed to compare each pair of survival curves ($P > 0.05$; ns, non-significant). Differences among groups were determined by two-way ANOVA with a Bonferroni *post hoc* test ($P > 0.05$; ns, non-significant).

Statistical tests were performed using GraphPad Prism version 6.0 (GraphPad Software, La Jolla, CA, USA).

RESULTS

rBCG1 and rBCG2 Vaccines Protect Mice Against *Mycobacterium tuberculosis* H37Ra

To determine whether our recombinant BCG vaccines rBCG1 and rBCG2 protect against MTB infection, we first conducted a vaccine efficacy test against the H37Ra strain in an ABSL2 facility. (We would have conducted this initial test in an ABSL3 facility with an aerosol virulent MTB Beijing strain, however our facility was not operational at the time.) We administered the vaccines to mice subcutaneously twice (at weeks 0 and 2) and then challenged the mice with MTB H37Ra via intravenous injection at week 4. The bacterial load and lung pathology were measured at weeks 8, 12, and 20 after the immunization. At week 2 (prior to H37Ra challenge), the lungs showed no sign of cellular infiltration (**Figures 1B,C**). At week 8 post-vaccination, the bacterial load of the PBS control group was high [CFU = $(115.2 \pm 47.91) \times 1{,}000$] compared to that of the BCG [CFU = $(5.0 \pm 2.822) \times 1{,}000$], rBCG1 [CFU = $(0 \pm 0) \times 1{,}000$] and rBCG2 [CFU = $(1.112 \pm 1.112) \times 1{,}000$] groups ($^{**}P < 0.001$; **Figure 1A**). Inflammation in the PBS control group was more severe than in the vaccination groups (**Figures 1B,C**). At week 12, the bacterial load in the PBS control was still high [CFU = $(74.72 \pm 14.13) \times 1{,}000$], whereas the bacterial loads were lower in the BCG, rBCG1, and rBCG2 groups [CFU = $(6.66 \pm 2.974) \times 1{,}000$, $(14.99 \pm 5.867) \times 1{,}000$, and $(1.667 \pm 1.054) \times 1{,}000$, respectively, $^{**}P < 0.001$; **Figure 1A**]. However, the cellular infiltration lesions had nearly disappeared by week 12 in the rBCG1 and rBCG2 groups (**Figures 1B,C**). Thus, the rBCG1 and rBCG2 vaccines protected mice against H37Ra infection at an early stage. At week 20, stable bacterial loads were detected for the PBS control group [CFU = $(68.57 \pm 6.904) \times 1{,}000$], but very low bacterial loads were measured in the rBCG1 and rBCG2 groups [CFU = $(16.67 \pm 5.236) \times 1{,}000$ and $(11.11 \pm 9.165) \times 1{,}000$, respectively; $^{*}P < 0.05$]. At 20 weeks, the bacterial load had dramatically increased in the BCG group [CFU = $(66.9 \pm 29.23) \times 1{,}000$, $P > 0.05$; **Figure 1A**). These CFU results paralleled the H&E staining patterns and pathologic scores (**Figures 1B,C**). Taken together, these results suggest that, whereas the parental BCG vaccine does not provide adequate protection against H37Ra infection, the rBCG1 and rBCG2 vaccines do. Thus, the efficacies of the rBCG1 and rBCG2 vaccines are higher than that of the parental BCG.

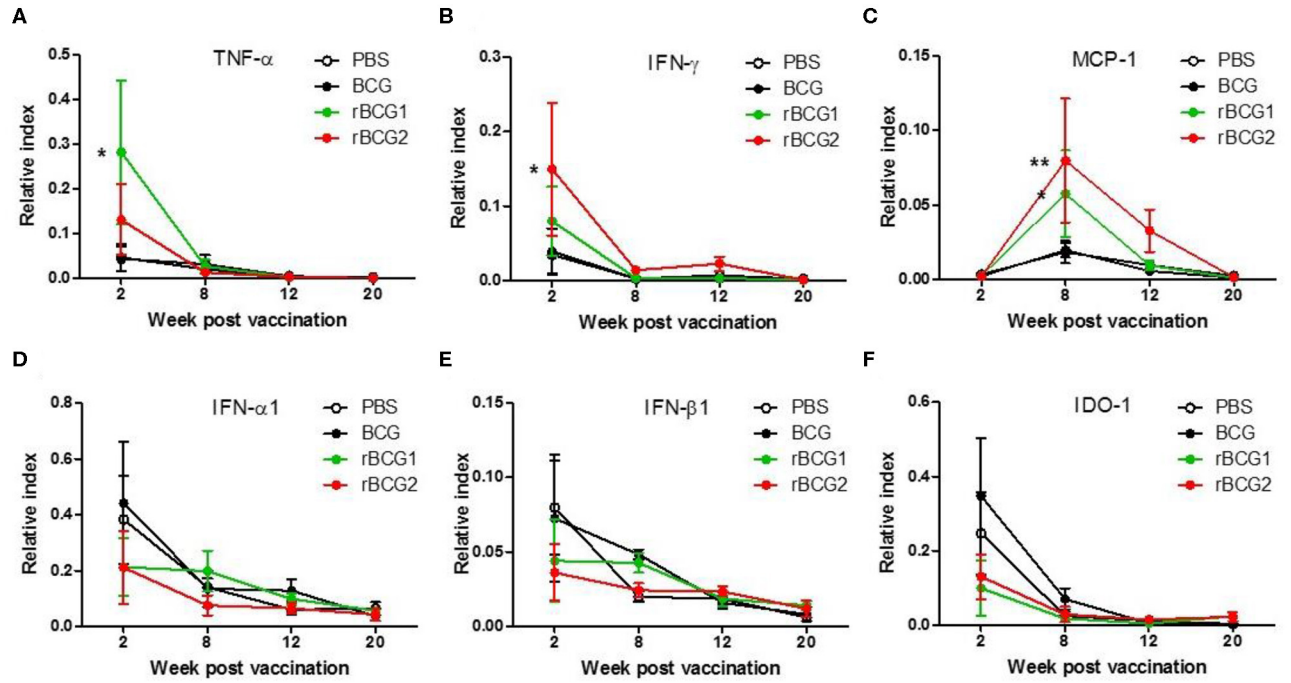

FIGURE 3 | Th1-mediated cytokine profiles expressed in murine lung following immunization with rBCG1 or rBCG2. C57BL/6 mice were immunized with BCG, rBCG1 or rBCG2 at weeks 0 and 2. They were then challenged with H37Ra at week 4 ($n = 6–7$, in two independent experiments). At 2, 8, 12, and 20 weeks, the mice were sacrificed, lung RNA was extracted and cytokine gene expression profiles were determined using qPCR. **(A)** TNF-α, **(B)** IFN-γ, **(C)** MCP-1, **(D)** IFN-α1, **(E)** IFN-β1, **(F)** IDO-1. Differences among groups were determined using two-way ANOVA with a Bonferroni *post hoc* test (*$P < 0.05$; **$P < 0.01$).

rBCG1 and rBCG2 Vaccines Are Safe in SCID Mice as Well as in C57BL/6 Wild-Type Mice

To test the safety of the rBCG1 and rBCG2 vaccines, we gave the same dose of BCG and rBCG vaccines to severe combined immunodeficiency (SCID) and C57BL/6 wild-type mice subcutaneously at weeks 0 and 2. All of the mice were monitored very closely until week 40 or an earlier humane endpoint. Mouse weight was recorded every week. After the vaccination, neither the SCID nor wild-type mice showed any adverse physical signs. The weights of both groups increased slightly every week, but the differences between groups were not significant (**Figures 2B,D**, $P > 0.05$, ns). Starting at week 21, one SCID mouse in each of the BCG, rBCG1 and rBCG2 groups was euthanized for humane reasons but there were no deaths in the PBS group (**Figure 2A**) or in any of the wild-type groups (**Figure 2C**). These results suggest that the rBCG1 and rBCG2 vaccines are safe, even in immunodeficient individuals.

mRNA Expression of Th1-Mediated Cytokines in Mouse Lung Tissue Following Immunization With BCG, rBCG1, and rBCG2

We next examined cytokine expression in the lungs using quantitative PCR (qPCR) to determine whether recombinant BCG vaccines stimulate Th1-mediated cytokine production. RNA was extracted from cells isolated from the lungs and spleens of the PBS control and vaccination groups before and after H37Ra challenge, at weeks 2, 8, 12, and 20, and qPCR was performed to detect cytokine gene expression in these tissues. TNF-α, IFN-γ, and MCP-1 were all increased in the BCG, rBCG1 and rBCG2 groups compared to the PBS control group, particularly during weeks 2 and 8 (**Figures 3A–C**). At weeks 12 and 20, TNF-α, IFN-γ, and MCP-1 were decreased in all groups (**Figures 3A–C**); presumably this reflects bacterial clearance, when cytokine production stops and normal resting levels are reached. These cytokines are the products of Th1-mediated immune responses. In contrast, IFN-α1, IFN-β1, and IDO-1, which are secreted by some of the surrounding infected immune cells, were detected at higher levels in the PBS and BCG groups compared to the rBCG1 and rBCG2 groups (**Figures 3D–F**). Cytokines IL-1β, IL-4, IL-6, IL-10, IL-12, IL-17, and IDO-2 were unchanged or undetectable for all groups (data not shown). These results suggest that rBCG1 and rBCG2 can induce host Th1 responses to clear MTB bacteria.

Macrophages, Th1 Cells and Th17 Cells Dominate Following Immunization With BCG, rBCG1, and rBCG2

We analyzed immune cell profiles from murine lung and spleen tissue using flow cytometry. Single cells were isolated from the lung and spleen in the PBS control and vaccination groups

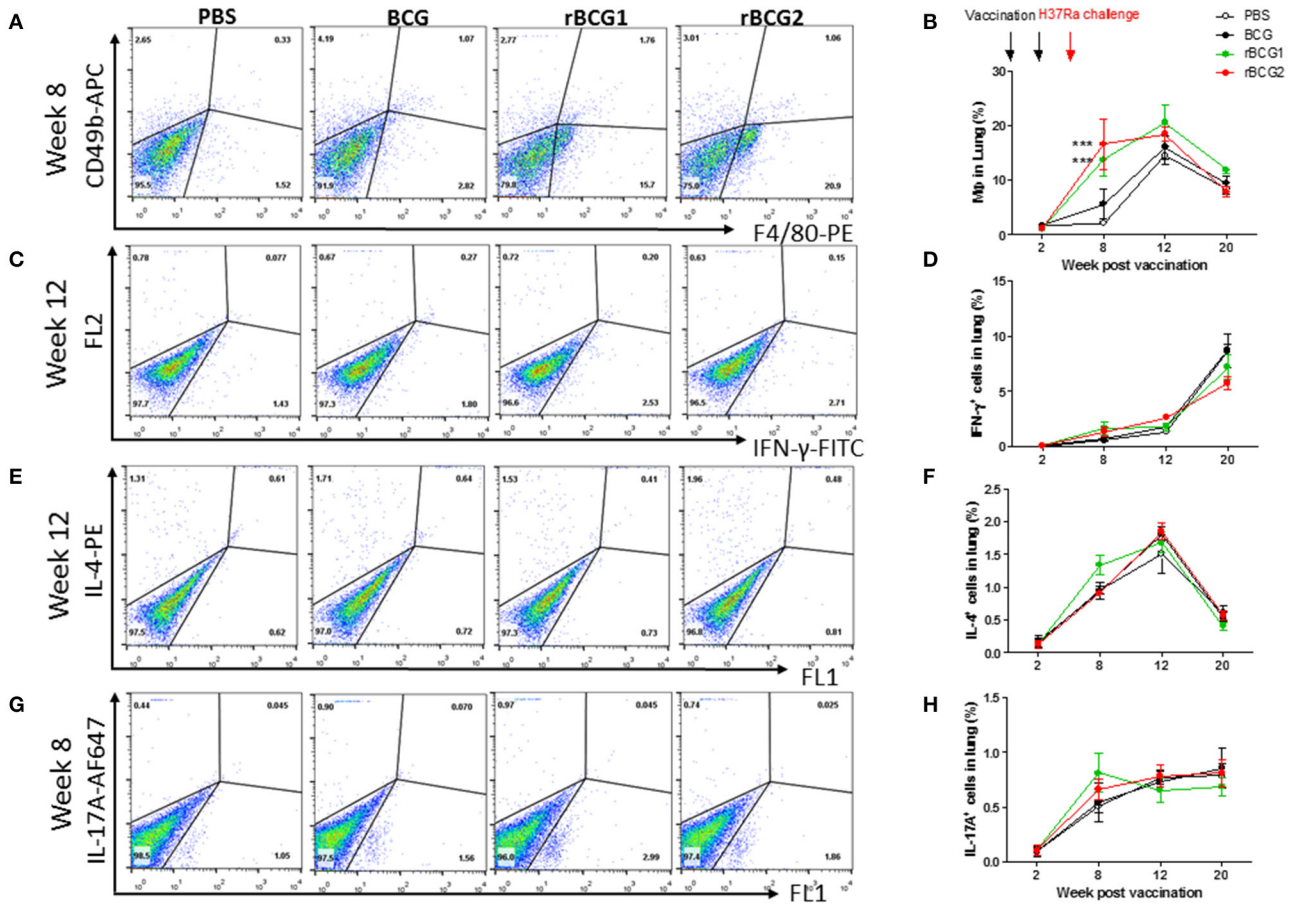

FIGURE 4 | Innate and adaptive immune cell profiles pulsed with tuberculosis-specific peptides from mice immunized with BCG, rBCG1, or rBCG2. C57BL/6 mice were immunized with BCG, rBCG1 or rBCG2 at weeks 0 and 2, and then challenged with H37Ra at week 4 ($n = 6$–7, in two independent experiments). At 2, 8, 12, and 20 weeks, the mice were sacrificed, and lungs were homogenized to single-cell suspensions. The cells were stimulated with tuberculosis-specific TB peptides (described in the Materials and Methods) for 68 h and then Golgi-stop for 4 h, stained for surface and intracellular markers, and then subjected to flow cytometry to determine the percentage of cytokine-producing cells within $CD4^+$ T cells. **(A)** Percentage of macrophages ($F4/80^+$ cells) in lung post-vaccination at week 8. **(B)** Percentage of macrophages ($F4/80^+$ cells) in lung post-vaccination at weeks 2–20. **(C)** Percentage of IFN-γ^+ cells in lung post-vaccination at week 12. **(D)** Percentage of IFN-γ^+ cells in lung post-vaccination at weeks 2–20. **(E)** Percentage of IL-4^+ cells in lung post-vaccination at week 12. **(F)** Percentage of IL-4^+ cells in lung post-vaccination at weeks 2–20. **(G)** Percentage of IL-17^+ T cells in lung post-vaccination at week 8. **(H)** Percentage of IL-17^+ T cells in lung post-vaccination at weeks 2–20. Differences among groups were determined by one-way or two-way ANOVA with a Tukey or Bonferroni *post hoc* test (***$P < 0.001$).

before and after H37Ra challenge, at weeks 2, 8, 12, and 20. After conducting surface marker and intracellular staining, FACS was used to analyze immune cell profiles. At week 2, all immune cell levels were very low, with no differences among the four groups (**Figures 4B,D,F,H**). At week 8 (i.e., 4 weeks after H37Ra challenge), macrophage numbers ($F4/80^+$ cells) had increased dramatically in the rBCG1 and rBCG2 vaccination groups compared to the PBS control and BCG groups (**Figures 4A,B**; *$P < 0.05$). There were few NK cells ($CD49b^+$ cells) and resident macrophages in all groups at 2 weeks (data not shown). Increased IFN-γ^+ T cells (**Figures 4C,D**) and IL-$17A^+$ T cells (**Figures 4G,H**) (but not IL-4^+ T cells, **Figures 4E,F**) were also detected in all BCG vaccination groups, but especially in the rBCG1 and rBCG2 groups. Thus, the induced cellular immunity was higher in mice immunized with rBCG1 and rBCG2 compared to parental BCG.

Monocyte Chemoattractant Protein-1 (MCP-1) Is the Dominant Cytokine Produced in Serum Following rBCG1 and rBCG2 Vaccination

Cytokine production was measured for serum and tissue (lung and spleen) using cultured supernatant samples and a multiple cytokine inflammation kit (BD Biosciences). The cytokine detection kit measured all inflammatory cytokines, including TNF-α, IFN-γ, IL-6, IL-10, IL-12, and MCP-1. No cytokines were found in tissue culture supernatant samples (data not shown) as they were below the limit of detection. Interestingly, MCP-1 was the only cytokine detected in serum. MCP-1 increased in the serum of mice immunized with rBCG1 and rBCG2 at 2 and 8 weeks (**Figure 5**; **$P < 0.01$). MCP-1 also increased in the PBS control and BCG groups beginning at week 8 and

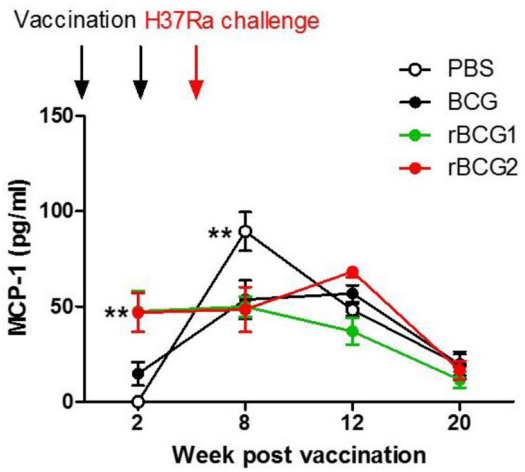

FIGURE 5 | High MCP-1 expression in serum during early-stage recombinant BCG vaccination. C57BL/6 mice were immunized with BCG, rBCG1, and rBCG2 at weeks 0 and 2, and then challenged with H37Ra at week 4 ($n = 6$–7, in two independent experiments). At 2, 8, 12, and 20 weeks, sera were collected, diluted 20,000 times, and assayed using a multiple cytokine kit. Differences among groups were determined by two-way ANOVA with a Bonferroni *post hoc* test (**$P < 0.01$).

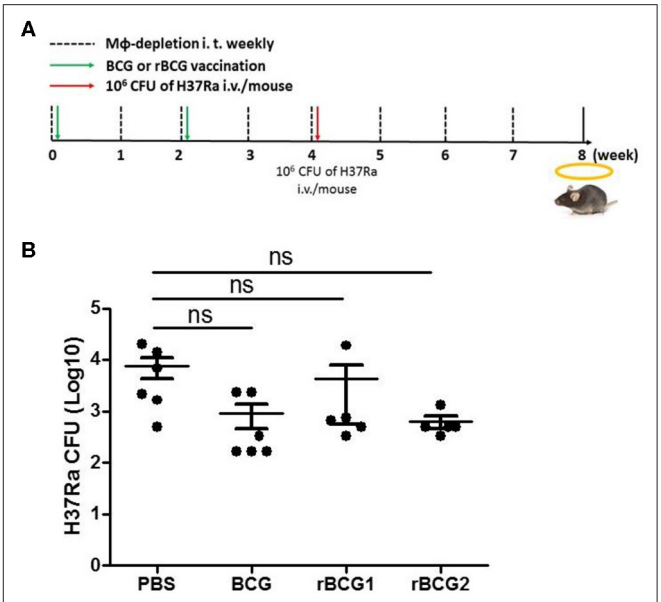

FIGURE 6 | Macrophages are significant for protection against *Mycobacterium* infection. C57BL/6 mice were given a two-dose vaccination of parental BCG, rBCG1, and rBCG2 (5×10^5 CFU per mouse) subcutaneously at weeks 0 and 2 ($n = 6$), and a challenge of H37Ra at week 4; they also received 50 μl of encapsome® (control) or clodrosome® intratracheally weekly for 8 weeks to deplete macrophages. Mice were sacrificed at week 8. **(A)** Timeline for vaccination, challenge, and intratracheal inoculation in mice. **(B)** CFU of bacterial growth in murine lung at week 8. Each plate contained 100 μl of tissue homogenate, and each sample was titrated for two dilutions (5 × and 50×) and repeated in triplicate. Differences among groups were determined using one-way ANOVA with a Tukey *post hoc* test ($P > 0.05$, ns, non-significant).

continuing until week 12. MCP-1 then decreased in all groups at week 20. The high MCP-1 production (weeks 2 and 8) coincided with reduced bacterial loads (**Figure 1A**) and increased lung macrophage levels in the rBCG1 and rBCG2 groups (**Figure 4A**).

Macrophages Are Key Mediators of the Immune Response at the Early Stage of H37Ra Infection

Based on the qPCR results, the increased MCP-1 production, and the higher numbers of macrophages in the lungs, macrophage function is obviously of central importance in the response to MTB infection. To evaluate the role of macrophages early in infection, we attempted to deplete macrophages by administering clodronate-liposomes intratracheally every week following the vaccination and challenge (**Figure 6A**). After 3–4 weeks, we counted and calculated the bacterial load among the control and vaccination groups. The bacterial load of the PBS control group was still high [CFU = (7.611 ± 3.282) × 1,000] (**Figure 6B**); however, the bacterial loads of each of the vaccination groups (BCG [CFU = (0.9167 ± 0.4488) × 1,000], rBCG1 [CFU = (4.283 ± 3.722) × 1,000], rBCG2 [CFU = (0.6333± 0.178) × 1,000]) were dramatically increased (compared with the results shown in **Figure 1A**), but were not significantly different compared to the PBS group (**Figure 6B**, $P > 0.05$, ns). This result suggests that macrophages are the main immune cells involved in protection against *Mycobacterium* infection early on. After macrophage depletion, the mice were no longer protected against the infection.

Increased Levels of Inflammatory M1-Polarized Macrophages Especially in rBCG1 and rBCG2 Vaccinated Mice

Macrophages adapt to the microenvironment and differentiate to express different functional phenotypes. M1 macrophages produce high levels of pro-inflammatory cytokines and have a strong ability to kill pathogens. In contrast, M2 macrophages are involved in clearance of parasites, tissue remodeling and immune regulation (30). We believe that rBCG1 and rBCG2 enhance the ability of M1 macrophages to clear pathogens. Using the remaining tissue samples fixed in paraffin blocks, we sought to compare the levels of M1 macrophages in the vaccination groups, especially in the rBCG1 and rBCG2 groups. We examined paraffin sections collected at week 8 because they showed the highest macrophage numbers and MCP-1 production. After deparaffinization, rehydration, antigen retrieval and blocking, the serial sections were stained to measure inducible nitric oxide synthase (iNOS, M1 macrophage marker) and mannose receptor (MR, M2 macrophage marker). In general, each treatment group expressed different levels of iNOS (**Figure 7A**); however, iNOS-expression was raised dramatically in the rBCG1 and rBCG2 groups (the mean M1 number for rBCG1 was ∼35, for rBCG2 ∼50, compared to PBS ∼18 and BCG ∼22; **Figures 7A,B**,

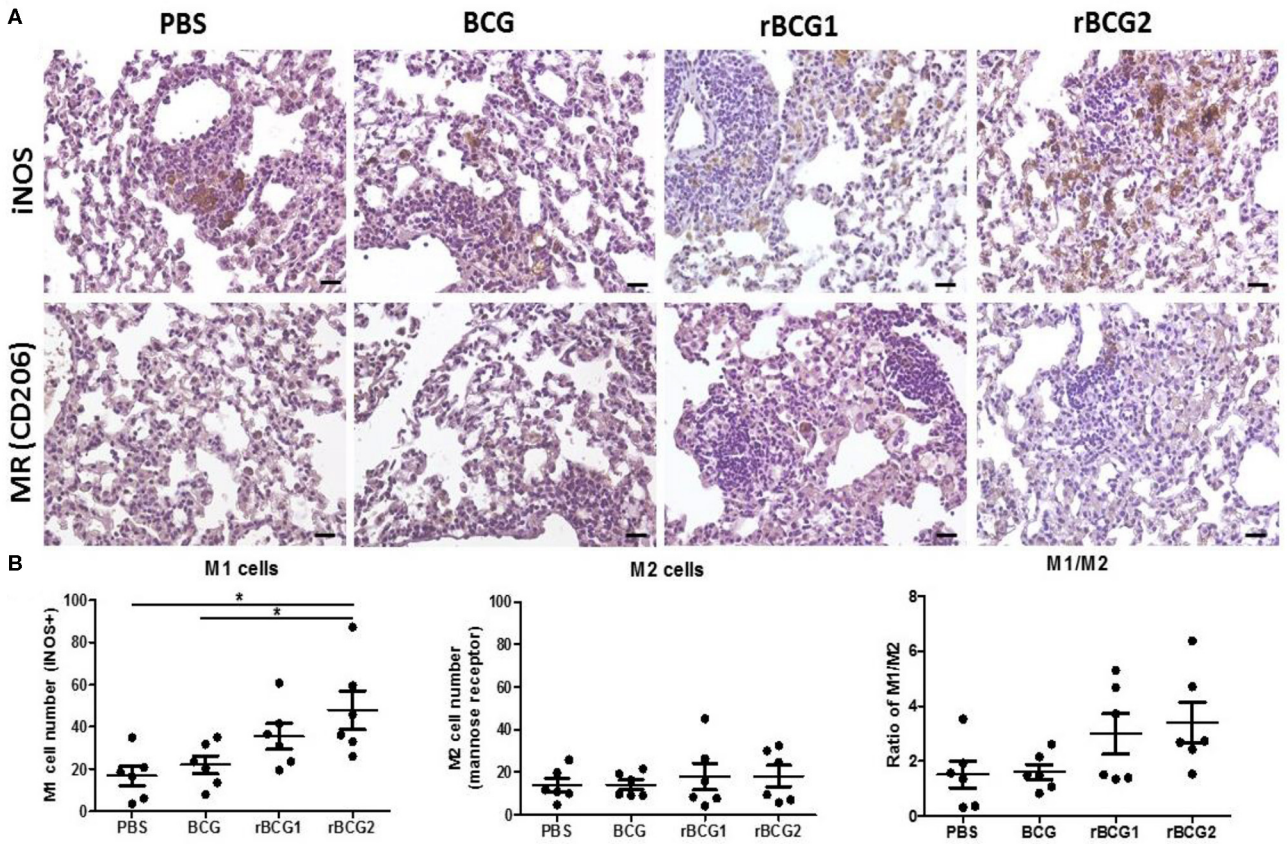

FIGURE 7 | Increased M1-polarized macrophage cells in lung tissue sections from mice vaccinated with rBCG1 or rBCG2. C57BL/6 mice were immunized with BCG, rBCG1, or rBCG2 at weeks 0 and 2, and then challenged with H37Ra at week 4 ($n = 6–7$). At week 8, the mice were sacrificed. One lung from each mouse was homogenized and the other lung was fixed in 3.7% formaldehyde. **(A)** After fixation, lung samples were embedded in paraffin, sectioned, and stained for iNOS (M1 marker) and MR (M2 marker); scale bar = 20 μm. The images are representative of slides from the four groups. **(B)** Lung tissue from six or seven animals per group was examined, and the number of DAB^+ plus hematoxylin-positive cells for each slide, based on five or six random views (each field of view has an area of 8.4×10^3 μm^2), was calculated. Differences among groups were determined by one-way ANOVA with a Tukey *post hoc* test (*$P < 0.05$).

*$P < 0.05$). The expression of MR was similar in all groups (the mean M2 value was ∼15–20, **Figures 7A,B**). These results indicate that, among the tested vaccines, rBCG2 induces the greatest increase in the number of M1 macrophages to clear bacteria in the lungs.

DISCUSSION

Ag85B and CFP-10 are well-known MTB antigens that strongly induce IFN-γ production (31) and enhance T cell proliferation (31, 32). Both proteins are considered good vaccine candidates for tuberculosis. Notably, IL-12 is believed to play an important role in cell-mediated immunity against intracellular infection, primarily by acting on T and NK cells. Recent study findings reveal that IL-12 can activate macrophages potently during intracellular infection, and this activating effect is mediated primarily through its effect on macrophage IFN-γ release (33). Therefore, rBCG2 expressing *Mycobacterium*-specific Ag85B and CFP10 combined with human IL-12 was constructed and investigated in this study. In our previous study, protection efficacy was tested by using splenocytes from vaccine-immunized mice and co-culturing them with *ex vivo* murine bone-marrow-derived macrophages to measure the survival ability of the MTB strains (34). The results showed that rBCG2 induced a strong immune response against MTB infection compared with the parental BCG strain (34). In the present study, we first tested rBCG1 and rBCG2 against the MTB strain H37Ra. We found that rBCG1 and rBCG2 produced a stronger immune response to MTB infection compared to the parental BCG vaccine in mice. Previous *ex vivo* murine bone-marrow-derived macrophage infection experiments with H37Rv also showed that rBCG1 and rBCG2 provide stronger immunity compared to parental BCG (35, 36). In the present study, during early infection, all three tested vaccines (BCG, rBCG1 and rBCG2) inhibited H37Ra growth. However, at week 20, the bacterial load in the BCG group rebounded and increased. In contrast, the bacterial loads in the rBCG1 and rBCG2 groups remained low and nearly undetectable. If the murine age is converted to human age, the period of protection of BCG (20 weeks) found in this study would

be equivalent to 15–20 years; this finding is consistent with that of a previous epidemiologic study of BCG vaccination in humans (37). Thus, rBCG1 and rBCG2 could provide more effective and longer protection against H37Ra compared to parental BCG.

We showed that macrophages, IFN-γ^+ cells and IL-17^+ cells increase soon after vaccination, particularly following rBCG1 and rBCG2 vaccination. Detection of high-level RNA expression of TNF-α, IFN-γ and MCP-1 in lung tissue of mice immunized with rBCG1 and rBCG2 further supports the immuno-protective results for these two candidate vaccines. MCP-1 produced in response to infection recruits monocytes, dendritic cells and T cells to the site of inflammation caused by infection. More importantly, in the present study, MCP-1 was the only cytokine detectable in mouse sera in the early stages following rBCG1 and rBCG2 vaccination. Although MCP-1 expression also increased in the PBS control group at 8 weeks, this finding is expected in the natural course of infection. These results also fit with our finding of increased macrophages in lung tissue following rBCG1 and rBCG2 vaccination. Thus, macrophages are vital to the early host immune response following rBCG1 and rBCG2 vaccination, but not parental BCG vaccination. Furthermore, the bacterial loads in the vaccination groups (BCG, rBCG1, and rBCG2) depleted of alveolar macrophages rose significantly, illustrating the importance of the protective role of macrophages early in MTB infection, which has not been shown previously. Moreover, we also found more inflammatory M1 cells in the two rBCG groups compared to the PBS control and parental BCG groups. This latter finding supports our argument that macrophages play a more important role in early and adaptive immunity to H37Ra than previously believed. Functional M1 macrophage assays will be needed to further clarify their roles. Over the past decades, most efforts to develop TB vaccine candidates have focused on enhancing adaptive immunity. However, in phase 2b clinical trials, while these vaccines have induced strong immune responses, they have been unable to confer significant protection against TB infection (38, 39). Recent studies suggest that trained immunity, particularly involving macrophages, may play a more important role than T cells in vaccine-mediated immunity (40–44), creating a new prospective view for vaccine development. Notably, our results suggest that both innate and adaptive immunity play important roles against *Mycobacterium* infection.

This study had some limitations. First, because our ABSL3 facility was not operational during the initial study period, we first conducted a vaccine efficacy test against the H37Ra strain in an ABSL2 facility. The present study not only focused on pathogenesis but also on the protective effect of vaccines against H37Ra, which is often used in vaccine or drug efficacy evaluation (45–47). To evaluate the efficacy of the new recombinant BCG, both *in vivo* (H37Ra infection, this study) and *ex vivo* models [H37Rv infection (34)] have been performed in our laboratory. Our results suggest that rBCG vaccines can provide good, safe and long-term protection against H37Ra infection. Second, functional M1 macrophage assays will be needed to further clarify the roles of macrophages. Our results showed that rBCG vaccination stimulated the greatest increase in the number of M1 macrophages, presumably to clear bacteria in the lungs, which may be involved in long-term protection.

In summary, this study showed that our rBCG vaccines are safe in SCID mice, and that they induced a significant increase in the number of M1 macrophages. Moreover, to further verify vaccine efficacy, an animal model incorporating a protective assay and challenged with virulent MTB strains should be investigated forthwith. Our results suggest that rBCG1 and rBCG2 may be good candidates as a novel TB vaccine.

DATA AVAILABILITY STATEMENT

All datasets generated for this study are included in the article/supplementary material.

ETHICS STATEMENT

The animal study was reviewed and approved by National Health Research Institutes Institutional Animal Care and Use Committee (NHRI-IACUC).

AUTHOR CONTRIBUTIONS

S-JY designed, performed the experiments, analyzed the data and wrote the manuscript. C-HH, Y-YC, C-WH, C-YC, and J-RC performed and assisted in the experiments. H-YD supervised this work and interpreted the data. All authors contributed to the article and approved the submitted version.

FUNDING

This project was supported by grants from Intramural grants provided by the National Health Research Institutes, Taiwan (IV-107PP-11 and IV-107-SP-09) and extramural grants supported by National Health Research Institute, and Central Government S & T grant, Taiwan (107-0324-01-19-13).

ACKNOWLEDGMENTS

We thank the Core Instrument Center of Pathology, Flow Cytometry, and the Laboratory Animal Center of the National Health Research Institutes for technical assistance and consultation.

REFERENCES

1. WHO. *Tuberculosis.* (2015). Available online at: http://www.whoint/mediacentre/factsheets/fs104/en/ (accessed March 24, 2016).
2. WHO. *Tuberculosis.* (2019). Available online at: https://www.whoint/tb/en/ (accessed March 24, 2020).
3. Calmette A. Preventive vaccination against tuberculosis with BCG. *Proc R Soc Med.* (1931) 24:1481–90. doi: 10.1177/003591573102401109

4. Sterne JA, Rodrigues LC, Guedes IN. Does the efficacy of BCG decline with time since vaccination? *Int J Tuberc Lung Dis.* (1998) 2:200–7.
5. Colditz GA, Brewer TF, Berkey CS, Wilson ME, Burdick E, Fineberg HV, et al. Efficacy of BCG vaccine in the prevention of tuberculosis. Meta-analysis of the published literature. *JAMA.* (1994) 271:698–702. doi: 10.1001/jama.271.9.698
6. Fine PEM. Variation in protection by BCG: implications of and for heterologous immunity. *Lancet.* (1995) 346:1339–45. doi: 10.1016/S0140-6736(95)92348-9
7. Brewer TF. Preventing tuberculosis with Bacillus Calmette-Guérin vaccine: a meta-analysis of the Literature. *Clin Infect Dis.* (2000) 31:S64–7. doi: 10.1086/314072
8. Kremer K, van-der-Werf MJ, Au BK, Anh DD, Kam KM, van-Doorn HR, et al. Vaccine-induced immunity circumvented by typical Mycobacterium tuberculosis Beijing strains. *Emerg Infect Dis.* (2009) 15:335–9. doi: 10.3201/eid1502.080795
9. Lopez B, Aguilar D, Orozco H, Burger M, Espitia C, Ritacco V, et al. A marked difference in pathogenesis and immune response induced by different Mycobacterium tuberculosis genotypes. *Clin Exp Immunol.* (2003) 133:30–7. doi: 10.1046/j.1365-2249.2003.02171.x
10. Tsenova L, Harbacheuski R, Sung N, Ellison E, Fallows D, Kaplan G. BCG vaccination confers poor protection against M. tuberculosis HN878-induced central nervous system disease. *Vaccine.* (2007) 25:5126–32. doi: 10.1016/j.vaccine.2006.11.024
11. Belisle JT, Vissa VD, Sievert T, Takayama K, Brennan PJ, Besra GS. Role of the major antigen of Mycobacterium tuberculosis in cell wall biogenesis. *Science.* (1997) 276:1420–2. doi: 10.1126/science.276.5317.1420
12. Roche PW, Triccas JA, Avery DT, Fifis T, Billman-Jacobe H, Britton WJ. Differential T cell responses to mycobacteria-secreted proteins distinguish vaccination with bacille Calmette-Guerin from infection with Mycobacterium tuberculosis. *J Infect Dis.* (1994) 170:1326–30. doi: 10.1093/infdis/170.5.1326
13. Mustafa AS, Amoudy HA, Wiker HG, Abal AT, Ravn P, Oftung F, et al. Comparison of antigen-specific T-cell responses of tuberculosis patients using complex or single antigens of Mycobacterium tuberculosis. *Scand J Immunol.* (1998) 48:535–43. doi: 10.1046/j.1365-3083.1998.00419.x
14. Aung H, Toossi Z, Wisnieski JJ, Wallis RS, Culp LA, Phillips NB, et al. Induction of monocyte expression of tumor necrosis factor alpha by the 30-kD alpha antigen of Mycobacterium tuberculosis and synergism with fibronectin. *J Clin Invest.* (1996) 98:1261–8. doi: 10.1172/JCI118910
15. Horwitz MA, Harth G, Dillon BJ, Masleša-Galić S. Recombinant bacillus Calmette–Guérin (BCG) vaccines expressing the Mycobacterium tuberculosis 30-kDa major secretory protein induce greater protective immunity against tuberculosis than conventional BCG vaccines in a highly susceptible animal model. *Proc Natl Acad Sci USA.* (2000) 97:13853–8. doi: 10.1073/pnas.250480397
16. Horwitz MA, Harth G. A new vaccine against tuberculosis affords greater survival after challenge than the current vaccine in the Guinea pig model of pulmonary tuberculosis. *Infect Immun.* (2003) 71:1672–9. doi: 10.1128/IAI.71.4.1672-1679.2003
17. Prendergast KA, Counoupas C, Leotta L, Eto C, Bitter W, Winter N, et al. The Ag85B protein of the BCG vaccine facilitates macrophage uptake but is dispensable for protection against aerosol Mycobacterium tuberculosis infection. *Vaccine.* (2016) 34:2608–15. doi: 10.1016/j.vaccine.2016.03.089
18. Berthet FX, Rasmussen PB, Rosenkrands I, Andersen P, Gicquel B. A Mycobacterium tuberculosis operon encoding ESAT-6 and a novel low-molecular-mass culture filtrate protein (CFP-10). *Microbiology.* (1998) 144 (Pt 11):3195–203. doi: 10.1099/00221287-144-11-3195
19. Pym AS, Brodin P, Brosch R, Huerre M, Cole ST. Loss of RD1 contributed to the attenuation of the live tuberculosis vaccines Mycobacterium bovis BCG and Mycobacterium microti. *Mol Microbiol.* (2002) 46:709–17. doi: 10.1046/j.1365-2958.2002.03237.x
20. Lewis KN, Liao R, Guinn KM, Hickey MJ, Smith S, Behr MA, et al. Deletion of RD1 from mycobacterium tuberculosis mimics bacille calmette-guérin attenuation. *J Infect Dis.* (2003) 187:117–23. doi: 10.1086/345862
21. Dietrich J, Aagaard C, Leah R, Olsen AW, Stryhn A, Doherty TM, et al. Exchanging ESAT6 with TB10.4 in an Ag85B fusion molecule-based tuberculosis subunit vaccine: efficient protection and ESAT6-based sensitive monitoring of vaccine efficacy. *J Immunol.* (2005) 174:6332–9. doi: 10.4049/jimmunol.174.10.6332
22. Larrouy-Maumus G, Layre E, Clark S, Prandi J, Rayner E, Lepore M, et al. Protective efficacy of a lipid antigen vaccine in a guinea pig model of tuberculosis. *Vaccine.* (2017) 35:1395–402. doi: 10.1016/j.vaccine.2017.01.079
23. Wiker HG, Harboe M, Bennedsen J, Closs O. The antigens of Mycobacterium tuberculosis, H37Rv, studied by crossed immunoelectrophoresis. Comparison with a reference system for Mycobacterium bovis, BCG. *Scand J Immunol.* (1988) 27:223–39. doi: 10.1111/j.1365-3083.1988.tb02342.x
24. Closs O, Harboe M, Axelsen NH, Bunch-Christensen K, Magnusson M. The antigens of Mycobacterium bovis, strain BCG, studied by crossed immunoelectrophoresis: a reference system. *Scand J Immunol.* (1980) 12:249–63. doi: 10.1111/j.1365-3083.1980.tb00065.x
25. O'Donnell MA, Aldovini A, Duda RB, Yang H, Szilvasi A, Young RA, et al. Recombinant Mycobacterium bovis BCG secreting functional interleukin-2 enhances gamma interferon production by splenocytes. *Infect Immun.* (1994) 62:2508–14. doi: 10.1128/IAI.62.6.2508-2514.1994
26. Murray PJ, Aldovini A, Young RA. Manipulation and potentiation of antimycobacterial immunity using recombinant bacille Calmette-Guérin strains that secrete cytokines. *Proceedings of the National Academy of Sciences.* (1996) 93:934. doi: 10.1073/pnas.93.2.934
27. Lin CW, Su IJ, Chang JR, Chen YY, Lu JJ, Dou HY. Recombinant BCG coexpressing Ag85B, CFP10, and interleukin-12 induces multifunctional Th1 and memory T cells in mice. *Apmis.* (2012) 120:72–82. doi: 10.1111/j.1600-0463.2011.02815.x
28. Dormans J, Burger M, Aguilar D, Hernandez-Pando R, Kremer K, Roholl P, et al. Correlation of virulence, lung pathology, bacterial load and delayed type hypersensitivity responses after infection with different Mycobacterium tuberculosis genotypes in a BALB/c mouse model. *Clin Exp Immunol.* (2004) 137:460–8. doi: 10.1111/j.1365-2249.2004.02551.x
29. Fett C, Zhao J, Perlman S. Measurement of CD8 and CD4 T cell responses in mouse lungs. *Bio-protocol.* (2014) 4:e1083. doi: 10.21769/BioProtoc.1083
30. Martinez FO, Gordon S. The M1 and M2 paradigm of macrophage activation: time for reassessment. *F1000Prime Reports.* (2014) 6:13. doi: 10.12703/P6-13
31. Arend SM, Andersen P, van Meijgaarden KE, Skjøt RLV, Subronto YW, van Dissel JT, et al. Detection of active tuberculosis infection by T cell responses to early-secreted antigenic target 6-kDa protein and culture filtrate protein 10. *J Infect Dis.* (2000) 181:1850–4. doi: 10.1086/315448
32. Arend SM, Geluk A, van Meijgaarden KE, van Dissel JT, Theisen M, Andersen P, et al. Antigenic equivalence of human T-Cell responses to Mycobacterium tuberculosis-specific RD1-encoded protein antigens ESAT-6 and culture filtrate protein 10 and to mixtures of synthetic peptides. *Infect Immun.* (2000) 68:3314–21. doi: 10.1128/IAI.68.6.3314-3321.2000
33. Xing Z, Zganiacz A, Santosuosso M. Role of IL-12 in macrophage activation during intracellular infection: IL-12 and mycobacteria synergistically release TNF-α and nitric oxide from macrophages via IFN-γ induction. *J Leukoc Biol.* (2000) 68:897–902. doi: 10.1189/jlb.68.6.897
34. Chen YY, Lin CW, Huang WF, Chang JR, Su IJ, Hsu CH, et al. Recombinant bacille Calmette–Guerin coexpressing Ag85b, CFP10, and interleukin-12 elicits effective protection against Mycobacterium tuberculosis. *J Microbiol Immunol Infect.* (2017) 50:90–6. doi: 10.1016/j.jmii.2014.11.019
35. Hu Z, Wong KW, Zhao HM, Wen HL, Ji P, Ma H, et al. Sendai virus mucosal vaccination establishes lung-resident memory CD8 T cell immunity and boosts BCG-primed protection against TB in mice. *Mol Ther.* (2017) 25:1222–33. doi: 10.1016/j.ymthe.2017.02.018
36. Moguche AO, Musvosvi M, Penn-Nicholson A, Plumlee CR, Mearns H, Geldenhuys H, et al. Antigen availability shapes T cell differentiation and function during tuberculosis. *Cell Host Microbe.* (2017) 21:695–706.e5. doi: 10.1016/j.chom.2017.05.012
37. Colditz GA, Brewer TF, Berkey CS, et al. Efficacy of bcg vaccine in the prevention of tuberculosis: Meta-analysis of the published literature. *JAMA.* (1994) 271:698–702. doi: 10.1001/jama.1994.03510330076038
38. Nemes E, Geldenhuys H, Rozot V, Rutkowski KT, Ratangee F, Bilek N, et al. Prevention of M. tuberculosis Infection with H4:IC31 Vaccine or BCG Revaccination. *N Engl J Med.* (2018) 379:138–49. doi: 10.1056/NEJMoa1714021
39. Tameris MD, Hatherill M, Landry BS, Scriba TJ, Snowden MA, Lockhart S, et al. Safety and efficacy of MVA85A, a new tuberculosis vaccine, in infants

previously vaccinated with BCG: a randomised, placebo-controlled phase 2b trial. *Lancet.* (2013) 381:1021–8. doi: 10.1016/S0140-6736(13)60177-4
40. Kaufmann E, Sanz J, Dunn JL, Khan N, Mendonça LE, Pacis A, et al. BCG educates hematopoietic stem cells to generate protective innate immunity against tuberculosis. *Cell.* (2018) 172:176–90.e19. doi: 10.1016/j.cell.2017.12.031
41. Cheng SC, Quintin J, Cramer RA, Shepardson KM, Saeed S, Kumar V, et al. mTOR- and HIF-1α-mediated aerobic glycolysis as metabolic basis for trained immunity. *Science.* (2014) 345:1250684. doi: 10.1126/science.1250684
42. Yoshida K, Maekawa T, Zhu Y, Renard-Guillet C, Chatton B, Inoue K, et al. The transcription factor ATF7 mediates lipopolysaccharide-induced epigenetic changes in macrophages involved in innate immunological memory. *Nat Immunol.* (2015) 16:1034–43. doi: 10.1038/ni.3257
43. Arts RJW, Carvalho A, La Rocca C, Palma C, Rodrigues F, Silvestre R, et al. Immunometabolic pathways in BCG-induced trained immunity. *Cell Rep.* (2016) 17:2562–71. doi: 10.1016/j.celrep.2016.11.011
44. Kleinnijenhuis J, Quintin J, Preijers F, Benn CS, Joosten LAB, Jacobs C, et al. Long-lasting effects of BCG vaccination on both heterologous Th1/Th17 responses and innate trained immunity. *J Innate Immun.* (2014) 6:152–8. doi: 10.1159/000355628
45. Gupta N, Garg S, Vedi S, Kunimoto DY, Kumar R, Agrawal B. Future path toward TB vaccine development: boosting BCG or re-educating by a new subunit vaccine. *Front Immunol.* (2018) 9:2371. doi: 10.3389/fimmu.2018.02371
46. Kim BJ, Kim BR, Kook YH, Kim BJ. A temperature sensitive Mycobacterium paragordonae induces enhanced protective immune responses against mycobacterial infections in the mouse model. *Sci Rep.* (2017) 7:15230. doi: 10.1038/s41598-017-15458-7
47. Khalil ZG, Hill TA, De Leon Rodriguez LM, Lohman RJ, Hoang HN, Reiling N, et al. Structure-activity relationships of wollamide cyclic hexapeptides with activity against drug-resistant and intracellular Mycobacterium tuberculosis. *Antimicrob Agents Chemother.* (2019) 3:e01773. doi: 10.1128/AAC.01773-18

Conflict of Interest: The authors declare that the research was conducted in the absence of any commercial or financial relationships that could be construed as a potential conflict of interest.

frontiers in Immunology

CORRECTION
published: 30 March 2021
doi: 10.3389/fimmu.2021.669616

Corrigendum: Activation of M1 Macrophages in Response to Recombinant TB Vaccines With Enhanced Antimycobacterial Activity

Shiu-Ju Yang[1], *Yih-Yuan Chen*[2], *Chih-Hao Hsu*[1], *Chia-Wei Hsu*[1], *Chun-Yu Chang*[1], *Jia-Ru Chang*[1] *and Horng-Yunn Dou*[1]*

[1] National Institute of Infectious Diseases and Vaccinology, National Health Research Institutes, Zhunan, Taiwan, [2] Department of Biochemical Science and Technology, National Chiayi University, Chia-Yi, Taiwan

OPEN ACCESS

Edited and reviewed by:
Juraj Ivanyi,
King's College London.
United Kingdom

***Correspondence:**
Horng-Yunn Dou
hydou@nhri.edu.tw

Specialty section:
This article was submitted to Microbial Immunology, a section of the journal Frontiers in Immunology

Received: 19 February 2021
Accepted: 16 March 2021
Published: 30 March 2021

Citation:
Yang S-J, Chen Y-Y, Hsu C-H, Hsu C-W, Chang C-Y, Chang J-R and Dou H-Y (2021) Corrigendum: Activation of M1 Macrophages in Response to Recombinant TB Vaccines With Enhanced Antimycobacterial Activity. Front. Immunol. 12:669616. doi: 10.3389/fimmu.2021.669616

Keywords: recombinant Bacille Calmette–Guérin, *Mycobacterium tuberculosis*, innate immunity, macrophage, vaccine

A Corrigendum on

Activation of M1 Macrophages in Response to Recombinant TB Vaccines With Enhanced Antimycobacterial Activity

By Shiu-Ju Yang, Yih-Yuan Chen, Chih-Hao Hsu, Chia-Wei Hsu, Chun-Yu Chang, Jia-Ru Chang, Horng-Yunn Dou (2020) Front. Immunol. 23 June 2020 doi: 10.3389/fimmu.2020.01298

In the original article, there was a mistake in **Figure 4G**. When analyzing the original data, the authors mistakenly took raw data of the second image of 4G, which caused the third and second images to be duplicated. The corrected **Figure 4** appears below.

The authors apologize for this error and state that this does not change the scientific conclusions of the article in any way. The original article has been updated.

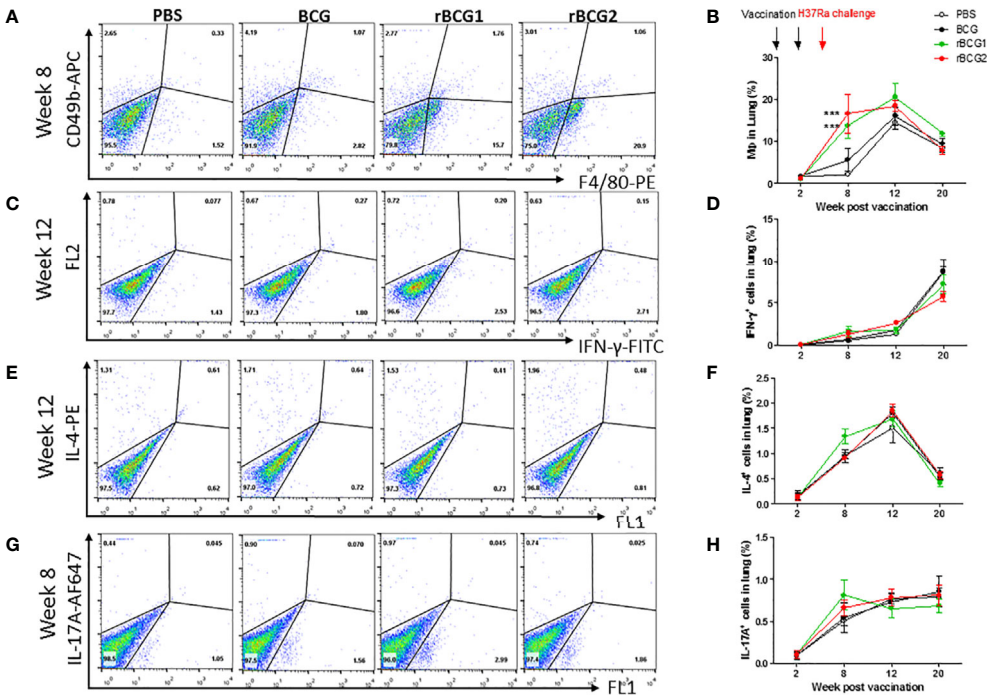

FIGURE 4 | Innate and adaptive immune cell profiles pulsed with tuberculosis-specific peptides from mice immunized with BCG, rBCG1, or rBCG2. C57BL/6 mice were immunized with BCG, rBCG1 or rBCG2 at weeks 0 and 2, and then challenged with H37Ra at week 4 (n = 6 to 7, in two independent experiments). At 2, 8, 12, and 20 weeks, the mice were sacrificed, and lungs were homogenized to single-cell suspensions. The cells were stimulated with tuberculosis-specific TB peptides (described in the Materials and Methods) for 68 h and then Golgi-stop for 4 h, stained for surface and intracellular markers, and then subjected to flow cytometry to determine the percentage of cytokine-producing cells within $CD4^+$ T cells. **(A)** Percentage of macrophages ($F4/80^+$ cells) in lung post-vaccination at week 8. **(B)** Percentage of macrophages ($F4/80^+$ cells) in lung post-vaccination at weeks 2 to 20. **(C)** Percentage of IFN-γ^+ cells in lung post-vaccination at week 12. **(D)** Percentage of IFN-γ^+ cells in lung post-vaccination at weeks 2 to 20. **(E)** Percentage of IL-4^+ cells in lung post-vaccination at week 12. **(F)** Percentage of IL-4^+ cells in lung post-vaccination at weeks 2 to 20. **(G)** Percentage of IL-17^+ T cells in lung post-vaccination at week 8. **(H)** Percentage of IL-17^+ T cells in lung post-vaccination at weeks 2 to 20. Differences among groups were determined by one-way or two-way ANOVA with a Tukey or Bonferroni *post hoc* test (***$P < .001$).

frontiers in Immunology

OPINION
published: 07 July 2020
doi: 10.3389/fimmu.2020.01465

Are There Sex-Specific Differences in Response to Adjunctive Host-Directed Therapies for Tuberculosis?

Noton K. Dutta[1]* *and Bianca E. Schneider*[2]

[1] Center for Tuberculosis Research, Department of Medicine, Johns Hopkins University School of Medicine, Baltimore, MD, United States, [2] Junior Research Group Coinfection, Priority Research Area Infections, Research Center Borstel - Leibniz Lung Center, Borstel, Germany

Keywords: ***Mycobacterium tuberculosis*, tuberculosis, host directed therapy, statins, treatment outcome, sex-specific differences, male-bias, mouse models**

INTRODUCTION

Tuberculosis (TB) appears to afflict men more than women, but the underlying reasons for this disparity and whether there are sex-based differences in TB treatment responses are unknown. Based on a knowledge gap in previously published studies, a pertinent research question is being asked: Are there sex-specific differences in response to adjunctive host-directed therapy (HDT) for TB? Using statins as a prototype, we also highlight the incorporation of appropriately designed studies on sex differences in HDT.

There is an important need for new drugs to help control the TB pandemic, counteract the emergence of drug resistance worldwide, and supplement the limited number of antimicrobials that are currently in the TB drug discovery pipeline. Therefore, the repurposing of existing drugs, including host-directed therapies (1), is being investigated as a means of accelerating the development of novel TB regimens in the clinical setting. We hypothesize that there is a sex difference in responses to adjunctive HDT because males are more susceptible to TB and various HDTs may have differential, sex-dependent impacts on inflammation. This question is important in the context of ongoing clinical trials that are investigating the potential roles of various HDTs as adjunctive therapy for TB, including the lipid-lowering agents, statins (StAT-TB, NCT03882177), the hypoglycemic agent, metformin (CTRI/2018/01/011176), and the anticancer agent, imatinib (IMPACT-TB, NCT03891901). Mayer-Barber and colleagues reported that the 5-lipoxygenase inhibitor zileuton, which is FDA-approved for the treatment of asthma, increased prostaglandin E2 (PGE2) levels in the lungs of *Mycobacterium tuberculosis*-infected mice and prevent acute mortality, while decreasing pulmonary bacillary loads, tissue necrosis, and type I IFN levels (2). Data from Pace et al. suggested that zileuton is less effective in males, prompting consideration of sex-based differences in leukotriene biosynthesis blockade for respiratory and cardiovascular diseases (3).

INCREASED TB INCIDENCE IN MEN

Despite over a century of research, TB still kills ∼1.5 million people every year (4). Globally, TB notification data show a male-to-female ratio of bacteriologically-confirmed pulmonary TB ranging from 1.2 in Ethiopia to 4.9 in Viet Nam (4), but the underlying reasons for this male bias remain elusive. Presumably, both gender- and sex-related factors contribute to higher TB rates in men. Socioeconomic and cultural factors influence exposure and help-seeking behavior, and confounding factors, such as smoking, alcohol and drug use, which are known risk factors for TB, are more common in men (5, 6). However, these factors are unlikely to explain the consistent global male bias, and biological

OPEN ACCESS

Edited by:
Rogelio Hernandez Pando, Instituto Nacional de Ciencias Médicas y Nutrición Salvador Zubirán (INCMNSZ), Mexico

Reviewed by:
Oscar Bottasso, National University of Rosario, Argentina
Haiko Schurz, Stellenbosch University, South Africa

***Correspondence:**
Noton K. Dutta
ndutta1@jhmi.edu

Specialty section:
This article was submitted to Microbial Immunology, a section of the journal Frontiers in Immunology

Received: *08 April 2020*
Accepted: *05 June 2020*
Published: *07 July 2020*

Citation:
Dutta NK and Schneider BE (2020) Are There Sex-Specific Differences in Response to Adjunctive Host-Directed Therapies for Tuberculosis? Front. Immunol. 11:1465. doi: 10.3389/fimmu.2020.01465

differences between the sexes likely affect susceptibility to mycobacterial infection and disease outcome (7, 8). Despite the well-known sex-based differences in human TB incidence rates, due to practical considerations, most animal studies have either used only one sex or do not report the sex of the animals at all.

THE ROLE OF BIOLOGICAL SEX IN TB

Recent data suggest that male C57BL/6 mice are less able to control *M. tuberculosis* infection relative to their female counterparts due to impaired innate and adaptive immune responses, as manifested by increased lung bacillary burdens and accelerated death (9). Divergent innate immune priming events occurring early in an infection influence both the bacterial load "set-point" and the ensuing adaptive immune response (10).

Innate recognition of pathogens and the induction of inflammatory and antimicrobial immune responses differ between the sexes (11). Factors that have been shown to account for the sex-based disparity in immune responses include genetic factors and hormonal mediators. Estrogen was shown to boost the ability of macrophages to kill *Streptococcus pneumoniae* (12), and the antimicrobial activity of peritoneal macrophages from female mice was significantly more potent against *Mycobacterium intracellulare* than that of male mice (13). IFNγ, a critical cytokine mainly produced by $CD4^+$ and $CD8^+$ T cells, increases the anti-bacterial effector functions of macrophages (14). Invariant natural killer T (iNKT) cells are a subset of T cells that bridge innate and adaptive immunity, recognize *M. tuberculosis*-infected macrophages, produce IFNγ, and kill intracellular bacteria (15). Estradiol induces iNKT cells from female mice to produce more IFNγ than their male counterparts (16). Moreover, IFNγ production by iNKT cells is impaired by female castration or genetic ablation of the estradiol receptor, and the normal phenotype is restored by estradiol injection (16, 17) In contrast, testosterone was shown to exert anti-inflammatory effects in macrophages and other innate immune cells that express the androgen receptor (AR), by inhibiting pro-inflammatory factors such as TNF-α and nitric oxide (NO), and increasing the synthesis of interleukin (IL)-10 (18). Male castration also increases TNF-α secretion in macrophages (19). These results illustrate the general, but probably simplistic, perception of estradiol as an immunity-sustaining or immunity-enhancing mediator, and of testosterone as a mediator that inhibits the immune response. Similarly, male mice are more susceptible to TB than female mice, which can be prevented by male castration (20), suggesting that testosterone could be a TB susceptibility factor. Sex hormones not only regulate innate but also adaptive responses. Generally, females show higher T cell activity including the production of T_h1-type cytokines such as IFNγ, and greater antibody responses than males (11). Differences in adaptive immunity might contribute to the impaired long-term containment of *M. tuberculosis* observed in mice (9, 20, 21). Indeed, we recently showed that increased male susceptibility in *M. tuberculosis* infection is associated with reduced B cell follicle formation in the lung (21).

Sex differences in TB can be mediated by more than hormonal influence. The X chromosome expresses a number of immune-related genes, as well as a number of immune-associated microRNAs (11). Females have two X chromosomes and benefit from a genetic diversity due to cellular mosaicism and genes escaping X chromosome inactivation which is often advantageous because it ameliorates the deleterious effects of X-linked mutations. Thus, sex disparity in TB may be a result of both hormonal and genetic influences.

STATINS AS ADJUNCTIVE HDT FOR TB

In addition to their cholesterol-lowering properties, β-Hydroxy β-methylglutaryl-CoA (HMG-CoA) reductase inhibitors (statins) have been shown to have broad anti-inflammatory and immunomodulatory properties (22, 23), and their use has been associated with significantly decreased risk of TB (24). Statins have been shown to have antimicrobial and immunomodulatory activity in mouse models of infection against intracellular pathogens, including *Salmonella enterica* and *Chlamydia pneumoniae*. Statins' mode of action in antimicrobial therapy is centered on controlling the infection rate in macrophages and monocytes. Mature macrophages respond to diverse environmental signals by expressing many functional phenotypes, from the *classical* phenotype (M1, proinflammatory) to the *alternative* phenotype (M2, anti-parasitic, immunoregulatory). Early secreted antigenic target of 6-kDa of *M. tuberculosis* induces M1 phenotype in the early stage and then polarizes to M2 phenotype in the later stage of TB infection (25). Heat-Shock Protein 16.3 of *M. tuberculosis* induces M2 polarization in the mouse bone marrow-derived macrophage model via CCRL2/CX3CR1 and may be mediated by the AKT/ ERK/p38-MAPK signaling pathway. In fact, adoptive transfer of M2 macrophages is effective in controlling TB infection apart from its role in controlling tissue damage (26)

In a recent publication (27), we screened eight different statins for a cytotoxic effect, anti-tubercular activity, synergy with first-line drugs in macrophages, pharmacokinetics, and adjunctive bactericidal activity in two different mouse models as a potential adjunctive therapy to existing first-line TB drugs (27). Pravastatin exhibited the most favorable therapeutic index *in vitro* and better anti-TB activity in the standard BALB/c mouse model and in the C3HeB/FeJ mouse model of human-like necrotic TB lung granulomas (27). Previous studies already demonstrated that pravastatin modulated phagosomal maturation characteristics in macrophages via phenocopying macrophage activation, and its use as an adjunctive agent in chronically infected mice altered lung and peripheral immune responses (27, 28). We also found that simvastatin adjunctive therapy enhanced the first-line TB regimen's antimicrobial activity and shortened the time required to achieve cure in a BALB/c mouse model of chronic TB infection (29). Bruiners et al. recently demonstrated that simvastatin inhibits mechanistic target of rapamycin complex 1 (mTORC1) activity and regulates transcription factor EB (TFEB) nuclear translocation to induce autophagy and lysosomal biogenesis (30). In addition, statins show synergy with the key sterilizing drug,

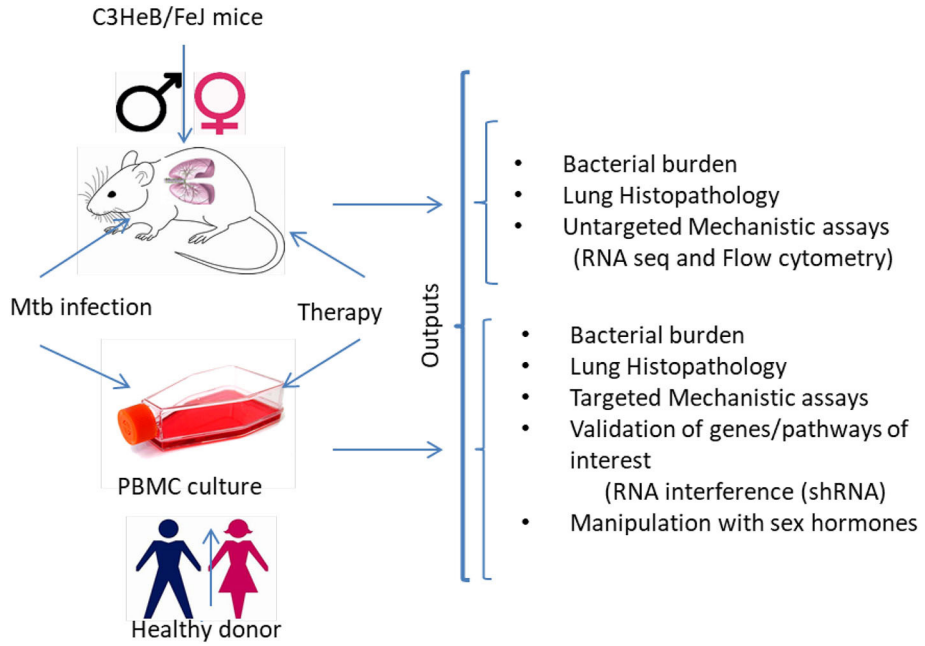

FIGURE 1 | Experimental sketch for preclinical examination of sex-differences in responsiveness to HDTs. The experimental strategy would help to determine sex-based differences in clinical, microbiological, immunological and histopathological outcomes in *M. tuberculosis* infected (i) C3HeB/FeJ male and female mice and (ii) human monocyte-derived macrophages from healthy male and female donors before and after treatment with HDTs. Several untargeted and targeted approaches can be used to investigate the molecular mechanisms associated with the sex-specific anti-TB activity of HDTs. MDMs, monocyte-derived macrophages; shRNA, Small hairpin RNA.

rifampin. Retrospective cohort studies found that statin use was associated with a reduced incidence of active TB disease (31, 32). However, studies focusing on anti-TB effect of statin on the basis of sex of the patients are lacking. Also, the preclinical studies were conducted exclusively in female mice, and it is unknown whether the adjunctive, host-directed anti-TB properties of statins are sex-specific, which is an important consideration for their potential clinical utility.

SEX DIFFERENCES IN THE EFFECTIVENESS OF STATINS

Previous studies (33) have shown sex-based differences for statins with respect to mortality following myocardial infarction (34) and in reducing the risk of Alzheimer's disease (35). These effects may result from differences in drug metabolism, but hormonal effects have not been explored. In some animal studies, the simvastatin metabolism rate was found to be considerably higher in males than in females (36); this statin might, therefore, be expected to have a greater clinical effect in males. This hypothesis was not confirmed in studies that enrolled human volunteers, while, in contrast, a lower rate of simvastatin and lovastatin metabolism was observed in men than in women (37). Moreover, several epidemiological studies have reported greater statin-induced reductions in both LDL and total cholesterol in women than in men (38).

CONCLUSIONS AND FUTURE DIRECTIONS

It has already been established that sex must be considered in preclinical studies, although clearly defined "go/no-go" endpoints to justify further testing of various HDT agents in clinical trials have yet to be defined. It is unknown if the anti-TB activity of statins and other promising HDTs are sex specific. The study of animals and cells of both sexes is essential to include preclinical study designs that will control drug exposure, efficacy, metabolism, and immune response variabilities on HDT for TB. Here, we propose to understand if sex influences the adjunctive anti-TB activity and immune responses of HDTs in: (i) a murine model of chronic TB infection with human-like necrotic lung granulomas; and (ii) *ex vivo* infection of human monocyte-derived macrophages (MDMs) (**Figure 1**). *M. tuberculosis* residing in necrotic mouse lung lesions may be more akin to persisters in human lesions with a reduced response to direct-acting anti-TB drugs; further, these areas represent relative pharmacological sanctuaries. Because of these favorable features, we and other groups have begun to use C3HeB/FeJ mice to test the efficacy of various antitubercular regimens and novel anti-inflammatory therapies (27, 39). An MDM system was chosen because macrophages are the key cell type harboring *M. tuberculosis* during infection and because this model is amenable to testing under multiple, controlled perturbations. Moreover, circulating monocytes are natural precursors of lung tissue-resident macrophages. In addition,

using primary cells, researchers will be able to validate the key findings *in vivo* in macrophages from both males and females by applying RNA interference technology. Downstream "omics" data will provide the opportunity to investigate the mechanisms underlying sex-based differences in host control of *M. tuberculosis* infection, as well as potential differences in response to standard antitubercular therapy and HDT between the sexes. Such results will improve the predictive value of animal models to evaluate treatment efficacy by HDT agents with respect to variables such as sex and potential clinical utility of particular immunomodulators. The identification of the biological pathways underlying sex differences in HDTs for TB will play an essential role in the development of more effective personalized healthcare. One unanswered question is to what extent the mouse model will be predictive of HDTs for TB in humans.

AUTHOR CONTRIBUTIONS

ND and BS have made substantial, direct and intellectual contribution to the work, critically reading an earlier version of this manuscript, and approved it for publication. All authors contributed to the article and approved the submitted version.

REFERENCES

1. Frank DJ, Horne DJ, Dutta NK, Shaku MT, Madensein R, Hawn TR, et al. Remembering the host in tuberculosis drug development. *J Infect Dis*. (2019) 219:1518–24. doi: 10.1093/infdis/jiy712
2. Mayer-Barber KD, Andrade BB, Oland SD, Amaral EP, Barber DL, Gonzales J, et al. Host-directed therapy of tuberculosis based on interleukin-1 and type I interferon crosstalk. *Nature*. (2014) 511:99–103. doi: 10.1038/nature13489
3. Pace S, Pergola C, Dehm F, Rossi A, Gerstmeier J, Troisi F, et al. Androgen-mediated sex bias impairs efficiency of leukotriene biosynthesis inhibitors in males. *J Clin Invest*. (2017) 127:3167–76. doi: 10.1172/JCI92885
4. WHO. *Global Tuberculosis Report 2019*. Geneva: World Health Organization. (2019).
5. Neyrolles O, Quintana-Murci L. Sexual inequality in tuberculosis. *PLoS Med*. (2009) 6:e1000199. doi: 10.1371/journal.pmed.1000199
6. Hargreaves JR, Boccia D, Evans CA, Adato M, Petticrew M, Porter JD. The social determinants of tuberculosis: from evidence to action. *Am J Public Health*. (2011) 101:654–62. doi: 10.2105/AJPH.2010.199505
7. Nhamoyebonde S, Leslie A. Biological differences between the sexes and susceptibility to tuberculosis. *J Infect Dis*. (2014) 209 (Suppl. 3):S100–106. doi: 10.1093/infdis/jiu147
8. Hertz D, Schneider B. Sex differences in tuberculosis. *Semin Immunopathol*. (2019) 41:225–37. doi: 10.1007/s00281-018-0725-6
9. Dibbern J, Eggers L, Schneider BE. Sex differences in the C57BL/6 model of *Mycobacterium tuberculosis* infection. *Sci Rep*. (2017) 7:10957. doi: 10.1038/s41598-017-11438-z
10. Chamekh M, Deny M, Romano M, Lefevre N, Corazza F, Duchateau J, et al. Differential susceptibility to infectious respiratory diseases between males and females linked to sex-specific innate immune inflammatory response. *Front Immunol*. (2017) 8:1806. doi: 10.3389/fimmu.2017.01806
11. Klein SL, Flanagan KL. Sex differences in immune responses. *Nat Rev Immunol*. (2016) 16:626–38. doi: 10.1038/nri.2016.90
12. Yang Z, Huang YC, Koziel H, De Crom R, Ruetten H, Wohlfart P, et al. Female resistance to pneumonia identifies lung macrophage nitric oxide synthase-3 as a therapeutic target. *Elife*. (2014) 3:e03711. doi: 10.7554/eLife.03711.013
13. Yamamoto Y, Tomioka H, Sato K, Saito H, Yamada Y, Setogawa T. Sex differences in the susceptibility of mice to infection induced by Mycobacterium intracellulare. *Am Rev Respir Dis*. (1990) 142:430–3. doi: 10.1164/ajrccm/142.2.430
14. Kak G, Raza M, Tiwari BK. Interferon-gamma (IFN-gamma): exploring its implications in infectious diseases. *Biomol Concepts*. (2018) 9:64–79. doi: 10.1515/bmc-2018-0007
15. Sada-Ovalle I, Chiba A, Gonzales A, Brenner MB, Behar SM. Innate invariant NKT cells recognize *Mycobacterium tuberculosis*-infected macrophages, produce interferon-gamma, and kill intracellular bacteria. *PLoS Pathog*. (2008) 4:e1000239. doi: 10.1371/journal.ppat.1000239
16. Gourdy P, Araujo LM, Zhu R, Garmy-Susini B, Diem S, Laurell H, et al. Relevance of sexual dimorphism to regulatory T cells: estradiol promotes IFN-gamma production by invariant natural killer T cells. *Blood*. (2005) 105:2415–20. doi: 10.1182/blood-2004-07-2819
17. Janele D, Lang T, Capellino S, Cutolo M, Da Silva JA, Straub RH. Effects of testosterone, 17beta-estradiol, and downstream estrogens on cytokine secretion from human leukocytes in the presence and absence of cortisol. *Ann N Y Acad Sci*. (2006) 1069:168–82. doi: 10.1196/annals.1351.015
18. D'agostino P, Milano S, Barbera C, Di Bella G, La Rosa M, Ferlazzo V, et al. Sex hormones modulate inflammatory mediators produced by macrophages. *Ann N Y Acad Sci*. (1999) 876:426–9. doi: 10.1111/j.1749-6632.1999.tb07667.x
19. Rettew JA, Huet-Hudson YM, Marriott I. Testosterone reduces macrophage expression in the mouse of toll-like receptor 4, a trigger for inflammation and innate immunity. *Biol Reprod*. (2008) 78:432–7. doi: 10.1095/biolreprod.107.063545
20. Bini EI, Mata Espinosa D, Marquina Castillo B, Barrios Payan J, Colucci D, Cruz AF, et al. The influence of sex steroid hormones in the immunopathology of experimental pulmonary tuberculosis. *PLoS ONE*. (2014) 9:e93831. doi: 10.1371/journal.pone.0093831
21. Hertz D, Dibbern J, Eggers L, Von Borstel L, Schneider BE. Increased male susceptibility to *Mycobacterium tuberculosis* infection is associated with smaller B cell follicles in the lungs. *Sci Rep*. (2020) 10:5142. doi: 10.1038/s41598-020-61503-3
22. Hennessy E, Adams C, Reen FJ, O'gara F. Is there potential for repurposing statins as novel antimicrobials? *Antimicrob Agents Chemother*. (2016) 60:5111–21. doi: 10.1128/AAC.00192-16
23. Dutta NK, Karakousis PC. Reply to Hu et al: Could there be detrimental effects of statin adjunctive TB therapy on immune responses? *J Infect Dis*. (2019). doi: 10.1093/infdis/jiz676. [Epub ahead of print].
24. Duan H, Liu T, Zhang X, Yu A, Cao Y. Statin use and risk of tuberculosis: a systemic review of observational studies. *Int J Infect Dis*. (2020) 93:168–74. doi: 10.1016/j.ijid.2020.01.036
25. Refai A, Gritli S, Barbouche MR, Essafi M. *Mycobacterium tuberculosis* virulent factor ESAT-6 drives macrophage differentiation toward the pro-inflammatory M1 phenotype and subsequently switches it to the anti-inflammatory M2 phenotype. *Front Cell Infect Microbiol*. (2018) 8:327. doi: 10.3389/fcimb.2018.00327
26. Pineros AR, Campos LW, Fonseca DM, Bertolini TB, Gembre AF, Prado RQ, et al. M2 macrophages or IL-33 treatment attenuate ongoing *Mycobacterium tuberculosis* infection. *Sci Rep*. (2017) 7:41240. doi: 10.1038/srep41240
27. Dutta NK, Bruiners N, Zimmerman MD, Tan S, Dartois V, Gennaro ML, et al. Adjunctive host-directed therapy with statins improves tuberculosis-related outcomes in mice. *J Infect Dis*. (2019) 221:1079–87. doi: 10.1093/infdis/jiz517
28. Parihar SP, Guler R, Khutlang R, Lang DM, Hurdayal R, Mhlanga MM, et al. Statin therapy reduces the *Mycobacterium tuberculosis* burden in human macrophages and in mice by enhancing autophagy and phagosome maturation. *J Infect Dis*. (2014) 209:754–63. doi: 10.1093/infdis/jit550
29. Dutta NK, Bruiners N, Pinn ML, Zimmerman MD, Prideaux B, Dartois V, et al. Statin adjunctive therapy shortens the duration of TB treatment in mice. *J Antimicrob Chemother*. (2016) 71:1570–7. doi: 10.1093/jac/dkw014
30. Bruiners N, Dutta NK, Guerrini V, Salamon H, Yamaguchi KD, Karakousis PC, et al. The anti-tubercular activity of simvastatin is mediated by cholesterol-dependent regulation of autophagy via the AMPK-mTORC1-TFEB axis. *bioRxiv [Preprint]*. (2020). doi: 10.2139/ssrn.3552811

31. Lai CC, Lee MT, Lee SH, Hsu WT, Chang SS, Chen SC, et al. Statin treatment is associated with a decreased risk of active tuberculosis: an analysis of a nationally representative cohort. *Thorax*. (2016) 71:646–51. doi: 10.1136/thoraxjnl-2015-207052
32. Su VY, Su WJ, Yen YF, Pan SW, Chuang PH, Feng JY, et al. Statin use is associated with a lower risk of TB. *Chest*. (2017) 152:598–606. doi: 10.1016/j.chest.2017.04.170
33. Baigent C, Keech A, Kearney PM, Blackwell L, Buck G, Pollicino C, et al. Efficacy and safety of cholesterol-lowering treatment: prospective meta-analysis of data from 90,056 participants in 14 randomised trials of statins. *Lancet*. (2005) 366:1267–78. doi: 10.1016/S0140-6736(05)67394-1
34. Karp I, Chen SF, Pilote L. Sex differences in the effectiveness of statins after myocardial infarction. *CMAJ*. (2007) 176:333–8. doi: 10.1503/cmaj.060627
35. Zissimopoulos JM, Barthold D, Brinton RD, Joyce G. Sex and race differences in the association between statin use and the incidence of Alzheimer Disease. *JAMA Neurol*. (2017) 74:225–32. doi: 10.1001/jamaneurol.2016.3783
36. Ohtawa M, Uchiyama N. Sex difference in metabolism of simvastatin by rat hepatic microsomes. *Eur J Drug Metab Pharmacokinet*. (1992) 17:175–81. doi: 10.1007/BF03190142
37. Vree TB, Dammers E, Ulc I, Horkovics-Kovats S, Ryska M, Merkx I. Differences between lovastatin and simvastatin hydrolysis in healthy male and female volunteers:gut hydrolysis of lovastatin is twice that of simvastatin. *ScientificWorldJournal*. (2003) 3:1332–43. doi: 10.1100/tsw.2003.121
38. Nakajima K. Sex-related differences in response of plasma lipids to simvastatin: the saitama postmenopausal lipid intervention study. *S-POLIS Group Clin Ther*. (1999) 21:2047–57. doi: 10.1016/S0149-2918(00)87236-7
39. Vilaplana C, Marzo E, Tapia G, Diaz J, Garcia V, Cardona PJ. Ibuprofen therapy resulted in significantly decreased tissue bacillary loads and increased survival in a new murine experimental model of active tuberculosis. *J Infect Dis*. (2013) 208:199–202. doi: 10.1093/infdis/jit152

Conflict of Interest: The authors declare that the research was conducted in the absence of any commercial or financial relationships that could be construed as a potential conflict of interest.

frontiers in Immunology

ORIGINAL RESEARCH
published: 23 July 2020
doi: 10.3389/fimmu.2020.01609

Inhibiting Histone Deacetylases in Human Macrophages Promotes Glycolysis, IL-1β, and T Helper Cell Responses to *Mycobacterium tuberculosis*

Donal J. Cox, Amy M. Coleman, Karl M. Gogan, James J. Phelan, Cilian Ó Maoldomhnaigh, Pádraic J. Dunne, Sharee A. Basdeo† and Joseph Keane†*

Trinity Translational Medicine Institute, St. James's Hospital, Trinity College, The University of Dublin, Dublin, Ireland

OPEN ACCESS

Edited by:
Juraj Ivanyi, King's College London, United Kingdom

Reviewed by:
Martha Torres, Instituto Nacional de Enfermedades Respiratorias, Mexico
Carmen Fernández, Stockholm University, Sweden

***Correspondence:**
Sharee A. Basdeo
basdeos@tcd.ie

†These authors have contributed equally to this work

Specialty section:
This article was submitted to Microbial Immunology, a section of the journal Frontiers in Immunology

Received: *21 February 2020*
Accepted: *16 June 2020*
Published: *23 July 2020*

Citation:
Cox DJ, Coleman AM, Gogan KM, Phelan JJ, Ó Maoldomhnaigh C, Dunne PJ, Basdeo SA and Keane J (2020) Inhibiting Histone Deacetylases in Human Macrophages Promotes Glycolysis, IL-1β, and T Helper Cell Responses to Mycobacterium tuberculosis. Front. Immunol. 11:1609. doi: 10.3389/fimmu.2020.01609

Tuberculosis (TB) is the leading infectious killer in the world. *Mycobacterium tuberculosis* (Mtb), the bacteria that causes the disease, is phagocytosed by alveolar macrophages (AM) and infiltrating monocyte-derived macrophages (MDM) in the lung. Infected macrophages then upregulate effector functions through epigenetic modifications to make DNA accessible for transcription. The metabolic switch to glycolysis and the production of proinflammatory cytokines are key effector functions, governed by epigenetic changes, that are integral to the ability of the macrophage to mount an effective immune response against Mtb. We hypothesised that suberanilohydroxamic acid (SAHA), an FDA-approved histone deacetylase inhibitor (HDACi), can modulate epigenetic changes upstream of the metabolic switch and support immune responses during Mtb infection. The rate of glycolysis in human MDM, infected with Mtb and treated with SAHA, was tracked in real time on the Seahorse XFe24 Analyzer. SAHA promoted glycolysis early in the response to Mtb. This was associated with significantly increased production of IL-1β and significantly reduced IL-10 in human MDM and AM. Since innate immune function directs downstream adaptive immune responses, we used SAHA-treated Mtb-infected AM or MDM in a co-culture system to stimulate T cells. Mtb-infected macrophages that had previously been treated with SAHA promoted IFN-γ, GM-CSF, and TNF co-production in responding T helper cells but did not affect cytotoxic T cells. These results indicate that SAHA promoted the early switch to glycolysis, increased IL-1β, and reduced IL-10 production in human macrophages infected with Mtb. Moreover, the elevated proinflammatory function of SAHA-treated macrophages resulted in enhanced T helper cell cytokine polyfunctionality. These data provide an *in vitro* proof-of-concept for the use of HDACi to modulate human immunometabolic processes in macrophages to promote innate and subsequent adaptive proinflammatory responses.

Keywords: glycolysis, tuberculosis, human alveolar macrophage, T cell, immunomodulation, HDACi, SAHA, Vorinostat

INTRODUCTION

Tuberculosis (TB) is the world's leading infectious killer (1). Current treatment regimens require many months of multiple drugs which are often not completed (2). Moreover, there is a significant rise in the incidence of multi-drug resistant TB, thus there is an urgent need for new therapeutic and vaccine strategies (1).

Mycobacterium tuberculosis (Mtb), the bacteria that causes TB, is phagocytosed by resident alveolar macrophages (AM), and infiltrating monocyte-derived macrophages (MDM) which then upregulate bactericidal effector functions. These effector functions are governed by changes in chromatin structure and gene transcription (3–5). DNA is tightly packed and condensed around histones, which inhibits access to genes. One of the major regulators of gene transcription is the acetylation status of histones which is controlled via two families of enzymes; histone acetyl transferases (HAT) and histone deacetylases (HDAC) (6). In general, acetylation of histones opens the packed DNA to make it accessible for transcription and therefore active, whereas HDAC close the DNA by removing acetyl groups from histones. Mtb infection can target host HDAC to modulate the immune response (7, 8). In keeping, HDAC inhibitors (HDACi) are being explored for their ability to modulate the development of TB (3, 9, 10).

We have previously established that glycolytic metabolism has a critical role in human AM function during Mtb infection (11). Metabolic changes and the switch to a pro-inflammatory macrophage phenotype are governed by epigenetics (12–16), and since previous studies have suggested that HDACi modulate macrophage function (3, 17–22), we sought to determine whether the pan HDACi suberanilohydroxamic acid (SAHA; also known as Vorinostat) could modulate macrophage function during Mtb infection.

Macrophages can direct memory T cell responses in the lung. T cells, activated in the lymph nodes, traffic to the lung, and require restimulation by tissue-resident antigen presenting cells (APC). Moreover, the suppressive lung environment promotes regulatory T (Treg) cells (23) and dampens effector T cells. We hypothesised that inhibiting histone deacetylases (HDAC) may improve macrophage responses to Mtb and subsequently elicit T cells with enhanced effector function.

We examined the ability of the FDA-approved HDAC inhibitor, SAHA, to modulate early clearance events in macrophages infected with Mtb. SAHA increased glycolysis in human macrophages early in the response to stimulation with Mtb. Furthermore, SAHA increased IL-1β and decreased IL-10 production in human AM and MDM. Infected macrophages treated with SAHA enhanced T helper (Th) cell responses, resulting in increased IFN-γ and GM-CSF production.

MATERIALS AND METHODS

MDM Cell Culture

Peripheral blood mononuclear cells (PBMC) were isolated from the buffy coats of healthy donors (Irish Blood Transfusion Services) or from the venous blood of Interferon Gamma Release Assay (IGRA) positive antibiotic-treated, otherwise healthy individuals attending St. James's Hospital respiratory outpatients' clinic (as approved by the Ethics Board), by density-gradient centrifugation over Lymphoprep (StemCell Technologies). Cells were washed, resuspended at 2.5×10^6 PBMC/ml in RPMI (Gibco) supplemented with 10% AB human serum (Sigma-Aldrich) and 1 ml of cell suspension was plated on to non-treated 24-well-tissue culture plates (Costar). Cells were maintained in humidified incubators for 6–7 days at 37°C and 5% CO_2. Non-adherent cells were removed by washing every 2–3 days. The purities of MDM were assessed by flow cytometry and were routinely >95% pure. Approximately 10% of the PBMC differentiate into MDM. PBMC were also cryopreserved for co-culture assays.

AM Acquisition and Culture

Human AM were retrieved at bronchoscopy, as approved by the Ethics Board of St. James's Hospital, and previously reported by us (24). All donors were patients undergoing clinically indicated bronchoscopy and written informed consent for retrieving additional bronchial washings for research was obtained prior to the procedure. Patients were not remunerated for participation in this study. Exclusion criteria included age under 18 years, inability to provide written informed consent or a known (or ensuing) diagnosis of malignancy, sarcoidosis, HIV, or Hepatitis C. Patients undergoing biopsy as part of bronchoscopy were also excluded. For the seven subjects recruited to this study, clinical indications for bronchoscopy included haemoptysis (3/7), cough (2/7), bronchitis (1/7), and atelectasis (1/7). Two patients were non-smokers, while five were either current or ex-smokers, of which two had diagnosed chronic obstructive pulmonary disease.

Sample acquisition during bronchoscopy: Conscious sedation was achieved using intravenous midazolam and lignocaine gel was administered to the nostril. Flexible video-bronchoscope was inserted through the nostril and advanced to the level of the vocal cords by posterior approach. Further lignocaine spray was administered prior to and subsequent to traversing the vocal cords. Following routine bronchoscopy, the bronchoscope was wedged in the right middle lobe bronchus. A total of 180 ml of sterile saline was administered as 60 ml boluses via a connector inserted into the bronchoscope and aspirated within 5–10 s under low suction. The bronchoalveolar lavage fluid (BALF) was then transported directly to the laboratory for AM isolation. Pre- and post-bronchoscopy patient care was not altered by participation in the study. The procedure was prolonged by ∼12 min.

Cells were seeded at 5×10^5 cells per ml (2.5×10^5 per well in a 48 well-plate) in RPMI (Gibco) supplemented with 10% FBS (Gibco), fungizone (2.5 μg/ml; Gibco) and cefotaxime (50 μg/ml; Melford Biolaboratories). Cells were incubated for 24 h at 37°C and 5% CO_2 before washing to remove non-adherent cells. Adherent cells (predominantly AM) were then used for experiments.

Mycobacterial Culture and Infection of Macrophages

Mtb H37Ra was obtained from The American Type Culture Collection (ATCC 25177™; Manassas, VA) and propagated in

Middlebrook 7H9 medium supplemented with ADC (Beckton Dickinson), to log phase. Irradiated H37Rv (iH37Rv) was gifted by BEI Resources. The multiplicity of infection (MOI) and donor variation in phagocytosis of Mtb was adjusted for by Auramine-O staining, as previously described (25). MDM or AM were plated on 8-well Lab-Tek chamber slides (Nunc). Macrophages were infected with a range of bacterial concentrations for 3 h before extracellular bacteria were thoroughly washed off. Cells were fixed with 2% PFA, stained with Hoechst 33342 (10 μg/ml; Sigma-Aldrich), and rapid Auramine O staining set (Scientific Device Laboratory Inc). The numbers of bacilli per cell were counted in at least 30 fields of vision per well on a fluorescent microscope (Olympus IX51). The volume of bacterial suspension required to yield an MOI of 1–10 bacteria per cell (∼70% of macrophages infected with at least 1 bacillus; median number of 5, average 4–6, mode 2–4 bacilli per cell, as plotted in **Supplemental Figures 2D,E**) was determined. Macrophages were infected in the presence of SAHA (20 μM) or equivalent volumes of vehicle control (0.1% DMSO; both Sigma-Aldrich). After 3 h extracellular bacteria were washed off and macrophages were incubated as indicated. Uninfected macrophages were assayed in parallel as controls.

Seahorse Analysis of Metabolic Function

The impact of SAHA on macrophage metabolic function was assessed using the Seahorse XFe Analyzer (Agilent). PBMC were isolated from healthy control buffy coats and MDM were adherence purified in non-treated 6 well-plates (Costar; 2.5×10^6 cells/ml, 4 ml/well). MDM were gently scraped, counted using trypan blue, and seeded onto Seahorse plates (1×10^5 viable cells per well, seeded in low volume for 2 h to facilitate adherence then topped up to 500 μl and allowed to rest overnight in a humidified incubator at 37°C and 5% CO_2 before analysis on the Seahorse XFe24 Analyzer. The extracellular acidification rate (ECAR) and the oxygen consumption rate (OCR), surrogates for glycolysis, and oxidative phosphorylation, respectively, were measured approximately every 10–20 min for 600 min. Human MDM were stimulated by injecting iH37Rv into wells through the Seahorse Analyzer ports 30 min after initiation. DMSO or SAHA were injected into corresponding wells 2 h post-infection. ECAR and OCR were tracked in real time for the following 10 h. Alternatively, the ECAR and OCR of MDM were examined 24 h post infection and treatment with SAHA or DMSO.

Macrophage Assays

The concentrations of IL-1β, IL-10 (BioLegend ELISA Max Deluxe kits), and TNF (Invitrogen ready-set-go kit) present in the supernatants were quantified by ELISA, according to the manufacturer's protocol.

To assess the impact of SAHA (20 μM; Sigma-Aldrich) on the viability of human MDM, cells were stained with propidium iodide (PI), and Hoechst 33258 and 33342 at the indicated time-points post-infection with Mtb or treatment with cycloheximide (positive control; 50 μg/ml). Cells were incubated for 30 min at room temperature in the dark and analysed on the Cytell Cell Imaging System (GE Healthcare Life Sciences).

The effect of SAHA on macrophage phagocytosis was assessed using fluorescent latex beads (2 μm; Sigma-Aldrich); healthy control human MDM were treated with fluorescent latex beads (125 μg/ml) for 60 min at 37°C in the presence of SAHA or vehicle control. Cells were thoroughly washed, fixed with 2% paraformaldehyde, gently removed from the plastic by scraping and acquired on a BD FACSCanto II. Additionally, MDM or AM were plated onto Lab-Teks (Nunc) and infected at a known MOI of 1–10 bacteria per cell (∼70% infectivity) in the presence of SAHA or vehicle control. After 3 h, Lab-Teks were washed with PBS and fixed with 2% paraformaldehyde prior to staining with rapid Auramine O staining set (Scientific Device Laboratory Inc) and Hoechst 33342 (Sigma-Aldrich). The numbers of bacteria per cell were counted using a fluorescent microscope (Olympus IX51) as described above.

T Cell Co-culture Assays

MDM from IGRA positive individuals, infected with H37Ra in the presence of SAHA or DMSO, were washed after 24 h and co-cultured with thawed, CFSE-labelled (BioLegend; 0.5 μM, according to the manufacturer's protocol) autologous PBMC (2.5×10^6 cells/ml; 10:1 ratio of PBMC to MDM). AM were co-cultured with allogeneic CFSE-labelled PBMC from a BCG-vaccinated, IGRA negative healthy control donor (2.5×10^6 cells/well; 10:1 ratio of PBMC to AM). Half the volume of supernatant was removed and replaced with fresh medium at indicated timepoints. The concentrations of IFN-γ, GM-CSF, IL-10 (all BioLegend ELISA Max Deluxe kits), and TNF (Invitrogen ready-set-go kit) were quantified by ELISA, according to the manufacturer's protocol. On day 10 post co-culture, cells were Fc blocked (BioLegend Human TruStain FcX) and stained with fluorochrome-conjugated antibodies specific for CD4 (PerCP-Cy5.5), CD25 (APC; both eBioscience), CD3 (BV510), CD8 (APC-Fire750; both BioLegend). Cells were fixed and permeabilised for intranuclear staining (FoxP3 staining buffer set; eBiosciences) and stained with fluorochrome-conjugated antibodies specific for FoxP3 (PE; eBioscience). Cells were analysed on a BD FACS Canto II flow cytometer, as previously described (26). Alternatively, cells were restimulated with PMA (50 ng/ml) and ionomycin (500 ng/ml) in the presence of brefeldin A (5 μg/ml; all Sigma-Aldrich) for 5 h to assess intracellular cytokine production. PMA-stimulated cells were Fc blocked and stained with fluorochrome-conjugated antibodies specific for CD3 (BV510) and CD8 (APC-Fire750). Cells were fixed, permeabilised (Fix perm kit; Invitrogen) and stained with fluorochrome conjugated antibodies specific for GM-CSF (PE), IFN-γ (APC; both BioLegend), and TNF (PerCP-Cy5.5; eBioscience). Cells were acquired on the BD FACSCanto II. Cytokine production from $CD3^+$ $CD8^+$ and $CD3^+$ $CD8^-$ (CD4) $CFSE^{lo}$ proliferating cells was analysed using FlowJo software as previously described (27).

Colony Forming Units (CFU)

CFU were determined at day 0 (3 h post-infection), 3, 6, or 10, as indicated; cells were lysed with triton-X 100 (0.1%) and pooled with bacterial pellets (at all timepoints except day 0) from the centrifugation of supernatants. Bacteria were diluted

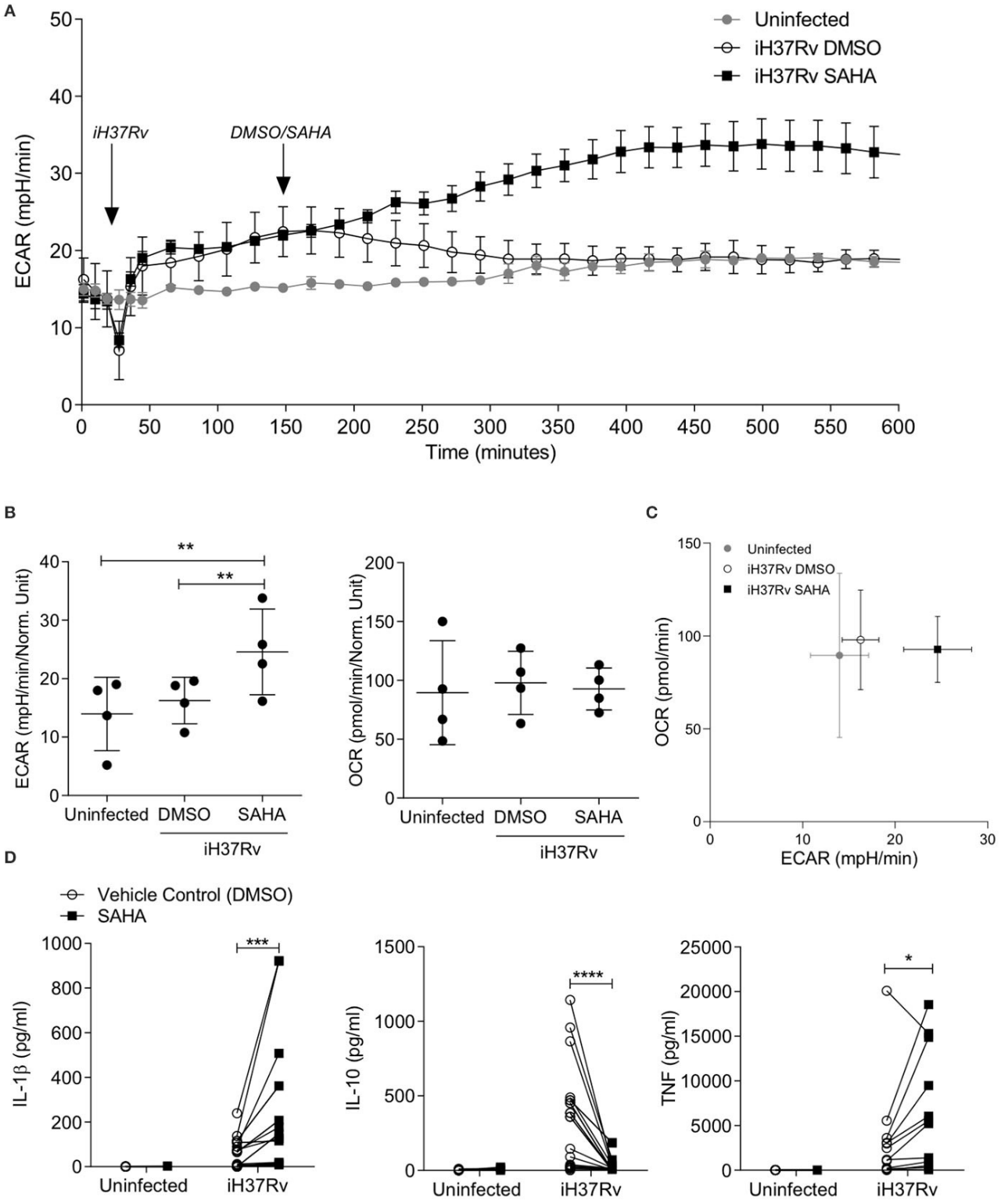

FIGURE 1 | SAHA supports aerobic glycolysis and modulates cytokine production in human macrophages during early Mtb infection. Monocyte derived macrophages (MDM) were analysed on the Seahorse XFe24 Analyzer. The extracellular acidification rates (ECAR) and oxygen consumption rate (OCR) were recorded

(Continued)

FIGURE 1 | approximately every 20 min. After 30 min, the Seahorse Analyzer injected iH37Rv (MOI 1-10) into assigned wells. Two hours later, DMSO or SAHA were injected through the Seahorse Analyzer (at 150 min; as indicated by the arrows). The ECAR and OCR readings were then continually sampled in real time. **(A)** Representative time-course graph illustrating the ECAR of MDM in real-time response to stimulation with iH37Rv and treatment with SAHA or vehicle control (DMSO); 3 technical replicates ± SD. **(B)** Collated data (error bars indicate mean ± SD) from $n = 4$ independent experiments for ECAR and OCR at 500 min. **(C)** The phenogram illustrates the energetic profile of MDM by plotting ECAR vs. OCR at 500 min (±SD, $n = 4$). **(D)** MDM were stimulated with iH37Rv for 24 h and concentrations of IL-1β ($n = 18$), IL-10 ($n = 18$), and TNF ($n = 12$) present in the supernatants were quantified by ELISA. Each paired data point represents the average of technical replicates from a single donor treated with DMSO (empty circles) or SAHA (closed squares). Statistically significant differences between DMSO and SAHA were determined by one-way ANOVA with Tukey's multiple comparison test **(B)** or two-way ANOVA with Sidak's multiple comparison test **(D)**; $^{*}P < 0.05$, $^{**}P < 0.01$, $^{***}P < 0.001$, $^{****}P < 0.0001$.

in Middlebrook 7H9 broth and plated onto Middlebrook 7H10 agar supplemented with OADC (both Becton Dickinson) and cycloheximide (Sigma-Aldrich). CFU counts were performed 14- and 21-days post incubation at 37°C.

Statistical Analysis

Statistical analyses were performed using GraphPad Prism 6 software. Statistically significant differences between two normally distributed groups were determined using Student's paired *t*-tests with two-tailed *P*-values. Differences between three or more groups were determined by one-way ANOVA with Tukey's multiple comparisons tests. Differences between two or more groups containing more than one variable were determined by two-way ANOVA with Sidak's multiple comparisons tests. $P < 0.05$ were considered statistically significant and denoted using an asterisk.

RESULTS

SAHA Supports Aerobic Glycolysis and IL-1β Production in Human Macrophages Early in Response to Mtb

The metabolic function of human macrophages changes upon infection with Mtb toward increased utilisation of aerobic glycolysis (11). Mtb, however, perturbs host metabolism (28–30) to evade clearance by the innate immune response. Additionally people with increased risk of contracting TB, such as smokers, have an impaired ability to shift toward aerobic glycolysis in response to infection with Mtb (31). Therefore, drugs with the ability to promote glycolysis may be beneficial as treatment strategies for people with increased risk of TB.

The upregulation of macrophage effector functions, including changes in cellular metabolism, is governed by gene transcription and thus is under the control of HDAC. We, therefore, hypothesised that the HDAC inhibitor SAHA would modulate the metabolic function of human macrophages infected with Mtb. Emerging evidence suggests that SAHA modulates both pathogen and host epigenetics (32–36). Since HDAC inhibitors could potentially impact the deacetylation activity within Mtb, we first used iH37Rv to assess the impact of SAHA on the host independent of its effects on the bacteria.

We analysed the extracellular acidification rate (ECAR) and the oxygen consumption rate (OCR) of human monocyte derived macrophages (MDM) in response to stimulation with Mtb and treatment with SAHA (20 μM) in a Seahorse XFe24 Analyzer (**Figure 1**). Baseline measurements of ECAR and OCR, surrogates for glycolysis and oxidative phosphorylation, respectively, were recorded for 30 min prior to the addition of Mtb iH37Rv. MDM were then treated with SAHA or the vehicle control (DMSO) 120 min post the addition of iH37Rv. ECAR and OCR were tracked in real-time over a 10-h period. The glycolytic rate (ECAR) of human MDM increased 15 min post the addition of iH37Rv (at 45 min; **Figure 1A**). The addition of SAHA at 150 min augmented the increasing glycolytic rate between 200 and 400 min, whereas the ECAR of MDM that received vehicle control returned to the baseline rate of the uninfected, untreated control (**Figure 1A**). Collated data from $n = 4$ independent experiments demonstrates that, at 500 min, SAHA significantly increased the ECAR (glycolysis) of human MDM stimulated with Mtb compared with DMSO-treated controls and uninfected MDM (**Figure 1B**, left; $P < 0.01$). Conversely, the OCR (oxidative phosphorylation) was not affected by the addition of SAHA (**Figure 1B**, right). A phenogram illustrating ECAR vs. OCR at 500 min shows the metabolic state of MDM infected in the presence of SAHA or vehicle control compared with uninfected cells (**Figure 1C**). The addition of SAHA in the absence of infection did not alter the metabolic profile of human MDM (data not shown). Twenty-four hours post stimulation with iH37Rv, SAHA-treated macrophages exhibited significantly reduced ECAR with no effect on OCR (**Supplemental Figure 1**). These data indicate that SAHA supports the rapid shift to glycolysis in human macrophages during the early response to Mtb infection.

Increased glycolysis in proinflammatory murine M1-type macrophages is associated with increased production of mature IL-1β but does not affect TNF production (37), whereas increased oxidative phosphorylation in homeostatic M2-type macrophages is linked to IL-10 production (38). In addition, IL-1β production and increased aerobic glycolysis promotes early clearance of Mtb from human and murine macrophages (11, 29). We assessed the effect of SAHA at a range of concentrations (from 5 to 40 μM) on the production of IL-1β and IL-10 in human MDM stimulated with iH37Rv (**Supplemental Figure 2A**). SAHA at 20 and 40 μM optimally induced IL-1β production whereas SAHA abrogated IL-10 at all concentrations examined. Since IL-1β release can result from pyroptosis (39), we analysed the effect of SAHA (20 μM) on human MDM cell death (**Supplemental Figure 2B**). MDM were treated with SAHA or vehicle control and stimulated with iH37Rv, infected with H37Ra or treated with cycloheximide as a positive control for cell death. After 24 h, MDM were stained with propidium iodide and Hoechst; cell death was analysed.

SAHA- and DMSO-treated MDM were washed and cultured in RPMI containing 10% FBS for the remaining time-points. SAHA was therefore used at a concentration of 20 μM which did not significantly promote cell death apart from in cycloheximide-treated MDM on day 3 ($P < 0.05$) when compared with control (**Supplemental Figure 2B**).

MDM from healthy control donors were stimulated with iH37Rv in the presence of SAHA (20 μM) or vehicle control. Since IL-1β and TNF are fundamental during the early host response to Mtb (11, 40–42) whereas IL-10 promotes TB disease progression in mice (43) and interrupts host defence in humans (44), we determined the concentrations of IL1-β, IL-10, and TNF by ELISA 24 h post stimulation (**Figure 1D**). SAHA significantly increased the production of IL-1β ($P < 0.001$) and TNF ($P < 0.05$) in human MDM stimulated with iH37Rv (**Figure 1D**). Conversely, SAHA significantly decreased production of IL-10 ($P < 0.0001$; **Figure 1D**).

To ensure that the increased glycolytic rate and increased IL-1β production were not a result of increased bacterial load inside SAHA-treated macrophages, we examined the effect of SAHA on phagocytosis in human MDM and AM (**Supplemental Figures 2C–E**). SAHA did not significantly alter the uptake of latex beads or Mtb.

Collectively, these data indicate that SAHA significantly increased glycolysis early in the response to stimulation with Mtb in human macrophages. Furthermore, SAHA significantly increased IL-1β and TNF production and significantly reduced IL-10, compared with vehicle control, in human macrophages stimulated with iH37Rv. These effects were not associated with increased cell death or increased bacterial load.

SAHA Modulates Cytokine Production in the Context of Live Mtb Infection in Human MDM and Alveolar Macrophages

To ensure this phenotype was recapitulated in the context of a live infection, we infected human MDM from healthy control donors with Mtb H37Ra in the presence of SAHA or vehicle control. After 24 h, the concentrations of IL-1β, IL-10, and TNF were quantified by ELISA (**Figure 2A**). Although the overall magnitude of the cytokine response was reduced in MDM infected with live H37Ra (**Figure 2A**) compared with iH37Rv (**Figure 1D**), SAHA significantly increased IL-1β production ($P < 0.0001$) and significantly reduced IL-10 production ($P < 0.05$) without affecting TNF production. Cells were lysed on day 0 (3 h post-infection), day 3, and day 6, and CFU were enumerated on Middlebrook agar supplemented with OADC (**Figure 2B**). SAHA did not significantly affect bacterial killing in human MDM.

The alveolar macrophage is the first cell to encounter Mtb and is thought to be ineffective at killing the bacteria (45–47). Therefore, the AM is a target cell for potential inhalable adjunctive therapies aimed at boosting immune function. We isolated human alveolar macrophages from BALF and infected them with Mtb in the presence of SAHA or vehicle control (**Figure 2C**). We found that HDAC inhibition with SAHA significantly increased IL-1β production ($P < 0.05$) and significantly reduced IL-10 production ($P < 0.05$) without altering TNF production in human alveolar macrophages infected with Mtb. Five out of seven of the AM donors were smokers; when we excluded non-smokers from the analysis SAHA maintained the ability to significantly boost IL-1β ($P < 0.05$; data not shown).

Treating MDM With SAHA Enhances Downstream Effector T Cell Responses to Mtb

Infiltrating monocytes that are recruited to the lung during infection and then become MDM are critical to controlling and killing Mtb (47). Moreover, both MDM and tissue resident AM are crucial for reactivating infiltrating effector T cells in the tissue. We utilised blood from interferon gamma release assay (IGRA) positive individuals to allow us to determine if treating Mtb-infected macrophages with SAHA had an effect on T cell responses. First we analysed the effect of SAHA on MDM from IGRA-positive donors (**Figure 3A**). HDAC inhibition with SAHA in infected MDM from IGRA positive donors significantly promoted IL-1β ($P < 0.05$) and reduced IL-10 ($P < 0.0001$) and did not significantly affect TNF production. We then established a co-culture assay in order to assess the impact of the increased glycolysis and IL-1β production and concomitantly reduced IL-10 production in infected macrophages treated with SAHA on the downstream T cell response.

T cells can be both protective and pathogenic during Mtb infection depending on their function and the stage of TB disease (48). IFN-γ and GM-CSF have emerged as critical T cell cytokines in the control of Mtb and have been shown to have additive effects on macrophage-mediated killing of Mtb (49). Therefore, we assessed if SAHA-treated macrophages could modulate T cell production of IFN-γ and GM-CSF.

MDM from IGRA-positive donors were infected with Mtb H37Ra in the presence of SAHA or vehicle control. After 24 h, MDM were thoroughly washed to remove SAHA/DMSO and co-cultured with autologous CFSE-labelled PBMC. The concentrations of IFN-γ, GM-CSF, IL-10, and TNF were quantified by ELISA on day 3, 7, and 10 post co-culture (**Figure 3B**). PBMC co-cultures containing SAHA-treated MDM infected with Mtb exhibited significantly increased concentrations of IFN-γ and GM-CSF at day 7 ($P < 0.05$) and day 10 ($P < 0.01$, $P < 0.001$, respectively) compared with PBMC co-cultured with DMSO-treated, Mtb-infected MDM. No differences were observed in the production of TNF or IL-10 (**Figure 3B**).

In order to determine which cells in the co-culture system were producing these cytokines, we used flow cytometry to assess cytokine production in subpopulations of the proliferating ($CFSE^{lo}$) cells. Representative histograms illustrate the frequencies of proliferating cells ($CFSE^{lo}$) in response to stimulation by uninfected autologous MDM, or MDM infected with Mtb in the presence of SAHA or DMSO (**Supplemental Figure 3A**). The frequencies of proliferating PBMC stimulated by Mtb-infected MDM

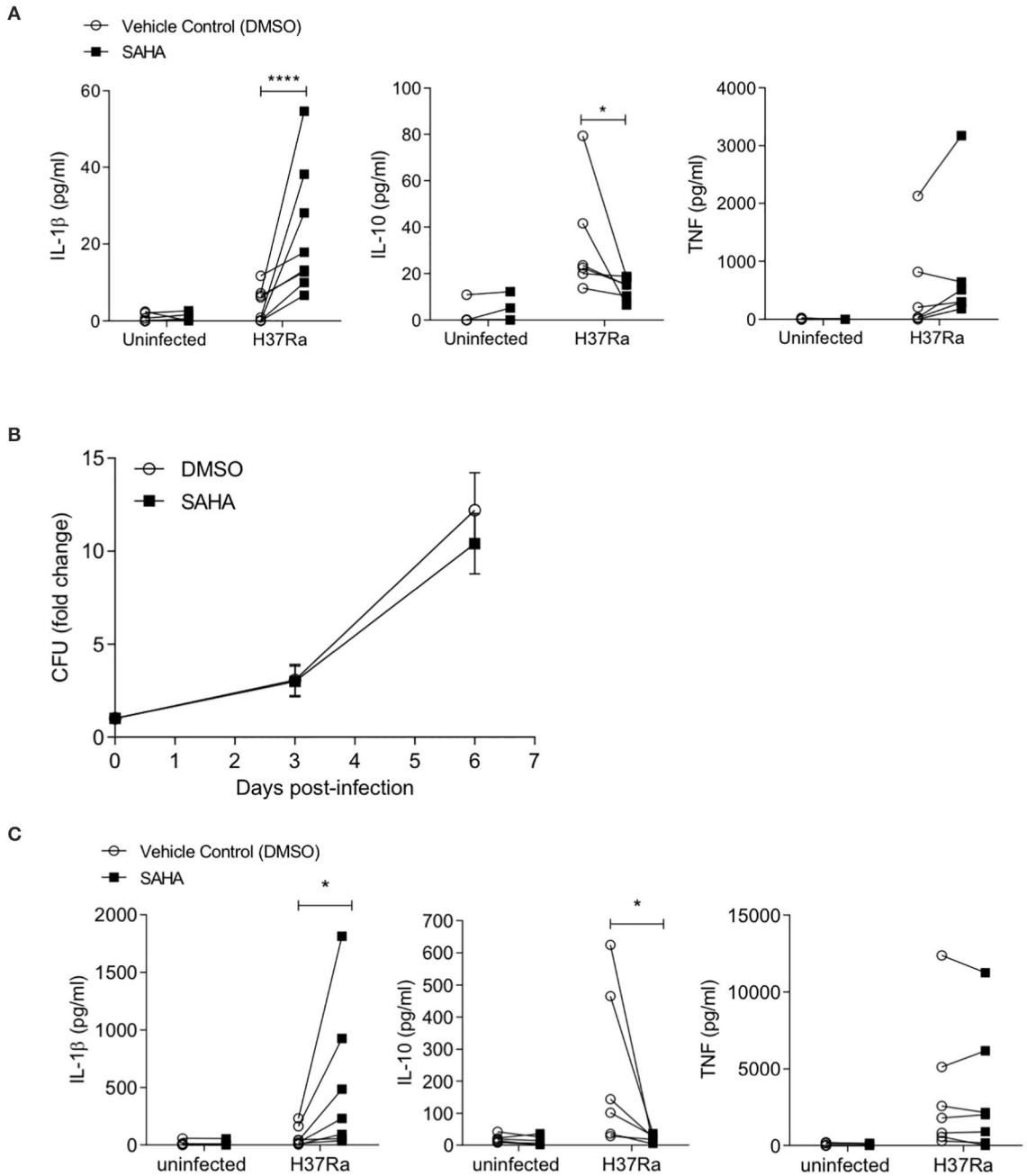

FIGURE 2 | SAHA modulates cytokine production in the context of live Mtb H37Ra infection in human healthy control MDM and alveolar macrophages. **(A)** MDM were infected with Mtb H37Ra (MOI 1-10) in the presence of SAHA or vehicle control (DMSO) for 24 h. The concentrations of IL-1β ($n = 8$), IL-10 ($n = 6$), and TNF ($n = 8$) present in the supernatants were quantified by ELISA. **(B)** MDM infected with Mtb H37Ra (MOI 1-10) were lysed on day 0 (3 h post-infection), day 3, and day 6. CFU were enumerated on Middlebrook 7H10 agar supplemented with OADC on day 21 post lysis. CFU are presented as fold change from day 0 and data points represent the average ± SD of $n = 3$ independent experiments. **(C)** Human AM ($n = 7$) were infected with H37Ra (MOI 1-10) in the presence of SAHA or DMSO. After 24 h, the concentrations of IL-1β, IL-10, and TNF present in the supernatants were measured by ELISA. Each paired data point represents the average of technical replicates from a single donor treated with DMSO (empty circles) or SAHA (closed squares). Statistically significant differences between DMSO and SAHA were determined by two-way ANOVA with Sidak's multiple comparison test **(A,C)** or by paired Student's *t*-test **(B)**; $^{*}P < 0.05$, $^{****}P < 0.0001$.

treated with SAHA were not significantly altered compared with DMSO (**Supplemental Figure 3A**; collated data, right). Furthermore, over 90% of proliferating cells were $CD3^{+}$ T cells, and this was not altered by treating the MDM with SAHA (**Supplemental Figure 3B**). In addition, SAHA did not significantly alter the frequencies of $CD4^{+}$ T helper (Th)

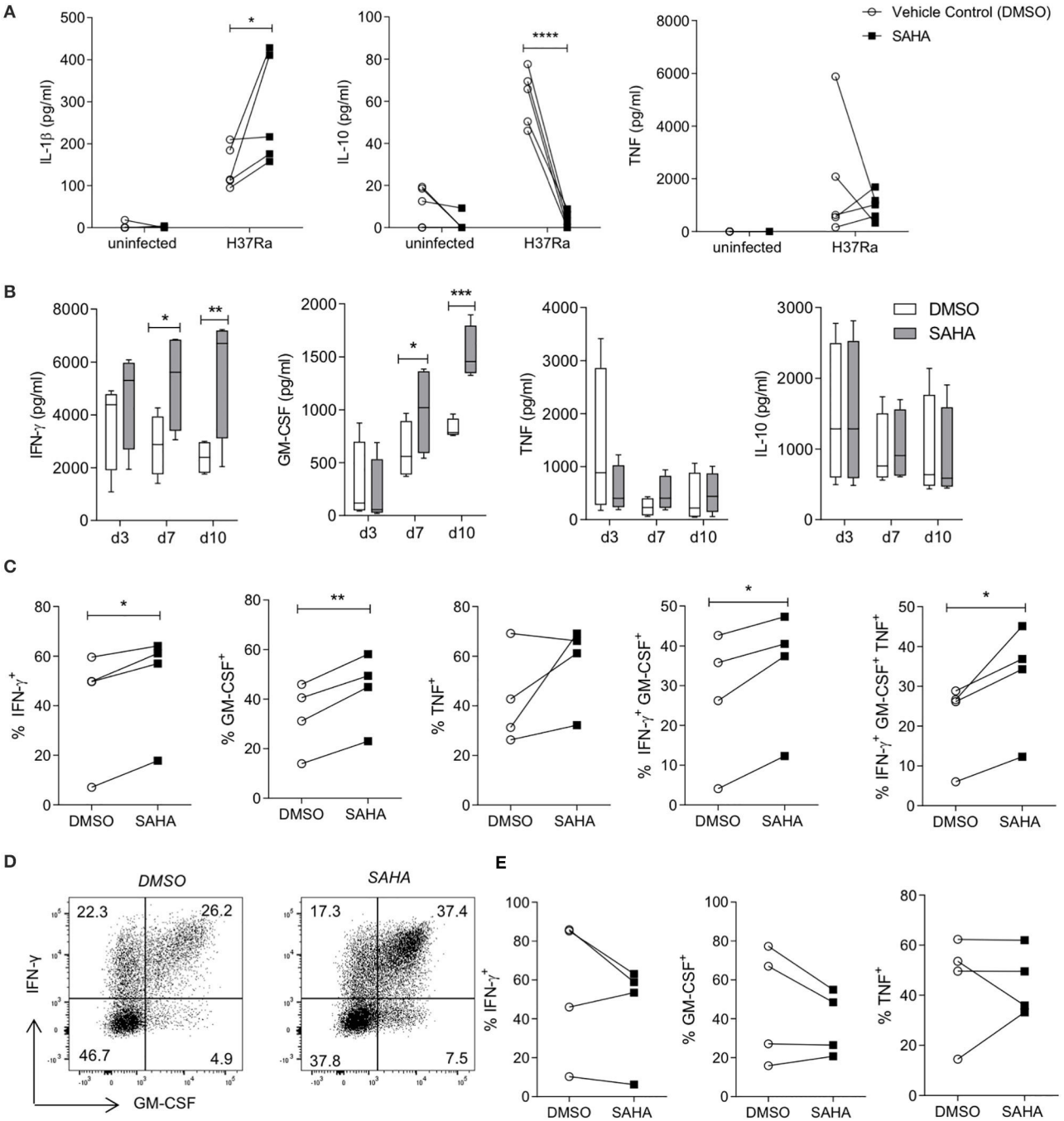

FIGURE 3 | SAHA-treated MDM enhanced downstream effector CD4 T cell responses to Mtb. MDM differentiated from the PBMC of IGRA positive individuals were infected with H37Ra (MOI 1-10) in the presence of SAHA or vehicle control (DMSO). **(A)** After 24 h, the concentrations of IL-1β, IL-10 and TNF were quantified by ELISA (n = 5). MDM were washed and co-cultured with CFSE-labelled PBMC from autologous donors. **(B)** The concentrations of IFN-γ, GM-CSF, TNF, and IL-10 present in the co-cultured supernatants on the indicated days were analysed by ELISA; collated data from $n = 4$ experiments, error bars indicate ± SD. **(C–E)** On day 10 post co-culture, PBMC were removed, stimulated with PMA/ionomycin in the presence of brefeldin A, or left unstimulated. Cells were stained with fluorochrome-conjugated antibodies specific for CD3, CD8, IFN-γ, TNF and GM-CSF, and analysed by flow cytometry. **(C)** Graphs illustrate collated data for the frequencies of cells producing cytokines in the population of $CD3^+CD8^-$ ($CD4^+$) T helper cells that are proliferating ($CFSE^{lo}$) in response to stimulation with Mtb infected macrophages ($n = 4$). Cells were gated on the basis of forward and side scatter, doublets were then excluded and the population of proliferating $CFSE^{lo}$ cells were gated. The Th cell subpopulation was gated within proliferating cells, then cytokines were examined within these populations. **(D)** Representative dot plots illustrate co-staining of GM-CSF with IFN-γ from proliferating CD4 ($CD3^+$ $CD8^-$) T cells. **(E)** Cytokine production from proliferating $CD8^+$ T cells was assessed. Statistically significant differences between DSMO and SAHA treated groups were determined by two-way ANOVA with Sidak's multiple comparisons test **(A,B)** or paired t-test **(C,E)**; $^*P < 0.05$, $^{**}P < 0.01$, $^{***}P < 0.001$.

cells or $CD8^+$ cytotoxic T (Tc) cells compared with DMSO (**Supplemental Figure 3C**).

PBMC were restimulated with PMA and ionomycin in the presence of brefeldin A to assess cytokine production from proliferating T cell populations. Proliferating CD4 Th cells (gated on $CD3^+$ $CD8^-$ cells as PMA stimulation reduces CD4 surface expression), stimulated by autologous SAHA-treated MDM infected with Mtb, exhibited significantly increased frequencies of IFN-γ^+ ($P < 0.05$), GM-CSF^+ ($P < 0.01$), IFN-γ^+ GM-CSF^+ ($P < 0.05$), and IFN-γ^+ GM-CSF^+ TNF^+ ($P < 0.05$) cells (**Figure 3C**). Representative dot plots illustrate the co-staining of IFN-γ and GM-CSF (**Figure 3D**). No significant differences were observed in cytokine production within proliferating $CD8^+$ Tc cells stimulated by autologous DMSO/SAHA-treated MDM infected with Mtb (**Figure 3E**).

These results indicate that treating human macrophages from IGRA-positive donors with SAHA promoted downstream effector Th cell responses.

SAHA Treated AM Enhance BCG-Primed CD4 Th Cell Responses to Mtb Infection

Having established that treating Mtb-infected MDM with SAHA resulted in increased effector Th cell function, we next sought to determine whether SAHA-treated AM infected with Mtb would promote effector T cell responses in healthy control individuals (IGRA negative) who had been BCG vaccinated and are therefore able to respond to Mtb antigens (PPD) *in vitro*. Due to clinical and ethical restrictions, AM and PBMC were isolated from different donors, therefore the allogeneic response was controlled for throughout the experiment.

AM were infected with Mtb H37Ra in the presence of SAHA or vehicle control. After 24 h, AM were thoroughly washed to remove SAHA/DMSO and co-cultured with CFSE-labelled PBMC from a BCG-vaccinated donor (IGRA negative but responds to PPD antigens *in vitro*). Uninfected AM co-cultured with PBMC (background allogeneic response) and AM infected with Mtb H37Ra and not co-cultured with PBMC were assayed as controls.

The concentrations of IFN-γ produced on day 2, day 5, day 7, and day 10 post co-culture were quantified by ELISA (**Figure 4A**). Notably, allogeneic PBMC co-cultured with Mtb-infected AM produced increased IFN-γ compared with background allogeneic responses or AM cultured alone. On day 2, PBMC stimulated with Mtb-infected, SAHA-treated AM exhibited significantly reduced IFN-γ production compared with DMSO control ($P < 0.05$). However, on day 5 and day 7, PBMC stimulated with Mtb-infected, SAHA-treated AM exhibited significantly increased IFN-γ production compared with PBMC stimulated with DMSO-treated, Mtb-infected AM ($P < 0.05$ and $P < 0.001$, respectively). By day 10, there was no significant difference in IFN-γ production. The concentrations of GM-CSF, TNF, and IL-10 present in the supernatant on day 5 are not significantly altered by treating the AM with SAHA compared with control (**Supplemental Figure 4A**).

$CFSE^{lo}$ proliferating PBMC were analysed by flow cytometry on day 10, as above (section Treating MDM with SAHA Enhances Downstream Effector T Cell Responses to Mtb). Treating infected AM with SAHA significantly increased the frequencies of $CD4^+$ proliferating T cells (**Figure 4B**; $P < 0.01$) and significantly reduced the frequencies of proliferating $CD8^+$ T cells (**Figure 4C**; $P < 0.0001$). Proliferating $CD4^+$ Th cells activated by SAHA-treated, infected AM exhibited significantly increased frequencies of cells producing IFN-γ ($P < 0.05$) and GM-CSF ($P < 0.05$) compared with control (**Figure 4B**). Treating the AM with SAHA did not significantly impact the ability of $CD4^+$ Th cells to produce TNF. In addition, treating the AM with SAHA had no impact on the ability of $CD8^+$ Tc to produce cytokine (**Figure 4C**). Representative dot plots show the co-staining of IFN-γ and GM-CSF in proliferating CD4 T cells (**Figure 4D**). Collated data indicates that SAHA-treated, Mtb infected AM promote significantly higher frequencies of IFN-γ^+ GM-CSF^+ double-positive ($P < 0.01$) and IFN-γ^+ GM-CSF^+ TNF^+ triple-positive ($P < 0.05$) $CD4^+$ Th cells compared with control (**Figure 4E**).

Our group have previously shown that the lung environment and specifically AM can promote the induction of Treg cells (23). Taken together with the data demonstrating that SAHA abrogated IL-10 production from AM, and since IL-10 is a major driver of Treg induction, we analysed the frequencies of Treg cells present in the co-culture. Representative plots showing the gating strategy for Treg cells and collated data indicate that treating infected AM with SAHA did not significantly alter the frequencies of $CD4^+$ Treg cells compared with control (**Supplemental Figures 4B,C**).

The autologous MDM-PBMC co-culture (of BCG vaccinated, IGRA negative donor who positively responds to PPD antigens *in vitro*) was assayed (**Supplemental Figures 4D–F**) as a control for the allogeneic AM-PBMC co-culture and also to assess if the findings could be recapitulated in the context of IGRA negative donors. The concentrations of IFN-γ present in the supernatants were analysed (**Supplemental Figure 4D**). Similar to the PBMC co-cultured with allogeneic AM and the IGRA-positive autologous model, IGRA negative PBMC stimulated with SAHA-treated, Mtb-infected autologous MDM exhibited significantly reduced IFN-γ production at day 3 ($P < 0.0001$) however; by day 7 and 10, PBMC secreted significantly more IFN-γ compared with controls ($P < 0.0001$; **Supplemental Figure 4D**). Dot plots show increased frequencies of Th cells co-producing IFN-γ and GM-CSF (**Supplemental Figure 4E**). CFU were enumerated at on day 0, day 3, and day 10 (**Supplemental Figure 4F**). MDM treated with SAHA exhibit reduced CFU at day 10 compared with control. MDM co-cultured with PBMC exhibit profoundly reduced CFU compared to MDM alone, as expected, but without a substantial difference between the treatment groups.

These data demonstrate that in the context of lung resident AM from healthy donors, SAHA can promote downstream Th cell responses, similar to the effects observed in the cells isolated from IGRA-positive individuals.

Taken together, these data illustrate that SAHA modulates metabolic function and affects the cytokine profile of macrophages infected with Mtb, and this results in enhanced Th cell effector function.

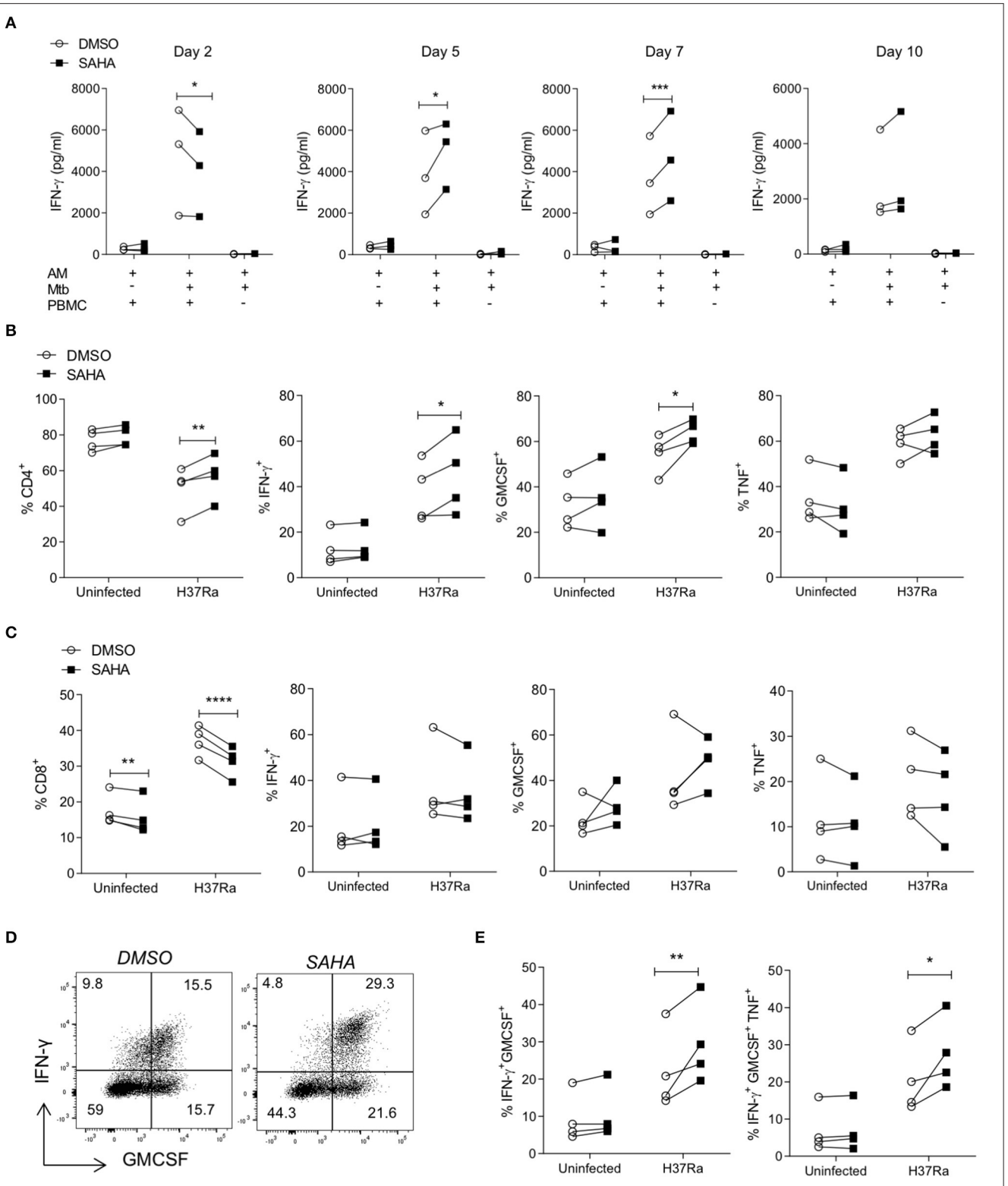

FIGURE 4 | SAHA treated AM enhanced BCG-primed CD4 Th cell responses to Mtb infection. Human AM were infected with H37Ra (MOI 1-10) in the presence of SAHA or DMSO. After 24 h, AM were washed and co-cultured with CFSE-labelled PBMC from a BCG-vaccinated healthy donor (IGRA negative) who responds to

(Continued)

FIGURE 4 | PPD antigens *in vitro*. Uninfected AM co-cultured with PBMC and Mtb-infected AM not co-cultured with PBMC were assayed in parallel as controls. **(A)** The concentrations of IFN-γ present in the supernatants on the indicated days were analysed by ELISA ($n = 3$). On day 10 post co-culture, PBMC were removed, stimulated with PMA/ionomycin in the presence of brefeldin A, or left unstimulated. **(B,C)** Cells were stained with fluorochrome-conjugated antibodies specific for CD3, CD4, CD8, IFN-γ, TNF and GM-CSF, and analysed by flow cytometry. Cells were gated on the basis of forward and side scatter, doublets were then excluded and the population of proliferating $CFSE^{lo}$ cells were gated. The CD4 and CD8 cell subpopulations were gated within proliferating cells, then cytokines were examined within these populations. Graphs illustrated collated data ($n = 4$) from unstimulated samples for the frequencies of proliferating cells expressing CD4 (**B**; left) or CD8 (**C**; left) and cytokine production from stimulated samples within the population of proliferating ($CFSE^{lo}$) $CD3^+$ $CD8^-$ ($CD4^+$) T helper cells **(B)** and $CD3^+$ $CD8^+$ cytotoxic T cells **(C)**. **(D)** Representative dot plots illustrate co-staining of IFN-γ and GM-CSF within the $CFSE^{lo}$ $CD3^+$ $CD8^-$ Th cell gate. **(E)** Collated data shows the frequencies of IFN-γ^+ GM-CSF^+ double-positive and IFN-γ^+ GM-CSF^+ TNF^+ triple-positive cells in the CD4 Th cell population that are proliferating. Statistically significant differences between DSMO and SAHA treated groups were determined by two-way ANOVA with Sidak's multiple comparisons test; $^*P < 0.05$, $^{**}P < 0.01$, $^{***}P < 0.001$, $^{****}P < 0.0001$.

DISCUSSION

The metabolic function of macrophages is emerging in the literature as a gatekeeping node in mediating the immune response to danger signals. Moreover, perturbance of macrophage metabolic function by Mtb or other environmental cues is associated with increased risk of TB disease and enhanced pathogenicity of the bacteria (24, 28, 29). Therefore, modulating the metabolic function of macrophages will be key to translating the burgeoning field of immunometabolism toward clinical benefit for patients.

Our hypothesis-driven human research aimed to provide proof-of-concept data for repurposing the FDA approved HDACi, SAHA, as an immune-augmenting therapy. These data can be used to inform further experimental models of infection *in vivo*.

Our data indicates that the use of the HDACi, SAHA, on human macrophages modulates both innate and adaptive immune function in response to infection with Mtb. Treating macrophages with SAHA resulted in significantly increased glycolysis early in the response to Mtb infection. Importantly this effect could be solely attributed to host macrophage responses to HDACi since iH37Rv was used to ensure direct effects of SAHA on the bacteria did not confound the experiment. HDACi have been reported to increase mitochondrial reactive oxygen species (ROS) in human macrophages infected with *S. Typhimurium* or *E. coli* (22). This is in keeping with our observation that SAHA promoted the early shift to glycolysis since mitochondrial ROS is associated with increased glycolysis in macrophages (50). The evidence for this increased glycolysis was further supported by the macrophage shift toward a more proinflammatory phenotype; producing more IL-1β and less IL-10. This increased glycolysis coupled with increased IL-1β is a well-documented phenotype in activated macrophages (37) and has previously been shown by our group in the context of Mtb infection (11, 29, 51). Inhibiting glycolysis *in vitro* has been reported to have no effect on TNF production from macrophages (11, 37). Infecting MDM with H37Ra in the presence of SAHA did not affect TNF production, in keeping with published literature that demonstrates the TNF is not associated with the shift to glycolysis *in vitro*. However, we also report here that treating human MDM with SAHA not only promoted glycolysis and IL-1β but also promoted TNF production in response to stimulation with iH37Rv. This indicates that TNF may be directly or indirectly linked to increased glycolysis in the context of iH37Rv stimulation in human macrophages. Work recently published by our group supports this data by showing that promoting glycolysis using an iron chelator also increased TNF production in human macrophages stimulated with iH37Rv (51). Furthermore, inhibition of glycolysis using 2-deoxyglucose in an *in vivo* mouse model of Mtb infection resulted in decreased *ex vivo* TNF production from interstitial macrophages from the lung (47). These data collectively suggest that the relationship between the metabolic function of macrophages and their ability to produce TNF is complex and therefore warrants further study.

We and others have previously shown that IL-1β (11, 40, 41) and TNF (41, 42) are critical for control of Mtb, whereas IL-10 inhibits bacterial clearance (44). The observed increase in IL-1β production and concomitant decrease in IL-10 may shift the immune response in favour of the host. Although SAHA promoted TNF production in the context of iH37Rv stimulation, it did not increase TNF production in the context of infection with H37Ra. This suggests that whilst the net proinflammatory effect is greater in the context of iH37Rv (with both IL-1β and TNF increased in response to SAHA), there is still a shift toward increased proinflammatory responses in the live infection (increased IL-1β, unchanged TNF, and decreased anti-inflammatory IL-10). Interestingly, SAHA promoted IL-1β production in murine bone marrow derived macrophages and human dendritic cells stimulated with LPS (52), suggesting SAHA may have wider applications as a modulator of macrophage function in other settings of infectious disease and cancer.

AM exhibit reduced capacity to shift toward aerobic glycolysis (47), which is accentuated in smokers, who are at increased risk of TB (31). In addition, emerging evidence suggests that multidrug-resistant Mtb does not induce a shift toward glycolysis in macrophages (28). Therefore, drugs with the ability to promote this shift toward utilising glycolysis, independent of the bacteria, may have significant clinical promise.

In the context of liver cancer, SAHA has been shown to inhibit HIF-1α expression and nuclear translocation (53, 54). Because the shift toward utilising aerobic glycolysis in proinflammatory macrophages is governed by HIF-1α stabilisation (55), this finding in cancer may appear incongruous to our findings that SAHA promoted the shift to glycolysis. These disparities may, at least in part, be due to timing; although SAHA promoted

glycolysis early in response to stimulation with iH37Rv, it reduced glycolysis at the later timepoint of 24 h.

The activation status, cytokine production, and metabolic function of APC can influence T cell activation (56), therefore, we analysed the effect of treating Mtb-infected macrophages with SAHA on downstream T cell responses. We found significantly increased IFN-γ and GM-CSF production. Importantly, the flow cytometry data demonstrates that the responding Th cells were able to produce IFN-γ, GM-CSF, and TNF concurrently. Increased IFN-γ and GM-CSF production is thought to be protective during TB disease (57, 58) and these cytokines exhibit an additive effect in promoting macrophage killing of Mtb *in vivo* (49). Moreover, cytokine polyfunctionality is thought to be beneficial over monofunctional T cell responses (59).

Although SAHA completely abrogated the production of IL-10 in macrophages infected with Mtb, the co-culture of macrophages with PBMC is IL-10 replete; indicating that the early abrogation of IL-10 production in macrophages is later rescued by subsequent responding T cells. This is important in order to ensure that these increased early inflammatory responses are balanced to limit excessive inflammation and damage to the lung (60).

Since IL-10 is a well-established suppressor of T cell activation (61), the ability of SAHA to reduce IL-10 production in infected macrophages likely contributes toward the enhanced T cell responses observed. In addition, IL-1β has been shown to drive a polyfunctional non-classical Th1-type response in the context of *Listeria monocytogenes* infection (62). We have previously shown that increased IFN-γ^+ GM-CS$^+$ TNF$^+$ polyfunctional cells are associated with the non-classical Th1 cell phenotype (27), therefore, the increased IL-1β in SAHA-treated Mtb-infected macrophages may be directly driving the enhanced polyfunctional Th1-type response. It is also plausible that the reduced ECAR observed in infected SAHA-treated macrophages after 24 h may promote better antigen presentation and T cell responses, consistent with published observations in dendritic cells whereby an initial increase in glycolysis is required for activation but subsequently reduced glucose uptake increases bioavailability of glucose for T cell activation (56). Thus, the metabolic phenotype induced by SAHA may be beneficial *in vivo* to support early clearance events by macrophages and then subsequently promote T helper cell responses.

The recapitulation of these findings in AM from healthy donors and T cells from a BCG-vaccinated healthy donor suggests that SAHA may have potential as a vaccine adjuvant delivered directly to the lungs. Additionally, because of SAHA's ability to promote IL-1β in AM from smokers, this approach may be useful in contexts where sessile, metabolically exhausted AM fail to support early clearance (31). BCG vaccination can induce trained immunity which confers non-specific protection against unrelated infections (63). The mechanisms underpinning trained immunity are changes in epigenetics and metabolic function (13, 14). Therefore, we hypothesise that SAHA may be able to modulate the "trained" phenotype in macrophages which may in turn effect the subsequent T cell response.

SAHA is directly cytotoxic to T cells in the context of cutaneous T cell lymphoma (64). Our data, however, indicates that SAHA can indirectly promote T helper cell function downstream of human macrophages in the context of Mtb infection. The role of the T cell in mediating protection vs. pathology in TB is debatable (65–70). We hypothesise that targeted delivery of SAHA to the lung may be beneficial; firstly to promote macrophage-mediated immunity to Mtb and secondly to refresh the population of T cells present in the lung during the disease state. Newly infiltrating T cells will therefore be reactivated *in situ* by SAHA-treated macrophages, that can enhance T helper cell effector functions.

Research around host-directed therapies have focused on anti-inflammatories to limit pathology in established TB disease, however, there is also a role for cell targeted immune-augmentation (51, 71). This strategy might have a role in early infection events, or to improve myeloid killing of drug resistant bacilli (28). We recently demonstrated *in vivo* efficacy of this approach, using inhaled macrophage homing micro-particles that contain all-trans retinoic acid which drives macrophage anti-TB responses (72, 73). Targeting HDACs has previously been postulated to have potential as an adjunct host-directed therapy for TB (10, 74). Our data is also supported by published *in vivo* data showing that Tubastatin A, a selective HDAC6 inhibitor, reduced IL-10, and enhanced Th1 responses in mice infected with Mtb H37Ra (9). Based on the current cellular study and on recently published data indicating that HDACi enhanced anti-mycobacterial responses in human macrophages (10), SAHA warrants further investigation as an immunosupportive agent.

Study Limitations

Although treating human macrophages with SAHA showed promising effects on innate and adaptive immune responses to Mtb, our study ambiguously did not show any significant effects on bacterial load. SAHA has previously been shown to have no direct effect on growth of Mtb in an *in vitro* axenic culture model, however, it elicited a modest reduction in bacterial burden in THP1 macrophages co-treated with SAHA and rifampicin compared to rifampicin alone (35). Considering this and our current study, we postulate that combining SAHA with conventional antibiotic therapies may aid killing of the pathogen through innate and adaptive mechanisms. Moreover, HDACi including SAHA have been shown to prevent ototoxic hearing loss (75) caused by aminoglycoside antibiotics and may therefore have beneficial off-target affects.

Our data indicates that SAHA augments the innate immune response to Mtb via increased glycolysis. This boosted innate immune response propagates enhanced polyfunctional Th cell responses *in vitro*. Although SAHA may have therapeutic potential in settings where the immune response is impaired, we also recognise that such an approach may be detrimental during active TB disease.

The effects observed on T cells stimulated with Mtb-infected AM are confounded by the allogeneic nature of this co-culture. Although the T cell response is increased over the background allogeneic response, the differences in Th cell function may be

due to a bystander effect. Whilst we cannot fully rule this out, we have observed that SAHA-treated AM stimulated with LPS exhibit increased IL-1β and decreased IL-10 production and when these AM are co-cultured with PBMC, they do not elicit a T cell response over the background allogeneic response and no differences were observed between the treatment groups (data not shown).

We used an avirulent Mtb strain to model the successful host immune response, though we have previously shown that this is a good model for the viable virulent pathogen in these ex-vivo experiments (11, 29). Additionally, the use of irradiated H37Rv allows us to analyse the effects of SAHA on the host without the confounding factor of the drug manipulating mycobacterial epigenetics and causing an effect.

Whilst it is likely that SAHA induces epigenetic changes via HDAC inhibition, the current study cannot rule out the possibility of non-specific hyperacetylation of other proteins, as HDAC also deacetylate non-histone proteins (76).

Conclusion

Treating human macrophages with SAHA enhanced proinflammatory function by promoting the early shift to glycolysis. In turn, these SAHA-treated, Mtb infected macrophages enhanced the T helper cell response downstream compared with vehicle control-treated infected macrophages.

Our data provides a proof-of-concept in primary human macrophages and T cells to advance SAHA toward pre-clinical *in vivo* studies. It also provides new promising rationale for targeting epigenetics to modulate human immunometabolic processes in macrophages.

DATA AVAILABILITY STATEMENT

The datasets generated for this study are available on request to the corresponding author.

ETHICS STATEMENT

The studies involving human participants were reviewed and approved by St. James's Hospital and Tallaght University Hospital Research Ethics Committee. The patients/participants provided their written informed consent to participate in this study.

AUTHOR CONTRIBUTIONS

SB, DC, JK, and PD were responsible for the experimental conception, design, and analysis. SB, DC, AC, CÓ, KG, and JP carried out the experimental work. SB co-wrote the manuscript with DC and it was revised by all authors. JK was responsible for obtaining clinical samples. All authors contributed to the article and approved the submitted version.

FUNDING

This work was supported by grants from the Irish Research Council (awarded to SB), the Health Research Board, and the Royal City of Dublin Hospital Trust (awarded to JK).

SUPPLEMENTARY MATERIAL

The Supplementary Material for this article can be found online at: https://www.frontiersin.org/articles/10.3389/fimmu.2020.01609/full#supplementary-material

REFERENCES

1. WHO. *Global Tuberculosis Report 2019*. Geneva: WHO. (2019).
2. Mekonnen HS, Azagew AW. Non-adherence to anti-tuberculosis treatment, reasons and associated factors among TB patients attending at gondar town health centers, Northwest Ethiopia. *BMC Res Notes.* (2018) 11:691. doi: 10.1186/s13104-018-3789-4
3. Moores RC, Brilha S, Schutgens F, Elkington PT, Friedland JS. Epigenetic regulation of matrix metalloproteinase-1 and−3 expression in *Mycobacterium tuberculosis* infection. *Front Immunol.* (2017) 8:602. doi: 10.3389/fimmu.2017.00602
4. Kathirvel M, Mahadevan S. The role of epigenetics in tuberculosis infection. *Epigenomics.* (2016) 8:537–49. doi: 10.2217/epi.16.1
5. Koeken V, Verrall AJ, Netea MG, Hill PC, van Crevel R. Trained innate immunity and resistance to *Mycobacterium tuberculosis* infection. *Clin Microbiol Infect.* (2019) 25:1468–72. doi: 10.1016/j.cmi.2019.02.015
6. Bannister AJ, Kouzarides T. Regulation of chromatin by histone modifications. *Cell Res.* (2011) 21:381–95. doi: 10.1038/cr.2011.22
7. Seshadri C, Sedaghat N, Campo M, Peterson G, Wells RD, Olson GS, et al. Transcriptional networks are associated with resistance to *Mycobacterium tuberculosis* infection. *PLoS ONE.* (2017) 12:e0175844. doi: 10.1371/journal.pone.0175844
8. Chandran A, Antony C, Jose L, Mundayoor S, Natarajan K, Kumar RA. *Mycobacterium tuberculosis* infection induces HDAC1-mediated suppression of IL-12B gene expression in macrophages. *Front Cell Infect Microbiol.* (2015) 5:90. doi: 10.3389/fcimb.2015.00090
9. Wang X, Tang X, Zhou Z, Huang Q. Histone deacetylase 6 inhibitor enhances resistance to *Mycobacterium tuberculosis* infection through innate and adaptive immunity in mice. *Pathogens and Disease.* (2018) 76:fty064. doi: 10.1093/femspd/fty064
10. Moreira JD, Koch BEV, van Veen S, Walburg KV, Vrieling F, Mara Pinto Dabés Guimarães T, et al. Functional inhibition of Host Histone Deacetylases (HDACs) enhances *in vitro* and *in vivo* anti-mycobacterial activity in human macrophages and in zebrafish. *Front Immunol.* (2020) 11:36. doi: 10.3389/fimmu.2020.00036
11. Gleeson LE, Sheedy FJ, Palsson-McDermott EM, Triglia D, O'Leary SM, O'Sullivan MP, et al. Cutting edge: *Mycobacterium tuberculosis* induces aerobic glycolysis in human alveolar macrophages that is required for control of intracellular bacillary replication. *J Immunol.* (2016) 196:2444–9. doi: 10.4049/jimmunol.1501612
12. Ivashkiv LB. Epigenetic regulation of macrophage polarization and function. *Trends Immunol.* (2013) 34:216–23. doi: 10.1016/j.it.2012.11.001
13. Saeed S, Quintin J, Kerstens HH, Rao NA, Aghajanirefah A, Matarese F, et al. Epigenetic programming of monocyte-to-macrophage differentiation and trained innate immunity. *Science.* (2014) 345:1251086. doi: 10.1126/science.1251086
14. Arts RJW, Novakovic B, ter Horst R, Carvalho A, Bekkering S, Lachmandas E, et al. Glutaminolysis and fumarate accumulation integrate immunometabolic

and epigenetic programs in trained immunity. *Cell Metab.* (2016) 24:807–19. doi: 10.1016/j.cmet.2016.10.008
15. Phan AT, Goldrath AW, Glass CK. Metabolic and epigenetic coordination of T cell and macrophage immunity. *Immunity.* (2017) 46:714–29. doi: 10.1016/j.immuni.2017.04.016
16. Donohoe DR, Bultman SJ. Metaboloepigenetics: interrelationships between energy metabolism and epigenetic control of gene expression. *J Cell Physiol.* (2012) 227:3169–77. doi: 10.1002/jcp.24054
17. Aung HT, Schroder K, Himes SR, Brion K, van Zuylen W, Trieu A, et al. LPS regulates proinflammatory gene expression in macrophages by altering histone deacetylase expression. *FASEB J.* (2006) 20:1315–27. doi: 10.1096/fj.05-5360com
18. Poralla L, Stroh T, Erben U, Sittig M, Liebig S, Siegmund B, et al. Histone deacetylase 5 regulates the inflammatory response of macrophages. *J Cell Mol Med.* (2015) 19:2162–71. doi: 10.1111/jcmm.12595
19. Wang H, Cheng F, Woan K, Sahakian E, Merino O, Rock-Klotz J, et al. Histone deacetylase inhibitor LAQ824 augments inflammatory responses in macrophages through transcriptional regulation of IL-10. *J Immunol.* (2011) 186:3986–96. doi: 10.4049/jimmunol.1001101
20. Van den Bossche J, Neele AE, Hoeksema MA, de Heij F, Boshuizen MC, van der Velden S, et al. Inhibiting epigenetic enzymes to improve atherogenic macrophage functions. *Biochem Biophys Res Commun.* (2014) 455:396–402. doi: 10.1016/j.bbrc.2014.11.029
21. Nieto-Patlan E, Serafin-Lopez J, Wong-Baeza I, Perez-Tapia SM, Cobos-Marin L, Estrada-Parra S, et al. Valproic acid promotes a decrease in mycobacterial survival by enhancing nitric oxide production in macrophages stimulated with IFN-gamma. *Tuberculosis.* (2019) 114:123–6. doi: 10.1016/j.tube.2018.12.007
22. Ariffin JK, das Gupta K, Kapetanovic R, Iyer A, Reid RC, Fairlie DP, et al. Histone deacetylase inhibitors promote mitochondrial reactive oxygen species production and bacterial clearance by human macrophages. *Antimicrob Agents Chemother.* (2015) 60:1521–9. doi: 10.1128/AAC.01876-15
23. Coleman MM, Ruane D, Moran B, Dunne PJ, Keane J, Mills KH. Alveolar macrophages contribute to respiratory tolerance by inducing FoxP3 expression in naive T cells. *Am J Respir Cell Mol Biol.* (2013) 48:773–80. doi: 10.1165/rcmb.2012-0263OC
24. O'Leary SM, Coleman MM, Chew WM, Morrow C, McLaughlin AM, Gleeson LE, et al. Cigarette smoking impairs human pulmonary immunity to Mycobacterium tuberculosis. *Am J Respir Crit Care Med.* (2014) 190:1430–6. doi: 10.1164/rccm.201407-1385OC
25. Coleman MM, Basdeo SA, Coleman AM, Ni Cheallaigh C, Peral de Castro C, McLaughlin AM, et al. All-trans retinoic acid augments autophagy during intracellular bacterial infection. *Am J Respir Cell Mol Biol.* (2018) 59:548–56. doi: 10.1165/rcmb.2017-0382OC
26. Basdeo SA, Moran B, Cluxton D, Canavan M, McCormick J, Connolly M, et al. Polyfunctional, pathogenic CD161+ Th17 lineage cells are resistant to regulatory T cell-mediated suppression in the context of autoimmunity. *J Immunol.* (2015) 195:528–40. doi: 10.4049/jimmunol.1402990
27. Basdeo SA, Cluxton D, Sulaimani J, Moran B, Canavan M, Orr C, et al. Ex-Th17 (Nonclassical Th1) cells are functionally distinct from classical Th1 and Th17 cells and are not constrained by regulatory T cells. *J Immunol.* (2017) 198:2249–59. doi: 10.4049/jimmunol.1600737
28. Howard NC, Marin ND, Ahmed M, Rosa BA, Martin J, Bambouskova M, et al. *Mycobacterium tuberculosis* carrying a rifampicin drug resistance mutation reprograms macrophage metabolism through cell wall lipid changes. *Nat Microbiol.* (2018) 3:1099–108. doi: 10.1038/s41564-018-0245-0
29. Hackett EE, Charles-Messance H, O'Leary SM, Gleeson LE, Munoz-Wolf N, Case S, et al. *Mycobacterium tuberculosis* limits host glycolysis and IL-1beta by restriction of PFK-M via MicroRNA-21. *Cell Rep.* (2020) 30:124–36. doi: 10.1016/j.celrep.2019.12.015
30. Russell SL, Lamprecht DA, Mandizvo T, Jones TT, Naidoo V, Addicott KW, et al. Compromised metabolic reprogramming is an early indicator of CD8(+) T cell dysfunction during chronic *Mycobacterium tuberculosis* infection. *Cell Rep.* (2019) 29:3564–79.e5. doi: 10.1016/j.celrep.2019.11.034
31. Gleeson LE, O'Leary SM, Ryan D, McLaughlin AM, Sheedy FJ, Keane J. Cigarette smoking impairs the bioenergetic immune response to *Mycobacterium tuberculosis* infection. *Am J Respir Cell Mol Biol.* (2018) 59:572–9. doi: 10.1165/rcmb.2018-0162OC
32. Guo F, Zhang H, Zhu G, McNair NN, Mead JR. The existing drug vorinostat as a new lead against cryptosporidiosis by targeting the parasite histone deacetylases. *J Infect Dis.* (2018) 217:1110–7. doi: 10.1093/infdis/jix689
33. Archin NM, Liberty AL, Kashuba AD, Choudhary SK, Kuruc JD, Crooks AM, et al. Administration of vorinostat disrupts HIV-1 latency in patients on antiretroviral therapy. *Nature.* (2012) 487:482–5. doi: 10.1038/nature11286
34. Tiffon C, Adams J, van der Fits L, Wen S, Townsend P, Ganesan A, et al. The histone deacetylase inhibitors vorinostat and romidepsin downmodulate IL-10 expression in cutaneous T-cell lymphoma cells. *Br J Pharmacol.* (2011) 162:1590–602. doi: 10.1111/j.1476-5381.2010.01188.x
35. Rao M, Valentini D, Zumla A, Maeurer M. Evaluation of the efficacy of valproic acid and suberoylanilide hydroxamic acid (vorinostat) in enhancing the effects of first-line tuberculosis drugs against intracellular *Mycobacterium tuberculosis*. *Int J Infect Dis.* (2018) 69:78–84. doi: 10.1016/j.ijid.2018.02.021
36. Tran K, Risingsong R, Royce DB, Williams CR, Sporn MB, Pioli PA, et al. The combination of the histone deacetylase inhibitor vorinostat and synthetic triterpenoids reduces tumorigenesis in mouse models of cancer. *Carcinogenesis.* (2013) 34:199–210. doi: 10.1093/carcin/bgs319
37. Tannahill GM, Curtis AM, Adamik J, Palsson-McDermott EM, McGettrick AF, Goel G, et al. Succinate is an inflammatory signal that induces IL-1beta through HIF-1alpha. *Nature.* (2013) 496:238–42. doi: 10.1038/nature11986
38. Ip WKE, Hoshi N, Shouval DS, Snapper S, Medzhitov R. Anti-inflammatory effect of IL-10 mediated by metabolic reprogramming of macrophages. *Science.* (2017) 356:513–9. doi: 10.1126/science.aal3535
39. Cunningham CC, Corr EM, Cox DJ, Dunne A. Investigating inflammasome activation under conditions of cellular stress and injury. *Methods Mol Biol.* (2015) 1292:105–13. doi: 10.1007/978-1-4939-2522-3_8
40. Mayer-Barber KD, Barber DL, Shenderov K, White SD, Wilson MS, Cheever A, et al. Caspase-1 independent IL-1beta production is critical for host resistance to *Mycobacterium tuberculosis* and does not require TLR signaling *in vivo*. *J Immunol.* (2010) 184:3326–30. doi: 10.4049/jimmunol.0904189
41. Bourigault ML, Segueni N, Rose S, Court N, Vacher R, Vasseur V, et al. Relative contribution of IL-1alpha, IL-1beta and TNF to the host response to *Mycobacterium tuberculosis* and attenuated M. bovis BCG. *Immun Inflamm Dis.* (2013) 1:47–62. doi: 10.1002/iid3.9
42. Keane J, Gershon S, Wise RP, Mirabile-Levens E, Kasznica J, Schwieterman WD, et al. Tuberculosis associated with infliximab, a tumor necrosis factor alpha-neutralizing agent. *N Engl J Med.* (2001) 345:1098–104. doi: 10.1056/NEJMoa011110
43. Beamer GL, Flaherty DK, Assogba BD, Stromberg P, Gonzalez-Juarrero M, de Waal Malefyt R, et al. Interleukin-10 promotes *Mycobacterium tuberculosis* disease progression in CBA/J Mice. *J Immunol.* (2008) 181:5545. doi: 10.4049/jimmunol.181.8.5545
44. O'Leary S, O'Sullivan MP, Keane J. IL-10 blocks phagosome maturation in mycobacterium tuberculosis-infected human macrophages. *Am J Respir Cell Mol Biol.* (2011) 45:172–80. doi: 10.1165/rcmb.2010-0319OC
45. Cohen SB, Gern BH, Delahaye JL, Adams KN, Plumlee CR, Winkler JK, et al. Alveolar macrophages provide an early *Mycobacterium tuberculosis* niche and initiate dissemination. *Cell Host Microbe.* (2018) 24:439–46. doi: 10.1016/j.chom.2018.08.001
46. Dodd CE, Pyle CJ, Glowinski R, Rajaram MV, Schlesinger LS. CD36-Mediated uptake of surfactant lipids by human macrophages promotes intracellular growth of mycobacterium tuberculosis. *J Immunol.* (2016) 197:4727–35. doi: 10.4049/jimmunol.1600856
47. Huang L, Nazarova EV, Tan S, Liu Y, Russell DG. Growth of *Mycobacterium tuberculosis in vivo* segregates with host macrophage metabolism and ontogeny. *J Exp Med.* (2018) 215:1135. doi: 10.1084/jem.20172020
48. Orme IM, Robinson RT, Cooper AM. The balance between protective and pathogenic immune responses in the TB-infected lung. *Nat Immunol.* (2015) 16:57–63. doi: 10.1038/ni.3048
49. Rothchild AC, Stowell B, Goyal G, Nunes-Alves C, Yang Q, Papavinasasundaram K, et al. Role of granulocyte-macrophage colony-stimulating factor production by T cells during *Mycobacterium tuberculosis* infection. *mBio.* (2017) 8:e01514–7. doi: 10.1128/mBio.01514-17
50. Mills EL, Kelly B, Logan A, Costa ASH, Varma M, Bryant CE, et al. Succinate dehydrogenase supports metabolic repurposing of mitochondria to drive inflammatory macrophages. *Cell.* (2016) 167:457–70.e13. doi: 10.1016/j.cell.2016.08.064

51. Phelan JJ, McQuaid K, Kenny C, Gogan KM, Cox DJ, Basdeo SA, et al. Desferrioxamine supports metabolic function in primary human macrophages infected with *Mycobacterium tuberculosis*. *Front Immunol.* (2020) 11:836. doi: 10.3389/fimmu.2020.00836
52. Stammler D, Eigenbrod T, Menz S, Frick JS, Sweet MJ, Shakespear MR, et al. Inhibition of histone deacetylases permits lipopolysaccharide-mediated secretion of bioactive IL-1beta via a caspase-1-independent mechanism. *J Immunol.* (2015) 195:5421–31. doi: 10.4049/jimmunol.1501195
53. Hutt DM, Roth DM, Vignaud H, Cullin C, Bouchecareilh M. The histone deacetylase inhibitor, Vorinostat, represses hypoxia inducible factor 1 alpha expression through translational inhibition. *PLoS ONE.* (2014) 9:e106224. doi: 10.1371/journal.pone.0106224
54. Zhang C, Yang C, Feldman MJ, Wang H, Pang Y, Maggio DM, et al. Vorinostat suppresses hypoxia signaling by modulating nuclear translocation of hypoxia inducible factor 1 alpha. *Oncotarget.* (2017) 8:56110–25. doi: 10.18632/oncotarget.18125
55. Corcoran SE, O'Neill LAJ. HIF1α and metabolic reprogramming in inflammation. *J Clin Invest.* (2016) 126:3699–707. doi: 10.1172/JCI84431
56. Lawless SJ, Kedia-Mehta N, Walls JF, McGarrigle R, Convery O, Sinclair LV, et al. Glucose represses dendritic cell-induced T cell responses. *Nat Commun.* (2017) 8:15620. doi: 10.1038/ncomms15620
57. Robinson RT. T cell production of GM-CSF protects the host during experimental tuberculosis. *mBio.* (2017) 8:e02087–17. doi: 10.1128/mBio.02087-17
58. Flynn JL, Chan J, Triebold KJ, Dalton DK, Stewart TA, Bloom BR. An essential role for interferon gamma in resistance to *Mycobacterium tuberculosis* infection. *J Exp Med.* (1993) 178:2249–54. doi: 10.1084/jem.178.6.2249
59. Geldenhuys H, Mearns H, Miles DJ, Tameris M, Hokey D, Shi Z, et al. The tuberculosis vaccine H4:IC31 is safe and induces a persistent polyfunctional CD4 T cell response in South African adults: a randomized controlled trial. *Vaccine.* (2015) 33:3592–9. doi: 10.1016/j.vaccine.2015.05.036
60. Cox DJ, Keane J. Platelets and tuberculosis: small cells, not so innocent bystanders. *Am J Respir Crit Care Med.* (2018) 198:153–4. doi: 10.1164/rccm.201802-0279ED
61. Akdis CA, Blaser K. Mechanisms of interleukin-10-mediated immune suppression. *Immunology.* (2001) 103:131–6. doi: 10.1046/j.1365-2567.2001.01235.x
62. Uchiyama R, Yonehara S, Tsutsui H. Fas-mediated inflammatory response in *Listeria monocytogenes* infection. *J Immunol.* (2013) 190:4245–54. doi: 10.4049/jimmunol.1203059
63. Kleinnijenhuis J, Quintin J, Preijers F, Joosten LAB, Ifrim DC, Saeed S, et al. Bacille calmette-Guérin induces NOD2-dependent nonspecific protection from reinfection via epigenetic reprogramming of monocytes. *Proc Natl Acad Sci USA.* (2012) 109:17537. doi: 10.1073/pnas.1202870109
64. Horwitz SM. Targeting histone deacetylases in T-cell lymphoma. *Leuk Lymphoma.* (2017) 58:1306–19. doi: 10.1080/10428194.2016.1247956
65. Kaufmann E, Sanz J, Dunn JL, Khan N, Mendonca LE, Pacis A, et al. BCG educates hematopoietic stem cells to generate protective innate immunity against tuberculosis. *Cell.* (2018) 172:176–90.e119. doi: 10.1016/j.cell.2017.12.031
66. Tzelepis F, Blagih J, Khan N, Gillard J, Mendonca L, Roy DG, et al. Mitochondrial cyclophilin D regulates T cell metabolic responses and disease tolerance to tuberculosis. *Sci Immunol.* (2018) 3:aar4135. doi: 10.1126/sciimmunol.aar4135
67. Elkington P, Tebruegge M, Mansour S. Tuberculosis: an infection-initiated autoimmune disease? *Trends Immunol.* (2016) 37:815–8. doi: 10.1016/j.it.2016.09.007
68. Behar SM. Antigen-specific CD8(+) T cells and protective immunity to tuberculosis. *Adv Exp Med Biol.* (2013) 783:141–63. doi: 10.1007/978-1-4614-6111-1_8
69. Kaufmann SH. Protection against tuberculosis: cytokines, T cells, and macrophages. *Ann Rheum Dis.* (2002) 61(Suppl. 2):ii54–8. doi: 10.1136/ard.61.suppl_2.ii54
70. Torrado E, Fountain JJ, Liao M, Tighe M, Reiley WW, Lai RP, et al. Interleukin 27R regulates CD4+ T cell phenotype and impacts protective immunity during *Mycobacterium tuberculosis* infection. *J Exp Med.* (2015) 212:1449–63. doi: 10.1084/jem.20141520
71. Condos R, Rom WN, Schluger NW. Treatment of multidrug-resistant pulmonary tuberculosis with interferon-gamma via aerosol. *Lancet.* (1997) 349:1513–5. doi: 10.1016/S0140-6736(96)12273-X
72. O'Connor G, Krishnan N, Fagan-Murphy A, Cassidy J, O'Leary S, Robertson BD, et al. Inhalable poly(lactic-co-glycolic acid) (PLGA) microparticles encapsulating all-trans-Retinoic acid (ATRA) as a host-directed, adjunctive treatment for *Mycobacterium tuberculosis* infection. *Eur J Pharm Biopharm.* (2019) 134:153–65. doi: 10.1016/j.ejpb.2018.10.020
73. Lawlor C, O'Connor G, O'Leary S, Gallagher PJ, Cryan S-A, Keane J, et al. Treatment of mycobacterium tuberculosis-infected macrophages with poly(lactic-co-glycolic acid) microparticles drives NFκB and autophagy dependent bacillary killing. *PLoS ONE.* (2016) 11:e0149167. doi: 10.1371/journal.pone.0149167
74. Zumla A, Rao M, Dodoo E, Maeurer M. Potential of immunomodulatory agents as adjunct host-directed therapies for multidrug-resistant tuberculosis. *BMC Med.* (2016) 14:89. doi: 10.1186/s12916-016-0635-1
75. Layman WS, Williams DM, Dearman JA, Sauceda MA, Zuo J. Histone deacetylase inhibition protects hearing against acute ototoxicity by activating the NF-κB pathway. *Cell Death Discov.* (2015) 1:15012. doi: 10.1038/cddiscovery.2015.12
76. Glozak MA, Sengupta N, Zhang X, Seto E. Acetylation and deacetylation of non-histone proteins. *Gene.* (2005) 363:15–23. doi: 10.1016/j.gene.2005.09.010

Conflict of Interest: The authors declare that the research was conducted in the absence of any commercial or financial relationships that could be construed as a potential conflict of interest.

frontiers in Immunology

PERSPECTIVE
published: 23 July 2020
doi: 10.3389/fimmu.2020.01599

GM-CSF Dependent Differential Control of *Mycobacterium tuberculosis* Infection in Human and Mouse Macrophages: Is Macrophage Source of GM-CSF Critical to Tuberculosis Immunity?

Abhishek Mishra[1†], *Vipul Kumar Singh*[1†], *Jeffrey K. Actor*[2], *Robert L. Hunter*[2], *Chinnaswamy Jagannath*[1], *Selvakumar Subbian*[3] *and Arshad Khan*[1*]

[1] Department of Pathology and Genomic Medicine, Houston Methodist Research Institute, Houston, TX, United States, [2] Department of Pathology and Laboratory Medicine, McGovern Medical School, University of Texas Health Sciences Center-Houston, Houston, TX, United States, [3] Department of Medicine, New Jersey Medical School, Public Health Research Institute, Newark, NJ, United States

OPEN ACCESS

Edited by:
Rogelio Hernandez Pando, Instituto Nacional de Ciencias Médicas y Nutrición Salvador Zubirán (INCMNSZ), Mexico

Reviewed by:
Shashank Gupta, Brown University, United States
Marc Jacobsen, Heinrich Heine University of Düsseldorf, Germany

***Correspondence:**
Arshad Khan
akhan5@houstonmethodist.org

[†] These authors have contributed equally to this work

Specialty section:
This article was submitted to Microbial Immunology, a section of the journal Frontiers in Immunology

Received: 18 February 2020
Accepted: 16 June 2020
Published: 23 July 2020

Citation:
Mishra A, Singh VK, Actor JK, Hunter RL, Jagannath C, Subbian S and Khan A (2020) GM-CSF Dependent Differential Control of Mycobacterium tuberculosis Infection in Human and Mouse Macrophages: Is Macrophage Source of GM-CSF Critical to Tuberculosis Immunity? Front. Immunol. 11:1599. doi: 10.3389/fimmu.2020.01599

Although classically associated with myelopoiesis, granulocyte-macrophage colony-stimulating factor (GM-CSF) is being increasingly recognized for its potential role in innate resistance against tuberculosis (TB). While the GM-CSF is produced by a variety of host cells, including conventional and non-conventional T cells, macrophages, alveolar epithelial cells, the cell population that promotes GM-CSF mediated innate protection against *Mycobacterium tuberculosis* infection remains unclear. This is because studies related to the role of GM-CSF so far have been carried out in murine models of experimental TB, which is inherently susceptible to TB as compared to humans, who exhibit a resolution of infection in majority of cases. We found a significantly higher amount of GM-CSF production by human macrophages, compared to mouse macrophages, after infection with *M. tuberculosis in vitro*. The higher levels of GM-CSF produced by human macrophages were also directly correlated with their increased life span and ability to control *M. tuberculosis* infection. Other evidence from recent studies also support that *M. tuberculosis* infected human macrophages display heterogeneity in their antibacterial capacity, and cells with increased expression of genes involved in GM-CSF signaling pathway can control intracellular *M. tuberculosis* growth more efficiently. Collectively, these emerging evidence indicate that GM-CSF produced by lung resident macrophages could be vital for the host resistance against *M. tuberculosis* infection in humans. Identification of GM-CSF dependent key cellular pathways/processes that mediate intracellular host defense can lay the groundwork for the development of novel host directed therapies against TB as well as other intracellular infections.

Keywords: *Mycobacterium tuberculosis*, granulocyte monocyte colony stimulating factor, macrophage, cell death, innate immunity, tuberculosis

Traditionally, it is thought that protective immunity to tuberculosis (TB) is primarily mediated by T cells, with $CD4^+$ T cells playing a central role. However, many population-based immunological and genetic studies support the belief that innate immunity is equally important in TB immunopathogenesis (1–3). Macrophages, a critical part of the innate immune system, have paradoxically been also recognized as a primary intracellular niche for the growth and survival of *Mycobacterium tuberculosis* (MTB) (4). While the molecular details of the MTB-macrophage interaction continue to be elucidated, emerging evidence suggest that the phenotypes and functional capacities of the recruited macrophage may play a crucial role in determining the outcome of infection (5). Currently, the elements that govern the tremendous phenotypic heterogeneity and functional plasticity of macrophages are not precisely known. More recent studies indicate that GM-CSF-driven differentiation of monocytes toward a macrophage is critical for its increased responsiveness to microbial pathogens (6–8). The importance of GM-CSF in mediating MTB infection control and inflammation *in vivo* has previously been reported by us and others (9, 10). However, GM-CSF can be produced by a variety of host cells, including conventional and non-conventional T cells, macrophages, and alveolar epithelial cells. Most of the studies that have been conducted in murine models of TB suggest that the production of GM-CSF by lung epithelial cells, conventional, and non-conventional T cells are essential for generating a protective immune response and restricting MTB growth in the lungs (8–11). A recent study, clearly suggested that human macrophages were also able to produce GM-CSF upon infection with MTB, and their antimycobacterial properties correlated with their ability to produce GM-CSF (12). While MTB-infected human macrophages displayed cell-to-cell variability in their antibacterial capacity, cell populations with increased expression of genes involved in the GM-CSF signaling pathway were able to better control MTB growth. The reduced ability of HIV-infected macrophages to produce GM-CSF and control MTB infection further suggests that GM-CSF signaling mediates host defenses.

Murine macrophages are also known to produce GM-CSF in the lung compartment during MTB infection (8). However, in previous studies, it was unclear whether GM-CSF produced by macrophages could also contribute to the protective response against MTB infection in mice, especially during the early phase of infection when conventional T cells (CD4) have not come into effect. It is also important to consider that mice are naturally more susceptible to MTB infection, as compared to humans; therefore, it was intriguing to examine whether differential GM-CSF production occurs in human vs. mouse macrophages.

We thus examined the level of GM-CSF produced by mouse MDMs (monocyte-derived macrophages) compared to human MDMs before and after infection with MTB (**Figure 1A**). While intrinsic levels of GM-CSF were very low in both human and mouse MDMs, the human MDMs produced relatively higher levels of GM-CSF than did mouse MDMs, even without MTB infection. After infection with MTB, human MDMs produced 2.5- to 5-fold higher levels of GM-CSF compared to mouse MDMs when measured over 7 days. When the ratio of GM-CSF produced by infected and uninfected MDMs was calculated (from **Figure 1A**), human MDMs (3.02–4.66) were found to have a higher ratio as compared to mouse MDMs (2.62–3.48). This ratio also constantly increased with time in human MDMs whereas it remained more or less stable in mouse MDMs. The comparison of GM-CSF production of infected and uninfected MDMs further indicated that infection with MTB increased the production of GM-CSF more robustly in human macrophages as compared to mouse macrophages. The bacterial burden in mouse MDMs was also significantly higher compared to human MDMs (**Figure 1B**). Notably, the level of GM-CSF production by human vs. mouse MDMs was different even before infection as well as at the beginning of infection (Day 1) when both of them had similar uptake of the bacilli, which suggests that the differential production of GM-CSF by human vs. mouse MDMs was most likely not driven by their respective bacterial load. We also examined if the induction of GM-CSF production could specifically be related to MTB infection only. Thus, LPS was added to human and mouse MDMs separately before infection with MTB. We, however, and did not find LPS to increase a significant level of GM-CSF production in both human and mouse MDMs (**Figure S1**) as compared to MTB infection (**Figure 1A**). This indicated that induction of GM-CSF production by mouse and human macrophages could be driven independent of pattern recognition receptor (TLR4) activation and be more specifically related to MTB infection. Also, when other cytokines produced by MDMs were examined, no significant difference in TNF-α, IL-4, and IL-10 but higher levels of IL-12 production by human MDMs were observed as compared to mouse MDMs after infection with MTB (**Figure S2**). IL-12 is known to be critical for the maturation and differentiation of antigen presenting cells (13). A positive correlation between GM-CSF and IL-12 production by human MDMs after infection with MTB thus indicates that higher levels of GM-CSF could have driven an alternate maturation, differentiation, and activation of human MDMs as compared to mouse MDMs.

Interestingly, the viability decreased significantly, while the bacterial burden increased, with time in mouse MDMs (**Figure 1C**). In contrast, human MDMs exhibited less cell death after infection with MTB. Surprisingly, even uninfected mouse MDMs were unable to survive beyond 7 days as compared to human MDMs, which were able to maintain nearly 50% viability until day 21 (**Figure 1D**).

Because human MDMs produced more GM-CSF as compared to mouse MDMs, we hypothesized that GM-CSF may contribute to the increased survival of human MDMs. To test this hypothesis, we supplemented mouse GM-CSF to mouse MDMs cultivated *in vitro* and examined their viability before and after MTB infection. As expected, the addition of GM-CSF to mouse MDMs significantly increased the longevity of both uninfected and MTB-infected mouse MDMs (**Figure 1E**). The uninfected and MTB-infected mouse MDMs supplemented with 2 ng of mouse GM-CSF were able to maintain more than 60% cell viability until day 21. The overall bacterial burden in both mouse and human MDMs was significantly reduced with supplementary GM-CSF (**Figure 1F**).

We also observed that exogenous addition of GM-CSF enhanced secretion of IL-2 by antigen 85B specific T cells (F9A6) upon overlay to infected human MDMs, indicating

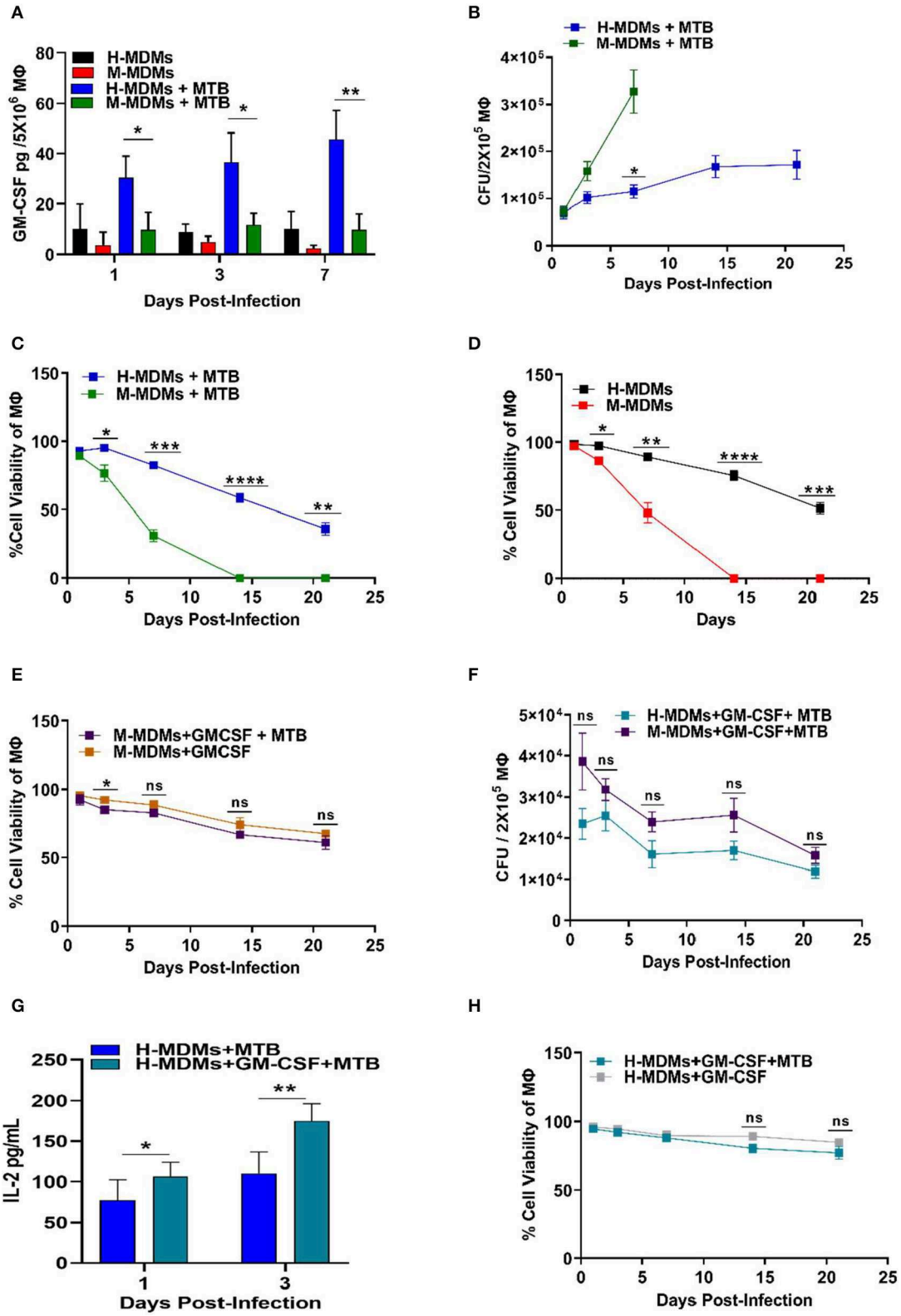

FIGURE 1 | Variability between human and mouse MDMs in their ability to secrete GM-CSF, control MTB infection and cell viability, and present antigens in the presence or absence of exogenous GM-CSF. **(A)** GM-CSF secreted by uninfected and MTB-infected human and mouse MDMs. **(B)** Changes in intracellular bacterial

(Continued)

FIGURE 1 | burden of mouse and human MDMs over 21 days. Bacterial burden in mouse MDMs could not be measured after 7 days because of complete death of host cells beyond this time point. **(C)** Cell viability of MTB-infected human and mouse MDMs over 21 days as measured by Alamar blue assay. **(D)** Cell viability of uninfected human and mouse MDMs over 21 days as measured by Alamar blue assay. **(E)** Effect of exogenous addition of GM-CSF on cell viability of MTB-infected and uninfected mouse MDMs with time. **(F)** Changes in bacterial burden with time in human and mouse MDMs after exogenous addition of GM-CSF (2 ng/mL/2 × 10^5 macrophages). **(G)** Antigen presentation levels (secreted IL-2 levels by MTB Ag85B specific T cells) of untreated and GM-CSF (2 ng/mL/2 × 10^5 macrophages) treated human MDMs at day 1 and 3 post-infection. **(H)** Effect of exogenous addition of GM-CSF on cell viability of MTB-infected and uninfected human MDMs with time. Data represent the average of three independent experiments carried out in duplicate. Bars and error bars represent means and SD, respectively. $*p \leq 0.05$, $**p \leq 0.005$, $***p \leq 0.0005$, $****p \leq 0.0001$.

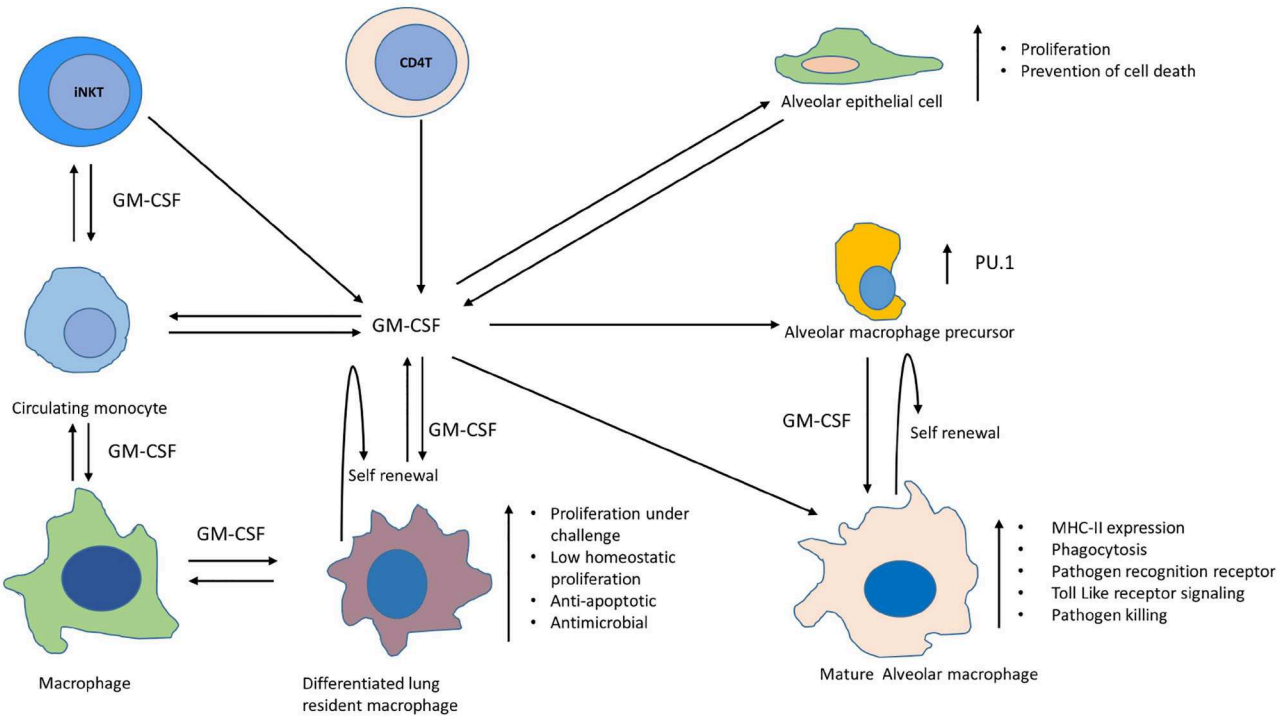

FIGURE 2 | Involvement of GM-CSF in differentiation, self-renewal, proliferation, and expansion of antimicrobial functions of different macrophage populations within lungs. Depicted are macrophages, monocytes, alveolar macrophages, alveolar epithelial cells, and other non-myeloid cells that produce GM-CSF in lungs during homeostasis and infection. Maturation of alveolar macrophage occurs in presence of GM-CSF leading to augmentation of their antimicrobial functions, such as increased expression of MHC-II, pathogen recognition receptors, activation of toll like receptor signaling and enhanced pathogen killing (14). GM-CSF is also required for self-renewal of AMs (15). Transcription factor PU.1 mediates this GM-CSF-dependent effects on differentiation of AMs and their innate immune functions during infections (16). Circulating monocytes can also be recruited to lungs during infections and GM-CSF assists in their differentiation into macrophages (17–19). GM-CSF further helps these differentiated macrophage in maintaining their self-renewal and a low homeostatic proliferation in the lungs during health, whereas challenge with infection/injury/inflammation can induce their proliferation in a GM-CSF dependent manner. These fully differentiated macrophages also exhibit strong anti-apoptotic and antimicrobial properties. Alveolar epithelial cells also produce GM-CSF which not only helps in clearance of surfactant proteins and lipids but also supports the differentiation of alveolar and recruited macrophages along with their innate effector functions against infections within lungs (9, 10, 20, 21). GM-CSF can also be produced by CD4 T and iNK T cells which can further contribute to the optimum level of this cytokine required for sustained macrophage effector functions against TB pathogen (11, 22).

a role for GM-CSF in improving antigen processing and presentation (**Figure 1G**). The GM-CSF-mediated increased antigen presentation by MTB-infected human MDMs became more prominent with time, indicating that GM-CSF gradually increased the fusion of bacteria-containing phagosomes with lysosomes. This could explain the observed decrease in bacterial load in the human cells (**Figure 1F**). Remarkably, human MDMs were also able to maintain their cell viability for a more extended period of time when GM-CSF was externally added to infected/uninfected cells (**Figure 1H**).

These results indicate that GM-CSF helped macrophage control MTB by decreasing bacterial load, while also preventing host cell death. These findings on human vs. murine monocyte-derived macrophages also indicate that the ability of macrophages to contain MTB infection could be due to the dual role of GM-CSF in prolonging the host cell survival as well as stimulating intracellular anti-MTB effector functions. Though not studied during MTB infection, GM-CSF has been known to modulate the developmental as well as effector functions of different lung macrophage populations (14). GM-CSF can stimulate oxidative metabolism, Fc-dependent phagocytosis,

and expression of class II major histocompatibility complex to boost the effector functions of macrophages (**Figure 2**). Based on these evidence together, it is intriguing to investigate whether lung resident macrophages that produce GM-CSF or respond to GM-CSF signaling could influence the outcome of MTB infection.

The role of GM-CSF is also well-defined in the self-renewal of macrophages, which is one of the mechanisms used to maintain a physiologically stable macrophage pool *in vivo* (23). Bone marrow-derived monocytes can settle in the lung during health as well as infection, and maintain their longevity through self-renewal (24, 25). Similarly, alveolar macrophages (AMs) also have the capacity of local self-renewal throughout life (15). GM-CSF is one of the critical intrinsic mitogenic signals required for self-renewal of both alveolar as well as bone marrow-derived macrophages in the lungs (**Figure 2**) (23). Macrophages of embryonic origin also require GM-CSF signaling to maintain the long-lived resident macrophage pool in the lungs. During the infection, increased production of GM-CSF has been shown to induce proliferation and differentiation of AMs which contributes to innate immunity in the lung (**Figure 2**) (16). Differentiation of AMs during infection is mediated through GM-CSF dependent increase in the expression of PU.1. Innate functions of AMs, such as cell adhesion, phagocytosis, pathogen killing, mannose-, and Toll-like receptor expression is promoted through PU.1. Macrophages derived from circulating monocytes also retain the capacity to proliferate and differentiate in the lungs during infection or inflammation and GM-CSF plays a pivotal role in the process (**Figure 2**) (17–19). While these fully differentiated macrophages can maintain a low homeostatic proliferation in the lungs during health, the challenge with infection/injury/inflammation can induce their proliferation strongly via GM-CSF. These differentiated lung macrophages also demonstrate increased antimicrobial properties. Though not studied in the context of MTB infection, evidences from earlier studies suggest that GM-CSF is essential to prevent apoptosis of macrophages during their differentiation (**Figure 2**) (26). We also observed a direct relationship between the levels of GM-CSF produced by macrophages and their ability to prevent cell death during MTB infection (**Figures 1A,C,D**). It is thus worth exploring whether this characteristic of self-renewal through GM-CSF helps against MTB infection *in vivo* as well. Simultaneous examination of these cellular processes during MTB infection can help us conclude whether GM-CSF signaling, cell differentiation, and cell death/survival pathways are linked with protective innate responses of macrophages. Because the lung is the primary site of MTB infection, and alveolar and resident macrophages are the primary host cells for the pathogen, relative levels of GM-CSF in the lung may determine macrophage function and their biological properties that, in turn, may influence the outcome of infection. Though in a murine model of TB, the protective role of GM-CSF producing non-myeloid cells, such as iNKT and CD4 T cells has also been reported during MTB infection which suggests that perhaps these cells could also be contributing to maintain an optimum level of GM-CSF required for the effective functioning of macrophages (**Figure 2**) (11, 22). While the local proliferation of alveolar and resident macrophages has been reported in humans as well as mice (27, 28), the latter is naturally more susceptible to TB. Infection of mice with MTB leads to progressive disease in all animals resulting in their premature death, in contrast to human populations that do not develop the primary disease in 90% cases. Considering this difference, how the levels and cellular source of GM-CSF in mice vs. human lungs differ before and after infection with MTB is important to understand. Multiple prolonged investigations so far have failed to find any consistent correlates of immunity that can distinguish adults who develop clinical TB from those who remain healthy. Most of these investigations have been carried out in experimental animal models that do not resemble the true immunopathological events that naturally occur during different outcomes in humans after exposure to MTB. In order to find the immune correlates and GM-CSF mediated mechanism of protection against TB, it is imperative to compare the immunopathological events that unfold in TB susceptible vs. TB resistant individuals/animal models after exposure to pathogen. While it is challenging to conduct such studies in humans, experimental animal models of rhesus macaque, cynomolgus macaque, and rabbit, have been developed in the past which could be explored to investigate the role of GM-CSF during different outcomes of MTB infection (29–31). It is also worth investigating if differences in GM-CSF levels and cellular sources within and outside of the lungs exist in TB-susceptible vs. TB-resistant human populations. The existence of polymorphisms in the GM-CSF gene or its receptor/s also needs to be analyzed to further validate the role of GM-CSF in innate immunity to TB. Answers to these unresolved questions through future studies may well envision a therapeutic role for GM-CSF, either through host-directed therapies or vaccines that elicit optimal GM-CSF production to control MTB.

DATA AVAILABILITY STATEMENT

All datasets generated for this study are included in the article/**Supplementary Material**.

ETHICS STATEMENT

The studies involving human participants were reviewed and approved by UTHSC-Houston IRB. Written informed consent for participation was not required for this study in accordance with the national legislation and the institutional requirements.

AUTHOR CONTRIBUTIONS

AK designed the study. AM and VS led the project, conducted the experiments and analyzed the data. AK wrote the manuscript. SS edited the manuscript. CJ, JA, and RH provided the feedback on the manuscript.

SUPPLEMENTARY MATERIAL

The Supplementary Material for this article can be found online at: https://www.frontiersin.org/articles/10.3389/fimmu.2020.01599/full#supplementary-material

REFERENCES

1. Morrison J, Pai M, Hopewell PC. Tuberculosis and latent tuberculosis infection in close contacts of people with pulmonary tuberculosis in low-income and middle-income countries: a systematic review and meta-analysis. *Lancet Infect Dis.* (2008) 8:359–68. doi: 10.1016/S1473-3099(08)70071-9
2. Netea MG, Joosten LAB, Latz E, Mills KHG, Natoli G, Stunnenberg HG, et al. Trained immunity: a program of innate immune memory in health and disease. *Science.* (2016) 352:aaf1098. doi: 10.1126/science.aaf1098
3. Gupta N, Kumar R, Agrawal B. New players in immunity to tuberculosis: the host microbiome, lung epithelium, and innate immune cells. *Front Immunol.* (2018) 9:709. doi: 10.3389/fimmu.2018.00709
4. Pieters J. Mycobacterium tuberculosis and the macrophage: maintaining a balance. *Cell Host Microbe.* (2008) 3:399–407. doi: 10.1016/j.chom.2008.05.006
5. Khan A, Singh VK, Hunter RL, Jagannath C. Macrophage heterogeneity and plasticity in tuberculosis. *J Leukoc Biol.* (2019) 106:275–82. doi: 10.1002/JLB.MR0318-095RR
6. van der Does AM, Bogaards SJP, Ravensbergen B, Beekhuizen H, van Dissel JT, Nibbering PH. Antimicrobial peptide hLF1-11 directs granulocyte-macrophage colony-stimulating factor-driven monocyte differentiation toward macrophages with enhanced recognition and clearance of pathogens. *Antimicrob Agents Chemother.* (2010) 54:811–6. doi: 10.1128/AAC.00652-09
7. Pasula R, Azad AK, Gardner JC, Schlesinger LS, McCormack FX. Keratinocyte growth factor administration attenuates murine pulmonary mycobacterium tuberculosis infection through granulocyte-macrophage colony-stimulating factor (GM-CSF)-dependent macrophage activation and phagolysosome fusion. *J Biol Chem.* (2015) 290:7151–9. doi: 10.1074/jbc.M114.591891
8. Benmerzoug S, Marinho FV, Rose S, Mackowiak C, Gosset D, Sedda D, et al. GM-CSF targeted immunomodulation affects host response to M. tuberculosis infection. *Sci Rep.* (2018) 8:8652. doi: 10.1038/s41598-018-26984-3
9. Szeliga J, Daniel DS, Yang CH, Sever-Chroneos Z, Jagannath C, Chroneos ZC. Granulocyte–macrophage colony stimulating factor-mediated innate responses in tuberculosis. *Tuberculosis.* (2008) 88:7–20. doi: 10.1016/j.tube.2007.08.009
10. Gonzalez-Juarrero M, Hattle JM, Izzo A, Junqueira-Kipnis AP, Shim TS, Trapnell BC, et al. Disruption of granulocyte macrophage-colony stimulating factor production in the lungs severely affects the ability of mice to control *Mycobacterium tuberculosis* infection. *J Leukoc Biol.* (2005) 77:914–22. doi: 10.1189/jlb.1204723
11. Rothchild AC, Jayaraman P, Nunes-Alves C, Behar SM. iNKT cell production of GM-CSF controls *Mycobacterium tuberculosis*. *PLoS Pathog.* (2014) 10:e1003805. doi: 10.1371/journal.ppat.1003805
12. Bryson BD, Rosebrock TR, Tafesse FG, Itoh CY, Nibasumba A, Babunovic GH, et al. Heterogeneous GM-CSF signaling in macrophages is associated with control of *Mycobacterium tuberculosis*. *Nat Commun.* (2019) 10:2329. doi: 10.1038/s41467-019-10065-8
13. Liu J, Cao S, Kim S, Chung EY, Homma Y, Guan X, et al. Interleukin-12: an update on its immunological activities, signaling and regulation of gene expression. *Curr Immunol Rev.* (2005) 1:119–37. doi: 10.2174/1573395054065115
14. Coleman DL, Chodakewitz JA, Bartiss AH, Mellors JW. Granulocyte-macrophage colony-stimulating factor enhances selective effector functions of tissue-derived macrophages. *Blood.* (1988) 72:573–8. doi: 10.1182/blood.V72.2.573.bloodjournal722573
15. Tarling JD, Lin H, Hsu S. Self-renewal of pulmonary alveolar macrophages: evidence from radiation chimera studies. *J Leukoc Biol.* (1987) 42:443–6. doi: 10.1002/jlb.42.5.443
16. Shibata Y, Berclaz PY, Chroneos ZC, Yoshida M, Whitsett JA, Trapnell BC. GM-CSF regulates alveolar macrophage differentiation and innate immunity in the lung through PU.1. *Immunity.* (2001) 15:557–67. doi: 10.1016/S1074-7613(01)00218-7
17. Sieweke MH, Allen JE. Beyond stem cells: self-renewal of differentiated macrophages. *Science.* (2013) 342:1242974. doi: 10.1126/science.1242974
18. Shi C, Pamer EG. Monocyte recruitment during infection and inflammation. *Nat Rev Immunol.* (2011) 11:762–74. doi: 10.1038/nri3070
19. McClean CM, Tobin DM. Macrophage form, function, and phenotype in mycobacterial infection: lessons from tuberculosis and other diseases. *Pathog Dis.* (2016) 74:ftw068. doi: 10.1093/femspd/ftw068
20. Rösler B, Herold S. Lung epithelial GM-CSF improves host defense function and epithelial repair in influenza virus pneumonia—a new therapeutic strategy? *Mol Cell Pediatr.* (2016) 3:29. doi: 10.1186/s40348-016-0055-5
21. Huffman JA, Hull WM, Dranoff G, Mulligan RC, Whitsett JA. Pulmonary epithelial cell expression of GM-CSF corrects the alveolar proteinosis in GM-CSF-deficient mice. *J Clin Invest.* (1996) 97:649–55. doi: 10.1172/JCI118461
22. Rothchild AC, Stowell B, Goyal G, Nunes-Alves C, Yang Q, Papavinasasundaram K, et al. Role of granulocyte-macrophage colony-stimulating factor production by T cells during mycobacterium tuberculosis infection. *MBio.* (2017) 8:e01514–17. doi: 10.1128/mBio.01514-17
23. Röszer T. Understanding the biology of self-renewing macrophages. *Cells.* (2018) 7:103. doi: 10.3390/cells7080103
24. Hashimoto D, Chow A, Noizat C, Teo P, Beasley MB, Leboeuf M, et al. Tissue-resident macrophages self-maintain locally throughout adult life with minimal contribution from circulating monocytes. *Immunity.* (2013) 38:792–804. doi: 10.1016/j.immuni.2013.04.004
25. Belhareth R. Macrophage populations and self-renewal: changing the paradigm. *World J Immunol.* (2015) 5:131. doi: 10.5411/wji.v5.i3.131
26. Zhang Y, Morgan MJ, Chen K, Choksi S, Liu Z-G. Induction of autophagy is essential for monocyte-macrophage differentiation. *Blood.* (2012) 119:2895–905. doi: 10.1182/blood-2011-08-372383
27. Huang L, Nazarova E V., Tan S, Liu Y, Russell DG. Growth of *Mycobacterium tuberculosis in vivo* segregates with host macrophage metabolism and ontogeny. *J Exp Med.* (2018) 215:1135–52. doi: 10.1084/jem.20172020
28. Nakata K, Gotoh H, Watanabe J, Uetake T, Komuro I, Yuasa K, et al. Augmented proliferation of human alveolar macrophages after allogeneic bone marrow transplantation. *Blood.* (1999) 93:667–73. doi: 10.1182/blood.V93.2.667
29. Lin PL, Rodgers M, Smith L, Bigbee M, Myers A, Bigbee C, et al. Quantitative comparison of active and latent tuberculosis in the cynomolgus macaque model. *Infect Immun.* (2009) 77:4631–42. doi: 10.1128/IAI.00592-09
30. Mehra S, Golden NA, Dutta NK, Midkiff CC, Alvarez X, Doyle LA, et al. Reactivation of latent tuberculosis in rhesus macaques by coinfection with simian immunodeficiency virus. *J Med Primatol.* (2011) 40:233–43. doi: 10.1111/j.1600-0684.2011.00485.x
31. Subbian S, Tsenova L, O'Brien P, Yang G, Kushner NL, Parsons S, et al. Spontaneous latency in a rabbit model of pulmonary tuberculosis. *Am J Pathol.* (2012) 181:1711–24. doi: 10.1016/j.ajpath.2012.07.019

Conflict of Interest: The authors declare that the research was conducted in the absence of any commercial or financial relationships that could be construed as a potential conflict of interest.

frontiers in Microbiology

ORIGINAL RESEARCH
published: 07 August 2020
doi: 10.3389/fmicb.2020.01901

Decreased Expression of CD69 on T Cells in Tuberculosis Infection Resisters

Zhen-Yan Chen[1†], Lei Wang[2†], Ling Gu[1], Rong Qu[3], Douglas B. Lowrie[1,4], Zhidong Hu[1,4], Wei Sha[2*] and Xiao-Yong Fan[3,4*]*

[1] Shanghai Public Health Clinical Center, Key Laboratory of Medical Molecular Virology of MOE/MOH, Fudan University, Shanghai, China, [2] Shanghai Pulmonary Hospital, Tongji University, Shanghai, China, [3] School of Laboratory Medicine and Life Science, Wenzhou Medical University, Wenzhou, China, [4] TB Center, Shanghai Emerging and Re-emerging Institute, Shanghai, China

OPEN ACCESS

Edited by:
Rogelio Hernandez Pando, Instituto Nacional de Ciencias Médicas y Nutrición Salvador Zubirán (INCMNSZ), Mexico

Reviewed by:
Yvonne Rosenstein, National Autonomous University of Mexico, Mexico
Jiezuan Yang, Zhejiang University, China

***Correspondence:**
Zhidong Hu
huzhidong2008@163.com
Wei Sha
shfksw@126.com
Xiao-Yong Fan
xyfan008@fudan.edu.cn

[†] These authors have contributed equally to this work

Specialty section:
This article was submitted to Microbial Immunology, a section of the journal Frontiers in Microbiology

Received: 30 April 2020
Accepted: 20 July 2020
Published: 07 August 2020

Citation:
Chen Z-Y, Wang L, Gu L, Qu R, Lowrie DB, Hu Z, Sha W and Fan X-Y (2020) Decreased Expression of CD69 on T Cells in Tuberculosis Infection Resisters. Front. Microbiol. 11:1901. doi: 10.3389/fmicb.2020.01901

Background: CD69 is a biomarker of T-cell activation status, but its activation status in human *Mycobacterium tuberculosis* (*Mtb*) infection remains elusive.

Methods: A set of cohorts of patients with different tuberculosis (TB) infection status including active TB patients (ATB), latent tuberculous infection patients (LTBI) and close contacts (CCs) of ATB was designed, and the expression profiles of CD69 and several T-cell markers were determined on *Mtb* antigen-stimulated T cells by flow cytometry.

Results: The frequencies of $CD4^+$ and $CD8^+$ T cells were both comparable among *Mtb*-infected individuals including ATB and LTBI, which guaranteed the consistency of the background level. A t-Distributed Stochastic Neighbor Embedding (tSNE) analysis on a panel of six phenotypic markers showed a unique color map axis gated on T cells in the CCs group compared with ATB and LTBI populations. By further gating on cells positive for each individual marker and then overlaying those events on top of the tSNE plots, their distribution suggested that some markers were expressed differently in the CCs group. Further analysis showed that the expression levels of CD69 on both $CD4^+$ and $CD8^+$ T cells were significantly lower in the CCs group, especially in interferon-γ-responding T cells.

Conclusion: Our findings suggest that the T-cell activation status of CD69 is associated with *Mtb* infection and may have the potential to distinguish LTBI from those populations who have been exposed continuously to *Mtb* but have not become infected.

Keywords: tuberculosis, CD69, T-cell, latent infection, close contacts, resister

INTRODUCTION

Tuberculosis (TB) is the leading cause of death due to a single infectious disease in the world, there were an estimated 10 million new TB cases and 1.5 million deaths in the year of 2018 (WHO, 2019). Host-directed therapy is a promising strategy for TB treatment but it has not yielded persuasive results due to our incomplete understanding of immunological mechanism against this disease.

About a quarter of the world's population has latent TB infection (LTBI), and their lifetime risk of developing TB disease is around 5%∼15% (WHO, 2019). *Mycobacterium tuberculosis* (*Mtb*)

infection is defined by standard clinical tests including tuberculin skin tests (TST) and interferon (IFN)-γ release assays (IGRAs). Recently, it was reported that nine months of isoniazid or four months of rifampin treatment can prevent the development of active TB disease in persons with LTBI (Samanovic and Darwin, 2016), illustrating the feasibility of sterile eradiation of *Mtb* in latent infection. However, the exact risk and timing of disease resulting from the exposure of close contacts (CCs) to active TB patients (ATB) have not been determined (Reichler et al., 2018). Recently, particular attention has been placed on the group of CCs with persistently negative TST/IGRA results despite prolonged exposure, a group termed "resisters" (Simmons et al., 2018; Kaipilyawar and Salgame, 2019). Identification of differential epidemiological and immunological characteristics of the CCs that are either "resisters" or LTBI will provide greater biological insights to prevent or clear early TB infections and develop novel diagnostic methods.

T cells, especially Th1 $CD4^+$ T cells, are a crucial part of anti-TB immunity. T-cell activation and exhaustion represent the different immune status at different stages of *Mtb* infection, distinguished by the expression of specific biomarkers. Our previous work demonstrated that the expression of KLRG1, regarded as a T-cell terminal differentiation biomarker, was associated with the progression of human TB (Hu et al., 2018). In animal infection/vaccination models, the expression of several T-cell biomarkers, such as CD38 (Dintwe et al., 2013), CD69 (Andersen and Smedegaard, 2000; Kauffman et al., 2018), CTLA-4 (Kirman et al., 1999; Nandakumar et al., 2014), LAG-3 (Workman et al., 2004; Phillips et al., 2015), Tim-3 (Jayaraman et al., 2016), and PD-1 (Lazar-Molnar et al., 2010; Reiley et al., 2010), has been reported to be related to TB infection. However, association with clinical TB has not been shown for all of them, especially their expression profiles in CCs remain to be defined.

In this study, the expression profiles of six biomarkers related to TB infection were compared among ATB, LTBI and CCs populations by flow cytometry in a designed cohort. As a result, Although the frequency of T cells was identical among these groups, a t-Distributed Stochastic Neighbor Embedding (tSNE) analysis on a panel including the phenotypic markers showed a unique color map axis gated on T cells in the CCs group compared with ATB and LTBI populations. By further gating on cells positive for each marker and then overlaying those events on top of the tSNE plots, their distribution suggested that some makers were differently expressed in the CCs group. Further analysis showed that the expression levels of CD69 on both $CD4^+$ and $CD8^+$ T cells were significantly lower in CCs group, especially on antigen-specific T cells. Thus, our data suggest that the activation status of CD69 might be associated with TB disease progression, and showed the potential to distinguish CCs from LTBI populations.

MATERIALS AND METHODS

Subjects

This study was approved by the Ethical Committee of Shanghai Pulmonary Hospital (approval number K18-215Z), and informed consent was obtained from all subjects. As shown in **Table 1**, the cohort comprised 45 ATB, 15 LTBI, 13 CCs and 17 non-TB-infected/close contacted persons (Non-TB). ATB was identified on the basis of sputum or effusion smear or polymerase chain reaction amplification positivity, confirmed by radiological findings and clinical syndromes, alongside with a final clinical diagnosis of ATB. LTBI was defined as IGRA-positive without clinical syndromes of active TB infection. CCs populations who were highly exposed to *Mtb* without infection fulfilled the following criteria: persons who had shared air space with an individual with pulmonary TB in the household or other indoor setting for > 15 hr per week or > 180 hr total during an infectious period (an infectious period was defined as the interval from 3 months before collection of the first culture-positive sputum specimen or the date of onset of cough, whichever was longer, through 2 weeks after the initiation of appropriate anti-tuberculosis treatment) and they were IGRA/TST negative without clinical syndromes of active TB infection. Non-TB subjects were defined as not *Mtb*-infected (IGRA-negative) and not having had close contact with ATB patients. All subjects were HIV/HCV-negative and were not taking immunosuppressive drugs.

Peripheral Blood Mononuclear Cells (PBMCs) Isolation

An equal volume of heparinized peripheral venous blood and RPMI-1640 cell culture medium (Hyclone) were mixed and slowly added onto an equal volume of lymphocyte separation solution Ficoll at room temperature (HMK). The diluted whole blood was layered on top of the lymphocyte separation solution with a clear interface. After centrifugation at 600 x *g* for 20 min, PBMCs were collected and washed two times with RPMI 1640 medium. The cells were suspended in 1 mL R10 medium (RPMI-1640 medium containing 10% (v/v) fetal bovine serum [FBS]). Viability and numbers of cells were determined using trypan blue in a counting chamber.

T-Spot Assay

T-Spot assay uses an ELISpot (enzyme-linked immune absorbent spot) platform for diagnosing TB infection (Beijing Jinhao, China). The test was performed according to the instructions of the manufacturer (Li et al., 2017). Briefly, PBMCs were added into a 96-well plate which was pre-coated with antibodies against IFN-γ in a volume of 100 μL/well with or without ESAT-6 and CFP10 peptides added as stimulants. After incubation at 37° in a 5% CO_2 incubator for 18∼20 h, the wells were washed and a working solution of a second antibody conjugated to biotin was added (100 μL/well). After incubation for 1 h at room temperature, the wells were washed and the enzyme conjugate working solution was added (100 μL/well) and incubated for another 1 h at room temperature. After washing again, the chromogenic substrate AEC working solution was added (100 μL/well) and incubated at room temperature for 7 min in the dark. Purified water was added to stop the reaction. The spots were counted by using an ImmunoSpot Reader (ChampSpot III, Beijing Sage Creation Science, China).

TABLE 1 | Clinical characteristics of study participants.

Groups	Patients with Active Tuberculosis (*n* = 45)	Latent Tuberculosis Infection (*n* = 15)	Close Contacts (*n* = 13)	Non-TB populations (*n* = 17)
Age, yr	41.82 (14–77)	43.27 (17–73)	44.02 (33–75)	43.71 (23–76)
Tuberculosis manifestation				
Pulmonary	33.33	N/A	N/A	N/A
Extrapulmonary	0	N/A	N/A	N/A
Both	66.67	N/A	N/A	N/A
Smear/culture/ PCR positivity	100	0	N/A	N/A
Sex, %				
Male	60	66.67	69.23	64.71
Female	40	33.33	30.77	35.29
BCG vaccinated	100	100	100	100
HIV	0	0	0	0

Data are median values (range) or percentage of participants. N/A, not applicable; PCR, polymerase chain reaction.

The results were defined as positive if the spots in the detection hole numbered at least 6 when the spots in negative control hole were fewer than 6, or the spots in the detection well were twice as many as the spots in the negative control when the number in the negative control hole was greater than 6.

Intracellular Cytokine Staining (ICS) and Flow Cytometric Analysis

The ICS assay was measured as described elsewhere (Hu et al., 2017). Briefly, the freshly isolated PBMCs were stimulated with peptide pools of ESAT-6 and CFP10 (5 μg/mL, synthesized by GL Biochem, China) in the presence of Brefeldin A and Monensin (both 1 μg/mL, BD Biosciences) in a round-bottom 96-well plate at 37° and 5% CO_2 for 12 h. After centrifugation at 600 x *g* for 5 min at 4°, the cells were surface-stained with 50 μL of the appropriate antibody panel diluted in PBS buffer containing 2% FBS for 30 min at 4° in the dark, followed by washing, fixation and permeabilization with Cytofix/Cytoperm (BD Biosciences) for 20 min at 4° in the dark. The fixed cells were washed then treated with a panel of antibodies against intracellular cytokines in a final volume of 50 μL and incubated for another 30 min at 4° in the dark. Finally, the cells were washed and transferred into the flow tube and analyzed by flow cytometry (LSR Fortessa, BD Biosciences). The data were analyzed by FlowJo 10 software (Ashland, OR).

t-Distributed Stochastic Neighbor Embedding (tSNE) Analysis

tSNE is a machine learning dimensionality-reducing algorithm that compares similarities of data points in high dimensional space and plots it in two dimensions through a way that preserves the structure of the dataset. In this study, firstly, all of the flow cytometry data from the ATB, LTBI and CCs groups were electronically concatenated into a single FCS file using FlowJo 10 software. Then the large concatenated files were down-sampled to create separate files for each group at a size of 50, 000 events/group. The equal-sized files were then gated on $CD4^+$ T cells based on the antibodies of CD3 and CD4, and tSNE analysis was performed in FlowJo using iterations = 1000 and perplexity = 30. The number of iterations refers to the number of loops in the repeated execution of the program, the default number (=1000) was used in this study. Perplexity is associated with the number of nearest neighbors that are used in learning algorithms and can be regarded as a knob that sets the number of effective nearest neighbors in tSNE analysis. The most appropriate value depends on the density of the data, a relatively large value (=30) was used since a large dataset was analyzed in this study.

Antibodies

The antibodies used in this study: CD3-PE/Dazzle594 (clone OKT3), CD38-FITC (clone 303504), CD69-Alexa Fluor 700 (clone 310922), Tim-3-Brilliant Violet 421 (clone F38-2E2) and CTLA-4-Percp-Cy5.5 (clone BN13) were from Biolegend. CD4-PE-Cy5 (clone RPA-T4), HLA-DR-APC (clone LN3), PD-1-APC-eFluor780 (clone EbioJ105) and IFN-γ-PE-Cy7 (clone 4S.B3) were from eBioscience.

Statistical Analysis

Statistical analyses were done using GraphPad Prism 7 software (La Jolla, CA). The data had a normal distribution and homogeneity of variance. The statistical differences between groups were assessed using one-way ANOVA tests. $P < 0.05$ was considered statistically significant.

RESULTS

Comparable T-Cell Frequencies Among ATB, LTBI, and CCs Groups

To explore the role of T cells in close contacts of TB patients, we firstly compared the frequencies of $CD4^+$ and $CD8^+$ T cells among TB, LTBI and CCs groups (the gating strategy is shown in **Supplementary Figure S1**). As shown in **Figures 1A,B**, the percentages of $CD4^+$ and $CD8^+$ T cells were comparable among groups as expected.

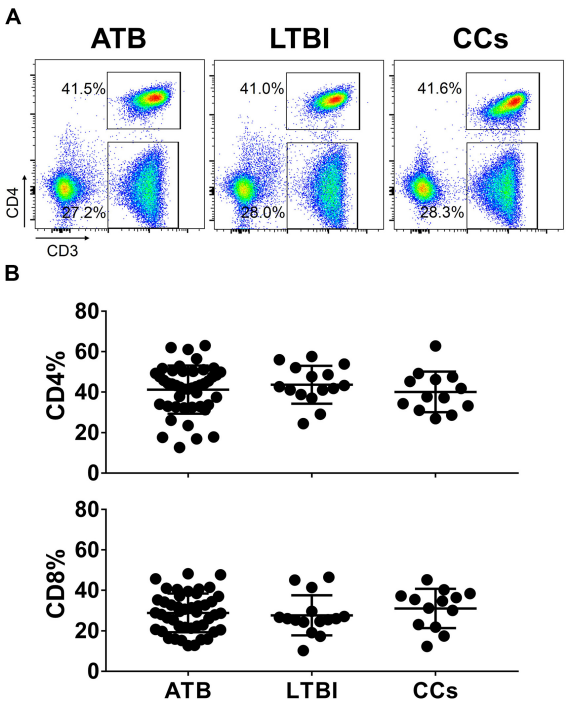

FIGURE 1 | The frequencies of $CD4^+$ and $CD8^+$ T cell subsets among groups. The freshly isolated PBMCs were stimulated with peptide pools for 12 h, and the percentage of $CD4^+$ T cells and $CD8^+$ T cells were determined by flow cytometry. Representative flow cytometric dot plots are shown in **(A)**. $CD4^+$ T cells were gated as $CD3^+CD4^+$ cells and $CD8^+$ T cells were defined as $CD3^+CD4^-$ cells. Summarized data are shown as scatter dots in **(B)**.

tSNE Analysis of a Panel Including Several Phenotypic Markers on T Cells

To further delineate the profiles of T cell-mediated immune responses in the CCs group, six T-cell biomarkers that had been reported to be associated with *Mtb* infection in mouse models were used. By gating on cells positive for each marker and then overlaying those events on top of the tSNE plots, we found that the cell distribution was similar between ATB and LTBI groups in a 2D scatterplot. Interestingly, the CCs group showed a unique plot map compared with the other two groups (**Figure 2**). This led us to further analysis of the different expression profiles of these markers.

CD69 Is Under-Expressed on $CD4^+$ and $CD8^+$ T Cells in CCs

As shown in **Figures 3A,B**, the percentage of $CD69^+$ cells among $CD4^+$ T cells was significantly lower in household contacts and non-TB infected/close-contacted populations, compared with patients infected or latently infected with TB. The expression of CD69 showed no significant differences between the ATB and LTBI groups. The CCs and Non-TB groups also showed comparable CD69 expression on $CD4^+$ T cells (**Figure 3**). The differences between groups in mean fluorescence intensity (MFI) values of CD69 on $CD4^+$ T cells did not reach statistical significance (**Supplementary Figure S2**). Similarly, CD69 was also under-expressed on $CD8^+$ T cells in CCs and Non-TB groups compared with TB infection groups (**Figure 4**). In contrast, the expression profiles of CD38, CTLA-4, HLA-DR, PD, and Tim-3 were comparable on both $CD4^+$ T cells and $CD8^+$ T cells, except that the expression of CD38 on $CD8^+$ T cells was lower in CCs groups than in ATB patients (**Figure 5**). Thus, these data suggest that the activation status of CD69 is associated with *Mtb* infection and may have the potential to distinguish LTBI from those populations who are exposed continuously to *Mtb* but are not infected.

The Expression of CD69 on IFN-γ-Responding T Cells

To further characterize the association of CD69 with the status of TB infection, we tested the frequency of CD69 on *Mtb*-specific T cells, which were defined as T cells that responded to produce IFN-γ after stimulation with *Mtb* antigens ESAT-6 and CFP10. Although most CCs were IGRA-negative, they showed a slight IFN-γ secretion at a background level in ICS assay, thus facilitating our analysis. Interestingly, our data showed that the expression levels of CD69 on IFN-γ^+ $CD4^+$ T cells were significantly lower in the CCs group compared with the ATB ($P < 0.01$) and LTBI ($P < 0.05$) groups (**Figure 6**), which was a higher degree of significance than found with the total $CD4^+$ T cells (**Figure 3**). In addition, the $CD69^+$ frequency was also significantly lower in IFN-γ^+ $CD8^+$ T cells in CCs compared with ATB ($P < 0.05$) and LTBI ($P < 0.05$) groups (**Figure 7**).

Taken together, our data showed a lower expression of CD69 on T cells, especially on *Mtb* antigen-stimulated IFN-γ-responding T cells, in the CCs group compared with TB infection groups, indicating that persistent CD69 activation is associated with the impaired host defense against *Mtb* infection that culminates in disease. It was recently shown that "resisters", defined as CCs with persistent TST/IGRA negativity, displayed enhanced antibody avidity and distinct *Mtb*-specific IgG Fc profiles instead of IFN-γ T-cell responses to ESAT-6 and CFP10 (Lu et al., 2019). Thus, our data support the contention that a CD69-expressing/IFN-γ-secreting non-T-cell host response to *Mtb* exposure might exist within the CCs population. Furthermore, lower CD69 expression in response to the *Mtb* antigen stimulation might be a clinically significant characteristic that could serve to distinguish CCs from TB-infected populations.

DISCUSSION

Despite significant progress over the past few decades, TB remains the world's leading killer infectious disease (WHO, 2019), suggesting that a more thorough understanding of the immune characteristics of *Mtb* infection is needed.

Especially needed are TB-specific biomarkers as indicators to predict infection reactivation, disease prognosis or vaccine-induced immune protection, and to differentiate various TB infection stages. Measurement of differences in T-cell activation

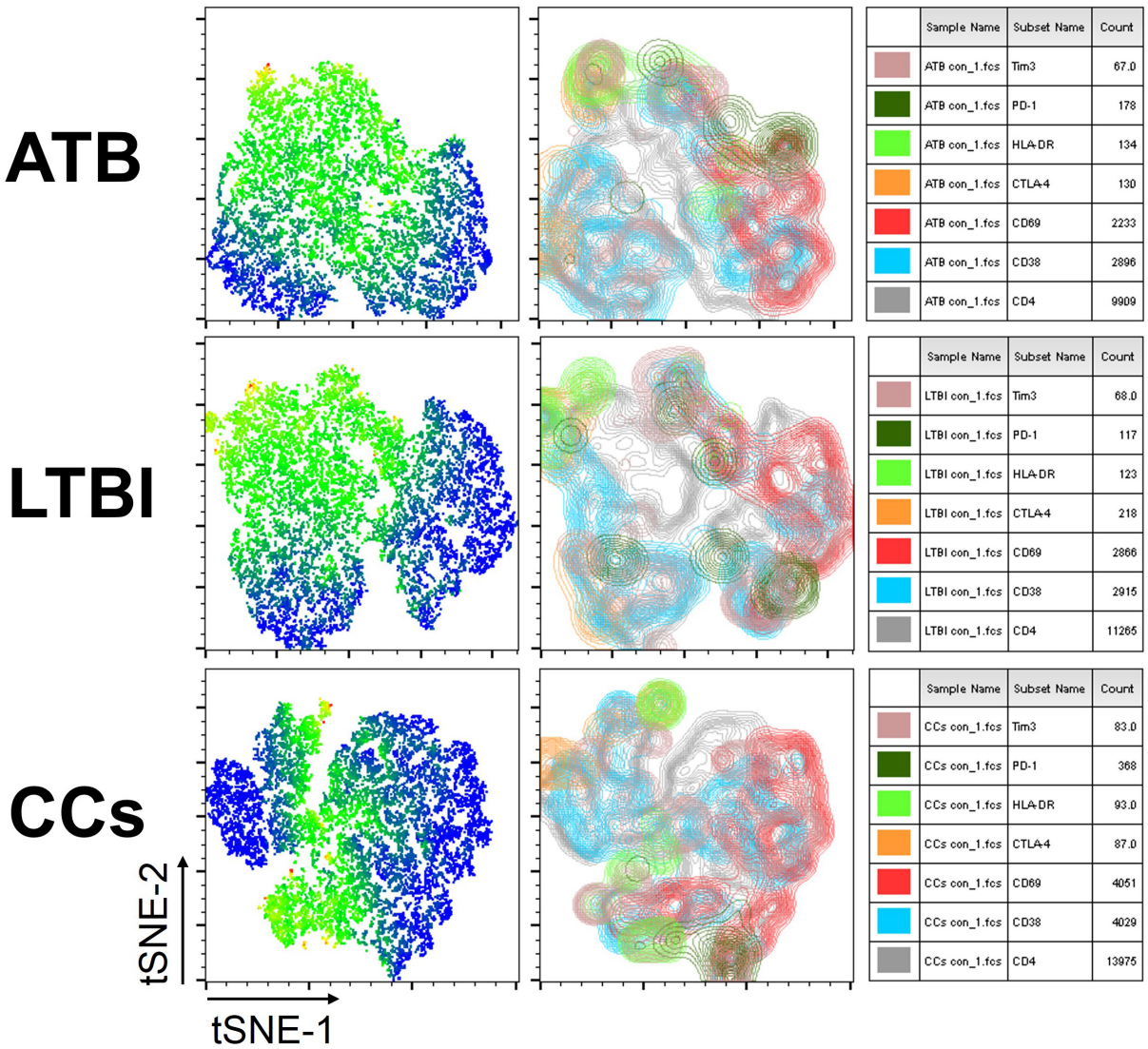

FIGURE 2 | tSNE map for six biomarkers on $CD4^+$ T cells. The expression levels and distribution of different biomarkers in each group demonstrated by tSNE. The heat map shows the degree of activity of different cells expressing various biomarkers, the most active is indicated by red, and the least active is indicated by blue (left panel). The classic tSNE map indicates different signs with different colors, which more intuitively shows their expression on $CD4^+$ T cells (middle panel). Combining heat map and classic map, the biomarkers for each color and the numbers of lymphocytes that express each biomarker are shown (right panel).

or exhaustion levels will be helpful. Previously, we demonstrated the role of T-cell surface maker KLRG1 in human $CD4^+$ T-cell immunity against TB (Hu et al., 2018). Recently, the concept of "resisters", defined as CCs who are persistently TST/IGRA negative, was described. "Resisters" were found to generate a non-IFN-γ-centric, *Mtb*-specific, $CD4^+$ T-cell-mediated immune response to TB exposure, marked by high levels of up-regulated CD40L/CD154 in a clinical cohort study (Lu et al., 2019). This finding served to highlight the importance of T-cell surface marker expression in anti-TB T-cell-mediated immunity. Although a range of biomarkers was found associated with TB infection in mouse models, not all have been clinically verified and in particular, their expression profiles in CCs remain to be defined.

Our new finding, that CD69 was under-expressed in CCs group, suggested that it might be associated with *Mtb* infection. Considering that the sample size in our current cohort was not large, we also determined CD69's expression profiles in non-*Mtb* infected/close contact (Non-TB) persons. Consistent with our expectation, the CD69's expression was significantly lower in the Non-TB persons compared with ATB and LTBI, further supporting our conclusion that activation status of CD69 on T cells was affected by *Mtb* infection.

CD69, a type II glycoprotein, is one of the earliest cell surface antigens expressed by T cells following activation, and potentially plays an important role in the activation and differentiation of a wide variety of hematopoietic cells (Ziegler et al., 1994). Numerous viral and bacterial infection models showed

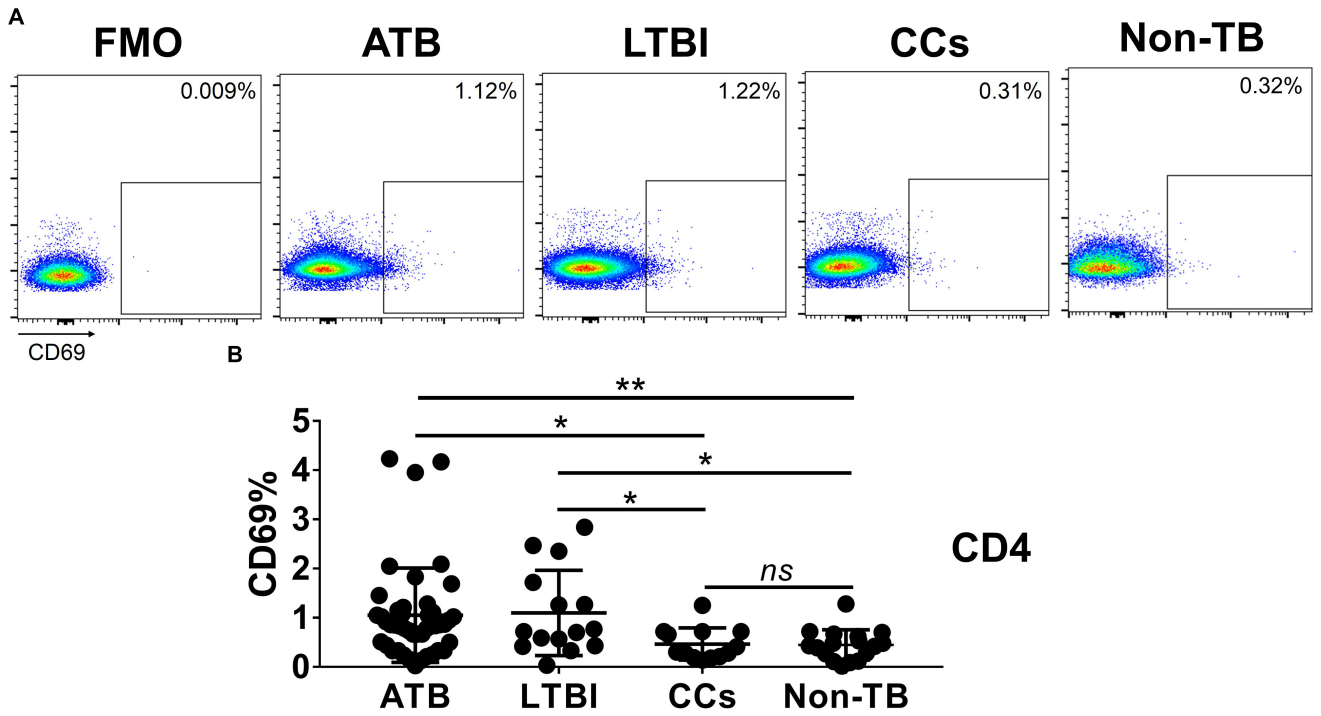

FIGURE 3 | The expression levels of CD69 on $CD4^+$ T cells. Representative flow cytometric plots of CD69 staining and "fluorescence minus one" (FMO) staining control on $CD4^+$ T cells are shown in **(A)** and the summarized data are shown as dot scatter plots in **(B)**. Values are expressed as mean ± SD. The *P* values were calculated by one-way ANOVA and were labeled in the figures. $^*P < 0.05$, $^{**}P < 0.01$ and *ns* indicates no significant difference, when compared as indicated.

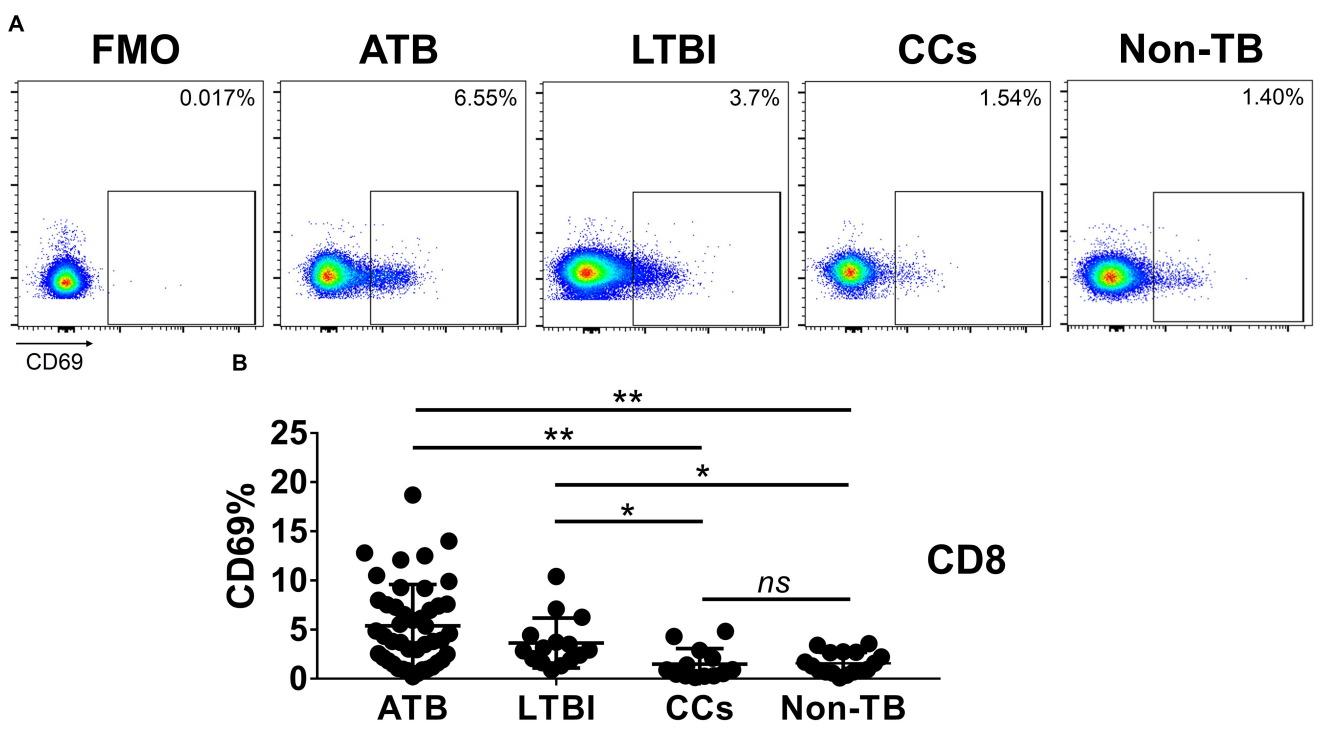

FIGURE 4 | The expression levels of CD69 on $CD8^+$ T cells. Representative flow cytometric plots of CD69 staining and FMO staining control on $CD8^+$ T cells are shown in **(A)** and the summarized data are shown as dot scatter plots in **(B)**. Values are expressed as mean ± SD. The *P* values were calculated by one-way ANOVA and are labeled in the figures. $^*P < 0.05$, $^{**}P < 0.01$ and *ns* indicates no significant difference, when compared as indicated.

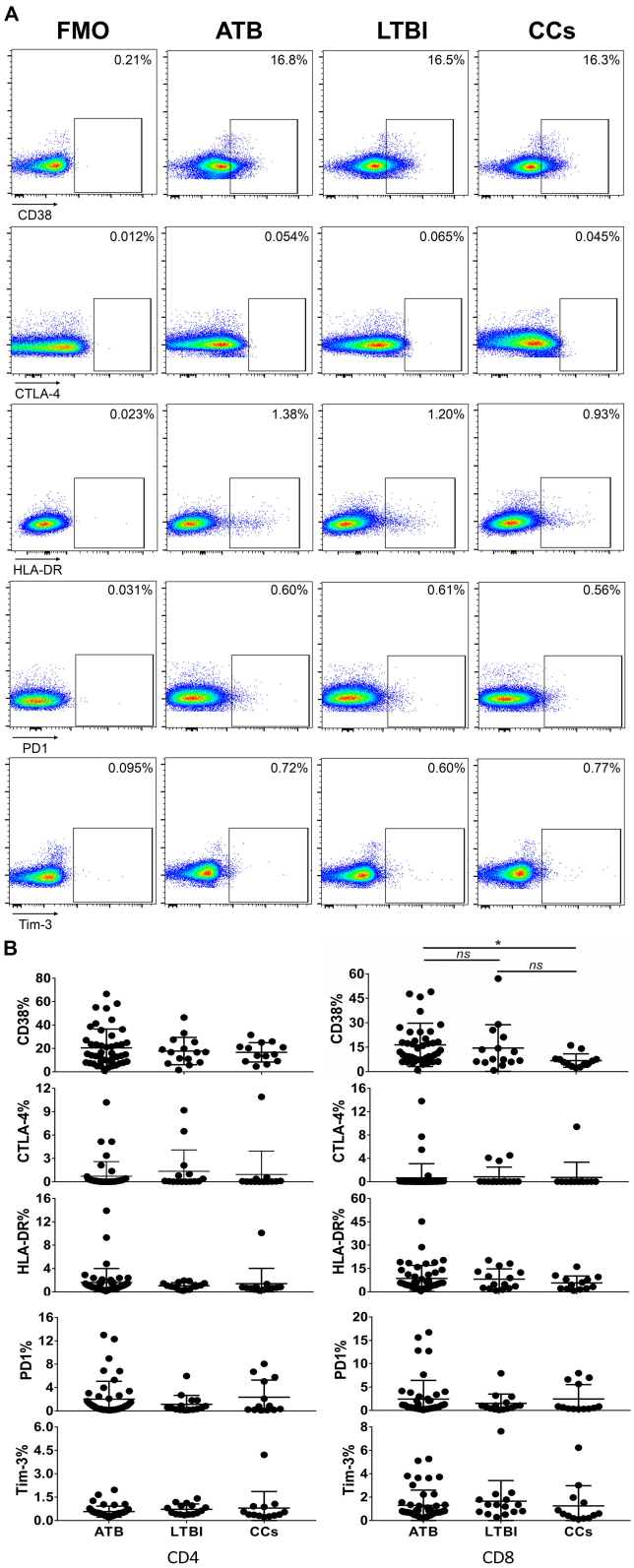

FIGURE 5 | The expression profiles of CD38, CTLA-4, HLA-DR, PD1, and Tim-3 on $CD4^+$ T cells and $CD8^+$ T cells. Representative flow cytometric plots of CD38, CTLA-4, HLA-DR, PD1, and Tim-3 staining and FMO staining controls are shown in **(A)** and the summarized data are shown as dot scatter plots in **(B)**. Values are expressed as mean ± SD. The *P* values were calculated by one-way ANOVA and are labeled in the figures. $^*P < 0.05$ and *ns* indicates no significant difference, when compared as indicated.

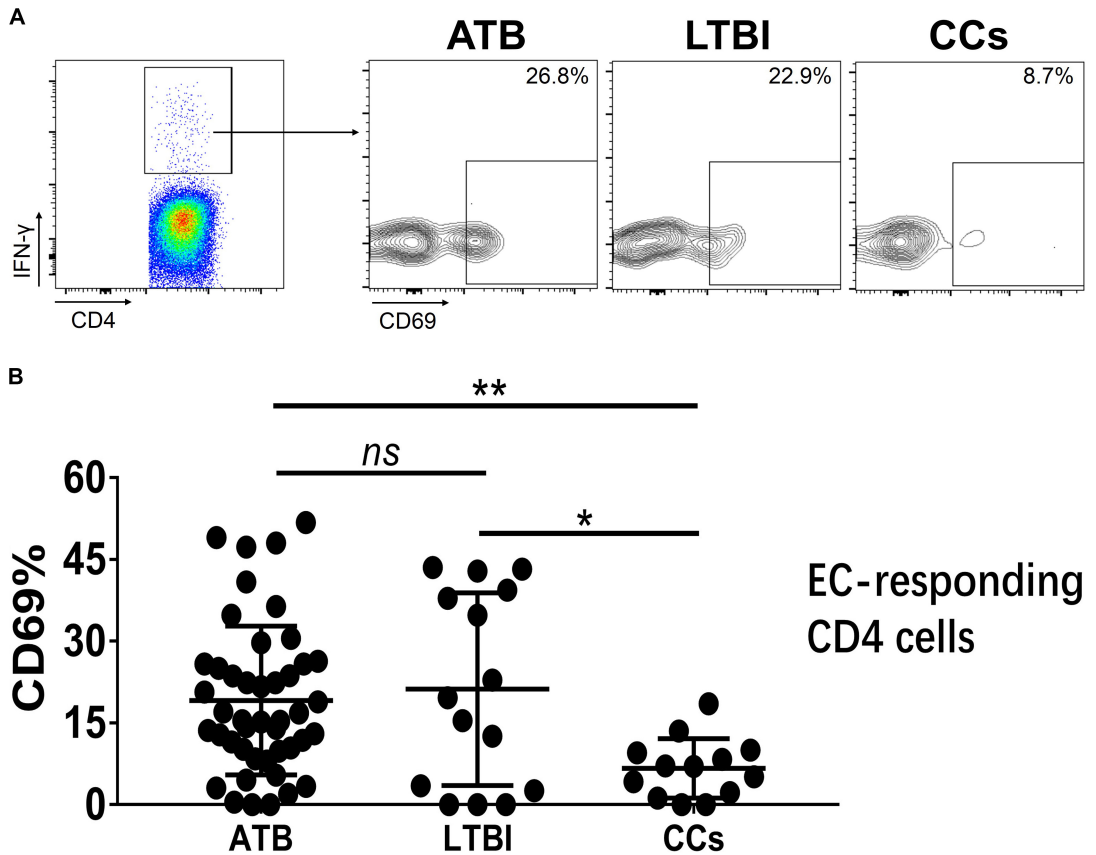

FIGURE 6 | The expression levels of CD69 on IFN-γ-responding $CD4^+$ T cells. Representative flow cytometric plots of IFN-γ and CD69 staining on $CD4^+$ T cells are shown in **(A)** and the summarized data are shown as dot scatter plots in **(B)**. EC, ESAT-6, and CFP10 peptide pools. Values are expressed as mean ± SD. The *P* values were calculated by one-way ANOVA and are labeled in the figures. $^*P < 0.05$, $^{**}P < 0.01$ and *ns* indicates no significant difference, when compared as indicated.

increased CD69 expression on T cells (Hodge et al., 2004; Vega-Ramos et al., 2010; Ishikawa et al., 2013). CD69 is also a co-stimulatory biomarker commonly expressed on $CD8^+$ T cells that bind to corresponding ligands that are expressed on DCs (Maimela et al., 2018). CD69 activation stimulates an influx of calcium ions and the activation of extracellular kinases ERK1/2, thereby facilitating $CD8^+$ T cell proliferation. In addition, CD69 activation stimulates the secretion of IL-2 and IFN-γ that promotes the cytotoxic function of $CD8^+$ T cells (Gonzalez-Amaro et al., 2013). CD69 is preferentially expressed on cells that activate the memory phenotype ($CD45RO^+$ $HLA\text{-}DR^+$), with an increase in the mucosal homing signal CCR6 and a decrease in the secondary lymphoid tissues homing signals CCR7 and CD62L. This suggests that CD69 may help lymphocytes migrate to the site of infection (Sallusto et al., 1999; Yong et al., 2017). The expression levels of CD69 on T cells fluctuated during anti-TB chemotherapy (Portales-Pérez et al., 2002) and in HIV-1/TB co-infected patients, the percentage of CD4+ T cells expressing $CD69^+$ was related to TST and IGRA results (Hsieh et al., 2000) confirming an association with disease status. Because here we have demonstrated that there is increased CD69 expression on $CD4^+$ and $CD8^+$ T cell in ATB and LTBI we speculate that blockage of CD69 by a specific antibody might influence the function of $CD4^+$ T cells. This remains to be investigated.

It was reported that primary viral infection might cause an IFN-I-dependent and systemic "partial" activation of T lymphocytes that was characterized by up-regulated expression of early activation marker CD69 and co-stimulatory molecule CD86 (Alsharifi et al., 2006). These partially activated T cells survived better and developed into effector cells more efficiently and thereby helped to eliminate virus infection in the early infection phase (Wijesundara et al., 2010). However, during chronic viral/bacterial infection and tumor formation, the ability of T cells to function and to establish memory might be impaired due to persistent/chronic antigen stimulation and then ultimately weaken the ability of the cells to confer host protection. This phenomenon was termed "T-cell exhaustion" (Blank et al., 2019). Exhausted T cells display high levels of surface markers such as PD-1, Tim-3, CTLA-4, LAG-3, and CD69 (Yi et al., 2010). Although the application of so-called "immune checkpoint blockade" therapies that target these molecules has become a major weapon in fighting cancer, a greater understanding of T-cell exhaustion is imperative to establish rational

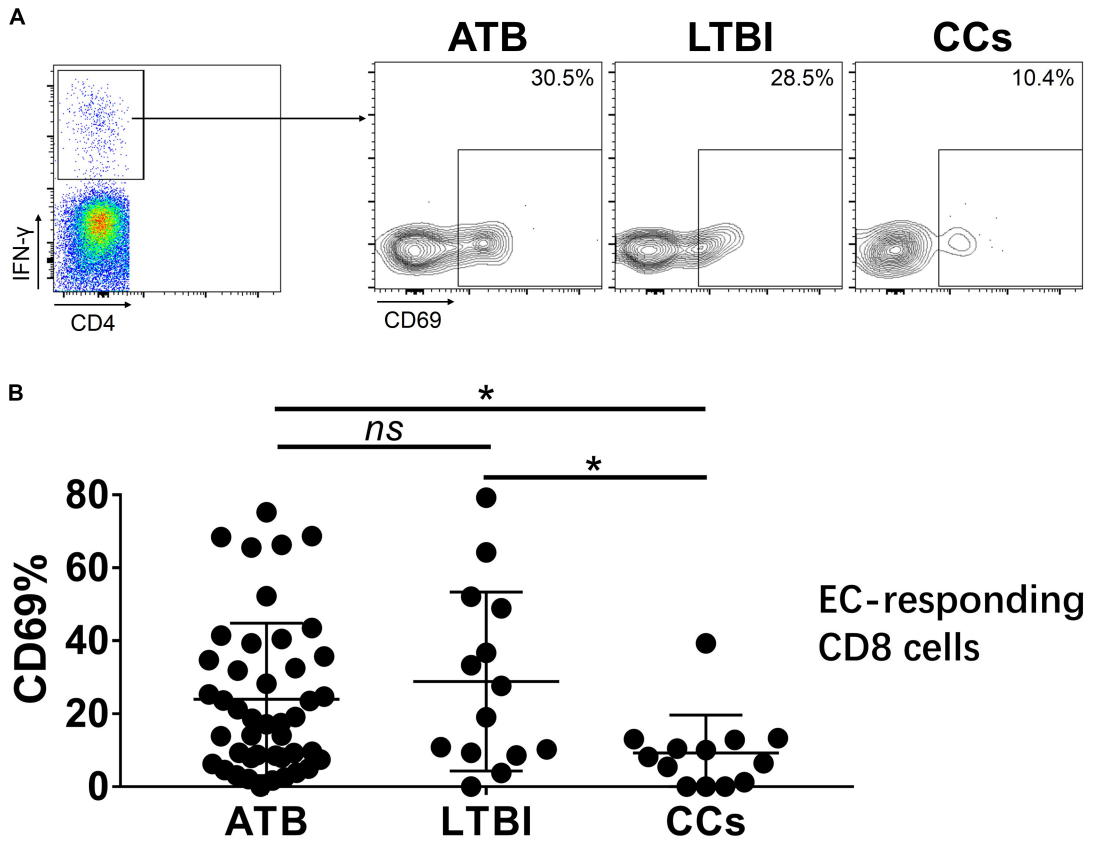

FIGURE 7 | The expression levels of CD69 on IFN-γ-responding $CD8^+$ T cells. Representative flow cytometric plots of IFN-γ and CD69 staining on $CD8^+$ T cells are shown in **(A)** and the summarized data are shown as dot scatter plots in **(B)**. Values are expressed as mean ± SD. The *P* values were calculated by one-way ANOVA and were labeled in the figures. $^*P < 0.05$ and *ns* indicates no significant difference, when compared as indicated.

immunotherapeutic interventions (Hashimoto et al., 2018). Previously, we showed that the expression of KLRG1, a maker of terminally differentiated T cells, was significantly increased during persistent TB infection, leading to an inadequate T-cell immune response (Hu et al., 2018). With regard to CD69, it was reported that targeting CD69 enhanced the early control of virus infection which related to increased numbers of cytokine-producing T cells and NK cells in the periphery (Notario et al., 2019). The attenuation of tumor progression in CD69 knockout mice was related to the increased levels of tumor infiltrating T cells and the decreased levels of CD8 T-cell exhaustion, and anti-CD69 antibody treatment enhanced the anti-tumor activity (Mita et al., 2018). In this study, we showed that *Mtb* infection similarly led to increased levels of CD69 expression on T cells, whereas CCs population showed levels of CD69 expression similar to those in non-TB infected/close contacted population. Thus, our data suggest that persistent CD69 activation might impair host defense against *Mtb* infection.

Considering all the subjects were immunized with BCG vaccines, ESAT-6 and CFP10, which are *Mtb*-specific antigens and not secreted by BCG strains, were used throughout the study, to avoid potential confounding factors (Yang et al., 2013). Even though, BCG-specific T-cell immune memory might also be associated with TB disease status, and it was showed that BCG increased CD69's expression on both CD4 (Hougardy et al., 2007) and natural killer cells (Marcenaro et al., 2008) in human cohort studies. Thus, it's reasonable to speculate that BCG-stimulated CD69's expression might also be used to define TB infection status, which worth further exploration.

It should be noted that CD8 T cells were roughly defined as $CD3^+CD4^-$ cells in this study, however, several T-cell subsets such as γδ T cells, NKT cells and mucosal-associated invariant T cells might be $CD3^+CD4^-CD8^-$, and they are not rare in peripheral blood (D'Acquisto and Crompton, 2011). Indeed, these T-cell subsets have been shown to participate in human host defense against *Mtb* infection in patients with active TB (Behr-Perst et al., 1999; Gansert et al., 2003; Jiang et al., 2014) and a decrease of CD69 expression on TCR $V\alpha7.2^+$ $CD4^-$ T cells was reported to be associated with impaired cytotoxic functions in chronic hepatitis B virus-infected patients (Yong et al., 2017). Thus, the surface markers such as CD69 on these subsets also have the potential to differentiate between LTBI and CC groups, which is a possibility worth further evaluation.

In conclusion, this study demonstrated that an up-regulation of the T-cell phenotype that expresses CD69 might be associated

with the progression of *Mtb* infection to disease. The potential of CD69 as an indicator to predict infection reactivation, to decrease immune protection, and to differentiate between CCs with LTBI and ATB remains to be further defined.

DATA AVAILABILITY STATEMENT

All datasets presented in this study are included in the article/**Supplementary Material**.

ETHICS STATEMENT

The studies involving human participants were reviewed and approved by the Ethical Committee of Shanghai Pulmonary Hospital (approval number K18-215Z), and informed consent was obtained from all subjects. The patients/participants provided their written informed consent to participate in this study.

AUTHOR CONTRIBUTIONS

X-YF, WS, and ZH conceived and designed this study. LW, Z-YC, LG, and RQ collected clinical samples and performed experiments. ZH performed statistical analyses. X-YF, ZH, and Z-YC interpreted the pooled results. ZH and Z-YC drafted the manuscript. X-YF and DL revised the manuscript. All authors approved the final manuscript.

FUNDING

This work was supported by Grants from the Chinese National Mega Science and Technology Program on Infectious Diseases (2018ZX10302301, 2018ZX10731301, and 2020ZX09201001-006-002), National Natural and Science Foundation of China (81873884 and 31771004), and Shanghai Outstanding Academic Leaders Program (19XD1403100 and 2019LJ13).

SUPPLEMENTARY MATERIAL

The Supplementary Material for this article can be found online at: https://www.frontiersin.org/articles/10.3389/fmicb.2020.01901/full#supplementary-material

FIGURE S1 | Flow cytometry gating strategy. Representative flow cytometric dot plots are shown. Briefly, $CD4^+$ T cells were gated as $CD3^+$ $CD4^+$ cells and $CD8^+$ T cells were defined as $CD3^+$ $CD4^-$ cells.

FIGURE S2 | The MFI values of CD69 on CD4 T cells are shown.

REFERENCES

Alsharifi, M., Regner, M., Blanden, R., Lobigs, M., Lee, E., Koskinen, A., et al. (2006). Exhaustion of type I interferon response following an acute viral infection. *J. Immunol.* 177, 3235–3241. doi: 10.4049/jimmunol.177.5.3235

Andersen, P., and Smedegaard, B. (2000). CD4(+) T-cell subsets that mediate immunological memory to *Mycobacterium tuberculosis* infection in mice. *Infect. Immun.* 68, 621–629. doi: 10.1128/iai.68.2.621-629.2000

Behr-Perst, S. I., Munk, M. E., Schaberg, T., Ulrichs, T., Schulz, R. J., and Kaufmann, S. H. (1999). Phenotypically activated gammadelta T lymphocytes in the peripheral blood of patients with tuberculosis. *J. Infect. Dis.* 180, 141–149. doi: 10.1086/314844

Blank, C. U., Haining, W. N., Held, W., Hogan, P. G., Kallies, A., Lugli, E., et al. (2019). Defining 'T cell exhaustion'. *Nat. Rev. Immunol.* 19, 665–674.

D'Acquisto, F., and Crompton, T. (2011). CD3+CD4-CD8- (double negative) T cells: saviours or villains of the immune response? *Biochem. Pharmacol.* 82, 333–340. doi: 10.1016/j.bcp.2011.05.019

Dintwe, O. B., Day, C. L., Smit, E., Nemes, E., Gray, C., Tameris, M., et al. (2013). Heterologous vaccination against human tuberculosis modulates antigen-specific CD4+ T-cell function. *Eur. J. Immunol.* 43, 2409–2420. doi: 10.1002/eji.201343454

Gansert, J. L., Kiessler, V., Engele, M., Wittke, F., Rollinghoff, M., Krensky, A. M., et al. (2003). Human NKT cells express granulysin and exhibit antimycobacterial activity. *J. Immunol.* 170, 3154–3161. doi: 10.4049/jimmunol.170.6.3154

Gonzalez-Amaro, R., Cortes, J. R., Sanchez-Madrid, F., and Martin, P. (2013). Is CD69 an effective brake to control inflammatory diseases? *Trends Mol. Med.* 19, 625–632. doi: 10.1016/j.molmed.2013.07.006

Hashimoto, M., Kamphorst, A. O., Im, S. J., Kissick, H. T., Pillai, R. N., Ramalingam, S. S., et al. (2018). CD8 t cell exhaustion in chronic infection and cancer: opportunities for interventions. *Annu. Rev. Med.* 69, 301–318. doi: 10.1146/annurev-med-012017-043208

Hodge, G., Hodge, S., Han, P., and Haslam, R. (2004). Multiple leucocyte activation markers to detect neonatal infection. *Clin. Exp. Immunol.* 135, 125–129. doi: 10.1111/j.1365-2249.2004.02346.x

Hougardy, J. M., Verscheure, V., Locht, C., and Mascart, F. (2007). In vitro expansion of CD4+CD25highFOXP3+CD127low/- regulatory T cells from peripheral blood lymphocytes of healthy *Mycobacterium tuberculosis*-infected humans. *Microbes Infect.* 9, 1325–1332. doi: 10.1016/j.micinf.2007.06.004

Hsieh, S. M., Hung, C. C., Pan, S. C., Wang, J. T., Tsai, H. C., Chen, M. Y., et al. (2000). Restoration of cellular immunity against tuberculosis in patients coinfected with HIV-1 and tuberculosis with effective antiretroviral therapy: assessment by determination of CD69 expression on T cells after tuberculin stimulation. *J. Acquir. Immune. Defic. Syndr.* 25, 212–220. doi: 10.1097/00126334-200011010-00002

Hu, Z., Wong, K. W., Zhao, H. M., Wen, H. L., Ji, P., Ma, H., et al. (2017). Sendai virus mucosal vaccination establishes lung-resident memory CD8 T cell immunity and boosts BCG-primed protection against TB in mice. *Mol. Ther.* 25, 1222–1233. doi: 10.1016/j.ymthe.2017.02.018

Hu, Z., Zhao, H., Li, C., Liu, X., Barkan, D., Lowrie, D. B., et al. (2018). The role of KLRG1 in human CD4+ T-cell immunity against tuberculosis. *J. Infect. Dis.* 217, 1491–1503. doi: 10.1093/infdis/jiy046

Ishikawa, C., Kawakami, H., Uchihara, J., Senba, M., and Mori, N. (2013). CD69 overexpression by human T-cell leukemia virus type 1 Tax transactivation. *Biochim. Biophys. Acta* 1833, 1542–1552. doi: 10.1016/j.bbamcr.2013.03.006

Jayaraman, P., Jacques, M. K., Zhu, C., Steblenko, K. M., Stowell, B. L., Madi, A., et al. (2016). TIM3 mediates T cell exhaustion during *Mycobacterium tuberculosis* infection. *PLoS Pathog.* 12:e1005490. doi: 10.1371/journal.ppat.1005490

Jiang, J., Wang, X., An, H., Yang, B., Cao, Z., Liu, Y., et al. (2014). Mucosal-associated invariant T-cell function is modulated by programmed death-1 signaling in patients with active tuberculosis. *Am. J. Respir. Crit. Care Med.* 190, 329–339.

Kaipilyawar, V., and Salgame, P. (2019). Infection resisters: targets of new research for uncovering natural protective immunity against *Mycobacterium tuberculosis*. *F1000Res.* 8.F1000.

Kauffman, K. D., Sallin, M. A., Hoft, S. G., Sakai, S., Moore, R., Wilder-Kofie, T., et al. (2018). Limited pulmonary mucosal-associated invariant t cell accumulation and activation during *Mycobacterium tuberculosis* infection in rhesus macaques. *Infect. Immun.* 86:e00431-18.

Kirman, J., McCoy, K., Hook, S., Prout, M., Delahunt, B., Orme, I., et al. (1999). CTLA-4 blockade enhances the immune response induced by mycobacterial infection but does not lead to increased protection. *Infect. Immun.* 67, 3786–3792. doi: 10.1128/iai.67.8.3786-3792.1999

Lazar-Molnar, E., Chen, B., Sweeney, K. A., Wang, E. J., Liu, W., Lin, J., et al. (2010). Programmed death-1 (PD-1)-deficient mice are extraordinarily sensitive to tuberculosis. *Proc. Natl. Acad. Sci. U.S.A.* 107, 13402–13407. doi: 10.1073/pnas.1007394107

Li, G., Li, F., Zhao, H. M., Wen, H. L., Li, H. C., Li, C. L., et al. (2017). Evaluation of a new IFN-gamma release assay for rapid diagnosis of active tuberculosis in a high-incidence setting. *Front. Cell Infect. Microbiol.* 7:117. doi: 10.3389/fcimb.2017.00117

Lu, L. L., Smith, M. T., Yu, K. K. Q., Luedemann, C., Suscovich, T. J., Grace, P. S., et al. (2019). IFN-γ-independent immune markers of *Mycobacterium tuberculosis* exposure. *Nat. Med.* 25, 977–987. doi: 10.1038/s41591-019-0441-3

Maimela, N. R., Liu, S., and Zhang, Y. (2018). Fates of CD8+ T cells in tumor microenvironment. *Comput. Struct. Biotec.* 17, 1–13. doi: 10.1016/j.csbj.2018.11.004

Marcenaro, E., Ferranti, B., Falco, M., Moretta, L., and Moretta, A. (2008). Human NK cells directly recognize Mycobacterium bovis via TLR2 and acquire the ability to kill monocyte-derived DC. *Int. Immunol.* 20, 1155–1167.

Mita, Y., Kimura, M. Y., Hayashizaki, K., Koyama-Nasu, R., Ito, T., Motohashi, S., et al. (2018). Crucial role of CD69 in anti-tumor immunity through regulating the exhaustion of tumor-infiltrating T cells. *Int. Immunol.* 30, 559–567. doi: 10.1093/intimm/dxy050

Nandakumar, S., Kannanganat, S., Posey, J. E., Amara, R. R., and Sable, S. B. (2014). Attrition of T-cell functions and simultaneous upregulation of inhibitory markers correspond with the waning of BCG-induced protection against tuberculosis in mice. *PLoS One* 9:e113951. doi: 10.1371/journal.pone.0113951

Notario, L., Redondo-Antón, J., Alari-Pahissa, E., Albentosa, A., Leiva, M., Lopez, D., et al. (2019). CD69 targeting enhances anti-vaccinia virus immunity. *J. Virol.* 93, e519–e553.

Phillips, B. L., Mehra, S., Ahsan, M. H., Selman, M., Khader, S. A., and Kaushal, D. (2015). LAG3 expression in active *Mycobacterium tuberculosis* infections. *Am. J. Pathol.* 185, 820–833. doi: 10.1016/j.ajpath.2014.11.003

Portales-Pérez, D. P., Baranda, L., Layseca, E., Fierro, N. A., de la Fuente, H., Rosenstein, Y., et al. (2002). Comparative and prospective study of different immune parameters in healthy subjects at risk for tuberculosis and in tuberculosis patients. *Clin. Diagn. Lab. Immunol.* 9, 299–307. doi: 10.1128/cdli.9.2.299-307.2002

Reichler, M. R., Khan, A., Sterling, T. R., Zhao, H., Moran, J., McAuley, J., et al. (2018). Risk and timing of tuberculosis among close contacts of persons with infectious tuberculosis. *J. infect. Dis.* 218, 1000–1008.

Reiley, W. W., Shafiani, S., Wittmer, S. T., Tucker-Heard, G., Moon, J. J., Jenkins, M. K., et al. (2010). Distinct functions of antigen-specific CD4 T cells during murine *Mycobacterium tuberculosis* infection. *Proc. Natl. Acad. Sci. U.S.A.* 107, 19408–19413. doi: 10.1073/pnas.1006298107

Sallusto, F., Lenig, D., Forster, R., Lipp, M., and Lanzavecchia, A. (1999). Two subsets of memory T lymphocytes with distinct homing potentials and effector functions. *Nature* 401, 708–712. doi: 10.1038/44385

Samanovic, M. I., and Darwin, K. H. (2016). Game of 'Somes: protein destruction for *Mycobacterium tuberculosis* pathogenesis. *Trends Microbiol.* 24, 26–34. doi: 10.1016/j.tim.2015.10.001

Simmons, J. D., Stein, C. M., Seshadri, C., Campo, M., Alter, G., Fortune, S., et al. (2018). Immunological mechanisms of human resistance to persistent *Mycobacterium tuberculosis* infection. *Nat. Rev. Immunol.* 18, 575–589. doi: 10.1038/s41577-018-0025-3

Vega-Ramos, J., Alari-Pahissa, E., Valle, J. D., Carrasco-Marín, E., Esplugues, E., Borràs, M., et al. (2010). CD69 limits early inflammatory diseases associated with immune response to *Listeria monocytogenes* infection. *Immunol. Cell Biol.* 88, 707–715. doi: 10.1038/icb.2010.62

WHO (2019). *Global Tuberculosis Report 2019*. Geneva: WHO.

Wijesundara, D. K., Kumar, S., Alsharifi, M., Mullbacher, A., and Regner, M. (2010). Antigen-specific activation thresholds of CD8+ T cells are independent of IFN-I-mediated partial lymphocyte activation. *Int. Immunol.* 22, 757–767. doi: 10.1093/intimm/dxq064

Workman, C. J., Cauley, L. S., Kim, I. J., Blackman, M. A., Woodland, D. L., and Vignali, D. A. (2004). Lymphocyte activation gene-3 (CD223) regulates the size of the expanding T cell population following antigen activation in vivo. *J. Immunol.* 172, 5450–5455. doi: 10.4049/jimmunol.172.9.5450

Yang, J., Xu, K., Zheng, J., Wei, L., Fan, J., and Li, L. (2013). Limited T cell receptor beta variable repertoire responses to ESAT-6 and CFP-10 in subjects infected with *Mycobacterium tuberculosis*. *Tuberculosis* 93, 529–537. doi: 10.1016/j.tube.2013.05.007

Yi, J. S., Cox, M. A., and Zajac, A. J. (2010). T-cell exhaustion: characteristics, causes and conversion. *Immunology* 129, 474–481. doi: 10.1111/j.1365-2567.2010.03255.x

Yong, Y. K., Tan, H. Y., Saeidi, A., Rosmawati, M., Atiya, N., Ansari, A. W., et al. (2017). Decrease of CD69 levels on TCR Valpha7.2(+)CD4(+) innate-like lymphocytes is associated with impaired cytotoxic functions in chronic hepatitis B virus-infected patients. *Innate. Immun.* 23, 459–467. doi: 10.1177/1753425917714854

Ziegler, S. F., Ramsdell, F., and Alderson, M. R. (1994). The activation antigen CD69. *Stem Cells* 12, 456–465. doi: 10.1002/stem.5530120502

Conflict of Interest: The authors declare that the research was conducted in the absence of any commercial or financial relationships that could be construed as a potential conflict of interest.

frontiers in Immunology

PERSPECTIVE
published: 03 September 2020
doi: 10.3389/fimmu.2020.02107

Harnessing Unconventional T Cells for Immunotherapy of Tuberculosis

Marco P. La Manna[1,2†], Valentina Orlando[1,2†], Bartolo Tamburini[1,2], Giusto D. Badami[1,2], Francesco Dieli[1,2‡] and Nadia Caccamo[1,2‡]*

[1] Central Laboratory of Advanced Diagnosis and Biomedical Research, Palermo, Italy, [2] Department of Biomedicine, Neurosciences and Advanced Diagnostics, University of Palermo, Palermo, Italy

Even if the incidence of tuberculosis (TB) has been decreasing over the last years, the number of patients with TB is increasing worldwide. The emergence of multidrug-resistant and extensively drug-resistant TB is making control of TB more difficult. *Mycobacterium bovis* bacillus Calmette–Guérin vaccine fails to prevent pulmonary TB in adults, and there is an urgent need for a vaccine that is also effective in patients with human immunodeficiency virus (HIV) coinfection. Therefore, TB control may benefit on novel therapeutic options beyond antimicrobial treatment. Host-directed immunotherapies could offer therapeutic strategies for patients with drug-resistant TB or with HIV and TB coinfection. In the last years, the use of donor lymphocytes after hematopoietic stem cell transplantation has emerged as a new strategy in the cure of hematologic malignancies in order to induce graft-versus leukemia and graft-versus-infection effects. Moreover, adoptive therapy has proven to be effective in controlling cytomegalovirus and Epstein-Barr virus reactivation in immunocompromised patients with *ex vivo* expanded viral antigen-specific T cells. Unconventional T cells are a heterogeneous group of T lymphocytes with limited diversity. One of their characteristics is that antigen recognition is not restricted by the classical major histocompatibility complex (MHC). They include CD1 (cluster of differentiation 1)–restricted T cells, MHC-related protein-1–restricted mucosal-associated invariant T (MAIT) cells, MHC class Ib–reactive T cells, and γδ T cells. Because these T cells are genotype-independent, they are also termed "donor unrestricted" T cells. The combined features of low donor diversity and the lack of genetic restriction make these cells suitable candidates for T cell–based immunotherapy of TB.

Keywords: host-directed therapy, tuberculosis, unconventional T cells, cytotoxicity, T cell receptor

OPEN ACCESS

Edited by:
Juraj Ivanyi,
King's College London,
United Kingdom

Reviewed by:
Goro Matsuzaki,
University of the Ryukyus, Japan
Arshad Khan,
McGovern Medical School,
The University of Texas Health Science Center at Houston,
United States

***Correspondence:**
Nadia Caccamo
nadia.caccamo@unipa.it

†These authors share first authorship

‡These authors share last authorship

Specialty section:
This article was submitted to Microbial Immunology, a section of the journal Frontiers in Immunology

Received: *28 April 2020*
Accepted: *04 August 2020*
Published: *03 September 2020*

Citation:
La Manna MP, Orlando V, Tamburini B, Badami GD, Dieli F and Caccamo N (2020) Harnessing Unconventional T Cells for Immunotherapy of Tuberculosis. Front. Immunol. 11:2107. doi: 10.3389/fimmu.2020.02107

INTRODUCTION

Tuberculosis (TB) is the deadliest infectious disease worldwide, even if the global incidence has declined over the past decades. The etiologic agent *Mycobacterium tuberculosis* still causes more than 10 million cases and 1.5 million deaths every year. Although drug treatment usually provides microbiological cure in patients treated with 6-month regimen for drug-sensitive strains, 1.1 million people remain sick (1), because of the spread of strains resistant to multiple drugs. Moreover, it is estimated that one-quarter of people worldwide are latently infected, and of these, 5 to 15% will develop TB during their lifetimes, due to the higher risk for people with

immunocompromised system, such as human immunodeficiency virus (HIV), malnutrition, or diabetes, or people who use alcohol or tobacco (2). Treatment for latently infected people is necessary for the global control of TB. The emergence of multidrug-resistant TB remains a growing threat to global public health; in fact, in the absence of a vaccine more efficient than *Mycobacterium bovis* bacillus Calmette–Guérin (BCG) vaccine to prevent primary infection or progression to active TB in latently infected people, TB global control needs novel therapeutic strategies in order to improve *M. tuberculosis* eradication and limit the excessive pathology.

In this context, the research of more effective and cheaper drugs represent one of the solutions (3, 4), while therapeutic interventions that can modulate the immune response have been proposed (5–7).

These interventions, termed "host-directed therapies" (HDTs), are directed to evaluate different aspects in order to better understand the inflammatory and immune pathways governing protective or detrimental outcomes of the disease. HDTs consider several mechanisms of action: the research of biological drugs useful to reduce treatment regimens strategy to reduce TB pathology targeting *M. tuberculosis* such as granuloma structure, autophagy induction, anti-inflammatory response, and cell- and antibody-mediated immune responses (8–10).

We review here developments and current advances in adoptive T cell therapy; in particular, we will focus on the role of unconventional T cells and discuss whether such approach may be helpful to offer a valid strategy for the cure of TB applicable also to other infectious diseases.

As the role of CD4 and CD8 T cells has been largely studied in TB, highlighting the limit of the high most polymorphic presentation of peptides antigens by MHC classes I and II molecules, the donor unrestricted nature of antigen presentation by molecules that are apparently non-polymorphic, elicits strong interest for vaccine or T cell immunotherapeutic approaches to target the entire global population without respect to host genetic factors.

NATURAL KILLER T AND MUCOSAL-ASSOCIATED INVARIANT T CELLS

Natural killer T (NKT) and MAIT cells constitute a subset of T cells that recognize antigens of non-peptidic nature. These cells are named as unconventional or "innate-like" T cells for their distinct features (11, 12). These cells have different memory, kinetics, and ligand recognition compared to conventional T cells (13).

MAIT and NKT cells recognize microbial metabolites and lipids presented by MHC-related protein 1 (MR1) and cluster of differentiation 1d (CD1d), respectively (**Figure 1**).

In *M. tuberculosis* infection, the role of NKT cell subsets has been investigated; here, we report some evidences of their role depending on the type of mycobacterial antigens specifically recognized.

NKT Cells

It has been shown that NKT cells play a key role in a variety of infectious and autoimmune diseases and cancer (14). NKT cells express a rearranged αβ T cell receptor (TCR) and NK cell receptors, which confer the capability to exert several effector functions in immune surveillance. Based on their TCR repertoire and antigen recognition, NKTs can be split up into invariant (iNKT) and diverse (dNKT). Both cell types are CD1d-restricted and respond to glycolipid and lipid antigens/CD1 complexes, respectively.

Invariant NKT

Invariant NKT cells, also termed classical type I cells, use an invariant TCRα chain (Vα14-Jα18 in mice, Vα24-Jα15 in humans) paired with limited TCRβ chains (Vβ7, 8.2 or 2 in mice, Vβ11 in humans), and constitute a majority of the overall CD1d-restricted repertoire (15, 16). iNKT cells specifically recognize the endogenous α-linked monoglycosylceramides, α-galactosyl ceramide (αGalCer) and α-glucosylceramide (αGalcCer). Similar to helper CD4 T cells, notwithstanding their specificity for αGalCer recognition, they are able to produce different cytokines such as interferon γ (IFN-γ), interleukin 4 (IL-4), or IL-17A, which designate them as iNKT1, iNKT2, and iNKT17.

Diverse NKT Cells

Diverse NKT cells have a more diverse repertoire and recognize a wider range of self and non-self lipids such as sphingolipids (e.g., sulfatides and βGalCer) and phospholipids (e.g., phosphatidylinositol, phosphatidylglycerol, and phosphatidylethanolamine).

Mycolipids, lipids belonging to the mycobacterial cell wall, can bind CD1d molecules and activate human NKT cells. dNKT cell activation in responses to different antigens has been detected in individuals infected with *M. tuberculosis* (17).

Their role has been investigated in *in vitro*, *in vivo*, and in preclinical models of *M. tuberculosis* infection (18–22). Active TB patients had a decreased percentage of iNKT cells in peripheral blood or bronchoalveolar lavage samples (23, 24), with respect to subjects with latent TB infection (25–30), even if these cells still maintained the capability to secrete high amounts of IFN-γ and displayed an activated phenotype (30, 31).

However, NKT cells from active TB patients express programmed death 1 (PD-1) molecule at cell surface that leads to their subsequent apoptosis, an event that can be abrogated through PD-1 blockade (23, 32). This finding is highly suggestive of an immunological approach to achieve a protective immune response against *M. tuberculosis*. In addition, iNKT cells present in pleural effusion in TB patients produce IL-21 and can then participate to local B cell activation and humoral immune response to *M. tuberculosis* (33).

While these studies do not clarify a key role for NKT cells in human TB, their rapid activation and the different role they can exert in TB infection poise them as an intriguing target for cell-based therapies (34).

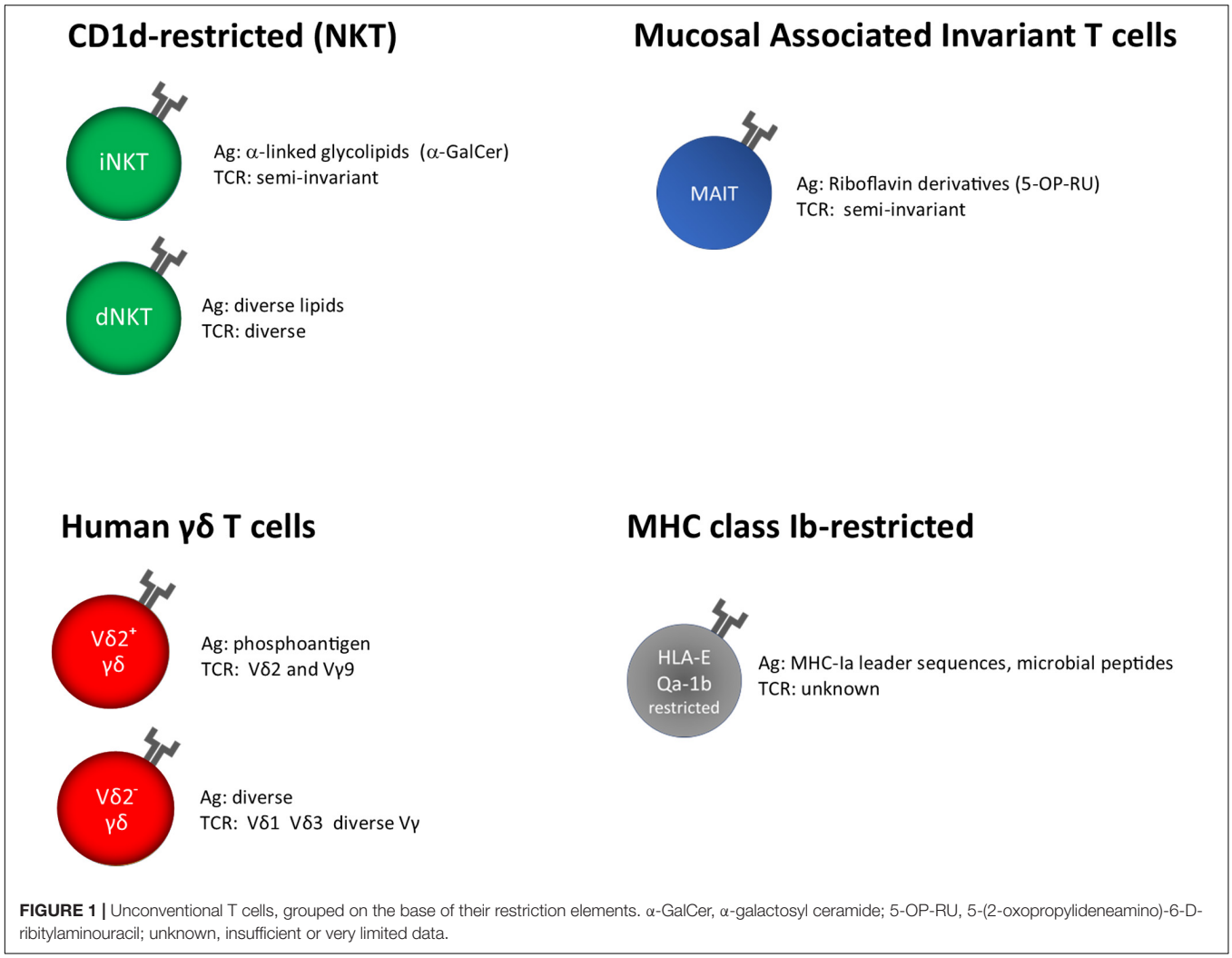

FIGURE 1 | Unconventional T cells, grouped on the base of their restriction elements. α-GalCer, α-galactosyl ceramide; 5-OP-RU, 5-(2-oxopropylideneamino)-6-D-ribitylaminouracil; unknown, insufficient or very limited data.

Finally, results from non-human primate (NHP) models of *M. tuberculosis* infection have demonstrated that $CD8^+$ iNKT cells play a protective role in preventing lung pathology (19, 35).

Altogether, these cells are promising tools for potential use as HDT in human TB, in a similar way to their use in cancer immunotherapy (36).

MAIT Cells

MAIT cells recognize very rapidly non-peptidic antigens presented by MR1 molecule (37). MAIT cells respond to Ag stimulation rapidly either because they are constitutively activated by Ags derived from commensal bacteria and maintain activated/memory phenotype, or their clonal size is larger than conventional T cells (38). In humans, MAIT cells express a Vα7.2-Jα33/12/20, TCRα chain preferentially paired with Vβ2 or Vβ13 (39–41). In their structure and function, MAIT cells represent a bridge between the innate and adaptive immunity. They are αβ T cells whose TCRs have restricted diversity and recognize small microbial metabolites. In the riboflavin synthesis process, many bacterial and fungal organisms produce small intermediates able to activate MAIT cells (42–45). There is also evidence that non–riboflavin-based antigens, also of microbial origin (46) and tumor cell–derived molecules (47), can bind to MR1 and activate some MR1-restricted T cells, although the identity of these antigens remains to be defined. MAIT cells comprise 1 to 10% of circulating $CD3^+$ T cells in healthy adults (48, 49) and have also been found in the gastrointestinal tract, liver, and airways (50–54).

The role of this population of T cells in the response against microorganisms is still a matter of studies. TCR-mediated activation of MAIT cells leads to cytokines production, cytotoxic effector function, migration, and proliferative expansion (12, 39, 55).

Because MAIT cells can respond to a range of bacteria and yeasts, several studies have supported the proposal of a peculiar and non-redundant role in protection against infectious diseases.

In particular, MAIT cells can contribute to the destruction of infected cells and activation of other immune cell types (56) through the release of perforin and granzymes; moreover, they are a source of several proinflammatory cytokines and chemokines, such as tumor necrosis factor α (TNF-α), IFN-γ, IL-17A, and MIP-1α. MAIT cells can also produce IL-22,

IL-13, IL-26, or IL-2, depending on the different cytokine milieus and tissue localization (57–60). Indeed, MAIT cells can even be activated by inflammatory stimuli in the absence of TCR-mediated antigen recognition (57–59, 61–68).

In animal models of mycobacterial infection, MAIT cells are able to reduce mycobacterial burden and increase the ability of macrophages to inhibit the growth of intracellular bacilli (56). MAIT cells were demonstrated to protect mice against mycobacterial infection (55, 69).

In human TB infection, several studies have evaluated MAIT cell frequencies in peripheral blood or in inflamed tissues, demonstrating that this cellular population decreases during active TB in diverse geographic settings (55, 70–72). Moreover, this decrease is paralleled by their enrichment in the inflamed tissue such as that found in the lungs and pleural effusions of TB patients (73), where they displayed a phenotype of activated/memory cells and a higher capacity to produce cytokines such as IFN-γ and TNF-α (74).

Studies have evaluated the relative increase or decrease of the absolute number or percentage with the progression of TB infection. In fact, in some circumstances, MAIT cell deficiency has been associated with the different clinical TB conditions. Moreover, their decrease has been inversely correlated with other biological parameters, such as high levels acid–fast bacilli in sputum of TB patients or with systemic markers of inflammation (72). Additionally, peripheral blood MAIT cells showed an impaired production of cytotoxic molecules and cytokines such as IFN-γ in patients with active pulmonary TB (75). These functionally impaired MAIT cells express higher levels of proapoptotic markers and PD-1 than MAIT cells from non-TB patients (71, 72, 74). PD-1$^+$ MAIT cell expression has been related to active TB status and declines with TB treatment (74, 76).

In vitro blockade of PD-1 can increase IFN-γ production in circulating MAIT cells from patients with TB, thus resembling the data obtained in studies on NKT cells.

Human data about MAIT cells still gave incomplete information about the role these cells play in bacterial disease, but it was stated that in active TB disease MAIT cells decrease in peripheral blood and those that remain show a dysfunctional, yet reversible phenotype. An immunological approach could be to use MR1 ligands in therapeutic settings, in order to potentiate the functional activities of MAIT cells in *M. tuberculosis* infection. This therapeutic approach would be applicable in the heterogeneous human populations because of the monomorphic nature of MR1, which displays very limited restriction barrier in human populations.

γδ T Cells

T cell receptor (TCR) of γδ T cells in humans consists of a γ and a δ chain; they are usually identified on the base of the δ chain expressed on the surface, Vδ1$^+$, Vδ2$^+$, and a minor subset Vδ3$^+$. The knowledge about their antigen recognition repertoire is not fully elucidated; in fact, some TCRs specifically recognize soluble antigens in the absence of Ag presentation, whereas other can bind antigens presented by MHC-I like molecules such as MICA, CD1, and EPCR (77, 78) (**Figure 1**).

The Vδ2$^+$ T cells are the major γδ subset in the blood, and their TCR consists of a Vδ2 and a Vγ9 chain that recognize microbially derived phosphorylated antigens associated with the monomorphic butyrophilin 3A1 (BTN3A1) molecule (79). Metabolites known as phosphoantigens (PAgs) activate Vγ9Vδ2 T cells (80, 81). One of these metabolites is isopentenyl pyrophosphate (IPP), produced in eukaryotes through the mevalonate pathway, a pathway involved in protein prenylation, and in cholesterol synthesis (82). A dysfunction of this pathway can lead to overproduction of endogenous IPP, as occurs in stressed cells (83, 84). Moreover, some drugs can manipulate the production of endogenous IPP. Another metabolite able to activate Vγ9Vδ2 T cells is hydroxymethyl-but-2-enylpyrophosphate (HMBPP), an intermediate of the alternative, non-mevalonate pathway of cholesterol used by some Eubacteria and by *Plasmodium falciparum*, the etiologic agent of malaria (85, 86).

Pags are recognized in a TCR-dependent manner, and very recently, the molecule BTN3A1, belonging to the butyrophilin (BTN) protein family, has been implicated as essential molecule in the PAgs activation pathway of Vγ9Vδ2 T cells (87–89).

BTN3A proteins are receptors expressed in several cell types, including immune cells and some malignant cells such as ovarian cancer. Even if the prominent role of BTN3A1 in PAg-induced Vγ9Vδ2 T cell activation is well documented, the mechanism of recognition of the PAg has not been fully delineated. There is strong evidence that Vγ9Vδ2 T cell activation is due to an intracellular sensing of PAg through the interaction with the B30.2 domain of BTN3A1 molecule (90–93).

Vγ9Vδ2 T cells can recognize another antigen belonging to *M. tuberculosis*, the 6-*O*-methylglucose-containing lipopolysaccharides.

Even if other two minor subsets of γδ T cells are less represented in blood, they are able to recognize mycobacterial lipid or glycolipids antigens presented by CD1c and CD1d molecules. Interestingly, some Vδ1$^+$γδ T cells are activated following recognition of α-GalCer presented by CD1d molecule (94), which might be relevant in human clinical trials.

Generally, any γδ T cell antigen could be used to design TB vaccines due to their ability to drive *in vivo* expansion of *M. tuberculosis*–reactive γδ or to generate *in vitro* γδ T cells to be used in adoptive cell therapy.

In human blood, γδ T cells are relatively abundant, so it is possible to isolate them in large numbers and characterize their effector mechanisms such as the ability to produce T_H 1-, T_H 2-, or T_H17-type cytokines and to exert potent cytotoxicity, this latter function being closely correlated to the elimination of infected or tumoral cells. These findings, together with their capacity to rapidly migrate to peripheral sites suggest that γδ T cells are good candidates for adoptive transfer models of therapy.

They are included in the cluster of unconventional T cells, because of their MHC unrestricted antigen recognition; therefore, they have been used and transferred from an MHC mismatched background without causing graft-versus-host disease (GVHD), which can be a life-threatening complication with adoptive transfer of conventional αβ T cells (95).

In *M. tuberculosis* infection, Vγ9Vδ2 T cells are activated rapidly after PAg stimulation, exerting effector mechanisms such as release TNF-α and IFN-γ (96), and cytotoxic molecules such as perforin, granzymes, and granulysin that are involved in the killing of *M. tuberculosis*–infected macrophages and in the reduction of the viability of intracellular and extracellular *M. tuberculosis* (97). In humans, BCG vaccination determines *in vivo* expansion of γδ T cell population with a memory phenotype, and similar findings have been observed in BCG or *M. tuberculosis*–infected rhesus macaques.

Moreover, adoptive transfer of activated Vγ9Vδ2 T cells in *M. tuberculosis*–infected macaques has demonstrated protection against this intracellular pathogen (79, 96). The adoptive transfer of γδ T cells in NHP reduced the bacterial burden and limited disease to the infected lobe by prevention of dissemination (98). In primates, this expansion is clonal and selects for $V\gamma9^{+}V\delta2^{+}$ TCR usage (79). This clonal expansion is due to the specific recognition of PAgs conserved among mycobacteria (99), recognized by butyrophilin-dependent manner (96, 100). Further advances in the use of γδ T cells, derived from the study in which responses in NHP can specifically be boosted by addition of PAgs to protein subunit vaccines are needed (101).

Therefore, clinical trials targeting γδ T cells may offer improved outcomes that can best be harnessed for immunotherapy approaches, as widely experienced in cancer immunotherapy (102).

HLA-E–Restricted T Cells

HLA-E has been classically defined by the ability to present signal sequence peptides from HLA class I, which inhibit NK cells cytolytic activity upon interaction with CD94/NKG2A receptors (103). However, it has been shown that HLA-E molecules are able to bind and present other self or pathogen-derived peptides, including *M. tuberculosis*, and can be recognized by adaptive T cells (104–106) (**Figure 1**).

HLA-E/mycobacterial peptide complexes are recognized differently from HLA-E/self-peptides; in fact, in our previous study, we have demonstrated that the latter are predominantly recognized by NK cells in a CD94 dependent manner; the former are specifically recognized by $CD8^{+}$ T cells in a CD3/TCR αβ-dependent manner (106).

The binding of peptides to HLA-E molecule has been described (107). The peptide-binding motif reveals that most of the peptides that bind to HLA-E are similar to HLA I leader sequence with P2 Met and PΩ Leu. This motif has been identified for 21 peptides, but the discovery of new HLA-E–specific peptides needs to be characterized in sharing anchor residues or motifs. In fact, the crystal structure analysis of HLA-E- bound to a mycobacterial peptide has revealed that the flexibility of the conformation of the bound peptides is also critical in the activation of CD8 T cells despite the preferred anchor residues (108).

Therefore, HLA-E plays a role in both innate and adaptive immune response, thanks to their interaction with both NK cells and antigen-specific $CD8^{+}$ T cells. One important aspect of HLA-E molecule is its low allelic variability, rendering this molecule an interesting candidate antigen-presenting molecule for peptide-based vaccination strategies (103, 109–111). These T cells can inhibit intracellular *M. tuberculosis* growth in human macrophages. Moreover, compared to class Ia molecules, HLA-E molecule is enriched in *M. tuberculosis* phagosomes and accessible for loading with *M. tuberculosis* peptides generated into the phagosome (112, 113).

Studies in mouse and NHP suggest a contribution of HLA-E–restricted T cells to protective immunity against TB.

It was found that the murine homolog of HLA-E, Qa-1 molecule, can bind and present human HLA-E–binding peptides to murine $CD8^{+}$ T cells, which display cytolytic and regulatory activities (114). Moreover, knockout studies confirmed a direct role for Qa-1 in regulating histopathology and bacterial burden and contributing to protection against *M. tuberculosis* (114).

MHC-E–restricted $CD8^{+}$ T cell responses are elicited in rhesus macaques (Rh) by an experimental rhesus cytomegalovirus (CMV) vaccine, which express genes coding for proteins specific for simian immunodeficiency virus (SIV). This attenuated Rh CMV vaccine showed strong protection against a subsequent challenge with SIV infection, and protection was due to activation of $CD8^{+}$ T cells that recognized SIV peptides bound to either MHC class II or MHC-E molecules, but not conventional MHC class Ia molecules, explaining in part the involvement of MHC-E–restricted T cells in protection (115–117). Further investigation revealed that naturally occurring SIV epitopes matched the Rh CMV vector–elicited $CD8^{+}$ T cell–restricted epitopes contributing to protection against a subsequent SIV challenge (112). Similarly to the model described above, Rh CMV-TB antigen vectors induced strong protection against TB following vaccination in 41% of treated NHPs (118). Moreover, Hansen et al. (118) demonstrated that one of three tested Rh CMV strain 68-1 vectored vaccines expressing six or nine protein from *M. tuberculosis* was able to elicit unconventionally restricted MHC class II and MHC-E restricted $CD8^{+}$ T cell responses. Therefore, viral-vectored vaccines can be developed in order to induce immunogenicity of HLA-E–restricted T cells against many pathogens in human patients.

Recently, we have demonstrated that *M. tuberculosis*–specific and HLA-E–restricted $CD8^{+}$ T cells are abundant but exhausted in peripheral blood of TB–HIV-1–coinfected patients, and this dysfunctional phenotype is correlated with high levels of PD-1 molecule expression. The use of anti-PD1 mAb may restore, even partially, the number and the functions of *M. tuberculosis*–specific and HLA-E–restricted $CD8^{+}$ T cells (119). Like NKT and MAIT cells, HLA-E–restricted $CD8^{+}$ T cells are associated with exhaustion. This abnormal phenotype is probably caused by the direct recognition of *M. tuberculosis*–infected cells and the exposure to high levels of inflammatory cytokines. Further research is needed to develop strategies for restoring this subset in patients with *M. tuberculosis* infection/disease, with or without HIV coinfection, in order to better define the therapeutic potential of immune checkpoint blockade.

Taking advantage for the relative monomorphism of HLA-E molecule and for its stable expression in HIV–*M. tuberculosis* infection, which represents an important issue of global health, the use of antigen recognition through HLA-E molecule, should

be considered as another valuable approach to promote or boost activation of $CD8^+$ T cells in vaccine formulation or immunotherapy.

PERSPECTIVE

Translational research can begin to use the knowledge of unconventional T cell biology to develop new immunotherapeutic approaches. Vaccine or immunotherapy development could represent a good strategy in infectious diseases prevention, but obviously, it is very important to demonstrate that identified ligands for unconventional T cells are expressed at the surface of infected cells at densities and durations that are able to engage TCRs and induce T cell activation and immunological memory phenotype. In fact, the efficacy of vaccine or immune protection in case of the re-encounter with the same pathogen could be reached by the induction of memory T cells.

Therefore, unconventional T cells can be used to improve T cell immunotherapy, thanks to several aspects, such as the rapid cytokine release without the need to previous clonal expansion due to their presence at high number of available experienced antigen-specific cells that have developed as memory-like state (77). Another important aspect is represented by the monomorphic model of antigen recognition by unconventional T cells that could be universally effective in human infectious diseases and cancer context. Moreover, their TCRs will not be able to give alloreactive responses and to cause GVHD, making these cells more suitable in cellular therapy such as chimeric antigen receptor (CAR) T cell therapy (120, 121).

MAIT, NKT, and γδ T cells are crucial players in the development and maintenance of immunity. These aspects have been demonstrated by the array of infectious, inflammatory, and malignant diseases in which they play diverse roles (81, 122–127).

Depending on the nature of the infectious or inflammatory setting, these can range from host protective functions, for example, antimicrobial or antitumor responses, to the augmentation of disease (122–126). A number of clinical trials based on γδ T cell therapy have been conducted or are ongoing to evaluate the safety and antitumor efficacy (128). Moreover, several clinical trials have assessed the safety and efficacy of Vγ9Vδ2 T cells for immunotherapy. Because of their high plasticity, studies using CAR- γδT cells could be of great interest also in infectious diseases.

Until now, no clinical trials have investigated on the efficacy of unconventional T cells in inducing protection toward *M. tuberculosis* disease.

Because of the role that these cellular populations play during the early stages of infection, they could be studied as promising tools in immunotherapy against the intracellular pathogen.

Finally, therapy using anti–PD-1 and anti–CTLA-4 monoclonal antibodies, important checkpoints of the immune response, has demonstrated to play an important and valid approach to treat some types of cancer (129), where it is assumed primarily to enhance $CD8^+$ T cell–mediated tumor destruction.

Given that unconventional T cells also express the inhibitory receptors such as PD-1 upon activation and that blockade of these receptors can enhance their effector activities and antitumor capacity (74, 130–132), the potential role that unconventional T cells play should be considered in infectious disease and the immunotherapy for infectious diseases, and the incorporation of unconventional T cells into these studies has the potential to provide novel approaches to this important area of medicine.

DATA AVAILABILITY STATEMENT

The original contributions presented in the study are included in the article/supplementary material, further inquiries can be directed to the corresponding author/s.

AUTHOR CONTRIBUTIONS

FD and NC wrote the manuscript. All authors have reviewed the manuscript and have made intellectual contributions to the work.

FUNDING

This work was supported by grants from the European Commission within the Horizon 2020 Program TBVAC2020 (contract no. 643381) and EMI-TB (contract no. 643558). The text represents the authors' views and does not necessarily represents position of the European Commission, which will not be liable for the use made of such information.

REFERENCES

1. World Health Organization. *Global Tuberculosis Report 2019*. Geneva: World Health Organization (2019).
2. UNOPS. *Stop TJUNOfPS, UNOPS, Geneva Switzerland. Partnership: The Paradigm Shift. 2016-2020. Global Plan to End TB*. Geneva: UNOPS (2015).
3. Andronis C, Sharma A, Virvilis V, Deftereos S, Persidis A. Literature mining, ontologies and information visualization for drug repurposing. *Brief Bioinform.* (2011) 12:357–68. doi: 10.1093/bib/bbr005
4. Rani J, Silla Y, Borah K, Ramachandran S, Bajpai U. Repurposing of FDA-approved drugs to target MurB and MurE enzymes in *Mycobacterium tuberculosis*. *J Biomol Struct Dyn.* (2019) 38:2521–32. doi: 10.1080/07391102.2019.1637280
5. Nunes-Alves C, Booty MG, Carpenter SM, Jayaraman P, Rothchild AC, Behar SM. In search of a new paradigm for protective immunity to TB. *Nat Rev Microbiol.* (2014) 12:289–99. doi: 10.1038/nrmicro3230
6. Raviglione MC, Ditiu L. Setting new targets in the fight against tuberculosis. *Nat Med.* (2013) 19:263. doi: 10.1038/nm.3129
7. Zumla A, Maeurer M. Rational development of adjunct immune-based therapies for drug-resistant tuberculosis: hypotheses and experimental designs. *J Infect Dis.* (2012) 205(Suppl. 2):S335–9. doi: 10.1093/infdis/jir881
8. Sachan M, Srivastava A, Ranjan R, Gupta A, Pandya S, Misra A. Opportunities and challenges for host-directed therapies in tuberculosis. *Curr Pharm Design.* (2016) 22:2599–604.
9. Kolloli A, Subbian S. Host-directed therapeutic strategies for tuberculosis. *Front Med.* (2017) 4:171. doi: 10.3389/fmed.2017.00171

10. Young C, Walzl G, Du Plessis N. Therapeutic host-directed strategies to improve outcome in tuberculosis. *Mucosal Immunol.* (2020) 13:190–204. doi: 10.1038/s41385-019-0226-5
11. Beckman EM, Porcelli SA, Morita CT, Behar SM, Furlong ST, Brenner MB. Recognition of a lipid antigen by CD1-restricted αβ+ T cells. *Nature.* (1994) 372:691–4. doi: 10.1038/372691a0
12. Kjer-Nielsen L, Patel O, Corbett AJ, Le Nours J, Meehan B, Liu L, et al. MR1 presents microbial vitamin B metabolites to MAIT cells. *Nature.* (2012) 491:717–23. doi: 10.1038/nature11605
13. Godfrey DI, Uldrich AP, McCluskey J, Rossjohn J, Moody DB. The burgeoning family of unconventional T cells. *Nat Immunol.* (2015) 16:1114–23. doi: 10.1038/ni.3298
14. Dhodapkar MV, Kumar V. Type II NKT cells and their emerging role in health and disease. *J Immunol.* (2017) 198:1015. doi: 10.4049/jimmunol.1601399
15. Park S-H, Weiss A, Benlagha K, Kyin T, Teyton L, Bendelac A. The mouse Cd1d-restricted repertoire is dominated by a few autoreactive T cell receptor families. *J Exp Med.* (2001) 193:893–904. doi: 10.1084/jem.193.8.893
16. Cardell S, Tangri S, Chan S, Kronenberg M, Benoist C, Mathis D. CD1-restricted CD4+ T cells in major histocompatibility complex class II-deficient mice. *J Exp Med.* (1995) 182:993–1004. doi: 10.1084/jem.182.4.993
17. Sieling PA, Chatterjee D, Porcelli SA, Prigozy TI, Mazzaccaro RJ, Soriano T, et al. CD1-restricted T cell recognition of microbial lipoglycan antigens. *Science.* (1995) 269:227. doi: 10.1126/science.7542404
18. Huang S. Targeting innate-like T cells in Tuberculosis. *Front Immunol.* (2016) 7:594. doi: 10.3389/fimmu.2016.00594
19. Dieli F, Taniguchi M, Kronenberg M, Sidobre S, Ivanyi J, Fattorini L, et al. An anti-inflammatory role for Vα14 NK T cells in *Mycobacterium bovis* Bacillus calmette-Guérin-infected mice. *J Immunol.* (2003) 171:1961–8. doi: 10.4049/jimmunol.171.4.1961
20. Kawakami K, Kinjo Y, Uezu K, Miyagi K, Kinjo T, Yara S, et al. Interferon-γ production and host protective response against *Mycobacterium tuberculosis* in mice lacking both IL-12p40 and IL-18. *Microb Infect.* (2004) 6:339–49. doi: 10.1016/j.micinf.2004.01.003
21. Emoto M, Emoto Y, Buchwalow IB, Kaufmann SHE. Induction of IFN-γ-producing CD4+ natural killer T cells by *Mycobacterium bovis* bacillus Calmette Guérin. *Eur J Immunol.* (1999) 29:650–9. doi: 10.1002/(sici)1521-4141
22. Sada-Ovalle I, Chiba A, Gonzales A, Brenner MB, Behar SM. Innate invariant NKT cells recognize *Mycobacterium tuberculosis*-infected macrophages, produce interferon-gamma, and kill intracellular bacteria. *PLoS Pathog.* (2008) 4:e1000239. doi: 10.1371/journal.ppat.1000239
23. Kee S-J, Kwon Y-S, Park Y-W, Cho Y-N, Lee S-J, Kim T-J, et al. Dysfunction of natural killer T cells in patients with active *Mycobacterium tuberculosis* infection. *Infect Immun.* (2012) 80:2100. doi: 10.1128/IAI.06018-11
24. Paquin-Proulx D, Costa PR, Terrassani Silveira CG, Marmorato MP, Cerqueira NB, Sutton MS, et al. Latent *Mycobacterium tuberculosis* infection is associated with a higher frequency of mucosal-associated Invariant T and invariant natural killer T cells. *Front Immunol.* (2018) 9:1394. doi: 10.3389/fimmu.2018.01394
25. Montoya CJ, Cataño JC, Ramirez Z, Rugeles MT, Wilson SB, Landay AL. Invariant NKT cells from HIV-1 or *Mycobacterium tuberculosis*-infected patients express an activated phenotype. *Clin Immunol.* (2008) 127:1–6. doi: 10.1016/j.clim.2007.12.006
26. Snyder-Cappione JE, Nixon DF, Loo CP, Chapman JM, Meiklejohn DA, Melo FF, et al. Individuals with pulmonary Tuberculosis have lower levels of circulating CD1d-restricted NKT cells. *J Infect Dis.* (2007) 195:1361–4. doi: 10.1086/513567
27. Sutherland JS, Jeffries DJ, Donkor S, Walther B, Hill PC, Adetifa IMO, et al. High granulocyte/lymphocyte ratio and paucity of NKT cells defines TB disease in a TB-endemic setting. *Tuberculosis.* (2009) 89:398–404. doi: 10.1016/j.tube.2009.07.004
28. Berzins SP, Smyth MJ, Baxter AG. Presumed guilty: natural killer T cell defects and human disease. *Nat Rev Immunol.* (2011) 11:131–42. doi: 10.1038/nri2904
29. Im JS, Kang T-J, Lee S-B, Kim C-H, Lee S-H, Venkataswamy MM, et al. Alteration of the relative levels of iNKT cell subsets is associated with chronic mycobacterial infections. *Clin Immunol.* (2008) 127:214–24. doi: 10.1016/j.clim.2007.12.005
30. Veenstra H, Baumann R, Carroll NM, Lukey PT, Kidd M, Beyers N, et al. Changes in leucocyte and lymphocyte subsets during tuberculosis treatment; prominence of CD3dimCD56+ natural killer T cells in fast treatment responders. *Clin Exp Immunol.* (2006) 145:252–60. doi: 10.1111/j.1365-2249.2006.03144
31. Li Z, Yang B, Zhang Y, Ma J, Chen X, Lao S, et al. *Mycobacterium tuberculosis*-specific memory NKT cells in patients with Tuberculous pleurisy. *J Clin Immunol.* (2014) 34:979–90. doi: 10.1007/s10875-014-0090-8
32. Singh A, Dey AB, Mohan A, Mitra DK. Programmed death-1 receptor suppresses γ-IFN producing NKT cells in human tuberculosis. *Tuberculosis.* (2014) 94:197–206. doi: 10.1016/j.tube.2014.01.005
33. Wu C, Li Z, Fu X, Yu S, Lao S, Yang B. Antigen-specific human NKT cells from tuberculosis patients produce IL-21 to help B cells for the production of immunoglobulins. *Oncotarget.* (2015) 6:28633–45. doi: 10.18632/oncotarget.5764
34. Zhao J, Siddiqui S, Shang S, Bian Y, Bagchi S, He Y, et al. Mycolic acid-specific T cells protect against *Mycobacterium tuberculosis* infection in a humanized transgenic mouse model. *eLife.* (2015) 4:e08525. doi: 10.7554/eLife.08525
35. Chancellor A, White A, Tocheva AS, Fenn JR, Dennis M, Tezera L, et al. Quantitative and qualitative iNKT repertoire associations with disease susceptibility and outcome in macaque tuberculosis infection. *Tuberculosis.* (2017) 105:86–95. doi: 10.1016/j.tube.2017.04.011
36. Zhang Y, Springfield R, Chen S, Li X, Feng X, Moshirian R, et al. α-GalCer and iNKT cell-based cancer immunotherapy: realizing the therapeutic potentials. *Front Immunol.* (2019) 10:1126. doi: 10.3389/fimmu.2019.01126
37. Hashimoto K, Hirai M, Kurosawa Y. A gene outside the human MHC related to classical HLA class I genes. *Science.* (1995) 269:693. doi: 10.1126/science.7624800
38. Godfrey DI, Koay H-F, McCluskey J, Gherardin NA. The biology and functional importance of MAIT cells. *Nat Immunol.* (2019) 20:1110–28. doi: 10.1038/s41590-019-0444-8
39. Reantragoon R, Corbett AJ, Sakala IG, Gherardin NA, Furness JB, Chen Z, et al. Antigen-loaded MR1 tetramers define T cell receptor heterogeneity in mucosal-associated invariant T cells. *J Exp Med.* (2013) 210:2305–20. doi: 10.1084/jem.20130958
40. Porcelli S, Yockey CE, Brenner MB, Balk SP. Analysis of T cell antigen receptor (TCR) expression by human peripheral blood CD4-8- alpha/beta T cells demonstrates preferential use of several V beta genes and an invariant TCR alpha chain. *J Exp Med.* (1993) 178:1–16. doi: 10.1084/jem.178.1.1
41. Lepore M, Kalinichenko A, Colone A, Paleja B, Singhal A, Tschumi A, et al. Parallel T-cell cloning and deep sequencing of human MAIT cells reveal stable oligoclonal TCRβ repertoire. *Nat Commun.* (2014) 5:3866. doi: 10.1038/ncomms4866
42. Hinks TSC, Marchi E, Jabeen M, Olshansky M, Kurioka A, Pediongco TJ, et al. Activation and in vivo evolution of the MAIT cell transcriptome in mice and humans reveals tissue repair functionality. *Cell Rep.* (2019) 28:3249–62.e5. doi: 10.1016/j.celrep.2019.07.039
43. Kelly J, Minoda Y, Meredith T, Cameron G, Philipp M-S, Pellicci DG, et al. Chronically stimulated human MAIT cells are unexpectedly potent IL-13 producers. *Immunol Cell Biol.* (2019) 97:689–99. doi: 10.1111/imcb.12281
44. Leng T, Akther HD, Hackstein C-P, Powell K, King T, Friedrich M, et al. TCR and inflammatory signals tune human MAIT cells to exert specific tissue repair and effector functions. *Cell Rep.* (2019) 28:3077–91.e5. doi: 10.1016/j.celrep.2019.08.050
45. Serriari N-E, Eoche M, Lamotte L, Lion J, Fumery M, Marcelo P, et al. Innate mucosal-associated invariant T (MAIT) cells are activated in inflammatory bowel diseases. *Clin Exp Immunol.* (2014) 176:266–74. doi: 10.1111/cei.12277
46. Meermeier EW, Laugel BF, Sewell AK, Corbett AJ, Rossjohn J, McCluskey J, et al. Human TRAV1-2-negative MR1-restricted T cells detect S. pyogenes and alternatives to MAIT riboflavin-based antigens. *Nature Commun.* (2016) 7:12506. doi: 10.1038/ncomms12506
47. Lepore M, Kalinichenko A, Calogero S, Kumar P, Paleja B, Schmaler M, et al. Functionally diverse human T cells recognize non-microbial antigens presented by MR1. *eLife.* (2017) 6:e24476. doi: 10.7554/eLife.24476

48. Lee OJ, Cho Y-N, Kee S-J, Kim M-J, Jin H-M, Lee S-J, et al. Circulating mucosal-associated invariant T cell levels and their cytokine levels in healthy adults. *Exp Gerontol.* (2014) 49:47–54. doi: 10.1016/j.exger.2013.11.003
49. Treiner E, Lantz O. CD1d- and MR1-restricted invariant T cells: of mice and men. *Curr Opin Immunol.* (2006) 18:519–26. doi: 10.1016/j.coi.2006.07.001
50. Dusseaux M, Martin E, Serriari N, Péguillet I, Premel V, Louis D, et al. Human MAIT cells are xenobiotic-resistant, tissue-targeted, CD161hi IL-17–secreting T cells. *Blood.* (2011) 117:1250–9. doi: 10.1182/blood-2010-08-303339
51. Kawachi I, Maldonado J, Strader C, Gilfillan S. MR1-restricted Vα19 mucosal-associated invariant T cells are innate T cells in the gut lamina propria that provide a rapid and diverse cytokine response. *J Immunol.* (2006) 176:1618–27. doi: 10.4049/jimmunol.176.3.1618
52. Billerbeck E, Kang Y-H, Walker L, Lockstone H, Grafmueller S, Fleming V, et al. Analysis of CD161 expression on human CD8 T cells defines a distinct functional subset with tissue-homing properties. *Proc Natl Acad Sci USA.* (2010) 107:3006–11. doi: 10.1073/pnas.0914839107
53. Jo J, Tan AT, Ussher JE, Sandalova E, Tang X-Z, Tan-Garcia A, et al. Toll-like receptor 8 agonist and bacteria trigger potent activation of innate immune cells in human liver. *PLoS Pathog.* (2014) 10:e1004210. doi: 10.1371/journal.ppat.1004210
54. Leeansyah E, Loh L, Nixon DF, Sandberg JK. Acquisition of innate-like microbial reactivity in mucosal tissues during human fetal MAIT-cell development. *Nat Commun.* (2014) 5:3143. doi: 10.1038/ncomms4143
55. Le Bourhis L, Martin E, Péguillet I, Guihot A, Froux N, Coré M, et al. Antimicrobial activity of mucosal-associated invariant T cells. *Nat Immunol.* (2010) 11:701–8. doi: 10.1038/ni.1890
56. Kurioka A, Ussher JE, Cosgrove C, Clough C, Fergusson JR, Smith K, et al. MAIT cells are licensed through granzyme exchange to kill bacterially sensitized targets. *Mucosal Immunol.* (2015) 8:429–40. doi: 10.1038/mi.2014.81
57. Ussher JE, Bilton M, Attwod E, Shadwell J, Richardson R, de Lara C, et al. CD161++CD8+ T cells, including the MAIT cell subset, are specifically activated by IL-12+IL-18 in a TCR-independent manner. *Eur J Immunol.* (2014) 44:195–203. doi: 10.1002/eji.201343509
58. Sattler A, Dang-Heine C, Reinke P, Babel N. IL-15 dependent induction of IL-18 secretion as a feedback mechanism controlling human MAIT-cell effector functions. *Eur J Immunol.* (2015) 45:2286–98. doi: 10.1002/eji.201445313
59. Leeansyah E, Svärd J, Dias J, Buggert M, Nyström J, Quigley MF, et al. Arming of MAIT cell cytolytic antimicrobial activity is induced by IL-7 and defective in HIV-1 infection. *PLoS Pathog.* (2015) 11:e1005072. doi: 10.1371/journal.ppat.1005072
60. Tang X-Z, Jo J, Tan AT, Sandalova E, Chia A, Tan KC, et al. IL-7 Licenses activation of human liver intrasinusoidal mucosal-associated invariant T Cells. *J Immunol.* (2013) 190:3142–52. doi: 10.4049/jimmunol.1203218
61. Chen Z, Wang H, D'Souza C, Sun S, Kostenko L, Eckle SBG, et al. Mucosal-associated invariant T-cell activation and accumulation after in vivo infection depends on microbial riboflavin synthesis and co-stimulatory signals. *Mucosal Immunol.* (2017) 10:58–68. doi: 10.1038/mi.2016.39
62. Slichter CK, McDavid A, Miller HW, Finak G, Seymour BJ, McNevin JP, et al. Distinct activation thresholds of human conventional and innate-like memory T cells. *JCI Insight.* (2016) 1:e86292. doi: 10.1172/jci.insight.86292
63. Turtle CJ, Delrow J, Joslyn RC, Swanson HM, Basom R, Tabellini L, et al. Innate signals overcome acquired TCR signaling pathway regulation and govern the fate of human CD161hi CD8α+ semi-invariant T cells. *Blood.* (2011) 118:2752–62. doi: 10.1182/blood-2011-02-334698
64. Salio M, Gasser O, Gonzalez-Lopez C, Martens A, Veerapen N, Gileadi U, et al. Activation of human mucosal-associated invariant T Cells induces CD40L-dependent maturation of monocyte-derived and primary dendritic cells. *J Immunol.* (2017) 199:2631. doi: 10.4049/jimmunol.1700615
65. Havenith SHC, Yong SL, Henson SM, Piet B, Idu MM, Koch SD, et al. Analysis of stem-cell-like properties of human CD161++IL-18Rα+ memory CD8+ T cells. *Int Immunol.* (2012) 24:625–36. doi: 10.1093/intimm/dxs069
66. van Wilgenburg B, Scherwitzl I, Hutchinson EC, Leng T, Kurioka A, Kulicke C, et al. MAIT cells are activated during human viral infections. *Nat Commun.* (2016) 7:11653. doi: 10.1038/ncomms11653
67. Gracey E, Qaiyum Z, Almaghlouth I, Lawson D, Karki S, Avvaru N, et al. IL-7 primes IL-17 in mucosal-associated invariant T (MAIT) cells, which contribute to the Th17-axis in ankylosing spondylitis. *Ann Rheum Dis.* (2016) 75:2124. doi: 10.1136/annrheumdis-2015-208902
68. Gold MC, Eid T, Smyk-Pearson S, Eberling Y, Swarbrick GM, Langley SM, et al. Human thymic MR1-restricted MAIT cells are innate pathogen-reactive effectors that adapt following thymic egress. *Mucosal Immunol.* (2013) 6:35–44. doi: 10.1038/mi.2012.45
69. Chua W-J, Truscott SM, Eickhoff CS, Blazevic A, Hoft DF, Hansen TH. Polyclonal mucosa-associated invariant T cells have unique innate functions in bacterial infection. *Infect Immun.* (2012) 80:3256. doi: 10.1128/IAI.00279-12
70. Sharma PK, Wong EB, Napier RJ, Bishai WR, Ndung'u T, Kasprowicz VO, et al. High expression of CD26 accurately identifies human bacteria-reactive MR1-restricted MAIT cells. *Immunology.* (2015) 145:443–53. doi: 10.1111/imm.12461
71. Jiang J, Yang B, An H, Wang X, Liu Y, Cao Z, et al. Mucosal-associated invariant T cells from patients with tuberculosis exhibit impaired immune response. *J Infection.* (2016) 72:338–52. doi: 10.1016/j.jinf.2015.11.010
72. Kwon Y-S, Cho Y-N, Kim M-J, Jin H-M, Jung H-J, Kang J-H, et al. Mucosal-associated invariant T cells are numerically and functionally deficient in patients with mycobacterial infection and reflect disease activity. *Tuberculosis.* (2015) 95:267–74. doi: 10.1016/j.tube.2015.03.004
73. Gold MC, Cerri S, Smyk-Pearson S, Cansler ME, Vogt TM, Delepine J, et al. Human mucosal associated invariant T cells detect bacterially infected cells. *PLoS Biol.* (2010) 8:e1000407. doi: 10.1371/journal.pbio.1000407
74. Jiang J, Wang X, An H, Yang B, Cao Z, Liu Y, et al. Mucosal-associated invariant T-cell function is modulated by programmed death-1 signaling in patients with active tuberculosis. *Am J Respir Care Med.* (2014) 190:329–39. doi: 10.1164/rccm.201401-0106OC
75. Meierovics A, Yankelevich W-JC, Cowley SC. MAIT cells are critical for optimal mucosal immune responses during in vivo pulmonary bacterial infection. *Proc Natl Acad Sci USA.* (2013) 110:E3119–28. doi: 10.1073/pnas.1302799110
76. Sakala IG, Kjer-Nielsen L, Eickhoff CS, Wang X, Blazevic A, Liu L, et al. Functional heterogeneity and antimycobacterial effects of mouse mucosal-associated invariant T cells specific for riboflavin metabolites. *J Immunol.* (2015) 195:587–601. doi: 10.4049/jimmunol.1402545
77. Godfrey DI, Le Nours J, Andrews DM, Uldrich AP, Rossjohn J. Unconventional T cell targets for cancer immunotherapy. *Immunity.* (2018) 48:453–73. doi: 10.1016/j.immuni.2018.03.009
78. Vantourout P, Hayday A. Six-of-the-best: unique contributions of γδ T cells to immunology. *Nat Rev Immunol.* (2013) 13:88–100. doi: 10.1038/nri3384
79. Shen Y, Zhou D, Qiu L, Lai X, Simon M, Shen L, et al. Adaptive immune response of Vγ2Vδ2 T cells during mycobacterial infections. *Science.* (2002) 295:2255–8. doi: 10.1126/science.1068819
80. Kabelitz D, Glatzel A, Wesch D. Antigen recognition by human γδ T lymphocytes. *Int Arch Allergy Immunol.* (2000) 122:1–7. doi: 10.1159/000024353
81. Chien Y-H, Meyer C, Bonneville M. γδ T cells: first line of defense and beyond. *Annu Rev Immunol.* (2014) 32:121–55. doi: 10.1146/annurev-immunol-032713-120216
82. Gruenbacher G, Nussbaumer O, Gander H, Steiner B, Leonhartsberger N, Thurnher M. Stress-related and homeostatic cytokines regulate Vγ9Vδ2 T-cell surveillance of mevalonate metabolism. *OncoImmunology.* (2014) 3:e953410. doi: 10.4161/21624011.2014.953410
83. Tanaka Y, Morita CT, Tanaka Y, Nieves E, Brenner MB, Bloom BR. Natural and synthetic non-peptide antigens recognized by human gamma delta T cells. *Nature.* (1995) 375:155–8. doi: 10.1038/375155a0
84. Gober H Jr., Kistowska M, Angman L, Jenö P, Mori L, De Libero G. Human T cell receptor γδ cells recognize endogenous mevalonate metabolites in tumor cells. *J Exp Med.* (2003) 197:163–8. doi: 10.1084/jem.20021500
85. Eberl M, Hintz M, Reichenberg A, Kollas A-K, Wiesner J, Jomaa H. Microbial isoprenoid biosynthesis and human γδ T cell activation. *FEBS Lett.* (2003) 544:4–10. doi: 10.1016/S0014-5793(03)00483-6
86. Morita CT, Jin C, Sarikonda G, Wang H. Nonpeptide antigens, presentation mechanisms, and immunological memory of human Vγ2Vδ2 T cells: discriminating friend from foe through the recognition of prenyl pyrophosphate antigens. *Immunol Rev.* (2007) 215:59–76. doi: 10.1111/j.1600-065X.2006.00479.x

87. Abeler-Dörner L, Swamy M, Williams G, Hayday AC, Bas A. Butyrophilins: an emerging family of immune regulators. *Trends Immunol.* (2012) 33:34–41. doi: 10.1016/j.it.2011.09.007
88. Afrache H, Gouret P, Ainouche S, Pontarotti P, Olive D. The butyrophilin (BTN) gene family: from milk fat to the regulation of the immune response. *Immunogenetics.* (2012) 64:781–94. doi: 10.1007/s00251-012-0619-z
89. Vavassori S, Kumar A, Wan GS, Ramanjaneyulu GS, Cavallari M, El Daker S, et al. Butyrophilin 3A1 binds phosphorylated antigens and stimulates human γδ T cells. *Nat Immunol.* (2013) 14:908–16. doi: 10.1038/ni.2665
90. Palakodeti A, Sandstrom A, Sundaresan L, Harly C, Nedellec S, Olive D, et al. The molecular basis for modulation of human Vγ9Vδ2 T cell responses by CD277/Butyrophilin-3 (BTN3A)-specific antibodies. *J Biol Chem.* (2012) 287:32780–90.
91. Peigné C-M, Léger A, Gesnel M-C, Konczak F, Olive D, Bonneville M, et al. The juxtamembrane domain of butyrophilin BTN3A1 controls phosphoantigen-mediated activation of human Vγ9Vδ2 T cells. *J Immunol.* (2017) 198:4228–34. doi: 10.4049/jimmunol.1601910
92. Sandstrom A, Peigné C-M, Léger A, Crooks James E, Konczak F, Gesnel M-C, et al. The intracellular B30.2 domain of butyrophilin 3A1 binds phosphoantigens to mediate activation of human Vγ9Vδ2 T cells. *Immunity.* (2014) 40:490–500. doi: 10.1016/j.immuni.2014.03.003
93. Harly C, Guillaume Y, Nedellec S, Peigné C-M, Mönkkönen H, Mönkkönen J, et al. Key implication of CD277/butyrophilin-3 (BTN3A) in cellular stress sensing by a major human γδ T-cell subset. *Blood.* (2012) 120:2269–79. doi: 10.1182/blood-2012-05-430470
94. Uldrich AP, Le Nours J, Pellicci DG, Gherardin NA, McPherson KG, Lim RT, et al. CD1d-lipid antigen recognition by the γδ TCR. *Nat Immunol.* (2013) 14:1137–45. doi: 10.1038/ni.2713
95. Godder KT, Henslee-Downey PJ, Mehta J, Park BS, Chiang KY, Abhyankar S, et al. Long term disease-free survival in acute leukemia patients recovering with increased γδ T cells after partially mismatched related donor bone marrow transplantation. *Bone Marrow Transplant.* (2007) 39:751–7. doi: 10.1038/sj.bmt.1705650
96. Chen CY, Yao S, Huang D, Wei H, Sicard H, Zeng G, et al. Phosphoantigen/IL2 expansion and differentiation of Vγ2Vδ2 T cells increase resistance to tuberculosis in nonhuman primates. *PLoS Pathog.* (2013) 9:e1003501. doi: 10.1371/journal.ppat.1003501
97. Meraviglia S, Caccamo N, Salerno A, Sireci G, Dieli F. Partial and ineffective activation of Vγ9Vδ2 T cells by *Mycobacterium tuberculosis*-infected dendritic cells. *J Immunol.* (2010) 185:1770–6. doi: 10.4049/jimmunol.1000966
98. Qaqish A, Huang D, Chen CY, Zhang Z, Wang R, Li S, et al. Adoptive transfer of phosphoantigen-specific γδ T cell subset attenuates *Mycobacterium tuberculosis* infection in nonhuman primates. *J Immunol.* (2017) 198:4753–63. doi: 10.4049/jimmunol.1602019
99. Huang D, Chen CY, Zhang M, Qiu L, Shen Y, Du G, et al. Clonal immune responses of Mycobacterium-specific γδ T cells in tuberculous and non-tuberculous tissues during *M. tuberculosis* infection. *PLoS One.* (2012) 7:e30631. doi: 10.1371/journal.pone.0030631
100. Pinheiro MB, Antonelli LR, Sathler-Avelar R, Vitelli-Avelar DM, Spindola-de-Miranda S, Guimarães TM, et al. CD4-CD8-αβ and γδ T cells display inflammatory and regulatory potentials during human tuberculosis. *PLoS One.* (2012) 7:e50923. doi: 10.1371/journal.pone.0050923
101. Cendron D, Ingoure S, Martino A, Casetti R, Horand F, Romagné F, et al. A tuberculosis vaccine based on phosphoantigens and fusion proteins induces distinct γδ and αβ T cell responses in primates. *Eur J Immunol.* (2007) 37:549–65. doi: 10.1002/eji.200636343
102. Caccamo N, Todaro M, Sireci G, Meraviglia S, Stassi G, Dieli F. Mechanisms underlying lineage commitment and plasticity of human γδ T cells. *Cell Mol Immunol.* (2013) 10:30–4. doi: 10.1038/cmi.2012.42
103. Braud VM, Allan DSJ, O'Callaghan CA, Söderström K, D'Andrea A, Ogg GS, et al. HLA-E binds to natural killer cell receptors CD94/NKG2A, B and C. *Nature.* (1998) 391:795–9. doi: 10.1038/35869
104. Prezzemolo T, van Meijgaarden KE, Franken KLMC, Caccamo N, Dieli F, Ottenhoff THM, et al. Detailed characterization of human *Mycobacterium tuberculosis* specific HLA-E restricted CD8+ T cells. *Eur J Immunol.* (2018) 48:293–305. doi: 10.1002/eji.201747184
105. van Meijgaarden KE, Haks MC, Caccamo N, Dieli F, Ottenhoff THM, Joosten SA. Human CD8+ T-cells recognizing peptides from *Mycobacterium tuberculosis* (Mtb) presented by HLA-E have an unorthodox Th2-like, multifunctional, Mtb inhibitory phenotype and represent a novel human T-cell subset. *PLoS Pathog.* (2015) 11:e1004671. doi: 10.1371/journal.ppat.1004671
106. Caccamo N, Pietra G, Sullivan LC, Brooks AG, Prezzemolo T, La Manna MP, et al. Human CD8 T lymphocytes recognize *Mycobacterium tuberculosis* antigens presented by HLA-E during active tuberculosis and express type 2 cytokines. *Eur J Immunol.* (2015) 45:1069–81. doi: 10.1002/eji.201445193
107. Grant EJ, Nguyen AT, Lobos CA, Szeto C, Chatzileontiadou DSM, Gras S. The unconventional role of HLA-E: the road less traveled. *Mol Immunol.* (2020) 120:101–12. doi: 10.1016/j.molimm.2020.02.011
108. Joosten SA, Ottenhoff THM, Lewinsohn DM, Hoft DF, Moody DB, Seshadri C. Harnessing donor unrestricted T-cells for new vaccines against tuberculosis. *Vaccine.* (2019) 37:3022–30. doi: 10.1016/j.vaccine.2019.04.050
109. Ulbrecht M, Honka T, Person S, Johnson JP, Weiss EH. The HLA-E gene encodes two differentially regulated transcripts and a cell surface protein. *J Immunol.* (1992) 149:2945–53. doi: 10.5282/ubm/epub.3019
110. Grimsley C, Kawasaki A, Gassner C, Sageshima N, Nose Y, Hatake K, et al. Definitive high resolution typing of HLA-E allelic polymorphisms: Identifying potential errors in existing allele data. *Tissue Antigens.* (2002) 60:206–12. doi: 10.1034/j.1399-0039.2002.600302
111. Robinson J, Halliwell JA, Hayhurst JD, Flicek P, Parham P, Marsh Steven GE. The IPD and IMGT/HLA database: allele variant databases. *Nucleic Acids Res.* (2014) 43:D423–31. doi: 10.1093/nar/gku1161
112. Grotzke JE, Harriff MJ, Siler AC, Nolt D, Delepine J, Lewinsohn DA, et al. The *Mycobacterium tuberculosis* phagosome is a HLA-I processing competent organelle. *PLoS Pathog.* (2009) 5:e1000374. doi: 10.1371/journal.ppat.1000374
113. Cohen GB, Gandhi RT, Davis DM, Mandelboim O, Chen BK, Strominger JL, et al. The selective downregulation of class I major histocompatibility complex proteins by HIV-1 protects HIV-infected cells from NK cells. *Immunity.* (1999) 10:661–71. doi: 10.1016/S1074-7613(00)80065-5
114. Bian Y, Shang S, Siddiqui S, Zhao J, Joosten SA, Ottenhoff TH, et al. MHC Ib molecule Qa-1 presents *Mycobacterium tuberculosis* peptide antigens to CD8+ T cells and contributes to protection against infection. *PLoS Pathog.* (2017) 13:e1006384. doi: 10.1371/journal.ppat.1006384
115. Hansen SG, Wu HL, Burwitz BJ, Hughes CM, Hammond KB, Ventura AB, et al. Broadly targeted CD8 T cell responses restricted by major histocompatibility complex E. *Science.* (2016) 351:714–20. doi: 10.1126/science.aac9475
116. Hansen SG Jr., Piatak M Jr., Ventura AB, Hughes CM, Gilbride RM, Ford JC, et al. Immune clearance of highly pathogenic SIV infection. *Nature.* (2013) 502:100–4. doi: 10.1038/nature12519
117. Hansen SG, Sacha JB, Hughes CM, Ford JC, Burwitz BJ, Scholz I, et al. Cytomegalovirus vectors violate CD8 T cell epitope recognition paradigms. *Science.* (2013) 340:1237874. doi: 10.1126/science.1237874
118. Hansen SG, Zak DE, Xu G, Ford JC, Marshall EE, Malouli D, et al. Prevention of tuberculosis in rhesus macaques by a cytomegalovirus-based vaccine. *Nat Med.* (2018) 24:130–43. doi: 10.1038/nm.4473
119. La Manna MP, Orlando V, Prezzemolo T, Di Carlo P, Cascio A, Delogu G, et al. HLA-E–restricted CD8+ T lymphocytes efficiently control Mycobacterium tuberculosis and HIV-1 coinfection. *Am J Respir Cell Mol Biol.* (2020) 62:430–9. doi: 10.1165/rcmb.2019-0261OC
120. Heczey A, Liu D, Tian G, Courtney AN, Wei J, Marinova E, et al. Invariant NKT cells with chimeric antigen receptor provide a novel platform for safe and effective cancer immunotherapy. *Blood.* (2014) 124:2824–33. doi: 10.1182/blood-2013-11-541235
121. Tian G, Courtney AN, Jena B, Heczey A, Liu D, Marinova E, et al. CD62L+ NKT cells have prolonged persistence and antitumor activity in vivo. *J Clin Invest.* (2016) 126:2341–55. doi: 10.1172/JCI83476
122. Rouxel O, Lehuen A. Mucosal-associated invariant T cells in autoimmune and immune-mediated diseases. *Immunol Cell Biol.* (2018) 96:618–29. doi: 10.1111/imcb.12011
123. Ussher JE, Willberg CB, Klenerman P. MAIT cells and viruses. *Immunol Cell Biol.* (2018) 96:630–41. doi: 10.1111/imcb.12008

124. Salou M, Franciszkiewicz K, Lantz O. MAIT cells in infectious diseases. *Curr Opin Immunol.* (2017) 48:7–14. doi: 10.1016/j.coi.2017.07.009
125. Haeryfar SMM, Shaler CR, Rudak PT. Mucosa-associated invariant T cells in malignancies: a faithful friend or formidable foe? *Cancer Immunol Immunother.* (2018) 67:1885–96. doi: 10.1007/s00262-018-2132-1
126. Hill TM, Bezbradica JS, Van Kaer L, Joyce S. CD1d-restricted natural killer T cells. In: *eLS*. Chichester: John Wiley & Sons, Ltd (2016). p. 1–27. doi: 10.1002/9780470015902.a0020180.pub2
127. Carding SR, Egan PJ. γδ T cells: functional plasticity and heterogeneity. *Nat Rev Immunol.* (2002) 2:336–45. doi: 10.1038/nri797
128. Lo Presti E, Pizzolato G, Gulotta E, Cocorullo G, Gulotta G, Dieli F, et al. Current advances in γδ T cell-based tumor immunotherapy. *Front Immunol.* (2017) 8:1401. doi: 10.3389/fimmu.2017.01401
129. Melero I, Berman DM, Aznar MA, Korman AJ, Gracia JLP, Haanen J. Evolving synergistic combinations of targeted immunotherapies to combat cancer. *Nat Rev Cancer.* (2015) 15:457–72. doi: 10.1038/nrc3973
130. Chang W-S, Kim J-Y, Kim Y-J, Kim Y-S, Lee J-M, Azuma M, et al. Cutting edge: programmed death-1/programmed death ligand 1 interaction regulates the induction and maintenance of invariant NKT cell anergy. *J Immunol.* (2008) 181:6707–10. doi: 10.4049/jimmunol.181.10.6707
131. Durgan K, Ali M, Warner P, Latchman YE. Targeting NKT cells and PD-L1 pathway results in augmented anti-tumor responses in a melanoma model. *Cancer Immunol Immunother.* (2011) 60:547–58. doi: 10.1007/s00262-010-0963-5
132. Iwasaki M, Tanaka Y, Kobayashi H, Murata-Hirai K, Miyabe H, Sugie T, et al. Expression and function of PD-1 in human γδ T cells that recognize phosphoantigens. *Eur J Immunol.* (2011) 41:345–55. doi: 10.1002/eji.201040959

Conflict of Interest: The authors declare that the research was conducted in the absence of any commercial or financial relationships that could be construed as a potential conflict of interest.

frontiers in Immunology

MINI REVIEW
published: 09 September 2020
doi: 10.3389/fimmu.2020.557809

Advancing Immunotherapeutic Vaccine Strategies Against Pulmonary Tuberculosis

*Sam Afkhami[1,2,3], Anne Drumond Villela[1,2,3], Michael R. D'Agostino[1,2,3], Mangalakumari Jeyanathan[1,2,3], Amy Gillgrass[1,2,3] and Zhou Xing[1,2,3]**

[1] McMaster Immunology Research Center, McMaster University, Hamilton, ON, Canada, [2] Department of Pathology and Molecular Medicine, McMaster University, Hamilton, ON, Canada, [3] Michael G. DeGroote Institute for Infectious Disease Research, McMaster University, Hamilton, ON, Canada

Chemotherapeutic intervention remains the primary strategy in treating and controlling tuberculosis (TB). However, a complex interplay between therapeutic and patient-related factors leads to poor treatment adherence. This in turn continues to give rise to unacceptably high rates of disease relapse and the growing emergence of drug-resistant forms of TB. As such, there is considerable interest in strategies that simultaneously improve treatment outcome and shorten chemotherapy duration. Therapeutic vaccines represent one such approach which aims to accomplish this through boosting and/or priming novel anti-TB immune responses to accelerate disease resolution, shorten treatment duration, and enhance treatment success rates. Numerous therapeutic vaccine candidates are currently undergoing pre-clinical and clinical assessment, showing varying degrees of efficacy. By dissecting the underlying mechanisms/correlates of their successes and/or shortcomings, strategies can be identified to improve existing and future vaccine candidates. This mini-review will discuss the current understanding of therapeutic TB vaccine candidates, and discuss major strategies that can be implemented in advancing their development.

Keywords: tuberculosis, therapeutic vaccine, chemotherapy, immunotherapy, respiratory mucosa, mycobacterial life cycle

OPEN ACCESS

Edited by:
Juraj Ivanyi,
King's College London,
United Kingdom

Reviewed by:
Helen McShane,
University of Oxford, United Kingdom
Rajko Reljic,
St George's, University of London,
United Kingdom

****Correspondence:***
Zhou Xing
xingz@mcmaster.ca

Specialty section:
This article was submitted to Microbial Immunology, a section of the journal Frontiers in Immunology

Received: *30 April 2020*
Accepted: *18 August 2020*
Published: *09 September 2020*

Citation:
Afkhami S, Villela AD, D'Agostino MR, Jeyanathan M, Gillgrass A and Xing Z (2020) Advancing Immunotherapeutic Vaccine Strategies Against Pulmonary Tuberculosis. Front. Immunol. 11:557809. doi: 10.3389/fimmu.2020.557809

INTRODUCTION

In 2014, the World Health Organization (WHO) supported a post-2015 END TB Resolution that aimed to curb 90% of both cases and deaths associated with tuberculosis (TB) by 2035 (1). Although measurable progress toward these goals has been made to-date, recent reports show that many interim goals originally set for 2020 will not be met globally (2). A major proportion of these shortcomings stem from current anti-TB chemotherapy regimens including fragmented patient adherence, treatment failure, and emergence of multi- and extensively drug resistant disease (3). Novel strategies to be administered in adjunct with conventional chemotherapy, known as Host-Directed Therapies (HDT), are designed to combat such shortcomings by improving patient adherence, improving cure rates, and preventing disease relapse (4, 5). In this mini-review, we focus on therapeutic vaccination strategies as HDTs for TB. We discuss current requirements for therapeutic vaccines in accordance with WHO standards, their mechanisms of action, detail the current pipeline, and expand on strategies to improve therapeutic vaccines.

CURRENT TB CHEMOTHERAPY LANDSCAPE AND ITS SHORTCOMINGS

Chemotherapy for drug-susceptible TB requires two months of continuous treatment with a cocktail of rifampicin, isoniazid, ethambutol, and pyrazinamide followed by four months of rifampicin and isoniazid. Although this regimen has remained largely unchanged for the last 35 years, numerous healthcare policies such as Direct Observed Treatment Short course have allowed for cure rates as high as 85% (2, 6). This, however, starkly contrasts the low success rate (56%) for drug-resistant disease, for which treatment can last upwards of 24 months (2). Although there are numerous factors that contribute to such low rates, many arise from, and are further exacerbated by poor patient adherence due to the duration of treatment required to successfully treat disease.

It is important to note that novel drugs and drug regimens progressing through the clinical pipeline continue to substantially improve TB treatment outcomes. Novel chemotherapeutics such as bedaquiline and pretomanid have allowed for regimens as short as nine months to be effective in curing drug-resistant forms of TB (7). However, despite such continued improvements, patient adherence remains poor. Chemotherapy durations remain longwinded and costly, and novel antibiotics pose the threat of off-target toxicities such as peripheral neuropathy and cardiac manifestations (8). Non-compliance additionally drives drug resistance which has alarmingly already been documented for bedaquiline (9). These, alongside other socioeconomic issues, are entangled with the longevity of treatment and therefore remain a major roadblock toward the success of chemotherapy against TB.

The development of novel immunotherapeutic strategies that synergize with antibiotics to further shorten the duration of chemotherapy required to successfully treat disease is an alluring platform for improving patient compliance and treatment success.

RATIONALE BEHIND PROLONGED MULTI-DRUG REGIMENS

Logically, multiple drugs are required to treat TB as to avoid the selection of resistant mycobacterial subpopulations that arise from single-drug monotherapy (defined as genetic tolerance) (10). Therefore, individuals with a higher bacillary burden are statistically more likely to carry intrinsically resistant mutants. In stark contrast, the rationale behind the length of therapy is perhaps less intuitive and requires scrutinization of the host-pathogen interface.

Airway macrophages comprise the major niche for *Mycobacterium tuberculosis* (*M.tb*) infection and outgrowth (11, 12). Infected macrophages deploy numerous mechanisms to eliminate *M.tb* which include phagolysosome fusion, upregulation of antimicrobial peptides, and autophagy (13–15). Eventual priming and recruitment of adaptive Th1 immunity further enhances mycobacterial control in part by promoting innate-mediated killing (16). Unfortunately, innate and adaptive immune responses together are often unable to fully eliminate the pathogen. This necessitates addition of chemotherapeutic interventions to further enhance mycobacterial clearance through inhibition of cell wall synthesis (isoniazid and pyrazinamide), and transcription (rifampicin) (10).

However, *M.tb* is fully capable of adapting to both the immunological and pharmacological pressures placed upon it. Examples of such bacterial countermeasures include inhibiting phagosome acidification, delaying adaptive responses, and upregulation of drug efflux pumps (15–18). In addition, immunological and chemotherapeutic stresses also cause *M.tb* to undergo transcriptomic and metabolic shifts leading to a state of dormancy. In this non-replicative state, the antigenic profile of *M.tb* shifts toward expression of stress/dormancy associated genes (19–25). Collectively, this not only further circumvents adaptive immune responses established against the replication antigens, but it also thwarts the efficacy of such therapies (defined as phenotypic tolerance) since the majority of TB chemotherapeutics only target actively replicating bacilli. These phenotypically tolerant, non-replicating mycobacteria are a major and under-investigated subpopulation responsible for disease relapse and the need for prolonged antibiotic therapy (26). As such, there has been a growing interest in strategies which can address such problems. Host-directed therapies represent a promising therapeutic category designed to accomplish this goal.

IMPROVING TREATMENT OUTCOME WITH HOST-DIRECTED THERAPIES

Host-directed therapies are administered in tandem with conventional chemotherapy to improve treatment success and reduce disease relapse. Depending on the strategy, HDTs accomplish this by (1) augmenting the host anti-TB immune response, (2) limiting lung pathology, and/or (3) enhancing mycobacterial sensitivity to chemotherapy. Numerous drug-based HDTs are currently under pre-clinical and clinical investigation. For example, the antihyperglycemic agent metformin has shown promise as it enhances macrophage intracellular mycobacterial killing by increasing phagolysosome fusion and production of reactive oxygen species (27, 28). Drug-based HDTs have been reviewed extensively elsewhere and will not be the focus of this review (4, 5, 29).

VACCINES AS HOST-DIRECTED THERAPIES AGAINST TB

Tuberculosis vaccination strategies encompass those administered prophylactically (to prevent infection), therapeutically (to improve treatment of active disease), and post-exposure (to prevent re-infection/re-activation) (30). Therapeutic vaccines continue to gain traction as leading candidates for TB HDTs.

Therapeutic vaccines are administered in adjunct (at the start or during) with conventional chemotherapy to accelerate treatment, shorten chemotherapy duration, and improve

treatment completion rates. The WHO has generated a detailed list of parameters necessary for an ideal therapeutic vaccine candidate, of which the major targets/goals are presented in **Figure 1** (31). Therapeutic TB vaccines aspire to accomplish these goals by boosting host anti-TB immunity, priming novel immune responses, and modulating the host inflammatory response. The following section briefly outlines the most recent advancements in emerging therapeutic TB vaccines, as identified by the TuBerculosis Vaccine Initiative (TBVI)[1] and the 2018 WHO Global TB Report (**Figure 2**).

[1]https://www.tbvi.eu/

MYCOBACTERIAL-BASED THERAPEUTIC TB VACCINES

Vaccae™

Vaccae™ consists of a heat-killed *Mycobacterium vaccae* (*M vaccae*) variant (32). This non-tuberculous mycobacterium is currently the most advanced therapeutic TB vaccine candidate and is approved for administration alongside standard chemotherapy in patients with active TB in China (33, 34). Although clinical data pertaining to Vaccae™ efficacy is conflicting (with certain meta-analyses indicating little-to-no improvement), recent studies have highlighted its

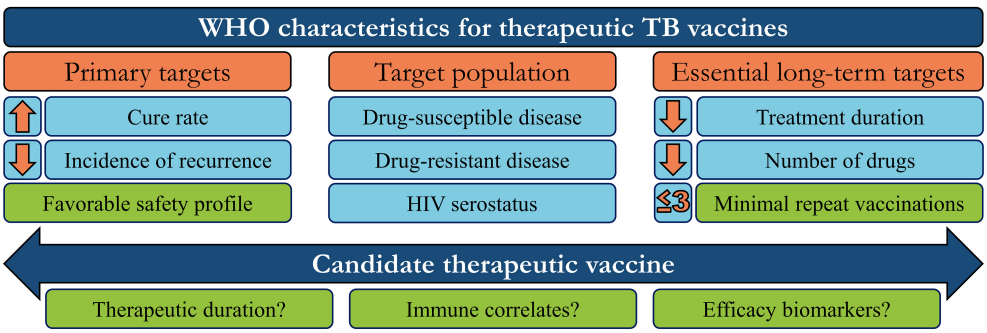

FIGURE 1 | WHO target characteristics for therapeutic tuberculosis vaccines. In order to guide research and development, the WHO has set aspirational targets/characteristics for candidate therapeutic TB vaccines. These include three major areas to address (orange boxes): Vaccine targets that determine efficacy, the target population, and the subsequent long-term impact on the chemotherapy regimen. Candidates which meet some/all of these targets must also be safe, efficacious in a minimum number of repeated doses, and investigated to define their mechanism-of-action or potential efficacy biomarkers, to further refine/guide future vaccination strategies (green boxes).

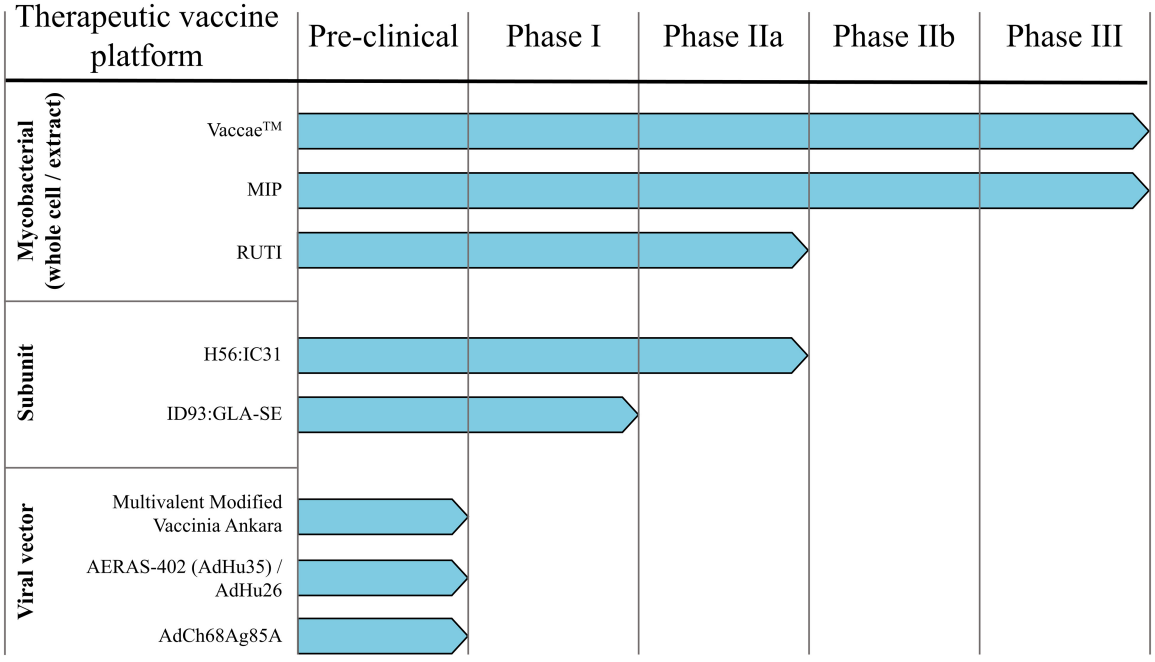

FIGURE 2 | Therapeutic TB vaccine pipeline. Numerous TB vaccine candidates under pre-clinical and/or clinical testing for their prophylactic efficacy are also evaluated as immunotherapies.

therapeutic efficacy (35, 36). In particular, such studies have highlighted the ability of orally administered Vaccae™ to accelerate negative sputum smear conversion. A large-scale phase III trial with 10,000 recruited participants is ongoing with interim results showing high retention rates (clinicaltrials.gov, NCT01979900). However immunological data pertaining to Vaccae™ mechanism of action is limited. Pre-clinical and clinical immunological studies have suggested that induction of robust Th1 (and conversely skewing away from Th2) immune responses, alongside induction of cytotoxic CD8 T lymphocytes are correlatives of efficacy (37).

Mycobacterium indicus pranii

Mycobacterium indicus pranii (MIP) is a non-pathogenic mycobacterium whose heat-killed variant has been successfully used as an immunotherapeutic for leprosy (38, 39). Characterization of the antigenic profile of MIP has shown broad antigenic congruency with *M.tb*, warranting further investigation toward its potential as a therapeutic vaccine. A recently published phase II trial where MIP was intradermally administered in adjunct to chemotherapy showed success in enhancing bacterial clearance, and improved lung pathology in patients with bi-lateral, drug-resistant disease (40). Pre-clinical studies in numerous animal models (including hyper-susceptible guinea pigs) have correlated the therapeutic efficacy of MIP to its ability to drive robust Th1-skewed immunity (41–43). Interestingly, these studies also compared the contribution of immunization route to efficacy, showing that respiratory mucosal vaccination was immunologically superior to the parenteral route.

RUTI®

In contrast to whole, heat-killed mycobacteria, RUTI® is composed of liposomes containing detoxified fragments of *M.tb* grown under hypoxic/stress conditions (44, 45). The growth of virulent *M.tb* under these conditions drives expression of an array of stress and latency associated antigens, thereby expanding the antigenic breadth of the RUTI® formulation, theoretically allowing for adaptive immune responses to target latent bacilli (46). The added advantage of this strategy is targeting the latent bacillary population which, as stated previously, is a major contributor to disease relapse. RUTI® is currently being investigated as a subcutaneously administered post-exposure vaccine in individuals with drug-resistant disease who have completed chemotherapy (45, 47). As such, RUTI® remains to be tested therapeutically in patients with active disease, potentially due to issues related to the Koch phenomenon (45).

RECOMBINANT-BASED THERAPEUTIC TB VACCINES

H56:IC31

H56:IC31 is a recombinant fusion protein of three *M.tb* antigens: Ag85B, ESAT-6, and Rv2660c combined in a stabilizing agent containing a TLR9 agonist as an adjuvant (48). By expressing replication and pathogenicity-based antigens (Ag85B, and ESAT-6, respectively) and latency-associated antigens (Rv2660c), H56:IC31 is designed to drive multi-functional Th1 immunity against both actively replicating and dormant bacilli, and has been shown to prevent *M.tb* reactivation in macaques following parenteral delivery (48, 49). H56:IC31 has undergone extensive clinical testing as a prophylactic vaccine in phase 1 and 2 trials showing a favorable safety and immunogenicity profile in IGRA− and IGRA+ individuals (50). In line with its success and clinical advancement as a prophylactic vaccine, H56:IC31 is also being investigated as an intramuscularly administeredtherapeutic for TB. This includes a phase 1 combinatorial HDT regimen with a Cyclooxygenase-2 inhibitor etoricoxib (clinicaltrials.gov, NCT02503839), and a phase II efficacy trial in South Africa addressing prevention of disease reoccurrence (clinicaltrials.gov, NCT03512249).

ID93/GLA-SE

ID93/GLA-SE is a recombinant vaccine expressing three virulence (Rv2608, Rv3619, and Rv3620) and one latency-associated (Rv1913) antigen in combination with a synthetic TLR4 agonist in an oil-in-water emulsion (51, 52). Similar to the other vaccine candidates described in this review, ID93/GLA-SE has been extensively characterized in pre-clinical animal models. Such studies have shown that ID93/GLA-SE drives robust and sustained anti-TB specific CD4 and CD8 T cell responses following parenteral delivery, correlating with significantly improved prophylactic protection against pulmonary TB (53). Therapeutic vaccination by the intramuscular route with ID93/GLA-SE in non-human primate models significantly reduced pulmonary mycobacterial burden, pathology, and improved survival (53). Thus far, a phase I trial has shown that ID93/GLA-SE is safe and immunogenic in QuantiFERON positive individuals, thereby supporting its further assessment as an immunotherapeutic (54).

VIRAL-VECTORED THERAPEUTIC TB VACCINES

Modified Vaccinia Ankara

Modified Vaccinia Ankara (MVA)-based TB vaccines have a checkered history with a phase IIb trial of MVA85A failing to enhance prophylactic immunity following parenteral immunization in BCG-vaccinated infants (55). Regardless, MVA-vectors remain widely utilized as TB vaccines given their remarkable ability to accommodate large transgene inserts and drive long-lived Th1 immunity (56). A recently developed MVA-based vaccine expressing 10 *M.tb* antigens has been assessed for its therapeutic efficacy in a murine model. Interestingly, this vaccine provided minimal reduction of bacterial burden within the lungs and a modest reduction in relapse (57). This was observed following parenteral, but not respiratory mucosal immunization. Additionally, immunological studies revealed that immune responses against some antigens were not induced. These observations highlight certain key considerations for vaccine design which will be addressed further in this review.

Adenovirus

Adenoviruses represent the most widely used viral vector platform for vaccine design (58). Human adenoviruses, in particular human adenovirus serotype 5 (AdHu5), have been extensively tested as a prophylactic vaccine platform delivered both parenterally and via the respiratory mucosal route (58–62). Unfortunately, in some instances the high seroprevalence of antibodies against this common respiratory pathogen has limited its efficacy. This has prompted the development of platforms founded in serotypes exotic to humans (63).

Non-human adenoviruses, such as chimpanzee adenoviruses have gained traction as vaccine vector candidates given their robust immunogenicity and low seroprevalence (63).

We previously characterized the prophylactic potential of a chimpanzee adenoviral-vectored vaccine expressing *M.tb* Ag85A (AdCh68Ag85A) (64). Our study showcased the superior immunogenicity and efficacy of this vector following respiratory mucosal administration in comparison to its AdHu5 counterpart. Additionally, utilizing a clinically relevant murine model of chemotherapy treated active TB disease, our group has shown that respiratory mucosal therapeutic immunization with AdCh68Ag85A accelerated bacterial clearance, limited lung pathology, and limited disease relapse following pre-mature chemotherapy cessation (65).

ADVANCING THERAPEUTIC TB VACCINE DESIGN

Although definite protective immune correlates for TB remain elusive, insights from ongoing pre-clinical and clinical trials provide invaluable information to steer development of efficacious therapeutic TB vaccination strategies. Such insights stem from both the immunological as well as the mycobacterial areas of research. In this section we highlight three categories (**Figure 3**) which we believe are most important in advancing therapeutic TB vaccine design: Vector formulation and immunization route, antigen/epitope optimization, and antigen selection dictated by the mycobacterial life cycle.

Vector Choice

Factors such as feasibility, safety, and immunogenicity are largely dictated by vector choice. As such, this represents a major consideration when developing novel TB therapeutic vaccine strategies. Whole organism-based vaccines (Vaccae^{TM} and PIM) are advantageous given their antigenic breadth. These vectors however may not be amenable for delivery via the respiratory mucosal route in humans due to potential safety considerations. Additionally, utilization of whole mycobacteria/mycobacterial fragments can potentially skew and/or mask immunological responses against less immunogenic, yet protective antigens (see below). As such, utilization of recombinant molecular biology techniques allows for construction of recombinant vaccines that focus immune responses against well-recognized protective antigens. This is the case for recombinant protein and viral-vectored vaccination strategies (58, 66).

In addition, through careful adjuvant selection, antigen-specific immunity can be polarized toward certain immune profiles. Use of TLR agonists (such as TLR9 in H56:IC31and TLR4 in ID93:GLA-SE) enhance both the cytokine functionality and longevity of Th1 immune responses which are critical for anti-TB immunity (67). Identification of adjuvants capable of inducing cytotoxic CD8 T cell responses can be challenging however and may represent a roadblock in developing optimal therapeutic TB vaccines. We have recently shown that antigen-specific CD8 T cells are the major cell type involved in the therapeutic efficacy of AdCh68Ag85A, thereby providing supporting evidence of their importance in anti-TB immunity (65).

Viral vectors, particularly adenoviruses, remain the most widely utilized platforms for vaccine design given their genetic malleability, safety, and amenability for respiratory mucosal administration (58). However as echoed by us and others, viral serotype selection is a major consideration in the downstream immunogenicity and efficacy of a vaccine candidate. For example, human adenovirus serotype 35 (AdHu35) has been used in place of AdHu5 given its low seroprevalence, which allows it to circumvent anti-vector immunity (68). Thus, this vector has been extensively tested as a putative prophylactic TB vaccine candidate (AERAS-402) (69). Unfortunately, recent studies have shown that parenteral administration of this vaccine did not significantly induce antigen-specific immunity (70, 71). In line with this observation, it is well documented that AdHu35 induces robust type 1 interferon responses, leading to downstream loss of vector transgene expression, which may negatively impact T cell immunity (72). Alongside the choice of immunization route (explained below), this also may explain why AERAS-402 failed to confer efficacy when administered therapeutically (73).

Progress in the development of other novel vaccine platforms provide new opportunities in further advancing therapeutic TB vaccine development. For example, nanoparticle-based vaccines have shown tremendous progress against a plethora of infectious diseases (74). Nanoparticles not only act as antigen carriers, but also possess intrinsic immunogenic properties (often not requiring adjuvants) which can be fine-tuned by altering their physiochemical properties (75). Recent studies have shown that nanoparticle-based TB vaccines are not only amenable for respiratory mucosal delivery, but can drive robust Th1-skewed immune responses which provide similar-to-grater immunity than BCG alone (76, 77).

Immunization Route

Compelling evidence suggests that protection against mucosal pathogens such as *M.tb* is heavily reliant on the presence of pathogen-specific immune cells at the primary site of infection (78–80). As seen during natural *M.tb* infection, bacterial control is observed when anti-TB specific T cells appear in the lung (81). Specifically, it is the presence of such immune responses within the airways that is critical in anti-TB immunity. Immunization route largely determines the anatomical location of antigen-specific T cells and therefore, vaccine efficacy (82). Pre-clinical studies show that parenteral immunization with TB vaccines drives robust antigen-specific T cell immune responses. However,

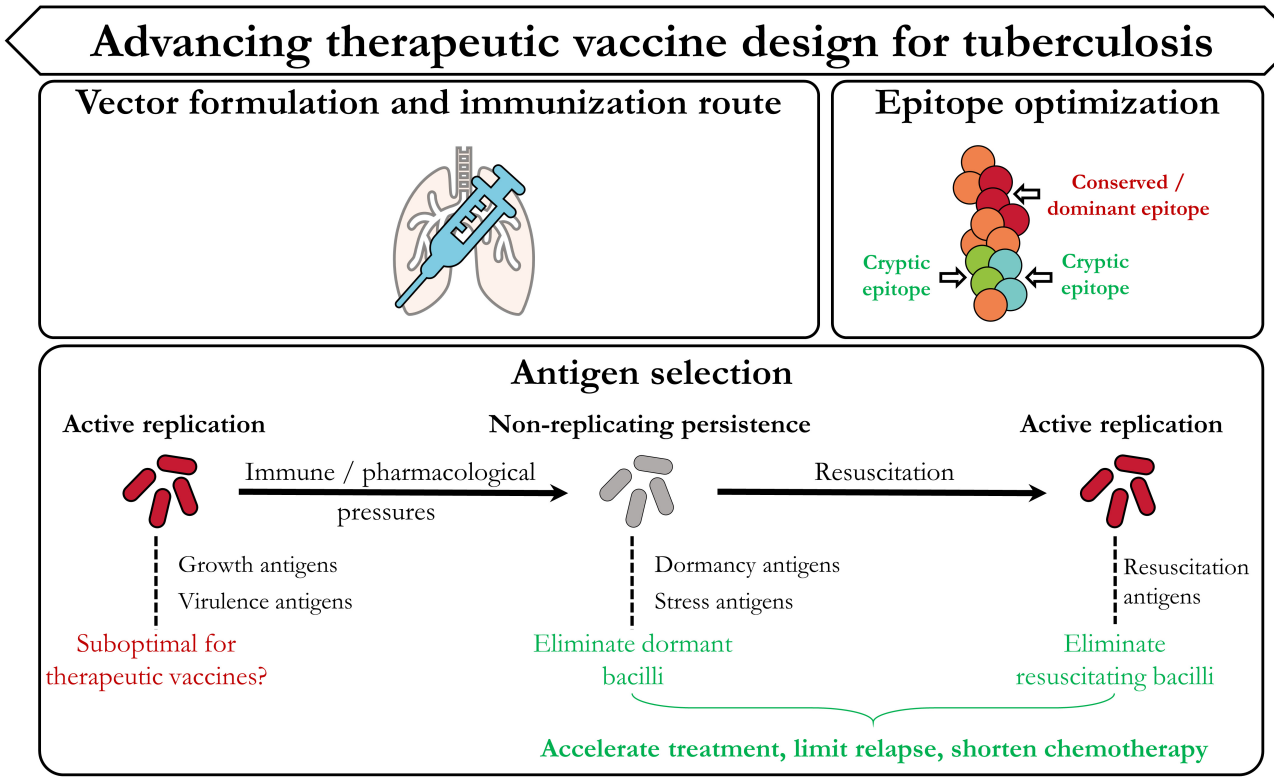

FIGURE 3 | Designing improved therapeutic TB vaccination strategies. In accordance with **Figure 1**, the current TB vaccine landscape has provided invaluable evidence which can be used to improve therapeutic vaccination strategies. These include the type of vaccine vector, the route of immunization, the selection and design of the epitope(s)/antigen(s), and further focus on identifying targets from the different stages of the mycobacterial life cycle.

such cells are primarily restricted to the periphery, unable to quickly enter the lung interstitium and airway lumen, and largely fail to confer protection against pulmonary TB (83). In stark contrast, respiratory mucosal immunization generates a long-lasting population of tissue-resident polyfunctional T cells that are primed to express homing molecules to allow preferential migration and residence in the airway lumen and lungs (80, 82, 84, 85). These immune cells, located at the portal of infection, are able to rapidly respond and carry out their effector function, providing markedly enhanced protection against pulmonary *M.tb* infection.

Antigen/Epitope Optimization

Most TB vaccine candidates in development continue to utilize antigens that are widely characterized in *M.tb*-infected individuals and are proven to be immunogenic (e.g., Ag85A, ESAT6, TB10.4). Seminal studies however have shown that *M.tb* infection in humans is characterized by adaptive T cell responses which are skewed toward hyper conserved epitopes (86, 87). Broad conservation of immune responses against such epitopes is a non-prototypic measure of immune evasion which *M.tb* is speculated to have evolved to control and concentrate the host immune response against non-protective antigens. As most vaccine strategies are formulated to include such immunodominant antigens and have been ineffective, it suggests that these candidates may be suboptimal for vaccine-derived protection. Consequently, targeting non-dominant (cryptic) antigens may represent a superior avenue for designing efficacious vaccines (88).

Expanding the repertoire of T cell immunity through immunization with cryptic antigens has been evaluated in TB in pre-clinical models (89, 90). Such studies have shown that T cell responses against cryptic antigens are significantly more functional than those elicited against classical immunodominant antigens and provide enhanced protection. Importantly, T cell responses against such cryptic antigens are longer-lived, and are less prone to exhaustion, making them ideal for long-lasting immunity. Collectively, such observations warrant the inclusion of cryptic antigens in therapeutic vaccination strategies.

Antigen Selection

Following pulmonary infection, adaptive immune responses are primarily skewed toward replication and virulence-associated antigens. As previously mentioned, immunological and pharmacological stresses proceed to drive *M.tb* into a non-replicating, dormant state. Antigenically, this is associated with a shift from replication-associated antigens to those involved in the stress and the dormancy response. Consequently this

allows *M.tb* to evade existing adaptive immune responses that have already been primed against such antigens. Two major conclusions can be inferred from this: Only targeting replication-associated antigens may be suboptimal for therapeutic vaccination platforms, and including dormancy/stress-associated antigens may improve therapeutic vaccine efficacy. A plethora of dormancy antigens are currently under investigation as tantalizing vaccine antigen candidates. As detailed earlier, H56:IC31 expresses the latency antigen Rv2660c and ID93:GLA-SE expresses Rv1813 (48, 53). These represent just two of many potential dormancy candidates (such as those controlled by the DosR Regulon) that warrant further investigation. In addition, it will be critical to assess whether immune responses to such antigens are able to specifically eliminate dormant bacilli. To do so will require implementation and standardization of experimental techniques that delineate between these mycobacterial subpopulations, which have been described previously (91).

In addition, targeting *M.tb* populations resuscitating from dormancy would also be critical in the development of therapeutic vaccines, as to eliminate/minimize reactivation. Mycobacterial resuscitation is a complex process and is regulated in a coordinated transcriptional burst preceding expression of metabolic and growth-related pathways (92). Resuscitation promoting factors (RPFs) represent a major class of antigens involved in this process and may represent promising vaccine antigen targets (92–94).

Evidence supporting further investigation of RPFs as vaccine antigens stems from clinical studies that correlated the long term maintenance of multifunctional adaptive immunity against these antigens in *M.tb*-infected non-progressors (95). This strongly supports the role of such immune responses in controlling reactivation from latency. Although RPFs have been included in numerous pre-clinical prophylactic vaccine candidates, no study to-date has investigated the contribution of RPF-specific immunity in restricting resuscitation (96, 97). Given the significant contribution of resuscitating *M.tb* populations to disease relapse, developing therapeutic vaccines to improve immune surveillance during or post-chemotherapy against such subpopulations would have substantial benefits.

CONCLUDING STATEMENT

Reaching the END TB set goals for 2035 remains a daunting task which we are unlikely to meet short of a revolution in current treatments. Investigation into therapeutic vaccines has expanded rapidly in the last several years offering novel insights toward vector design, and targeted antigen selection from differing stages of the bacterial lifecycle. While this field lags behind the development of prophylactic strategies, therapeutic vaccines have the potential to enhance treatment success rates, even for difficult-to-treat drug-resistant forms of TB. As this emerging field of TB vaccine development continues to flourish, there are several factors that will be critical to assessing their potential success, and eventual utilization. Namely, to what extent are these vaccines able to shorten the duration of existing chemotherapeutic regimens? How will we evaluate the efficacy of these vaccines under realistic situations such as fragmented or incomplete therapy? Can therapeutic immunization protect against recurrent infection? Intertwined with this are establishing correlates to measure efficacy, and the standardization of complex, pre-clinical models necessary to account for the myriad of moving parts at play. This includes, but is not limited to, dissecting immune responses from vaccines versus those induced from infection, the role of chemotherapy in driving dormancy/escape from immunological pressures, and safety/efficacy in individuals living with HIV.

AUTHOR CONTRIBUTIONS

SA, AV, and ZX designed the manuscript. SA and AV wrote the manuscript. ZX approved the manuscript. All authors revised and edited the manuscript.

ACKNOWLEDGMENTS

We acknowledge the support from the Canadian Institutes of Health Research Foundation Program and the Natural Sciences and Engineering Research Council of Canada.

REFERENCES

1. World Health Organization Executive Board. *Global Strategy and Targets for Tuberculosis Prevention, Care and Control After 2015*. Geneva: WHO (2015). p. 1–23.
2. World Health Organization. *Global Tuberculosis Report 2019*. Geneva: WHO (2019).
3. World Health Organization. *Consolidated Guidelines on Tuberculosis Treatment*. Geneva: WHO (2019).
4. Wallis RS, Hafner R. Advancing host-directed therapy for tuberculosis. *Nat Rev Immunol.* (2015) 15:255–63. doi: 10.1038/nri3813
5. Young C, Walzl G, Du Plessis N. Therapeutic host-directed strategies to improve outcome in tuberculosis. *Mucosal Immunol.* (2020) 13:190–204. doi: 10.1038/s41385-019-0226-5
6. World Health Organization. *What is DOTS? A Guide to Understanding the WHO-recommended TB Control Strategy Known as DOTS*. Geneva: WHO (1999). p. 1–39.
7. Conradie F, Diacon AH, Ngubane N, Howell P, Everitt D, Crook AM, et al. Treatment of highly drug-resistant pulmonary tuberculosis. *N Engl J Med.* (2020) 382:893–902. doi: 10.1056/NEJMoa1901814
8. Diacon AH, Pym A, Grobusch MP, de los Rios JM, Gotuzzo E, Vasilyeva I, et al. Multidrug-resistant tuberculosis and culture conversion with bedaquiline. *N Engl J Med.* (2014) 371:723–32. doi: 10.1056/NEJMoa1313865
9. de Vos M, Ley SD, Wiggins KB, Derendinger B, Dippenaar A, Grobbelaar M, et al. Bedaquiline microheteroresistance after cessation of tuberculosis treatment. *N Engl J Med.* (2019) 380:2178–80. doi: 10.1056/NEJMc1815121
10. Colijn C, Cohen T, Ganesh A, Murray M. Spontaneous emergence of multiple drug resistance in tuberculosis before and during therapy. *PLoS One.* (2011) 6:e18327. doi: 10.1371/journal.pone.0018327
11. Cohen SB, Gern BH, Delahaye JL, Adams KN, Plumlee CR, Winkler JK, et al. Alveolar macrophages provide an early *Mycobacterium tuberculosis* niche and initiate dissemination. *Cell Host Microbe.* (2018) 24:439–46.e4. doi: 10.1016/j.chom.2018.08.001

12. Huang L, Nazarova EV, Tan S, Liu Y, Russell DG. Growth of *Mycobacterium tuberculosis* in vivo segregates with host macrophage metabolism and ontogeny. *J Exp Med.* (2018) 215:1135–52. doi: 10.1084/jem.20172020
13. Kimmey JM, Huynh JP, Weiss LA, Park S, Kambal A, Debnath J, et al. Unique role for ATG5 in neutrophil-mediated immunopathology during *M. tuberculosis* infection. *Nature.* (2015) 528:565–9. doi: 10.1038/nature16451
14. Songane M, Kleinnijenhuis J, Netea MG, van Crevel R. The role of autophagy in host defence against *Mycobacterium tuberculosis* infection. *Tuberculosis.* (2012) 92:388–96. doi: 10.1016/j.tube.2012.05.004
15. Levitte S, Adams KN, Berg RD, Cosma CL, Urdahl KB, Ramakrishnan L. Mycobacterial acid tolerance enables phagolysosomal survival and establishment of tuberculous infection in vivo. *Cell Host Microbe.* (2016) 20:250–8. doi: 10.1016/j.chom.2016.07.007
16. Lai R, Jeyanathan M, Shaler CR, Damjanovic D, Khera A, Horvath C, et al. Restoration of innate immune activation accelerates Th1-cell priming and protection following pulmonary mycobacterial infection. *Eur J Immunol.* (2014) 44:1375–86. doi: 10.1002/eji.201344300
17. Romagnoli A, Etna MP, Giacomini E, Pardini M, Remoli ME, Corazzari M, et al. ESX-1 dependent impairment of autophagic flux by *Mycobacterium tuberculosis* in human dendritic cells. *Autophagy.* (2012) 8:1357–70. doi: 10.4161/auto.20881
18. Lai R, Jeyanathan M, Afkhami S, Zganiacz A, Hammill JA, Yao Y, et al. CD11b + dendritic cell–mediated anti– *Mycobacterium tuberculosis* Th1 activation is counterregulated by CD103 + dendritic cells via IL-10. *J Immunol.* (2018) 200:1746–60. doi: 10.4049/jimmunol.1701109
19. Karakousis PC, Yoshimatsu T, Lamichhane G, Woolwine SC, Nuermberger EL, Grosset J, et al. Dormancy phenotype displayed by extracellular *Mycobacterium tuberculosis* within artificial granulomas in mice. *J Exp Med.* (2004) 200:647–57. doi: 10.1084/jem.20040646
20. Voskuil MI, Schnappinger D, Visconti KC, Harrell MI, Dolganov GM, Sherman DR, et al. Inhibition of respiration by nitric oxide induces a *Mycobacterium tuberculosis* dormancy program. *J Exp Med.* (2003) 198:705–13. doi: 10.1084/jem.20030205
21. Gengenbacher M, Kaufmann SHE. *Mycobacterium tuberculosis*?: success through dormancy. *FEMS Microbiol Rev.* (2012) 36:514–32. doi: 10.1111/j.1574-6976.2012.00331.x
22. Raffetseder J, Pienaar E, Blomgran R, Eklund D, Patcha Brodin V, Andersson H, et al. Replication rates of *Mycobacterium tuberculosis* in human macrophages do not correlate with mycobacterial antibiotic susceptibility. *PLoS One.* (2014) 9:e112426. doi: 10.1371/journal.pone.0112426
23. Park H-D, Guinn KM, Harrell MI, Liao R, Voskuil MI, Tompa M, et al. Rv3133c/dosR is a transcription factor that mediates the hypoxic response of *Mycobacterium tuberculosis*. *Mol Microbiol.* (2003) 48:833–43. doi: 10.1046/j.1365-2958.2003.03474.x
24. Mehra S, Foreman TW, Didier PJ, Ahsan MH, Hudock TA, Kissee R, et al. The DosR regulon modulates adaptive immunity and is essential for *Mycobacterium tuberculosis* persistence. *Am J Respir Crit Care Med.* (2015) 191:1185–96. doi: 10.1164/rccm.201408-1502OC
25. Bartek IL, Rutherford R, Gruppo V, Morton RA, Morris RP, Klein MR, et al. The DosR regulon of *M. tuberculosis* and antibacterial tolerance. *Tuberculosis.* (2009) 89:310–6. doi: 10.1016/j.tube.2009.06.001
26. Hu Y, Pertinez H, Liu Y, Davies G, Coates A. Bedaquiline kills persistent *Mycobacterium tuberculosis* with no disease relapse: an in vivo model of a potential cure. *J Antimicrob Chemother.* (2019) 74:1627–33. doi: 10.1093/jac/dkz052
27. Singhal A, Jie L, Kumar P, Hong GS, Leow MK-S, Paleja B, et al. Metformin as adjunct antituberculosis therapy. *Sci Transl Med.* (2014) 6:263ra159. doi: 10.1126/scitranslmed.3009885
28. Lachmandas E, Eckold C, Böhme J, Koeken VACM, Marzuki MB, Blok B, et al. Metformin alters human host responses to *Mycobacterium tuberculosis* in healthy subjects. *J Infect Dis.* (2019) 220:139–50. doi: 10.1093/infdis/jiz064
29. Torfs E, Piller T, Cos P, Cappoen D. Opportunities for overcoming *Mycobacterium tuberculosis* drug resistance: emerging mycobacterial targets and host-directed therapy. *Int J Mol Sci.* (2019) 20:2868. doi: 10.3390/ijms20122868
30. Orme IM. Tuberculosis vaccine types and timings. *Clin Vaccine Immunol.* (2015) 22:249–57. doi: 10.1128/CVI.00718-14
31. World Health Organization. *WHO Preferred Product Characteristics for Therapeutic Vaccines to Improve Tuberculosis Treatment Outcomes*. Geneva: WHO (2019). doi: 10.1128/cvi.00718-14
32. Stanford JL, Rook GAW, Bahr GM, Dowlati Y, Ganapati R, Ghazi Saidi K, et al. *Mycobacterium vaccae* in immunoprophylaxis and immunotherapy of leprosy and tuberculosis. *Vaccine.* (1990) 8:525–30. doi: 10.1016/0264-410X(90)90002-4
33. Huang C, Hsieh W. Efficacy of *Mycobacterium vaccae* immunotherapy for patients with tuberculosis: a systematic review and meta-analysis. *Hum Vaccin Immunother.* (2017) 13:1960–71. doi: 10.1080/21645515.2017.1335374
34. Weng H, Huang J-Y, Meng X-Y, Li S, Zhang G-Q. Adjunctive therapy of *Mycobacterium vaccae* vaccine in the treatment of multidrug-resistant tuberculosis: a systematic review and meta-analysis. *Biomed Rep.* (2016) 4:595–600. doi: 10.3892/br.2016.624
35. de Bruyn G, Garner P. *Mycobacterium vaccae* immunotherapy for treating tuberculosis. *Cochrane Database Syst Rev.* (2003) CD001166.
36. Yang XY, Chen QF, Cui XH, Yu Y, Li YP. *Mycobacterium vaccae* vaccine to prevent tuberculosis in high risk people: a meta-analysis. *J Infect.* (2010) 60:320–30. doi: 10.1016/j.jinf.2010.02.005
37. Skinner MA, Yuan S, Prestidge R, Chuk D, Watson JD, Tan PLJ. Immunization with heat-killed *Mycobacterium vaccae* stimulates CD8+ cytotoxic T cells specific for macrophages infected with *Mycobacterium tuberculosis*. *Infect Immun.* (1997) 65:4525–30. doi: 10.1128/IAI.65.11.4525-4530.1997
38. Burdick AE, Ramirez CC. The role of mycophenolate mofetil in the treatment of leprosy reactions. *Int J Lepr Other Mycobact Dis.* (2005) 73:127–8.
39. Zaheer SA, Mukherjee R, Ramkumar D, Misra RS, Sharma AK, Kar HK, et al. Combined multidrug and Mycobacterium w vaccine therapy in patients with multibacillary leprosy. *J Infect Dis.* (1993) 167:401–10. doi: 10.1093/infdis/167.2.401
40. Sharma SK, Katoch K, Sarin R, Balambal R, Kumar Jain N, Patel N, et al. Efficacy and safety of *Mycobacterium indicus* pranii as an adjunct therapy in category II pulmonary tuberculosis in a randomized trial. *Sci Rep.* (2017) 7:3354. doi: 10.1038/s41598-017-03514-1
41. Guleria I, Mukherjee R, Kaufmann SE. In vivo depletion of CD4 and CD8 T lymphocytes impairs Mycobacterium w vaccine-induced protection against *M. tubercolosis* in mice. *Med Microbiol Immunol.* (1993) 182:129–35. doi: 10.1007/BF00190265
42. Gupta A, Ahmad FJ, Ahmad F, Gupta UD, Natarajan M, Katoch VM, et al. Protective efficacy of *Mycobacterium indicus* pranii against tuberculosis and underlying local lung immune responses in guinea pig model. *Vaccine.* (2012) 30:6198–209. doi: 10.1016/j.vaccine.2012.07.061
43. Das S, Chowdhury BP, Goswami A, Parveen S, Jawed J, Pal N, et al. *Mycobacterium indicus* pranii (MIP) mediated host protective intracellular mechanisms against tuberculosis infection: involvement of TLR-4 mediated signaling. *Tuberculosis.* (2016) 101:201–9. doi: 10.1016/j.tube.2016.09.027
44. Cardona P-J, Amat I, Gordillo S, Arcos V, Guirado E, Díaz J, et al. Immunotherapy with fragmented *Mycobacterium tuberculosis* cells increases the effectiveness of chemotherapy against a chronical infection in a murine model of tuberculosis. *Vaccine.* (2005) 23:1393–8. doi: 10.1016/j.vaccine.2004.09.008
45. Nell AS, D'lom E, Bouic P, Sabaté M, Bosser R, Picas J, et al. Safety, tolerability, and immunogenicity of the novel antituberculous vaccine RUTI: randomized, placebo-controlled phase II clinical trial in patients with latent tuberculosis infection. *PLoS One.* (2014) 9:e89612. doi: 10.1371/journal.pone.0089612
46. Guirado E, Gil O, Caìceres N, Singh M, Vilaplana C, Cardona P-J. Induction of a specific strong polyantigenic cellular immune response after short-term chemotherapy controls bacillary reactivation in murine and guinea pig experimental models of tuberculosis. *Clin Vaccine Immunol.* (2008) 15:1229–37. doi: 10.1128/CVI.00094-08
47. Vilaplana C, Montané E, Pinto S, Barriocanal AM, Domenech G, Torres F, et al. Double-blind, randomized, placebo-controlled Phase I clinical trial of the therapeutical antituberculous vaccine RUTI®. *Vaccine.* (2010) 28:1106–16. doi: 10.1016/j.vaccine.2009.09.134
48. Lin PL, Dietrich J, Tan E, Abalos RM, Burgos J, Bigbee C, et al. The multistage vaccine H56 boosts the effects of BCG to protect cynomolgus macaques against active tuberculosis and reactivation of latent *Mycobacterium tuberculosis* infection. *J Clin Invest.* (2012) 122:303–14. doi: 10.1172/JCI46252

49. Aagaard C, Hoang T, Dietrich J, Cardona P-J, Izzo A, Dolganov G, et al. multistage tuberculosis vaccine that confers efficient protection before and after exposure. *Nat Med.* (2011) 17:189–94. doi: 10.1038/nm.2285
50. Luabeya AKK, Kagina BMN, Tameris MD, Geldenhuys H, Hoff ST, Shi Z, et al. First-in-human trial of the post-exposure tuberculosis vaccine H56:IC31 in *Mycobacterium tuberculosis* infected and non-infected healthy adults. *Vaccine.* (2015) 33:4130–40. doi: 10.1016/j.vaccine.2015.06.051
51. Coler RN, Bertholet S, Moutaftsi M, Guderian JA, Windish HP, Baldwin SL, et al. Development and characterization of synthetic glucopyranosyl lipid adjuvant system as a vaccine adjuvant. *PLoS One.* (2011) 6:e16333. doi: 10.1371/journal.pone.0016333
52. Bertholet S, Ireton GC, Kahn M, Guderian J, Mohamath R, Stride N, et al. Identification of human T cell antigens for the development of vaccines against *Mycobacterium tuberculosis*. *J Immunol.* (2008) 181:7948–57. doi: 10.4049/jimmunol.181.11.7948
53. Coler RN, Bertholet S, Pine SO, Orr MT, Reese V, Windish HP, et al. Therapeutic immunization against *Mycobacterium tuberculosis* is an effective adjunct to antibiotic treatment. *J Infect Dis.* (2013) 207:1242–52. doi: 10.1093/infdis/jis425
54. Penn-Nicholson A, Tameris M, Smit E, Day TA, Musvosvi M, Jayashankar L, et al. Safety and immunogenicity of the novel tuberculosis vaccine ID93 + GLA-SE in BCG-vaccinated healthy adults in South Africa: a randomised, double-blind, placebo-controlled phase 1 trial. *Lancet Respir Med.* (2018) 6:287–98. doi: 10.1016/S2213-2600(18)30077-8
55. Tameris MD, Hatherill M, Landry BS, Scriba TJ, Snowden MA, Lockhart S, et al. Safety and efficacy of MVA85A, a new tuberculosis vaccine, in infants previously vaccinated with BCG: a randomised, placebo-controlled phase 2b trial. *Lancet.* (2013) 381:1021–8. doi: 10.1016/S0140-6736(13)60177-4
56. Cottingham MG, Carroll MW. Recombinant MVA vaccines: dispelling the myths. *Vaccine.* (2013) 31:4247–51. doi: 10.1016/j.vaccine.2013.03.021
57. Leung-Theung-Long S, Coupet C, Gouanvic M, Schmitt D, Ray A, Hoffmann C, et al. A multi-antigenic MVA vaccine increases efficacy of combination chemotherapy against *Mycobacterium tuberculosis*. *PLoS One.* (2018) 13:e0196815. doi: 10.1371/journal.pone.0196815
58. Afkhami S, Yao Y, Xing Z. Methods and clinical development of adenovirus-vectored vaccines against mucosal pathogens. *Mol Ther Methods Clin Dev.* (2016) 3:16030. doi: 10.1038/mtm.2016.30
59. Tchilian E, Ahuja D, Hey A, Jiang S, Beverley P. Immunization with different formulations of *Mycobacterium tuberculosis* antigen 85A induces immune responses with different specificity and protective efficacy. *Vaccine.* (2013) 31:4624–31. doi: 10.1016/j.vaccine.2013.07.040
60. Smaill F, Jeyanathan M, Smieja M, Medina MF, Thanthrige-Don N, Zganiacz A, et al. A human type 5 adenovirus-based tuberculosis vaccine induces robust T cell responses in humans despite preexisting anti-adenovirus immunity. *Sci Transl Med.* (2013) 5:205ra134. doi: 10.1126/scitranslmed.3006843
61. Jeyanathan M, Shao Z, Yu X, Harkness R, Jiang R, Li J, et al. AdHu5Ag85A respiratory mucosal boost immunization enhances protection against pulmonary tuberculosis in BCG-primed non-human primates. *PLoS One.* (2015) 10:e0135009. doi: 10.1371/journal.pone.0135009
62. Yao Y, Lai R, Afkhami S, Haddadi S, Zganiacz A, Vahedi F, et al. Enhancement of antituberculosis immunity in a humanized model system by a novel virus-vectored respiratory mucosal vaccine. *J Infect Dis.* (2017) 216:135–45. doi: 10.1093/infdis/jix252
63. Colloca S, Barnes E, Folgori A, Ammendola V, Capone S, Cirillo A, et al. Vaccine vectors derived from a large collection of simian adenoviruses induce potent cellular immunity across multiple species. *Sci Transl Med.* (2012) 4:115ra2. doi: 10.1126/scitranslmed.3002925
64. Jeyanathan M, Thanthrige-Don N, Afkhami S, Lai R, Damjanovic D, Zganiacz A, et al. Novel chimpanzee adenovirus-vectored respiratory mucosal tuberculosis vaccine: overcoming local anti-human adenovirus immunity for potent TB protection. *Mucosal Immunol.* (2015) 8:1373–87. doi: 10.1038/mi.2015.29
65. Afkhami S, Lai R, D'Agostino MR, Vaseghi-Shanjani M, Zganiacz A, Yao Y, et al. Single-dose mucosal immunotherapy with chimpanzee adenovirus-based vaccine accelerates TB disease control and limits its rebound following antibiotic cessation. *J Infect Dis.* (2019) 220:1355–66. doi: 10.1093/infdis/jiz306
66. Nascimento IP, Leite LCC. Recombinant vaccines and the development of new vaccine strategies. *Brazilian J Med Biol Res.* (2012) 45:1102–11. doi: 10.1590/s0100-879x2012007500142
67. Schellack C, Prinz K, Egyed A, Fritz JH, Wittmann B, Ginzler M, et al. IC31, a novel adjuvant signaling via TLR9, induces potent cellular and humoral immune responses. *Vaccine.* (2006) 24:5461–72. doi: 10.1016/j.vaccine.2006.03.071
68. Thorner AR, Vogels R, Kaspers J, Weverling GJ, Holterman L, Lemckert A, et al. Age dependence of adenovirus-specific neutralizing antibody titers in individuals from sub-saharan Africa. *J Clin Microbiol.* (2006) 44:3781–3. doi: 10.1128/JCM.01249-06
69. Abel B, Tameris M, Mansoor N, Gelderbloem S, Hughes J, Abrahams D, et al. The novel tuberculosis vaccine, AERAS-402, induces robust and polyfunctional CD4 + and CD8 + T cells in adults. *Am J Respir Crit Care Med.* (2010) 181:1407–17. doi: 10.1164/rccm.200910-1484OC
70. van Zyl-Smit RN, Esmail A, Bateman ME, Dawson R, Goldin J, van Rikxoort E, et al. Safety and immunogenicity of adenovirus 35 tuberculosis vaccine candidate in adults with active or previous tuberculosis. A Randomized Trial. *Am J Respir Crit Care Med.* (2017) 195:1171–80. doi: 10.1164/rccm.201603-0654OC
71. Darrah PA, Bolton DL, Lackner AA, Kaushal D, Aye PP, Mehra S, et al. Aerosol vaccination with AERAS-402 elicits robust cellular immune responses in the lungs of rhesus macaques but fails to protect against high-dose *Mycobacterium tuberculosis* challenge. *J Immunol.* (2014) 193:1799–811. doi: 10.4049/jimmunol.1400676
72. Johnson MJ, Björkström NK, Petrovas C, Liang F, Gall JGD, Loré K, et al. Type I interferon-dependent activation of NK cells by rAd28 or rAd35, but not rAd5, leads to loss of vector-insert expression. *Vaccine.* (2014) 32:717–24. doi: 10.1016/j.vaccine.2013.11.055
73. Alyahya SA, Nolan ST, Smith CMR, Bishai WR, Sadoff J, Lamichhane G. Immunogenicity without efficacy of an adenoviral tuberculosis vaccine in a stringent mouse model for immunotherapy during treatment. *PLoS One.* (2015) 10:e0127907. doi: 10.1371/journal.pone.0127907
74. Pati R, Shevtsov M, Sonawane A. Nanoparticle vaccines against infectious diseases. *Front Immunol.* (2018) 9:2224. doi: 10.3389/fimmu.2018.02224
75. Gregory AE, Titball R, Williamson D. Vaccine delivery using nanoparticles. *Front Cell Infect Microbiol.* (2013) 3:1–13. doi: 10.3389/fcimb.2013.00013
76. Stylianou E, Diogo GR, Pepponi I, Dolleweerd C, Arias MA, Locht C, et al. Mucosal delivery of antigen−coated nanoparticles to lungs confers protective immunity against tuberculosis infection in mice. *Eur J Immunol.* (2014) 44:440–9. doi: 10.1002/eji.201343887
77. Ballester M, Nembrini C, Dhar N, de Titta A, de Piano C, Pasquier M, et al. Nanoparticle conjugation and pulmonary delivery enhance the protective efficacy of Ag85B and CpG against tuberculosis. *Vaccine.* (2011) 29:6959–66. doi: 10.1016/j.vaccine.2011.07.039
78. Jeyanathan M, Heriazon A, Xing Z. Airway luminal T cells: a newcomer on the stage of TB vaccination strategies. *Trends Immunol.* (2010) 31:247–52. doi: 10.1016/j.it.2010.05.002
79. Xing Z, Jeyanathan M, Smaill F. New approaches to TB vaccination. *Chest.* (2014) 146:804–12. doi: 10.1378/chest.14-0439
80. Wang J, Thorson L, Stokes RW, Santosuosso M, Huygen K, Zganiacz A, et al. Single mucosal, but not parenteral, immunization with recombinant adenoviral-based vaccine provides potent protection from pulmonary tuberculosis. *J Immunol.* (2004) 173:6357–65. doi: 10.4049/jimmunol.173.10.6357
81. Cooper AM. Cell-mediated immune responses in tuberculosis. *Annu Rev Immunol.* (2009) 27:393–422. doi: 10.1146/annurev.immunol.021908.132703
82. Lai R, Afkhami S, Haddadi S, Jeyanathan M, Xing Z. Mucosal immunity and novel tuberculosis vaccine strategies: route of immunisation determined T-cell homing to restricted lung mucosal compartments. *Eur Respir Rev.* (2015) 24:356–60. doi: 10.1183/16000617.00002515
83. Jeyanathan M, Afkhami S, Khera A, Mandur T, Damjanovic D, Yao Y, et al. CXCR3 signaling is required for restricted homing of parenteral tuberculosis vaccine–induced T cells to both the lung parenchyma and airway. *J Immunol.* (2017) 199:2555–69. doi: 10.4049/jimmunol.1700382
84. Haddadi S, Thanthrige-Don N, Afkhami S, Khera A, Jeyanathan M, Xing Z. Expression and role of VLA-1 in resident memory CD8 T cell responses to

respiratory mucosal viral-vectored immunization against tuberculosis. *Sci Rep.* (2017) 7:9525. doi: 10.1038/s41598-017-09909-4
85. Haddadi S, Vaseghi-Shanjani M, Yao Y, Afkhami S, D'Agostino MR, Zganiacz A, et al. Mucosal-pull induction of lung-resident memory CD8 T cells in parenteral TB vaccine-primed hosts requires cognate antigens and CD4 T cells. *Front Immunol.* (2019) 10:2075. doi: 10.3389/fimmu.2019.02075
86. Comas I, Chakravartti J, Small PM, Galagan J, Niemann S, Kremer K, et al. Human T cell epitopes of *Mycobacterium tuberculosis* are evolutionarily hyperconserved. *Nat Genet.* (2010) 42:498–503. doi: 10.1038/ng.590
87. Coscolla M, Copin R, Sutherland J, Gehre F, de Jong B, Owolabi O, et al. tuberculosis T cell epitope analysis reveals paucity of antigenic variation and identifies rare variable TB antigens. *Cell Host Microbe.* (2015) 18:538–48. doi: 10.1016/j.chom.2015.10.008
88. Woodworth JS, Andersen P. Reprogramming the T cell response to tuberculosis. *Trends Immunol.* (2016) 37:81–3. doi: 10.1016/j.it.2015.12.009
89. Woodworth JS, Aagaard CS, Hansen PR, Cassidy JP, Agger EM, Andersen P. Protective CD4 T cells targeting cryptic epitopes of *Mycobacterium tuberculosis* resist infection-driven terminal differentiation. *J Immunol.* (2014) 192:3247–58. doi: 10.4049/jimmunol.1300283
90. Aagaard CS, Hoang TTKT, Vingsbo-Lundberg C, Dietrich J, Andersen P. Quality and vaccine efficacy of CD4 + T cell responses directed to dominant and subdominant epitopes in ESAT-6 from *Mycobacterium tuberculosis*. *J Immunol.* (2009) 183:2659–68. doi: 10.4049/jimmunol.0900947
91. Loraine J, Pu F, Turapov O, Mukamolova GV. Development of an in vitro assay for detection of drug-induced resuscitation-promoting-factor-dependent mycobacteria. *Antimicrob Agents Chemother.* (2016) 60:6227–33. doi: 10.1128/AAC.00518-16
92. Salina EG, Grigorov AS, Bychenko OS, Skvortsova YV, Mamedov IZ, Azhikina TL, et al. Resuscitation of dormant "Non-culturable" *Mycobacterium tuberculosis* is characterized by immediate transcriptional burst. *Front Cell Infect Microbiol.* (2019) 9:272. doi: 10.3389/fcimb.2019.00272
93. Shleeva MO, Bagramyan K, Telkov MV, Mukamolova GV, Young M, Kell DB, et al. Formation and resuscitation of 'non-culturable' cells of Rhodococcus rhodochrous and *Mycobacterium tuberculosis* in prolonged stationary phase. *Microbiology.* (2002) 148:1581–91. doi: 10.1099/00221287-148-5-1581
94. Mukamolova GV, Turapov O, Malkin J, Woltmann G, Barer MR. Resuscitation-promoting factors reveal an occult population of Tubercle bacilli in sputum. *Am J Respir Crit Care Med.* (2010) 181:174–80. doi: 10.1164/rccm.200905-0661OC
95. Commandeur S, van Meijgaarden KE, Lin MY, Franken KLMC, Friggen AH, Drijfhout JW, et al. Identification of human T-cell responses to *Mycobacterium tuberculosis* resuscitation-promoting factors in long-Term latently infected individuals. *Clin Vaccine Immunol.* (2011) 18:676–83. doi: 10.1128/CVI.00492-10
96. Romano M, Aryan E, Korf H, Bruffaerts N, Franken CLMC, Ottenhoff THM, et al. Potential of *Mycobacterium tuberculosis* resuscitation-promoting factors as antigens in novel tuberculosis sub-unit vaccines. *Microbes Infect.* (2012) 14:86–95. doi: 10.1016/j.micinf.2011.08.011
97. Hansen SG, Zak DE, Xu G, Ford JC, Marshall EE, Malouli D, et al. Prevention of tuberculosis in rhesus macaques by a cytomegalovirus-based vaccine. *Nat Med.* (2018) 24:130–43. doi: 10.1038/nm.4473

Conflict of Interest: The authors declare that the research was conducted in the absence of any commercial or financial relationships that could be construed as a potential conflict of interest.

The reviewer HM declared a past co-authorship with one of the authors ZX to the handling editor.

frontiers in Immunology

REVIEW
published: 10 September 2020
doi: 10.3389/fimmu.2020.02006

Diagnosis for Latent Tuberculosis Infection: New Alternatives

Claudia Carranza[1], *Sigifredo Pedraza-Sanchez*[2], *Eleane de Oyarzabal-Mendez*[1] *and Martha Torres*[1,3]*

[1] Departamento de Microbiología, Instituto Nacional de Enfermedades Respiratorias, Mexico City, Mexico, [2] Unidad de Bioquímica Instituto Nacional de Ciencias Médicas y Nutrición, Salvador Zubirán, Mexico City, Mexico, [3] Subdirección de Investigación Biomédica, Instituto Nacional de Enfermedades Respiratorias Ismael Cosio Villegas, Mexico City, Mexico

Latent tuberculosis infection (LTBI) is a subclinical mycobacterial infection defined on the basis of cellular immune response to mycobacterial antigens. The tuberculin skin test (TST) and the interferon gamma release assay (IGRA) are currently used to establish the diagnosis of LTB. However, neither TST nor IGRA is useful to discriminate between active and latent tuberculosis. Moreover, these tests cannot be used to predict whether an individual with LTBI will develop active tuberculosis (TB) or whether therapy for LTBI could be effective to decrease the risk of developing active TB. Therefore, in this article, we review current approaches and some efforts to identify an immunological marker that could be useful in distinguishing LTBI from TB and in evaluating the effectiveness of treatment of LTB on the risk of progression to active TB.

Keywords: latent tuberculosis infection, LTBI, IGRA, TST, LTBI diagnosis

OPEN ACCESS

Edited by:
Juraj Ivanyi,
King's College London,
United Kingdom

Reviewed by:
Andre G. Loxton,
South African Medical Research Council, South Africa
Carmen Judith Serrano,
Mexican Social Security Institute (IMSS), Mexico

***Correspondence:**
Martha Torres
marthatorres98@yahoo.com

Specialty section:
This article was submitted to Microbial Immunology, a section of the journal Frontiers in Immunology

Received: *29 May 2020*
Accepted: *24 July 2020*
Published: *10 September 2020*

Citation:
Carranza C, Pedraza-Sanchez S, de Oyarzabal-Mendez E and Torres M (2020) Diagnosis for Latent Tuberculosis Infection: New Alternatives. Front. Immunol. 11:2006. doi: 10.3389/fimmu.2020.02006

INTRODUCTION

Approximately 5–10% of the individuals infected with *Mycobacterium tuberculosis (M. tuberculosis)* develop the disease during the first 2–5 years after infection (1). In the rest of them, the innate immune response will either fully eliminate the infection without leaving a trace of immunological response (resistance to TB infection) (2) or lead to a state of persistent immune response to *M. tuberculosis* antigens without clinical evidence of active disease (2, 3). This last outcome is indeed the basis to consider that one fourth of the world population is infected with *M. tuberculosis* (4). These are the individuals who persist with the so-called latent tuberculosis infection (LTBI) immunoreactivity even if bacterial clearance is achieved, becoming a potential reservoir for active tuberculosis. In this context, there is a clear need of diagnostic assays for LTBI that could be used as well to identify individuals at risk of developing active TB and to monitor response to LTBI treatment.

The identification of individuals in contact with active TB cases during the first 2 years of exposure is important for two reasons: first, because it allows the implementation of public health policies of disease control by identifying individuals with an increased risk of developing the active tuberculosis; in particular, those who acquired the infection recently (4, 5); and second, because it can lead to a better understanding of the immune response during infection, which could be instrumental in the development of better therapeutic and prophylactic interventions.

For a long time, the dominant paradigm for LTBI has been one of a fine balance between host immune response and pathogen metabolism so that progression to active disease occurs whenever this balance is disrupted. However, evidence has been emerging over the past decade that has redefined TB infection in terms of a spectrum of immune responses rather than a static condition (6).

In persons with LTBI, several factors increase the risk of developing active TB. Most of them are related to an impaired immune response, such as concurrent HIV infection, cancer, immunosuppressive therapy or renal transplant, and diabetes. This last condition is particularly important; the incidence of diabetes has been increasing in countries that also have high TB endemicity and because diabetic individuals are approximately three times more likely to develop TB than non-diabetic individuals (7, 8). Some other factors, though, are related to specific components of host response, such as macrophage activation, maintenance of granuloma structure, CD4 T cells, CD8 T cells, interferon-gamma (IFN-γ), and tumor necrosis factor alpha (TNF-α) production, all of them important for the control of the pathogen during LTBI (9). More recently, studies using whole-blood transcriptomic profiling have been performed to identify signatures that could differentiate between LTBI and active tuberculosis and predict different outcomes of treatment (10–12).

In this review, we discuss the strategies aimed at improving the accuracy of diagnosis of LTBI, the possible biomarkers linked to the latency of mycobacterial infection, as well as to the treatment and follow up of patients with a subclinical infection.

DIAGNOSIS OF LTBI

There is no gold standard test for LTBI (3). Indeed, the low tissue bacterial burden associated with LTBI works against any diagnostic strategy focused on the identification of the bacteria or its components. The diagnosis of LTBI is rather indirect and relies on evidence of a cellular immune response to mycobacterial antigens. The most commonly used tests for LTBI diagnosis are the intradermal tuberculin test (TST) and IGRA.

The TST was developed more than a 100 years ago by Robert Koch, also known as "old tuberculin," or Mantoux test after Charles Mantoux established the diagnosis criteria for reading a TST (13). TST is widely used around the world, in particular in developing countries due to its low cost and straightforward implementation compared to IGRAs. TST has also been used as an epidemiological tool to evaluate the prevalence of LTBI (14). The TST is carried out by injecting intradermal purified protein derivate (PPD) in the forearm of an individual. An induration reaction of 15 mm or larger, read after 48 or 72 h, is considered indicative of past or current mycobacterial infection. The TST requires trained personnel to apply, read, and interpret the test.

TST is based on delayed-type hypersensitivity (DTH) skin reactivation to tuberculin PPD. Tuberculin PPD is a mixture of protein precipitated of mycobacterial culture filtrates, which have undergone modifications (13). There are different manufacturers of PPD referred to as international standard (PPD-SI) and commercial brands under the US FDA standard PPD-S2, such as Aplisol (JHP Pharmaceuticals, Inc, Rochester, MI, USA) or Tubersol (Sanofi Pasteur Limited, Swiftwater, PA, USA). Besides PPD-S2, there are several other formulations such as PPD RT23 produced by Statens Serum Institut, which is the most widely used PPD in the world (13), and a variability of the potency among PPD may affect the TST result.

The question on which components of PPD are mainly responsible for the DTH reaction is an important and unresolved one. Molecular analysis of PPD-S2 has revealed highly conserved chaperone proteins among most of the mycobacterial species such as the 10-kDa chaperonin (GroES, BCG-a heat shock protein), the 60-kDa chaperonin 1 (GroEL), the probable chaperone protein (DnaK, heat shock protein 70), and the heat shock proteins (HspX, alpha-crystallin homolog), which constitute about 60% of the PPD proteomic content (15). Due to the abundance of these proteins, it would be reasonable to expect one or more of them to cause DTH reaction; however, little is known regarding which of them are responsible for it. Moreover, the presence of highly conserved proteins in PPD prevents the TST to distinguish among *M. tuberculosis* infection, Bacille Calmette–Guérin (BCG) vaccination, and exposure to environmental non-TB mycobacteria.

The immune response involved in TST has been the subject of several studies, which had revealed that biological variations among individuals, as those presented below, may explain in part why some persons have strong TST responses, while others present a weak or no response at all.

- The CD14 (−159C/T) polymorphism variant (a variant in the CD14 molecule present in monocytes and macrophages), which is associated with a higher probability to be TST negative even if vaccinated with BCG (16).
- Th1, Th2, or Th17 immune responses influence TST reactivity: since TST-positive individuals show significantly impaired interleukin (IL)-17 and IL-23 production, lack of Th17 upregulation may be a key feature of TST positivity, while Th2 cytokines could play a marginal role on TST (17). However, IL-17-producing cells are phenotypically and functionally heterogeneous and may play different roles in immune pathology and protection. The role for Th17 during *M. tuberculosis* infection is conflicting and may be protective during acute infection and harmful during chronic infection (18, 19).
- A decreased expression of cutaneous lymphocyte antigen (CLA) on skin-resident T cells is associated with later phases of the skin response. A reduced TST reaction in older individuals is not associated to a reduction in the numbers or function of PPD-specific CD4 T cells but to the low expression of CLA, as observed in an *ex vivo* study of the cells associated with the blisters produced by the PPD in the TST (20).
- TST anergy may reflect a reduced cell-mediated immune response related to a major codominant gene responsible for TST variability, as suggested by a study of familial segregation on TST reactivity in household contacts of TB index cases in Colombia (21).
- A major locus (TST2) on the chromosome region 5p15 controls the intensity of DTH to tuberculin. The absence

of TST reactivity has a genetic component and corresponds to the major locus (TST1) on chromosomal region 11p14, which controls TST response and reflect T-cell-independent resistance to *M. tuberculosis*, as per the results of a study in a hyperendemic region in South Africa (22).

- Some individuals living in highly endemic areas remain TST negative, suggesting that these individuals are more likely to be naturally resistant to *M. tuberculosis* infection rather than intrinsically deficient in eliciting DTH response (22).

Interestingly, there are other diseases or metabolic states that can also influence the reactivity to TST. Recently, Deniz and colleagues studied 371 patients with chronic kidney disease (which are more susceptible to tuberculosis infection and disease) and found that both high levels of parathormone (PTH) and vitamin D treatment correlate with a negative TST result, indicating that these factors may induce some degree of immunosuppresion (23).

Two interesting reports in children have suggested that helminth infestation may affect the result of immunological tests that evaluate infection with *M. tuberculosis* (24), while the IFN-γ/IL-10 ratio may correlate positively to the TST test, suggesting that the relationship of these two cytokines may be important in TST reactivity (25). This last report also showed that TST is affected by BCG administration but not by exposure to non-tuberculosis mycobacteria (25).

In summary, TST results are affected by a complex array of factors such as age, nutritional and immunological status, the time interval between antigen exposure and the test performance, BCG vaccination, immunosuppression, genetic background, and cross-reactivity with environmental non-tuberculosis mycobacteria and perhaps other pathogens.

The IGRA is a whole blood assay developed in the past decades to detect the IFN-γ produced *in vivo* by sensitized T cells after *in vitro* stimulation with mycobacterial antigens. The mycobacterial antigens used in these assays are the early secretory antigenic target (ESAT-6) and the 10-kDa culture filtrate protein (CFP-10). ESAT-6 and CFP-10 antigens are encoded in the region of differentiation 1 (RD1) present in the *M. tuberculosis* and *Mycobacterium bovis* genome and are absent in the Bacillus Calmette–Guerin vaccine (BCG) and most environmental mycobacteria (26, 27). Therefore, IGRA results are not affected by neither BCG vaccination nor exposure to environmental mycobacteria.

Until 2015, only two types of assays were commercially available: QuantiFERON (QFT) and QuantiFERON TB Gold in tubes (QFT-GIT), which contain long peptides derived from ESAT-6 and CFP-10 (TB7.7, or Rv2654c encoded by RD11 present in QFT-GIT has been removed). QuantiFERON-TB Gold Plus (QFT-Plus), a new generation assay, now includes both long peptides derived from ESAT-6 and CFP-10 (designed to induce a specific CD4 T-cell response) and shorter peptides in an additional tube, to induce IFN-γ production by CD4 and CD8 lymphocytes (28). The inclusion of peptides for stimulation of CD8 T cells has been reported to improve discrimination of LTBI from active TB (29, 30). In general, the QFT-Plus assay demonstrates a stronger association with increased *M. tuberculosis* exposure compared with QFT-GIT in adults with LTBI (28) and, even though both assays correlates well for LTBI diagnosis, the QFT-Plus exhibits a higher sensitivity with similar specificity regardless subject's age (28).

T-SPOT.TB, another commercially available assay, uses the *M. tuberculosis* antigens ESAT-6 and CFP-10. This assay is based on ELISPOT technique, which quantifies the number of IFN-γ-producing T cells (spot-forming cells). It requires expensive reader and software and specialized trained personnel, which restricts its clinical application in developing countries (31). Although The T-SPOT.TB and QuantiFERON assay correlate well, the T-SPOT.TB is less used (32). Considerable discrepancy between TST and T-SPOT-TB test in LTBI individuals has been reported (33).

In addition, different studies have reported a heritability of IFN-γ response to mycobacterial antigens including ESAT-6 and that the percentage of heritability was different in the population assessed, but the higher heritability was described in South African subjects using sibling pairs, and the estimated IFN-γ response heritability was 58% for ESAT-6 (34, 35).

Similar to what has been described for TST, the performance of the IGRA tests can be affected by several factors, mainly related to an impaired immune response and to technical issues. For example, the addition of IL-7 increases test positivity (36). The clinical accuracy of IGRAs seems to be negatively affected in patients with immune-mediated inflammatory diseases (IMIDs) (37) such as Crohn's disease, where the function of immune cells is suppressed (38), as well as in patients on immunomodulatory drugs such as teriflunomide, which exerts an inhibitory effect on T-cell activation, and outcome in QuantiFERON results changing from positive to negative with marked reduction in IFN-γ (39). In addition, high dose of corticosteroids have been associated a high proportion of indeterminate QTF-GIT results in rheumatoid arthritis patients and inflammatory bowel disease. Patients with these conditions, therefore, should be tested with QTF-GIT prior to steroid treatment (40). Interestingly, the IGRA sensitivity is not compromised by diabetes in TB patients; in fact, the sensitivity of QTF was significantly higher in TB patients with diabetes in comparison to those with no diabetes (41). The technical variations that may affect IGRA results include those related to blood sampling (time, volume), tube shaking, incubation or processing delay (cell viability in blood may be affected), incubation duration, analytical errors, and manufacturing defects (5).

COMPARING TST AND IGRA FOR THE DIAGNOSIS OF LTBI

Although both the TST and IGRA are used in medical practice for the diagnosis of LTBI, they evaluate different parameters of the immune response that are relevant in immunocompetent individuals.

TST performs an *in vivo* assessment of the delayed-type hypersensitivity in response to PPD of the bacilli, and the readout is the size of the skin induration area after 48–72 h. On the other hand, the IGRA test evaluates the cell-mediated immune

response *in vitro*, and the readout is based on the level of IFN-γ produced by circulating effector memory cells (42) and the frequency of effector T cells that produce IFN-γ.

The diversity of antigens used in these tests may account for most of the differences in specificity, but genetic diversity and differences in immune response among individuals also affect the performance and results of both tests. Meta-analyses have confirmed that IGRA is more specific in low-risk, BCG-vaccinated individuals (33, 43) and more sensitive in diagnosing *M. tuberculosis* coinfection in HIV-infected patients (44). Discordant results between TST and IGRA are common in individuals with LTBI, but in the case of IGRA (QuantiFERON-GIT), the accuracy of the test may be improved by a longer incubation period with the stimuli and by including IL-2 level measurements (45).

The diversity of immune response in patients with LTBI may also reflect differences in the participation of specific T-cell subsets. For example, an increased number of CD4CD25 high CD39+ cells (regulatory T cells, defined by these and other markers such as FoxP3) has been observed in individuals TST+ and IGRA+, compared to TST+ and IGRA–, suggesting that higher numbers of these cells allow patients to respond to both tests (46). In addition, the correlation of TST and IGRA varies among individuals from settings of high vs. low incidence, perhaps due to the effects of BCG vaccination, exposure to environmental mycobacteria, or the risk of reinfection (47, 48). This is why TST and IGRA results should be interpreted in the context of prevalence and exposure, as has been highlighted by several authors (49, 50).

Interestingly, fluctuations in IGRA results are observed in individuals with high exposure to *M. tuberculosis* such as healthcare workers, suggesting either a poor reproducibility of the assay or a reinfection causing reversion as a result of the continuous exposure to mycobacterial antigens (51). In addition, false conversions are more commonly seen with IGRAs than with TST in low-risk populations (52).

Generally speaking, both tests exhibit similar limitations. For example, their precision is low in immune-compromised individuals being screened for LTBI. This is a crucial constraint, since these individuals are the ones at higher risk of developing TB. Neither TST nor IGRA, QTF-GIT, or QTF are particularly useful in predicting progression to active tuberculosis. Although the newest QTF-Plus looks promising in discerning between LTBI and active TB and between recent and remote acquired TB infection, it needs further validation in both high- and low-risk populations.

Putting all these data into perspective, it is not difficult to understand why the current TST and IGRA cannot meet the requirements for a test that reliably predicts which individuals are more likely to control the infection and who are more likely to progress to active TB.

One strategy to tackle this problem is to build upon current TST and IGRA to develop better tests. One example of this approach is the C-TB, which is a promising hypersensitivity skin test that uses recombinant ESAT-6 and CFP-10 proteins (53). This test is supposed to combine the low cost of TST and the high specificity of IGRA. Another example is the use of different mycobacterial antigens to improve the IGRA test, such as the Esx-1 substrate protein C (EspC; Rv3615c). This is an ESAT-6-like protein that is as immunodominant as ESAT-6 and CFP-10 in people with TB and LTBI and which identifies *M. tuberculosis*-infected persons who do not react to neither ESAT-6 nor CFP-10 (54).

Building on the existing TST and IGRA tests may not be enough, though, given the diversity of factors that can affect them, including individual genetic background. For this reason, alternative strategies have been explored.

LATENCY ANTIGENS AS POTENTIAL FOR DIFFERENTIATING LTBI FROM ACTIVE TB

Since LTBI is defined in terms of immunoreactivity to mycobacterial antigens, the selection of the right antigens to evaluate is key in the diagnosis of LTBI and in the development of assays able to discriminate among different states of the infection and the risk of progression to active TB. Numerous studies have focused on the identification of mycobacterial antigens naturally expressed during LTBI.

In vitro models of latency combined with genome-wide transcriptome profiling have identified genes that remain upregulated during LTBI and code for proteins known as "latency antigens."

It should be noted that the term "latency" refers to the state of the, host while the term "dormancy" refers to the state of the bacteria during the latency state. Dormancy is a reversible metabolic shutdown, a state of low bacterial metabolism that is associated to a transition from replicating to non-replicating bacilli, in which cells are able to survive for a long time without replication displaying immune-evading strategies (55, 56). Oxygen deprivation and levels of nitric oxide are examples of factors that favor a low metabolic state.

The dormancy survival regulator (DosR) (also called DosR regulon, DevR, Rv3133c) regulates the initial response of *M. tuberculosis* to hypoxia (57). When DosR is phosphorylated by histidine kinases, it results in the induction of about 48 genes (58). Transcriptional analysis under hypoxic conditions has revealed that, while induction of the DosR regulon is transient, over 200 genes known as enduring hypoxic response (EHR) genes remain induced for a long time, showing more stability than the DosR genes and some overlap with those induced in the Wayne model of hypoxia and nutrient deprivation (59). In addition, some studies have demonstrated that DosR regulon-encoded proteins induce a stronger T-cell response in individuals with LTBI compared to patients with active TB, suggesting a potential use for LTBI diagnosis (60, 61). The accumulated (and sometimes conflicting) evidence that links specific latency antigens with cytokine responses include the following observations:

- Individuals with remote LTBI show a significantly higher IFN-γ response to Rv2628 (*M. tuberculosis* latency antigen) than individuals with recent infection, which suggests that responses to Rv2628 may be associated with immune-mediated protection against tuberculosis and could be useful to distinguish recent from remote infection (62).

- A short stimulation with Rv2031c induces significantly lower IFN-γ, TNF-α, and IL-10 concentrations in active TB patients compared to household contacts and healthy controls (63). Interestingly, some authors have not found differences in IFN-γ response to Rv2031c between TB, LTBI, and healthy controls (60, 62).
- A study that evaluated IFN-γ production in response to latency-associated antigens and EHR mycobacterial antigens (CFP10-1, Rv2031, Rv0849, Rv1986, Rv2659c, Rv2693c, and Rv1737) found that Rv1737 (NarK2) was among the DosR regulon-encoded antigens most frequently recognized by individuals with LTBI (64).
- There are significant differences in IFN-γ responses for DosR antigens (Rv1735c, Rv2006, Rv2625c, Rv1996, Rv2032, Rv2629, Rv3126c, Rv0081, Rv2631, Rv3130c, Rv2624c, Rv2007c, Rv2028c, and Rv3134) in healthy household contacts compared with patients with active TB, as reported by a study in whole blood that included a wide range of stage-specific antigens to assess IFN-γ response in a long-incubation assay (65).
- Antigens Rv1733c, Rv2029c, and Rv2628 have been reported to increase the concentrations of IFN-γ, Granzyme B, IL-17, and sIL-2 during treatment of active TB (66).
- The stimulation of peripheral blood mononuclear cells (PBMC) with Rv1737c and Rv2029c seem to increase the IFN-γ or TNF-α-producing CD4 and CD8 T cells in individuals with LTBI compared to active TB (67).
- The use of RV2004 induced a strong proinflammatory response (TNF-α, IL-8, IL-1b, and IL-12) in LTBI individuals compared with active TB and healthy controls (68).
- Stimulation with Rv2627c, Rv2629, and Rv2630 induced high concentrations of or TNF-α, IL-6, and IL-10 in patients with active TB. The detection of IL-6, IL-17, and IL-8 in supernatants of cultures with Rv0574c, Rv2630, Rv1998, Rv054, and Rv2028c might confirm the roles of these antigens in inflammation and the pathogenesis of TB (69).
- Finally, a meta-analysis that screened a total of 1,533 articles and selected 34 for the final analysis found that among a vast number of different mycobacterial antigens, the Rv0081, Rv1733c, Rv1737c, Rv2029c, Rv2031, and Rv2628, all encoded by DosR, were among the most widely studied and have the highest potential for differentiating LTBI from active TB (70).

POTENTIAL ROLE OF ANTIBODIES IN LTBI DIAGNOSIS

A widely held paradigm considers the role of the human antibody response against to *M. tuberculosis* in the protection against TB as marginal (71), at least compared with that offered by cell-mediated immunity. This paradigm has been supported by two kind of observations: the presence of high levels of antibodies in the active form of the disease, suggesting that antibodies do not confer protection (72), and the apparently unaffected risk of TB reactivation of patients receiving rituximab, a human/mouse chimeric anti-CD20 antibody that induces a rapid depletion of normal CD20-expressing B cells (73). Although the presence of antibodies in the serum from patients with active TB has led to the development of commercial diagnostic tests, the World Health Organization has not recommended their use as diagnostic tools on the grounds of suboptimal sensitivity and specificity (74).

More recently, however, our understanding of the role of antibodies specific to mycobacterial proteins has started to evolve. Indeed, emerging evidence suggests that, since the metabolism of *M. tuberculosis* changes over the course of the infection, the expression of immunodominant antigens should reflect these changes, leading in turn to differences in the antibody profile between LTBI and active TB that could be exploited for diagnostic purposes (75).

In support of this hypothesis, we can refer to these observations:

- Mycobacterial proteins of 36, 25, and 23 kDa, present in membrane vesicles, have been detected only in sera from TB patients but not in healthy controls, while titters of those antibodies are lower in individuals with LTBI (72).
- Vaccination with BCG induces immunoglobulin G (IgG) antibodies against Ag85A that are associated with a reduced risk of developing active TB (76).
- In another study on BCG vaccination, LAM-specific IgG antibodies have increased significantly after the first primary and booster doses (77).
- Neutrophils and monocytes/macrophages present increased internalization and killing of mycobacteria in the presence of specific antibodies (77).
- Specific IgG antibody levels against transmembrane protein Rv1733c are significantly higher in LTBI than in TB patients (78). In contrast, levels of antibodies against other specific *M. tuberculosis* proteins are significantly higher in TB patients than in healthy individuals living in the same endemic areas (78).
- High levels of antibodies against ESAT-6, P1c1 (membrane-associated phospholipase C1, Rv2351c), HspX, and TB8.4 (Rv1174c) are detected in the sera from TB patients using immuno-PCR based in ELISA assay (79).
- Individuals with established LTBI have higher plasma levels of anti-Rv2626c IgG than in recently infected individuals and patients with active TB (80).
- Levels of IgM antibodies against *M. tuberculosis* membrane-associated antigens (MtM), IgA antibodies against alpha crystallin (Acr), and a proliferative T-cell response to both antigens can potentially discriminate between LTBI and active TB disease (81).

EVALUATING THE EFFECT OF DRUG THERAPY OF LTBI

A successful treatment of LTBI is an important component in the control of TB at a global level (82). Patients should undergo thorough clinical evaluation to rule out active TB before initiating drug therapy for LTBI, since monotherapy with Isoniazid (INH), the most common frontline therapy for LTBI, would be highly inappropriate in the context of active TB. In

addition, the individual risk of reactivation must be balanced against potential risks of developing treatment-related adverse events (82). Therefore, patients with recently acquired LTBI should be evaluated for preexisting medical conditions that may increase the risk of such adverse events and should be tested for coinfection with HIV (83).

Although INH significantly reduces the risk of progression to TB, its effectiveness is limited by the need of a prolonged administration (6 and 12 months in immunocompetent and immunosuppressed individuals, respectively) as well as by the associated adverse events (84). In 2018, the World Health Organization issued new guidelines on the treatment of LTBI in children and adults living in countries with high and low incidence rates of TB. The new guidelines include an individualized risk assessment for preventive treatment of high-risk household contacts of patients with multidrug-resistant TB (3).

Although the effectiveness of INH prophylactic treatment for LTBI is weakly established, there is also some evidence of an associated increase in the vulnerability for TB reactivation and reinfection, which suggests a therapy-related immune impairment (85). In this regard, a study performed in a murine model of mycobacterial infection showed that, although treatment with INH decreases the number of bacteria, INH-treated mice present a more profound suppression of antigen-specific proliferative response compared to untreated mice, even when INH reduces the number of bacteria (85). Based on the above, it is clear that individuals at risk of TB should undergo a clinical evaluation before starting LTBI treatment and that the elimination of TB requires developing new, safer drugs for the treatment of LTBI that can be administered for shorter periods, as well as adequate biomarkers to assess the efficacy of LTBI treatment.

Assessing the effectiveness of LTBI therapy is not straightforward, since infected individuals have no symptoms and mycobacteria cannot be isolated. This has led to the search of immunological markers for this purpose (86). However, one important challenge intrinsic to LTBI is the great diversity of associated physiological and clinical conditions. While some individuals can harbor lifelong chronic non-progressive infection, others present some degree of transient immunodeficiency (e.g., related to other conditions such as HIV, diabetes, or immunosuppressive therapy) that allows LTBI to progress, without an effective treatment and monitoring, to an active form of the disease. Such diversity in the immune status may correlate with a diversity of granulomas containing dormant mycobacteria (6) and could be responsible, in part, for the differences observed in the response to drug therapy.

Since the diagnosis of LTBI is established on the basis of the immune response of individuals to mycobacterial antigens, the immunological tests used for the diagnosis have also been adopted to assess response to drug treatment. This assessment includes measuring IFN-γ in response to mycobacterial antigens, since IFN-γ is considered to be one of the prominent surrogate markers of protective immunity against *M. tuberculosis* (9, 87). So far, few studies have evaluated the effect of INH therapy on the immune response of people with LTBI, and these studies have yielded conflicting results (88–90). Such conflicting data could be associated to variables like the prevalence of TB, antibiotics used, treatment adherence, type of assay (QuantiFERON varieties vs. TB-SPOT), incubation periods (short vs. long), and antigen types (proteins vs. peptides).

In addition, not all studies agree on the target antigen. While studies using ELISPOT have focused on the response to ESAT-6, others have concentrated on the response to CFP-10 (91–93).

All in all, there is still no convincing evidence of the reliability of neither the IFN-γ levels nor the numbers of IFN-γ-producing cells in assessing the response to INH treatment, a view that is consistent with other authors (90, 94, 95).

The limitations of IGRAs have prompted proposals to measure several biomarkers as a mean to distinguish between patients with active tuberculosis and LTBI. Some of these proposals include the following:

- Using chemokine IP10 instead of IFN-γ (96)
- Measuring sCD14 or sMD2 levels in plasma, which are higher in active TB than in LTBI (97, 98)
- Monitoring a reduction in CXCL10 levels in plasma, which should decrease after 2 weeks of treatment of active TB (99) (perhaps not applicable in LTBI)
- Determining overexpression of CCL4 in lung tissue in patients with late-stage TB (100).
- Characterization of polyfunctional CD4 T cells with a higher proportion of bifunctional T cells producing IFN-γ and TNF-α and effector memory phenotype (EM) in response to CFP-10 and ESAT-6 in active TB and LTBI (101)
- Characterization of circulating marginal zone B cells (CD19+IgM+CD23–CD27+) and memory phenotypes to distinguish between active TB and end of treatment (102)
- Measuring circulating antibodies secreting cells, memory B cells, and antibodies specific to Cut4 (Rv3452) and CFP21 (Rv1984c) lipolytic enzymes antigens, hypothetically associated with reactivation (103).

On the other hand, studies of whole transcriptomics in patients with LTBI or active TB have revealed groups of genes that are over- or underexpressed in these patients. In the light of these findings, specific gene signatures that correspond to certain stages of the disease have been proposed. In addition, transcriptomic studies allow the study of changes in the expression of transcribed genes throughout the duration of therapy, which can in turn lead to the discovery of biomarkers of diagnostic and prognostic value. Some of these studies, performed in blood cells (10, 11), have already shown that one of the main pathways overexpressed during active tuberculosis is the IFN signaling pathway, which includes both IFN-γ and IFN-αβ induced responses (10, 12).

The next step after a candidate gene has been identified by genomics/transcriptomics is to confirm a differentiated expression by PCR. Following this approach, our group has found that USP18, IFI44L, IFT1, and IL12RA genes are overexpressed in LTBI patients treated with INH, while the expression of CCL4, CXCL11, and IFNA genes is reduced during the INH treatment. Based on this finding, we have proposed these genes

as potential biomarkers for the monitoring of response to LTBI treatment (104).

DETECTING PROGRESSION TO ACTIVE TB

Infection by *M. tuberculosis* can no longer be understood in terms of two fixed, mutually exclusive categories (LTBI vs. active TB). Instead, it represents a continuous spectrum of states that differ by the degree of interplay between pathogen replication and host resistance. Signs and symptoms are not always a reliable way to detect the evolution to an active disease, as many times they are subtle, pleomorphic, or easily confused with the clinical presentation of many other conditions. Therefore, the search for diagnostic biomarkers for LTBI and active TB must consider parameters relevant to the whole spectrum of the immune response.

The progression of LTBI to active TB is determined by factors related to the bacteria (e.g., strain virulence, inoculum size, etc.), host (e.g., state of immune response, treatment with steroids, and biologic agents such as antibodies against tumor necrosis factor, solid organ or hematological transplantation, HIV infection, age), and environment (e.g., smoking, occupational exposure in health care workers).

In previous works, IFN-inducible genes in neutrophils had been identified as a specific TB signature; 393 transcripts were identified in whole blood from active TB of intermediate and high burden settings, correlating with radiological extent of disease and reverting to that of healthy controls following treatment (10). TB signature consisting of both IFN-γ and type I IFNαβ signaling genes, contained in the 393 differentially expressed transcripts. Type I IFN-αβ-inducible transcripts has been described as having a dual role: they participate in bacterial control, but they also are associated to an increased susceptibility to TB, as suggested by the direct correlation between its levels in whole blood and the severity of the disease (10). Furthermore, it has been proposed that IFN-α signaling could be valuable to define predictive biomarkers of LTBI progression to active TB (11). The IFN signature comprises a series of genes that are overexpressed in active tuberculosis but revert during the first week of successful therapy, adopting the pattern seen in LTBI (10, 105). In addition, some data suggest that IL-15 and vitamin D levels differentiate active TB from LTBI (106).

Interestingly, in patients with LTBI, but not healthy or BCG-vaccinated individuals, neither patients after TB treatment presented a CD4 cell subset, which is $CD27^{-}PC\text{-}1^{+}$; these data were interpreted as evidence of *in vivo* induced cell differentiation driven by *M. tuberculosis* antigens, which suggest that these membrane markers could help to differentiate individuals with LTBI from healthy individuals and help to monitor TB drug treatment (107).

Another PPD-specific CD4 T-cell subset secreting TNF-α, but not IFN-γ or IL-2 and with a differentiated effector memory phenotype ($CD45RA^{-}CCR7^{-}CD127^{-}$), was shown useful to distinguish active TB from LTBI patients (108). In a recent study in which blood cells from patients with active TB or LTBI were stimulated with PPD or ESAT-6/CFP-10, as a result of this stimulation, the $CD4^{+}CD27^{-}CCR4^{+}$ T-cell subset was induced higher in subjects with active TB compared to those with LTBI. This may indicate that CD27 and CCR4 expression should be investigated as promising immunodiagnostic markers for TB (109).

A recent candidate-gene association study of polymorphisms has focused on ULK1, which encodes a component of an upstream protein complex that transduces signals to central autophagy effectors. ULK1 has been associated with susceptibility to LTBI in Asian individuals; rs12297124 minor allele, a non-coding ULK1 single-nucleotide polymorphism, conferred 80% reduction of LTBI. In addition, it was observed that the replication of *M. tuberculosis* is increased in ULK1-deficient monocytes, which in turn is associated with a decreased TNF-α response to stimulation with Toll-like receptor (TLR) ligands and an impaired autophagy (110).

A recent blood transcriptomic study on sorted memory CD4 T cells, aimed at detecting differentiated gene expression signatures between LTBI and uninfected individuals, found a 74-gene signature related to exposure to *M. tuberculosis*. This gene signature reflected the expansion of CD4 T cells subset containing TB-specific peptide reactivity in LTBI (111). Combining transcriptomic data with single-cell protein profiling and *in vitro* stimulation with Ag-specific peptide pools has allowed the identification of a TB-specific CD4 $CD62L^{-}GPA33^{-}$ subset of TH1 cells. However, this observation has been limited to the LTBI and healthy population, and therefore, no conclusion can be drawn on whether this profile could be useful in assessing long-term protection against active TB (111).

In addition, a study demonstrated that the frequency of purified protein derivate-specific CD4 T cells secreting TNF-α but not IFN-γ or IL-2 with a differentiated effector memory phenotype ($CD45RA^{-}CCR7^{-}CD127^{-}$, TNF-α-only T_{EFF}) was able to distinguish between active TB from LTBI and correlate with a risk factor for progression (108). Moreover, the proportion of TNF-α-only T_{EFF} with an effector memory phenotype $CD45RA^{-}CCR7^{-}CD127^{-}$ is significantly higher during recently acquired LTBI in comparison to remotely acquired LTBI, and the phenotype of TNF-α-only T_{EFF} has been associated with a progression risk and active TB in immunocompetent adults (112). During TB disease and recently acquired LTBI, there seems to be an expansion of a heterogeneous population of immature myeloid-derived suppressor cells (MDSCs) at intermediate stages of cell differentiation (113).

Since several studies have identified a biological heterogeneity of the cell immune subsets associated with status of TB infection, immune cell profiling may look promising at evaluating the risk of developing active TB in LTBI individuals.

Some reports indicate that most of the cellular-mediated immune responses are under the control of microRNAs (miRNAs), key regulators that posttranscriptionally repress the expression of target messenger RNAs (mRNAs) (114). miRNAs are 18–25 nucleotide long, non-coding RNAs that inhibit the translation into proteins by a direct interaction with the protein-specific messenger RNA (114).

Modulation of miRNA expression is induced by intracellular bacteria as a mechanism to survive inside host immune cells

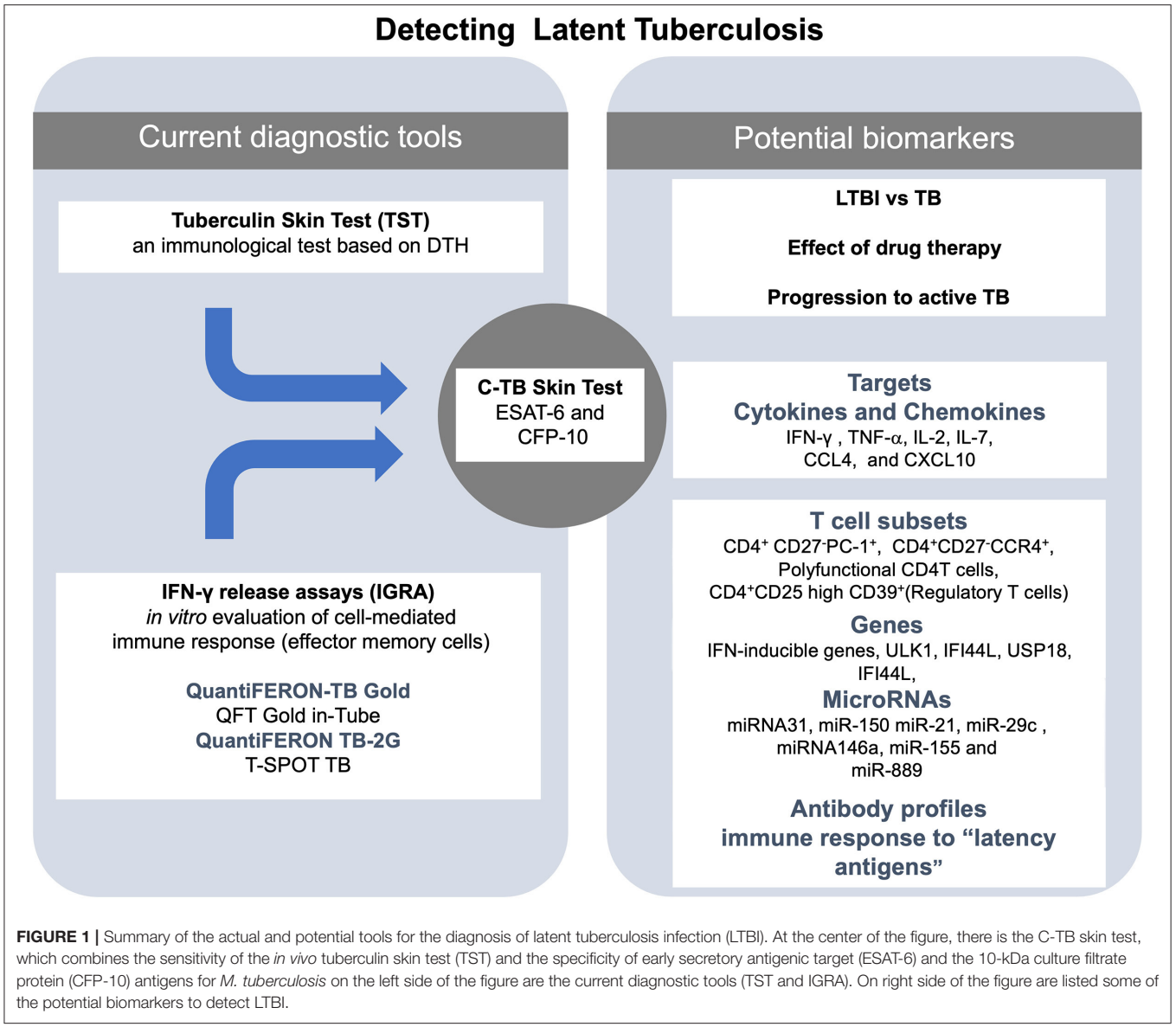

FIGURE 1 | Summary of the actual and potential tools for the diagnosis of latent tuberculosis infection (LTBI). At the center of the figure, there is the C-TB skin test, which combines the sensitivity of the *in vivo* tuberculin skin test (TST) and the specificity of early secretory antigenic target (ESAT-6) and the 10-kDa culture filtrate protein (CFP-10) antigens for *M. tuberculosis* on the left side of the figure are the current diagnostic tools (TST and IGRA). On right side of the figure are listed some of the potential biomarkers to detect LTBI.

(115). Differential expression of miRNAs in cells infected with *M. tuberculosis* suggests that the relevance of some miRNAs as biomarkers for LTBI and LTBI reactivation (116) deserves further exploration. This is supported by several observations:

- miRNA-31 expression in children with TB is significantly lower compared to healthy children (117).
- has-miR-150 is significantly downregulated, while both has-miR-21 and has-miR-29c are significantly upregulated in active TB patients in comparison to those with LTBI and healthy individuals (118).
- miR-146a and miR-155 are well-studied in TB infection models. Thus, downregulation of miR-146a expression in alveolar macrophages of patients with pulmonary TB is associated with disease progression, while the lack of miR-155 expression is associated with an increased susceptibility to *M. tuberculosis* infection (119, 120).
- miR-223, which regulates CXCL-2, CCL3, and IL-6, has a critical role in the control of TB in myeloid cells (121).
- miR-889 and TNF-like weak inducers of apoptosis (TWEAK, target of miR-889) may be considered as potential biomarkers of LTBI reactivation. In this regard, miR-889 expression is significantly higher in patients with rheumatoid arthritis who also have LTBI compared to those not infected or healthy individuals. By the same token, it decreases significantly in those receiving prophylactic LTBI therapy (122).
- miR-155 is significantly decreased in the serum of patients with TB in relation to healthy volunteers, suggesting that inhibition of miR-155 may be closely associated with the development of TB (123).

- has-miR-197-3p, has-miR-99b-5p, and has-miR-191-5p are expressed higher in different patterns in the neutrophils of healthy controls vs. that in patients with active TB (124).
- miR320, miR204, miR-331, miR-147, and miR-210 expressions in B cells are differentially expressed between TB cases and controls, but the biological relevance of these findings is still uncertain (124).

In summary, specific miRNAs have shown some power to distinguish between LTBI and active TB. Specifically, evidence rising from multiple independent groups of investigators point out to miR-889, miR223, miR-155, miR-150, miR146a, miR23, and miR-21 as the most promising candidates for this purpose. However, studies with a higher number of individuals to validate these markers are still needed. A general scheme of the laboratory techniques and molecular markers used for diagnosis and treatment of LTBI is shown in **Figure 1**.

CONCLUDING REMARKS

LTBI represents an occult face of the larger global health problem of TB. A reliable diagnosis and a successful treatment of individuals with LTBI is a paramount issue in the control of TB because they may, eventually, progress to the active form of TB.

The TST has been the most broadly used technique for the diagnosis of LTBI because of its simplicity and the *in vivo* evidence it provides for an antimycobacterial cellular immune response. However, it has the inconvenience of being positive in the BCG-vaccinated individual. The further introduction of IGRAs has added higher specificity, while the new version QTF-Plus looks promising in differentiating between active TB and LTBI. Despite this progress, the search for a reliable biomarker of LTBI and evaluating the efficacy of drug therapy in patients with LTBI remains open.

In this review, we have summarized the main strategies and some targets or immunological markers that have been proposed over the last decade for the differential diagnosis between LTBI and active TB and for evaluating the effectiveness of treatment of LTBI. One of them is the analysis of cellular profile such as the proportion of TNF-α-only T_{EFF} with an effector memory phenotype $CD45RA^{-}CCR7^{-}CD127^{-}$, which has been associated with a higher risk of progression to active TB in immunocompetent adults. Another is the expansion of a heterogeneous population of immature myeloid-derived suppressor cells (MDSCs), which has been linked to both active TB and recently acquired LTBI. In addition, the cellular response against mycobacterial latency-associated antigens, such as those encoded by the DosR regulon, have been found to be useful in identifying individuals with LTBI or active TB. Other potential candidates include the specific antibody response to distinct *M. tuberculosis* antigens, the identification of specific miRNA, and molecular signatures observed in the analysis of blood transcriptome, such as IFN-γ signaling. The challenges ahead include the validation of these tests in groups of individuals representative of distinct populations and their practicality in low-income countries, where tuberculosis is still a major public health problem. Such challenges, once overcome, may pave the way to a whole new way to deal with the disease.

AUTHOR CONTRIBUTIONS

CC, EO-M, and SP-S contributed to the manuscript writing and revision. MT contributed to the manuscript writing and provided the initial idea. All authors contributed to the article and approved the submitted version.

FUNDING

This study was funded by Instituto Nacional de Enfermedades Respiratorias Ismael Cosio Villegas.

ACKNOWLEDGMENTS

Thanks to Enrique Camacho Mezquita for reviewing our manuscript.

REFERENCES

1. Anderson L, Baddeley A, Dias HM, Floyd K, Baena IG, Gebreselassie N, et al. *Global Tuberculosis Report*. Geneva: WHO (2018).
2. Simmons JD, Stein CM, Seshadri C, Campo M, Alter G, Fortune S, et al. Immunological mechanisms of human resistance to persistent *Mycobacterium tuberculosis* infection. *Nat Rev Immunol*. (2018) 18:575–89. doi: 10.1038/s41577-018-0025-3
3. World Health Organization. *Latent tuberculosis Infection - Executive Summary*. Geneva: WHO (2018).
4. Behr MA, Edelstein PH, Ramakrishnan L. Revisiting the timetable of tuberculosis. *BMJ*. (2018) 362:1–10. doi: 10.1136/bmj.k2738
5. Pai M, Behr M. Latent *Mycobacterium tuberculosis* infection and interferon-gamma release assays. *Microbiol Spectrum*. (2016) 4:1–10. doi: 10.1128/microbiolspec.TBTB2-0023-2016
6. Barry CE, Boshoff HI, Dartois V, Dick T, Ehrt S, Flynn J, et al. The spectrum of latent tuberculosis: rethinking the biology and intervention strategies. *Nat Rev Microbiol*. (2009) 7:845–55. doi: 10.1038/nrmicro2236
7. Ayelign B, Negash M, Genetu M, Wondmagegn T, Shibabaw T. Immunological impacts of diabetes on the susceptibility of *Mycobacterium tuberculosis*. *J Immunol Res*. (2019). doi: 10.1155/2019/6196532. [Epub ahead of print].
8. Jeon CY, Murray MB. Diabetes mellitus increases the risk of active tuberculosis: a systematic review of 13 observational studies. *PLoS Med*. (2008) 5:e181. doi: 10.1371/journal.pmed.0050181
9. Flynn JL, Chan J. Tuberculosis: latency and reactivation MINIREVIEW tuberculosis: latency and reactivation. *Infect Immunity*. (2001) 69:4195–201. doi: 10.1128/IAI.69.7.4195-4201.2001
10. Berry MPR, Graham CM, McNab FW, Xu Z, Bloch SAA, Oni T, et al. An interferon-inducible neutrophil-driven blood transcriptional signature in human tuberculosis. *Nature*. (2010) 466:973–7. doi: 10.1038/nature09247
11. Ottenhoff THM, Dass RH, Yang N, Zhang MM, Wong HEE, Sahiratmadja E, et al. Genome-wide expression profiling identifies type 1 interferon response pathways in active tuberculosis. *PLoS ONE*. (2012) 7:e45839. doi: 10.1371/journal.pone.0045839
12. Thompson EG, Du Y, Malherbe ST, Shankar S, Braun J, Valvo J, et al. Host blood RNA signatures predict the outcome of tuberculosis treatment. *Tuberculosis*. (2017) 107:48–58. doi: 10.1016/j.tube.2017.08.004

13. Yang H, Kruh-Garcia NA, Dobos KM. Purified protein derivatives of tuberculin — past, present, and future. *FEMS Immunol Med Microbiol*. (2012) 66:273–80. doi: 10.1111/j.1574-695X.2012.01002.x
14. Dye C, Scheele S, Dolin P, Pathania V, Raviglione MC. Global Burden of Tuberculosis. *JAMA*. (1999) 282:677. doi: 10.1001/jama.282.7.677
15. Cho YS, Dobos KM, Prenni J, Yang H, Hess A, Rosenkrands I, et al. Deciphering the proteome of the in vivo diagnostic reagent "purified protein derivative" from *Mycobacterium tuberculosis*. *Proteomics*. (2012) 12:979–91. doi: 10.1002/pmic.201100544
16. Druszczynska M, Wlodarczyk M, Kielnierowski G, Seweryn M, Wawrocki S, Rudnicka W. CD14-159C/T polymorphism in the development of delayed skin hypersensitivity to tuberculin. *PLoS ONE*. (2017) 12:e0190106. doi: 10.1371/journal.pone.0190106
17. Babu S, Bhat SQ, Kumar NP, Kumaraswami V, Nutman BT. Regulatory T cells modulate Th17 responses in tuberculin skin test positive (TST+) individuals. *J Infect Dis*. (2010) 201:20–31. doi: 10.1086/648735
18. Gallegos AM, van Heijst JWJ, Samstein M, Su X, Pamer EG, Glickman MS. A gamma interferon independent mechanism of CD4 T cell mediated control of *M. tuberculosis* infection *in vivo*. *PLoS Pathog*. (2011) 7:e1002052. doi: 10.1371/journal.ppat.1002052
19. Gopal R, Monin L, Slight S, Uche U, Blanchard EA, Junecko BAF et al. Unexpected Role for IL-17 in Protective Immunity against Hypervirulent *Mycobacterium tuberculosis* HN878 Infection. *PLoS Pathog*. (2014) 10:e1004099. doi: 10.1371/journal.ppat.1004099
20. Akbar AN, Reed JR, Lacy KE, Jackson SE, Vukmanovic-Stejic M, Rustin MHA. Investigation of the cutaneous response to recall antigen in humans *in vivo*. *Clin Exp Immunol*. (2013) 173:163–72. doi: 10.1111/cei.12107
21. Cobat A, Barrera LF, Henao H, Arbeláez P, Abel L, García LF, et al. Tuberculin skin test reactivity is dependent on host genetic background in Colombian tuberculosis household contacts. *Clin Infect Dis*. (2012) 54:968–71. doi: 10.1093/cid/cir972
22. Cobat A, Gallant CJ, Simkin L, Black GF, Stanley K, Hughes J, et al. Two loci control tuberculin skin test reactivity in an area hyperendemic for tuberculosis. *J Exp Med*. (2009) 206:2583–91. doi: 10.1084/jem.20090892
23. Deniz S, Aydemir Y, Sengül A, Emre JÇ, Tanrisev M, Özhan MH, et al. Factors affecting TST level in patients undergoing dialysis: a multicenter study. *Hemodial Int*. (2019) 23:81–7. doi: 10.1111/hdi.12676
24. van Soelen N, Mandalakas AM, Kirchner HL, Walzl G, Grewal HMS, Jacobsen M, et al. Effect of ascaris lumbricoides specific IgE on tuberculin skin test responses in children in a high-burden setting: a cross-sectional community-based study. *BMC Infect Dis*. (2012) 12:1–8. doi: 10.1186/1471-2334-12-211
25. Burl S, Adetifa UJ, Cox M, Touray E, Whittle H, McShane H, et al. The tuberculin skin test (TST) is affected by recent BCG vaccination but not by exposure to non-tuberculosis mycobacteria (NTM) during early life. *PLoS ONE*. (2010) 5:e12287. doi: 10.1371/journal.pone.0012287
26. Arend SM, Geluk A, Van Meijgaarden KE, Van Dissel JT, Theisen M, Andersen P, et al. Antigenic equivalence of human T-cell responses to *Mycobacterium tuberculosis*-specific RD1-encoded protein antigens ESAT-6 and culture filtrate protein 10 and to mixtures of synthetic peptides. *Infect Immunity*. (2000) 68:3314–21. doi: 10.1128/IAI.68.6.3314-3321.2000
27. Harboe M, Oettinger T, Wiker HG, Rosenkrands I, Andersen P. Evidence for occurrence of the ESAT-6 protein in *Mycobacterium tuberculosis* and virulent *Mycobacterium bovis* and for its absence in *Mycobacterium bovis* BCG. *Infect Immunity*. (1996) 64:16–22. doi: 10.1128/IAI.64.1.16-22.1996
28. Barcellini L, Borroni E, Brown J, Brunetti E, Campisi D, Castellotti PF, et al. First evaluation of QuantiFERON-TB gold plus performance in contact screening. *Eur Respir J*. (2016) 48:1411–9. doi: 10.1183/13993003.00510-2016
29. Petruccioli E, Vanini V, Chiacchio T, Cuzzi G, Cirillo DM, Palmieri F, et al. Analytical evaluation of QuantiFERON- Plus and QuantiFERON- Gold In-tube assays in subjects with or without tuberculosis. *Tuberculosis*. (2017) 106:38–43. doi: 10.1016/j.tube.2017.06.002
30. Pourakbari B, Mamishi S, Benvari S, Mahmoudi S. Comparison of the QuantiFERON-TB gold plus and QuantiFERON-TB gold in-tube interferon-γ release assays: a systematic review and meta-analysis. *Adv. Med. Sci*. (2019) 64:437–43. doi: 10.1016/j.advms.2019.09.001
31. Chee CBE, Gan SH, KhinMar KW, Barkham TM, Koh CK, Liang S, et al. Comparison of sensitivities of two commercial gamma interferon release assays for pulmonary tuberculosis. *J Clin Microbiol*. (2008) 46:1935–40. doi: 10.1128/JCM.02403-07
32. King TC, Upfal M, Gottlieb A, Adamo P, Bernacki E, Kadlecek CP, et al. T-SPOTTB interferon-g release assay performance in healthcare worker screening at nineteen US Hospitals. *Am J Respir Crit Care Med*. (2015) 192:367–73. doi: 10.1164/rccm.201501-0199OC
33. Diel R, Goletti D, Ferrara G, Bothamley G, Cirillo D, Kampmann B, et al. Interferon-γ release assays for the diagnosis of latent *Mycobacterium tuberculosis* infection: a systematic review and meta-analysis. *Eur Respir J*. (2011) 37:88–99. doi: 10.1183/09031936.00115110
34. Cobat A, Gallant CJ, Simkin L, Black GF, Stanley K, Hughes J, et al. High heritability of antimycobacterial immunity in an area of hyperendemicity for tuberculosis disease. *J Infect Dis*. (2010) 201:15–9. doi: 10.1086/648611
35. Tao L, Zalwango S, Chervenak K, Thiel B, Malone LSL, Qiu F, et al. Genetic and shared environmental influences on interferon-γ production in response to mycobacterium tuberculosis antigens in a ugandan population. *Am J Trop Med Hygiene*. (2013) 89:169–73. doi: 10.4269/ajtmh.12-0670
36. Hiza H, Fenner L, Hella J, Kuchaka D, Sasamalo M, Blauenfeldt T, et al. Boosting effect of IL-7 in interferon gamma release assays to diagnose *Mycobacterium tuberculosis* infection. *PLoS ONE*. (2018) 13:e0202525. doi: 10.1371/journal.pone.0202525
37. Latorre I, Mínguez S, Carrascosa JM, Naves J, Villar-Hernández R, Muriel B, et al. Immune-mediated inflammatory diseases differently affect IGRAs' accuracy for latent tuberculosis infection diagnosis in clinical practice. *PLoS ONE*. (2017) 12:e0189202. doi: 10.1371/journal.pone.0189202
38. Pérez I, Roig C, Gil M, Torrent P, Albiol P, Carballido M, et al. Concordancia entre la prueba de la tuberculina y el interferon gamma release assay-IGRA en pacientes con enfermedades inflamatorias mediadas por la inmunidad. *Rev Española Quimioterapia*. (2019) 32:445–50.
39. Bua A, Ruggeri M, Zanetti S, Molicotti P. Effect of teriflunomide on QuantiFERON-TB gold results. *Med Microbiol Immunol*. (2017) 206:73–5. doi: 10.1007/s00430-016-0482-x
40. Hakimian S, Popov Y, Rupawala AH, Salomon-Escoto K, Hatch S, Pellish R. The conundrum of indeterminate QuantiFERON-TB gold results before anti-tumor necrosis factor initiation. *Biol Targets Therapy*. (2018) 12:61–7. doi: 10.2147/BTT.S150958
41. Walsh MC, Camerlin AJ, Miles R, Pino P, Martinez P, Mora-Guzmán F, et al. The sensitivity of interferon-gamma release assays is not compromised in tuberculosis patients with diabetes. *Int J Tuberculosis Lung Dis*. (2011) 15:179–84.
42. Pathakumari B, Devasundaram S, Raja A. Altered expression of antigen-specific memory and regulatory T-cell subsets differentiate latent and active tuberculosis. *Immunology*. (2018) 153:325–36. doi: 10.1111/imm.12833
43. Menzies D, Pai M, Zwerling A. Systematic review: T-cell-based assays for the diagnosis of latent tuberculosis infection: an update. *Ann Internal Med*. (2008) 149:177–84. doi: 10.7326/0003-4819-149-3-200808050-00241
44. Ramos JM, Robledano C, Masiá M, Belda S, Padilla S, Rodríguez JC, et al. Contribution of Interferon gamma release assays testing to the diagnosis of latent tuberculosis infection in HIV-infected patients: a comparison of QuantiFERON-TB Gold In Tube, T-SPOTTB and tuberculin skin test. *BMC Infect Dis*. (2012) 12:1–10. doi: 10.1186/1471-2334-12-169
45. Sauzullo I, Mastroianni CM, Mengoni F, Ermocida A, Mascia C, Salotti A, et al. Long-term IFN-γ and IL-2 response for detection of latent tuberculosis infection in healthcare workers with discordant immunologic results. *J Immunol Methods*. (2014) 414:51–7. doi: 10.1016/j.jim.2014.07.013
46. Serrano CJ, Castañeda-Delgado JE, Trujillo-Ochoa JL, González-Amaro R, Hernández-García MH, Enciso-Moreno JA. Regulatory T-cell subsets in response to specific *Mycobacterium tuberculosis* antigens *in vitro* distinguish among individuals with different QTF and TST reactivity. *Clin Immunol*. (2015) 157:145–55. doi: 10.1016/j.clim.2015.02.008
47. Diel R, Loddenkemper R, Nienhaus A. Predictive value of interferon-γ release assays and tuberculin skin testing for progression from latent TB infection to disease state: a meta-analysis. *Chest*. (2012) 142:63–75. doi: 10.1378/chest.11-3157
48. Dheda K, van Zyl Smit R, Badri M, Pai M. T-cell interferon-γ release assays for the rapid immunodiagnosis of tuberculosis: clinical utility in high-burden

vs. low-burden settings. *Curr Opin Pulmonary Med*. (2009) 15:188–200. doi: 10.1097/MCP.0b013e32832a0adc
49. Detjen AK, Loebenberg L, Grewal HMS, Stanley K, Gutschmidt A, Kruger C, et al. Short-term reproducibility of a commercial interferon gamma release assay. *Clin Vaccine Immunol*. (2009) 16:1170–5. doi: 10.1128/CVI.00168-09
50. Ringshausen FC, Nienhaus A, Costa JT, Knoop H, Schlösser S, Schultze-Werninghaus G, et al. Within-subject variability of *Mycobacterium tuberculosis*-specific gamma interferon responses in German health care workers. *Clin Vaccine Immunol*. (2011) 18:1176–82. doi: 10.1128/CVI.05058-11
51. Park JS, Lee JS, Kim MY, Lee CH, Il Yoon H, Lee SM, et al. Monthly follow-ups of interferon-γ release assays among health-care workers in contact with patients with TB. *Chest*. (2012) 142:1461–8. doi: 10.1378/chest.11-3299
52. Dorman SE, Belknap R, Graviss EA, Reves R, Schluger N, Weinfurter P, et al. Interferon-γ release assays and tuberculin skin testing for diagnosis of latent tuberculosis infection in healthcare workers in the united states. *Am J Respir Crit Care Med*. (2014) 189:77–87. doi: 10.1164/rccm.201302-0365OC
53. Aggerbeck H, Giemza R, Joshi P, Tingskov PN, Hoff ST, Boyle J, et al. Randomised clinical trial investigating the specificity of a novel skin test (C-Tb) for diagnosis of *M. tuberculosis* infection. *PLoS ONE*. (2013) 8:e64215. doi: 10.1371/journal.pone.0064215
54. Millington KA, Fortune SM, Low J, Garces A, Hingley-Wilson SM, Wickremasinghe M, et al. Rv3615c is a highly immunodominant RD1 (Region of difference 1)-dependent secreted antigen specific for *Mycobacterium tuberculosis* infection. *Proc Natl Acad Sci USA*. (2011) 108:5730–5. doi: 10.1073/pnas.1015153108
55. Caño-muñiz S, Anthony R, Niemann S, Alffenaar JC. New approaches and therapeutic options for mycobacterium. *Clin Microbiol Rev*. (2018) 31:1–13. doi: 10.1128/CMR.00060-17
56. Lewis K. Persister cells. *Annu Rev Microbiol*. (2010) 64:357–72. doi: 10.1146/annurev.micro.112408.134306
57. Park HD, Guinn KM, Harrell MI, Liao R, Voskuil MI, Tompa M, et al. Rv3133c/dosR is a transcription factor that mediates the hypoxic response of *Mycobacterium tuberculosis*. *Mol Microbiol*. (2003) 48:833–43. doi: 10.1046/j.1365-2958.2003.03474.x
58. Roberts DM, Liao RP, Wisedchaisri G, Hol WGJ, Sherman DR. Two sensor kinases contribute to the hypoxic response of *Mycobacterium tuberculosis*. *J Biol Chem*. (2004) 279:23082–7. doi: 10.1074/jbc.M401230200
59. Rustad TR, Harrell MI, Liao R, Sherman DR. The enduring hypoxic response of *Mycobacterium tuberculosis*. *PLoS ONE*. (2008) 3:e1502. doi: 10.1371/journal.pone.0001502
60. Hozumi H, Tsujimura K, Yamamura Y, Seto S, Uchijima M, Nagata T, et al. Immunogenicity of dormancy-related antigens in individuals infected with *Mycobacterium tuberculosis* in Japan. *Int J Tuberculosis Lung Dis*. (2013) 17:818–24. doi: 10.5588/ijtld.12.0695
61. Leyten EMS, Lin MY, Franken KLMC, Friggen AH, Prins C, van Meijgaarden KE, et al. Human T-cell responses to 25 novel antigens encoded by genes of the dormancy regulon of *Mycobacterium tuberculosis*. *Microbes Infect*. (2006) 8:2052–60. doi: 10.1016/j.micinf.2006.03.018
62. Goletti D, Butera O, Vanini V, Lauria FN, Lange C, Franken KLMC, et al. Response to Rv2628 latency antigen associates with cured tuberculosis and remote infection. *Eur Respir J*. (2010) 36:135–42. doi: 10.1183/09031936.00140009
63. Belay M, Legesse M, Mihret A, Bekele Y, Ottenhoff THM, Franken KLMC, et al. Pro- and anti-inflammatory cytokines against Rv2031 are elevated during latent tuberculosis: a study in cohorts of tuberculosis patients, household contacts and community controls in an endemic setting. *PLoS ONE*. (2015) 10:e124134. doi: 10.1371/journal.pone.0124134
64. Torres M, García-García L, Cruz-Hervert P, Guio H, Carranza C, Ferreyra-Reyes L, et al. Effect of isoniazid on antigen-specific interferon-γ secretion in latent tuberculosis. *Eur Respir J*. (2015) 45:473–82. doi: 10.1183/09031936.00123314
65. Chegou NN, Black GF, Loxton AG, Stanley K, Essone PN, Klein MR, et al. Potential of novel *Mycobacterium tuberculosis* infection phase-dependent antigens in the diagnosis of TB disease in a high burden setting. *BMC Infectious Diseases*. (2012) 12:10. doi: 10.1186/1471-2334-12-10
66. Mensah GI, Addo KK, Tetteh JA, Sowah S, Loescher T, Geldmacher C, et al. Cytokine response to selected MTB antigens in Ghanaian TB patients, before and at 2 weeks of anti-TB therapy is characterized by high expression of IFN-γ and Granzyme B and inter- individual variation. *BMC Infect Dis*. 14:1. doi: 10.1186/1471-2334-14-495
67. Arroyo L, Rojas M, Franken KLMC, Ottenhoff THM, Barrera LF. Multifunctional T cell response to DosR and Rpf antigens is associated with protection in long-Term mycobacterium tuberculosis-infected individuals in Colombia. *Clin Vaccine Immunol*. (2016) 23:813–24. doi: 10.1128/CVI.00217-16
68. Doddam SN, Peddireddy V, Ahmed N. *Mycobacterium tuberculosis* DosR regulon gene Rv2004c encodes a novel antigen with pro-inflammatory functions and potential diagnostic application for detection of latent tuberculosis. *Front Immunol*. (2017) 8:712. doi: 10.3389/fimmu.2017.00712
69. Kassa D, Ran L, Geberemeskel W, Tebeje M, Alemu A, Selase A, et al. Analysis of immune responses against a wide range of *Mycobacterium tuberculosis* antigens in patients with active pulmonary tuberculosis. *Clin Vaccine Immunol*. (2012) 19:1907–15. doi: 10.1128/CVI.00482-12
70. Meier NR, Jacobsen M, Ottenhoff THM, Ritz N. A systematic review on novel mycobacterium tuberculosisantigens and their discriminatory potential for the diagnosis of latent and active tuberculosis. *Front Immunol*. (2018) 9:2476. doi: 10.3389/fimmu.2018.02476
71. Jacobs AJ, Mongkolsapaya J, Screaton GR, McShane H, Wilkinson RJ. Antibodies and tuberculosis. *Tuberculosis*. (2016) 101:102–13. doi: 10.1016/j.tube.2016.08.001
72. Ziegenbalg A, Prados-Rosales R, Jenny-Avital ER, Kim RS, Casadevall A, Achkar JM. Immunogenicity of mycobacterial vesicles in humans: Identification of a new tuberculosis antibody biomarker. *Tuberculosis*. (2013) 93:448–55. doi: 10.1016/j.tube.2013.03.001
73. Kimby E. Tolerability and safety of rituximab (MabThera®). *Cancer Treat Rev*. (2005) 31:456–73. doi: 10.1016/j.ctrv.2005.05.007
74. WHO. *Commercial Serodiagnostic Tests for Diagnosis of Tuberculosis*. Geneva: WHO (2011). Available online at: https://www.ncbi.nlm.nih.gov/books/NBK304212/
75. de Araujo LS, da Silva N de BM, Leung JAM, Mello FCQ, Saad MHF. IgG subclasses' response to a set of mycobacterial antigens in different stages of *Mycobacterium tuberculosis* infection. *Tuberculosis*. (2018) 108:70–6. doi: 10.1016/j.tube.2017.10.010
76. Fletcher HA, Snowden MA, Landry B, Rida W, Satti I, Harris SA, et al. T-cell activation is an immune correlate of risk in BCG vaccinated infants. *Nat Commun*. (2016) 7:11290. doi: 10.1038/ncomms11290
77. De Vallière S, Abate G, Blazevic A, Heuertz RM, Hoft DF. Enhancement of innate and cell-mediated immunity by antimycobacterial antibodies. *Infect Immunity*. (2005) 73:6711–20. doi: 10.1128/IAI.73.10.6711-6720.2005
78. Coppola M, Arroyo L, van Meijgaarden KE, Franken KL, Geluk A, Barrera LF, et al. Differences in IgG responses against infection phase related *Mycobacterium tuberculosis* (Mtb) specific antigens in individuals exposed or not to Mtb correlate with control of TB infection and progression. *Tuberculosis*. (2017) 106:25–32. doi: 10.1016/j.tube.2017.06.001
79. Mehta PK, Dahiya B, Sharma S, Singh N, Dharra R, Thakur Z, et al. Immuno-PCR, a new technique for the serodiagnosis of tuberculosis. *J Microbiol Methods*. (2017) 139:218–29. doi: 10.1016/j.mimet.2017.05.009
80. Amiano NO, Morelli MP, Pellegrini JM, Tateosian NL, Rolandelli A, Seery V, et al. IFN-γ and IgG responses to *Mycobacterium tuberculosis* latency antigen Rv2626c differentiate remote from recent tuberculosis infection. *Sci Rep*. (2020) 10:1–9. doi: 10.1038/s41598-020-64428-z
81. Kumar SK, Arya S, Aggarwal A, Kapoor P, Nath A, Misra R, et al. Immune responses to *Mycobacterium tuberculosis* membrane-associated antigens including alpha crystallin can potentially discriminate between latent infection and active tuberculosis disease. *PLoS ONE*. (2020) 15:e228359. doi: 10.1371/journal.pone.0228359
82. Parekh MJ, Schluger NW. Treatment of latent tuberculosis infection. *Ther Adv Respir Dis*. (2013) 7:351–6. doi: 10.1177/1753465813503028
83. Dhar GC. Treatment of latent tuberculosis infection. *Ann Internal Med*. (2015) 162:394. doi: 10.7326/L15-5058-2
84. IUAT International Union Against Tb. Efficacy of various durations of isoniazid preventive therapy for tuberculosis: five years of follow-up in the IUAT trial. *Bull WHO*. (1982) 60:555–64.
85. Tousif S, Singh DK, Ahmad S, Moodley P, Bhattacharyya M, Van Kaer L, et al. Isoniazid induces apoptosis of activated CD4+ T cells: implications for

post-therapy tuberculosis reactivation and reinfection. *J Biol Chem*. (2014) 289:30190–5. doi: 10.1074/jbc.C114.598946
86. Goletti D, Parracino MP, Butera O, Bizzoni F, Casetti R, Dainotto D, et al. Isoniazid prophylaxis differently modulates T-cell responses to RD1-epitopes in contacts recently exposed to *Mycobacterium tuberculosis*: a pilot study. *Respir Res*. (2007) 8:1–10. doi: 10.1186/1465-9921-8-5
87. Singh M, Bhatt P, Sharma M, Varma-Basil M, Chaudhry A, Sharma S. Immunogenicity of late stage specific peptide antigens of *Mycobacterium tuberculosis*. *Infect Genet Evolut*. (2019) 74:103930. doi: 10.1016/j.meegid.2019.103930
88. Adetifa IM, Ota MOC, Jeffries DJ, Lugos MD, Hammond AS, Battersby NJ, et al. Interferon-γ ELISPOT as a biomarker of treatment efficacy in latent tuberculosis infection a clinical trial. *Am J Respir Crit Care Med*. (2013) 187:439–45. doi: 10.1164/rccm.201208-1352OC
89. Brock I, Munk ME, Kok-Jensen A, Andersen P. Performance of whole blood IFN-γ test for tuberculosis diagnosis based on PPD or the specific antigens ESAT-6 and CFP-10. *Int J Tuberculosis Lung Dis*. (2001) 5:462–7.
90. Johnson JL, Geldenhuys H, Thiel BA, Toefy A, Suliman S, Pienaar B, et al. Effect of isoniazid therapy for latent tb infection on quantiferon-Tb gold in-Tube responses in adults with positive tuberculin skin test results in a high tb incidence area. *Chest*. (2014) 145:612–7. doi: 10.1378/chest.13-1232
91. Chee C, Bin E, Khinmar KW, Gan SH, Barkham TMS, Pushparani M, et al. Latent tuberculosis infection treatment and T-cell responses to *Mycobacterium tuberculosis*-specific antigens. *Am J Respir Crit Care Med*. (2007) 175:282–7. doi: 10.1164/rccm.200608-1109OC
92. Ewer K, Millington KA, Deeks JJ, Alvarez L, Bryant G, Lalvani A. Dynamic antigen-specific T-cell responses after point-source exposure to *Mycobacterium tuberculosis*. *Am J Respir Crit Care Med*. (2006) 174:831–9. doi: 10.1164/rccm.200511-1783OC
93. Wilkinson KA, Kon OM, Newton SM, Meintjes G, Davidson RN, Pasvol G, et al. Effect of treatment of latent tuberculosis infection on the T cell response to *Mycobacterium tuberculosis* antigens. *J Infect Dis*. (2006) 193:354–9. doi: 10.1086/499311
94. Chiappini E, Bonsignori F, Mangone G, Galli L, Mazzantini R, Sollai S, et al. Serial T-Spot.Tb and quantiferon-tb-gold in-tube assays to monitor response to antitubercular treatment in Italian children with active or latent tuberculosis infection. *Pediatr Infect Dis J*. (2012) 31:974–7. doi: 10.1097/INF.0b013e31825d0d67
95. Lee SW, Lee SH, Yim J-J. Serial interferon-gamma release assays after chemoprophylaxis in a tuberculosis outbreak cohort. *Infection*. (2012) 40:431–5. doi: 10.1007/s15010-012-0265-2
96. Wergeland I, Pullar N, Assmus J, Ueland T, Tonby K, Feruglio S, et al. IP-10 differentiates between active and latent tuberculosis irrespective of HIV status and declines during therapy. *J Infect*. (2015) 70:381–91. doi: 10.1016/j.jinf.2014.12.019
97. Feruglio SL, Trøseid M, Damås JK, Kvale D, Dyrhol-Riise AM. Soluble markers of the toll-like receptor 4 pathway differentiate between active and latent tuberculosis and are associated with treatment responses. *PLoS ONE*. (2013) 8:e69896. doi: 10.1371/journal.pone.0069896
98. Mihret A, Bekele Y, Bobosha K, Kidd M, Aseffa A, Howe R, et al. Plasma cytokines and chemokines differentiate between active disease and non-active tuberculosis infection. *J Infect*. (2013) 66:357–65. doi: 10.1016/j.jinf.2012.11.005
99. Tonby K, Ruhwald M, Kvale D, Dyrhol-Riise AM. IP-10 measured by dry plasma spots as biomarker for therapy responses in *Mycobacterium tuberculosis* infection. *Sci Rep*. (2015) 5:1–6. doi: 10.1038/srep09223
100. Rangel-Santiago JF, Baay-Guzman GJ, Duran-Padilla MA, Lopez-Bochm KA, Garcia-Romero BL, Hernandez-Cueto DD, et al. A novel role of Yin-Yang-1 in pulmonary tuberculosis through the regulation of the chemokine CCL4. *Tuberculosis*. (2016) 96:87–95. doi: 10.1016/j.tube.2015.10.013
101. Chiacchio T, Petruccioli E, Vanini V, Cuzzi G, Pinnetti C, Sampaolesi A, et al. Polyfunctional T-cells and effector memory phenotype are associated with active TB in HIV-infected patients. *J Infect*. (2014) 69:533–45. doi: 10.1016/j.jinf.2014.06.009
102. Du Plessis WJ, Keyser A, Walzl G, Loxton AG. Phenotypic analysis of peripheral B cell populations during *Mycobacterium tuberculosis* infection and disease. *J Inflamm*. (2016) 13:1–8. doi: 10.1186/s12950-016-0133-4
103. Rénier W, Bourdin A, Rubbo PA, Peries M, Dedieu L, Bendriss S, et al. B cells response directed against Cut4 and CFP21 lipolytic enzymes in active and latent tuberculosis infections. *PLoS ONE*. (2018) 13:e196470. doi: 10.1371/journal.pone.0196470
104. De Oyarzabal E, García-García L, Rangel-Escareño C, Ferreyra-Reyes L, Orozco L, Herrera MT, et al. Expression of USP18 and IL2RA is increased in individuals receiving latent tuberculosis treatment with isoniazid. *J Immunol Res*. (2019). doi: 10.1155/2019/1297131. [Epub ahead of print].
105. Bloom CI, Graham CM, Berry MPR, Wilkinson KA, Oni T, Rozakeas F, et al. Detectable changes in the blood transcriptome are present after two weeks of antituberculosis therapy. *PLoS ONE*. (2012) 7:e46191. doi: 10.1371/journal.pone.0046191
106. Hong Y, Kim Y, Lee JJ, Lee MG, Lee CY, Kim Y, et al. Levels of vitamin D-associated cytokines distinguish between active and latent tuberculosis following a tuberculosis outbreak. *BMC Infect Dis*. (2019) 19:1–8. doi: 10.1186/s12879-019-3798-5
107. Adekambi T, Ibegbu CC, Kalokhe AS, Yu T, Ray SM, Rengarajan J. Distinct effector memory CD4 + T cell signatures in latent *Mycobacterium tuberculosis* infection, BCG vaccination and clinically resolved tuberculosis. *PLoS ONE*. (2012) 7:e36046. doi: 10.1371/journal.pone.0036046
108. Pollock KM, Whitworth HS, Montamat-Sicotte DJ, Grass L, Cooke GS, Kapembwa MS, et al. T-cell immunophenotyping distinguishes active from latent tuberculosis. *J Infect Dis*. (2013) 208:952–68. doi: 10.1093/infdis/jit265
109. Latorre I, Fernández-Sanmartín MA, Muriel-Moreno B, Villar-Hernández R, Vila S, De Souza-Galvão ML, et al. Study of CD27 and CCR4 markers on specific CD4+ T-cells as immune tools for active and latent tuberculosis management. *Front Immunol*. (2019) 10:3094. doi: 10.3389/fimmu.2018.03094
110. Horne DJ, Graustein AD, Shah JA, Peterson G, Savlov M, Steele S, et al. Human ULK1 variation and susceptibility to *Mycobacterium tuberculosis* infection. *J Infect Dis*. (2016) 214:1260–7. doi: 10.1093/infdis/jiw347
111. Burel JG, Lindestam Arlehamn CS, Khan N, Seumois G, Greenbaum JA, Taplitz R, et al. Transcriptomic analysis of CD4 + T cells reveals novel immune signatures of latent tuberculosis. *J Immunol*. (2018) 200:3283–90. doi: 10.4049/jimmunol.1800118
112. Halliday A, Whitworth H, Kottoor SH, Niazi U, Menzies S, Kunst H, et al. Stratification of latent mycobacterium tuberculosis infection by cellular immune profiling. *J Infect Dis*. (2017) 215:1480–7. doi: 10.1093/infdis/jix107
113. Du Plessis N, Loebenberg L, Kriel M, Von Groote-Bidlingmaier F, Ribechini E, Loxton AG, et al. Increased frequency of Myeloid-derived suppressor cells during active tuberculosis and after recent *Mycobacterium tuberculosis* infection suppresses T-cell function. *Am J Respir Crit Care Med*. (2013) 188:724–32. doi: 10.1164/rccm.201302-0249OC
114. Bartel D. P, Lee R, Feinbaum R. MicroRNAs: genomics, biogenesis, mechanism, and function genomics: the miRNA *Genes*. (2004) 116:281–97. doi: 10.1016/S0092-8674(04)00045-5
115. Das K, Garnica O, Dhandayuthapani S. Modulation of host miRNAs by intracellular bacterial pathogens. *Front Cell Infect Microbiol*. (2016) 6:79. doi: 10.3389/fcimb.2016.00079
116. Sabir N, Hussain T, Shah SZA, Peramo A, Zhao D, Zhou X. miRNAs in tuberculosis: new avenues for diagnosis and host-directed therapy. *Front Microbiol*. (2018) 9:602. doi: 10.3389/fmicb.2018.00602
117. Wang JX, Xu J, Han YF, Zhu YB, Zhang WJ. Diagnostic values of microRNA-31 in peripheral blood mononuclear cells for pediatric pulmonary tuberculosis in Chinese patients. *Genet Mol Res*. (2015) 14:17235–43. doi: 10.4238/2015.December.16.23
118. Latorre I, Leidinger P, Backes C, Domínguez J, De Souza-Galvão ML, Maldonado J, et al. A novel whole-blood miRNA signature for a rapid diagnosis of pulmonary tuberculosis. *Eur Respir J*. (2015) 45:1173–6. doi: 10.1183/09031936.00221514
119. Spinelli SV, Diaz A, D'Attilio L, Marchesini MM, Bogue C, Bay ML, et al. Altered microRNA expression levels in mononuclear cells of patients with pulmonary and pleural tuberculosis and their relation with components of the immune response. *Mol Immunol*. (2013) 53:265–9. doi: 10.1016/j.molimm.2012.08.008

120. Wu J, Lu C, Diao N, Zhang S, Wang S, Wang F, et al. Analysis of microRNA expression profiling identifies miR-155 and miR-155* as potential diagnostic markers for active tuberculosis: a preliminary study. *Hum Immunol*. (2012) 73:31–7. doi: 10.1016/j.humimm.2011.10.003
121. Dorhoi A, Iannaccone M, Farinacci M, Faé KC, Schreiber J, Moura-Alves P, et al. MicroRNA-223 controls susceptibility to tuberculosis by regulating lung neutrophil recruitment. *J Clin Investig*. (2013) 123:4836–48. doi: 10.1172/JCI67604
122. Chen DY, Chen YM, Lin CF, Lo CM, Liu HJ, Liao TL. MicroRNA-889 inhibits autophagy to maintain mycobacterial survival in patients with latent tuberculosis infection by targeting TWEAK. *MBio*. (2020) 11:1–17. doi: 10.1128/mBio.03045-19
123. Zhang C, Xi X, Wang Q, Jiao J, Zhang L, Zhao H, et al. The association between serum miR-155 and natural killer cells from tuberculosis patients. *Int J Clin Exp Med*. (2015) 8:9168–72.
124. van Rensburg IC, du Toit L, Walzl G, du Plessis N, Loxton AG. Decreased neutrophil–associated miRNA and increased B-cell associated miRNA expression during tuberculosis. *Gene*. (2018) 655:35–41. doi: 10.1016/j.gene.2018.02.052

Conflict of Interest: The authors declare that the research was conducted in the absence of any commercial or financial relationships that could be construed as a potential conflict of interest.

frontiers in Immunology

ORIGINAL RESEARCH
published: 02 October 2020
doi: 10.3389/fimmu.2020.577815

Selection of a Single Domain Antibody, Specific for an HLA-Bound Epitope of the Mycobacterial Ag85B Antigen

*Paola A. Ortega[1], Mayra Silva-Miranda[1,2], Alfredo Torres-Larios[3], Eduardo Campos-Chávez[3], Kees C. L. C. M. Franken[4], Tom H. M. Ottenhoff[4], Juraj Ivanyi[5] and Clara Espitia[1,5]**

[1] Departamento de Inmunología, Instituto de Investigaciones Biomédicas, Universidad Nacional Autónoma de México, Ciudad de México, México, [2] CONACyT-Instituto de Investigaciones Biomédicas, Universidad Nacional Autónoma de México, Ciudad de México, México, [3] Department of Biochemistry and Structural Biology, Instituto de Fisiología Celular, Universidad Nacional Autónoma de México, Ciudad de México, México, [4] Department of Infectious Diseases, University Medical Centre Leiden, Leiden, Netherlands, [5] Center for Host-Microbiome Interactions, King's College London, London, United Kingdom

OPEN ACCESS

Edited by:
Mario Alberto Flores-Valdez, CONACYT Centro de Investigación y Asistencia en Tecnología y Diseño del Estado de Jalisco (CIATEJ), Mexico

Reviewed by:
Eddie A. James, Benaroya Research Institute, United States
Armando Acosta, Universiti Sains Malaysia Health Campus, Malaysia

***Correspondence:**
Clara Espitia
espitia@iibiomedicas.unam.mx

Specialty section:
This article was submitted to Microbial Immunology, a section of the journal Frontiers in Immunology

Received: 30 June 2020
Accepted: 14 September 2020
Published: 02 October 2020

Citation:
Ortega PA, Silva-Miranda M, Torres-Larios A, Campos-Chávez E, Franken KCLCM, Ottenhoff THM, Ivanyi J and Espitia C (2020) Selection of a Single Domain Antibody, Specific for an HLA-Bound Epitope of the Mycobacterial Ag85B Antigen. Front. Immunol. 11:577815. doi: 10.3389/fimmu.2020.577815

T cells recognizing epitopes on the surface of mycobacteria-infected macrophages can impart protection, but with associated risk for reactivation to lung pathology. We aimed to identify antibodies specific to such epitopes, which carry potentials for development toward novel therapeutic constructs. Since epitopes presented in the context of major histocompatibility complex alleles are rarely recognized by naturally produced antibodies, we used a phage display library for the identification of monoclonal human single domain antibody producing clones. The selected 2C clone displayed T cell receptor-like recognition of an HLA-A*0201 bound $_{199}$KLVANNTRL$_{207}$ peptide from the Ag85B antigen, which is known to be an immunodominant epitope for human T cells. The specificity of the selected domain antibody was demonstrated by solid phase immunoassay and by immunofluorescent surface staining of peptide loaded cells of the T2 cell line. The antibody affinity binding was determined by biolayer interferometry. Our results validated the used technologies as suitable for the generation of antibodies against epitopes on the surface of *Mycobacterium tuberculosis* infected cells. The potential approaches forward the development of antibody in immunotherapy of tuberculosis have been outlined in the discussion.

Keywords: tuberculosis, single domain antibodies, peptide-human leukocyte antigen complex, mycobacterial Ag85B, T cell receptor-like antibodies

INTRODUCTION

Current problems of Tuberculosis (TB) control are due to the emergence of drug resistant strains, the failure of the existing BCG vaccination and the persistence of factors associated with poverty-stricken populations. Consequently, there is a global morbidity of 10 million people with the mortality of 1.2 million in HIV-negative people and 0.25 million in HIV positive subjects (1) New

approaches toward the control of TB involve the shortening of the current chemotherapy regimen (2) and prophylaxis for HIV-related TB without interfering with antiretroviral therapy (3). This pilot study, aiming at the immunotherapy of TB had an initial objective to identify monoclonal antibodies with T cell receptor (TCR)-like specificity, binding to peptide epitope/human leukocyte antigen (HLA) class I complexes on the surface of *M. tuberculosis* infected cells. This approach has been based in the evidence, that such antibodies can be developed for the specific killing of malignant and virus-infected cells (4–10).

The mycobacterial peptides epitopes complexed with MHC class I molecules on the surface of infected cells are known to be recognized and leading to the activation of CD8+ T cells (11–13). Therefore, antibodies with TCR-like specificity following conjugation with suitable apoptosis-inducing ligands could potentially become mycobactericidal and a suitable adjunct to the chemotherapy of TB. The identification of TCR-like antibodies with specificity against *M. tuberculosis* Acr1 peptides/HLA.A*0201, HLA.A*011 and HLA.A*24 class I complexes has recently been reported, using peptide/MHC complexes generated *via* UV-induced peptide exchange. The complexes were panned against human DAb (domain antibody) phage display library (14, 15). This approach can be expanded by testing immunodominant epitopes from other *M. tuberculosis* antigens recognized in the context of HLA class I alleles (16, 17). Our interest focused on the HLA-A*0201 restricted CD8+T-cell epitopes of Ag85B, a major secreted *M. tuberculosis* protein. Two Ag85B peptides $_{143}$FIYAGSLSA$_{151}$ and $_{199}$KLVANNTRL$_{207}$ had previously been identified in healthy humans and in immunized HLA-A2 transgenic mice (18), while HLA-A*0201 allele specific recognition of $_{37}$YLLDGLRAQ$_{45}$ and $_{199}$KLVANNTRL$_{207}$, was observed in patients with active TB (19). Since epitopes from Esat-6 and TB10.4, are recognized in the context of various HLA-A alleles, the HLA-A*0201 restricted, $_{199}$KLVANNTRL$_{207}$ epitope from Ag85B appeared to be the most immunodominant (17) and was therefore chosen as our target for the selection and characterization of a TCR-like antibody. Using a human DAb phage display library, we selected a clone producing a single domain antibody (sdAb) against the Ag85B$_{p199-207}$/HLA-A*0201 complex (Ag85Bp/HLA-A*0201). Its specificity was determined by ELISA, and by its binding capacity to the Ag85Bp/HLA-A*0201 expressed on cells of the human HLA-A*0201 positive T2 cell line.

MATERIALS AND METHODS

Mycobacterium tuberculosis Peptides/HLA-A*0201 Complexes

Three nonamer peptides, known to be HLA-A*0201 restricted CD8+T cell epitopes from: Ag85B ($_{199}$KLVANNTRL$_{207}$), Esat-6 ($_{82}$AMASTEGNV$_{90}$), or Acr1 ($_{120}$GILTVSVAV$_{128}$) proteins of *M. tuberculosis* (16) were synthesized by Anaspec, Inc. (USA). The peptides were of > 90% purity, and their homogeneity was confirmed by analytical reverse-phase high-performance liquid chromatography. The biotinylated recombinant complexes of Ag85Bp/HLA-A*0201, Esat-6$_{p82-90}$/HLA-A*0201 (Esat-6p/HLA-A*0201), and Acr1$_{p120-128}$/HLA-A*0201 (Acr1p/HLA-A*0201), were produced using extracellular HLA class I molecules, with C-terminal BirA recognition site, and β2-microglobulin (20). The insoluble aggregates expressed in *Escherichia coli* in the form of inclusion bodies were solubilized in urea and folded with peptide by dilution. Monomers were biotinylated using the BirA enzyme and purified by gel filtration on a Hiload 16/60 Superdex 75 prep grade.

Evaluation of Refolding of Peptide/HLA-A*0201 Complexes by ELISA

An ELISA was carried out to evaluate the correct conformation of the complexes by using the W6/32 mAb (Invitrogen/USA) which recognizes a conformational epitope on the intact heavy chain/β2microglobulin complex (21–23). Briefly, 0.5 μg/well of the biotinylated complexes in Phosphate Buffer Saline (PBS), were immobilized on streptavidin coated (ThermoScientific/USA) and on uncoated high protein-binding (ThermoScientific) plates. Samples were incubated overnight (ON) at 4°C. Next day, plates were washed twice with PBS and then incubated 1 h at room temperature (RT) with W6/32 mAb diluted 1/2,000 in PBS-tween-20 0.05%, Bovine Serum Albumin BSA 2% (PBS-TBSA). After 3 washes with PBS-T, wells were incubated by 1 h with Horseradish peroxidase conjugated goat anti-mouse IgG H+L antibody (anti-mouse IgG-HRP)[1/2,000 (Invitrogen/USA)]. Then, complexes on both streptavidin coated and uncoated plates, were incubated with streptavidin-HRP (Biosource/China), diluted 1/4,000 1 h at RT. Finally the reaction was revealed with TMB (3,3',5,5'-tetramethylbenzidine) (ThermoScientific), and stopped with 100 μl of 0.16M H_2SO_4. Absorbance values were measured at 450 nm using an ELISA plate reader (Multiskan Go, Thermo).

Panning of the Human Single Domain Antibody Phage Library Against the Ag85B$_{p199-207}$/HLA-A*0201 Complex

A human DAb phage display library, containing approximately 3×10^9 sdAb clones (Geneservice, Cambridge) was used following a modified protocol (24). A negative panning was carried out for elimination of the background reactivity against streptavidin as follow: 5 x10^{12} phage library particles were pre-incubated at 4°C for 1h with 30 μl of streptavidin magnetic beads M280 (Invitrogen/Norway), then tube was placed in a magnet and phage supernatant was incubated with a 7.5 μg of biotinylated Ag85Bp/HLA-A*0201 in PBS at 4°C for 1h. After that, 200 μl of streptavidin beads were added and sample was incubated for 15 min at 4°C with shaking. Beads were pulled down with the magnet and washed 15 times with PBS-T 0.1%. Finally, sdAb phage complexes were eluted by incubation with glycine–HCl pH 2.2 for 15 min at RT and sample was neutralized with Tris-HCl pH 9.0. For the second and the third round of selection, 2.5 and 1.25 μg of complexes were exposed to streptavidin beads and washed 15 and 25 times with PBS-T 0.1% respectively. After the third final round of panning, the eluted sdAb phages were used

to infect 5 ml freshly prepared *E. coli* TG1 culture. Bacteria were plated onto TYE medium supplemented with 4% glucose and carbenicillin 100 μg/ml ($TYG_{4\%}C_{100}$). After ON culture, 94 individual clones were picked onto a 96 wells plate, containing 200 μl of $2xTYG_{4\%}C_{100}$. Plates were incubated ON at 37°C, with shaking at 200 rpm. Next day, 5 μl of ON culture from each well was transferred to a new plate with 200 μl of fresh $2xTYG_{4\%}C_{100}$. After 3 h of culture at 37°C, 50 μl 2xTY supplemented with $4x10^8$ M13 phage was added to each well and plates were incubated for 1 h at 37°C. After centrifugation to 2,800 rpm during 10 min, pellet was re suspended in 200 μl of $2xTYC_{100}K_{100}$ (Kanamycin 100 μg/ml). Cultures were grown at 26°C with shaking at 250 rpm, during 16-24 h.

ELISA Phage

Phage supernatants from each well were collected and evaluated by ELISA. Biotinylated complexes at 0.5 μg/well were bound to coated streptavidin plates as described before, and incubated with 100 μl of phage supernatant for 1 h at RT. After several washes with PBS-T 0.05%, wells were incubated with anti-M13 HRP antibody (1/2,500) for 1 h at RT (GE Healthcare/USA). The reaction was developed with o-Phenylenediamine dihydrochloride OPD (SigmaAldrich/USA), and stopped adding 25 μl of 3M H_2SO_4. Absorbance values were measured at 492 nm using an ELISA plate reader Multiskan–GO. Phage supernatants from positive clones were also evaluated by phage ELISA against non-target complex; Esat-6p/HLA-A*0201 and Acr1p/HLA-A*0201 as described above.

Domain Antibody Sequencing

Double strand phagemid DNA extraction was performed from 3 selected clones in *E. coli* strain TG1 by using GeneJET Plasmid Miniprep kit (ThermoScientific/Lithuania), The primers used for sequencing were LMB3 (5′ CAGGAAACAGCTATGAC 3′) and pHEN (5′CTATGCGGCCCCATTCA 3′). Sequencing was carried out in the sequencing facility at Instituto de Investigaciones Biomédicas. For translation BioEdit 7.2 software was used and BLAST and Clustalw tools for sequences analysis and alignment.

Production of Soluble Domain Antibody

Transformation of *E. coli* HB2151 by phage infection and expression of sdAb were done with minor modifications according to (25). Once bacteria were transformed with phages, the positive clones (2C, 3C, and 7E), 50 μl of $1:10^{12}$ to $1:10^6$ cell dilutions were sub-cultured in $TYEC_{100}$ plates and incubated overnight at 37°C. Three random unit forming colony (UFC) were picked up from each sample and inoculated in a culture flask containing $2xTYC_{100}$. The culture was grown with shaking (250 rpm) at 37°C until OD_{600nm}=0.6 (26). Then, Isopropyl-β-D-1-thiogalactoside (IPTG) (Promega/USA) was added to a final concentration of 1 mM, culture was continued, at 26°C with shaking (250 rpm), ON. Cells were harvest by centrifugation at 4,500 rpm, and bacterial sediment was treated with an osmotic buffer (750 mM sucrose, 100 mM Tris pH 7.5) as described by (27). The periplasmic fractions obtained from each clone were subjected to affinity chromatography on Protein-A-agarose (Roche/Germany), in order to purify the sdAbs following the manufacturer protocol. The eluted protein fractions were shuffled and concentrated to 500 μl in PBS pH 7.4, using amicon-15ml, 10.000 WM (Merck/Ireland). Protein quantification was determined by BCA assay (Pierce/USA).

SDS-PAGE and Western Blot

Ten μg/well of recombinant periplasmic extracts and 1.4 μg/well from 2C and 7E clones, were resolved on pre-made SDS-PAGE 4%–20%, (ThermoScientific/USA) and transferred to PVDF membranes. After 1 h blocking with PBS-BSA at RT, membranes were incubated with anti-c-Myc mAb (Sigma/USA) diluted 1/750 in PBS-T-BSA and then after washes with PBS-T, membranes were incubated with anti-mouse IgG HRP diluted (1/2,000)(Invitrogen/USA) for 1 h, washed with PBS-T, and developed with 3 mg/ml of 3,3-diaminobenzidine in PBS and 30% hydrogen peroxide diluted 1:1,000.

Evaluation of Specificity of Single Domain Antibodies by ELISA

The specificity of the purified sdAb 2C and 7E, were evaluated by ELISA using 1μg of target Ag85Bp/HLA-A*0201 and non-targets Esat-6p/HLA-A*0201 and Acr1p/HLA-A*0201 as which were immobilized on streptavidin plates. Complexes were incubated with 5 μg of sdAb followed by incubation with 1/1,000 dilution of anti-c-Myc Ab labelled with HRP (Sigma-Aldrich/Ireland Ltd) by 1h. After several washes with PBS-T, the reaction was developed with 50 μl of TMB. The reaction was stopped with 1M of H_2SO_4. OD_{450nm} was measured in an Infinitum F50 microplate ELISA reader (Tecan/Switzerland). Three experiments were carried out by duplicated for 2C and 2 experiments for 7E.

Ex Vivo Specificity of Single Domain 2C on the Surface of T2 Cells

To assess the ability to sdAb 2C to recognize the Ag85Bp/HLA-A*0201 an *ex vivo* assay was performed, by using the HLA-A*0201 positive T2 lymphoblastic human cell line (kindly donate by Dr. Patricia Gorocica INER-México). These cells are characterized by export empty HLA class I molecules due to a processing defect by homozygous deletion of the MHC class II region located on chromosome 6 including the TAP1 and TAP2 (transporters associated with antigen processing) genes which encode the transporter proteins (28). Cells were maintained in RPMI-1640 medium supplemented with 20% (vol/vol) fetal bovine serum (FBS) (Gibco/USA), at 37°C, 5% $C0_2$. T2 cells ($6x10^5$) were placed on flat bottom, 24 well cell culture plates (Costar/USA) in RPMI free serum in absence and presence of peptides from Ag85B and Esat-6.

In order to confirm the presence of HLA-ABC on T2 cells, they were incubated with W6/32 mAb (1μg/million cells), for 30 min on ice, after 3 washes, goat anti-mouse IgG Alexa fluor 488 (Invitrogen/USA) at 1/2,000 dilution was added. Samples were fixating with 0.5% PFA and the slides were mounted with vectashield (Vector Laboratories/USA). Then, cells ($6x10^5$) were incubated with 80 μg of either $Ag85Bp_{(199-207)}$ target peptide and $Esat\text{-}6p_{(82-90)}$ as non-target. Twenty μg/ml of β2m (Sigma) was

added according to (29). Cells were incubated for 8 h at 37°C in 5% CO_2 atmosphere, after that cells were washed twice with PBS and incubated with 10 μg of sdAb 2C ON at 4°C in agitation, and then washed 2 times, with PBS, following by incubation with anti-c-Myc Ab (Santa Cruz-/Europe) (1/100) for 1 h at RT. After three washes, anti-mouse IgG Alexa fluor 488 (Invitrogen/USA) (1/2,000) was added and samples were incubated for 1 h at RT. After three washes, Hoechst 33343 (Life technologies/USA) diluted 1/9,000 was used for 10 min for nucleus staining. sdAb 2C was evaluated on cells in the absence of peptides and as a staining control in one condition, no domain was added. Fluorescence images were acquired with Olympus BX41, (Fluorescence-Microcopy) using the 100x magnifying lens, the digital images were captured with Zen 2.6 blue edition software, and the capture parameters, exposure time and intensity for each staining system, were applied in both control and problem samples.

Kinetic Binding Assays for the Assessment of the Interaction of sdAb 2C With Ag85B/HLA-A*0201 Complex by Biolayer Interferometry

The binding kinetics and the determination of the dissociation constant (K_D) for the sdAb 2C against the Ag85Bp/HLA-A*0201 complex were performed using Biolayer Interferometry (BLI) at 25°C. Streptavidin biosensors in an Octet RED96 system (FortéBio Inc. San Jose, CA, USA) were used. The assays were performed on black bottom 96-well microplates (Greiner Bio-One 655209) in a total volume of 200 μl with orbital shaking at 1000 rpm. Experiments were controlled with the software Data Acquisition 8.2 (ForteBio, Inc.) For the BLI experiment, a baseline was established using 1x Kinetics buffer (FortéBio Inc. San Jose, CA, USA). Then, the biotinylated Ag85Bp/HLA-A*0201 complex at 25 ng was allowed to bind to streptavidin sensor for 5 min, followed by washing with the same buffer to eliminate nonspecific binding. Next, the purified sdAb was bound to the Ag85Bp/HLA-A*0201 complex in the biosensor and the association rate was measured (k_a). In the last step, the dissociation rate (k_d) of the antibody-complex was obtained. The BLI experiment was done with six different concentrations of the sdAb 2C from (2.54 to 81.3 μM), one well with 200 μl without sdAb was used as a negative control. New streptavidin biosensors were used for each experiment. The binding of sdAb 2C at 10 μM, to non-target Esat-6p/HLA-A*0201 was also tested. The data were processed using the Octet Data Analysis Software version 8.2 (FortéBio Inc. San Jose, CA, USA) according to a 1:1 model.

Statistical Analysis

GraphPad Prism version 6.0c software was used to analyze the results. For the statistical analysis, one-way ANOVA multiple comparisons with Sidak`s post Hoc correction was used.

RESULTS

Evaluation of Peptide HLA-A Complexes With W6/32 Antibody

Ag85Bp/HLA-A*0201, Esat-6p/HLA-A*0201, and Acr1p/HLA-A*0201 immobilized on streptavidin plates were recognized by W6/32 mAb (**Figure 1A**), indicating this result that peptides HLA-A*0201 complexes were correctly folded. In contrast, the mAb did not recognize the complexes bound to non-coated streptavidin control plate (**Figure 1B**), showing the results that direct binding of the complexes in the plates could lead to a loss of conformation. The biotinylated complexes bound to streptavidin plates were not recognized for streptavidin-HRP, an indication that biotinylated complexes were correctly oriented by streptavidin on coated plates (**Figure 1A**). In contrast, the positive signal obtained with the complexes bound to the non-coated streptavidin plate (**Figure 1B**), was an indication that exposed biotin in unfolded complexes was being recognized by streptavidin-HRP.

Screening of the Human Single DAb Phage Library Binding to $Ag85B_{p199-207}$ HLA-A*0201/Complexes

The number of phage particles from sdAb library during the three rounds of selection was consistent with the published protocol (24). The final output titers of phage particles showed an enrichment factor of 25 (**Table 1**). From 94 clones evaluated by monoclonal phage-ELISA, only 7 clones showed absorbance 10 fold higher than the negative control (clone not reactive to the

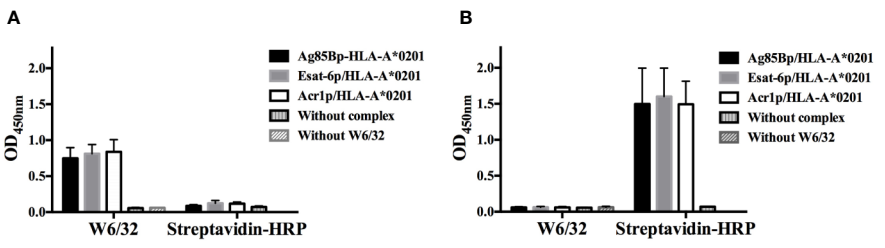

FIGURE 1 | Evaluation of complexes with conformational antibody W6/32. **(A)** Two groups of biotinylated complexes were immobilized on streptavidin coated plates, the group on the left was detected with W6/32 and the group on the right, was incubated with HRP-streptavidin. **(B)** The same as A, but both groups of biotinylated complexes were bound to uncoated streptavidin plates and detected with W6/32 and HRP-streptavidin respectively. The dates represent the media +/- standard deviation from three independent experiments.

TABLE 1 | Selective enrichment of phage domain antibody after 3 rounds of biopanning.

SelS Selection Round	Ag85Bp/ HLA-A*0201	Phages Input	Eluted phages/ml	Eluted/input	Enrichment Factor*	Amplified Phages/ml	Tween 20/ # washes
1	7.5µg	5.0×10^{12}	6.0×10^{6}	1.2×10^{-6}	1.0	84×10^{12}	1.0%/15
2	2.5µg	5.0×10^{12}	1.4×10^{8}	2.8×10^{-5}	23	7×10^{12}	0.1%/15
3	1.25µg	5.0×10^{12}	1.5×10^{8}	3.0×10^{-5}	25	—	0.1%/25

**Enrichment factor was determined by dividing the eluted/input ratio in each round by the ratio in the first round. according to Bagheri et al. (30) Zhang et al. (31).*

Ag85Bp/HLA-A*0201) (**Figure 2A**). From those, clones 2C, 3C, and 7E did not recognized streptavidin (**Figure 2B**) and all of them showed specific binding by ELISA to the target complex and but none bound to non-target complexes, Esat-6p/HLA-A*0201, and Acr1p/HLA-A*0201 (**Figure 2C**).

Domain Antibody Sequencing

BLAST search analysis of sdAb 2C, 3C, and 7E sequences, showed that all them matched with 122 amino acids length of immunoglobulin heavy chain variable region, partial (>ABM67233.1 Homo sapiens). Sequences corresponded to a human dAb with a length of 160 and 159 amino acids residues for 2C and 7E domains, respectively, the protein sequence of the 3C domain was exactly the same as 2C but shorter in length, 3C had only 151 amino acids due to the presence of a stop codon. For all sequences, the three complementarity determining regions (CDR) and the c-Myc tag sequence were identified. Clones 2C and 7E were selected to continue with de antibody expression phase.

Production of Single Domain Antibodies

sdAb 2C was produced in *E. coli* HB2151. The expression and purification of sdAb 2C is shown in **Figure 3A**. Purified sdAb 2C with the expected molecular mass of ≈15 kDa was detected by Coomassie blue staining (**Figure 3A**, line 3) and antibody was recognized by anti-c-Myc Ab on Western blot (**Figure 3A**, line 4). The yield of production of 2C was 1418 µg from 50 ml of culture, (Results obtained with 7E are not shown).

Specificity of Single Domain Antibodies by ELISA

The recognition of the Ag85Bp/HLA-A*0201 complex by sdAb 2C was evaluated by ELISA, using Esat-6p/HLA-A*0201 and Acr1p/HLA-A*0201 as non-targets. The results are shown in **Figure 3B**. The binding of sdAb 2C to Ag85Bp/HLA-A*0201 complex was highly specific, showing statistically significant differences with respect to non-targed complexes. On the other hand, sdAb 7E, showed a nonspecific signal absorbance ratios for both target and non-target complexes (Results not shown).

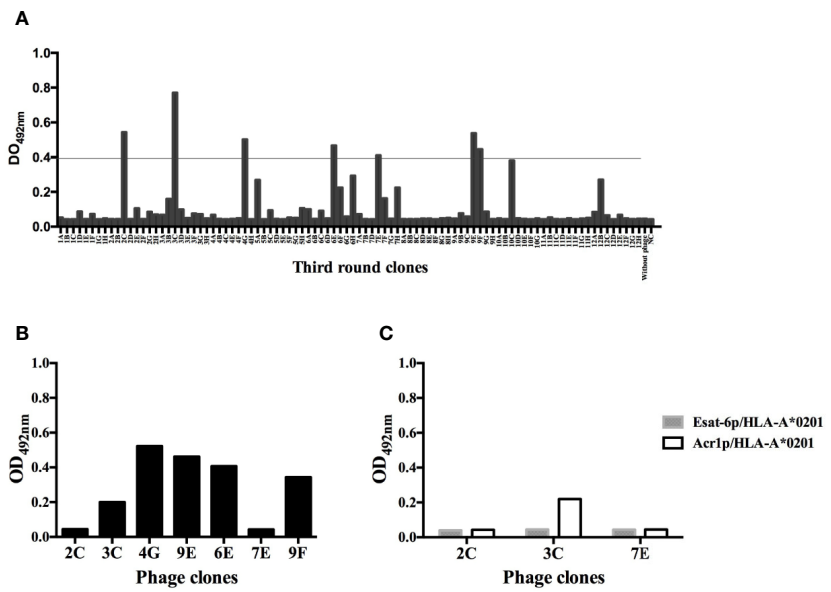

FIGURE 2 | Monoclonal phage-domain Immunoassay. **(A)** Clones from the third round of panning. Positives clones showed signal recognition to Ag85Bp/HLA-A*0201 of 10 fold higher than negative control (NC), well with unrelated sdAb. Line indicates the threshold used to define a positive result. **(B)** Positive clones exposed to streptavidin coated plates (without complex). **(C)** Clones 2C, 3C, and 7E that showed the lowest recognition signal towards streptavidin tested with non-target peptides.

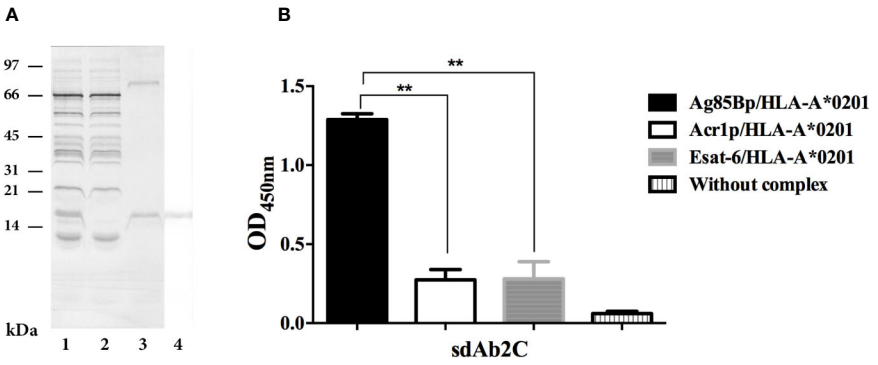

FIGURE 3 | Expression, purification and specificity evaluation of sdAb 2C. **(A)** Lanes 1 to 3. Line 1, Coomassie blue stained of periplasmatic extract. Line 2, unbound fraction to protein A sepharose column. Line 3, purified domain. Lane 4, Western blot of purified sdAb 2C recognized by anti-c-Myc Ab. **(B)** Evaluation of specificity of sdAb 2C by ELISA with target Ag85Bp/HLA-A*0201 and non-target (Esat-6p/HLA-A*0201 and Acr1p/HLA-A*0201) complexes. The results represent 3 independent experiments and significant differences are indicated by asterisk ($p < 0.05$).

Ex Vivo Specificity of Soluble Domain 2C on T2 Cells Surface

Surface expression of HLA-A molecules in T2 cells was demonstrable by binding of the W6/32 mAb in absence and in presence of either $Ag85Bp_{199\text{-}207}$ or $Esat\text{-}66_{p82\text{-}90}$ peptides (**Supplementary Figure S1**). However, sdAbs 2C showed different recognition patterns, whereby the sdAb 2C fluorescence signal was observed only on T2 cells exposed to the $Ag85Bp_{199\text{-}207}$ (**Figure 4**). About 6.4% of positive events were observed, but no positive signals were detected without sdAb 2C, or without $Ag85Bp_{199\text{-}207}$, or by incubation with the no-target Esat-6 peptide.

sdAb 2C Binding Affinity by Biolayer Interferometry

The association of sdAb 2C to Ag85Bp/HLA-A*0201 was measured by BLI. The affinity constant was calculated in terms of equilibrium dissociation constant (K_D) to be 15 + 0.20 μM (**Figure 5A**). The sdAb interacts with the target complex in a concentration dependent manner and confirms the dissociation constant value (**Figure 5B**). The interaction of sdAb with Esat-6p/HLA-A*0201 was very low and the binding parameters could not be determined.

DISCUSSION

CD8+ T cells recognizing peptide epitopes bound to MHC/HLA class I molecules have the capacity to lyse the *M. tuberculosis* infected cells, thus contributing to the intracellular killing of the infecting organisms (16). Hence, binding of antibodies with TCR-like recognition specificity seemed desirable for developing antibody constructs, with mycobactericidal potentials. TCR-like Ab recognizing MHC class I bound antigenic peptides on antigen presenting cells, have previously been reported for the treatment of cancer, viral infections and autoimmune diseases (6). The aim toward TB immunotherapy has recently been initiated by the selection of antibodies against the latency expressed Acr1/HLA class I restricted epitopes (14, 15). We report here on a TCR-like sdAb against an immunodominant HLA-A*0201 binding epitope of the Ag85B, selected by screening and selection from a human DAb phage display library. The secreted, fibronectin binding, mycolyl transferase protein is a strong immunogen in both infected and active TB cases and it has been used in several recombinant vaccine constructs (32–35). We chose the $_{p199}$KLVANNTRL$_{207}$ peptide as the target epitope in this study, because its known immunodominance for the human CD8+ T cell responses in the context of HLA-A*0201 and it's a conserved sequence in the genome (16, 17, 19). These properties favoured the previous application of TCR-like sdAbs for targeting tumors and cells infected with other pathogens (36, 37).

The procedures used for the selection and evaluation of TCR-like sdAbs ensure the specificity of recognition between for the target and non-target molecules. In this work, all the biotinylated complexes were first evaluated through a comparative ELISA, using plates with or without streptavidin. The results showed that the streptavidin coated plates ensured an adequate arrangement and orientation of p/HLA-A complexes, which is necessary for finding the specific TCR-like sdAbs. Similarly, Ag85Bp/HLA-A*0201 was bound to magnetic pearl cover with streptavidin for the selection of recombinant phages (26). From the third-round of selection, clones, 2C and 3C of identical sequence and clone 7E bound to the target complex. However, after conversion to the soluble form, sdAb 7E lost its specificity for the target complex. Such a change in specificity was previously reported to be due to loss of structural support by the phage scaffold pIII protein for the anti-H1N1 influenza virus antibody's antigen-binding site (38). The production of sdAb 2C and 7E in *E. coli* HB2151 from periplasmatic extracts was satisfactory, compared with the previously reported production outputs (25, 39).

Although sdAb 2C was highly specific against the target complex, its affinity is low, i.e., in the range of 1–100 μM

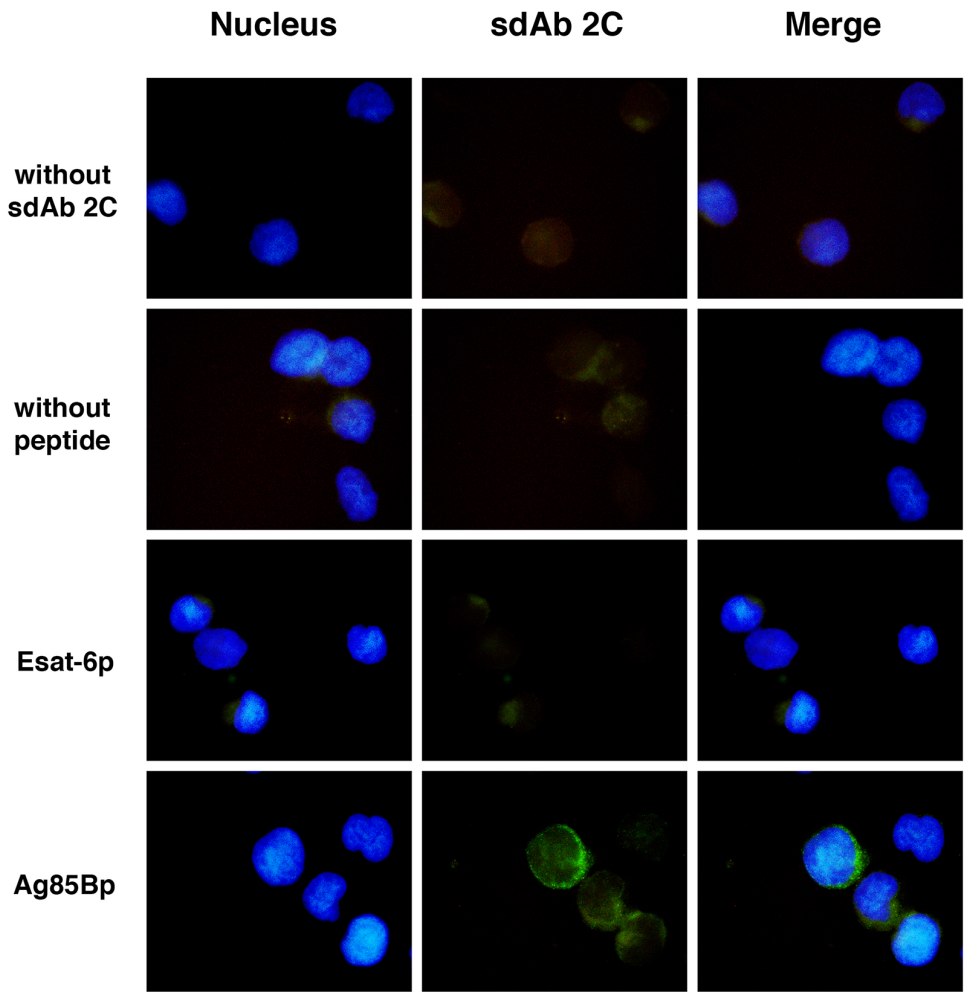

FIGURE 4 | Recognition of *M. tuberculosis* peptide/HLA-A*0201 complex on T2 cells surface by sdAb 2C. Cells were exposed to Ag85B and Esat-6 peptides. As negative control cells without peptide were used. Peptide/HLA-A*0201complexes were detected with sdAb 2C follow by anti-IgG coupled to Alexa Fluor 488 as secondary Ab. More than 200 fields were examined for each condition using the 100x magnification, by fluorescence microscopy.

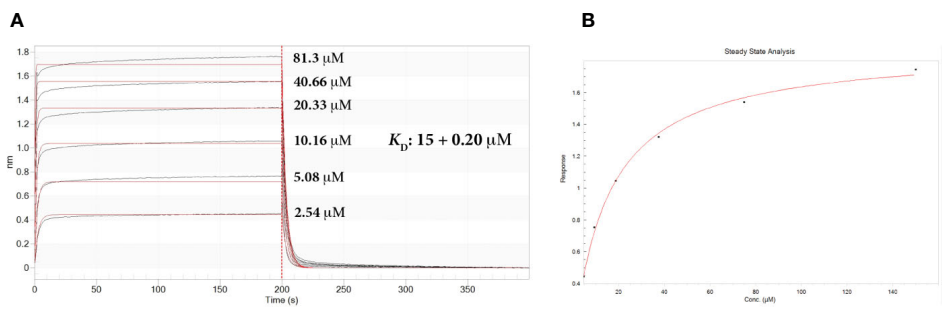

FIGURE 5 | Real-time biolayer interferometry sensorgrams for determination of the binding affinity. **(A)** Sensorgram showing reference substrate binding, on streptavidine biosensors, of Ag85Bp/HLA-A*0201 complex with increased concentrations of sdAb 2C. Calculated affinity constant K_D is shown in the upper right of the sensorgram. Association constant, k_a: 1.93 × 10^4 + 0.02 × 10^4 M^{-1} s^{-1}; dissociation constant, k_d: 0.289 + 0.003 s^{-1}. **(B)** Steady state analysis of the binding response (nm) as a function of sdAb. Calculated K_D 15.0 + 0.7 µM.

corresponding to the affinity binding interaction of TCR ligands. The low binding affinity known for TCR-like antibody fragments selected from human libraries can be improved using complementary technologies (40). An increased up to 100 fold of the initial affinity from scFv (single chain variable fragment) directed against the HLA-A2-pWT1$_{126}$ complex, was achived by mutagenesis combined with yeast display based on one specific scFv-clone (41). The affinity could also be improved by re-cloning and re-selection of clones or by conversion of sdAbs into multivalent formats with higher avidity (4, 42). Though antibody affinity can be significant for its potential for immunotherapy, most interestingly however, it was found that low, rather than high antibody affinity has been reported to essential for the passive antibody therapy of a drosophila based model of Alzheimer's disease (43, 44). This was interpreted on the grounds that the low affinity anti-tau antibody may loosen up intracellular tau aggregates allowing better access of lysosomal degrading enzymes, while high affinity antibody may make these aggregates more compact and therefore more difficult to degrade. Such interpretation may be relevant also for the desired intracellular mycobactericidal action on *M. tuberculosis* infected macrophages.

Antibodies generated in animals against MHC-I recombinant tetramers are rarely TCR-like, because many of them recognize the α3 domain of MHC-I and β2 microglobulin (β2m) (5) and also due to the reduced stability of recombinant p/HLA-A complex (45). However, the phage display antibody libraries have the advantage that the fusion proteins are exposed on the surface of phage particles, and recombinant p/HLA-A complex targets can be used through several selection rounds (37). The structure of human sdAbs also known as nanobodies, used in the present work represents a single variable domain based on the VH3-23 germline segment heavy chain with synthetic diversity introduced by PCR mutagenesis into all tree complementary determining regions (24). They are highly stable, easily produced in large quantity by *E. coli*, they are of low immunogenicity, small size (15 kDa), and can be fused with multiple tags (46–48). Consequently, sdAbs have been used for virus detection (49–51), for imaging *in vivo*, mainly in cancer due to their bio distribution, high tumor penetrance and fast clearance from the blood circulation (52). The immunotherapeutic potentials include therapeutic targets in cancer (53), antagonism of angiogenesis (54) and acting as metastasis inhibitors.

CONCLUSIONS AND PERSPECTIVES

The TCR-like identity of the sdAb 2C has been validated by its specific recognition of Ag85Bp/HLA-A*0201 on the surface of human T2 cell line. It will be of further interest to test, if the sdAb 2C can detect the expression of the HLA-A*0201-bound Ag85B peptide on human macrophages, which contain either replicating or dormant *M. tuberculosis* infection. A positive result would justify further engineering of the sdAb 2C to become an immunotoxin, by conjugation with suitable apoptosis inducing ligands, i.e., *Pseudomonas* exotoxin A, Granzyme B or BH3 peptide (55, 56), in endeavour to develop a mycobactericidal immunotherapeutic agent.

Further, development of sdAb 2C will need evaluation in both HLA-A*0201 transgenic mice and in humans with active TB disease. The obtained results are showing the feasibility of selecting TCR-like sdAbs to other immunodominant epitopes of *M. tuberculosis* and their future development as potential immunotherapeutic adjuncts to the chemotherapy of TB.

DATA AVAILABILITY STATEMENT

The raw data supporting the conclusions of this article will be made available by the authors, without undue reservation.

AUTHOR CONTRIBUTIONS

CE and JI conceived and supervised the study. CE, PO, MS-M, and KF performed experiments. TO, KF, MS-M, and PO designed experiments, analyzed data, and provided new tools and reagents. CE, JI, and PO wrote the manuscript. All authors contributed to the article and approved the submitted versión.

ACKNOWLEDGMENTS

We thank Cristina Parada for technical assistance, the University program PASPA-UNAM for a scholarships to CE to take out a Sabbatical stay in the Center for Host-Microbiome Interactions at the Guy's Campus of King's College London. This project was funded by a Research Institutional program "NUATEI" from Instituto de Investigaciones Biomédicas UNAM, México and by the EC/H2020-PHC-2014/EMI-TB grant entitled: Eliciting Mucosal Immunity to Tuberculosis. PO is a PhD student from Doctorado en Ciencias Bioquímicas at Universidad Nacional Autónoma de México (UNAM), and has a scholarship from the Consejo Nacional de Ciencia y 417 Tecnología (CONACYT), (CVU/707238).

SUPPLEMENTARY MATERIAL

The Supplementary Material for this article can be found online at: https://www.frontiersin.org/articles/10.3389/fimmu.2020.577815/full#supplementary-material

SUPPLEMENTARY FIGURE 1 | Recognition of HLA-A molecules on T2 cell surface. Cells were loaded with Ag85B and Esat-6 peptides and cells without peptide as negative control. HLA-A molecules were detected with W6/32 as primary Ab, by anti c-Myc Ab and anti IgG coupled to Alexa Fluor 488 as secondary Abs. More than 200 fields were observed for each condition evaluated using the 100x magnification, by fluorescence microscopy.

REFERENCES

1. World Health Organization. *Global tuberculosis report* (2018). Available at: https://www.who.int/es/news-room/fact-sheets/detail/tuberculosis (Accessed Jun 16, 2018).
2. Hoagland DT, Liu J, Lee RB, Lee RE. New agents for the treatment of drug-resistant *Mycobacterium tuberculosis*. *Adv Drug Deliv Rev* (2016) 102:55–72. doi: 10.1016/j.addr.2016.04.02
3. Pawlowski A, Jansson M, Sköld M, Rottenberg ME, Källenius G. Tuberculosis and HIV co-infection. *PLoS Pathog* (2012) 8(2):e1002464. doi: 10.1371/journal.ppat.1002464
4. Chames P, Hufton SE, Coulie PG, Uchanska-Ziegler B, Hoogenboom HR. Direct selection of a human antibody fragment directed against the tumor T-cell epitope HLA-A1-MAGE-A1 from a nonimmunized phage-Fab library. *Proc Natl Acad Sci* (2000) 97(14):7969–74. doi: 10.1073/pnas.97.14.796
5. Wittman VP, David W, Tiffany N, Francisca AN, Stephen W and Jon AW. Antibody targeting to a class I MHC-peptide epitope promotes tumor cell death. *J Immunol* (2006) 177:4187–95. doi: 10.4049/jimmunol.177.6.4187
6. Dahan R, Reiter Y. T-cell-receptor-like antibodies generation, function and applications. *Expert Rev Mol Med* (2012) 14:e6. doi: 10.1017/erm.2012.2
7. Saeed M, van BM, Zalba S, Schooten E, Rens JA, Koning GA, et al. Targeting melanoma with immunoliposomes coupled to anti-MAGE A1 TCR-like single-chain antibody. *Int J Nanomed* (2016) 11:955–75. doi: 10.2147/IJN.S96123
8. Porgador A, Yewdell JW, Deng Y, Bennink JR, Germain RN. Localization, quantitation, and in situ detection of specific peptide-MHC class I complexes using a monoclonal antibody. *Immunity* (1997) 6:715–26. doi: 10.1016/s1074-7613(00)80447-1
9. Cohen CJ, Sarig O, Yamano Y, Tomaru U, Jacobson S, Reiter Y. Direct phenotypic analysis of human MHC class I antigen presentation: visualization, quantitation, and in situ detection of human viral epitopes using peptide-specific, MHC-restricted human recombinant antibodies. *J Immunol* (2003) 170(8):4349–61. doi: 10.4049/jimmunol.170.8.4349
10. Denkberg G, Cohen CJ, Lev A, Chames P, Hoogenboom HR, Reiter Y. Direct visualization of distinct T cell epitopes derived from a melanoma tumor-associated antigen by using human recombinant antibodies with MHC-restricted T cell receptor-like specificity. *Proc Natl Acad Sci* (2002) 99 (14):9421–6. doi: 10.1073/pnas.132285699
11. Shams H, Klucar P, Weis SE, Lalvani A, Moonan PK, Safi H, et al. Characterization of a *Mycobacterium tuberculosis* peptide that is recognized by human CD4+ and CD8+ T cells in the context of multiple HLA alleles. *J Immunol* (2004) 173 (3):1966–77. doi: 10.4049/jimmunol.173.3.1966
12. Klein MR, Smith SM, Hammond AS, Ogg GS, King AS, Vekemans J, et al. HLA-B*35-restricted CD8 T cell epitopes in the antigen 85 complex of *Mycobacterium tuberculosis*. *J Infect Dis* (2001) 183(6):928–34. doi: 10.1086/319267
13. Lewinsohn DA, Winata E, Swarbrick GM, Tanner KE, Cook MS, Null MD, et al. Immunodominant tuberculosis CD8 antigens preferentially restricted by HLA-B. *PLoS Pathog* (2007) 13(9):1240–9. doi: 10.1371/journal.ppat.0030127
14. Dass SA, Norazmi MN, Dominguez AA, Miguel MESGS, Tye GJ. Generation of a T cell receptor (TCR)-like single domain antibody (sDAb) against a *Mycobacterium Tuberculosis* (Mtb) heat shock protein (HSP) 16kDa antigen presented by Human Leukocyte Antigen (HLA)-A*02. *Mol Immunol* (2018) 101:189–96. doi: 10.1016/j.molimm.2018.07.001
15. Dass SA, Norazmi MN, Acosta A, Sarmiento ME, Tye GJ. TCR-like domain antibody against *Mycobacterium tuberculosis* (Mtb) heat shock protein antigen presented by HLA-A*11 and HLA-A*24. *Int J Biol Macromol* (2020) 155:305–14. doi: 10.1016/j.ijbiomac.2020.03.229
16. Comas I, Chakravartti J, Small PM, Galagan J, Niemann S, Kremer K, et al. Human T cell epitopes of *Mycobacterium tuberculosis* are evolutionarily hyperconserved. *Nat Genet* (2010) 6:498–503. doi: 10.1038/ng.590
17. Axelsson –R, Loxton AG, Walzl G, Ehlers MM, Kock MM, Zumla A, et al. Broad profile of co-dominant epitopes shapes the peripheral *Mycobacterium tuberculosis* specific CD8+ T-cell immune response in South African patients with active tuberculosis. *PLoS One* (2013) 3:e58309. doi: 10.1371/journal.pone.0058309
18. Geluk A, van Meijgaarden KE, Franken KL, Drijfhout JW, D'Souza S, Necker A, et al. Identification of major epitopes of *Mycobacterium tuberculosis* AG85B that are recognized by HLA-A*0201-restricted CD8+ T cells in HLA-transgenic mice and humans. *J Immunol* (2000) 165(11):6463–71. doi: 10.4049/jimmunol.165.11.6463
19. Weichold FF, Mueller S, Kortsik C, Hitzler WE, Wulf MJ, Hone DM, et al. Impact of MHC class I alleles on the *M. tuberculosis* antigen-specific CD8+ T-cell response in patients with pulmonary tuberculosis. *Genes Immun* (2007) 8 (4):334–43. doi: 10.1038/sj.gene.6364392
20. Prezzemolo T, van Meijgaarden KE, Franken KLMC, Caccamo N, Dieli F, Ottenhoff, et al. Detailed characterization of human Mycobacterium tuberculosis specific HLA-E restricted CD8+ T cells. *Eur J Immunol* (2018) 48(2):293–305. doi: 10.1002/eji.201747184
21. Denkberg G, Cohen CJ, Segal D, Kirkin AF, Reiter Y. Recombinant human single-chain MHC-peptide complexes made from *E. coli* By in vitro refolding: functional single-chain MHC-peptide complexes and tetramers with tumor associated antigens. *Eur J Immunol* (2000) 30(12):3522–32. doi: 10.1002/1521-4141(2000012)30:12
22. Parham P, Barnstable CJ, Bodmer WF. Use of a monoclonal antibody (W6/32) in structural studies of HLA-A,B,C, antigens. *J Immunol* (1979) 23(1):342–9.
23. Mora GM de L, Duenas GA, Hernández MJ, De la Cruz HE, Pérez CE, Weiss SB, et al. Up-regulation of HLA class-I antigen expression and antigen-specific CTL response in cervical cancer cells by the demethylating agent hydralazine and the histone deacetylase inhibitor valproic acid. *J Transl Med* (2006) 4:55. doi: 10.1186/1479-5876-4-55
24. Lee CM, Iorno N, Sierro F, Christ D. Selection of human antibody fragments by phage display. *Nat Protoc* (2007) 2(11):3001–8. doi: 10.1038/nprot.2007.448
25. Abou El-Magd RM, Vozza NF, Tuszynski JA, Wishart DS. Isolation of soluble scFv antibody fragments specific for small biomarker molecule, L-Carnitine, using phage display. *J Immunol Methods* (2016) 428:9–19. doi: 10.1016/j.jim.2015.11.006
26. Santich BH, Liu H, Liu C, Cheung NK. "Generation of TCR-Like Antibodies Using Phage Display". In: G Houen, editor. *Methods in molecular biology*, vol. 1348 . New York: NY human Press (2015). p. 191–204.
27. Liu JL, Goldman ER, Zabetakis D, Walper SA, Turner KB, Shriver-Lake LC, et al. Enhanced production of a single domain antibody with an engineered stabilizing extra disulfide bond. *Microb Cell Fact* (2015) 14:158. doi: 10.1186/s12934-015-0340-3
28. DeMars R, Spies T. New genes in the MHC that encode proteins for antigen processing. *Trends Cell Biol* (1992) 3:81–6. doi: 10.1016/0962-8924(92)90077-z
29. Atzin-Méndez JA, López-González JS, Báez R, Arenas-Del Angel MC, Montaño LF, Silva-Adaya, et al. Expansion of quiescent lung adenocarcinoma CD8+ T cells by MUC1-8-mer peptide-T2 cell-β2 microglobulin complexes. *Oncol Rep* (2016) 1:33–42. doi: 10.3892/or.2015.4328
30. Bagheri S, Yousefi M, Safaie Qamsari E, Riazi-Rad F, Abolhassani M, Younesi V, et al. Selection of single chain antibody fragments binding to the extracellular domain of 4-1BB receptor by phage display technology. *Tumour Biol* (2017) 39 (3):1010428317695924. doi: 10.1177/1010428317695924
31. Zhang F, Chen Y, Ke Y, Zhang L, Zhang B, Yang L, et al. Single Chain Fragment Variable (scFv) Antibodies Targeting the Spike Protein of Porcine Epidemic Diarrhea Virus Provide Protection against Viral Infection in Piglets. *Viruses* (2019) 11(1):58. doi: 10.3390/v11010058
32. Kadir NA, Sarmiento ME, Acosta A, Norazmi MN. Cellular and humoral immunogenicity of recombinant *Mycobacterium smegmatis* expressing Ag85B epitopes in mice. *Int J Mycobacteriol* (2016) 5(1):7–13. doi: 10.1016/j.ijmyco.2015.09.006
33. Babaki M, Soleimanpour S, Rezaee SA. Antigen 85 complex as a powerful *Mycobacterium tuberculosis* immunogene: Biology, immune-pathogenicity, applications in diagnosis, and vaccine design. *Microb Pathog* (2017) 112:20–9. doi: 10.1016/j.micpath.2017.08.040
34. Horwitz MA, Harth G, Dillon BJ, Maslesa-Galic' S. Recombinant bacillus calmette-guerin (BCG) vaccines expressing the *Mycobacterium tuberculosis* 30-kDa major secretory protein induce greater protective immunity against tuberculosis than conventional BCG vaccines in a highly susceptible animal model. *Proc Natl Acad Sci U S A* (2000) 25:13853–8. doi: 10.1073/pnas.250480397
35. Olsen WA, van PLA, Meng OL, Birk RP, Andersen P. Protection of mice with a tuberculosis subunit vaccine based on a fusion protein of antigen 85b and esat-6. *Infect Immun* (2001) 5:2773–8. doi: 10.1128/IAI.69.5.2773-2778.2001

36. De Groeve K, Deschacht N, De Koninck C, Caveliers V, Lahoutte T, Devoogdt N, Muyldermans S, De Baetselier P, Raes G. Nanobodies as tools for in vivo imaging of specific immune cell types. *J Nucl Med* (2010) 51:782–9. doi: 10.2967/jnumed.109.070078
37. Ingram JR, Schmidt FI, Ploegh HL. Exploiting Nanobodies' Singular Traits. *Annu Rev Immunol* (2018) 36:695–715. doi: 10.1146/annurev-immunol-042617-053327
38. Kaku Y, Noguchi A, Okutani A, Inoue S, Tanabayashi K, Yamamoto Y, et al. Altered specificity of single-chain antibody fragments bound to pandemic H1N1-2009 influenza virus after conversion of the phage-bound to the soluble form. *BMC Res Notes* (2012) 5:483. doi: 10.1186/1756-0500-5-483
39. Ruano-Gallego D, Fraile GC, Fernández LÁ. Screening and purification of nanobodies from *E. coli* culture supernatants using the hemolysin secretion system. *Microb Cell Fact* (2019) 18(1):47. doi: 10.1186/s12934-019-1094-0
40. Høydahl L, Frick R, Sandlie I, Løset GÅ. Targeting the MHC Ligandome by Use of TCR-Like Antibodies. *Antibodies Basel* (2019) 8(2):32. doi: 10.3390/antib8020032
41. Zhao Q, Ahmed M, Tassev DV, Hasan A, Kuo TY, Guo HF, et al. Affinity maturation of T-cell receptor-like antibodies for Wilms tumor 1 peptide greatly enhances therapeutic potential. *Leukemia* (2015) 29(11):2238–47. doi: 10.1038/leu.2015.125
42. Zhu X, Wang L, Liu R, Flutter B, Li S, Ding J, et al. COMBODY: one-domain antibody multimer with improved avidity. *Immunol Cell Biol* (2010) 88 (6):667–75. doi: 10.1038/icb.2010.21
43. Krishnaswamy S, Huang HW, Marchal IS, Ryoo HD, Sigurdsson EM. Neuronally expressed anti-tau scFv prevents tauopathy-induced phenotypes in Drosophila models. *Neurobiol Dis* (2020) 137:104770. doi: 10.1016/j.nbd.2020.104770
44. Congdon E, Chukwu J, Shamir D, Deng J, Ujla D, Sait H, et al. Tau antibody chimerization alters its charge and binding, thereby reducing its cellular uptake and efficacy. *EBioMedicine* (2019) 42:157–73. doi: 10.1016/j.ebiom.2019.03.033
45. Cohen M, Reiter Y. T-Cell Receptor-Like Antibodies: Targeting the Intracellular Proteome Therapeutic Potential and Clinical Applications. *Antibodies* (2013) 2(3):517–34. doi: 10.3390/antib2030517
46. Salvador JP, Vilaplana L, Marco MP. Nanobody: outstanding features for diagnostic and therapeutic applications. *Anal Bioanal Chem* (2019) 411 (9):1703–13. doi: 10.1007/s00216-019-01633-4
47. Wang P, Li G, Yan J, Hu Y, Zhang C, Liu X, et al. Bactrian camel nanobody-based immunoassay for specific and sensitive detection of Cry1Fa toxin. *Toxicon* (2014) 92:186–92. doi: 10.1016/j.toxicon.2014.10.024
48. Mass DR, Sepulveda J, Pernthaner A, Shoemaker CB. Alpaca (Lama pacos) as a convenient source of recombinant camelid heavy chain antibodies (VHHs). *J Immunol Methods* (2007) 324(1-2):13–25. doi: 10.1016/j.jim.2007.04.008
49. Ma Z, Tianyu W, Zhiwei L, Xuyang G, Yangsheng T, Li Y, et al. A novel biotinylated nanobody-based blocking ELISA for the rapid and sensitive clinical detection of porcine epidemic diarrhea virus. *J Nanobiotechnol* (2019) 17(1):96. doi: 10.1186/s12951-019-0531-x
50. Gelkop S, Sobarzo A, Brangel P, Vincke C, Romão E, Fedida-Metula S, et al. The Development and Validation of a Novel Nanobody-Based Competitive ELISA for the Detection of Foot and Mouth Disease 3ABC Antibodies in Cattle. *Front Vet Sci* (2018) 5:250. doi: 10.3389/fvets.2018.00250
51. Zhu M, Gong X, Hu Y, Ou W, Wan Y. Streptavidin-biotin-based directional double Nanobody sandwich ELISA for clinical rapid and sensitive detection of influenza H5N1. *J Transl Med* (2014) 12:352. doi: 10.1186/s12967-014-0352-5
52. Oliveira S, Heukers R, Sornkom J, Kok RJ, van Bergen En Henegouwen PM. Targeting tumors with nanobodies for cancer imaging and therapy. *J Control Release* (2013) 172(3):607–17. doi: 10.1016/j.jconrel.2013.08.298
53. Ji L, Dong C, Fan R, Qi S. A high affinity nanobody against endothelin receptor type B: a new approach to the treatment of melanoma. *Mol Biol Rep* (2020) 47(3):2137–47. doi: 10.1007/s11033-020-05313-w
54. Ebrahimizadeh W, Mousavi SL, Javidan Z, Rajabibazl M. Production of Novel VHH Nanobody Inhibiting Angiogenesis by Targeting Binding Site of VEGF. *Appl Biochem Biotechnol* (2015) 176(7):1985–95. doi: 10.1007/s12010-015-1695-y
55. Rosenblum M. Immunotoxins and toxin constructs in the treatment of leukemia and lymphoma. *Adv Pharmacol* (2004) 51:209–28. doi: 10.1016/S1054-3589(04)51009-8
56. Walensky LD, Kung AL, Escher I, Malia TJ, Barbuto S, Wright RD, et al. Activation of apoptosis in vivo by a hydrocarbon-stapled BH3 helix. *Science* (2004) 305(5689):1466–70. doi: 10.1126/science.1099191

Conflict of Interest: The authors declare that the research was conducted in the absence of any commercial or financial relationships that could be construed as a potential conflict of interest.

frontiers in Immunology

ORIGINAL RESEARCH
published: 14 October 2020
doi: 10.3389/fimmu.2020.566710

A Direct Role for the CD1b Endogenous Spacer in the Recognition of a *Mycobacterium tuberculosis* Antigen by T-Cell Receptors

Frank Camacho[1], Ernesto Moreno[2], Luis F. Garcia-Alles[3], Glay Chinea Santiago[4], Martine Gilleron[5], Aleikar Vasquez[1], Yee Siew Choong[6], Fátima Reyes[1], Mohd Nor Norazmi[7]*, Maria E. Sarmiento[7]* and Armando Acosta[7]**

[1] Biologicals Sciences School, University of Concepcion, Concepcion, Chile, [2] Faculty of Basic Sciences, University of Medellin, Medellin, Colombia, [3] TBI, Université de Toulouse, CNRS, INRA, INSA, Toulouse, France, [4] Center for Genetic Engineering and Biotechnology, Havana, Cuba, [5] Institut de Pharmacologie et Biologie Structurale, Université de Toulouse, Toulouse, France, [6] Institute for Research in Molecular Medicine (INFORMM), Universiti Sains Malaysia, Minden, Malaysia, [7] School of Health Sciences, Health Campus, Universiti Sains Malaysia, Kubang Kerian, Malaysia

Lipids, glycolipids and lipopeptides derived from *Mycobacterium tuberculosis* (Mtb) are presented to T cells by monomorphic molecules known as CD1. This is the case of the Mtb-specific sulfoglycolipid Ac_2SGL, which is presented by CD1b molecules and is recognized by T cells found in tuberculosis (TB) patients and in individuals with latent infections. Our group, using filamentous phage display technology, obtained two specific ligands against the CD1b-Ac_2SGL complex: (i) a single chain T cell receptor (scTCR) from a human T cell clone recognizing the CD1b-AcSGL complex; and (ii) a light chain domain antibody (dAbκ11). Both ligands showed lower reactivity to a synthetic analog of Ac_2SGL (SGL12), having a shorter acyl chain as compared to the natural antigen. Here we put forward the hypothesis that the CD1b endogenous spacer lipid (EnSpacer) plays an important role in the recognition of the CD1b-Ac_2SGL complex by specific T cells. To support this hypothesis we combined: (a) molecular binding assays for both the scTCR and the dAbκ11 antibody domain against a small panel of synthetic Ac_2SGL analogs having different acyl chains, (b) molecular modeling of the CD1b-Ac_2SGL/EnSpacer complex, and (c) modeling of the interactions of this complex with the scTCR. Our results contribute to understand the mechanisms of lipid presentation by CD1b molecules and their interactions with T-cell receptors and other specific ligands, which may help to develop specific tools targeting Mtb infected cells for therapeutic and diagnostic applications.

Keywords: CD1b, *Mycobacterium tuberculosis*, sulfoglycolipids, Ac_2SGL, scTCR, endogenous spacer

Abbreviations: Ac_2SGL, 2-palmitoyl or 2-stearoyl-3-hydroxyphthioceranoyl-2′-sulfate-α-α'-d-trehalose; dAbκ11, domain antibody; EnSpacer, endogenous spacer that stabilizes the CD1b groove; Mtb, *Mycobacterium tuberculosis; scTCR, single chain TCR; TB, Tuberculosis*

OPEN ACCESS

Edited by:
Juraj Ivanyi, King's College London, United Kingdom

Reviewed by:
Gennaro De Libero, University of Basel, Switzerland
Patrick Brennan, Colorado State University, United States

***Correspondence:**
Ernesto Moreno
emoreno@udem.edu.co
Mohd Nor Norazmi
norazmimn@usm.my
Armando Acosta
armando@usm.my; aracosta2001@yahoo.com
Maria E. Sarmiento
mari@usm.my

Specialty section:
This article was submitted to Microbial Immunology, a section of the journal Frontiers in Immunology

Received: *28 May 2020*
Accepted: *10 September 2020*
Published: *14 October 2020*

Citation:
Camacho F, Moreno E, Garcia-Alles LF, Chinea Santiago G, Gilleron M, Vasquez A, Choong YS, Reyes F, Norazmi MN, Sarmiento ME and Acosta A (2020) A Direct Role for the CD1b Endogenous Spacer in the Recognition of a Mycobacterium tuberculosis Antigen by T-Cell Receptors. Front. Immunol. 11:566710. doi: 10.3389/fimmu.2020.566710

INTRODUCTION

Tuberculosis (TB) is a contagious disease mainly caused by *Mycobacterium tuberculosis* (Mtb) (1), being the leading cause of mortality due to infectious agents (1). The low sensitivity of diagnostic methods, the insufficient therapeutic coverage, the emergence of strains that are resistant to therapy, and the lack of an effective vaccine demand the development of new diagnostic and therapeutic approaches (2, 3).

Human leukocyte antigens (HLA), which are highly polymorphic (more than 26,000 alleles) (4, 5), present a variety of Mtb peptides to T-cells, which is considered a key element in the immune response against Mtb (6–8). On the other hand, lipids, glycolipids, and lipopeptides, are presented to T cells by the non-polymorphic CD1 molecules (9). Several Mtb lipid antigens are presented by CD1 molecules such as CD1a, CD1b, CD1c, and CD1d, increasing the breadth of the T-cell responses to Mtb (10–12).

A variety of Mtb lipid antigens are presented to T cells in association with CD1b (10–12). One mycobacterial antigen, in particular, belonging to the group of diacylated sulfoglycolipids and identified as 2-palmitoyl or 2-stearoyl-3-hydroxyphthioceranoyl-2′-sulfate-α-α'-d-trehalose (Ac_2SGL), was found to be expressed by virulent Mtb bacilli and presented by CD1b (13). This CD1b-Ac_2SGL complex was able to stimulate specific T cells found in TB patients and latently infected individuals, but not in healthy-tuberculin skin test (TST) negative individuals (13).

The process of identifying relevant Mtb antigens from purified lipid fractions carried out by Gilleron et al. (2004) (13) was based on the use of several CD1-restricted T cell clones from a healthy donor highly reactive to TST (13). One of these clones, named Z4B27, was specific for Ac_2SLG, thus allowing its identification as a novel Mtb antigen. The specificity of this clone, as well as the structural requirements conferring antigenicity to Ac_2SLG, were further studied using a panel of 17 synthetic analogs sharing the same sulfated trehalose head but differing in their lipid tails (14). Replacement of the multi-methyl-branched fatty acid by conventional fatty acids at the 3-position of the trehalose sulfate retained binding to CD1b but prevented T cell stimulation. Among the 17 synthetic sulfoglycolipids that were tested, the analog coded as SGL12 was one of the two most active, although with a lower potency as compared to the native antigen. The observed differences in T-cell stimulating capabilities were attributed to differences in length, methyl branches and stereochemistry between the acyl chains of these compounds (14).

CD1 molecules have a deep and hydrophobic antigen-binding groove that allow the presentation of large hydrophobic antigens (15). Among the members of the human CD1 family, CD1b shows the largest binding groove, capable of accommodating hydrophobic chains of about 70 carbons (16, 17). After biosynthesis, the integrity of the CD1b hydrophobic channels is maintained by association with endogenous phosphatidylcholine and a long endogenous spacer (EnSpacer). Together, these two lipids stabilize the CD1b groove (15).

The crystal structure of SGL12 in complex with CD1b [Protein Data Bank (PDB) entry 3T8X] (18) shows the sulfotrehalose head exposed on the binding groove, while the EnSpacer is fully embedded inside the CD1b internal channels. In this structure, the F' channel is closed due to a conformational rearrangement involving several binding groove residues, which prevents the EnSpacer from sliding outward (19). This, however, may not be the case for the natural Mtb sulfoglycolipid. While the synthetic analog SGL12 has a fixed-length lipid moiety, the Ac_2SGL antigen shows heterogeneous lengths, with its most abundant variant having a 32 carbon hydroxyphthioceranoic acid containing eight branched methyl groups. In contrast, the corresponding chain in SGL12 has 24 carbons in total, with only four branched methyl groups (14).

In consequence, presentation of the native Ac_2SGL antigen on CD1b most likely requires a repositioning of the EnSpacer.

The discovery of new specific ligands capable of specifically detecting Mtb-infected cells may contribute to the development of new diagnostic and therapeutic tools. On the other hand, the recognition of infected cells by ligands such as antibodies implies the recognition of Mtb-specific antigens presented on surface molecules such as HLA and CD1. In this sense, ligands recognizing HLA-Mtb-epitopes and CD1b-Mtb-lipids complexes have been reported (20–22), but the high polymorphism of the HLA molecules is a drawback for their use as universal markers for infected cells, so, antigens bound to the non-polymorphic CD1 molecules, offer an interesting alternative as universal markers of Mtb infected cells.

Using the phage display technology, our group obtained a single-chain T cell receptor (scTCR) construct, composed of the variable alpha and beta domains from the Z4B27 clone. This recombinant scTCR recognizes both the CD1b-Ac_2SGL and CD1b-SGL12 complexes, showing a higher reactivity for the complex with the natural antigen. The phage-displayed scTCR was also able to recognize Mtb-infected cells from a TB patient (23), showing the potential to become a diagnostic tool. Interestingly, a very similar behavior was found for a Vk (variable kappa) domain antibody fragment (dAbκ11) selected from a phage display library using CD1b-transfected cells loaded with Ac_2SGL (20).

Taken together, the experiments recapitulated here, both the functional studies, at the cellular level (using the Z4B27 clone, with cytokine-release assays) (13, 14, 24), and the binding studies at the molecular level (using the scTCR or dAbκ11 in ELISA studies) (20, 23), show a marked dependence between the acyl chain length and the TCR recognition of the CD1b-sulfoglycolipid complexes. On the other hand, and as pointed above, the crystal structure of the CD1b:SGL12 complex provides important clues on how a much larger acyl chain would push the EnSpacer, so much that it might not fit completely inside the CD1b channels. This, in turn, might directly affect the TCR binding event.

Here we put forward the hypothesis that the CD1b EnSpacer plays an important, direct role in the recognition of the CD1b-Ac_2SGL complex by specific T cells, and specifically by the scTCR derived from the Z4B27 clone. To give support to this hypothesis we first performed additional binding assays, for both

the scTCR and dAbκ11, against a small panel of synthetic Ac_2SGL analogs having different acyl chains, and then constructed a computer model of the CD1b-Ac_2SGL/EnSpacer complex, which was subsequently used for modeling of the interactions of this complex with the scTCR.

MATERIALS AND METHODS

CD1b:Lipid Complexes

Ac_2SGL, the synthetic analogs (SGL12, SL1, SL37, and SL38) and human sulfatide (hSulf), Avantis Polar Lipids (United States), were complexed in solution with recombinant human CD1b as described by Garcia-Alles et al. (18, 19).

Ligands

M13 phage displaying scTCR and a light chain κ domain antibody (dAbκ11) recognizing CD1b-Ac_2SGL were obtained as described by Camacho et al. (20, 23).

Enzyme-Linked Immunosorbent Assay

A 96-well Maxisorp microplate (Nunc, United States) was coated (16 h/4°C) with: (a) the anti-CD1b mAb BCD1b3.1 (Sigma, United States) to capture CD1b complexes and free CD1b; (b) the anti-CD1e mAb CD1e20.6 to capture the recombinant human CD1e. Both mAbs were diluted in carbonate-bicarbonate pH 9.6 coating buffer (3 μg/mL). The plate was then blocked with 3% PBS-skim milk (1 h/RT). Two washes (PBS-tween-20, 0.05%) were performed, and the complexes and free CD1b were added in PBS pH7.4 (1 μg/mL). After three washes (PBS-tween20, 0.05%), scTCR and dAbκ11, diluted in 3% PBS-skim milk (10^8 phages) were added and the plate was incubated for 1 h at RT. Subsequently, three washes were performed, and HRP/Anti-M13 monoclonal conjugate (GE, Healthcare, Life Sciences; diluted 1:5000 in 3% PBS-skim milk) was added. 1 h later, the plate was washed as above, TMB liquid substrate (Sigma, United States) was added, followed by incubation (10 min/RT). The reaction was stopped with 1 M sulfuric acid (Merck, Germany). Absorbance values (450 nm) were measured in a microplate reader (BioRad, United States). Each sample was studied in triplicate, and the experiment was repeated three times.

Statistical Analysis

Analysis of variance (ANOVA) was performed to compare absorbance values, and the Tukey multiple comparisons test was then performed to determine significant differences in the recognition of the different CD1b-lipid complexes by scTCR and dAbκ11. Statistical analyses were performed using GraphPad Prism version 4.0 (San Diego, California, United States).

Construction of the CD1b:Ac_2SGL:EnSpacer Complex

The program VMD v1.9.3 (25) was used for most modeling procedures. The crystal structure of the CD1b:SGL12 complex (19) (PDB entry 3T8X) was used as main template both for the protein and the lipid ligands. Most of the CD1b structure was in 3T8X was kept as is, with the exception of the backbone and side chain conformations of a group of residues surrounding the F' channel way out, which were copied from 1GZP (17). The program Avogadro v1.2 (26), was employed to modify the SGL12 structure into Ac_2SGL and to complete the modeled EnSpacer out of a fragment of the crystal spacer of 3T8X. Torsion angles in the Ac_2SGL acyl chain and in the EnSpacer were manipulated using the Molefacture plugin in VMD.

Construction of the CD1b:Ac_2SGL:EnSpacer Complex With the scTCR

The starting model for the scTCR was constructed with the Swiss Model Server (27), based on our manually curated alignment of the target and template sequences. The linker joining the alpha and beta chains was not modeled. The TCR of PDB entry 4EN3 was chosen among several possible templates because of the high percent of amino acid identity shown for both the alpha (88.7%) and beta (48.6%) variable domains. Then the full model of the CD1b:Ac_2SGL:EnSpacer:scTCR complex was assembled using the CD1b-TCR complex in 5WKI as template. The obtained models of CD1b:Ac_2SGL:EnSpacer and scTCR were superimposed on their protein counterparts in 5WKI using as reference atoms the alpha carbons of selected sequence segments corresponding to structurally conserved helices and/or beta sheet strands. The program CHARMM v43a1 (28) was used to run a one nanosecond (1 ns) molecular dynamics simulation at 400 K in vacuum only for the TCR, keeping fixed most of its structure and allowing to move selected CDR residues, including most of CDR3α and CDR3β. A representative conformation, sterically compatible with the lipid ligands, was then selected out from the collected 1,000 frames. The final model was obtained from a molecular dynamics simulation of the whole complex in a water box, aimed to refining the crude starting model and explore the intermolecular interactions.

RESULTS

Binding Data Shows a Decrease in Reactivity for Synthetic Analogs With Shorter Acyl Chains

To further assess the influence of different acyl chain lengths in recognition of the sulfotrehalose head by the scTCR, we used a panel of molecules consisting of the natural antigen Ac_2SGL and four synthetic analogs (**Figure 1A**). Their code names and the structures of their acyl chains are shown in **Figure 1A**. In three of the synthetic analogs (SL37, SGL12, and SL38), the acyl chain is tetramethylated, while in the SL1 analog it is completely linear.

Figure 1B shows the reactivity of the scTCR with these analogs presented on a recombinant CD1b receptor, as measured by enzyme-linked immunosorbent assay (ELISA). The natural antigen Ac_2SGL and the SL37 analog were recognized by the scTCR with the same strength. They both have acyl chains with the same length (32 carbons) but differing in the number of methyl branches (eight vs. four). Then we observed a

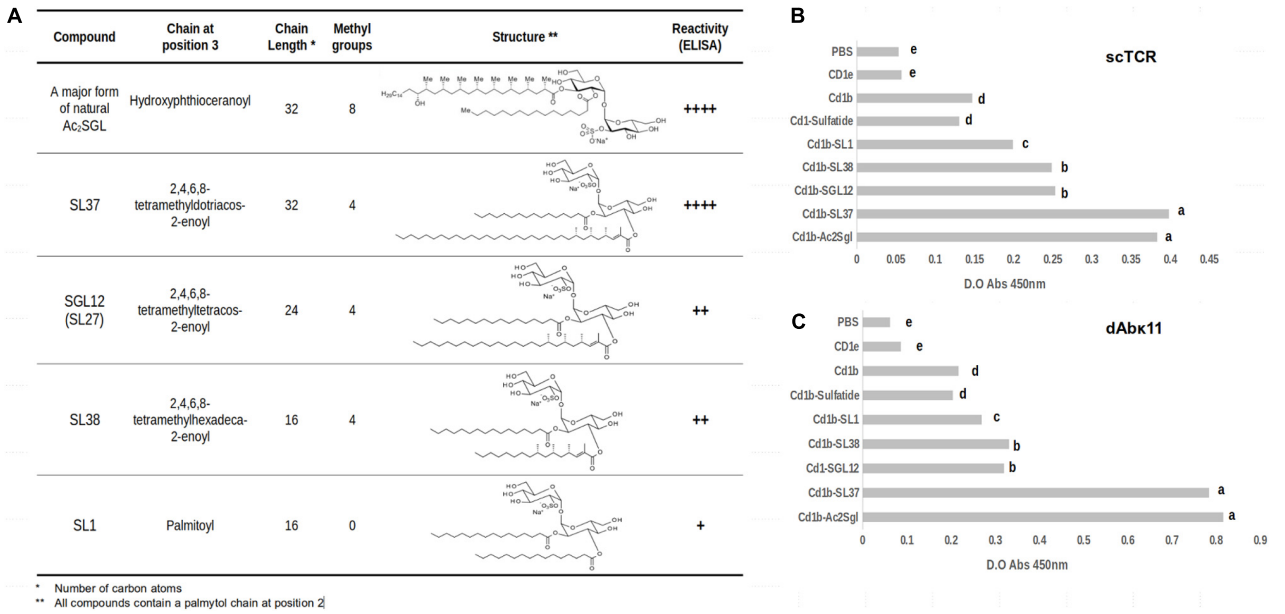

FIGURE 1 | Differential recognition of CD1b:Mtb lipid complexes by phage-displayed ligands. **(A)** Structures and characteristics of *M. tuberculosis* sulfoglycolipid (Ac_2SGL) and synthetic sulfoglycolipid analogs. **(B,C)** Recognition of CD1b:Mtb Ac_2SGL and its synthetic analogs complexes by the phage-displayed scTCR and dAbvk11 ligands, respectively, as measured by ELISA. The data represent the means of the absorbance values of three replicates +SD. Lowercase letters represent statistically significant differences.

marked decrease in reactivity for the SGL12 analog, whose acyl chain is tetramethylated as that of SL37 but is much shorter (24 carbons). Noteworthy, the crystal structure of SGL12 in complex with CD1b shows that three of the four methyl branches are exposed to the solvent on the CD1b binding groove, while the fourth branch is placed at the very entrance of the A' channel. Thus, taken together, these results suggest that the additional four methyl branches found in Ac_2SGL (namely in its most abundant variant), are inserted deeply in the A' channel and therefore have little or no influence in scTCR recognition. A further decrease in length of the acyl chain (down to 16 carbons, in SL38) but keeping the four methyl branches, did not have an additional effect in scTCR reactivity since the recognition levels for SGL12 and SL38 are practically the same. Finally, a further slight decrease in reactivity was observed for SL1, having a 16-carbon acyl chain, but completely linear.

A key point implicitly included in the above analyses is that the orientation of the sulfotrehalose head on the CD1b groove must be extremely similar for all these sulfoglycolipids. The reason for this is that the scTCR binds to all these antigens while docked to CD1b, which it does in a well conserved orientation, as discussed further below. In other words, in all these binding events the scTCR pocket that takes in the sulfotrehalose head is placed in the same conserved position on the CD1b groove. Curiously, the reactivity of the dAbκ11 antibody domain, which we tested here for binding to the same CD1b-bound synthetic analogs, followed the same pattern observed for the scTCR. However, the native antigen and SL37 were recognized with higher reactivity as compared to the rest of the analogs (**Figure 1C**).

These results led us to hypothesize that the cause behind the observed differences in recognition by the scTCR (and most likely also by dAbκ11) is a displacement of the EnSpacer due to the long fatty acid chain in Ac_2SGL and SL37, which forces the EnSpacer to protrude above the CD1b groove. The lipid presented this way, may interact with the TCR and, possibly, modulate its binding reactivity and the elicited immune response.

Analysis of EnSpacer Arrangement in CD1b Crystal Structures

We looked for CD1b crystal structures to investigate if any of them contained a protruding EnSpacer. A search in the PDB yielded 13 entries presenting different antigens (PDB codes: 1GZP, 1GZQ, 1UQS, 2H26, 3T8X, 5L2J, 5L2K, 5WKE, 5WKG, 5WKI, 5WL1, 6CUG, and 6D64); three of these entries contain CD1b-antigen complexes with T-cell receptors. The relatively small number of structures was tractable for individual visual inspection. None of the structures displayed the EnSpacer protruding above the level of the groove borders, namely above the level of the Tyr151 side chain (18). Moreover, several of these complexes showed a closed F' channel, holding the spacer completely buried.

Noteworthy, in one of the structures – 1UQS, CD1b in complex with glucose monomycolate (GMM) – the EnSpacer is absent because the long meromycolate chain of GMM spans all the way from the A' to the F' channel. In contrast, in the other 12 structures, the fatty acid chains are accommodated in the A' channel, with approximately half of them reaching up to the turn connecting the A' and T' channels. Compared to these

farther-reaching fatty acid chains, the end of the SGL12 acyl chain stays behind by about three carbon atoms. On the other hand, the EnSpacers modeled on the electronic density maps in these structures show different lengths, most of them between 34–40 carbon-atoms, except for the short lipids (≤26 carbons) seen in 5L2J, 5L2K, and 5WKI.

In summary, except for the large GMM antigen, EnSpacers of different lengths are lined up with the acyl chains of the other CD1 ligands along the T' and F' channels, without protruding above the CD1 binding groove. None of these acyl chains, however, is as long as the hydroxyphthioceranoic chain of Ac_2SGL.

Model of the CD1b:Ac_2SGL Complex With a Protruding EnSpacer

The fatty acid chain of the most abundant Ac_2SGL variant is 32-carbon long, which exceeds the length of the corresponding chain in SGL12 by eight carbons. If the sulfotrehalose head in both molecules adopts the same position on the CD1b binding groove, then the acyl chain of Ac_2SGL most likely enters the T' channel, displacing the EnSpacer toward the F' channel exit. To assess this effect, we constructed a homology model of the CD1b:Ac_2SGL complex, based mostly on the crystal structure of the CD1b:SGL12 complex (3T8X), with a few residues at the F' channel exit being modeled based on the crystal structure of the CD1b:GM2 complex [1GZP (17)].

Figure 2 shows the resulting model. As indicated above, the sulfotrehalose head of Ac_2SGL was kept in the same conformation and relative position as in the CD1b:SGL12 complex, therefore its interactions with the CD1b receptor are the same observed in the template structure. The hydroxyphthioceranoic chain of Ac_2SGL was built, as much as possible, on the SGL12 acyl chain, while the exceeding eight linear carbons were copied on the carbon chain of the crystal spacer (**Figure 2A**). Then we modeled a 40-carbon long EnSpacer, most of which (30 carbons) was built on the crystal spacer in 3T8X. The remaining 10 carbons were added following the stretched conformation observed in 1GZP as well as in several other CD1b structures. As expected, a six-carbon segment of the EnSpacer protrudes above the groove borders (**Figure 2B**). This segment was modeled bended over the closest trehalose ring. Still, because of its high flexibility, it may easily adopt other conformations, for example, bending over the hydrophobic patch formed by Phe84 and Leu147 at the F' channel way out. In any case, even for slightly shorter spacers, this extreme of the EnSpacer becomes exposed to possible interactions with T cell receptors.

A Model of the Complex of CD1b:Ac_2SGL:EnSpacer With the scTCR Shows Direct Participation of the EnSpacer in the Interaction

Having the model of the CD1b:Ac_2SGL:EnSpacer complex, we undertook the construction of a model of this molecular system in complex with the variable domains of the Ac_2SGL-specific scTCR derived from the Z4B27 clone. The three crystal structures of CD1b-antigen-TCR complexes deposited so far in the PDB 5L2K (29); 5WKI (30); and 6CUG (31) show that these TCRs are anchored on CD1b in a conserved orientation (31), which provides a reliable ground for homology modeling of the scTCR complex with CD1b:Ac_2SGL.

First, a model of the scTCR variable domains was constructed using the SwissModel server, after a careful selection of the TCR template (4EN3) and supervised alignment of its alpha and beta domain sequences with the corresponding scTCR sequences, aiming to produce an accurate model. Then, the models of the CD1b:Ac_2SGL:EnSpacer complex and the scTCR were superimposed on the corresponding CD1b and TCR molecules in PDB entry 5WKI, chosen as a template to assemble the full molecular model.

The obtained model needed some additional adjustments, in particular for the long CDRs 3 of both the alpha and beta variable regions, which play a principal role in the interaction with the presented antigen (31). While most of the scTCR structure, including CDRs 1 and 2 of both chains, could be modeled with confidence, the long and flexible CDRs 3 was built by the automated server in one its many possible conformations, in which these loops bump onto the trehalose head and the protruding EnSpacer. To explore the conformational space of both CDR3 loops for suitable binding geometries, we conducted a short (1 ns) molecular dynamics simulations in vacuum, in which the two CDRs 3 and a few amino acids at the tips of the other four CDRs were allowed to move, while the rest of the TCR structure remained fixed. From the collected ensemble of conformations (1,000 frames), we selected a representative geometry where both CDRs 3 embraced the trehalose and lipid heads. A final model was then obtained from a molecular dynamic simulation of the whole complex in a water box (**Figure 3**).

In the model, the sulfotrehalose head of Ac_2SGL fits well in a cavity formed mainly by CDR3α and CRD3β, with contributions also from CDR1β and CDR2β. The long and flexible CDR3β embraces the protruding segment of the EnSpacer together with a trehalose ring and its sulfate group and extends further over the CD1b surface (**Figure 2B**). On the opposite side, CDR3α covers the other trehalose ring and also the exposed part of the acyl chain containing the first three methyl branches. In general, the model provides a rational structural framework to explain the scTCR specificity.

DISCUSSION

The relevance of chain length and methylation of the fatty acids in Ac_2SGL synthetic analogs, regarding their capability to stimulate specific T-cell clones, has been demonstrated in several studies – longer acyl chains are more antigenic (14, 24). In this work, we propose and give support to a plausible structural explanation for these experimental findings, whose cornerstone is the direct participation of the EnSpacer, forced to protrude on the CD1b groove, in the interactions with T-cell receptors.

We selected a small panel of molecules consisting of the natural Mtb antigen Ac_2SGL and four synthetic analogs – three of them having tetramethylated acyl chains of different

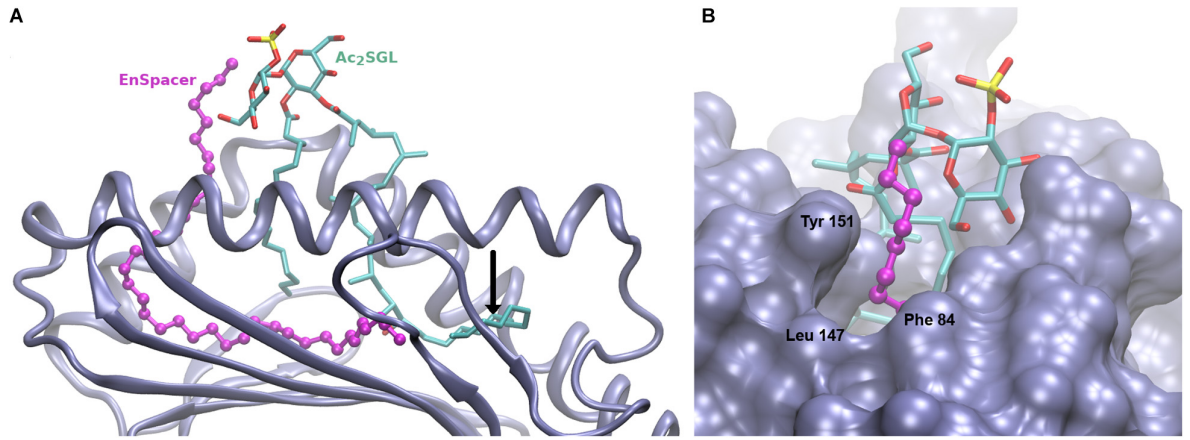

FIGURE 2 | Model of the CD1b:Ac_2SGL:lipid complex. **(A)** Overall view showing the Cd1b domains α1 and α2 (in ice blue cartoon), the Ac_2SGL antigen (in sticks, colored by atom type), and the 38-carbon endogenous lipid (in balls and sticks, magenta). The tail of the acyl chain of Ac2SGL makes a turn and enters into the T' channel, displacing the endogenous lipid. The vertical black arrow indicates the position that would be occupied by the last carbon atom of the 24-carbon long acyl chain of SGL2. The spacer in the CD1b:SGL12 crystal complex would then be positioned right after it, filling up the space occupied by the remaining Ac2SGL tail. **(B)** Zoom on the F' channel way out, showing the protruding extreme of the endogenous lipid above the binding groove. CD1b in molecular surface representation, Ac2SGL and the lipid as in panel **A**.

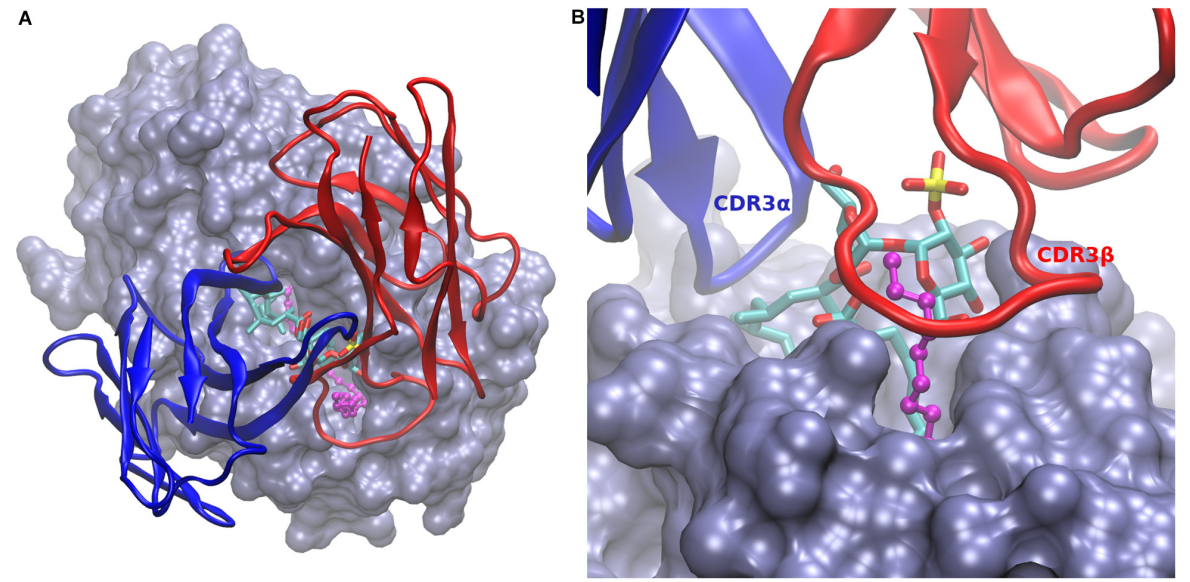

FIGURE 3 | Model of CD1b:Ac_2SGL:lipid in complex with the scTCR. **(A)** Overall view of the scTCR docked on top of the CD1b:Ac_2SGL:lipid complex. CD1b in ice blue molecular surface, Ac2SGL in sticks (colored by atom type), and the endogenous lipid in balls and sticks (magenta). The alpha (blue) and beta (red) TCR chains are represented in cartoon. **(B)** Zoom on the binding interactions from the TCR beta chain side. CDR3β (labeled in red) embraces the lipid together with the trehalose head, while CDR3α (labeled in blue) interacts with the sulfoglycolipid from the opposite side.

lengths (32, 24, and 16 carbons) and one analog having a 16-carbon linear chain – to further characterize the recognition capabilities of the recombinant scTCR derived from the CD1b-Ac_2SGL specific T cell clone Z4B27, in particular, its dependence on acyl chain length. In parallel, we also tested the antibody Vk domain dAbκ11. Our molecular panel included the SGL12 analog (C24, tetramethylated), previously tested for binding of both the scTCR and dAbκ 11.

As shown by Gau et al. (24), the length of tetramethylated fatty acyl chains is crucial for efficient T-cell activation – the longer the chain, the more stimulatory the analog. In fact, their synthetic analog 21c (32-carbon long) is almost identical to the SL37 analog used here, except for the saturation of the fatty acid, which was found to have no effect in the antigenic properties of the tested compounds (24). Our molecular binding assays showed a similar dependence on acyl chain length and methylation, found in previous cellular assays (14, 24).

By contrasting these binding and functional cellular-assays results with the available structural data, we inferred that a common EnSpacer (36–40 carbon long), when accommodated together with a long acyl chain (e.g., 32 carbon long), has to protrude above the F' channel way out. To support this hypothesis, we constructed a structural model of CD1b in complex with Ac_2SGL together with an average-length EnSpacer. A key result to back up our model was the observed equal binding of the scTCR and dAbκ11 to Ac_2SGL and SL37, which differ in their number of methyl branches but have the same acyl chain length. We interpreted this as a strong evidence that the trehalose units of both molecules are exposed in the same geometry on the CD1b binding groove. On the other hand, the acyl chains of both SL37 and SGL12 are tetramethylated, so they should accommodate themselves in practically the same way at the entrance of the A' channel.

Based on these experimental facts and arguments, we concluded that the sulfotrehalose heads of Ac_2SGL and SGL12 must be displayed on CD1b in the same spatial configuration and, therefore, the crystal structure of CD1b in complex with SGL12 (18) became an ideal template for homology modeling of the complex with Ac_2SGL. The model of the CD1b:Ac_2SGL:EnSpacer complex was built for the most abundant Ac_2SGL variant and for an EnSpacer of average length (38 carbons). Still, according to the model, any slightly shorter or longer EnSpacer (within a 36–40 carbon range), would have a carbon stretch protruding on the CD1b groove and exposed to T-cell receptors, together with the sulfoglycolipid.

Currently, no structural data is available on possible TCR interactions involving the EnSpacer, since in the three crystal structures of CD1b-antigen-TCR complexes deposited so far in the Protein Data Bank (29–31) the lipid is completely buried in the CD1b molecule. However, an inspection of these structures revealed that in all of them the CDR3β covers the F' channel exit, being in contact with CD1b amino acids at the closed end of the channel. Therefore, a protruding EnSpacer would most likely be in contact with CDR3β .

Our model of the whole CD1b:Ac_2SGL:EnSpacer:scTCR complex illustrates how such interactions may occur. The constructed model has strong as well as weak points. On the strong side: (a) the CD1b:Ac_2SGL component has a solid ground in the crystal structure of the CD1b:SGL12 complex; (b) most of the scTCR structure, specifically its framework and CDRs 1 and 2 of both the alpha and beta chains, could be reliably modeled based on highly similar in sequence TCR structures; and (c) the conserved TCR orientation observed in the CD1b-TCR crystal complexes (31) allowed a safe initial docking of the scTCR model onto the CD1b-antigen complex. On the other side, the weak points of the model are mainly two: (a) the conformations of the highly flexible backbones of the two long CDRs 3 (alpha and beta) and their side chains cannot be modeled with confidence; and (b) the protruding segment of the EnSpacer is highly flexible, making difficult to predict its right complexed conformation. But in spite of the uncertainties, inherent to most computer models of protein-protein complexes (32) the model of the CD1b:Ac_2SGL:EnSpacer:scTCR complex shows that even a short protruding segment of the EnSpacer would interact with the CDR3β of the scTCR and, most likely, with other Ac_2SGL-specific T-cell receptors as well.

CONCLUSION

In this study, we describe the interactions of Ac_2SGL with CD1b and provide support to the hypothesis that its long acyl chain forces the direct engagement of the EnSpacer in TCR recognition. These results contribute to understanding the mechanisms of lipid presentation by CD1b molecules and their interactions with T-cell receptors and other specific ligands, which will help to develop specific tools targeting Mtb infected cells for therapeutic and diagnostic applications.

DATA AVAILABILITY STATEMENT

The original contributions presented in the study are included in the article/Supplementary material, further inquiries can be directed to the corresponding author/s.

AUTHOR CONTRIBUTIONS

All authors have read and approved the manuscript and contributed significantly to this work.

FUNDING

This work was supported by LRGS Grant 203.PPSK.67212001 and 203.PPSK.67212002 (Ministry of Higher Education, Malaysia).

ACKNOWLEDGMENTS

Our group appreciate the contribution of Jacques Prandi in the preparation of the synthetic SGLs.

REFERENCES

1. World Health Organization. *Global Tuberculosis Report Geneva:(2019)*. Geneva: World Health Organization (2019).
2. Floyd K, Glaziou P, Zumla A, Raviglione M. The global tuberculosis epidemic and progress in care, prevention, and research: an overview in year 3 of the End TB era. *Lancet Respirat Med.* (2018) 6:299–314. doi: 10.1016/s2213-2600(18)30057-2
3. Acharya B, Acharya A, Gautam S, Ghimire SP, Mishra G, Parajuli N, et al. Advances in diagnosis of Tuberculosis: an update into molecular diagnosis of *Mycobacterium tuberculosis*. *Mol Biol Rep.* (2020) 47:4065–75. doi: 10.1007/s11033-020-05413-7
4. Hurley CK. Naming HLA diversity: a review of HLA nomenclature. *Hum Immunol.* (2020). doi: 10.1016/j.humimm.2020.03.005 (in press).
5. Robinson J, Guethlein LA, Cereb N, Yang SY, Norman PJ, Marsh SG, et al. Distinguishing functional polymorphism from random variation in

the sequences of> 10,000 HLA-A,-B and-C alleles. *PLoS Genet.* (2017) 13:e1006862. doi: 10.1371/journal.pgen.1006862
6. Scriba TJ, Coussens AK, Fletcher HA. Human immunology of tuberculosis. *Microbiol Spectr.* (2017) 5:213–37. doi: 10.1128/9781555819569.ch11
7. Sia JK, Rengarajan J. Immunology of *Mycobacterium tuberculosis* infections. *Gram Positive Pathogens.* (2019) 7:1056–86. doi: 10.1128/9781683670131.ch64
8. Bettencourt P, Müller J, Nicastri A, Cantillon D, Madhavan M, Charles PD, et al. Identification of antigens presented by MHC for vaccines against tuberculosis. *NPJ Vaccines.* (2020) 5:1–14. doi: 10.1038/s41541-019-0148-y
9. Chancellor A, Gadola SD, Mansour S. The versatility of the CD 1 lipid antigen presentation pathway. *Immunology.* (2018) 154:196–203. doi: 10.1111/imm.12912
10. Mori L, De Libero G. Presentation of lipid antigens to T cells. *Immunol Lett.* (2008) 117:1–8. doi: 10.1016/j.imlet.2007.11.027
11. Van Rhijn I, Moody DB. CD 1 and mycobacterial lipids activate human T cells. *Immunol Rev.* (2015) 264:138–53. doi: 10.1111/imr.12253
12. Lepore M, Mori L, De Libero G. The conventional nature of non-MHC-restricted T cells. *Front Immunol.* (2018) 9:1365. doi: 10.3389/fimmu.2018.01365
13. Gilleron M, Stenger S, Mazorra Z, Wittke F, Mariotti S, Böhmer G, et al. Diacylated sulfoglycolipids are novel mycobacterial antigens stimulating CD1-restricted T cells during infection with *Mycobacterium tuberculosis*. *J Exp Med.* (2004) 199:649–59. doi: 10.1084/jem.20031097
14. Guiard J, Collmann A, Garcia-Alles LF, Mourey L, Brando T, Mori L, et al. Fatty acyl structures of *Mycobacterium tuberculosis* sulfoglycolipid govern T cell response. *J Immunol.* (2009) 182:7030–7. doi: 10.4049/jimmunol.0804044
15. Garcia−Alles LF, Versluis K, Maveyraud L, Vallina AT, Sansano S, Bello NF, et al. Endogenous phosphatidylcholine and a long spacer ligand stabilize the lipid−binding groove of CD1b. *EMBO J.* (2006) 25:3684–92. doi: 10.1038/sj.emboj.7601244
16. Batuwangala T, Shepherd D, Gadola SD, Gibson KJ, Zaccai NR, Fersht AR, et al. The crystal structure of human CD1b with a bound bacterial glycolipid. *J Immunol.* (2004) 172:2382–8. doi: 10.4049/jimmunol.172.4.2382
17. Gadola SD, Zaccai NR, Harlos K, Shepherd D, Castro-Palomino JC, Ritter G, et al. Structure of human CD1b with bound ligands at 2.3 Å, a maze for alkyl chains. *Nat Immunol.* (2002) 3:721–6. doi: 10.1038/ni821
18. Garcia-Alles LF, Collmann A, Versluis C, Lindner B, Guiard J, Maveyraud L, et al. Structural reorganization of the antigen-binding groove of human CD1b for presentation of mycobacterial sulfoglycolipids. *Proc Natl Acad Sci USA.* (2011) 108:17755–60. doi: 10.1073/pnas.1110118108
19. Garcia-Alles LF, Giacometti G, Versluis C, Maveyraud L, de Paepe D, Guiard J, et al. Crystal structure of human CD1e reveals a groove suited for lipid-exchange processes. *Proc Natl Acad Sci USA.* (2011) 108:13230–5. doi: 10.1073/pnas.1105627108
20. Camacho F, Sarmiento ME, Reyes F, Kim L, Huggett J, Lepore M, et al. Selection of phage-displayed human antibody fragments specific for CD1b presenting the Mycobacterium tuberculosis glycolipid Ac2SGL. *Int J Mycobacteriol.* (2016) 5:120–7. doi: 10.1016/j.ijmyco.2015.12.002
21. Dass SA, Norazmi MN, Acosta A, Sarmiento ME, Tye GJ. TCR-like domain antibody against Mycobacterium tuberculosis (Mtb) heat shock protein antigen presented by HLA-A* 11 and HLA-A* 24. *Int J Biol Macromol.* (2020) 155:305–14. doi: 10.1016/j.ijbiomac.2020.03.229
22. Dass SA, Norazmi MN, Acosta A, Sarmiento ME, Tye GJ. Generation of a T cell receptor (TCR)-like single domain antibody (sDAb) against a Mycobacterium Tuberculosis (Mtb) heat shock protein (HSP) 16kDa antigen presented by Human Leukocyte Antigen (HLA)-A* 02. *Mol Immunol.* (2018) 101:189–96. doi: 10.1016/j.molimm.2018.07.001
23. Camacho F, Huggett J, Kim L, Infante JF, Lepore M, Perez V, et al. *Phage display of Functional αβ Single-Chain T-Cell Receptor Molecules Specific for CD1b: Ac 2 SGL Complexes From Mycobacterium Tuberculosis-Infected Cells, BMC Immunology*. London: BioMed Central (2013). p. S2. doi: 10.1186/1471-2172-14-S1-S2
24. Gau B, Lemétais A, Lepore M, Garcia-Alles LF, Bourdreux Y, Mori L, et al. Simplified deoxypropionate acyl chains for *Mycobacterium tuberculosis* sulfoglycolipid analogues: chain length is essential for high antigenicity. *ChemBioChem.* (2013) 14:2413–7. doi: 10.1002/cbic.201300482
25. Humphrey W, Dalke A, Schulten K. VMD: visual molecular dynamics. *J Mol Graphics.* (1996) 14:33–8. doi: 10.1016/0263-7855(96)00018-5
26. Hanwell MD, Curtis DE, Lonie DC, Vandermeersch T, Zurek E, Hutchison GR. Avogadro: an advanced semantic chemical editor, visualization, and analysis platform. *J Cheminform.* (2012) 4:17. doi: 10.1186/1758-2946-4-17
27. Waterhouse A, Bertoni M, Bienert S, Studer G, Tauriello G, Gumienny R, et al. SWISS-MODEL: homology modelling of protein structures and complexes. *Nucleic Acids Res.* (2018) 46:W296–303. doi: 10.1093/nar/gky427
28. Brooks BR, Brooks CL III, Mackerell AD Jr., Nilsson L, Petrella RJ, Roux B, et al. CHARMM: the biomolecular simulation program. *J Comput Chem.* (2009) 30:1545–614. doi: 10.1002/jcc.21287
29. Gras S, Van Rhijn I, Shahine A, Cheng T-Y, Bhati M, Tan LL, et al. T cell receptor recognition of CD1b presenting a mycobacterial glycolipid. *Nat Commun.* (2016) 7:1–12. doi: 10.1038/ncomms13257
30. Shahine A, Van Rhijn I, Cheng T-Y, Iwany S, Gras S, Moody DB, et al. A molecular basis of human T cell receptor autoreactivity toward self-phospholipids. *Sci Immunol.* (2017) 2:16. doi: 10.1126/sciimmunol.aao1384
31. Shahine A, Reinink P, Reijneveld JF, Gras S, Holzheimer M, Cheng T-Y, et al. A T-cell receptor escape channel allows broad T-cell response to CD1b and membrane phospholipids. *Nat Commun.* (2019) 10:1–12. doi: 10.1109/tmag.2013.2278570
32. Lensink MF, Velankar S, Wodak SJ. Modeling protein–protein and protein–peptide complexes: CAPRI 6th edition. *Proteins.* (2017) 85:359–77. doi: 10.1002/prot.25215

Conflict of Interest: The authors declare that the research was conducted in the absence of any commercial or financial relationships that could be construed as a potential conflict of interest.

frontiers in Immunology

ORIGINAL RESEARCH
published: 22 October 2020
doi: 10.3389/fimmu.2020.566319

Mycobacteria-Specific T Cells Are Generated in the Lung During Mucosal BCG Immunization or Infection With *Mycobacterium tuberculosis*

*Juan I. Basile†, Ruining Liu†, Wenjun Mou‡, Yu Gao, Berit Carow and Martin E. Rottenberg**

Department of Microbiology, Tumor and Cell Biology and Center for Tuberculosis Research, Karolinska Institutet, Stockholm, Sweden

Specific T cell responses are central for protection against infection with *M. tuberculosis*. Here we show that mycobacteria-specific CD4 and CD8 T cells accumulated in the lung but not in the mediastinal lymph node (MLN) at different time points after *M. tuberculosis* infection or BCG immunization. Proliferating specific T cells were found in the lung after infection and immunization. Pulmonary, but not MLN-derived CD4 and CD8 T cells, from *M. tuberculosis*-infected mice secreted IFN-γ after stimulation with different mycobacterial peptides. Mycobacteria-specific resident memory CD4 and CD8 T cells (TRM) expressing PD-1 accumulated in the lung after aerosol infection and intratracheal (i.t.) -but not subcutaneous (s.c.)- BCG immunization. Chemical inhibition of recirculation indicated that TRM were generated in the lung after BCG i.t. immunization. In summary, mycobacteria specific-TRM accumulate in the lung during i.t. but not s.c. immunization or *M. tuberculosis* infection. Collectively our data suggests that priming, accumulation and/or expansion of specific T cells during BCG immunization and *M. tuberculosis* infection occurs in the lung.

Keywords: *Mycobacterium tuberculosis*, T cell, lung, resident memory T cells, BCG- immunization

OPEN ACCESS

Edited by:
Rogelio Hernandez Pando, Instituto Nacional de Ciencias Médicas y Nutrición Salvador Zubirán (INCMNSZ), Mexico

Reviewed by:
Arshad Khan, University of Texas Health Science Center at Houston, United States
Mario Alberto Flores-Valdez, CONACYT Centro de Investigación y Asistencia en Tecnología y Diseño del Estado de Jalisco (CIATEJ), Mexico

****Correspondence:***
Martin E. Rottenberg
martin.rottenberg@ki.se

†These authors have contributed equally to this work

‡Present address:
Wenjun Mou, Laboratory of Tumor Immunology, Beijing Pediatric Research Institute, Beijing Children Hospital, Capital Medical University, Beijing, China

Specialty section:
This article was submitted to Microbial Immunology, a section of the journal Frontiers in Immunology

Received: *27 May 2020*
Accepted: *11 September 2020*
Published: *22 October 2020*

Citation:
Basile JI, Liu R, Mou W, Gao Y, Carow B and Rottenberg ME (2020) Mycobacteria-Specific T Cells Are Generated in the Lung During Mucosal BCG Immunization or Infection With Mycobacterium tuberculosis. Front. Immunol. 11:566319. doi: 10.3389/fimmu.2020.566319

INTRODUCTION

Tuberculosis (TB) is the leading cause of infectious death; in 2018, 10 million people developed and 1.5 million patients died from TB (1). The risk of developing TB increases during HIV and *Mycobacterium tuberculosis* co-infection, suggesting that impairment of T cell-mediated immune responses reactivates the asymptomatic infection.

The only TB vaccine, BCG (Bacille Calmette–Guérin) in use since 1921, offers substantial protection of infants against meningeal or miliary TB. However, protection against pulmonary TB in adults is not sufficient. The BCG vaccine, to a large extent and with some exceptions, mitigates only the most severe aspects of infection and exhibits a highly variable efficacy, especially in high-burden areas (2). Developing new and efficacious TB vaccines, a very effective intervention for containing the TB spread, is a critical unmet public health need (3).

The lung is the portal of entry for *M. tuberculosis* and experimental evidence indicates that local T-cell mediated immune defense mechanisms are crucial for successful bacterial control during latent infection with *M. tuberculosis*. Delivering a TB vaccine by aerosol to the respiratory mucosa, as a mimic of natural infection has been shown to augment protection of mice, guinea pigs and macaques as compared to immunization at a distal site (4–9). Following the classical paradigm naïve T cells will be activated in the draining mediastinal lymph nodes (MLNs) after *M. tuberculosis* infection or mucosal immunization. Activated T cells will then egress and migrate to the lung parenchyma for interaction with *M. tuberculosis*-infected phagocytes or differentiate into memory T cells that on re-exposure will mount a rapid and robust response to the pathogen (10). A subset of these, the resident memory cells T cell (T_{RM}) reside in the mucosal tissues including the lung and do not recirculate through the blood or the lymphatics (11). Positioned at the site of pathogen invasion, both CD4 and CD8 T_{RM} have been shown to contribute to the early clearance of pathogens such as influenza, LCMV, Sendai, RSV or herpex simplex viruses, or *Listeria sp*, *Yersinia sp,* and *Chlamydia sp* among others (12–17). T_{RM} are also generated after vaccination or infection with *M. tuberculosis* and have been shown play a role in protection (18). BCG-vaccinated mice sustained protection against *M. tuberculosis* infection even when egress of cells from the secondary lymphoid organs was blocked, suggesting that memory lymphocytes retained in the lung following vaccination were sufficient for protection (19, 20).

Here, we compared the generation of T cells in the lung and MLNs after infection and mucosal and distal BCG immunization. Contrary to expectations, mucosal BCG-vaccination and *M. tuberculosis* infection generated high levels of mycobacteria-specific T cells in the lung, specific T cells remained undetected or very low in the draining mediastinal lymph nodes at all time points tested. Mycobacteria-specific CD4 and CD8 T_{RM} were generated after aerosol *M. tuberculosis* infection and intratracheal (i.t.), but not subcutaneous (s.c.), BCG immunization. Moreover, T_{RM} accumulated in the lung in absence of lymphoid circulation after i.t. BCG immunization, altogether suggesting that upon mucosal immunization or infection mycobacteria specific T cells are generated in the lung. Our data strongly supports mucosal delivery for induction of protective adaptive immune responses against *M. tuberculosis*.

MATERIALS AND METHODS

Ethics Statement

The animals were housed and handled at the Department of Microbiology, Tumor and Cell Biology and the Astrid Fagreus Laboratory, Karolinska Institutet, Stockholm, according to directives and guidelines of the Swedish Board of Agriculture, the Swedish Animal Protection Agency, and the Karolinska Institute (djurskyddslagen 1988:534; djurskyddsförordningen 1988:539; djurskyddsmyndigheten DFS 2004:4). The study was performed under approval of the Stockholm North Ethical Committee on Animal Experiments permit number N397/13 and N487/11. Animals were housed under specific pathogen-free conditions.

Mice, Infection, and Infectivity Assay

BCG Montreal and *M. tuberculosis* Harlingen were grown in Middlebrook 7H9 (Difco, Detroit, MI) supplemented with albumin, dextrose and catalase.

Eight-10 week-old C57BL/6J mice were used for immunizations or infections. Mice were infected with 250 *M. tuberculosis* Harlingen strain by aerosol during 20 min using a nose-only exposure unit (In-tox Products, Uppsala, Sweden) (21), or immunized s.c. or i.t. with 10^7 BCG.

The intratracheal aerosol administration was performed using a MicroSprayer® Aerosolizer—Model IA-1C and a FMJ-250 High Pressure Syringe (Penn-Century, Wyndmoor, PA), a device that generates a air-free plume of liquid aerosol directly into the lungs. The tip of the device was inserted near to the carina of the anesthetized animal and 50 μl of BCG suspension containing 10^7 CFUs was aerosolized into the lungs.

To determine viable numbers of CFUs at time-points post-infection, the right lung of each mouse was homogenized in PBS with 0.05% Tween 80. Ten-fold serial dilutions were made in 0.05% Tween 80 and plated onto Middlebrook 7H11 agar containing 10% enrichment of oleic acid, albumin, dextrose, catalase, 5 μg of amphotericin B per ml and 8 μg/ml polymyxin B grown for 3 weeks at 37°C. Colonies were counted 3 weeks after incubation at 37°C and CFUs determined.

Flow Cytometry and Intracellular Cytokine Staining

Lungs were removed, mechanically minced into small pieces and digested with 3 mg/ml Collagenase D and 30 μg/ml DNase I for 1 h at 37° C, and single-cell suspensions prepared by filtering lung tissue through 70-μm nylon cell strainers. To further remove impurities cells were loaded in 40/70% Percoll gradient in PBS and centrifuged for 30 min at room temperature. The cells at the interphase were collected and washed. Single spleen cell suspensions were obtained by mechanical disruption, lysis of erythrocytes and straining over a 70-μm nylon mesh. Single cell suspensions were obtained after mechanical disruption of the mediastinal lymph node followed by filtering over a 70-μm nylon mesh.

Lung, lymph node cells and spleen cells were stained for CD3, CD4, CD8, CD69, CD44, CD11a, CD103, PD-1, and KRLG-1 (all from eBioscience) for 30 min 4° C and fixed before acquisition.

To discriminate between tissue-localized and blood-borne cells in an intravascular staining was performed as previously described (22). In short, mice were inoculated i.v. with 3 μg of FITC-labeled anti-CD45.2 (clone 104 BD), sacrificed 3–5 min after i.v. innoculation, and lungs and MLN leukocytes isolated immediately as described. Peripheral blood was sampled for every mouse as a control.

Data were acquired on a LSRII Flow cytometry and analyzed with FlowJo software (Tree star Inc., Ashland, OR).

Tetramer Staining

MHCII tetramers containing amino acids 1–20 of *M. tuberculosis* ESAT-6 or 240-254 of Ag85B and the MHCI tetramer containing amino acids 4–11 TB10.4 (all from the NIH Tetramer Core Facility) were used for detection of *M. tuberculosis* -specific

murine CD4 or CD8 T cells. Single-cell lung or MLN suspensions were stained at saturating concentrations with the tetramers and incubated at 37°C for 1 h for the MHCII tetramers and at 4°C for 30 min for the MHCI tetramer.

Intracellular Cytokine Staining

For determination of IFN-γ-producing cells, lung and MLN cells from *M. tuberculosis* infected mice were incubated with either 5 μg/ml $ESAT6_{1-15}$, 5 μg/ml $TB10.4_{4-11}$, 20 μg/ml purified protein derivative (PPD) (Statens Serum Institut, Denmark), or 50 ng/ml phorbol myristate acetate (PMA) and 2 μg/ml ionomycin (Sigma) for 6 at 37°C. Brefeldin (10 μg/ml) was added to the cultures the last 4 h of stimulation. Cells were then stained with cell population-specific antibodies, and live/dead staining, fixed, permeabilized using leukocyte permeabilization reagent IntraPrep™ (Immunotech, Marseille, France) and further stained with anti-IFN-γ (eBioscience). Data were acquired on a LSRII Flow cytometry and analyzed with FlowJo software (Tree star Inc., Ashland, OR).

Antigen-Specific T Cell Labeling *in situ*

The detection of antigen-specific T cells *in situ* was performed modified to a previously described protocol (23). Briefly, sections (ca 200–400 μm) from lungs from *M. tuberculosis*-infected mice kept in PBS containing heparin (100 μg/ml) were obtained using a scalpel. Sections were blocked with 2% normal goat serum, 0.025% triton for 1 h, as all incubations steps at 4°C. After PBS washing, APC-labeled TB10.4 tetramers at a concentration of 0.5 μg/ml with 1% goat serum and 0.5 μg/ml rat anti-CD8a were added to slices and incubated for 4 h. Sections were washed in PBS and then incubated with biotinylated anti-APC Abs and secondary FITC anti-rat antibody both diluted 1:100 overnight. Sections were washed with PBS and then incubated with APC-conjugated streptavidin diluted 1:100 in PBS for 3 h together with DAPI. Slices were washed with PBS and then fixed with PBS-buffered 2% formaldehyde for 2 h at 4°C. Finally, sections were washed three times with PBS and then mounted to slides using Fluoromount™ Aqueous Mounting Medium. Stained sections were analyzed using a confocal microscope (Zeiss LSM 710).

Statistics

Statistical analysis and graphical representation of data were done using GraphPad Prism 8 software (Grah Pad Prism, San Diego, CA). We have used the Welch's *t*-test, which assumes normal distribution but can be used when the two samples have unequal variances for comparisons (*t*-test). Statistical significance between 3 and more groups was determined using one- or two-way ANOVA. The Welch's test was also used for ANOVA comparisons. We have used used the Turkey's multiple comparisons test or *t-test* with Holm-Sidak correction for multiple comparisons of the same parameters (for example for analyzing kinetics).

RESULTS

Mycobacteria-Specific T Cells Accumulate in the Lung but Not the Mediastinal Lymph Node During BCG Immunization or Infection With *M. tuberculosis*

We first compared the frequency and numbers of mycobacterial $Ag85B_{240-254}$ and $ESAT6_{1-20}$ tetramer-binding CD4 T cells and $TB10.4_{4-11}$-specific CD8 T cells in the lungs and MLN of *M. tuberculosis*-infected mice (**Figures 1A–C**). $TB10.4_{4-11}$-tetramer-binding CD8 T cells constituted ∼1/3 of the total CD44+ CD8 T cells and showed a distinct accumulation early after infection (**Figures 1B,C**). In comparison, Ag85B-specific CD4 T cells were ∼1% of the activated CD4 T cells, with a relatively more delayed accumulation after infection (**Figure 1B**), while ESAT6 tetramer-binding cells constituted more than 5% of activated CD4 T cells, with a relatively early increase early after infection (**Figures 1B,C**).

Surprisingly, Ag85B, ESAT6, and TB10.4 tetramer-binding T cells were either not observed or detected at very low frequencies in the MLN of mice at all times after *M. tuberculosis*-infection measured, despite the presence of high frequencies of T cells of the same specificities in the lung (**Figures 1A,B**).

CD4 and CD8 T cells were activated in the MLN after infection with *M. tuberculosis* as measured by the expression of CD44 as compared to uninfected controls (**Figure 1D**). However, the frequencies of activated CD4 or CD8 T cells were lower than those in the lungs (**Figure 1D**).

To further support this observation, the frequencies of IFN-γ-secreting CD4 and CD8 T cells in response to $ESAT6_{1-15}$ and $TB10.4_{4-11}$ peptide stimulation were evaluated in the lung and MLNs of *M. tuberculosis*-infected mice. Lung T cells from mice infected with *M. tuberculosis* secreted IFN-γ after stimulation with the ESAT6 and TB-10.4 peptides, while no IFN-γ responses were determined in T cells from lungs from non-infected mice (**Figures 2A–C**). CD4, but not CD8 T cells, responded to ESAT-6 peptide stimulation by producing IFN-γ. Instead, CD8 but not CD4 T cells showed substantial IFN-γ responses to TB10.4 peptide stimulation (**Supplementary Figure 1A**).

In contrast to the response observed by lung CD4 and CD8 T cells, MLN T cells showed low frequencies or undetectable levels of IFN-γ-secreting cells in response to peptide stimulation (**Figures 2A–C**). CD4 T cells from lungs but not MLNs from *M. tuberculosis*-infected mice secreted IFN-γ in the absence of peptide stimulation (**Supplementary Figure 1B**). IFN-γ secretion was neither detected in unstimulated lung CD8 T cells from *M. tuberculosis*-infected mice nor in CD4 T cells from uninfected mice (**Supplementary Figures 1B,C**). CD4 and CD8 T cells from lungs or MLN from infected or control mice secreted IFN-γ in response to PMA/ionomycin stimulation. However, both CD4 and CD8 T cells from lungs from *M. tuberculosis*-infected mice secreted higher levels of IFN-γ as compared to MLN cells from infected mice, or to lung or MLN T cells from uninfected controls (**Supplementary Figures 1D–F**).

To exclude that T cell specific for other mycobacterial antigens are present in the MLN, we compared the IFN-γ responses

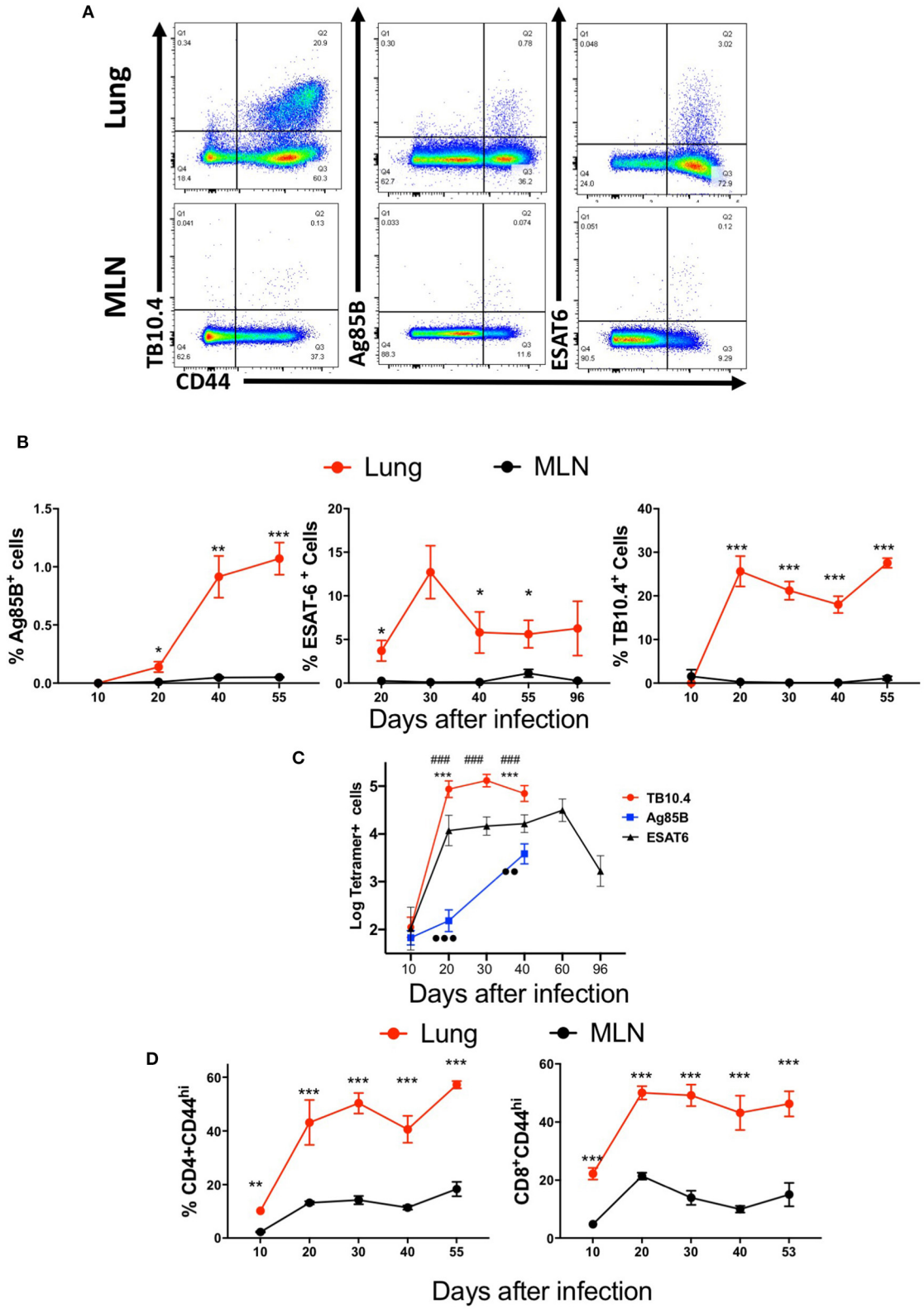

FIGURE 1 | Mycobacteria-specific T cells accumulate in the lung but not the mediastinal lymph node during immunization or infection with *M. tuberculosis*. C57BL/6 mice were infected via aerosol with 250 *M. tuberculosis*, and sacrificed at the indicated days after infection ($n \geq 5$ per time point). The T cell populations in lung and

(Continued)

FIGURE 1 | MLN were analyzed. **(A)** Representative dot plots of tetramer Ag85B, ESAT6, and TB10.4 binding T cells in the lungs and MLN from mice 40 days after infection with *M. tuberculosis* are depicted. **(B)** The mean percentage of tetramer Ag85B, ESAT6, and TB10.4 binding cells gated within the CD44+ CD4 and CD8 T cell populations in the lung or MLN from mice ($n \geq 5$ per time point) at different days after infection ± SEM are displayed. Differences in frequencies tetramer binding cells between lung and MLN at a given time point after infection are significant at $^{*}p \leq 0.05$, $^{**}p \leq 0.01$, and $^{***}p \leq 0.001$ (Welch's *t*-test with Holm-Sidak correction for multiple comparisons). **(C)** The mean $\log_1 0$ transformed number of tetramer^{+} Ag85B, ESAT6 and TB10.4 cells ± SD at the indicated days after aerosol infection with *M. tuberculosis.* Differences in cell numbers between *Ag85B and TB10.4; # TB10.4 and ESAT6; and •-Ag85B and ESAT6 are significant at $p < 0.01$ and $p < 0.001$ (2 or 3 symbols) were calculated using Welch's *t* test with Holm-Sidak correction for multiple comparisons. **(D)** The mean frequencies of CD44+ CD4 and CD8 T cells in the lung or MLN from mice at the indicated days after infection with *M. tuberculosis* are shown. Differences are significant at $^{**}p \leq 0.01$, and $^{***}p \leq 0.001$ (Welch's *t*-test with Holm-Sidak correction for multiple comparisons).

by lung and MLN T cells from *M. tuberculosis* infected mice stimulated with PPD were compared. PPD is a purified protein fraction isolated from culture media filtrates of *M. tuberculosis* that contains more than 300 different proteins (22, 24, 25). Lung CD4 and CD8 T cells but not MLN T cells produced IFN-γ in response to PPD stimulation (**Figures 2D,E**). The levels of IFN-γ secreted by MLN T cells stimulated with PPD were similar to those secreted by non-stimulated controls from infected mice (**Figure 2E**).

The frequency and expression levels of the proliferation marker Ki-67 in ESAT6 and TB10.4 tetramer-binding CD4 and CD8 T cells in the lung of *M. tuberculosis* infected mice were increased as compared with those in naïve T cells (**Figures 3A,B**). The frequency of cells non-tetramer binding activated CD4 and CD8 T cells was also increased compared to that of naïve T cells.

Moreover, the immunostaining of lung slices from *M. tuberculosis* infected mice with TB10.4 tetramer overlapped as expected with CD8 labeled cells and showed a clustered distribution in the lung lesions of infected mice. TB10.4 labeling was not observed in MLN sections of the same animal (**Figure 3C**, **Supplementary Figure 1G**).

Kinetics of Accumulation of Specific T_{RM} Cells in the Lungs of *M. tuberculosis*-Infected Mice

The frequency and numbers of pulmonary CD4 and CD8 T_{RM} during *M. tuberculosis* infection were then determined (**Figures 4A,B**). CD4 T_{RM} were distinguished from circulating T effector-memory cells based on upregulated expression of the early activation marker CD69 and the integrin CD11a (10, 26, 27), whereas CD8 T_{RM} were characterized by the expression of the αE integrin CD103 and CD69 (10). Lung T_{RM} were detected at all time points after 20 days of *M. tuberculosis* infection. While the number of mycobacteria-specific T_{RM} followed that of the total mycobacteria-specific T cells (**Figure 3C**), the frequencies and numbers of T_{RM} within the antigen-specific and total T cells showed important differences (**Figure 4D**, **Supplementary Figures 2A,B**). The frequencies of Ag85B and TB10.4-specific T_{RM} cells were higher than those of T_{RM} within tetramer-negative T cells. Instead, the frequency of ESAT6 tetramer-binding CD4 T_{RM} cells was lower than in the tetramer-negative population (**Figure 4D**). TB10.4 tetramer-binding T_{RM} constituted ca 50% of the total CD8 T_{RM} cell numbers in the infected lungs (**Supplementary Figures 2A,B**).

In order to further characterize the antigen-specific T cells induced locally in the lung during infection with *M. tuberculosis*, we measured the expression of the PD-1 and KLRG1. PD-1+ CD4 T cells have been shown to display proliferative and protective capacity and residence in the lung parenchyma after *M. tuberculosis* infection, while KLRG1 associated with short-lived terminally differentiated effector cells (28–30). The expression of KRLG1 in mycobacteria-specific T cells peaked at 3 weeks after infection and decreased thereafter (Figure 3E). Most T_{RM} cells in the lung did not express KRLG1 (**Supplementary Figure 2C**). The frequency of PD1+ Ag85B and TB10.4-specific CD4 and CD8 T cells increased during infection with *M. tuberculosis* and remained elevated at the late time points of infection (**Figure 4E**).

In order to confirm that CD8 and CD4 T_{RM} are bona fide parenchymal resident cells we performed intravascular labeling with anti-CD45.2 mAb. Mice were sacrificed 3–5 min after inoculation. Lymph nodes leukocytes remained unlabeled, all blood leukocytes were labeled by anti CD45.2 and ∼50% of lung leukocytes were labeled (**Supplementary Figure 2D** and not shown). Approximately 70% of CD4 and CD8 T cells from mice 30 days after infection with *M. tuberculosis* resided in the lung parenchyma (**Figure 2E**). While most tetramer ESAT6 binding CD4 T cells located in the parenchyma while TB10.4 tetramer labeled cells localized both in the vasculature and the parenchyma, indicating a skewed distribution of the mycobacterial specific T cells (**Figures 4F,G**). As expected, both CD4 and CD8 T_{RM} (total and tetramer TB10.4 binding cells) located in the lung parenchyma (**Figures 4H,I**, **Supplementary Figures 2F,G**). Thus, CD8 and CD4 T_{RM} are bona fide parenchymal resident cells.

Mycobacteria-Specific T Cells Accumulate in the Lung but Not the Mediastinal Lymph Node After Mucosal BCG Immunization

We then compared the kinetics of generation of mycobacteria-specific T cells in the lung and the MLN of mice 3 weeks after either i.t. or s.c. BCG immunization.

We found that the i.t. immunization induced a higher number of mycobacterial $Ag85B_{240-254}$ and $TB10.4_{4-11}$ tetramer-binding CD4 and CD8 T cells in the lung as compared to those immunized via the s.c. route (**Figures 5A,B**). Instead, Ag85B or TB10.4 tetramer-binding CD4 or CD8 T cells in the MLN were undetectable or had very low numbers after either i.t. or s.c. BCG immunization (**Figures 5A,B**).

The frequency of Ki-67 activated CD44+ CD4 and CD8 T cells increased in the lungs of i.t. BCG-immunized mice as compared to that of naïve mice, indicating that T cells proliferated in the

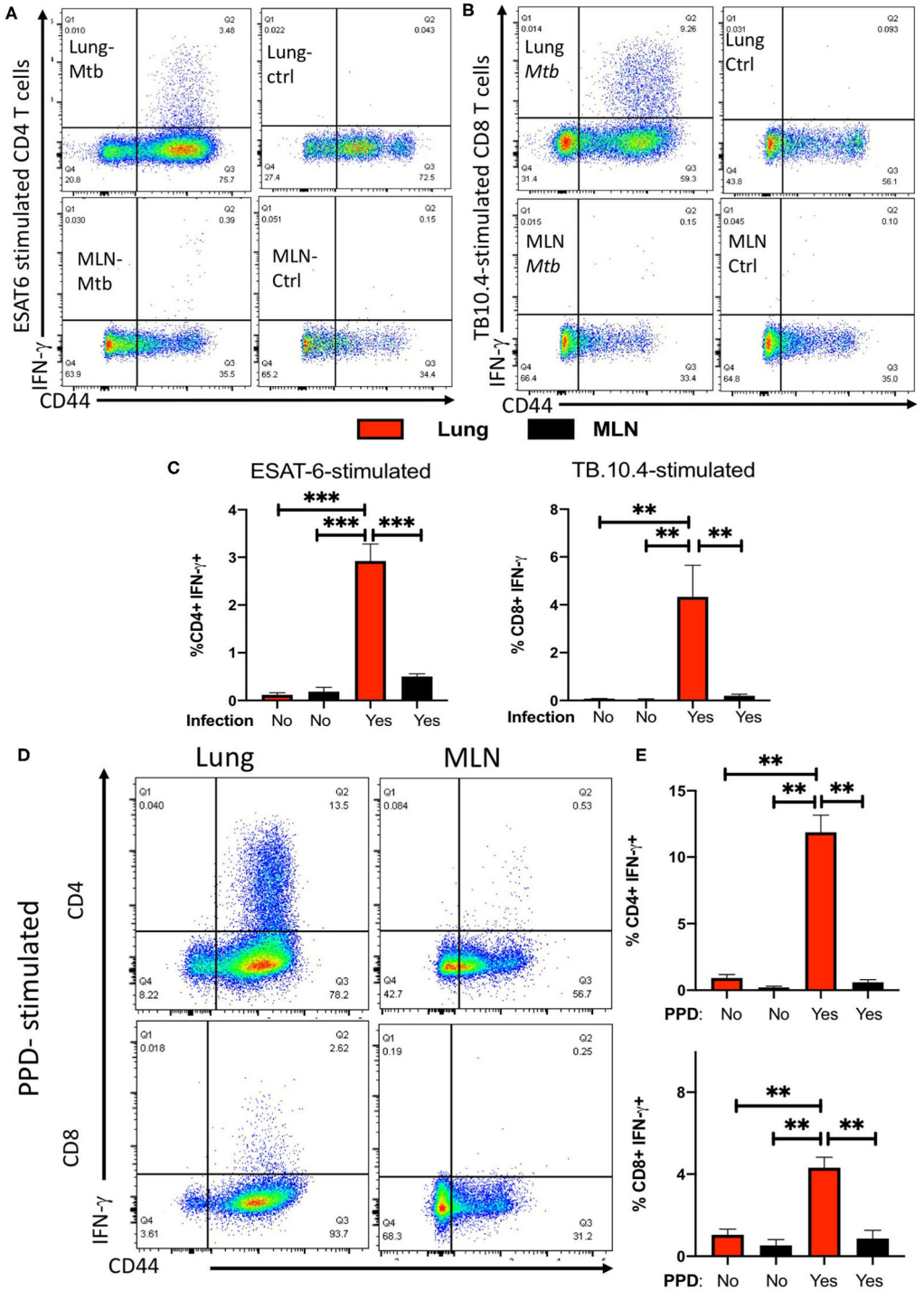

FIGURE 2 | Infection with *M. tuberculosis* results in the accumulation of ESAT-6 and TB10.4-specific IFN-γ-secreting T cells in the lung but not in the MLNs. Representative dot plots showing the CD44+ expression and IFN-γ secretion by lung or MLN CD4 **(A)** or CD8 **(B)** T cells from mice at 4 weeks after infection with *M.tuberculosis* or uninfected controls. Lung and MLN cell suspensions were stimulated with 20 μg/ml of either $ESAT6_{1-15}$ **(A)** or $TB10.4_{4-11}$ **(B)** peptides for 6 hrs. IFN-γ was determined by ICS after 4 h incubation with brefeldin A as described in the materials and methods section. **(C)** The mean frequencies of IFN-γ secretion ± SEM from lung or MLN CD4 and CD8 T cells from mice at 60 days after infection with *M. tuberculosis* or uninfected controls. Lung cell suspensions were stimulated with 10 μg/ml $ESAT6_{1-15}$ or $TB10.4_{4-11}$ peptides for 6 h or were left untreated. Differences of IFN-γ-secreting cell frequencies with stimulated lung cells are significant at $^{**}p \leq 0.01$, and $^{***}p \leq 0.001$ (2-way ANOVA). Representative dot plots **(D)** and the mean frequencies **(E)** of IFN-γ-secreting ± SEM lung or MLN CD4 and CD8 T cells from mice 30 days after infection with *M. tuberculosis* stimulated or not with PPD. Differences of between groups are significant at $^{**}p \leq 0.01$ (2-way ANOVA).

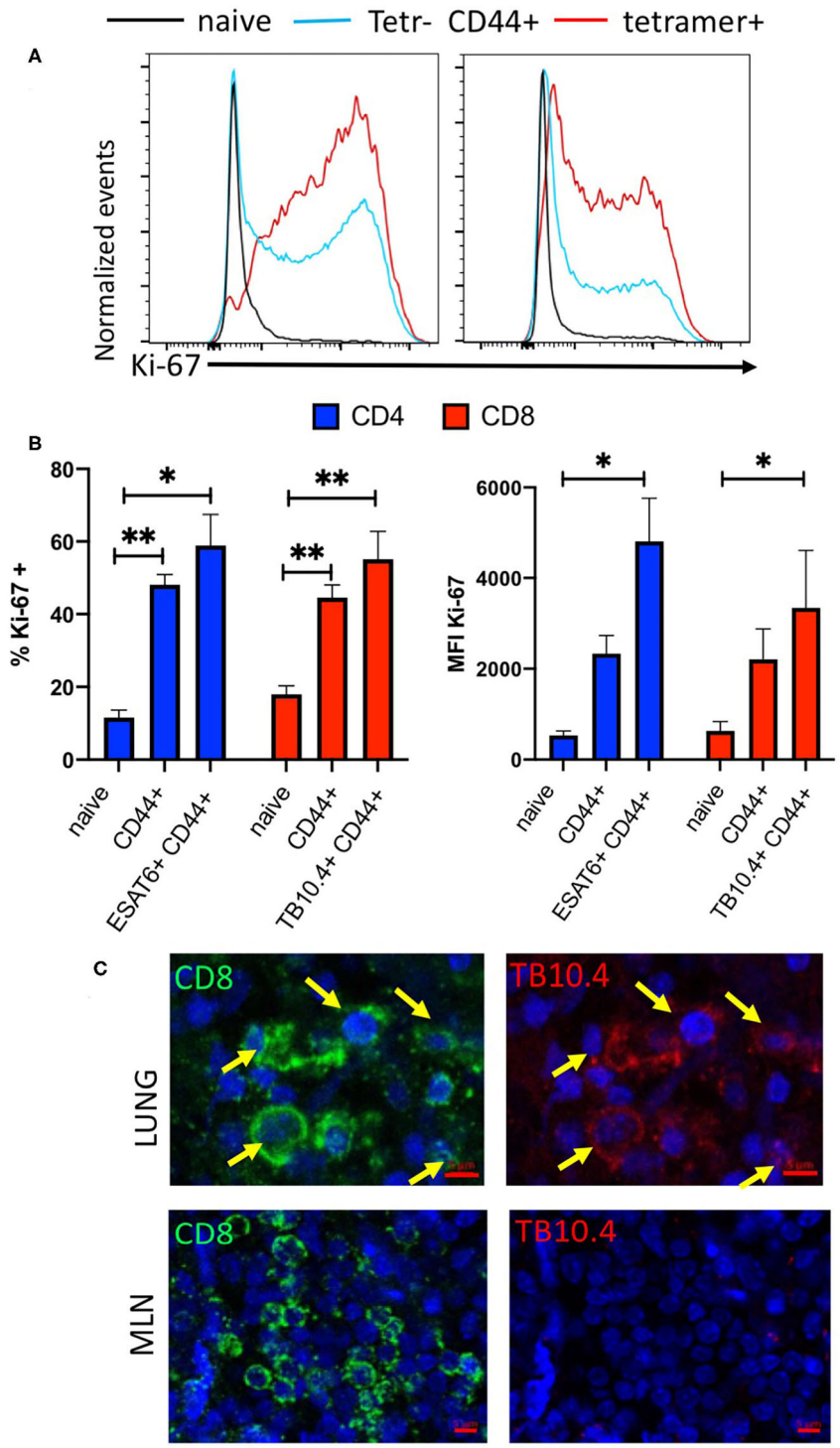

FIGURE 3 | Infection with *M. tuberculosis* results in the accumulation of *M. tuberculosis* specific proliferating T cells in the lung. **(A)** Representative histograms showing Ki67 expression in naïve (CD44 neg), CD44+ tetramer binding (ESAT6 or TB10.4 for CD4 or CD8 T cells, respectively) and non-binding CD44+ CD4 or CD8 T cells from mice at 4 weeks after infection with *M. tuberculosis*. **(B)** The mean frequency of Ki67+ CD4 and CD8 T cells ± SEM from lung of from mice either 4 weeks after infection with *M. tuberculosis*. Total CD44+ CD4 and CD8 T cells as well as tetramer ESAT6 or TB10.4+ CD4 or CD8 T cells are depicted ($n = 6$ per group). The frequencies of Ki67 cells are compared to those of CD44- naïve CD4 or CD8 T cell in the same lung. Differences with lung T cells from naïve cells are significant at $^{*}p \leq 0.05$ and $^{**}p \leq 0.01$ (one-way ANOVA). **(C)** Double immunolabelling with TB10.4 tetramer and CD8 in lung and MLN slices from mice ($n = 3$) 8 weeks after infection with *M. tuberculosis* was performed as described in the materials and methods section. Representative micrographs are shown.

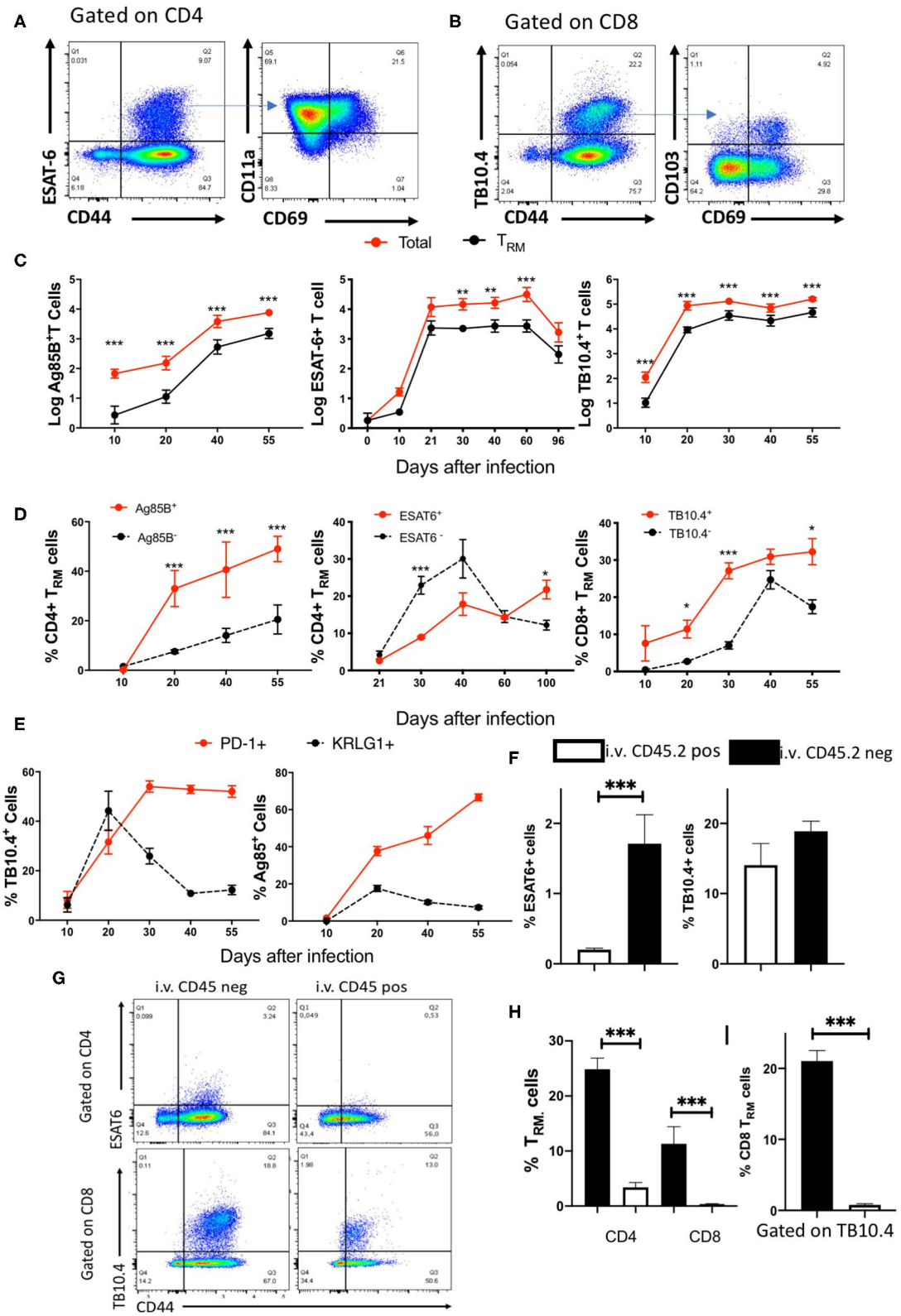

FIGURE 4 | Kinetics of specific TRM cell accumulation in the lungs of *M. tuberculosis*-infected mice. **(A)** Representative dot plots and gating strategy of tetramer ESAT-6 binding CD11a+CD69+ CD4TRM cells in the lungs of mice 4 weeks after *M. tuberculosis* infection. **(B)** Representative dot plots and gating strategy of

(Continued)

FIGURE 4 | tetramer TB10.4 binding and CD103+CD69+ CD8 TRM cells in the lungs of mice 4 weeks after *M. tuberculosis* infection. **(C)** The mean log10 of total and TRM tetramer binding Ag85B, ESAT6, and TB10.4 cell numbers in the lungs of mice at different time points after *M. tuberculosis* ± SEM are depicted. Differences between total and TRM cell numbers at each time point are significant (*$p \leq 0.05$, **$p \leq 0.05$, and ***$p \leq 0.001$, Welch's *t*-test with Holm-Sidak correction for multiple comparisons). **(D)** The mean frequencies of lung CD4 or CD8 TRM cells within tetramer positive or negative populations ± SEM at different times after infection with *M. tuberculosis* are shown. The frequencies of TRM are calculated with respect to total CD4 or CD8 CD44+ tetramer positive or negative T cells. Differences are significant at *$p \leq 0.05$, **$p \leq 0.05$, and ***$p \leq 0.001$ calculated using Welch's *t*-test with Holm-Sidak correction for multiple comparisons. **(E)** The mean frequencies of PD1+ and KRLG1+ within Ag85B and TB10.4 tetramer-binding cells in the lung of mice at different times after infection with *M. tuberculosis* ± SEM is shown. Ag85B and TB10.4 tetramer positive cells were gated on CD4 and CD8 cells, respectively. Differences in frequencies of PD1 and KRLG1 positive cell populations are significant at *$p \leq 0.05$ and ***$p \leq 0.001$(Student's *t*-test with Holm-Sidak correction for multiple comparisons). **(F)** The mean ± SEM ($n = 6$) of i.v. CD45.2 positive or negative ESAT6 and TB10.4 tetramer binding within CD4 and CD8T, respectively, cells in the lung of mice 30 days after infection with *M. tuberculosis* ($n = 6$). Differences are significant at ***$p \leq 0.001$ Welch's *t*-test. **(G)** Representative dot plots of i.v. CD45.2 labeled or unlabeled ESAT6 and TB10.4 tetramer binding T cells in the lung of mice 30 days after infection with *M. tuberculosis*. **(H)** The mean frequencies ± SEM ($n = 6$) of i.v. CD45.2 positive or negative CD11a+CD69+ CD4 TRM and CD103+ CD69+ CD8 TRM cells within activated CD4 and CD8 T cells, respectively, in the lung of mice 30 days after infection with *M. tuberculosis*. Differences are significant at ***$p \leq 0.001$ Welch's *t*-test. **(I)** The mean ± SEM ($n = 6$) of i.v. CD45.2 positive and i.v. CD45.2 negative TB10.4 tetramer binding CD103+CD69+ CD8 TRM cells in the lung parenchyma and vasculature of mice 30 days after infection with *M. tuberculosis*. Differences are significant at ***$p \leq 0.001$ Welch's *t*-test.

lung in both BCG-immunized as well as in *M. tuberculosis*-infected mice (**Figures 5C,D**). Thus, the results suggest that after BCG immunization or *M. tuberculosis* infection specific T cells are generated in the lungs.

The levels of lung T_{RM} after i.t. and s.c. BCG immunization were then evaluated (**Figure 6A**). We found increased frequencies of CD44+ CD4 T and CD4 T_{RM} cells in lungs from mice after i.t. as compared to s.c. BCG immunization (**Figure 6B**). CD4 T_{RM} were observed at 14 but not 7 days after i.t. immunization, and remained at high levels 45 days after BCG administration, while $CD4T_{RM}$ were undetectable at different time points after s.c. immunization (**Supplementary Figure 3A**). Ten-fold higher numbers of Ag85B tetramer-binding cells were present in the lungs of i.t. immunized compared to those immunized s.c. BCG (**Figure 6C**). Ag85B-specific lung CD4 T_{RM} in mice immunized s.c. were undetectable (**Figure 6C**).

We then compared the accumulation of $TB10.4_{4-11}$ tetramer-binding CD8 T cells in the lungs of mice 1 and 3 weeks after i.t. or s.c. BCG immunization (**Figure 6D**). The frequency of activated CD8 T cells and the number and frequency of TB10.4 tetramer-binding CD8 cells increased from 1 to 3 weeks after immunization (**Figures 6E–G**). The frequency of tetramer-binding TB10.4 T_{RM} within the lung CD8 T cells increased between 1 and 3 weeks after i.t. BCG immunization (**Figure 6F**). TB10.4-specific CD8 T cell were detected already 1 week after immunization and their numbers were higher in i.t. than in s.c. BCG-immunized mice (**Figure 6G**). T_{RM} were not detected within the TB10.4-specific CD8 T cells in the lungs of s.c. immunized mice, while their frequency increased 3 weeks after i.t. BCG immunization as compared to those detected 1 week after immunization (**Figures 6D,H**).

To further characterize the antigen-specific lung T cells following i.t. and s.c. BCG immunization PD1 and KRLG1 expression were assessed (**Supplementary Figure 3B**). We found that 30% of mycobacteria-specific CD8 T cells in the lung of mice immunized i.t. with BCG expressed PD1. In comparison, the percentage of PD1-expressing cells was reduced in TB10.4 tetramer-binding and in total CD8 T cells in the lungs of s.c. immunized mice (**Figure 6I**). In contrast, the frequency of KRLG1+ cells was increased in lungs of mice immunized via the s.c. route as compared to those obtained from i.t. vaccinated mice (Figure 5I).

Bona Fide T_{RM} Develop in the Lungs of Mice After Mucosal BCG Immunization

We used the S1PR agonist FTY720 (fingolimod) to block egress of T cells from the lungs or lymph nodes, in order to assess whether T cells could be generated in the mice during BCG immunization. All groups of mice were vaccinated s.c. with BCG and after 3 weeks mice were treated daily i.p. with 1 mg/kg FTY720. One day after the first FTY720 administration, mice were boosted i.t. with BCG (**Figure 7A**). The administration of FTY720 reduced by more than 90% the number of blood T cells already 15 h after inoculation of a single dose (**Supplementary Figure 4A**). The i.t. booster increased protection of mice against challenge with *M. tuberculosis* as shown by the reduced levels of bacteria in lungs and spleens (**Supplementary Figures 4B,C**).

The frequency of CD44+ CD4 and CD8 T cells in lungs increased in both groups (boosted or not) after FTY720 treatment due to the fall of naïve T cells (**Figures 7B–E**). The number of CD44+ CD4 T cells in the lung of i.t. BCG-boosted animals increased after FTY720 administration (**Figure 7C**), while both CD44+ CD4 and CD8 T cell numbers were reduced in the s.c. immunized group as compared to those not treated with FTY720. Moreover, the numbers and frequencies of CD4 and CD8 T_{RM} increased in i.t. BCG re-vaccinated mice treated with FTY720, while numbers of CD4 T_{RM} in s.c. BCG immunized but not re-vaccinated mice remained very low, been mostly undetectable (**Figures 7B–E**).

Since inoculation of FTY720 was done before i.t. immunization, our results indicate that T_{RM} generation and accumulation in the lung takes place in the absence of lymphoid recirculation after i.t. immunization, suggesting a minor role for MLN if any in this process.

DISCUSSION

Our data indicate that aerosol infection with *M. tuberculosis* and mucosal immunization with BCG results in the generation, proliferation and persistence of specific T cells (a fraction

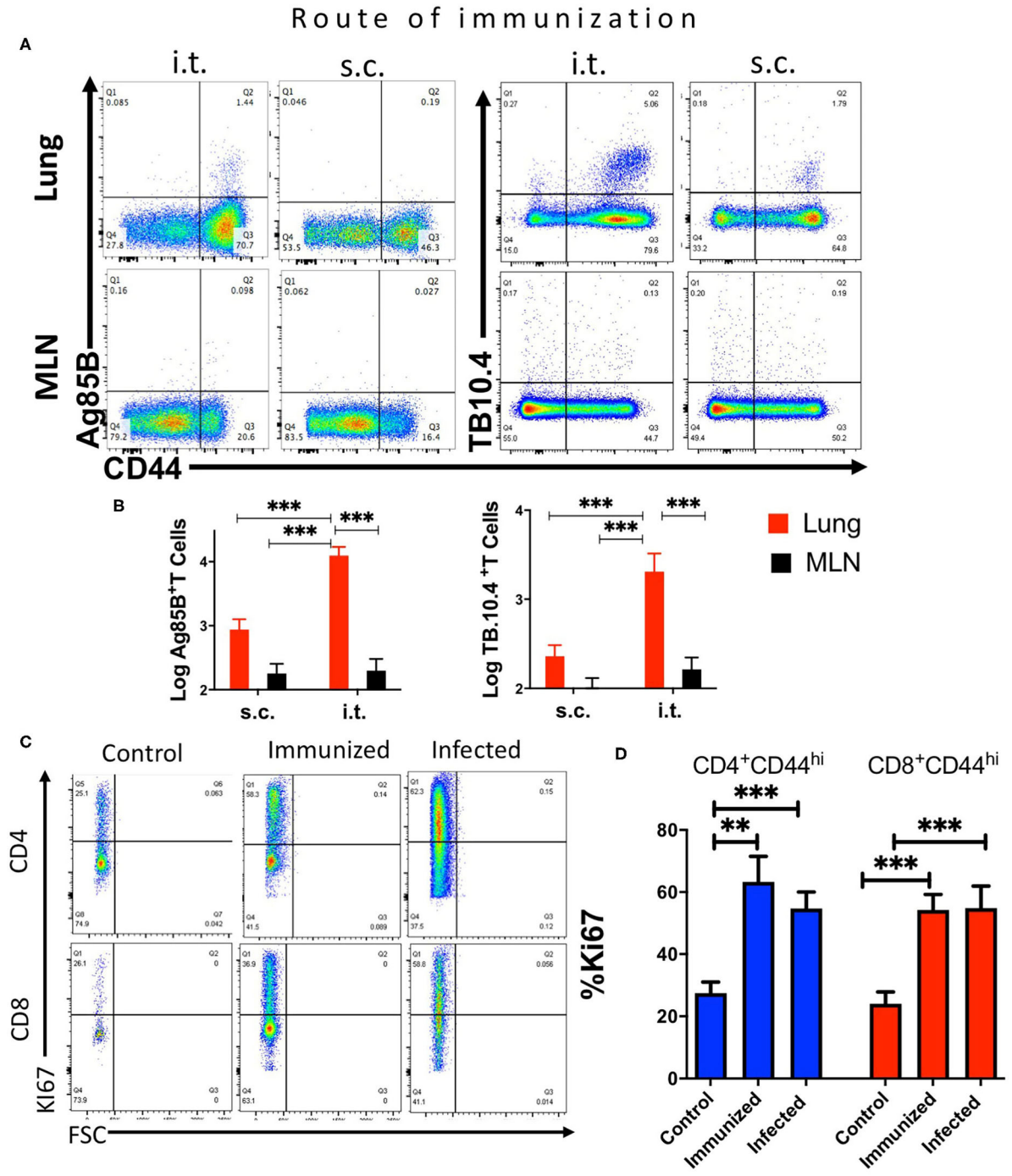

FIGURE 5 | Mycobacteria-specific T cells accumulate in the lung but not the mediastinal lymph node during immunization or infection with *M. tuberculosis*. C57BL/6 mice were immunized i.t. or s.c. with 107 BCG and T cell populations analyzed in the lung and MLN cell suspensions 3 weeks after immunization. **(A)** Representative dot plots of tetramer Ag85B and TB10.4 binding CD4 or CD8 T cells, respectively, in lungs and MLN from mice 3 weeks after i.t. or s.c. BCG immunization are shown. **(B)** The mean percentage of tetramer Ag85B and TB10.4 binding cells gated within the CD44+ CD4 and CD8 T cell populations in the lung or MLN from BCG-immunized mice. Differences in frequencies tetramer binding cells between lung and MLN at a given time point after infection are significant at $^{**}p \leq 0.01$, and $^{***}p \leq 0.001$(Welch's *t*-test with Holm-Sidak correction for multiple comparisons). **(C)** Representative dot plots showing the frequency of Ki67+ gated in CD44+ CD4 or CD8 T cells in the lung from mice either 4 weeks after infection with *M. tuberculosis*, 3 weeks after i.t. BCG immunization or left untreated are shown. **(D)** The mean frequency of Ki67+ CD4 and CD8 T cells ± SEM from lung of mice 4 weeks after infection with *M. tuberculosis*, 3 weeks after BCG immunization and non-immunized control mice ($n \geq 5$ per group) are shown. Differences with lung T cells from uninfected mice are significant at $^{**}p \leq 0.01$ and $^{***}p \leq 0.001$ (Welch's *t*-test with Holm-Sidak correction for multiple comparisons).

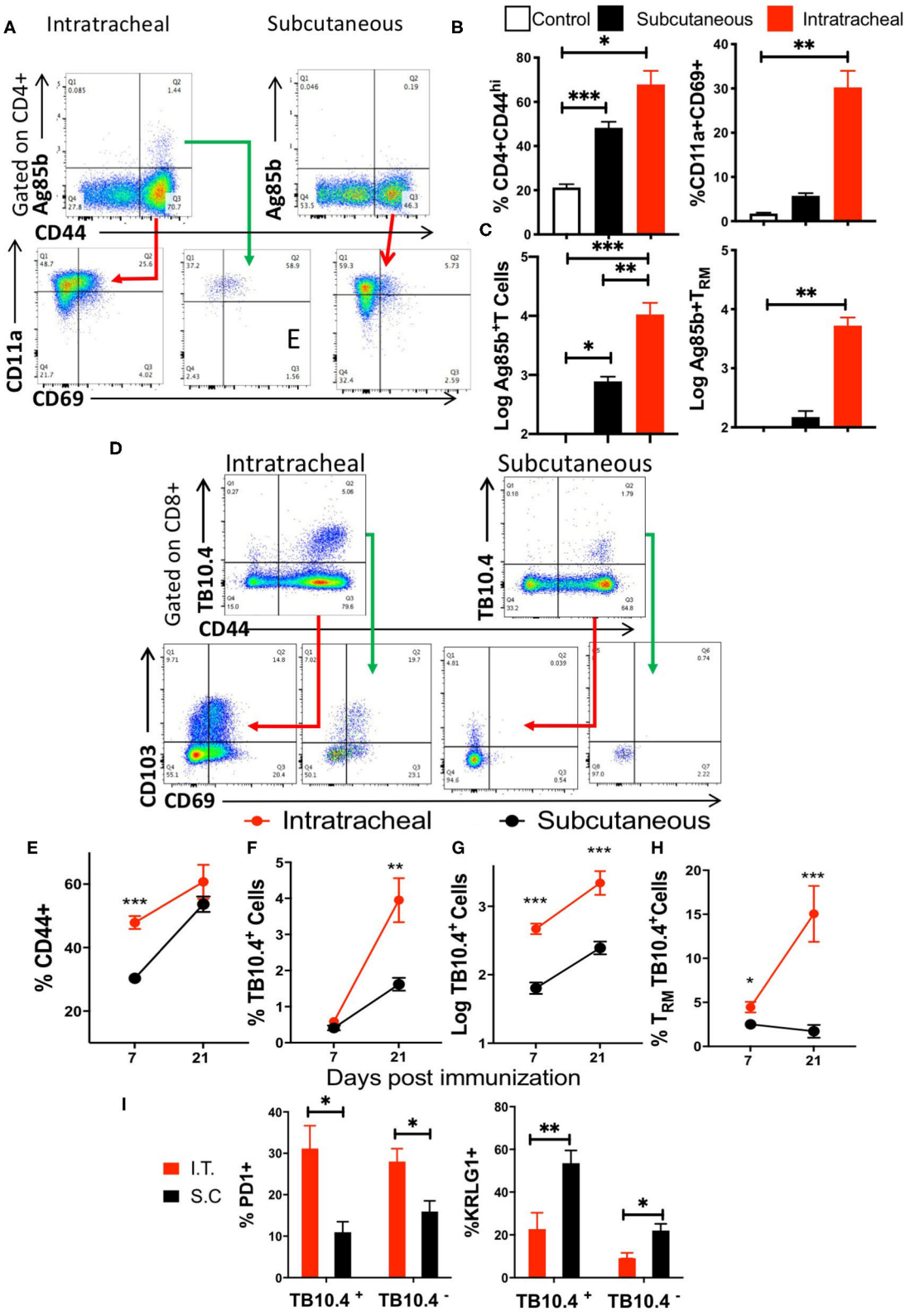

FIGURE 6 | Mycobacteria-specific Trm cells accumulate in the lung during BCG immunization. **(A)** Representative dot plots and gating strategy of tetramer Ag85B binding and CD11a+CD69+ CD4TRM cells in the lungs of mice 3 weeks after i.t. and s.c. BCG immunization. **(B)** Mice were immunized with BCG s.c. or i.t. and

(Continued)

FIGURE 6 | sacrificed 3 weeks later. A group of mice was left untreated. The frequency of CD44+ in gated CD3+ CD4 T cells from lungs and of CD4 TRM ± SEM gated on CD3+ CD44+ cells are shown. The mean % ± SEM of at least 4 animals per group are shown. Differences between groups are significant at $^{*}p \leq 0.05$ and $^{**}p \leq 0.001$ (Welch's *t*-test with Holm-Sidak correction for multiple comparisons). **(C)** The mean numbers ± SEM of tetramer Ag85B binding total and TRM CD4 T cells in the lungs of i.t. and s.c. BCG immunized mice are shown ($n \geq 5$ animals per group). Differences between groups are significant at $^{**}p \leq 0.001$ and $^{***}p \leq 0.001$ (one-way ANOVA). **(D)** Mice were immunized i.t. or s.c. with BCG and sacrificed 1 or 3 weeks later. The representative dot plots show the presence of tetramer TB10.4 binding CD44+ CD8 T cells in the lungs of i.t. or s.c. BCG-immunized mice. The CD69+CD103+ CD8 TRM within the tetramer TB10.4 positive or negative cells are also shown. **(E–H)** The frequency of CD44+ gated on CD3+ CD8 T cells **(E)**, of tetramer TB10.4+ within CD44+ CD8 T cells **(F)**, the numbers of tetramer TB10.4+ CD8 T cells **(G)** and the frequency of TRM cells within all TB10.4 tetramer binding cells **(H)** were determined in lungs from mice at 1 and 3 weeks after i.t. or s.c. immunization with BCG. The mean frequencies or log10 transformed cell numbers ± SEM ($n = 5$ per group) are shown. Differences between groups were statistically significant at $^{*}p \leq 0.05$, $^{**}p \leq 0.001$, and $^{***}p \leq 0.001$ (Welch's *t*-test with Holm-Sidak correction for multiple comparisons). **(I)** The mean frequencies of PD1+ and KRLG1+ cells within the TB10.4 tetramer + or−CD44+ CD8 T cells in the lungs of mice immunized i.t. or s.c. with BCG 3 weeks before sacrifice are shown. Differences between i.t. and s.c. immunized mice ($n = 5$ per group) were significant at $^{*}p \leq 0.05$ and $^{**}p \leq 0.01$ (Welch's *t*-test with Holm-Sidak correction for multiple comparisons).

exhibiting T_{RM} markers) in the lung, independently of the recirculation from the draining lymph nodes.

It is generally accepted that following antigen encounter in the lung, during infection or immunization dendritic cells (DCs) will migrate to the MLNs and present mycobacterial antigens and different co-stimulatory signals to specific naïve T-cells. The low frequency of naïve T cells specific for any one pathogen epitope means dependence on primary responses initiated in draining lymph nodes, often allowing time for a serious infection to develop. The activated T cells will proliferate and differentiate into effector T-cells and memory T-cells that are distributed more broadly throughout the body. Upon re-exposure to the pathogen, memory T-cells are able to mount a more rapid and robust antigen-specific responses (10, 31).

Our results argue that during infection with *M. tuberculosis* or i.t. BCG immunization, mycobacteria-specific T cells are generated in the lung. The absence or low numbers of tetramer-binding *M. tuberculosis*-specific T cells at all time points studied, the low frequencies or absence IFN- γ-secreting cells in the MLNs of infected mice in response to specific peptides well as to a PPD (containing several *M. tuberculosis* proteins), and the expression of the proliferation marker Ki67 in specific CD4 and CD8 T cells from the lung of *M. tuberculosis* -infected or BCG-immunized mice support this possibility.

Although i.t. aerosol immunization is not applicable for human vaccination for practical reasons, it allows for a more accurate delivery of defined doses than with intranasal or aerosol vaccination. While doses of 5×10^5 BCG CFU i.t. have been shown improved protection of mice against *M. tuberculosis* challenge as compared to the s.c. route (4), the 10^7 BCG dose was chosen for our studies since it has been shown to confer the largest reduction of lung *M. tuberculosis* levels, when compared to lower doses (32). The i.t. immunization with BCG generated higher mycobacteria-specific lung CD4 and CD8 T cells as compared to the s.c. route of delivery. After i.t. BCG immunization or booster an important fraction of total or antigen-specific CD4 and CD8 lung T cells displayed a T_{RM} phenotype. Instead, T_{RM} were low or absent after s.c. BCG administration, as also shown previously in the lung or bronchoalveolar fluid lavage cells (4, 33). Although most experiments were done in mice sacrificed at 3 weeks after immunization, T_{RM} were measured from 14 to 45 but not 7 days after BCG i.t. immunization, but were under detection level in s.c. immunized mice.

KRLG1+ T cells are short-lived terminally differentiated T cells (28). Upon infection, *M. tuberculosis*-specific CD4 T cells expressing KLRG1 exhibited a heightened capacity to secrete IFN-γ (29). PD-1+ T cells secreted less inflammatory cytokines than KLRG1+ counterparts upon re-stimulation, proliferated, showed a higher survival rate and the capacity to differentiate into KLRG1+ cells (29). PD-1+ CD4 T cells mediated protection against *M. tuberculosis*, and PD-1+ T cells and T_{RM} locate in the lung parenchyma as shown here and elsewhere (28, 33). Here we showed that levels of *M. tuberculosis*-specific KRLG1+ CD4 and CD8 T cells were high early (20 dpi) after infection and decreased thereafter, while the levels of PD1+ T cells increased during the first weeks of infection, remaining high at later time points. Most KRLG1+ cells did not express T_{RM} markers.

The i.t. BCG immunization generated higher levels of total or *M. tuberculosis*-specific PD1+ CD4 and CD8 T cells as compared to those generated after s.c. immunization, which showed higher frequency of KRLG1 expression. In line with this, we confirm previous studies showing that mucosal immunization or boosting with BCG or mycobacterial antigens improve vaccine activity compared to the commonly used intradermal BCG (4, 6–8, 32, 34).

T cells are restricted to using the S1P pathway to exit secondary lymphoid organs and enter the blood (35, 36). FTY720 is a S1P receptor modulator that impairs lymphocyte egress from the lymph nodes and other secondary organs (37). Previous studies have shown that once priming has occurred, recruitment from circulation is not needed, implying the protective T-cells locate in the lung (38). Here, FTY720 inoculation indicated that persistent T_{RM} were detected in lungs. The results also suggest that after i.t. immunization with BCG, T_{RM} are generated in the lung independently of recruitment of T cells from lymphoid stores since FTY720 was inoculated before the revaccination.

Immune responses to a variety of antigens have been shown to be initiated directly in the lung by using lymphotoxin (LT)-deficient mice that lack conventional secondary lymphoid organs (39, 40). By means of LT-deficient and splenectomized mice, it was shown that CD8+ T cells could be primed, proliferated, acquired a memory phenotype and cleared a challenge viral infection in the complete absence of secondary lymphoid organs

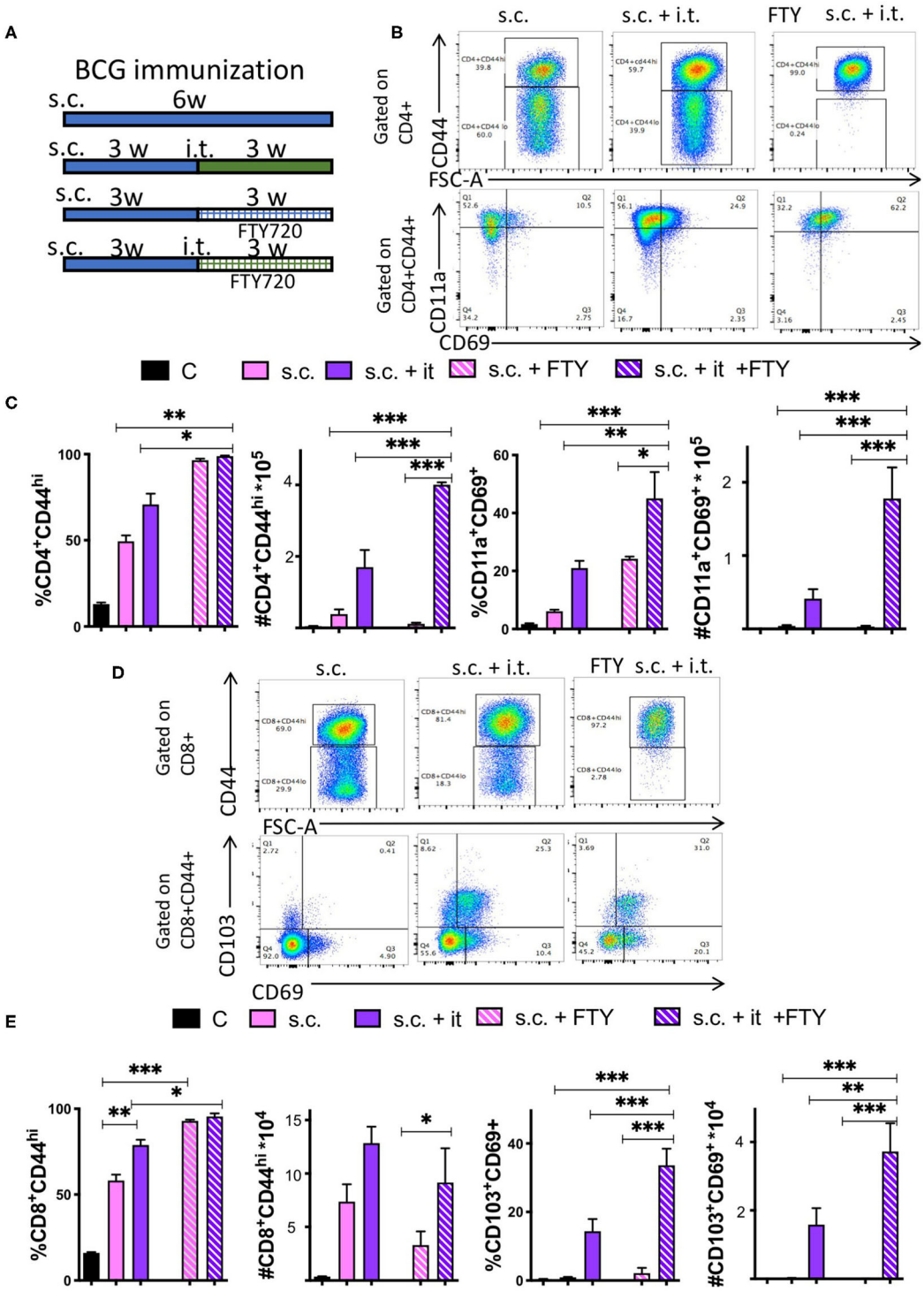

FIGURE 7 | Bona fide TRM develop in the lungs of mice after mucosal BCG immunization. **(A)** Mice were immunized s.c. with 107 BCG and revaccinated or not i.t. with BCG 3 weeks after. Group of immunized and revaccinated mice were treated with 1 mg/kg i.p. FTY320 daily starting 1 day after revaccination until sacrifice. Mice were sacrificed 3 weeks after revaccination. Representative dot plots **(B)** and the mean frequencies and cell numbers **(C)** of pulmonary CD4+CD44+ and of CD11a+CD69+ TRM ± SEM ($n \geq 5$) in the lung of mice are shown. Differences between experimental groups are significant at $^{*}p \leq 0.05$, $^{**}p \leq 0.01$, and $^{***}p \leq 0.001$ (one way ANOVA). **(D,E)** Mice were immunized with BCG and treated with FTY720 as described in A-B and **Supplementary Figure 2**. Representative dot plots **(D)** and the mean frequencies and numbers **(E)** of pulmonary CD8+CD44+ T cells and of CD103+CD69+ TRM in the lungs of mice 3 weeks after revaccination ± SEM ($n \geq 5$) are shown. Differences between groups are significant at $^{*}p \leq 0.05$, $^{**}p \leq 0.01$, and $^{***}p \leq 0.001$ (one way ANOVA).

(41). LT-deficient mice were also shown to generate protective T cell responses against *M. tuberculosis* (42–44). In lymph node deficient splenectomized mice infected with influenza, immune responses were initiated without delay (40). Our results indicate that T cells are generated in the lung, excluding functional compensations occurring in genetically deficient mice. We fall short of showing that T cell priming occurs in the lung of infected mice.

Leukocytes that infiltrate the lung have been shown to assemble into inducible bronchus-associated lymphoid tissue (iBALT) after inflammation or infection (45). Like conventional lymphoid organs, iBALT contains segregated B and T cell areas, specialized stromal cells, high endothelial venules, and lymphatic vessels (46). iBALTs might promote encounters between naive lymphocytes recruited from the blood and antigen-presenting cells that have migrated from the lumen of the airways. Naïve T cells were primed within the iBALT (47), and T cells in the iBALT have been suggested to participate in the protective secondary immune responses against pathogens (34, 48).

The pulmonary delivery of *M. tuberculosis* antigen-primed DCs has been shown to led to increased and rapid iBALT formation and improved disease outcome (49). B cell follicles are often observed in *M. tuberculosis* granulomas in mice (50), humans, and monkeys (51). Monkeys with latent *M. tuberculosis* infection maintain large, well-organized areas of iBALTs surrounding granulomas, whereas NHPs with active disease have fewer and less organized areas of iBALT (51).

Different studies have suggested that the antigen-specific T cell responses during *M. tuberculosis* infection show a delayed onset as compared to infection with other pathogens (52–55). These studies used transgenic or retrogenic specific T cell transfers to show T cell activation in the lymph nodes during *M. tuberculosis* infection (54–57). Our data studying suggest that T cell priming or activation in the draining lymph node is not required to generate antigen-specific T cell responses in the lungs. Whether a delay in T cell priming might be instead due to the process of formation of the iBALTs induced by *M. tuberculosis* infection or mucosal vaccination deserves further investigation. We showed qualitatively differences in the mucosal as compared to a distal route of immunization, supporting the use of mucosal immunization for achieving superior immune protection against infection with *M. tuberculosis*.

DATA AVAILABILITY STATEMENT

The datasets presented in this article are not readily available because all raw data from this article can be obtained upon request to the corresponding author. Requests to access the datasets should be directed to Martin E. Rottenberg, martin.rottenberg@ki.se.

ETHICS STATEMENT

The animal study was reviewed and approved by Stockholm North Ethical Committee.

AUTHOR CONTRIBUTIONS

JB, RL, WM, and BC performed the investigation. BC and MR wrote the original draft and reviewed the manuscript. MR conceived the study. All authors approved the final version of this manuscript to be published.

FUNDING

This study was supported by the Swedish Heart and Lung foundation 2018-20/20170491, the Swedish Research Council 2019-01691 and 2019-04725, the Swedish Institute for Internationalization of Research (STINT) 4-1796/2014, the European Community H2020 EMITB (Grant No. 643558), and the Karolinska Institutet.

ACKNOWLEDGMENTS

We thank the expert help of the staff of the Astrid Fagreus animal house, Department of Comparative Medicine, Karolinska Institutet. We would like to thank the National Institutes of Health Tetramer Core Facility for providing reagents. We also thank Dr. Benedict Chambers for comments.

SUPPLEMENTARY MATERIAL

The Supplementary Material for this article can be found online at: https://www.frontiersin.org/articles/10.3389/fimmu.2020.566319/full#supplementary-material

REFERENCES

1. WHO. *Global Tuberculosis Report 2019*. Geneva: World Health Organization (2019).
2. Zumla A, George A, Sharma V, Herbert RH, Baroness Masham of I, Oxley A, et al. The WHO 2014 global tuberculosis report–further to go. *Lancet Glob Health*. (2015) 3:e10–2. doi: 10.1016/S2214-109X(14)70361-4
3. Hingley-Wilson SM, Sambandamurthy VK, Jacobs WR Jr. Survival perspectives from the world's most successful pathogen, *Mycobacterium tuberculosis*. *Nat Immunol*. (2003) 4:949–55. doi: 10.1038/ni981
4. Perdomo C, Zedler U, Kuhl AA, Lozza L, Saikali P, Sander LE, et al. Mucosal BCG vaccination induces protective lung-resident memory t cell populations against tuberculosis. *MBio*. (216) 7:e01686–16. doi: 10.1128/mBio.01686-16
5. White AD, Sarfas C, West K, Sibley LS, Wareham AS, Clark S, et al. Evaluation of the Immunogenicity of *Mycobacterium bovis* BCG delivered by aerosol to the lungs of macaques. *Clin Vaccine Immunol*. (2015) 22:992–1003. doi: 10.1128/CVI.00289-15
6. Chen L, Wang J, Zganiacz A, Xing Z. Single intranasal mucosal *Mycobacterium bovis* BCG vaccination confers improved protection compared to subcutaneous vaccination against pulmonary tuberculosis. *Infect Immun*. (2004) 72:238–46. doi: 10.1128/IAI.72.1.238-246.2004
7. Goonetilleke NP, McShane H, Hannan CM, Anderson RJ, Brookes RH, Hill AV. Enhanced immunogenicity and protective efficacy against *Mycobacterium tuberculosis* of bacille Calmette-Guerin vaccine using mucosal administration and boosting with a recombinant modified vaccinia virus Ankara. *J Immunol*. (2003) 171:1602–9. doi: 10.4049/jimmunol.171.3.1602

8. Wang J, Thorson L, Stokes RW, Santosuosso M, Huygen K, Zganiacz A, et al. Single mucosal, but not parenteral, immunization with recombinant adenoviral-based vaccine provides potent protection from pulmonary tuberculosis. *J Immunol.* (2004) 173:6357–65. doi: 10.4049/jimmunol.173.10.6357
9. Xing Z, McFarland CT, Sallenave JM, Izzo A, Wang J, McMurray DN. Intranasal mucosal boosting with an adenovirus-vectored vaccine markedly enhances the protection of BCG-primed guinea pigs against pulmonary tuberculosis. *PLoS ONE*. (2009) 4:e5856. doi: 10.1371/journal.pone.0005856
10. Mueller SN, Gebhardt T, Carbone FR, Heath WR. Memory T cell subsets, migration patterns, and tissue residence. *Annu Rev Immunol.* (2013) 31:137–61. doi: 10.1146/annurev-immunol-032712-095954
11. Ariotti S, Haanen JB, Schumacher TN. Behavior and function of tissue-resident memory T cells. *Adv Immunol.* (2012) 114:203–16. doi: 10.1016/B978-0-12-396548-6.00008-1
12. Turner DL, Farber DL. Mucosal resident memory CD4 T cells in protection and immunopathology. *Front Immunol.* (2014) 5:331. doi: 10.3389/fimmu.2014.00331
13. Gebhardt T, Wakim LM, Eidsmo L, Reading PC, Heath WR, Carbone FR. Memory T cells in nonlymphoid tissue that provide enhanced local immunity during infection with herpes simplex virus. *Nat Immunol.* (2009) 10:524–30. doi: 10.1038/ni.1718
14. Steinbach K, Vincenti I, Kreutzfeldt M, Page N, Muschaweckh A, Wagner I, et al. Brain-resident memory T cells represent an autonomous cytotoxic barrier to viral infection. *J Exp Med.* (2016) 213:1571–87. doi: 10.1084/jem.20151916
15. Shin H, Iwasaki A. A vaccine strategy that protects against genital herpes by establishing local memory T cells. *Nature.* (2012) 491:463–7. doi: 10.1038/nature11522
16. Sheridan BS, Pham QM, Lee YT, Cauley LS, Puddington L, Lefrancois L. Oral infection drives a distinct population of intestinal resident memory CD8(+) T cells with enhanced protective function. *Immunity.* (2014) 40:747–57. doi: 10.1016/j.immuni.2014.03.007
17. Bergsbaken T, Bevan MJ, Fink PJ. Local inflammatory cues regulate differentiation and persistence of CD8(+) tissue-resident memory T cells. *Cell Rep.* (2017) 19:114–24. doi: 10.1016/j.celrep.2017.03.031
18. Ogongo P, Porterfield JZ, Leslie A. Lung tissue resident memory T-cells in the immune response to *Mycobacterium tuberculosis*. *Front Immunol.* (2019) 10:992. doi: 10.3389/fimmu.2019.00992
19. Florido M, Muflihah H, Lin LCW, Xia Y, Sierro F, Palendira M, et al. Pulmonary immunization with a recombinant influenza A virus vaccine induces lung-resident CD4(+) memory T cells that are associated with protection against tuberculosis. *Mucosal Immunol.* (2018) 11:1743–52. doi: 10.1038/s41385-018-0065-9
20. Connor LM, Harvie MC, Rich FJ, Quinn KM, Brinkmann V, Le Gros G, et al. A key role for lung-resident memory lymphocytes in protective immune responses after BCG vaccination. *Eur J Immunol.* (2010) 40:2482–92. doi: 10.1002/eji.200940279
21. Carow B, Qun Ye X, Gavier-Widen D, Bhuju S, Oehlmann W, Singh M, et al. Silencing suppressor of cytokine signaling-1 (SOCS1) in macrophages improves *mycobacterium tuberculosis* control in an interferon-gamma (IFN-gamma)-dependent manner. *J Biol Chem.* (2011) 286:26873–87. doi: 10.1074/jbc.M111.238287
22. Anderson KG, Mayer-Barber K, Sung H, Beura L, James BR, Taylor JJ, et al. Intravascular staining for discrimination of vascular and tissue leukocytes. *Nat Protoc.* (2014) 9:209–22. doi: 10.1038/nprot.2014.005
23. Li S, Mwakalundwa G, Skinner PJ. *In situ* MHC-tetramer staining and quantitative analysis to determine the location, abundance, and phenotype of antigen-specific CD8 T cells in tissues. *J Vis Exp*. (2017) 127:56130. doi: 10.3791/56130
24. Cho YS, Dobos KM, Prenni J, Yang H, Hess A, Rosenkrands I, et al. Deciphering the proteome of the *in vivo* diagnostic reagent "purified protein derivative" from *Mycobacterium tuberculosis*. *Proteomics.* (2012) 12:979–91. doi: 10.1002/pmic.201100544
25. Prasad TS, Verma R, Kumar S, Nirujogi RS, Sathe GJ, Madugundu AK, et al. Proteomic analysis of purified protein derivative of *Mycobacterium tuberculosis*. *Clin Proteomics.* (2013) 10:8. doi: 10.1186/1559-0275-10-8
26. Teijaro JR, Turner D, Pham Q, Wherry EJ, Lefrancois L, Farber DL. Cutting edge: tissue-retentive lung memory CD4 T cells mediate optimal protection to respiratory virus infection. *J Immunol.* (2011) 187:5510–4. doi: 10.4049/jimmunol.1102243
27. Turner DL, Bickham KL, Thome JJ, Kim CY, D'Ovidio F, Wherry EJ, et al. Lung niches for the generation and maintenance of tissue-resident memory T cells. *Mucosal Immunol.* (2014) 7:501–10. doi: 10.1038/mi.2013.67
28. Moguche AO, Shafiani S, Clemons C, Larson RP, Dinh C, Higdon LE, et al. ICOS and Bcl6-dependent pathways maintain a CD4 T cell population with memory-like properties during tuberculosis. *J Exp Med.* (2015) 212:715–28. doi: 10.1084/jem.20141518
29. Reiley WW, Shafiani S, Wittmer ST, Tucker-Heard G, Moon JJ, Jenkins MK, et al. Distinct functions of antigen-specific CD4 T cells during murine *Mycobacterium tuberculosis* infection. *Proc Natl Acad Sci USA.* (2010) 107:19408–13. doi: 10.1073/pnas.1006298107
30. Barber DL, Mayer-Barber KD, Feng CG, Sharpe AH, Sher A. CD4 T cells promote rather than control tuberculosis in the absence of PD-1-mediated inhibition. *J Immunol.* (2011) 186:1598–607. doi: 10.4049/jimmunol.1003304
31. Cauley LS, Lefrancois L. Guarding the perimeter: protection of the mucosa by tissue-resident memory T cells. *Mucosal Immunol.* (2013) 6:14–23. doi: 10.1038/mi.2012.96
32. Aguilo N, Toledo AM, Lopez-Roman EM, Perez-Herran E, Gormley E, Rullas-Trincado J, et al. Pulmonary *Mycobacterium bovis* BCG vaccination confers dose-dependent superior protection compared to that of subcutaneous vaccination. *Clin Vaccine Immunol.* (2014) 21:594–7. doi: 10.1128/CVI.00700-13
33. Bull NC, Stylianou E, Kaveh DA, Pinpathomrat N, Pasricha J, Harrington-Kandt R, et al. Enhanced protection conferred by mucosal BCG vaccination associates with presence of antigen-specific lung tissue-resident PD-1(+) KLRG1(-) CD4(+) T cells. *Mucosal Immunol.* (2019) 12:555–64. doi: 10.1038/s41385-018-0109-1
34. Kaushal D, Foreman TW, Gautam US, Alvarez X, Adekambi T, Rangel-Moreno J, et al. Mucosal vaccination with attenuated *Mycobacterium tuberculosis* induces strong central memory responses and protects against tuberculosis. *Nat Commun.* (2015) 6:8533. doi: 10.1038/ncomms9533
35. Bankovich AJ, Shiow LR, Cyster JG. CD69 suppresses sphingosine 1-phosophate receptor-1 (S1P1) function through interaction with membrane helix 4. *J Biol Chem.* (2010) 285:22328–37. doi: 10.1074/jbc.M110.123299
36. Matloubian M, Lo CG, Cinamon G, Lesneski MJ, Xu Y, Brinkmann V, et al. Lymphocyte egress from thymus and peripheral lymphoid organs is dependent on S1P receptor 1. *Nature.* (2004) 427:355–60. doi: 10.1038/nature02284
37. Brinkmann V, Davis MD, Heise CE, Albert R, Cottens S, Hof R, et al. The immune modulator FTY720 targets sphingosine 1-phosphate receptors. *J Biol Chem.* (2002) 277:21453–7. doi: 10.1074/jbc.C200176200
38. Delahaye JL, Gern BH, Cohen SB, Plumlee CR, Shafiani S, Gerner MY, et al. Cutting Edge: bacillus calmette-guerin-induced T cells shape *Mycobacterium tuberculosis* infection before reducing the bacterial burden. *J Immunol.* (2019) 203:807–12. doi: 10.4049/jimmunol.1900108
39. De Togni P, Goellner J, Ruddle NH, Streeter PR, Fick A, Mariathasan S, et al. Abnormal development of peripheral lymphoid organs in mice deficient in lymphotoxin. *Science.* (1994) 264:703–7. doi: 10.1126/science.8171322
40. Moyron-Quiroz JE, Rangel-Moreno J, Kusser K, Hartson L, Sprague F, Goodrich S, et al. Role of inducible bronchus associated lymphoid tissue (iBALT) in respiratory immunity. *Nat Med.* (2004) 10:927–34. doi: 10.1038/nm1091
41. Moyron-Quiroz JE, Rangel-Moreno J, Hartson L, Kusser K, Tighe MP, Klonowski KD, et al. Persistence and responsiveness of immunologic memory in the absence of secondary lymphoid organs. *Immunity.* (2006) 25:643–54. doi: 10.1016/j.immuni.2006.08.022
42. Day TA, Koch M, Nouailles G, Jacobsen M, Kosmiadi GA, Miekley D, et al. Secondary lymphoid organs are dispensable for the development of T-cell-mediated immunity during tuberculosis. *Eur J Immunol.* (2010) 40:1663–73. doi: 10.1002/eji.201040299
43. Kashino SS, Vallerskog T, Martens G, Troudt J, Keyser A, Taylor J, et al. Initiation of acquired immunity in the lungs of mice lacking lymph nodes after infection with aerosolized *Mycobacterium tuberculosis*. *Am J Pathol.* (2010) 176:198–204. doi: 10.2353/ajpath.2010.090446

44. Allie N, Keeton R, Court N, Abel B, Fick L, Vasseur V, et al. Limited role for lymphotoxin alpha in the host immune response to *Mycobacterium tuberculosis*. *J Immunol.* (2010) 185:4292–301. doi: 10.4049/jimmunol.1000650
45. Marin ND, Dunlap MD, Kaushal D, Khader SA. Friend or foe: the protective and pathological roles of inducible bronchus-associated lymphoid tissue in pulmonary diseases. *J Immunol.* (2019) 202:2519–26. doi: 10.4049/jimmunol.1801135
46. Hwang JY, Randall TD, Silva-Sanchez A. Inducible bronchus-associated lymphoid tissue: taming inflammation in the lung. *Front Immunol.* (2015) 7:258. doi: 10.3389/fimmu.2016.00258
47. Halle S, Dujardin HC, Bakocevic N, Fleige H, Danzer H, Willenzon S, et al. Induced bronchus-associated lymphoid tissue serves as a general priming site for T cells and is maintained by dendritic cells. *J Exp Med.* (2009) 206:2593–601. doi: 10.1084/jem.20091472
48. Mehra S, Golden NA, Dutta NK, Midkiff CC, Alvarez X, Doyle LA, et al. Reactivation of latent tuberculosis in rhesus macaques by coinfection with simian immunodeficiency virus. *J Med Primatol.* (2011) 40:233–43. doi: 10.1111/j.1600-0684.2011.00485.x
49. Griffiths KL, Ahmed M, Das S, Gopal R, Horne W, Connell TD, et al. Targeting dendritic cells to accelerate T-cell activation overcomes a bottleneck in tuberculosis vaccine efficacy. *Nat Commun.* (2016) 7:13894. doi: 10.1038/ncomms13894
50. Carow B, Hauling T, Qian X, Kramnik I, Nilsson M, Rottenberg ME. Spatial and temporal localization of immune transcripts defines hallmarks and diversity in the tuberculosis granuloma. *Nat Commun.* (2019) 10:1823. doi: 10.1038/s41467-019-09816-4
51. Slight SR, Rangel-Moreno J, Gopal R, Lin Y, Fallert Junecko BA, Mehra S, et al. CXCR5(+) T helper cells mediate protective immunity against tuberculosis. *J Clin Invest.* (2013) 123:712–26. doi: 10.1172/JCI65728
52. Ernst JD. The immunological life cycle of tuberculosis. *Nat Rev Immunol.* (2012) 12:581–91. doi: 10.1038/nri3259
53. Chackerian AA, Alt JM, Perera TV, Dascher CC, Behar SM. Dissemination of *Mycobacterium tuberculosis* is influenced by host factors and precedes the initiation of T-cell immunity. *Infect Immun.* (2002) 70:4501–9. doi: 10.1128/IAI.70.8.4501-4509.2002
54. Reiley WW, Calayag MD, Wittmer ST, Huntington JL, Pearl JE, Fountain JJ, et al. ESAT-6-specific CD4 T cell responses to aerosol *Mycobacterium tuberculosis* infection are initiated in the mediastinal lymph nodes. *Proc Natl Acad Sci USA.* (2008) 105:10961–6. doi: 10.1073/pnas.0801496105
55. Wolf AJ, Desvignes L, Linas B, Banaiee N, Tamura T, Takatsu K, et al. Initiation of the adaptive immune response to *Mycobacterium tuberculosis* depends on antigen production in the local lymph node, not the lungs. *J Exp Med.* (2008) 205:105–15. doi: 10.1084/jem.20071367
56. Carpenter SM, Nunes-Alves C, Booty MG, Way SS, Behar SM. A higher activation threshold of memory CD8+ T cells has a fitness cost that is modified by TCR affinity during tuberculosis. *PLoS Pathog.* (2016) 12:e1005380. doi: 10.1371/journal.ppat.1005380
57. Grace PS, Ernst JD. Suboptimal antigen presentation contributes to virulence of *mycobacterium tuberculosis in vivo*. *J Immunol.* (2016) 196:357–64. doi: 10.4049/jimmunol.1501494

Conflict of Interest: The authors declare that the research was conducted in the absence of any commercial or financial relationships that could be construed as a potential conflict of interest.

Advantages of publishing in Frontiers

OPEN ACCESS
Articles are free to read for greatest visibility and readership

FAST PUBLICATION
Around 90 days from submission to decision

HIGH QUALITY PEER-REVIEW
Rigorous, collaborative, and constructive peer-review

TRANSPARENT PEER-REVIEW
Editors and reviewers acknowledged by name on published articles

Frontiers
Avenue du Tribunal-Fédéral 34
1005 Lausanne | Switzerland

Visit us: www.frontiersin.org
Contact us: frontiersin.org/about/contact

REPRODUCIBILITY OF RESEARCH
Support open data and methods to enhance research reproducibility

DIGITAL PUBLISHING
Articles designed for optimal readership across devices

FOLLOW US
@frontiersin

IMPACT METRICS
Advanced article metrics track visibility across digital media

EXTENSIVE PROMOTION
Marketing and promotion of impactful research

LOOP RESEARCH NETWORK
Our network increases your article's readership